N O T I C E

THIS DOCUMENT HAS BEEN REPRODUCED FROM MICROFICHE. ALTHOUGH IT IS RECOGNIZED THAT CERTAIN PORTIONS ARE ILLEGIBLE, IT IS BEING RELEASED IN THE INTEREST OF MAKING AVAILABLE AS MUCH INFORMATION AS POSSIBLE

RI/RD80-218-2

(NASA-CR-161622) ORBIT TRANSFER VEHICLE ADVANCED EXPANDER CYCLE ENGINE POINT DESIGN STUDY. VOLUME 2: STUDY RESULTS (Rocketdyne) 365 p HC A16/MF A01 CSCL 21H

N81-15019

Unclas

G3/20 29619

NASA

ORBIT TRANSFER VEHICLE
ADVANCED EXPANDER CYCLE ENGINE
POINT DESIGN STUDY
(VOLUME II: STUDY RESULTS)

ROCKETDYNE
A DIVISION OF ROCKWELL INTERNATIONAL

PREPARED FOR

NATIONAL AERONAUTICS AND SPACE ADMINISTRATION
GEORGE C. MARSHALL SPACE FLIGHT CENTER
HUNTSVILLE, ALABAMA 35812

JAN 1981
RECEIVED
NASA STI FACILITY
ACCESS DEPT.

Rockwell International

Rocketdyne Division
6633 Canoga Avenue
Canoga Park, California 91304

RI/RD80-218-2

ORBIT TRANSFER VEHICLE
ADVANCED EXPANDER CYCLE ENGINE
POINT DESIGN STUDY
(Volume II: Study Results)

CONTRACT NO. NAS8-33568

12 DEC 1980

PREPARED FOR:

NATIONAL AERONAUTICS AND SPACE ADMINISTRATION
GEORGE C. MARSHALL SPACE FLIGHT CENTER
HUNTSVILLE, ALABAMA 35812

PREPARED BY

ADVANCED PROGRAMS
CANOGA PARK, CALIFORNIA

APPROVED BY

H. G. Diem

H. G. DIEM
PROGRAM MANAGER

ROCKETDYNE DIVISION, ROCKWELL INTERNATIONAL CORPORATION
6633 CANOGA AVENUE, CANOGA PARK, CALIFORNIA 91304

FOREWORD

This report presents the results of studies conducted during the Orbital Transfer Vehicle Advanced Expander Cycle Engine Point Design Study. Trade studies, component analysis, component design and engine design layouts were completed for an Advanced Expander Cycle Engine Point Design. A steady state off-design engine simulation model and a transient model were also completed which aided component sizing, selection and placement. The study was conducted by Rocketdyne, a Division of Rockwell International, under contract NAS8-33568 -- administered by Marshall Space Flight Center (MSFC) of the National Aeronautics and Space Administration (NASA). The NASA Contracting Officer's Representative was Mr. Dale Blount of MSFC. Mr. H. G. Diem was the Rocketdyne Program Manager. The technical effort was conducted under the direction of Mr. A. Martinez, Study Manager.

The Final Report is submitted in three parts:

- Vol. I , Executive Summary
- Vol. II , Study Results
- Vol. III, Supporting Research and Technology

The Engine Steady State and Transient simulation user's manuals are submitted separately:

RI/RD80-212, User's Manual for Expander Cycle Rocket Engine Steady-State Off-Design Code

RI/RD80-214, User's Manual for Expander Cycle Rocket Engine Transient Simulation Code

ACKNOWLEDGEMENT

The following personnel provided significant contributions to effort conducted under this contract.

CYCLE SYNTHESIS AND EVALUATION	J. Glass D. Nguyen
OPTIMIZATION CODE, FORMULATION AND IMPLEMENTATION	D. Nguyen J. Glass
COMPONENT HEAT TRANSFER, COMBUSTION, AERODYNAMICS, AND STRESS ANALYSIS	W. Wagner J. Shoji C. Laren J. Lobitz P. Mehegan V. Jaqua E. Fryk H. Otsuki
TURBOMACHINERY SELECTION, ANALYSIS AND DESIGN	A. Csomor G. Jackson R. Sutton R. Furst J. Boynton J. Zorad D. Swaim J. Galazin
THRUST CHAMBER COMPONENT DESIGN	R. Wahl A. Feight P. Jencek R. Saxelby G. Bartee
ENGINE SYSTEM CONTROLS, ANALYSIS AND DESIGN	L. Sack D. Nguyen C. Landis G. Tellier W. Gillon E. Lum
ENGINE DESIGN LAYOUT	H. Marker H. Dubrick C. Andel B. Hines

CONTENTS

	Page
Introduction and Summary	1
Engine System Configuration Definition (Task 1)	1-1
Power Cycle Configuration	1-1
Main Turbine Arrangement	1-1
Cycle Energy Source	1-7
High Pressure Pump Designs	1-9
Boost Pump Drive	1-11
Cooling Circuit Design	1-12
Combustor, Injector Design	1-19
Engine Power Balance and Performance	1-21
Engine Control System	1-31
Primary Valves	1-33
Secondary Valves	1-35
Closed Loop Control	1-36
Controller Redundancy	1-38
Sensors	1-35
Igniter	1-35
Thrust Chamber Design and Performance (Tasks 2, 3)	2-1
Injector Design Description	2-4
Injector Material Selection	2-11
Body and Closeout Materials	2-12
Injector Posts Material	2-13
Faceplate Materials	2-13
Injector Performance	2-14
Injector Face Heat Transfer	2-16
Injector Low Thrust Operation	2-18

CONTENTS (Cont'd)

	Page
Ignition System	2-19
Combustion Chamber Design	2-22
Combustion Chamber Heat Transfer Analysis	2-26
Acoustic Absorber Cooling	2-29
Combustion Chamber Liner Materials	2-35
Materials and Processing Considerations	2-40
Design Characteristics	2-42
Life Considerations	2-42
Material Experience	2-43
Liner Closeout Material	2-45
Manifold Materials	2-46
Combustor Life Evaluation	2-47
Structural Design Criteria and Requirements	2-53
Combustion Stability - Analysis and Design	2-56
Priem Analysis of Acoustic Instability	2-57
Stability Aids Design	2-60
Fixed Nozzle Design - 1 1/2 Pass	2-63
Fixed Nozzle Design - 1 3/4 Pass	2-65
Manifold Design	2-68
Nozzle Jacket	2-69
Recommended Nozzle Materials	2-70
Nozzle Tubes	2-71
Nozzle Jacket - Materials	2-72
Forward Manifold - Materials	2-72
Channel Wall Nozzle Liner - Material	2-73
Fixed Nozzle Cooling Analysis and Circuit Selection	2-74
Nozzle Flow Analysis and Wall Contour Selection	2-81

CONTENTS (Cont'd)

Page

Supersonic Contour Design 2-84

Optimum Thrust Nozzle 2-85

Parabolic Nozzle 2-85

Nozzle Contour Selection 2-88

Extendible Nozzle Design 2-90

Dump Cooled Nozzle Thermal Analysis 2-92

Nozzle Flow Balance 2-94

Dump Nozzle Drag and Heat Retention 2-98

Alternate Dump Nozzle Wall Construction Approaches 2-99

Alternate Extendible Nozzle Concepts 2-99

Regeneratively Cooled Nozzle Extension 2-99

Carbon-Carbon Nozzle 2-101

State-of-the-Art 2-102

Service Life 2-102

Manufacturing and Handling 2-102

Safety and Reliability 2-102

Cost to Manufacture 2-103

Maintainability 2-103

Weight Comparisons 2-103

Recommended Configurations 2-103

Turbomachinery Design and Performance (Tasks 2, 3) 3-1

Turbomachinery Description Summary 3-1

Turbomachinery Design Selection Summary 3-8

High Pressure Oxygen Turbopump 3-8

High Pressure Fuel Turbopump 3-13

Low Pressure Oxygen Turbopump 3-16

Low Pressure Fuel Turbopump 3-18

Hydrogen Turbomachinery — Detailed Design 3-20

Low Pressure Fuel Turbopump 3-20

CONTENTS (Cont'd)

	Page
Pump Performance	3-25
Low Pressure Fuel Turbopump Turbine Analysis	3-31
Technology and Development Issues	3-36
Rotordynamic Analysis	3-42
High Pressure Fuel Turbopump	3-42
Pump Performance	3-46
High Pressure Turbopump Turbine Analysis	3-56
High Pressure Fuel Turbopump	3-66
Off-Design Operation and Performance	3-73
Technology Requirements	3-80
Oxygen Turbomachinery Detail Design	3-81
Low Pressure LOX Boost Turbopump	3-81
Pump Performance Analysis	3-85
LPLTP Turbine Design and Performance Analysis	3-90
Rotordynamic Analysis	3-92
Turbopump Off-Design Operation and Performance	3-92
Technology Requirements	3-92
High Pressure LOX Turbopump	3-98
Pump Performance	3-102
High Pressure Oxidizer Pump Turbine Analysis	3-105
Rotordynamic Analysis	3-119
Turbopump Off-Design Operation and Performance	3-125
Technology Requirements	3-129
Turbomachinery Technology and Development Issue Summary	3-129
Engine Control System	4-1
Control System Selected	4-1
Control Point Selection	4-9
Closed Loop Control	4-12
Start and Shutdown	4-12
Controller Selection	4-13

CONTENTS (Cont'd)

	Page
Redundancy	4-16
Power Distribution	4-22
Conceptual Designs for Control Valves	4-27
Main Oxidizer Valve	4-28
Valving Element	4-28
Seals	4-28
Housing	4-30
Electric Motor Actuator	4-30
Pneumatic Override Piston and Clutch	4-31
Position Indicator	4-31
Materials	4-32
Maintenance	4-32
Main Fuel Valve	4-32
Turbines Bypass Valve	4-32
Oxidizer Turbine Bypass Valve	4-35
Gaseous Oxygen Valve	4-35
Dump Coolant Control Valve	4-35
Igniter Valves	4-39
Tank Pressurization Valves	4-39
Inlet Valves	4-39
Solenoid Control Valves	4-41
Valve Weights Summary	4-41
Engine Start Transient Simulation	4-43
Engine Starts from Pumped Idle Mode	4-43
Off-Design Mixture Ratio	4-45
Engine Power Accessories	5-1
LOX Heat Exchanger - Requirements and Candidate Configurations	5-1
Heat Exchanger Location	5-3
Pressurization System Requirements	5-5

CONTENTS (Cont'd)

	Page
Pressure-Drop Requirements	5-6
Concentric Tube Configuration	5-6
Plate-Stack Configuration	5-8
Selected Liquid, Oxidizer Gasifier Design	5-8
Turbine Gas Regenerator	5-10
Regenerator Location	5-12
Regenerator Configuration Selection	5-13
Heat Exchanger Geometry Optimization	5-15
Engine Configuration Layout	6-1
Engine Operation	6-1
Engine Assembly Layout	6-5
Engine Installation Drawing	6-11
Engine Data Summary	7-1
Mainstage Operation	7-1
Component Pressure-Drop Allocation	7-4
Engine Ducting Flow Velocities and Pressure Losses	7-7
Pressure-Loss Modeling	7-7
Flowrates	7-7
Pressures	7-10
Temperatures	7-10
Performance Prediction	7-11
Expander Cycle Point-Design Performance	7-13
Vaporization and Mixing Efficiency	7-13
Reaction Kinetics	7-18
Two-Dimensional Expansion Efficiency	7-19
Boundary Layer Analysis	7-22
Non-Boundary Layer Heat Loss Efficiency	7-23
Dump-Coolant Specific Impulse	7-26
Life Evaluation - Mainstage	7-26
Fatigue Life Evaluation - Methodology	7-26
Finite-Element Cycle Life Analysis Results	7-26

(CONTENTS (Cont'd)

	Page
Cycle Life Analysis-Regenerative Cooling Code	7-31
Cycle Life Without Regenerator	7-32
Cycle Life With Regenerator	7-32
Nozzle and Nozzle Extension Cycle Life	7-43
Operation at MR = 7	7-43
Performance Prediction - MR = 7	7-45
Combustor Cycle Life at MR = 7	7-47
Nozzle and Nozzle Extension Cycle Life at MR = 7	7-47
Low-Thrust Operation	7-47
Tanked-Idle Mode Operation	7-51
Pumped-Idle Operation	7-57
Oxidizer-Side Pressure Drops	7-57
Performance Prediction-Pumped Idle	7-63a
Weight and Mass-Property Breakdowns	7-63
NPSH Requirements and Capabilities	7-66
Cavitation Evaluation	7-69
Two-Phase Evaluation	7-70
Pump Inlet Conditions	7-73
Two-Phase Limits	7-74
Evaluation of Results	7-83
OTV Tank Vapor Pressure	7-86
10 Psia Tank Vapor Pressure	7-86
References	R-1
Appendix A - Control Valve Specification	A-1

ILLUSTRATIONS

		Page
Fig. 1	Advanced Expander Cycle Engine Point Design Configuration, Retracted Nozzle Not Shown.	4
Fig. 2	Advanced Expander Cycle Engine Point Design Study, Schedule .	5
Fig. 1-1	Advanced Expander Engine Point Design Evolved from NAS8-33568 Studies.	1-3
Fig. 1-2	Expander Engine Schematics.	1-4
Fig. 1-3	Expander Cycle Engine Point Design Schematic.	1-5
Fig. 1-4	Tee-Mounted Turbomachinery, Advanced Expander Cycle Engine Point Design.	1-10
Fig. 1-5	Advanced Expander Thrust Chamber Coolant Circuits, Optimized Flight-Weight Design.	1-13
Fig. 1-6	Advanced Expander Engine Thrust Chamber Coolant Circuit Designs	1-15
Fig. 1-7	Advanced Expander Thrust Chamber Coolant Circuit, Recommended Baseline Design for Test Verification	1-18
Fig. 1-8	Flow, Pressure, Temperature and Power Schedule, F=15Klb,MR=6.	1-23
Fig. 1-9	Flow, Pressure, Temperature and Power Schedule, F=15K,MR=7. .	1-24
Fig. 1-10	Flow, Pressure, Temperature, and Power Schedules, Pumped Idle	1-25
Fig. 1-11	Flow, Pressure, and Temperature Schedules, Tank Head Idle . .	1-26
Fig. 1-12	Advanced Expander Cycle Engine Specific Impulse vs.Area Ratio	1-28
Fig. 1-13	Normalized OTV Payload for 6:1 Mixture Ratio.	1-28
Fig. 1-14	Engine Control System	1-32
Fig. 1-15	Primary Valves, Advanced Expander Cycle Engine Point-Design .	1-34
Fig. 1-16	Dual-Dual Redundant Cross-Strapped System	1-39
Fig. 2-1	Advanced Expander Cycle Engine Point-Design, Thrust Chamber Assembly.	2-2
Fig. 2-3	Advanced Expander Cycle Injector Concept.	2-4
Fig. 2-2	OTV-Thrust Chamber Assembly Layout.	2-5
Fig. 2-4	Injector, Expander Point Design Engine Layout (Inertia Welded)	2-7
Fig. 2-5	Injector Element Components	2-10

Illustrations (Cont'd)

		Page
Fig. 2-6	Expander Cycle Injector Rigimesh Face Temperature Rise vs. H_2 Transpirant Flow.	2-17
Fig. 2-7	Expander Cycle Injector Rigimesh Face Temperature vs.Flowrate	
Fig. 2-8	Igniter, Assembly of OTV Dual.	2-17
Fig. 2-9	Advanced Expander Cycle Combustion Chamber	2-23
Fig. 2-10	OTV-Combustor Assembly	2-24
Fig. 2-11	Thrust Chamber Manufacturing Flow Chart.	2-26
Fig. 2-12	Candidate Combustor Controus	2-27
Fig. 2-13	Comparison of Total Heat Input to Coolant for Various Combustor Lengths	2-28
Fig. 2-14	LO_2/H_2 Expander (Tapered Controu) Combustor Heat Transfer Coefficient Test Data Correlation.	2-30
Fig. 2-15	Cylindrical Chamber Wall Heat Flux Distribution, Mixture Ratio Influence, LO_2/GH_2	2-30
Fig. 2-16	Comparison of Design with regard to Peak Heat Flux, Injector Region Heat Flux, and Combustor Integrated Heat Flux	2-31
Fig. 2-17	LO_2/H_2 Advanced Expander Cycle Engine Tapered Controu Combustion Channel Geometry.	2-32
Fig. 2-18	Advanced Expander Cycle Engine Combustor Temperature Profiles	2-33
Fig. 2-19	Acoustic Cavity Cooling Detail	2-34
Fig. 2-20	Acoustic Absorber Temperature Profile.	2-35
Fig. 2-21	Thrust Chamber Thermal Fatigue Analysis.	2-38
Fig. 2-22	NARloy-Z Ingot Processing and Inspection	2-41
Fig. 2-23	Life Analysis Logic Diagram	2-48
Fig. 2-24	Combustor Life Cycle Analysis Models	2-50
Fig. 2-25	Stability Parameter (A_p) Analysis	2-58
Fig. 2-26	Priem Analysis of Advanced Expander Thrust Chamber	2-59
Fig. 2-27	Acoustic Absorber Effectiveness.	2-62
Fig. 2-28	Stability Threshold Correlations and Design Point.	2-62
Fig. 2-29	OTV-Fixed Nozzle Assembly 1 1/2 - Pass	2-64
Fig. 2-30	Nozzle, Expander Cycle, 1 3/4 Pass Assembly of	2-66
Fig. 2-31	Nozzle Coolant Manifold Arrangement.	2-68

Illustrations (Cont'd)

		Page
Fig. 2-32	Nozzle Turnaround Manifold and Nozzle Extension Mechanism Interface	2-70
Fig. 2-33	Advanced Expander Cycle 1-3/4-Pass Fixed Nozzle Parametric Results	2-76
Fig. 2-34	Advanced Expander Cycle Nozzle Transition Channel Geometry	2-77
Fig. 2-35	Advanced Expander Cycle Nozzle Transition Temperature Profiles	2-77
Fig. 2-36	Advanced Expander Cycle Nozzle Tube Geometry	2-78
Fig. 2-37	Advanced Expander Cycle Nozzle Tube Temperature Profiles	2-79
Fig. 2-38	Throat Geometry for Transonic Flow Analysis	2-82
Fig. 2-39	Transonic Flowfield Solution for Advanced Expander Cycle	2-83
Fig. 2-40	Nozzle Design Method	2-84
Fig. 2-41	Nozzle Percent Length (15K Thrust)	2-86
Fig. 2-42	Normalized OTV Payload for 6:1 Mixture Ratio	2-86
Fig. 2-43	Expander Nozzle Contour	2-89
Fig. 2-44	Nozzle, Assembly of OTV Extendable	2-91
Fig. 2-45	Expander Thrust Chamber Dump-Cooled Nozzle Parametrics, Wall Thickness, 0.0045 In.	2-95
Fig. 2-46	Expander Cycle Thrust Chamber Dump-Cooled Nozzle Parametrics Wall Thickness, 0.0055 In.	2-96
Fig. 2-47	Expander Cycle Thrust Chamber Dump-Cooled Nozzle Parametrics Wall Thickness, 0.0065 In.	2-97
Fig. 2-45	Examples of Dump-Cooled Nozzle Wall Design Concept Considered	2-100
Fig. 3-1	Expander Cycle Engine Schematic	3-2
Fig. 3-2	Expander Cycle Liquid Oxygen Turbomachinery "T" Mount	3-4
Fig. 3-3	Expander Cycle Hydrogen Turbomachinery "T" Mount	3-7
Fig. 3-4	Expander Cycle LOX Pump Study	3-12
Fig. 3-5	Expander Cycle Fuel Pump Study	3-15
Fig. 3-6	Fuel Low Pressure Pump	3-22
Fig. 3-7	Fuel Low Pressure Turbopump Material Selection	3-23

Illustrations (Cont'd) Page

Fig. 3-8 Fuel Low Pressure Turbopump Development Instrumentation Selection. 3-24
Fig. 3-9 Low Pressure Fuel Pump Efficiency and Head Coefficient 3-29
Fig. 3-10 Fuel Boost Pump Suction Performance. 3-30
Fig. 3-11 Low Pressure Fuel Pump Normalized Performance. 3-32
Fig. 3-12 Low Pressure Fuel Turbopump Turbine Mean Diameter Optimization. 3-34
Fig. 3-13 Low Pressure Fuel Turbine, Velocity Vector Diagram 3-37
Fig. 3-14 Low Pressure Fuel Turbopump Turbine Performance. 3-40
Fig. 3-15 Low Pressure Fuel Turbopump Turbine Off-Design Performance . . 3-41
Fig. 3-16 Fuel Low Pressure Turbopump. 3-43
Fig. 3-17 Critical Speed vs. Bearing Stiffness 3-44
Fig. 3-18 Low Pressure Fuel Turbopump Critical Speeds. 3-45
Fig. 3-19 Fuel - High Pressure Turbopump 3-47
Fig. 3-20 Fuel - High Pressure Turbopump Material Selection. 3-48
Fig. 3-21 Fuel - High Pressure Turbopump Development Instrumentation Selection. 3-49
Fig. 3-22 Flowrate Profiles in High Pressure Fuel Pump 3-50
Fig. 3-23 Pressure and Density Profiles in High Pressure Fuel Pump . . . 3-51
Fig. 3-24 Temperature Profiles in High Pressure Fuel Pump. 3-52
Fig. 3-25 Head and Efficiency vs. Capacity, High Pressure Fuel Pump. . . 3-55
Fig. 3-26 Balance Piston Flow and Performance, High Pressure Fuel Pump . 3-57
Fig. 3-27 Mean Diameter Optimization, High Pressure Fuel Turbopump Turbine. 3-60
Fig. 3-28 Velocity Vector Diagrams, High Pressure Fuel Turbopump Turbine. 3-62
Fig. 3-29 HPFTP Turbine - Expander Engine Blade Path State Conditions. . 3-64
Fig. 3-30 HPFTP Turbine Preliminary Turbine Blade Path Data. 3-65
Fig. 3-31 Off-Design Performance, High Pressure Fuel Turbopump Performance 3-67
Fig. 3-32 Predicted Efficiency, High Pressure Fuel Turbopump Turbine . . 3-68
Fig. 3-33 Fuel - High Pressure Turbopump 3-69

Illustrations (Cont'd) Page

Fig. 3-34 Critical Speeds vs. Bearing Stiffness High Pressure Fuel Turbopump 3-71
Fig. 3-35 Critical Speeds and Mode Shapes High Pressure Fuel Turbopump . 3-72
Fig. 3-36 Off-Design Pump Flow Profiles 3-74
Fig. 3-37 Off-Design Pump Pressure, Density Profiles 3-75
Fig. 3-38 Off-Design Pump Temperature Profiles 3-76
Fig. 3-39 Pump Performance Characteristics at Pumped-Idle 3-79
Fig. 3-40 Oxidizer - Low Pressure Turbopump 3-82
Fig. 3-41 Oxidizer Low Pressure Turbopump Material Selection 3-83
Fig. 3-42 Oxidizer Low Pressure Turbopump Development Instrumentation Selection 3-84
Fig. 3-43 Overall Head and Efficiency, Low Pressure Pump 3-87
Fig. 3-44 Velocity Vector, Low Pressure LOX Pump 3-88
Fig. 3-45 Suction Performance, Low Pressure LOX Pump 3-89
Fig. 3-46 Turbine Efficiency, Low Pressure LOX Turbopump Turbine 3-93
Fig. 3-47 Critical Speeds vs. Bearing Stiffness Low Pressure LOX Turbopump 3-94
Fig. 3-48 Critical Speeds and Mode Shapes, Low Pressure LOX Turbopump . . 3-95
Fig. 3-49 Nodal Point Locations, Critical Speeds Study, Low Pressure LOX Turbopump 3-96
Fig. 3-50 Off-Design Performance, Low Pressure LOX Turbopump 3-97
Fig. 3-51 Oxidizer - High Pressure Turbopump 3-99
Fig. 3-52 Oxidizer - High Pressure Turbopump Material Selection 3-100
Fig. 3-53 Oxidizer - High Pressure Turbopump Development Instrumentation Selection 3-101
Fig. 3-54 Efficiency and Dimensionaless Headrise, High Pressure Oxidizer Pump 3-103
Fig. 3-55 Cavitation Performance, High Pressure Oxidizer Pump 3-106
Fig. 3-56 Balance Piston Thrust, High Pressure Oxidizer Pump 3-107
Fig. 3-57 High Pressure Oxidizer Turbopump Turbine Mean Diameter Optimization 3-110
Fig. 3-58 Velocity Vector Diagram, High Pressure LOX Turbopump Turbine . 3-112

Illustrations (Cont'd) Page

Fig. 3-59 Off-Design Efficiency, High Pressure Oxidizer Turbopump Turbine. 3-117

Fig. 3-60 Off-Design Flow Parameter, High Pressure Oxidizer Turbopump Turbine. 3-118

Fig. 3-61 Critical Speed vs. Bearing Stiffness, High Pressure LOX Turbopump. 3-120

Fig. 3-62 Oxidizer - High Pressure Turbopump, Critical Speed Node Locations. 3-121

Fig. 3-63 Critical Speeds and Mode Shapes, High Pressure Oxidizer Turbopump 3-122

Fig. 3-64 Critical Speed vs. Bearing Stiffness, First Re-design High Pressure LOX Turbopump 3-123

Fig. 3-65 Critical Speeds and Mode Shapes First Redesign High Pressure Turbopump. 3-124

Fig. 3-66 Critical Speed vs. Bearing Stiffness, Second Redesign High Pressure Oxidizer Pump 3-126

Fig. 3-67 Critical Speed and Mode Shapes, Second Redesign, High Pressure LOX Turbopump 3-127

Fig. 3-68 Efficiency and Head Ratio, High Pressure LOX Pump. 3-128

Fig. 3-69 Characteristics of Turbopump Operation 3-132

Fig. 4-1 Series Turbines Baseline Engine Main Propellant Controls . . . 4-3

Fig. 4-2 Schematic-Expander Cycle System (OTV). 4-4

Fig. 4-3 Dual-Dual Redundant Cross-Strapped System (Recommended System for OTV Engine). 4-6

Fig. 4-4 Primary Valves, Advanced Expander Cycle Engine Point-Design. . 4-8

Fig. 4-5 Effect on Thrust and Mixture Ratio of Varying Individual Valve Flow Areas 4-11

Fig. 4-6 Controller Comparisons 4-17

Fig. 4-7 Valve Position-Feedback Closed-Loop Control System 4-20

Fig. 4-8 Mainstage-Trim Closed-Loop Control 4-21

Fig. 4-9 Dual Redundant Rail System 4-23

Fig. 4-10 Dual Redundant Cross-Strapped System (SSME Configuration). . . 4-24

Fig. 4-11 Triple Redundant Cross-Strapped System 4-25

Illustrations (Cont'd) Page

Fig. 4-12 Dual-Dual Redundant Cross-Strapped System (Recommended for OTV Engine) 4-26
Fig. 4-13 Main Oxidizer Valve-OTV 4-29
Fig. 4-14 Main Fuel Valve-OTV 4-33
Fig. 4-15 GH_2 Turbine Bypass Valve - OTV 4-34
Fig. 4-16 Oxidizer Turbine Bypass Valve - OTV 4-36
Fig. 4-17 Gaseous Oxidizer Valve 4-37
Fig. 4-18 Dump-Coolant Control Valve 4-38
Fig. 4-19 LOX Inlet Valve 4-40
Fig. 4-20 Expander Engine Start from Tank-Head Idle Mode 4-44
Fig. 4-21 Expander Engine Closed-Loop Control of Thrust and Mixture Ratio 4-46
Fig. 5-1 Candidate Oxidizer Heat Exchangers 5-2
Fig. 5-2 Expander Engine Schematic 5-4
Fig. 5-3 Concentric Tube Heat Exchanger Length Requirements 5-7
Fig. 5-4 Liquid Oxygen Gasifier 5-9
Fig. 5-5 Expander Engine Schematics 5-14
Fig. 5-6 Sample Regenerator Model Output 5-16
Fig. 5-7 Turbine Gas Regenerator 5-17
Fig. 6-1 Hydrogen Flow in Advanced Expander Engine Point Design 6-2
Fig. 6-2 Oxygen Flow in Advanced Expander Engine Point Design 6-4
Fig. 6-3 Engine System Assembly & Interface - Expander Cycle System (OTV) 6-6
Fig. 6-4 Gimbal/Thrust Mount Layout 6-10
Fig. 6-5 Latching Mechanism Details 6-12
Fig. 6-6 Engine System Installation-Expander Cycle System (OTV) 6-13
Fig. 7-1 Flow, Pressure, Temperature and Power Schedule F=15K LB.,MR=6. 7-5
Fig. 7-2 JANNAF Simplified Performance Procedures, Performance Parameters and Computer Programs 7-2
Fig. 7-3 Injector Mixing Efficience Comparison 7-16
Fig. 7-5 Injector Performance from CICM Model Analyses 7-17
Fig. 7-6 Parametric and Point-Design Kinetic Analysis 7-20
Fig. 7-7 Parametric and Point-Design Two-Dimensional Nozzle Efficiency. 7-21

Illustrations (Cont'd) Page

Fig. 7-8 Nozzle Boundary Layer Drag Losses. 7-24

Fig. 7-9 Boundary Layer Efficiency Correlation. 7-25

Fig. 7-10 Heated Hydrogen Specific Impulse 7-27

Fig. 7-11 Life Analysis Logic Diagram. 7-29

Fig. 7-12 Flow, Pressure, Temperature and Power Schedule, F=15K LB,MR=7. 7-44

Fig. 7-13 Flow, Pressure, and Temperature Schedules - Tank Head Idle . . 7-55

Fig. 7-14 Flow, Pressure, Temperature, and Power Schedules, Pumped Idle. 7-61

Fig. 7-15 Thermodynamic Suppression Head Factor for Various Propellants as a Function of Vapor Pressure. 7-71

Fig. 7-16 Liquid Flow Densities. 7-75

Fig. 7-17 Vapor Fraction Differential Changes for Isentropic Expansions from a Saturated Liquid. 7-76

Fig. 7-18 Vapor to Liquid Density Ratios 7-77

Fig. 7-19 Approximate Acoustic Parameter 7-82

Fig. 7-20 Inducer Blade Vapor Pumping Capacity for OTV Boost Pumps . . . 7-84

TABLES

		Page
Table 1	Engine Requirements	2
Table 1-1	Performance-Optimized Advanced Expander Cycle Engine Baseline Design Characteristics	1-2
Table 1-2	Optimization Aspects Impacting Thrust Chamber Design	1-2
Table 1-3	Thrust Chamber Heat Load Capabilities (60-Inch Engine Length, ε = 625)	1-7
Table 1-4	Thrust Chamber Heat Load Capabilities (60-Inch Engine Length, ε = 625)	1-8
Table 1-5	Coolant Circuit Design, Parameters, Optimized Flightweight Expander Thrust Chamber	1-16
Table 1-6	Comparison of Nozzle Configuration Parameters	1-17
Table 1-7	Advanced Expander Cycle Engine Point Design Performance	1-22
Table 1-8	Control System Selection	1-37
Table 2-1	Advanced Expander Thrust Chamber Design Summary (Thrust Chamber Length = 107 Inches)	2-3
Table 2-2	Injector Component Materials	2-12
Table 2-3	Injector Element Design Parameters	2-15
Table 2-4	Advanced Expander Thrust Chamber Efficiency Parameters	2-16
Table 2-5	Initial ASE Ignition Test Summary	2-22
Table 2-6	Room Temperature Properties for Candidate Alloys	2-36
Table 2-7	Combustion Chamber Liner Experience	2-44
Table 2-8	Resistance to Softening During Exposure to a Temperature of 1000F	2-45
Table 2-9	Properties of Electrodeposited Nickel	2-46
Table 2-10	Thermal Gradient Loading	2-49
Table 2-11	Life Summary of Coolant Channel Section at Critical Throat Region	2-51
Table 2-12	Fusion Weld Joint Efficiency Factors	2-55
Table 2-13	Electron Beam Weld Joint Efficiency Factors	2-55
Table 2-14	Expander Cycle Fixed Nozzle Parameters	2-67
Table 2-15	Recommended Nozzle Materials	2-71
Table 2-16	Mechanical Properties of A286 and Type 347 CRES	2-71

TABLES (Cont'd) Page

Table 2-17 Candidate Materials for Nozzle Manifolds (Room Temperature) . 2-73

Table 2-18 Advanced Expander Cycle Thrust Chamber, 1-3/4 Pass Nozzle Parameters, F=15K Thrust, P_c = 1540 PSIA. 2-80

Table 2-19 Advanced Expander Cycle Thrust Chamber Parameters, F=15K Thrust, P_c = 1540 PSIA, 1 1/2 Pass Circuit. 2-81

Table 2-20 Performance of Parabolic Nozzle Contours for Fixed Length and Area Ratio. 2-88

Table 2-21 Advanced Expander Cycle Engine Point Design Dump-Cooled Nozzle Parameters 2-93

Table 3-1 Expander Cycle Turbomachinery Description Summary 3-3

Table 3-2 Preliminary Turbomachinery Selection Rankings 3-9

Table 3-3 Expander Cycle High Pressure Oxygen Turbopump Trade Study . . 3-10

Table 3-4 Expander Cycle High Pressure Fuel Turbopump Trade Study . . . 3-14

Table 3-5 Expander Cycle Low Pressure Oxygen Boost Pump Drive Trade Study 3-17

Table 3-6 Expander Cycle Low Pressure Fuel Boost Pump Drive Trade Study.3-19

Table 3-7 Expander Cycle Engine Point-Design Turbomachinery, Operating Parameters. 3-21

Table 3-8 Low Pressure Fuel Pump Design 3-27
3-28

Table 3-9 Low Pressure Fuel Turbopump Turbine Performance Parameters. 3-33

Table 3-10 Low Pressure Fuel Turbopump Turbine, Flange-to-Flange Efficiency and Performance. 3-35

Table 3-11 Low Pressure Fuel Turbopump Turbine, Blade Path State Conditions. 3-38

Table 3-12 Low Pressure Fuel Turbopump Turbine, Prelinary Turbine Blade Path Data 3-39

Table 3-13 Low Pressure Fuel Turbopump Turbine, Blade Path Geometry Assumptions 3-42

Table 3-14 Expander Cycle High Pressure Fuel Pump at 110,000 RPM 3-54

Table 3-15 High Pressure Fuel Turbopump Turbine, Performance Parameters. 3-59

Table 3-16 High Pressure Fuel Turbopump Turbine, Flange to Flange Efficiency and Performance. 3-61

TABLES (Cont'd) Page

Table 3-17 High Pressure Fuel Turbopump Turbine, Blade Path Geometry Assumptions. 3-66
Table 3-18 Expander Cycle High Pressure Fuel Pump 3-78
Table 3-19 LOX Boost Pump Inducer Design. 3-86
Table 3-20 Expander Cycle High Pressure Oxidizer Pump 3-104
Table 3-21 High Pressure Oxidizer Turbopump Expander Turbine Performance Parameters. 3-109
Table 3-22 High Pressure Oxidizer Turbopump Expander Engine Flange to Flange Efficiency and Performance. 3-111
Table 3-23 High Pressure Oxidizer Turbopump Turbine 3-114
Table 3-24 High Pressure Oxidizer Turbopump Turbine - Preliminary Turbine Blade Path Data. 3-115
Table 3-25 High Pressure Oxidizer Turbopump - Blade Path Geometry Assumptions. 3-116

Table 4-1 Engine Controls System Concepts Definition 4-2
Table 4-2 Expander Cycle Performance 4-10
Table 4-3 Actuator Requirements. 4-14
Table 4-4 OTV Expander Cycle Start and Shutdown Controller Requirements. 4-15
Table 4-5 Controller Functions for Manned OTV. 4-18
Table 4-6 Controller Trade Study Summary 4-19
Table 4-7 Valve Name, Symbol, Weight 4-42

Table 5-1 LOX Heat Exchanger Flowrates, (lb/sec) 5-5
Table 5-2 LOX Heat Exchanger Geometry. 5-10
Table 5-3 LOX Heat Exchanger Requirements. 5-11

Table 6-1 Preliminary OTV Ducting Design 6-7

Table 7-1 Engine Design Point Balance. 7-2, 7-3 7-4
Table 7-2 Design-Point Valve Characteristics 7-6
Table 7-3 Component ΔP Allocation. 7-6
Table 7-4 Design Engine Ducting Preliminary Characteristics. 7-8

TABLES (Cont'd)

		Page
Table 7-5	Expander Cycle Secondary Flows.	7-9
Table 7-6	JANNAF Methodology Thrust Chamber Performance Efficiency Factors.	7-11
Table 7-7	Advanced Expander Cycle Engine Point Design Performance (Thrust = 15K, MR - 6.0).	7-14
Table 7-8	Expander Injector η_{c*} Values.	7-18
Table 7-9	Life Summary of Coolant Channel Section at Critical Throat Region.	7-31
Table 7-10	Combustor Cycle Life Analysis, MR = 6.45, Stations 0-29	7-33 7-34 7-35
Table 7-11	Combustor Cycle Life Analysis, MR-6.45, Stations 43-72, with Turbine Gas Regenerator	7-36
Table 7-12	Combustor/Nozzle Transition Section Cycle Life Analysis, Mr - 6.45, 1-3/4 Pass Nozzle.	7-37
Table 7-13	Fixed Nozzle (1-3/4 Pass) Cycle Life Analysis, MR=6	7-38
Table 7-14	Nozzle Extension Cycle Life Analysis, Mr = 6. . . .	7-39
Table 7-15	Engine Balance, Mr = 7.	7-40 7-41 7-42
Table 7-16	Advanced Expander Engine Point Design Performance (Thrust = 15K, MR = 7.0).	7-46
Table 7-17	Combustor Cycle Life Analysis, MR = 7.7, with Turbine Gas Regenerator	7-48
Table 7-18	Combustor Nozzle Transition Section, Cycle Life 1-3/4 Pass, MR - 7.7, with Turbine Gas Regenerator.	7-49
Table 7-19	Fixed Nozzle Cycle Life, 1-3/4 Pass, MR - 7.7, with Turbine Gas Regenerator	7-50
Table 7-20	Engine Balance at Tanked Idle	7-52 7-53 7-54
Table 7-21	Advanced Expander Performance at Tanked Idle. . . .	7-56

TABLES (Cont'd)

		Page
Table 7-22	Engine Balance - Pumped Idle	7-58, 7-59, 7-60
Table 7-23	Advanced Expander Thrust Chamber Performance (Thrust = 1.8K, MR = 4.0)	7-62
Table 7-24	Expander Cycle Engine Point Design Weight Characteristics	7-64
Table 7-25	Expander Cycle Engine Mass Properties	7-65
Table 7-26	Original OTV Suction Requirements	7-66
Table 7-27	Feed Line Geometries	7-67
Table 7-28	Assumptions for Predicting Pump Inlet Conditions	7-68
Table 7-29	OTV Boost Pump operating Conditions	7-68
Table 7-30	Thermodynamic Suppression Head Effects	7-72
Table 7-31	OTV Boost Pump Two Phase* Pumping Evaluation Under Full Flow Conditions	7-78
Table 7-32	OTV Boost Pump Two Phase* Pumping Evaluation Under Pump Idle Mode Flow Conditions	7-79
Table 7-33	Two Phase Pumping Limits	7-81
Table 7-34	Conclusions and Recommendations	7-85

INTRODUCTION AND SUMMARY

NASA-sponsored studies of the Orbit Transfer Vehicle (OTV) have evaluated during recent years the use of a high-energy oxygen/hydrogen upper stage employing advanced engines for the Space Transportation System. Engine studies resulting from NAS 8-32996 efforts indicated that expander cycle engine components can be optimized for delivery of the high performance and reliability required of the OTV engines. NAS 8-33568 study results reported herein, have led to an optimized expander engine point design concept which delivers high performance and reliability and provides growth and design margin capabilities. These studies have concentrated on the thrust chamber and turbomachinery as the key components of the engine power cycle and have provided component and system designs of sufficient depth to produce accurate engine and component weights, accurate engine and turbomachinery performance, engine control techniques and technology verification requirements.

The Orbit Transfer Vehicle (OTV) has as a goal the same basic characteristics as its parent system, the Space Shuttle, i.e., reusability, operational flexibility, and payload retrieval with high reliability and low operating cost. The OTV is thus planned to be a manned, reusable cryogenic upper stage of high performance and reliability. The requirements for the engine of a vehicle of this type have been derived from a large number of NASA-sponsored vehicle and engine studies. For the advanced expander cycle engine, these requirements were outlined in the Statement of Work of the recently completed Advanced Expander Cycle Engine Point Design Study Contract, NAS8-33568, and appear in Table 1.

The Advanced Expander Cycle Engine Point Design identified in these studies relies on increased combustor surface area and on turbine gas regeneration to obtain significant increases in hydrogen coolant bulk temperature The higher temperature hydrogen derives the turbine power required to achieve chamber pressures approximately four times those realized in the conventional expander cycle engines. Increased chamber length or wetted perimeter provide added heat transfer surface area and increased heat loads, while turbine gas regeneration provides higher hydrogen bulk temperature without increasing combustor heat

TABLE 1. ENGINE REQUIREMENTS

1. The engine will operate as an expander cycle with liquid hydrogen and liquid oxygen propellants.

2. Engine vacuum thrust will be 15K pounds at an engine O_2/H_2 weight flowrate mixture ratio of 6.0, with programmed mixture ratio in the range 6 to 7.

3. Engine length with the two-position extendible nozzle retracted will be no greater than 60 inches.

4. Engine design and materials technology are to be based on 1980 state of the art.

5. The engine must be capable of accommodating programmed and/or command variations in mixture ratio over an operating range of 6:1 to 7:1 during a given mission. The effects on engine operation and lifetime must be predictable over the operating mixture ratio range.

6. The propellant inlet temperature will be 162.7 R for the oxygen boost pump and 37.8 R for the hydrogen pump. The boost pump inlet NPSH at full thrust will be 2 feet for the oxygen pump and 15 feet for the hydrogen pump.

7. The service free life of the engine cannot be less than 60 start/shutdown cycles or 2 hours accumulated run time, and the service life between overhauls cannot be less than 300 start/shutdown cycles or 10 hours accumulated run time. The engine will have provisions for ease of access, minimum maintenance, and economical overhaul.

8. The engine when operating within the nominal prescribed range of thrust, mixture ratio, and propellant inlet conditions will not incur during its service life chamber pressure oscillation, disturbances, or random spikes greater than ±5% of the mean steady-state chamber pressure. Deviations to be expected in emergency modes will be predictable.

9. The engine nozzle is to be a contoured bell with an extendible/retractable section.

10. Engine gimbal requirements are +15 degrees and -6 degrees in the pitch plane and ±6 degrees in the yaw plane.

11. The engine is to provide gaseous hydrogen and oxygen autogenous pressurization for the propellant tanks.

12. The engine is to be manrated and capable of providing abort return of the vehicle to the Orbiter orbit.

13. The engine design will meet all of the necessary safety and environmental criteria of being carried in the Orbiter payload bay and operating in the vicinity of the manned orbiter.

14. The engine must be adaptable to extended low-thrust operation of approximately 1K vacuum thrust. Kitting of the engine's injectors, turbine flow area, and other constraining components may be considered as well as the inclusion of a heat exchanger to gasify the LOX for low-thrust operation. Engine mixture ratio will be maintained as high as cooling and power constraint allow (but no greater than 7:1).

input. These hydrogen temperature augmentation procedures place the increased demands of pump power generation on the combustor and led to wall temperature, cycle life, and pressure drop limitations not previously found in the conventional expander cycle engine. To ease the demands placed on the thrust chamber, efficient utilization of the thermal energy is made in the turbomachinery, valves, heat exchangers, ducts, and other components. The NAS8-33568 effort has selected component designs, cooling schemes, structural designs, and fabrication procedures which allow the system to deliver high performance and meet the prescribed cycle life.

The engine system design (Fig. 1) was chosen from engine trade and optimization studies conducted in Contracts NAS8-32996 and NAS8-33568. These studies indicated that the limit of chamber pressure and specific impulse obtained within a given engine length is reached when combustor material temperature limits are reached, when the increased coolant pressure drops cancel the benefits of the turbine temperature increases, or when the nozzle length is compromised, affecting specific impulse adversely. Not all conditions that maximize chamber pressure necessarily led to specific impulse maximization. It was found that specific impulse optimized at chamber pressures lower than the maximum values attainable. Engine system optimization procedures and tradeoffs were performed to provide an engine system design where specific impulse is maximized but yet adequate margins are provided in engine power, thrust chamber life, and operating temperatures; and where cost, weight, technology level and reliability considerations play an important role.

The engine as configured in NAS8-33568 studies delivers 480.8 sec. of specific impulse operating at a chamber pressure of 1,540 psia and mixture ratio of 6:1. The engine system achieves a nozzle area ratio of 625:1 within a total engine length of 117 in. In the retracted nozzle configuration the engine occupies a length of 60 in. The engine has been designed to satisfy the requirements of Table 1.

To accomplish the effort described in the Statement of Work (SOW), nine technical tasks were defined and a program schedule outlined as indicated in Fig. 2.

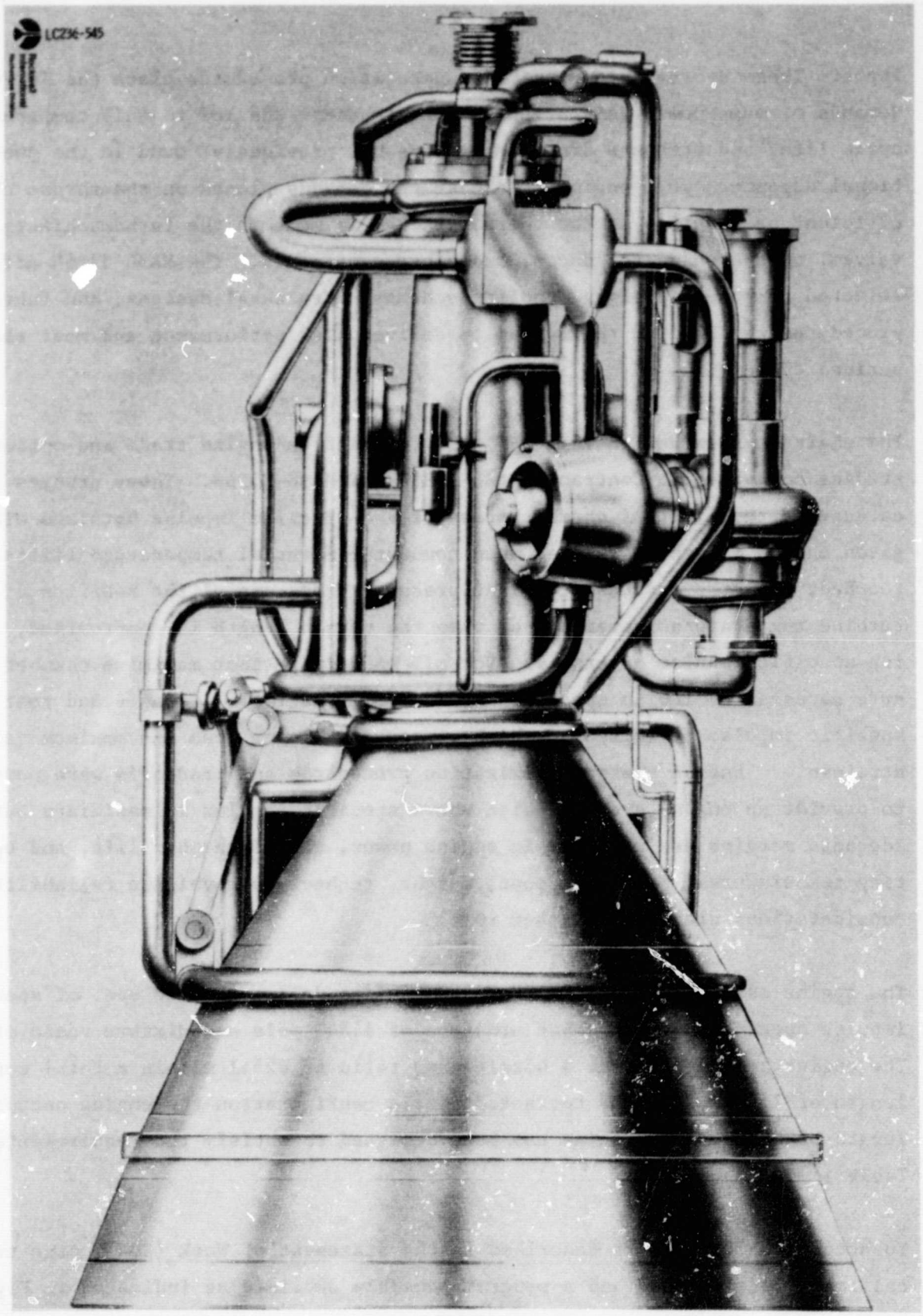

Figure 1. Advanced Expander Cycle Engine Point Design Configuration, Retracted Nozzle Not Shown

ORIGINAL PAGE IS
OF POOR QUALITY

FIG. 2 **ADVANCED EXPANDER CYCLE ENGINE POINT DESIGN STUDY**

(NAS8-33568)

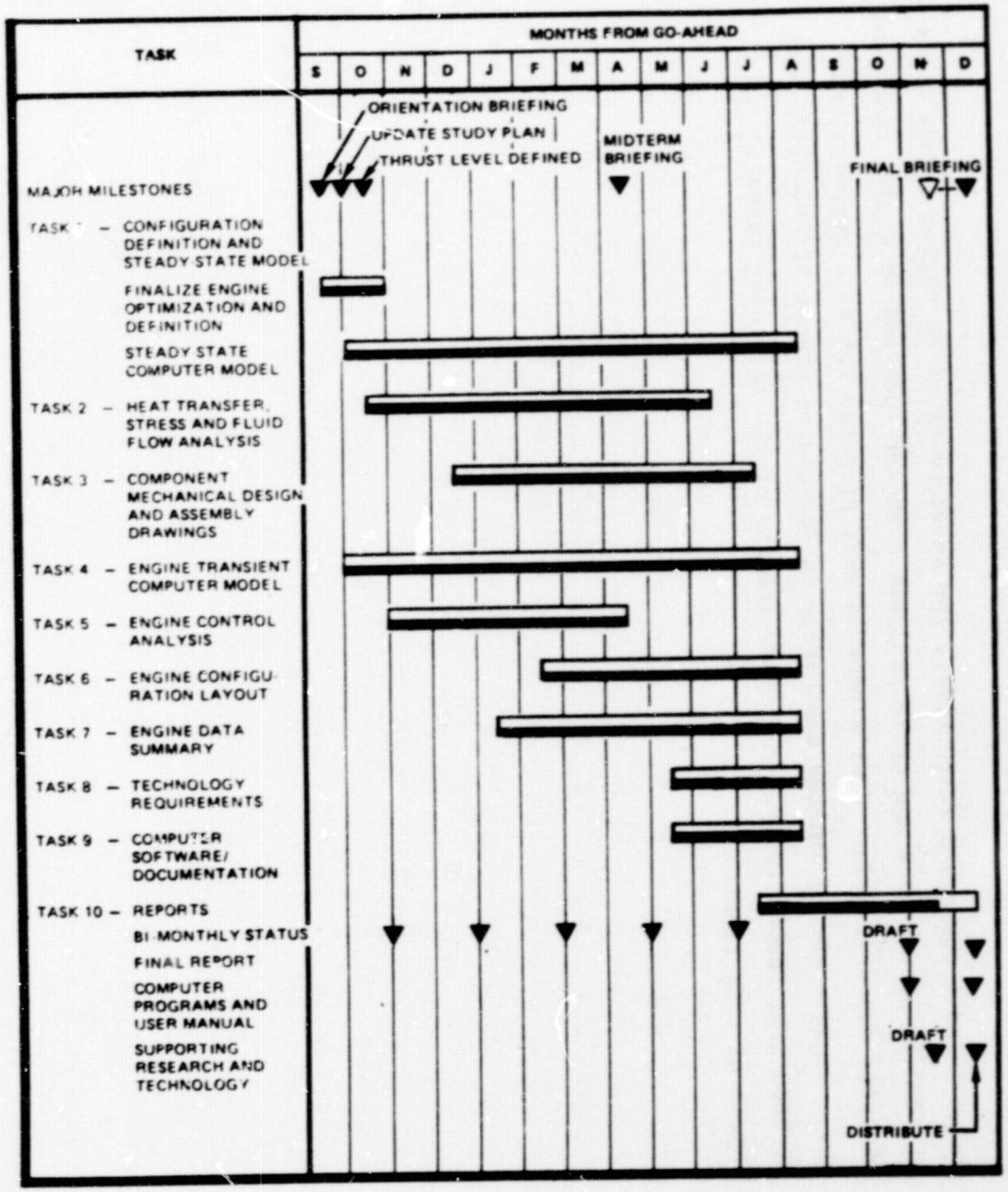

ORIGINAL PAGE IS OF POOR QUALITY

Tasks 1 and 4 comprised respectively the development of an engine steady state off-design performance and cycle analysis computer code and an engine transient analysis computer code. User's manuals were prepared for each computer code. These manuals are documented separately in Rocketdyne report RI/RD80-212, and RI/RD80-214, respectively. The study results of the remaining tasks is the object of this report.

ENGINE SYSTEM CONFIGURATION DEFINITION (TASK 1)

The design characteristics of the baseline engine configuration selected from the trade and optimization studies performed in Task 1 are presented in Table 1-1 This selection resulted from specific impulse performance and weight optimization of the engine in the 10K to 20K pound-thrust range. Selection of component design and performance levels was made to provide design margins that will reduce engine development risks. Although, for the engine length selected, performance optimizes near an area ratio of 800:1, the recommended design (Fig. 1-1) utilizes a nozzle with expansion area ratio of 625:1 in an extended engine legnth of 117 in. The lower area ratio value facilities altitude testing in idle mode, reduces test and fabrication costs, results in a lower engine weight, and causes a negligible loss in payload performance. Engine optimization aspects considered in the study and which directly impact the design of the baseline thrust chamber are shown in Table 1-2 and discussed below.

POWER CYCLE CONFIGURATION

Four major areas of power cycle optimization were examined: main turbine arrangement, cycle energy source, high-pressure pump design, and boost pump drive. Cycle configurations resulting from the first two areas were: parallel main turbines, series main turbines, turbine gas regeneration and turbine gas reheat. These cycles and combinations thereof are illustrated in Fig. 1-2. They were evaluated with smooth-wall combustors and with thermally enhanced combustor configurations.

Main Turbine Arrangement

The selected chamber pressure of 1,540 psia is consistent with 1980 technology and was obtained with optimized turbomachinery operating in a series main turbine arrangement (Fig. 1-3) for maximum utilization of available energy in the hydrogen coolant. For the selection of series over parallel main turbine arrangement, an engine cycle optimizer code was allowed to optimize engine specific impulse under the following constraints: turbine/pump geometry, and

TABLE 1-1. PERFORMANCE-OPTIMIZED ADVANCED EXPANDER CYCLE ENGINE BASELINE DESIGN CHARACTERISTICS

BASELINE DESIGN CHARACTERISTICS	
FULL THRUST (VACUUM), POUNDS	15,000
MIXTURE RATIO	6
CHAMBER PRESSURE, PSIA	1540
EXPANSION AREA RATIO	625
SPECIFIC IMPULSE, SECONDS	480.8
PUMP DISCHARGE PRESSURE, PSIA	
OXYGEN	2650
HYDROGEN	4670
PUMP SPEEDS, RPM	
OXYGEN	52,800
HYDROGEN	110,000
TURBINE INLET TEMPERATURE, R	875
RETRACTED LENGTH, INCHES	60
EXTENDED LENGTH, INCHES	117
ENGINE DRY WEIGHT, POUNDS	475
TECHNOLOGY BASIS	1980
DESIGN FEATURES	
FULL-FLOW REGENERATIVE COOLING	
SERIES MAIN TURBINES	
GH_2 DRIVEN LOW PRESSURE HYDROGEN PUMP	
GASEOUS HYDROGEN TURBINE DRIVEN LOW-PRESSURE LOX PUMP	
SMOOTH-WALL 20-INCH-LONG COMBUSTION CHAMBER	
AUTOGENOUS TANK PRESSURIZATION	
TURBINE GAS REGENERATION	

TABLE 1-2. OPTIMIZATION ASPECTS IMPACTING THRUST CHAMBER DESIGN

POWER CYCLE	OPTIMIZED/SELECTED VALUES
TURBOPUMP SYSTEM (NUMBER OF PUMP STAGES)	
FUEL	3
OXIDIZER	1
TURBINE ARRANGEMENT	SERIES
LOW-PRESSURE TURBINE AND PUMP DRIVES, FUEL/OXIDIZER	GH_2/FULL-FLOW HYDRAULIC
HIGH-PRESSURE TURBINE AND PUMP DRIVES, FUEL/OXIDIZER	GH_2/GH_2
THRUST CHAMBER	
HEAT LOADS REQUIREMENTS, BTU/SEC	10,000
COOLING CIRCUIT	FULL-FLOW REGEN
CYCLE LIFE	300 x 4
COOLANT PRESSURE DROP, PSID	370
TURBINE GAS REGENERATION	
DRIVE GAS DELTA TEMPERATURE, R	100
ENGINE CONTROL AND POWER MARGINS	
FLOWRATE, %	10
PRESSURE DROP, %	10
ENGINE OFF-DESIGN OPERATION	
MIXTURE RATIO	7
THRUST, % OF NORMAL	10

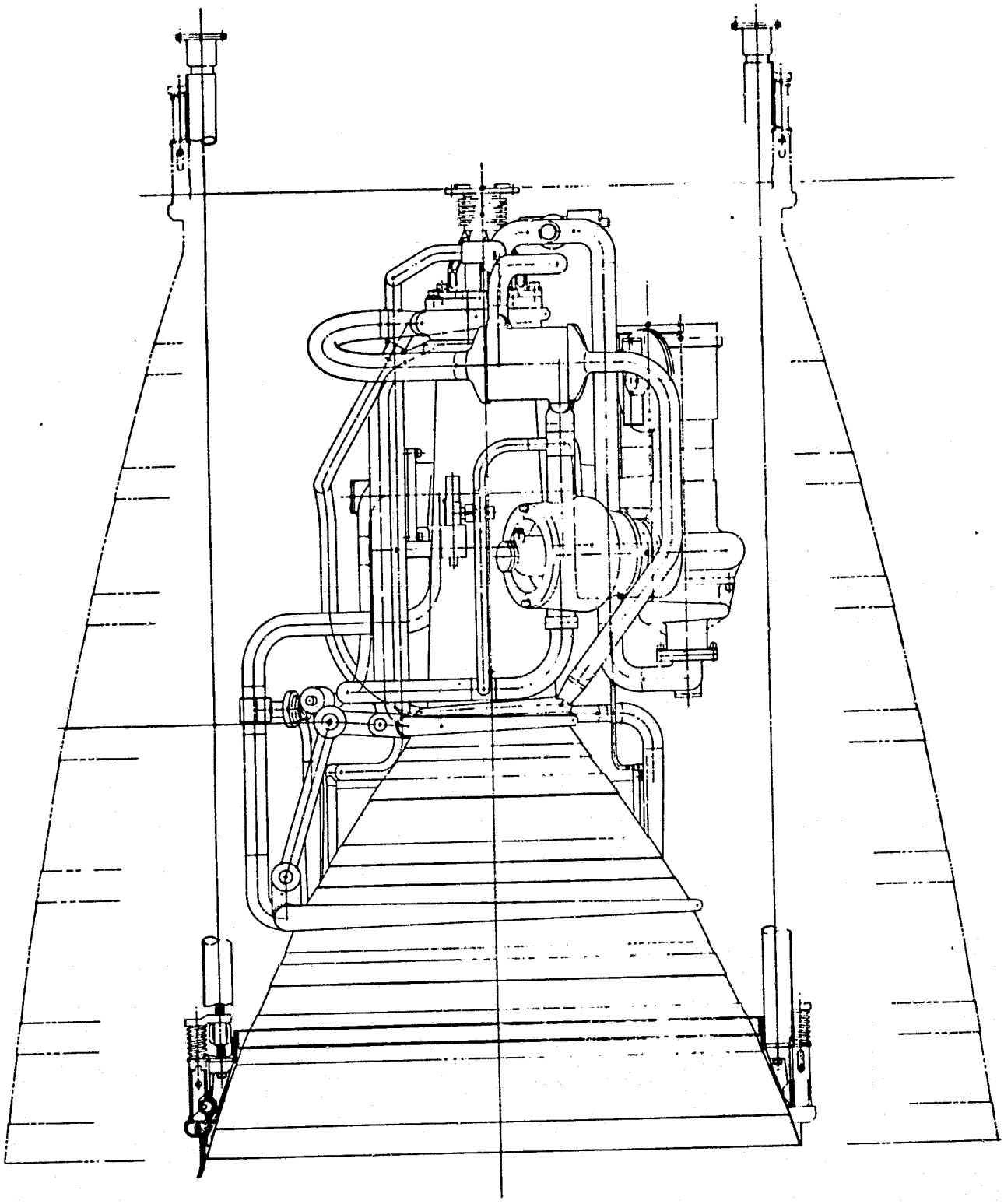

Figure 1-1. Advanced Expander Engine Point Design Evolved From NAS8-33568 Studies

ORIGINAL PAGE IS
POOR QUALITY

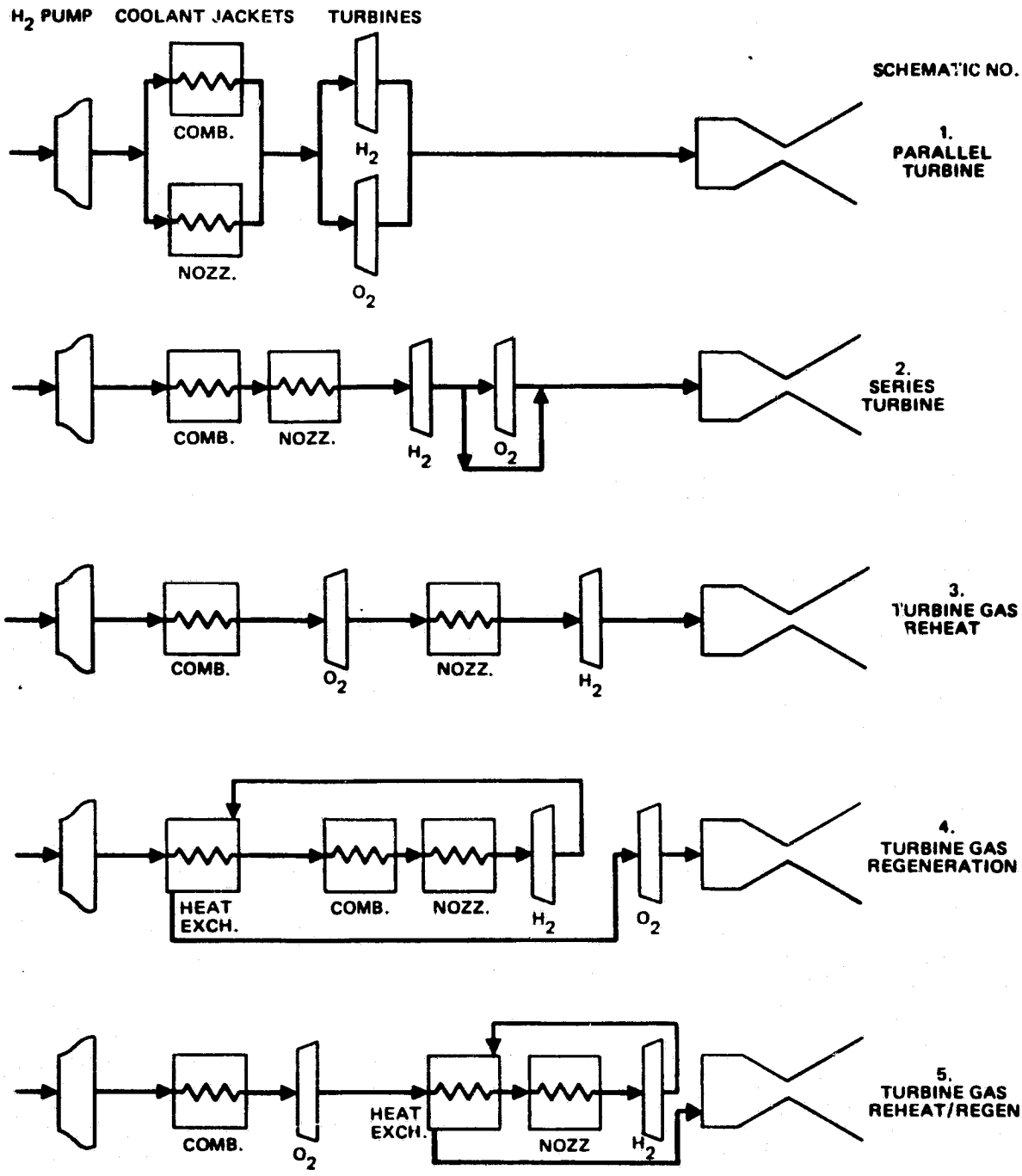

Figure 1-2 Expander Engine Schematics

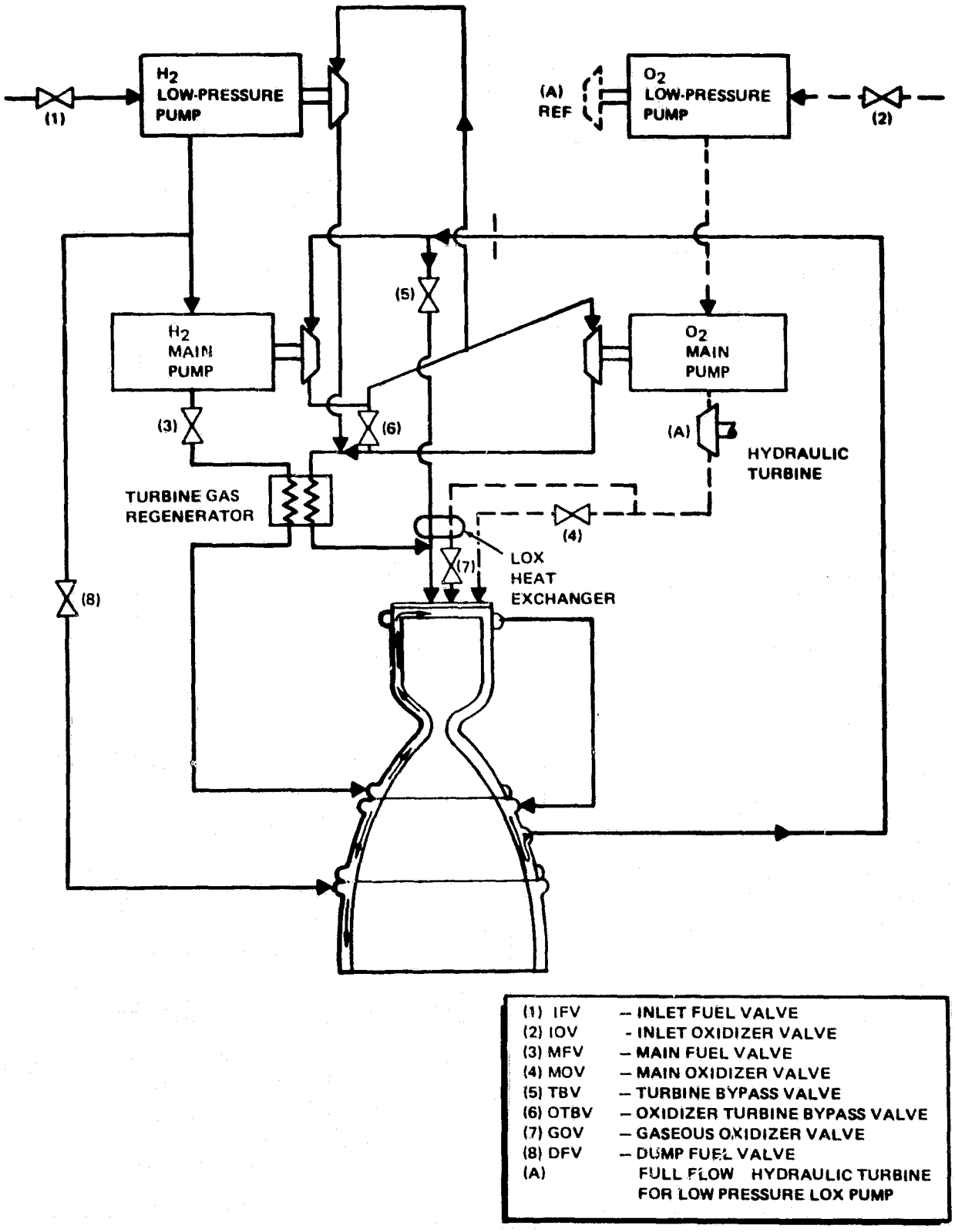

Figure 1-3. Expander Cycle Engine Point Design Schematic

bearing DN compatible with 1980 technology; combustor length limits of 10 to 20 inches; coolant jacket bulk temperature limits of 1000 and 1260 R, respectively for combustor and nozzle; and certain flow and pressure drop margins. The optimizer was allowed to vary nozzle expansion area ratio, pump speed, chamber pressure, pressure ratio, and combustor length to arrive at an optimum delivered specific impulse and a corresponding chamber pressure. Results for the series versus parallel turbine case, for a thrust level of 15,000 pounds demonstrated that the series turbine arrangement can attain approximately 230 psi higher in chamber pressure than the parallel turbine arrangement. The reason for this is that more flow is available to each turbine in the series configuration than in the parallel arrangement. The higher flowrate allows higher turbine power. It allows also higher volume flow in the turbines and, therefore, improved turbine efficiencies and higher turbine arc of admission. The higher chamber pressure in the series turbine arranged engine results in higher nozzle expansion area ratio and thus, approximately 2 seconds higher specific impulse.

A turbine inlet temperature of 875 R is required to develop the necessary turbine power. This is achieved through high thermal input to the hydrogen in the combustor and nozzle, and through recycling of part of this heat in a turbine gas regenerator to boost turbine inlet temperature.

Turbine power margins are provided in the form of a pressure drop reserve of 10 percent built into a calibrated system orifice, and in the form of a turbine gas bypass reserve of 10 percent. These combined reserves are set aside for engines where worst-case probable variations in turbomachinery efficiencies and uncertainties in the component pressure drop and heat load determination would create system power loss deviations from the average engine and, therefore, lower chamber pressures. Use of the pressure drop and/or flow reserve will return the engine chamber pressure and thrust to the required value. Thrust chamber heat loads, turbine gas regeneration and power margin requirements are discussed in the following section.

Cycle Energy Source

Approximately 10,000 Btu/sec transferred from the hot gas to the hydrogen coolant in the thrust chamber is required to provide enough pump power to support a chamber pressure of 1400 psia (Table 1-3), and provide the power margins levels discussed in the previous section. This required combustor heat load was determined using procedures correlated to heat load values demonstrated experimentally in the 8.6-inch-long combustor of the Advanced Space Engine (ASE). In the expander cycle, a combustor of conventional length (10 inches), similar to the ASE combustor, can only deliver 866 psi chamber pressure with efficient turbomachinery (Table 1-3).

TABLE 1-3. THRUST CHAMBER HEAT LOAD CAPABILITIES
(60-INCH ENGINE LENGTH, ε = 625)

COMBUSTOR CONFIGURATION	TOTAL THRUST CHAMBER HEAT LOAD, BTU/SEC	COMBUSTOR HEAT LOAD, BTU/SEC	NOZZLE HEAD LOAD, BTU/SEC	TURBINE INLET TEMPERATURE, R	POWER MARGINS		P_c* PSIA	NOZZLE PERCENT LENGTH	I_s, SECONDS
					ΔP	$\dot{W}$			
10-INCH CYLINDRICAL	6416	3675	2741	472	10	10	866	66.2	471.5
20-INCH CYLINDRICAL	9502	6601	2901	702	10	10	1300	73.1	478.4
20-INCH TAPERED	10093	7218	2875	760	10	10	1400	75.7	479.9

*MAXIMUM CHAMBER PRESSURE CAPABILITY WITHOUT A REGENERATOR

A 20-inch cylindrical combustor provides a 40 percent increase in heat loads and a significantly increased chamber pressure (1300 psia). Longer combustor lengths would provide higher total heat loads and higher chamber pressure but would result in nozzle percent lengths below 80 percent and consequently lower specific impulse performance.

Gradual tapering of the nozzle combustor wall starting at a station 3 inches from the injector provides reduced heat flux at the nozzle throat and a more evenly distributed heat flux profile. It also provides more favorable boundary layer conditions approaching the throat and reduces the tendency of boundary layer separation. The improved heat loads resulting from wall tapering allow attainment of 1400 psia chamber pressure without turbine gas regenerator effects as discussed below.

Turbine Gas Regenerator Effects

The turbine inlet gas temperature obtained with the 20-inch combustor length is not sufficient to sustain chamber pressures higher than 1400 psia. Within the 1980 state-of-the-art technology, it is not possible to increase heat loads in a length restricted chamber through thermal enhancement schemes. With the 20-inch tapered combustor, the calculated maximum wall temperature is 810 F, a value still below the imposed limit of 1000 F (Table 1-4), above which hot gas wall erosion becomes a factor.

TABLE 1-4. THRUST CHAMBER HEAT LOAD CAPABILITIES
(60-INCH ENGINE LENGTH, ε = 625)

COMBUSTOR CONFIGURATION	TOTAL THRUST CHAMBER HEAT LOAD, BTU/SEC	COMBUSTOR MAXIMUM WALL TEMPERATURE, F	TURBINE INLET TEMPERATURE R,	POWER MARGINS		P_c, PSIA	NOZZLE PERCENT LENGTH	I_s, SECONDS
				ΔP	$\dot{W}$			
20-INCH CYLINDRICAL	9502	913	702	10	10	1300	73.1	478.4
20-INCH TAPERED	10093	810	760	10	10	1400	75.7	479.9
20-INCH TAPERED WITH REGENERATOR	9987	858	872	10	10	1540	79.4	480.8

Turbine gas regeneration can be employed to increase the turbine gas inlet temperature at the expense of increasing the wall temperature, as long as the required thrust chamber cycle life is not compromised. It was found feasible to achieve a 100 degree increase in turbine inlet temperature with only a moderate increase in wall temperatures without a decrease in cycle life. The turbine gas regenerator thus provided a viable scheme for a significantly increased chamber pressure (1540 psia, Table 1-4) making it possible to retain the power margins previously adopted for contingencies arising during development of the engine. This design approach was selected as the baseline configuration.

Turbine gas regeneration is accomplished within a countercurrent heat exchanger. The thermal capacitance of fluids and components comprising the regenerator power cycle accumulates the additional heat reflected in the higher turbine inlet temperature.

This heat is picked up by the cold hydrogen liquid from the pump prior to entry into the coolant chamber. The heat pumping process increases the bulk temperature of the hydrogen exiting the nozzle coolant jacket, which is used to drive the main turbines in series arrangement. The thermal effectiveness required of the heat exchanger is low (18 percent) because only a small quantity of heat (1800 Btu/sec) is required to obtain the desired turbine temperature rise of 100 R. For this effectiveness, a counter current platelet heat exchanger design of low weight (16 pounds) is utilized which provides an AMOTV round trip increase of 70 pounds in payload* through the increase in chamber pressure and specific impulse (Table 1-4).

Within limits established by the chamber hot-gas wall temperature, the turbine gas regenerator design can be altered to furnish a certain amount of additional engine power margin. This would provide for unforseen contingencies in system and component pressure drops, turbomachinery efficiencies, or combustor and nozzle heat loads.

HIGH PRESSURE PUMP DESIGN

The high pressure turbomachinery make use of a three-stage fuel pump, with partial admission two-stage gaseous hydrogen driven turbine stages; and a single stage oxidizer pump, with partial admission single-stage gaseous turbine drive. These pumps are supplied with required suction head by a set of low pressure pumps which are each integrated with their respective high pressure pumps in a "T"configuration (Fig. 1-4). The low pressure oxygen pump is hydraulically driven which reduces the number of interpropellant seals. The"T"configuration takes full advantage of the full-flow hydraulic drive feature to provide a compact set of low/high pressure oxygen turbomachinery with good packaging capabilities, reduction of interconnecting duct lengths and hydraulic losses, and improved integration with the inlet valve. The T-mounted hydrogen turbomachinery also results in compact packaging. This type of mounting needs experimental development and evaluation on effects of orientation on pump head and suction

*Aeromaneuvering Orbit Transfer Vehicle as defined in NASA TMX-73394.

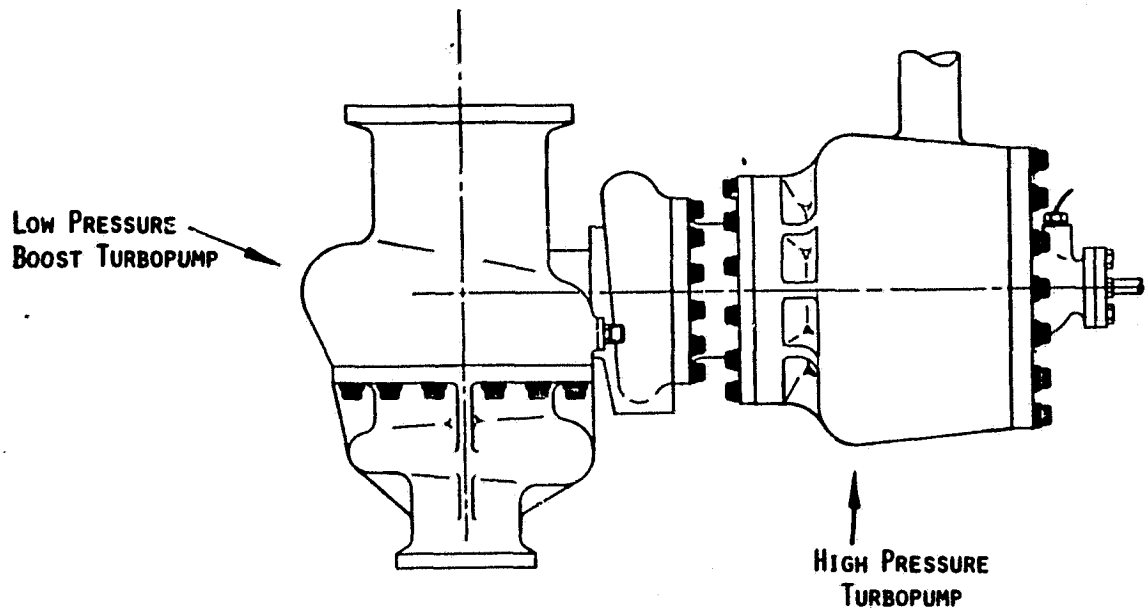

a) Oxidizer Turbomachinery

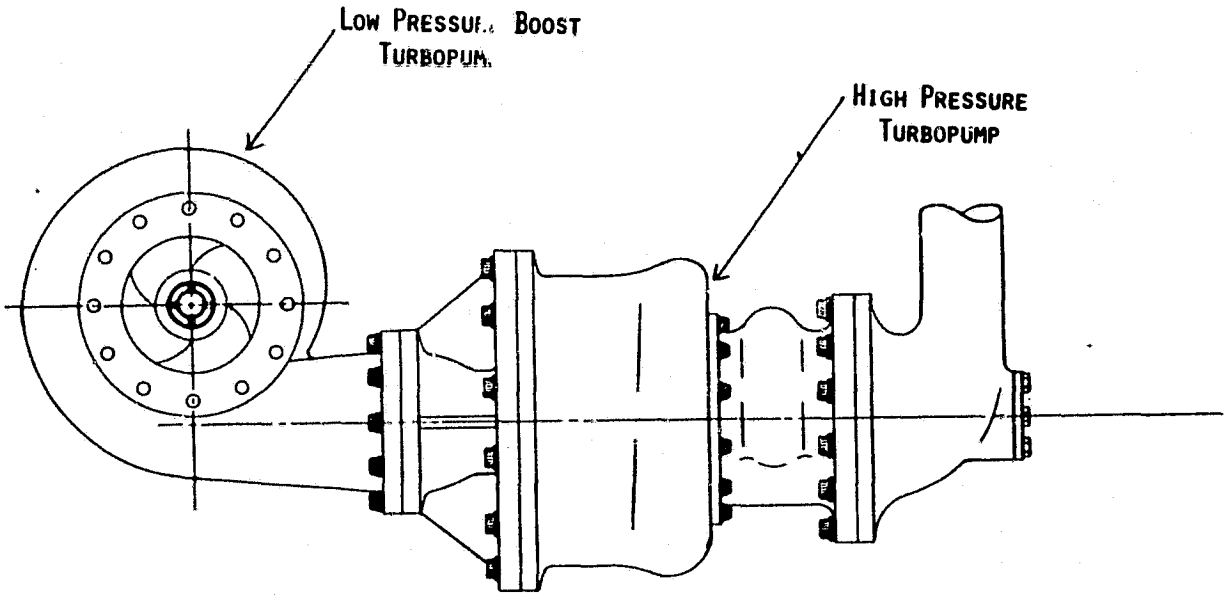

b) Fuel Turbomachinery

Figure 1-4. Tee-Mounted Turbomachinery, Advanced Expander Cycle Engine Point Design

performance. The design allows for separate fabrication of the turbopump for development and verification of performance capabilities, and later integration for evaluation of performance effects of the T-orientation.

Within the bearing DN limits established by the 1980 technology ground rule and other ground rules for pump and turbine parameters, high-pressure hydrogen pump speeds of 110,000 rpm are required to provide maximum efficiency of utilization of turbine derived power. The engine pump speeds and bearing DN are consistent with 17 mm diameter bearings. Similar size bearings (20 mm) have received extensive testing in the Advanced Space Engine (ASE) fuel (MK 48F) and oxidizer (MK 48-Ø) pump technology development programs. Speeds of 52,800 rpm are sufficient to provide acceptable performance in the high pressure oxygen pump whose power consumption is approximately 1/4 that of the hydrogen pump.

Because of the high torque required to drive both main pumps from a single turbine and the resultant impact on gear life, a single turbine with geared drives was ruled out for the high pressure turbomachinery. Similar life considerations and the added requirement of off-design mixture ratio of 7:1 operation ruled out dual turbines with synchronizing gears even though this scheme may be advantageous for ease of engine control during engine transient buildup and decay.

The fuel pump design is a three-stage centrifugal machine with inducer and axial inlet, similar to the successful design of the ASE. The fuel impellers are 3.8 inches in diameter with a tip speed and stage specific speed of 1824 ft/sec and 669, respectively. The oxidizer pump is a single stage centrifugal pump of 2.55 inches impeller diameter, 590 ft/sec tip speed and 1122 specific speed. Pump thermodynamic efficiencies are 64 percent and 66.6 percent, respectively for the hydrogen and oxygen pumps.

Boost Pump Drive

The impact of boost pump drive method upon overall engine performance is small because of the low horsepower requirements for these pumps, therefore, other factors provide the basis for selection of the boost pump drive method.

A gaseous hydrogen turbine drive was chosen for the low pressure hydrogen pump based upon trade studies considering performance, transient characteristics, flexibility of design, complexity, and packaging and testing flexibility. The hydrogen boost pump turbine is placed in parallel arrangement with the main oxidizer turbine. Adequate flow and pressure ratio is obtained for this turbine at this location. The gaseous hydrogen turbine drive approach provides for the possibility of some degree of control over the start transient. Operation is initiated early in the sequence of events and thus enhances system chilldown during tank head idle mode (THI). This turbine drive allows for maximum flexibility of packaging, provides flexibility in off-design operation, has good life capability, and provides flexibility during development testing since boost pump components can be tested separate from the main pump.

The oxygen boost pump employs a full-flow hydraulic turbine placed in series with the main pump high pressure discharge outlet, utilizing the full main pump flow. The advantages of the full-flow hydraulic boost pump drive are integrated packaging, no interpropellant seal usage, high efficiency, zero leakage and thus zero nonpropulsive propellant losses, low speed and good life capability.

Geared drives were studied and eliminated on the basis of the maximum life demonstrated (5.56 hours) at a pitch line velocity of 16,000 fpm (Ref. 1-1) A pitch line velocity of 25,000 fpm would be required to maintain high main pump performance. This high pitch line velocity coupled with a 10 hour life requirement could result in a significant development problem.

COOLING CIRCUIT DESIGN

The cooling circuit optimized in the engine trade and optimization studies is a full-flow regenerative scheme depicted in Fig. 1-5 . All of the hydrogen flow, except for pump seal leakage, bearing cooling flows and that used in the dump-cooled nozzle, is used in cooling the combustion chamber and fixed nozzle in series arrangement. This hydrogen flow enters the combustor coolant jacket from the turbine-gas regenerator outlet at an expansion area ratio of approximately 14:1 and cools the combustor by flowing in an up-pass manner. Entrance at this

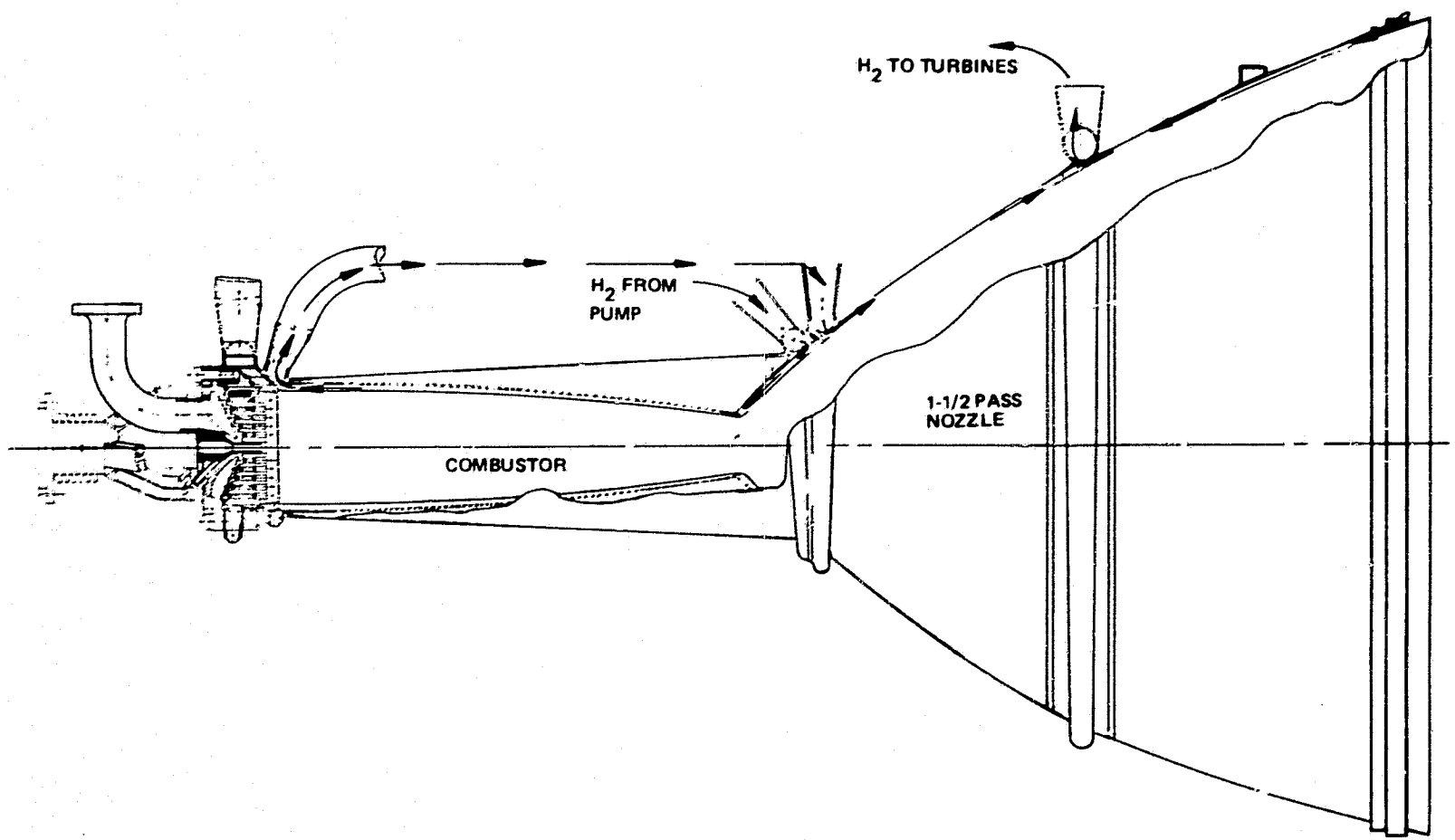

Figure 1-5. Advanced Expander Thrust Chamber Coolant Circuits, Optimized Flightweight Design

area ratio allows for low coolant bulk temperatures at the most critical chamber cross section (upstream of throat) governing chamber life. It also results in the lowest hydrogen bulk temperatures exiting the combustor coolant jacket, and therefore, enhances chamber life.

The coolant flow is collected at the injector plane and is routed to the nozzle coolant distributing manifold at an expansion area ratio of approximately 14:1. From here it flows to the end of the fixed nozzle (ε = 225) in a downpass manner, turned around and returned in uppass manner to exit the nozzle at an area ratio of 95:1. This results in a 1-1/2 coolant passes in the fixed nozzle. Lower pressure drops and lower manifold weights result from the 1-1/2-pass scheme. The heated hydrogen is then directed to the fuel turbine. This circuit allows for the highest fuel turbine inlet temperatures since the coolant exit temperature is governed by the maximum allowable nozzle coolant bulk temperatures. This limit of 1260 R for the fixed nozzle is higher than that of the combustor (1000 R) since because of lower heat fluxes, the nozzle cycle life is higher than the combustor. Coolant circuit design parameters are shown in Table

A 1-1/2 uppass circuit starting part way down the nozzle (Fig. 1-6) and having as final point the injector plane was considered but not selected since the maximum hydrogen bulk temperature is controlled by the maximum allowable combustor wall temperature and results in the lowest fuel turbine inlet temperatures (1000 R).

Split-flow regenerative cooling as used in the ASE thrust chamber (Fig. 1-6) was evaluated for the advanced expander thrust chamber and eliminated on the basis of high coolant pressure drops. The higher surface area of the 20-inch combustor length and lower coolant flowrate of the split-flow regenerative cooling scheme led to higher coolant velocities and attendant higher coolant pressure drops for the required chamber life.

A single downpass cooling scheme for the fixed nozzle starting at an area ratio of approximately 14:1 and ending at an area ratio of 225:1 results in a simpler

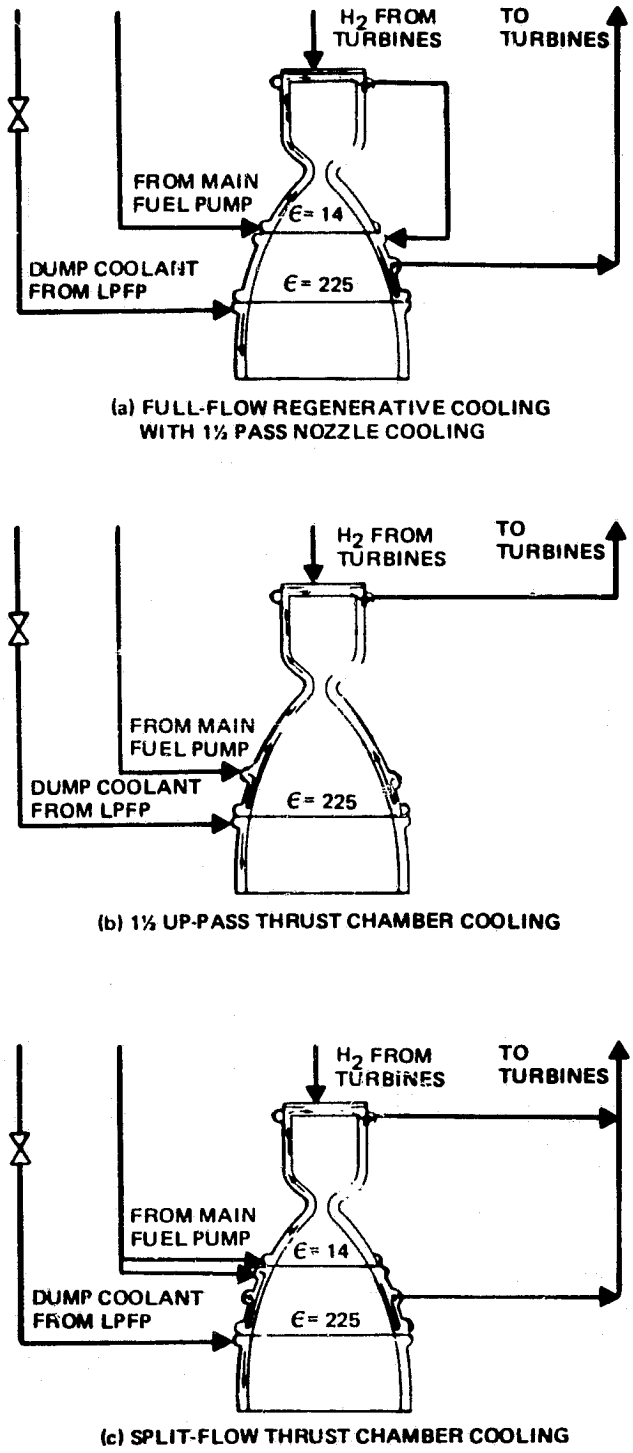

Figure 1-6. Advanced Expander Engine Thrust Chamber Coolant Circuit Designs

TABLE 1-5. COOLANT CIRCUIT DESIGN, PARAMETERS, OPTIMIZED FLIGHTWEIGHT EXPANDER THRUST CHAMBER

	COMBUSTOR	FIXED NOZZLE	EXTENDIBLE NOZZLE
CIRCUIT TYPE	SINGLE UPPASS REGENERATIVE	1-1.2 PASS REGENERATIVE	SINGLE DOWNPASS DUMP COOLED
AREA RATIOS (ε)	ε = 14 TO INJECTOR	ε = 14 TO ε = 225 TO ε = 95 TO TURBINE	ε = 225 to ε = 625
NUMBER OF CHANNELS (TUBES)	98	280/560	1080
WALL THICKNESS, INCH	0.025 TO 0.035	0.010	0.0045
CLOSED-OUT WALL THICKNESS, INCH	0.060	--	--
MINIMUM LAND WIDTH, INCH	0.040	--	--

nozzle mechanical design that can provide fabrication cost savings for test-demonstration hardware. This configuration can provide similar heat loads (Table 1-5) and pressure drops as the 1-1/2 pass scheme but will result in a heavier fixed nozzle because of the bigger diameter coolant collection manifold. To obtain a lower weight and to facilitate incorporation of the nozzle retracting mechanism and attach hardware, the flight weight nozzle hardware would require the 1-1/2 pass scheme.

Chamber pressures resulting from single pass, 1-1/2 pass and full 2-pass coolant circuit designs are shown in Table 1-6 . A full 2-pass circuit from an attach area ratio of 14:1 results in high coolant pressure drops. A large portion of the pressure drop occurs near the exit of the full 2-pass circuit where the coolant densities are the lowest and velocities are high. Although the heat pickup is slightly higher in the 2-pass, its coolant pressure drop reduces chamber pressure ~ 100 psi below the reference 1-1/2-pass system.

Fabrication complexity of the 1-1/2 pass nozzle can be improved with a 1-3/4-pass nozzle construction which makes use of a transition milled channel copper piece between the combustor and tubular nozzle to provide a coolant departure plane midway between that of the full 2-pass circuit and the 1-1/2 circuit. By avoiding the last 4 inches of the 2-pass flow circuit, a large portion of the coolant pressure drop is avoided so that chamber pressure is not compromised in the 1-3/4-pass nozzle (Table 1-6). The milled channel piece, however, adds

TABLE 1-6. COMPARISON OF NOZZLE CONFIGURATION PARAMETERS

Nozzle Design Parameters	1 Pass	1-1/2 Pass	1-3/4 Pass	Full 2 Pass
N, Number of Tubes	360	280	180/180	180/180
ΣQ, Btu/sec	2608	2494	2548	2565
ΔP, Psi	42	50	68	340
ΔT, R	180	175	177	182
$T_{wg_{MAX}}$, F	724	718	593	683
Projected Flight Weight, Pounds	70.8	62.6	67.9	ND
P_c, psia	1540	1540	1540	1437

*ND = No Design Layout Made

extra weight (Table 1-6) to the flightweight nozzle assembly. For test demonstration purposes, added weight is not objectionable since performance and operation of the nozzle is not affected. Because of these considerations, the 1-3/4-pass cooling scheme was selected as an alternate for the thrust chamber design and as a recommended design for thrust chamber test verification effort (Fig. 1-7).

EXTENDIBLE NOZZLE DESIGN

Because metallic fuel cooled nozzles are considered state-of-the-art, a hydrogen dump-cooled retractable nozzle was selected for the advanced expander baseline engine configuration. This type of nozzle has been constructed under the ASE program and has received some experimental evaluation. The retractable nozzle extends from an area ratio range of 225 to 625 (Table 1-5). The single downpass cooling circuit is formed by 1080 round tapered tubes. To offset favorably the mixture ratio shift in the combustor caused by dump cooling, the coolant is discharged at the end of the tubes through an area ratio of 30:1. This action develops dump-flow performance higher than the main thrust chamber specific impulse , offsetting the loss caused by the main chamber mixture ratio shift. A

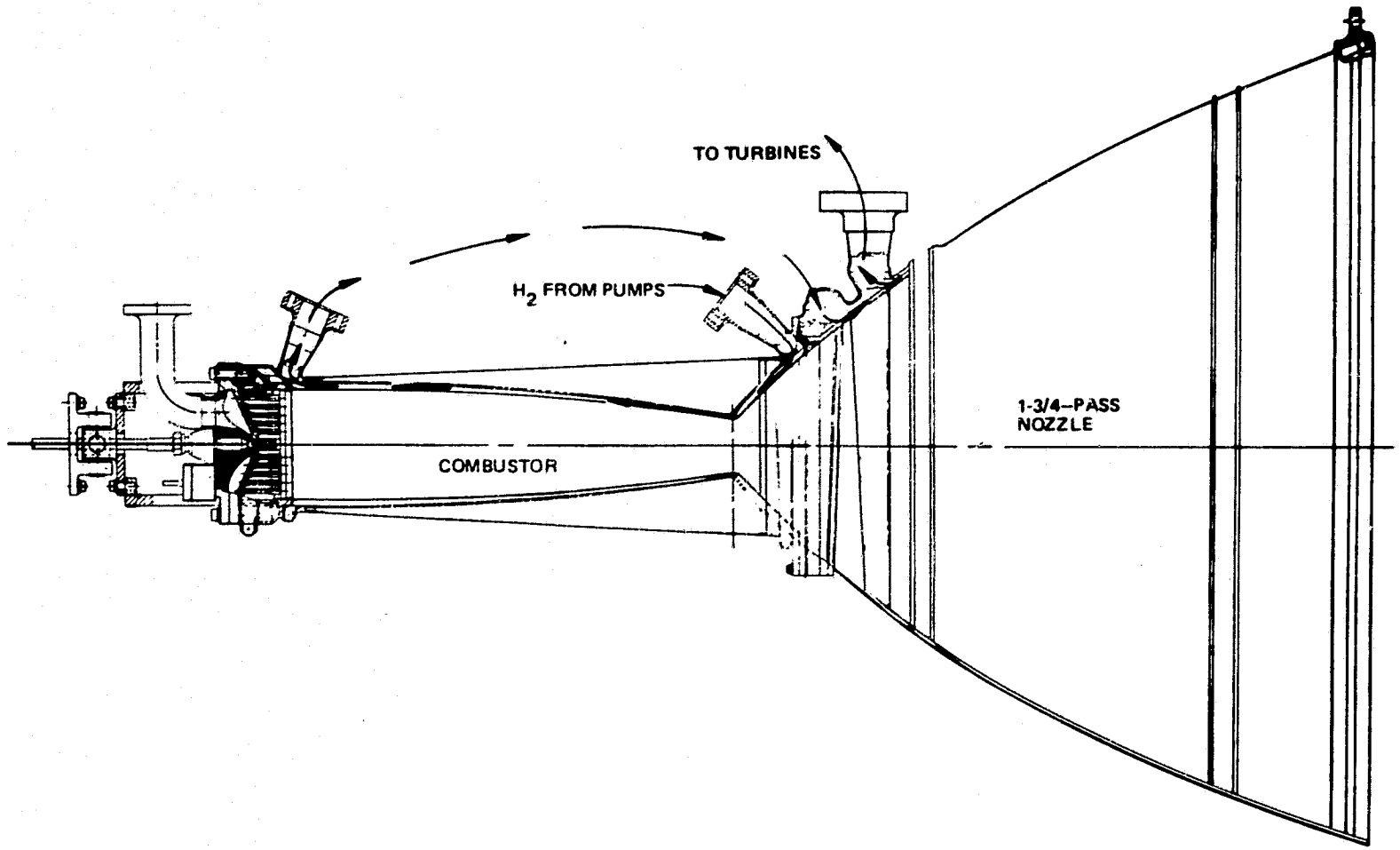

Figure 1-7. Advanced Expander Thrust Chamber Coolant Circuit, Recommended Baseline Design for Test Demonstration

metallic, radiation-cooled, extendible nozzle was considered and not selected because of inability of this concept to meet required cycle life within current state-of-the-art nozzle fabrication techniques, A carbon-carbon, radiation-cooled extendible nozzle, though weight-wise attractive, was not considered current state-of-the-art. Unknown carbon erosion rates in the presence of hot LOX/hydrogen combustion products (especially steam), and during on- and off-design thrust chamber operation, are considered an obstacle in meeting nozzle life requirements.

COMBUSTION CHAMBER AND INJECTOR DESIGN

Injector

Coaxial injection elements and a transpiration cooled rigimesh faceplate have been selected for the baseline engine design. This configuration offers proven performance, reliability, and complete fabrication experience for minimum iteration during design and development. The coaxial/rigimesh concept has been applied successfully, using liquid oxygen and gaseous hydrogen, to numerous Rocketdyne injector designs varying in chamber pressure from 700 psi to 4000 psi, with corresponding thrust levels from 3000 to 470,000 pounds of thrust.

Detailed analyses using the CICM Computer Program and Priem instability model confirm that the point-design expander cycle injector and combustion chamber will operate with a very high level of inherent stability for the transverse acoustic modes. To enhance the stability margin for off-design operating points, such as the start transient, 18 Helmholtz cavity acoustic absorbers have been added at the injector plane of the combustion chamber. These have been very conservatively sized, so as to ensure acoustic stability under all operating conditions. Design analyses using performance models (CICM) anchored on J-2, J-25, SSME and ASE coaxial injector test results show the injector combustion efficiency will be 99.9 percent at design thrust and mixture ratio and 99.8 percent at off-design MR=7.

The Advanced Expander Engine combustion chamber is configured with a smooth hot wall and a length of 20 inches. The hot wall is regeneratively cooled with hydrogen flowing in axial channels from the throat region toward the injector face. The coolant channel geometry favors a contraction ratio of 4. The chamber configuration represents 1980 technology. Existing chamber fabrication technology is directly applicable to this design; heat pickup correlation is traced to directly applicable ASE thrust chamber testing. Structurally, the mechanism responsible for low cycle fatigue in the channel geometry as understood, is directly applicable to the design, and finds basis in SSME, ASE, and 40K thrust chamber testing.

The smooth wall chamber is conventional in cross section, but unconventional in length at 20 inches. It offers the design and fabrication advantages of current technology easily extrapolated to a 20-inch length. The concept is currently employed on the SSME and ASE concepts, specific design heat pickup verification exists; the capability of (NARloy-Z) the liner material is documented for both low-cycle fatigue and strength; and no new manufacturing processes are needed. The coolant channel configuration employs geometry limits developed and used in the SSME and ASE programs. The fabrication process is well documented for use with the proposed chamber. The channels are closed out with an 0.005 copper electroplating and a 0.055 nickel structural electroplate over the copper.

Although a number of alloys were considered, only two contenders (NARloy-Z and AMZIRC) qualify for serious consideration as combustion chamber liners for the Expander Cycle Engine. Both are copper-base alloys--NARloy-Z was developed by Rocketdyne specifically for use in regenerating cooled rocket engine hardware; AMZIRC was developed as a commercial alloy aimed at the electronic equipment market. NARloy-Z was selected as the best qualified material for the following reasons:

1. A successful history in the SSME, with over 83,000 seconds of cumulative hot-firing exposure during 608 tests on 17 engines without a single engine failure due to the NARloy-Z liners.

2. The demonstrated strain-softening feature of AMZIRC alloy, which leads to surface rumpling and rapid loss in load-bearing ability during repeated thermal cycles.

3. The presense of oxide stringers and inclusions in commercial AMZIRC.

4. The necessity of developing fabrication processes to produce oxide-free AMZIRC products and proving their capability to withstand combustion liner operating conditions.

ENGINE POWER BALANCE AND PERFORMANCE

Four operating points have been defined for the advanced expander cycle engine point design, as required by study ground rules in Table 1. These are: (1) rated 15K lb thrust at mixture ratio of 6:1, (2) rated 15K lb thrust at mixture ratio of 7:1, (3) pump-idle engine thrust at its corresponding mixture ratio, and (4) tank-head idle thrust. The pump-idle conditions has been defined as 1800 pounds thrust and mixture ratio of 4:1. At these conditions, the engine system operates without any flow/pressure instabilities. The tank-head idle conditions are engine pressure fed mode conditions governed by the system resistances and the vapor pressures in the propellant tanks. Engine balances have been obtained at all four operating conditions. Key performance parameters for the thrust chamber and engine are summarized in Table 1-7 . Flow, pressure, power, and temperature schedules for the four engine operating points are indicated in Figs.1-8 through 1-11. More specific details of the power balance appear in the Engine Data Summary section.

The high-performance thrust chamber design configuration, developed in these point-design engine studies, reflects optimum utilization of the prescribed engine length. The chamber pressure has been maximized consistent with realistic turbomachinery and thrust chamber component efficiencies (margins). Combustion chamber and nozzle geometries have been configured to optimize specific impulse and payload performance within the axial length allocated to the thrust

TABLE 1-7. ADVANCED EXPANDER CYCLE ENGINE POINT DESIGN PERFORMANCE

Operating Mode	Full Power	Off-Design (MR=7)	Pump-Idle (MR=4)	Tank-Head Idle
Engine Thrust, Pounds	15,000	15,000	1800	61.3
Engine Specific Impulse	480.8	468.0	471.3	450.4
Engine Mixture Ratio	6.00	7.00	4.0	2.85
Chamber Pressure, Psia	1,540	1,515	203	7.2
Throat Area, In.^{2}	4.697	4.697	4.697	4.697
Area Ratio				
Full Nozzle	625	625	625	625
Fixed Nozzle	225	225	225	225
Thrust Chamber Thrust, Pounds(1)	14,807	14,807	1,773	59.9
Dump-Coolant Thrust, Pounds	193	193	27	1.4
Thrust Chamber Mixture Ratio	6.59	7.74	4.31	3.11
Thrust Chamber Specific Impulse				
Full Nozzle (ε = 625)	481.2	468.3	471.79	456.2
Fixed Nozzle (ε = 225)	TBD(2)	TBD	TBD	TBD
Injector Flowrates, lb/sec				
Fuel	4.05	3.615	0.708	0.0319
Oxidizer	26.71	28.006	3.051	0.0993
Propellant Injection Temperature, R				
Fuel	660	721	633	647
Oxidizer	183	183	167	163
Propellant Injection Pressure, Psia				
Fuel	1,805	1,744	252	10.4
Oxidizer	2,144	2,168	210	10.1
Coolant Flowrate, lb/sec				
Combustor	4.09	3.65	0.724	0.032
Fixed Nozzle	4.09	3.65	0.724	0.032
Expendable Nozzle	0.36	0.36	0.05	0.003
Coolant Inlet Temperature, R				
Combustor	224	225	161	37.8
Nozzle	696	747	598	633
Coolant Inlet Pressure, Psia				
Combustor	4,577	4.083	709	18.3
Nozzle	4,257	3,791	485	18.3

(1) Thrust Exclusive of Dump-Coolant Thrust
(2) TBD = To Be Determined

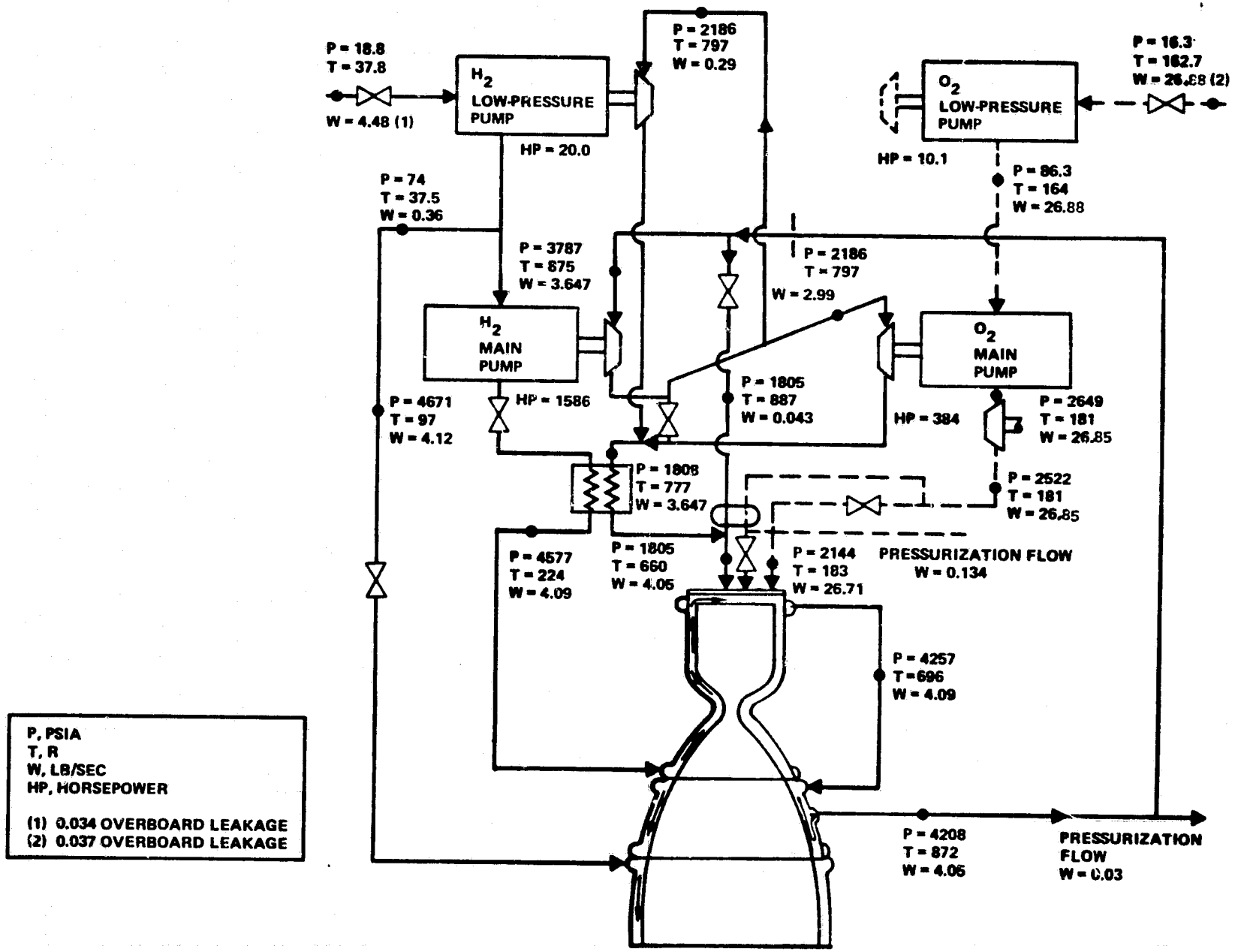

Figure 1-8. Flow, Pressure, Temperature and Power Schedule, F = 15K LB., MR = 6

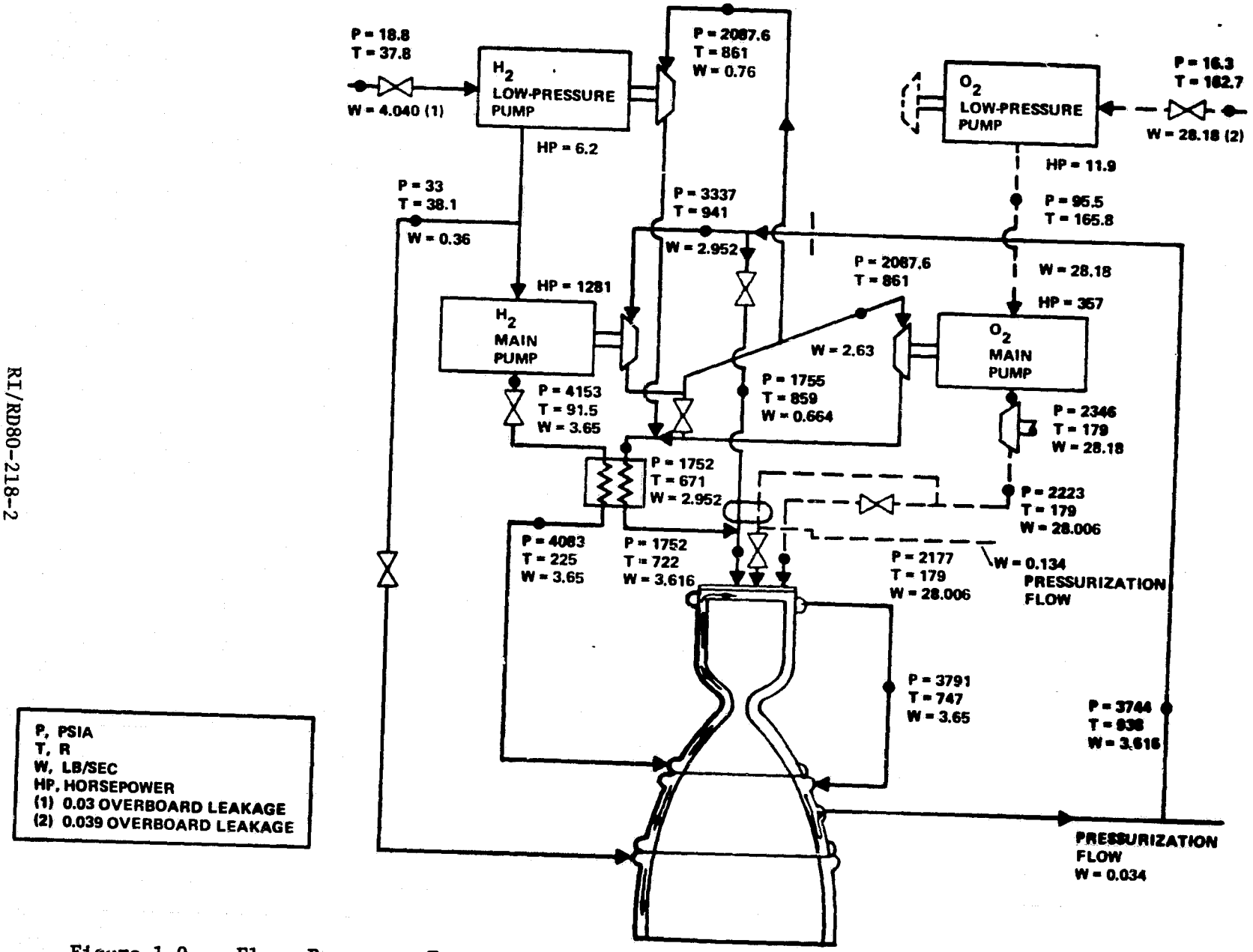

Figure 1-9. Flow, Pressure, Temperature, and Power Schedule, F = 15K LB., MR = 7

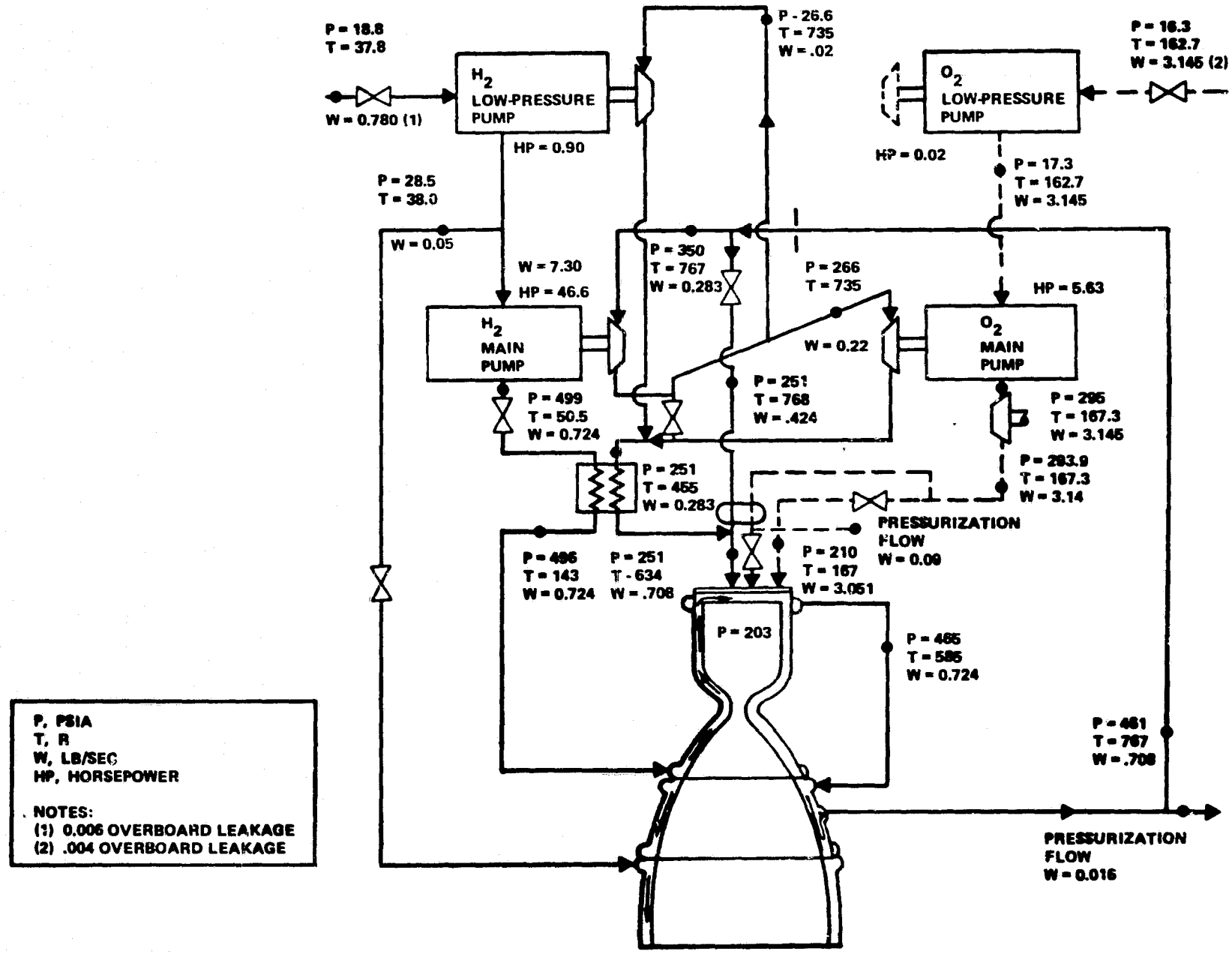

Figure 1-10. Flow, Pressure, Temperature, and Power Schedules, Pumped Idle

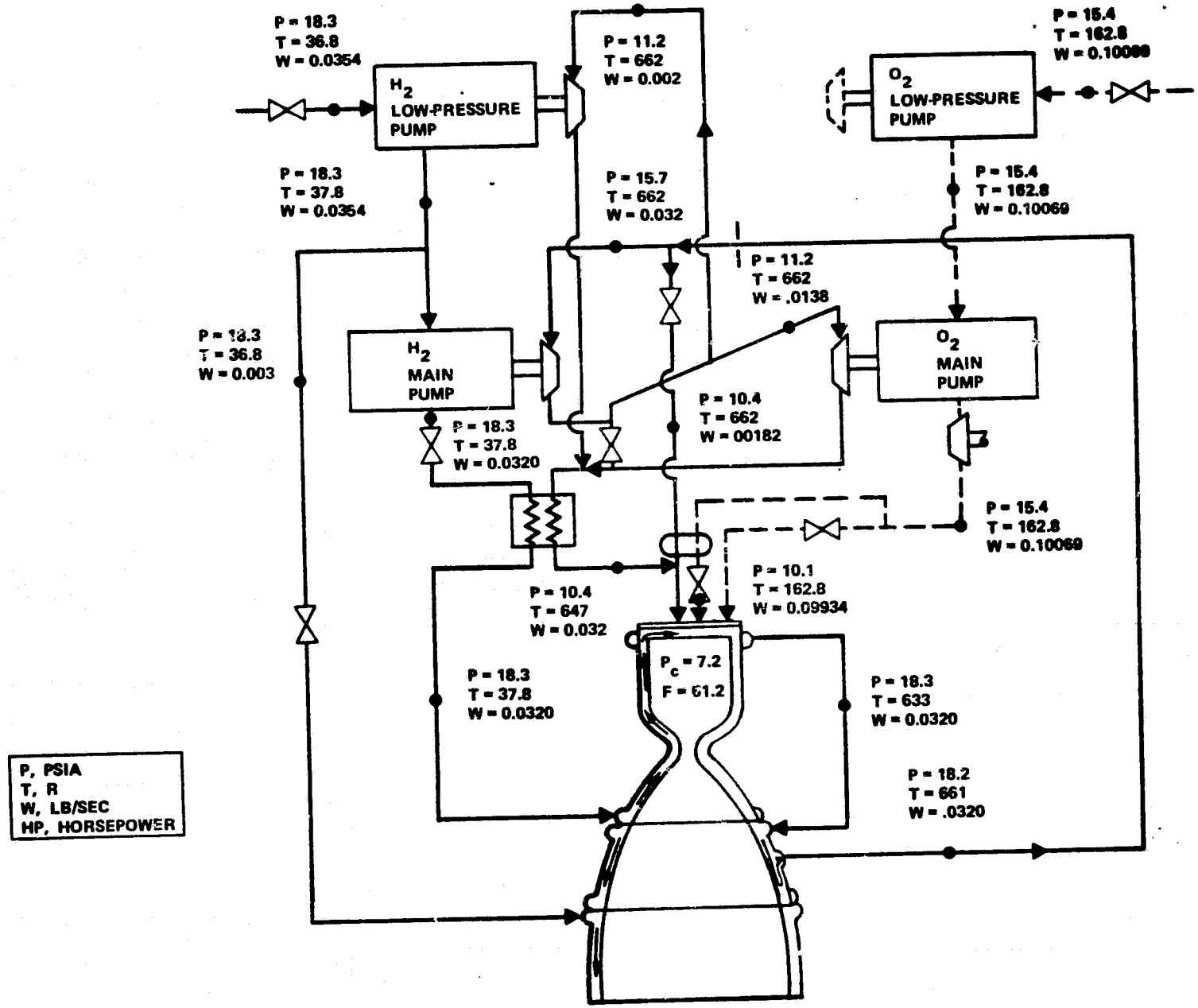

Figure 1-11. Flow, Pressure, and Temperature Schedules, Tank Head Idle

chamber. The selected combustion chamber length (20 in.) provides high combustion efficiency (0.999 at design thrust and mixture ratio), high thermal input to the turbine drive gas, and allows near-optimum specific impulse delivery of the resulting nozzle length. The nozzle contour, area ratio, and percent length (Table 1-1) have been the result of a selection process aimed at providing a reasonable balance between performance, weight, payload delivery, ease of altitude testing, handling, and fabrication costs.

How the engine places impulse and payload-wise relative to engines of other thrusts and area ratios but of equal engine length is shown in Fig. 1-12 and 1-13. The engine specific impulse is approximately one second lower than the highest impulse achievable in the prescribed length; attained by the 10K engines (Fig. 1-12). However, because of engine weight and gravity-loss considerations, the engine payload delivery is highest for the 15K lb, engine (Fig. 1-13). The selected engine area ratio (625) provides payload delivery very near the maximum attainable in the prescribed envelope.

The engine performance in Table 1-1 reflects the refinements resulting from performance efficiency studies of each engine component conducted in the Expander Cycle Point Design Engine Study. JANNAF specified performance procedures have been used in obtaining the engine delivered performance. Details of these performance procedures for the subject engine are presented in the Engine Data Summary section.

Off-Design Mixture Ratio

Mixture ratio of 6:1 operation is required for one-way Orbit Transfer Vehicle mission while the mixture ration of 7:1 operation is required for two-way missions. Commonality of propellant tanks between the two vehicles dictates the different operating mixture ratios for the two missions. The long chamber length and high performance coaxial type injector result in very little performance degradation when the thrust chamber operates off-design at an engine mixture ratio of 7:1. The injector element design assures near complete mixing while the long combustor length results in complete vaporization between injector and throat planes.

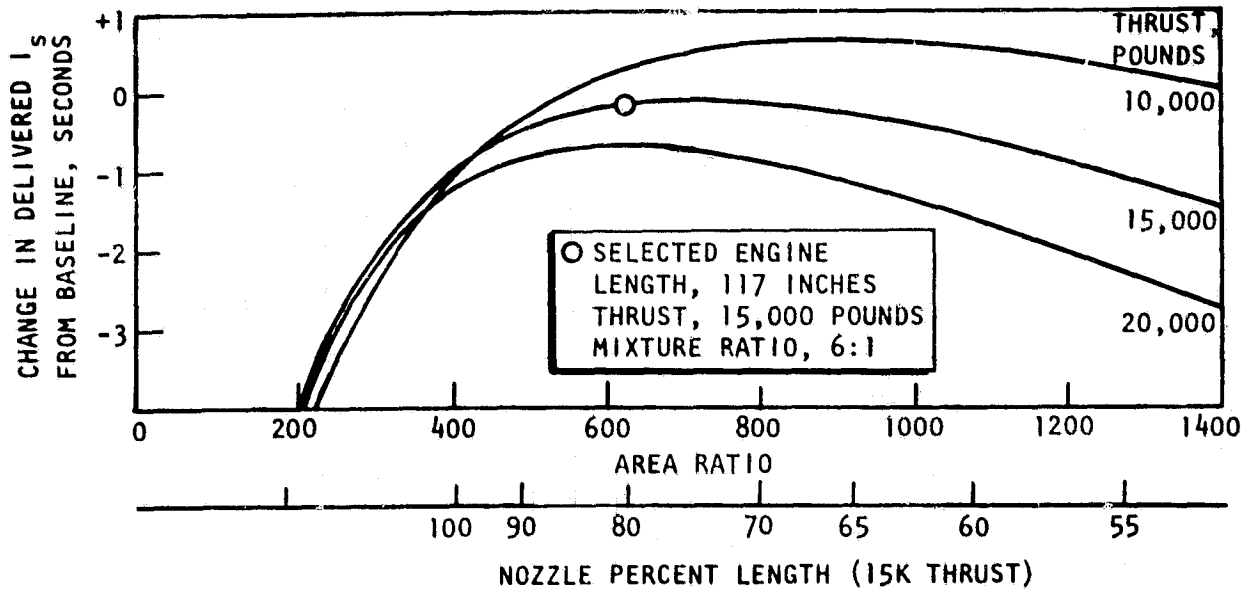

Figure 1-12. Advanced Cycle Engine Specific Impulse vs Area Ratio

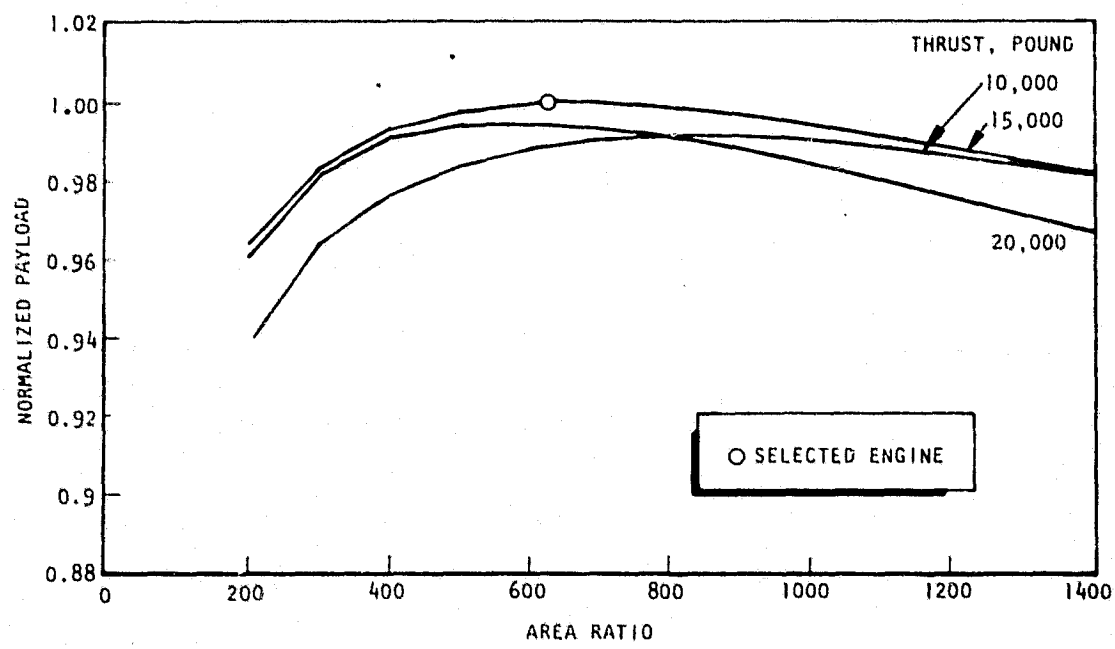

Figure 1-13. Normalized OTV Payload for 6:1 Mixture Ratio

The thrust chamber coolant channels and tubes are designed at on-design mixture ratio conditions (6:1) with sufficient pressure drop to allow operation at off-design mixture ratio of 7:1 without degradation in cycle-life. The chamber walls are essentially overcooled at MR = 6 and properly cooled at MR = 7.

Pumped-Idle Operation

Low engine thrust pumped-idle operation (1800 pounds) is required in either the one-way or two-way missions to provide autogeneous tank pressurization and thus pump-required NPSH for each mainstage firing during execution of the mission. A thrust of 1800 pounds with its corresponding engine mixture ratio of 4:1 was selected because at these conditions the coolant jackets and pump flow hydraulic resistances lead to stable operation of the engine. Lower fuel flowrates and pressures result in low fuel pump flow coefficients and the possibility of two-phase flow in the coolant jackets. These two conditions can lead to pump-coolant jacket coupled instabilities characterized by "chugging" of the flow. For these reasons the thrust and mixture ratio conditions of Table 1-7 were selected.

High lox-side injector pressure drops at design thrust conditions allow for sufficiently high pressure drops at pumped-idle flows. With the relatively high pressure drop of the main oxidizer valve the lox injector pressure drops provide required stability in the liquid oxygen system at pumped-idle conditions. Injection velocities of the hydrogen and oxygen injection elements result in 100 percent complete combustion at pumped-idle as indicated by the Coaxial Injector Combustion Model (CICM) Analysis Program.

Tank Head Idle

Engine starts to full thrust are effected from idle mode conditions. Idle mode occurs in two stages. The first, tank-head-idle, provides pump and system conditioning flows under existing tank vapor pressures. The second, pumped idle mode, provides autogeneous pressurization of the propellant tanks enabling the engine pumps to obtain required NPSH during mainstage operation.

In tank-head idle the main propellant pumps are restrained from rotation while the low pressure pumps are allowed to operate and aid in the delivery of flow for thermal conditioning of the system. The gas driven hydrogen boost turbines starts the fuel boost pump ahead of the main hydrogen pump to provide the latter with required NPSH and to aid in start conditioning and priming of the fuel system.

A heat exchanger is used to vaporize the liquid oxygen prior to entry into the thrust chamber. It is located in the turbine bypass circuit just upstream of the main injector (Fig 1-3). The heat exchanger provides stability on the thrust chamber oxygen side during tank head idle. With turbine bypass valves closed in tank head idle, maximum hydrogen flow is routed through the heat exchanger and through the low pressure pump turbines.

Kitted Engine For Low Thrust Mission

There are missions in which the subject design point engine, equipped with a minimum number of component modifications, will perform efficiently at a main thrust of approximately 1500 pounds. This dedicated-low-thrust engine will utilize the same thrust chamber as the 15,000-pound-thrust engine. No modification is required to the combustor or nozzle. A high 15K thrust LOX-side injector pressure drop ensures stable operation of the injector at the low thrust with the aid of the high-pressure drop in the main LOX valve located near the injector. As shown by injector performance calculations, the combustion efficiency at the low thrust mixture ratio of 6:1 conditions is improved to 0.993 by using a smaller Rigimesh retainer nut, effectively reducing flow area and thus increasing hydrogen velocity.

High mixture ratios at this thrust mean low hydrogen flows in the turbine and pump with respectively decreased turbine power and low fuel pump flow coefficient. The end result of both of these is a tendency of the engine to lack in pump power and flow stability. Engine transient simulation studies conducted in NAS8-33568 have indicated that a thrust mixture ratio operation of 4:1 is stable at a thrust of 1800 pounds but tends to instability as thrust is reduced.

Operation at a thrust of 1500 pounds is stable with a mixture ratio of 2.5:1. Higher mixture ratio (6:1) is desired for higher specific impulse and payload performance ,, which will require some modification of the fuel pump to provide higher flow coefficients. These could be provided in the form of pump flow recirculation. Other means have been explored and are reported in NAS8-32996 final report. Engine MR = 6 operation at a thrust of 1500 pounds will require further evaluation of turbomachinery and other components to ensure engine stability and power balance.

Sufficient hydrogen is present in the engine cycle at low thrust to provide effective cooling at the various mixture ratio conditions. What is required is proper split of coolant flows between the dump-cooled nozzle and the remaining part of the thrust chamber. This is accomplished with a 3-position dump-fuel control valve. These conditions enable the proper flow split at mainstage, pumped idle, and tank-head idle.

ENGINE CONTROL SYSTEM

The engine control system selected (Fig.1-14) provides the elements of sensing and monitoring engine performance, the electronic controller (one of whose functions is to generate electronic commands to modulate and sequence the valves), the final control elements (valves) to execute those commands, the ignition system, and the electrical harness to interconnect the engine control system.

The control of the engine and its operating modes during start, mainstage and shutdown account for approximately 11 percent of the functions required of the engine controller and control system. Other major function categories comprise the following percentages of the total function; Checkout and Status Monitoring 34 percent, Input/Output Data Processing 21 percent, and Protection of Engine and Man-Rated Capability 34 percent.

Checkout and status monitoring includes those functions starting during engine preparation for flight and continuing during engine operation. They ascertain the viability of each component to operate and to continue operating during the

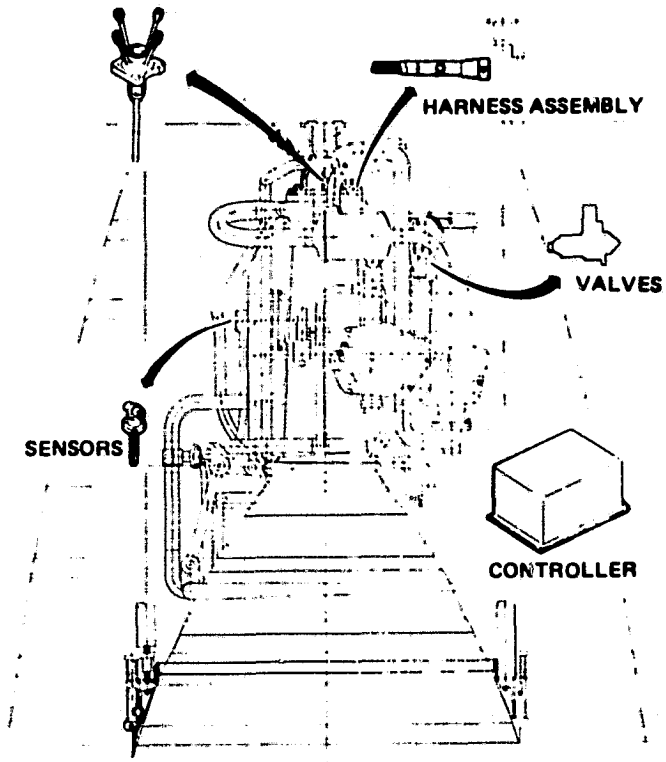

Figure 1-14. Engine Control System

flight. The input/output data processing includes all those listed functions for engine maintenance and performance evaluation, the processing of commands and monitoring of status, failures and initial conditions. The protection of engine and manrated capability group includes all the functions concerned with safe and reliable operation of the engine. It is believed that all of these functions must be present in the Advanced Expander Cycle Engine Point Design control system to provide the reliability required of this reusable engine as used in the OTV manned missions. The man rating and safety requirements for the OTV cannot be met without the engine control, engine health monitoring and checkout provided by the controller.

Primary Valves

To enable control of thrust and mixture ratio level during mainstage and start, a simple three-valve closed-loop control system has been defined. The control points selected have capability to fully control the engine thrust and mixture ratio over the full range of required engine operating conditions. The control modulates the areas of the main oxidizer valve (MOV), the turbine bypass valve (TBV), and the oxidizer turbine bypass valve (OTBV) to achieve independently the proper balance of propellant flows for independent control of thrust and mixture ratio. The main fuel valve (MFV), the fuel inlet valve (FIV), and the oxidizer inlet valve (OIV) complete the set of six primary valves. These valves are designed as on-off valves requiring no modulation.

In mainstage, closed loop thrust and mixture ratio control are exercised as required by the system controller and vehicle commands. The three modulated valves depicted on schematic in Fig. 1-3 are used for control of thrust during start transients and mainstage, and for control of mixture ratio between 6:1 and 7:1. Thrust control is more sensitive to modulation of the turbine bypass valve located in parallel arrangement with the two main turbines. Mixture ratio control is more sensitive to the main oxidizer valve situated in the liquid oxygen line downstream of the main oxidizer pump. An oxidizer turbine bypass valve (OTBV) increases the sensitivity of the thrust control valve during mixture ratio extremes. It performs its function by varying the flow-split between oxidizer and fuel turbines. The OTBV is required for pumped-idle mode operation.

Design of the primary valves is based on rotary valve element configurations utilizing common electric actuator designs. Four of these valves are shown in Fig. 1-15. Electrical fail operational function in the actuator is provided by dual electric motors and coils in the L.V.D.T.[1] position transducer. Fail safe engine shutdown is provided by pneumatic override pistons in the MOV an TBV actuated from separate three solenoid valves. The MOV and MFV employ a common design rotary sector ball valve closure with positive shutoff seat seal. The TBV and OTBV utilize a more simple rotary plug configuration without tight shutoff seal requirements.

(1) Linear Variable Differential Transformer

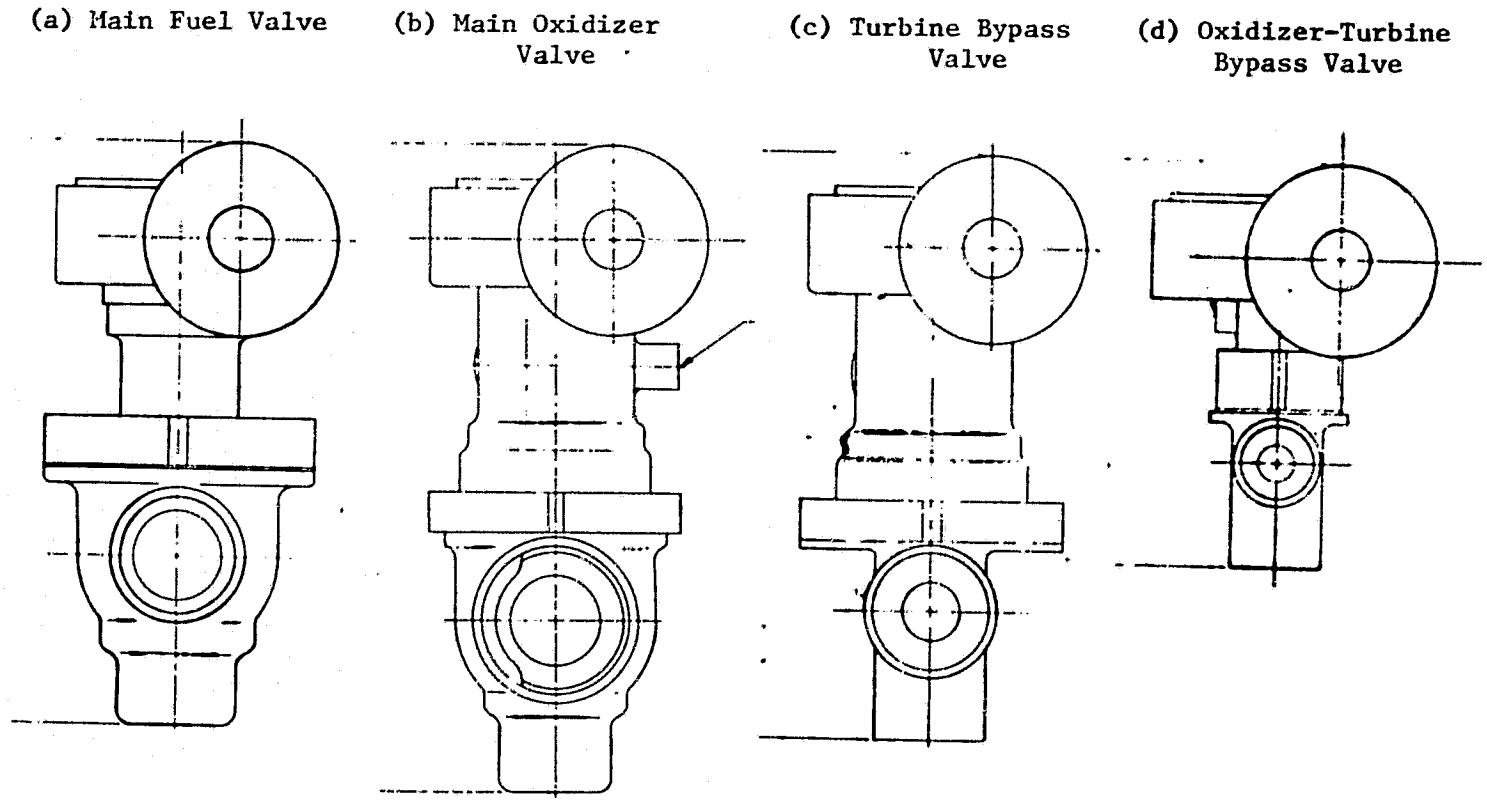

Figure 1-15. Primary Valves, Advanced Expander Cycle Engine Point-Design

Engine inlet shutoff valves (FIV and OIV) are required to isolate propellants from turbopump seals before and after firing. These two valves are similar in design to the MOV valve and provide straight through line diameters equal to pump inlet diameters to minimize pressure drop and flow disturbances upstream of pumps. The design layouts presented in the Valve Section shows a lightweight ball valve with shaft and seat seals identical with the MOV.

Secondary Valves

Secondary valves include the gaseous oxidizer valve (GOX), the dump coolant valve (DCV), the two igniter propellant valves and the two tank pressurization valves. Design details of these valves are discussed in the Valves Section.

Closed Loop Control

The thrust and mixture ratio levels are variable upon vehicle command. The control is required to maintain engine thrust and mixture ratio, within anticipated values of ± 5 percent and ± 2 percent, respectively of the commanded mainstage values. This type of precision is similar to Centaur upper stage engine thrust and mixture ratio precision requirements of ± 2 percent. These can be relaxed somewhat for the OTV, especially on the thrust requirement. Space Shuttle Main Engine (SSME) precision requirements are ± 1.25 percent in thrust and ± 2 percent in mixture ratio. A closed-loop control is required for this type of precision. As determined from SSME test data, much wider variation would be incurred if the engine is not closed-loop controlled. Large variations in mixture ratio during startup and mainstage would be detrimental to both engine performance and engine life. A sequencing type control (which is an open-loop control) does not have the precision to control variable thrust and mixture ratio without greatly relaxed precision.

Open-loop control with limited authority trim adds a closed loop to a scheduled open loop control. This control achieves the precision of closed loop for steady-state performance via the trim loop. It does not achieve the dynamic response precision of a closed-loop control system because the trim loop is

ineffective for large transients. This type of control is thus not effective during start and shutdown. A closed-loop control is necessary to meet the projected OTV requirements. It has the following advantages:

1. It allows replacement of a larger number of the engine components without hot-fire of the engine.

2. It minimizes the need for calibrating control valves and actuators.

3. It maintains engine component operation during start and shutdown within prescribed limits, even with a change in operating characteristics of components, thus allowing engine to meet required life.

Of the four control system concepts examined in the trade studies (Table 1-8), the Full-Range Controls concept was selected. The Mainstage Trim Control and Full-Range Controls both provide the accuracy required at mainstage as shown in Table 1-8. Because valve position control is required during start, idle mode and shutdown operation; and an electronic controller is required for sequencing and monitoring a manned OTV, the full-range control is essentially available due to the above requirements (Table 1-9).

Table 1-9 OTV System Requirements Define Control System

- Valve Trim or Valve Control Required for Mainstage Thrust and Mixture Ratio Accuracy
- Position Control Required for Start, Idle Mode, and Shutdown
- Electronic Controller Required for Sequencing and Health Monitoring of Manned OTV Engine
- Full Range Control Available due to above requirements.

TABLE 1-8 CONTROL SYSTEM SELECTION

ENGINE CONTROL SYSTEM CONCEPTS	CHARACTERISTICS
A. Minimum Electronic Systems No Controller Mechanical Sequencing Monitoring Instrumentation for Reusable Engine Redline Monitoring for Man-Rating Checkout by Off-Engine Means	● Run-to-Run Variations Thrust - 20% MR - 13% ● No Start and Shutdown Control Flexibility
B. Open Loop Electrical Sequence Control No Valve Positioning Control Monitoring Instrumentation and Redline Monitoring Checkout and Status Monitoring on Engine	● Run-to-Run Variations Thrust - 20% MR - 13% ● No Start and Shutdown Control Flexibility
C. Mainstage Trim Controls Electrical Sequence Control No Valve Positioning Control During Start and Shutdown Monitoring Instrumentation and Redline Monitoring Performance Instrumentation Feedback During M/S to Trim F & MR Checkout and Status Monitoring by Engine	● Run-to-Run Variations Thrust - 2% MR - 2% ● Limited Start, Shutdown Control Capability
D. Full Range Controls Controller Performing Valve Position Control Feedback to Control F & MR as Required Monitoring Instrumentation and Redline Monitoring Performance Instrumentation Checkout & Status Monitoring by Engine	● Run-to-Run Variations Thrust - 2% MR - 2% ● Full Start, Shutdown Control Capability

Controller Redundancy

The controller is considered the most reliable component in the control system. Redundancy is included to provide for random failure of electronic components. The dual-dual cross-strapped system (Fig. 1-16) was selected as the least complex, most effective approach toward achieving high probability of mission success.

Sensors

Instruments are required for engine performance and control, and for engine health and safety monitoring. Redundancy in the sensors is also provided to increase reliability. Sensor requirements are indicated in Table 1-9.

Table 1-9 Instrumentation Requirements

	Number	Engine Penetrations
Monitoring Instruments	30	15
Performance Instruments	26	9

Igniter

Redundancy in the ignition system required for man rating engine capability is achieved with a dual plasma torch igniter. This ASE type igniter provided electrode durability and predictability of ignition. It consists of dual exciters, harnesses, and igniter injection elements, in a single combustion chamber and flame tube.

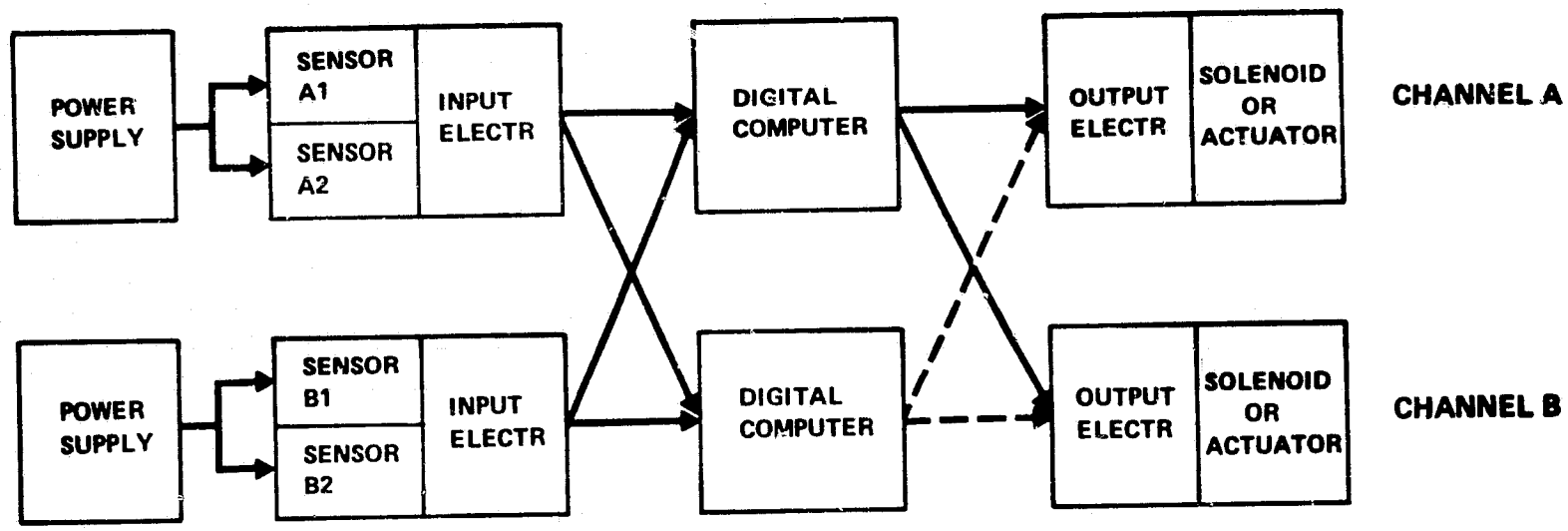

PRO

- GREATEST CHANCE OF MISSION SUCCESS
- STRENGTHENS WEAKEST LINK
- SOME EXPERIENCE ON SSME

CON

- NOT FO/FO/FS AT ALL LEVELS

Figure 1-16. Dual-Dual Redundant Cross-Strapped System

THRUST CHAMBER DESIGN AND PERFORMANCE (TASKS 2 AND 3)

The Advanced Expander Cycle Point Design Thrust Chamber (Figure 2-1) has been designed to provide a chamber pressure of 1540 psia with a turbine gas regenerator and full cycle-life capabilities. This design will also provide a chamber pressure of 1540 psia with reduced engine power margins. The design also has the capability to provide an interim chamber pressure of 1400 psia with full power margins and without any form of thermal enhancement. Expander cycle thrust chamber concept growth has been provided by definition of alternate thermal enhancement concepts. These concepts will provide alternate future state-of-the-art schemes to the use of a turbine gas regenerator and when their potential is fully developed, could provide chamber pressure and power margin growth. The evaluation of these alternatives is being actively pursued in company funded effort.

The design selection for the advanced expander thrust chamber concept is summarized in Table 2-1. The combustion chamber configuration selection consisting of a chamber diameter of 4.8 inches and a length of 20 inches provides the thermal energy required for a chamber pressure of 1540 psia. This combustion chamber length maximizes the coaxial injector vaporization performance and within the allowable thrust chamber length of 107 inches, optimizes nozzle length (87 inches), nozzle percent length (79.4) and payload. The nozzle overall expansion area ratio of 625 results in near-optimum payload delivery and simplifies engine fabrication, handling and test. The nozzle attach area ratio of 14:1 and cooling circuit chosen (Table 2-1) result in satisfaction of cycle-life requirements (300 x 4) with high coolant bulk temperatures, maximum turbine power, and ease of fabrication. The principal material of NARloy-Z and the channel wall construction in the combustion chamber have received extensive test evaluation in ASE and SSME programs. The tubular A286 fixed-nozzle construction has an extensive experience base in the SSME program.

The Advanced Expander Cycle Thrust Chamber Assembly (Figure 2-1) is comprised of the injector, igniter, combustion chamber, primary nozzle and retractable nozzle subassemblies. A layout of the thrust chamber assembly is presented in

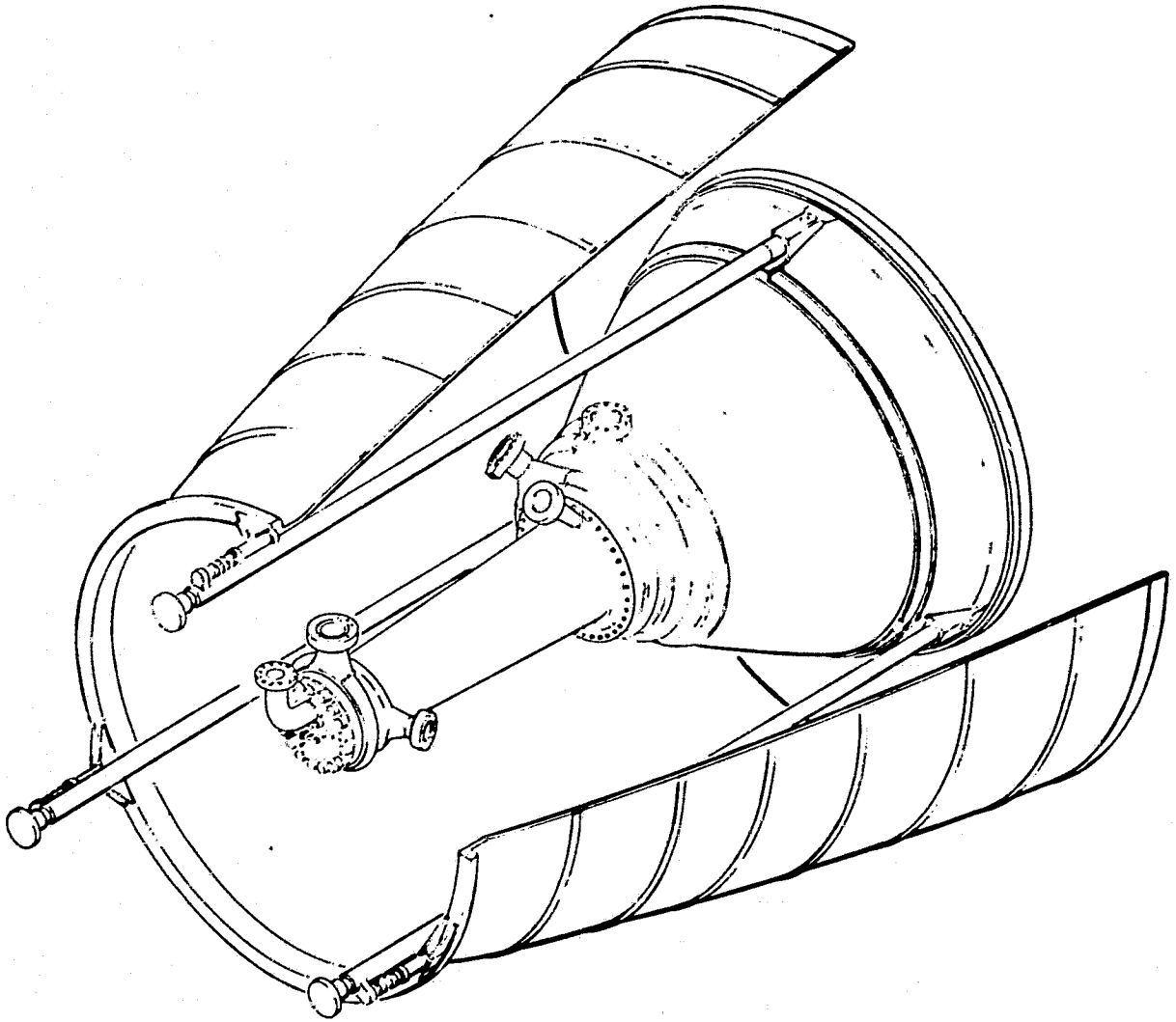

Figure 2-1. Advanced Expander Cycle Engine Point-Design, Thrust Chamber Assembly

TABLE 2-1. ADVANCED EXPANDER THRUST CHAMBER DESIGN SUMMARY (THRUST CHAMBER LENGTH = 107 INCHES)*

• GEOMETRY	
COMBUSTION CHAMBER	
CHAMBER PRESSURE, PSIA	1540
CHAMBER THROAT DIAMETER, INCHES	2.4454
CHAMBER CONTRACTION RATIO	3.853
CHAMBER INLET DIAMETER, INCHES	4.80
CHAMBER LENGTH, INCHES	20.0
CHAMBER/NOZZLE ATTACH AREA RATIO	14:1
NOZZLE	
TOTAL NOZZLE LENGTH, INCHES	87
FIXED NOZZLE LENGTH, INCHES	30
NOZZLE OVERALL AREA RATIO	625
FIXED NOZZLE AREA RATIO	225
OVERALL NOZZLE PERCENT LENGTH	79.44
NOZZLE INSIDE EXIT DIAMETER	61.135
• DESIGN CONCEPTS	
INJECTOR TYPE	COAXIAL
COMBUSTOR COOLING	UPPASS, FULL-FLOW
NOZZLE TYPE	OPTIMUM BELL
NOZZLE COOLING	1-3/4 PASS, FULL-FLOW
COMBUSTOR MATERIALS/CONSTRUCTION	NARloy-Z/CHANNEL-WALL
NOZZLE TUBE MATERIAL	A286

*PROPELLANT INJECTION TO NOZZLE EXIT PLANES

Figure 2-2. The primary nozzle is attached to the combustion chamber at an area ratio of 14:1 extending to an area ratio of 225:1 to 625:1. All thrust chamber assembly components are representative of a lightweight configuration with welded flanges where appropriate and bolted flanges at propellant inlet and discharge locations and at line replaceable units.

The major components in the assembly (igniter, injector, combustor, and fixed and retractable nozzles) are all easily removable from the assembly to facilitate repair, inspection, and modification.

INJECTOR DESIGN DESCRIPTION

A coaxial element injector (Figure 2-3) was selected for the Advanced Expander Cycle Point Design Thrust Chamber Assembly. This selection was based on experience indicating that high performance, stable combustion, low weight, and ease of fabrication can be achieved with this type of injector. Similar coaxial element injector designs using LOX/hydrogen have been successfully used on the J-2, J-2S, SSME, and ASE engines.

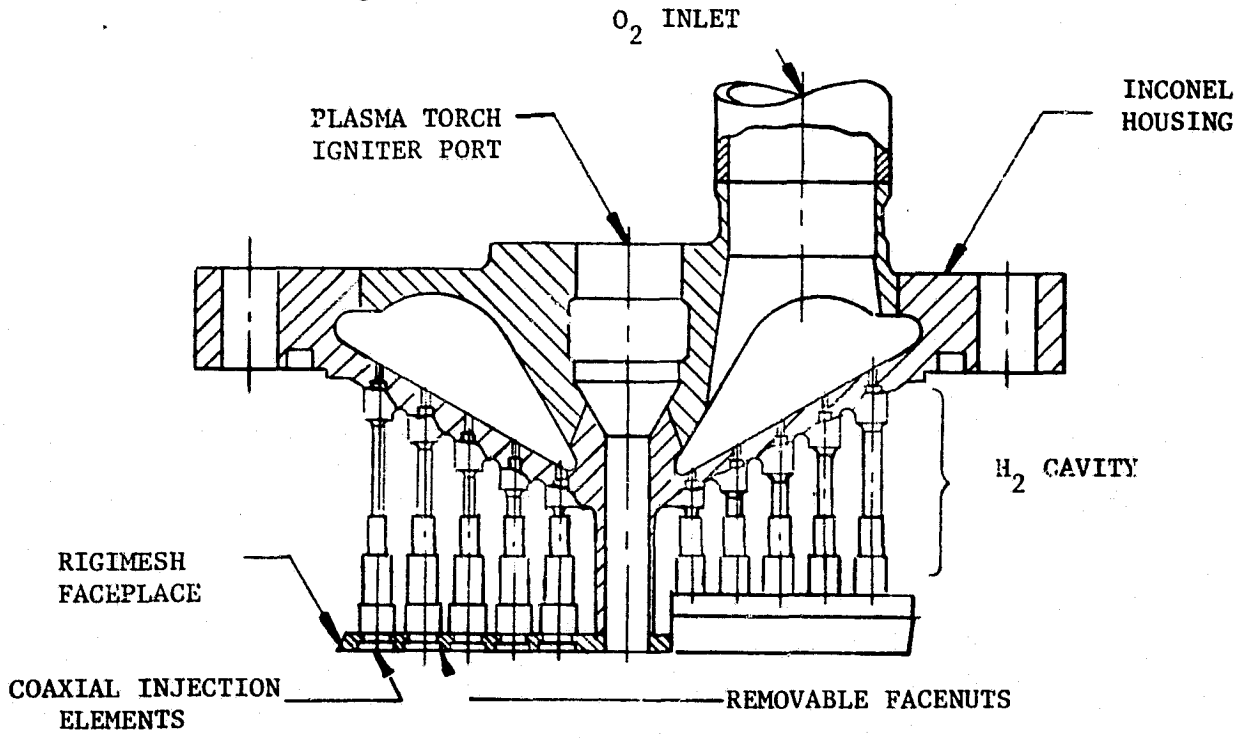

Figure 2-3. Advanced Expander Cycle Injector Concept

ORIGINAL PAGE IS
OF POOR QUALITY

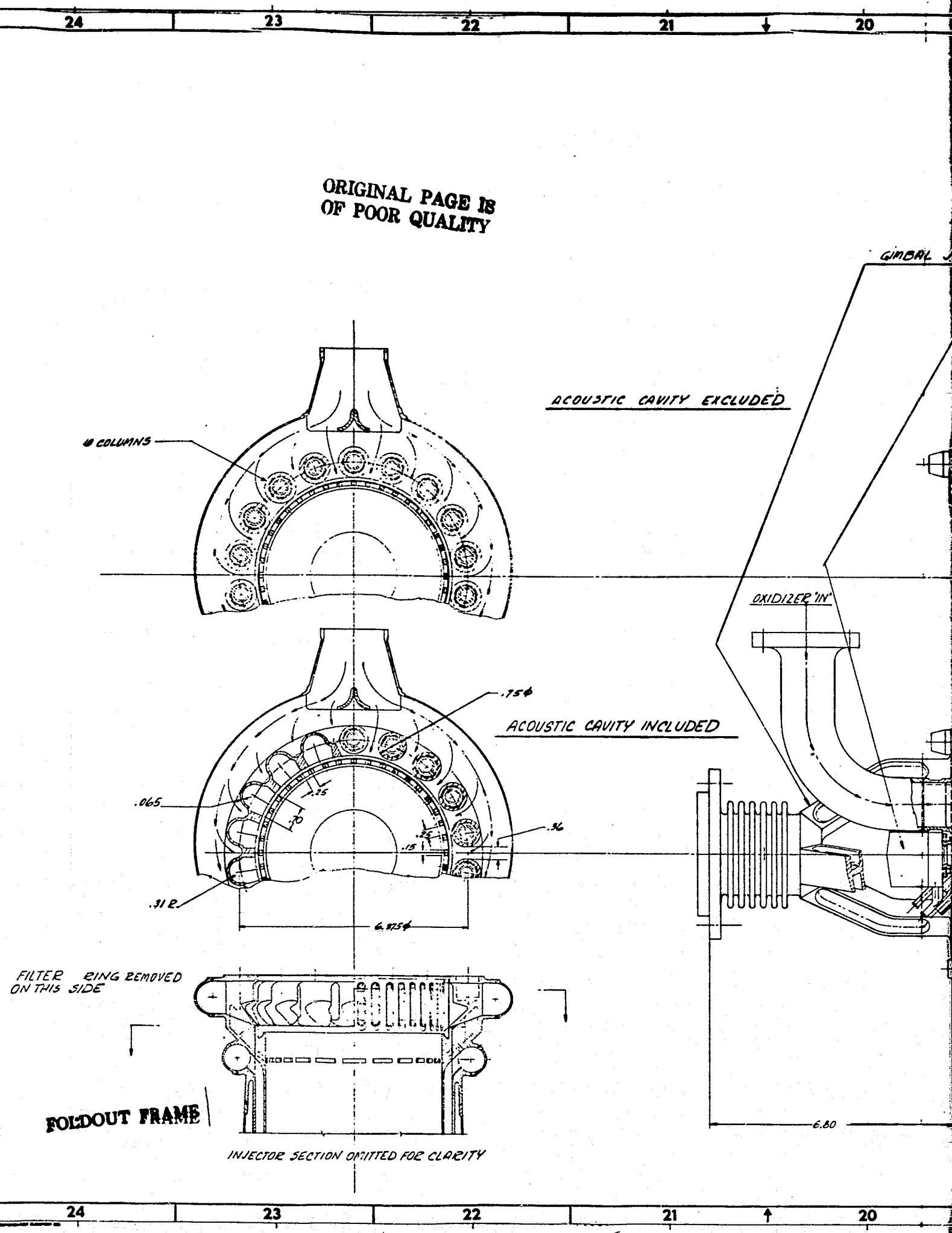

FOLDOUT FRAME

MICROFILM OVERLAP AREA

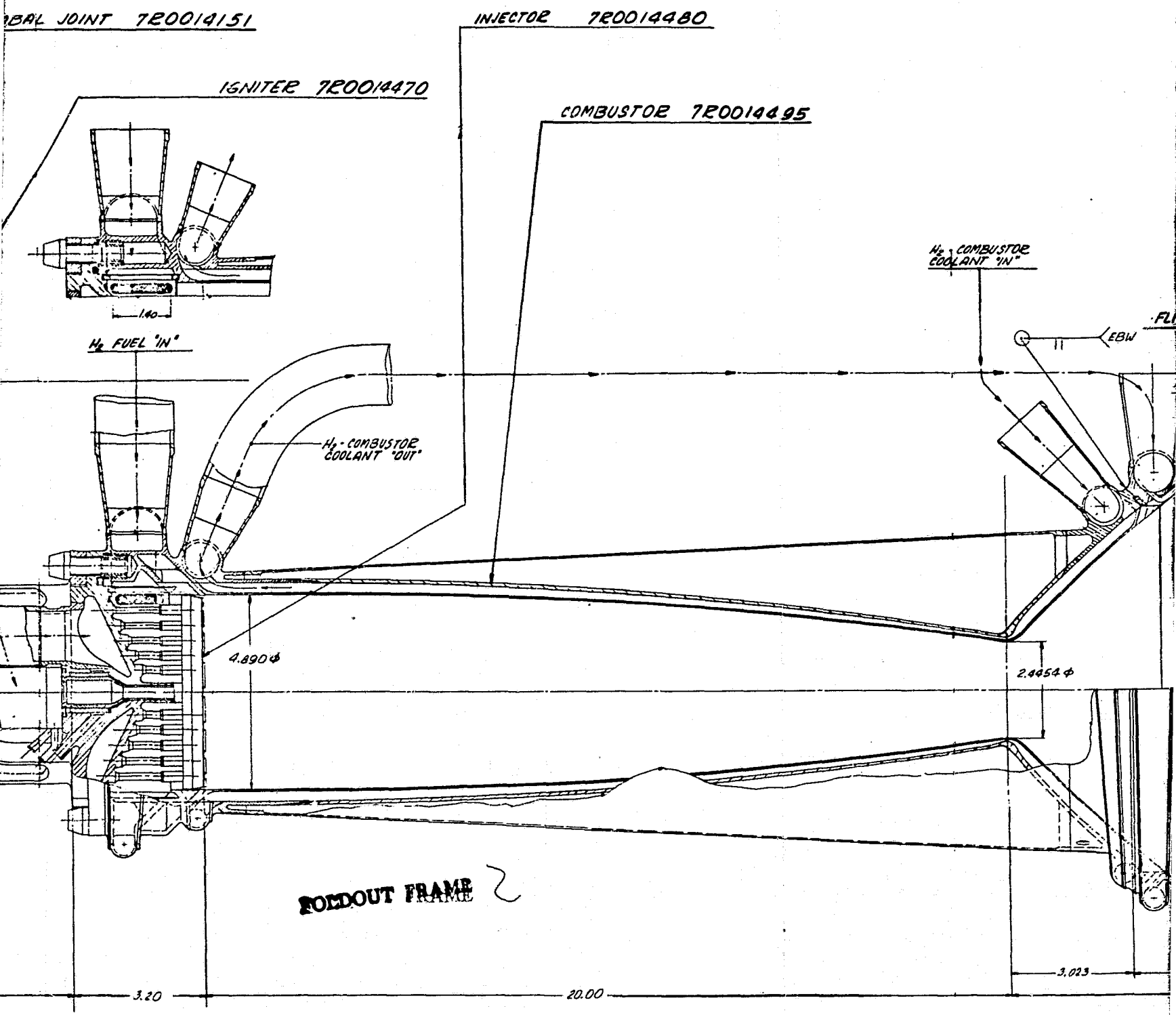

FOLDOUT FRAME 2

Rockwell International Corporation
Rocketdyne Division
Canoga Park, California

FSCM NO 02682	FRAME 1		
7R0014500		SH	REV

MICROFILM OVERLAP AREA

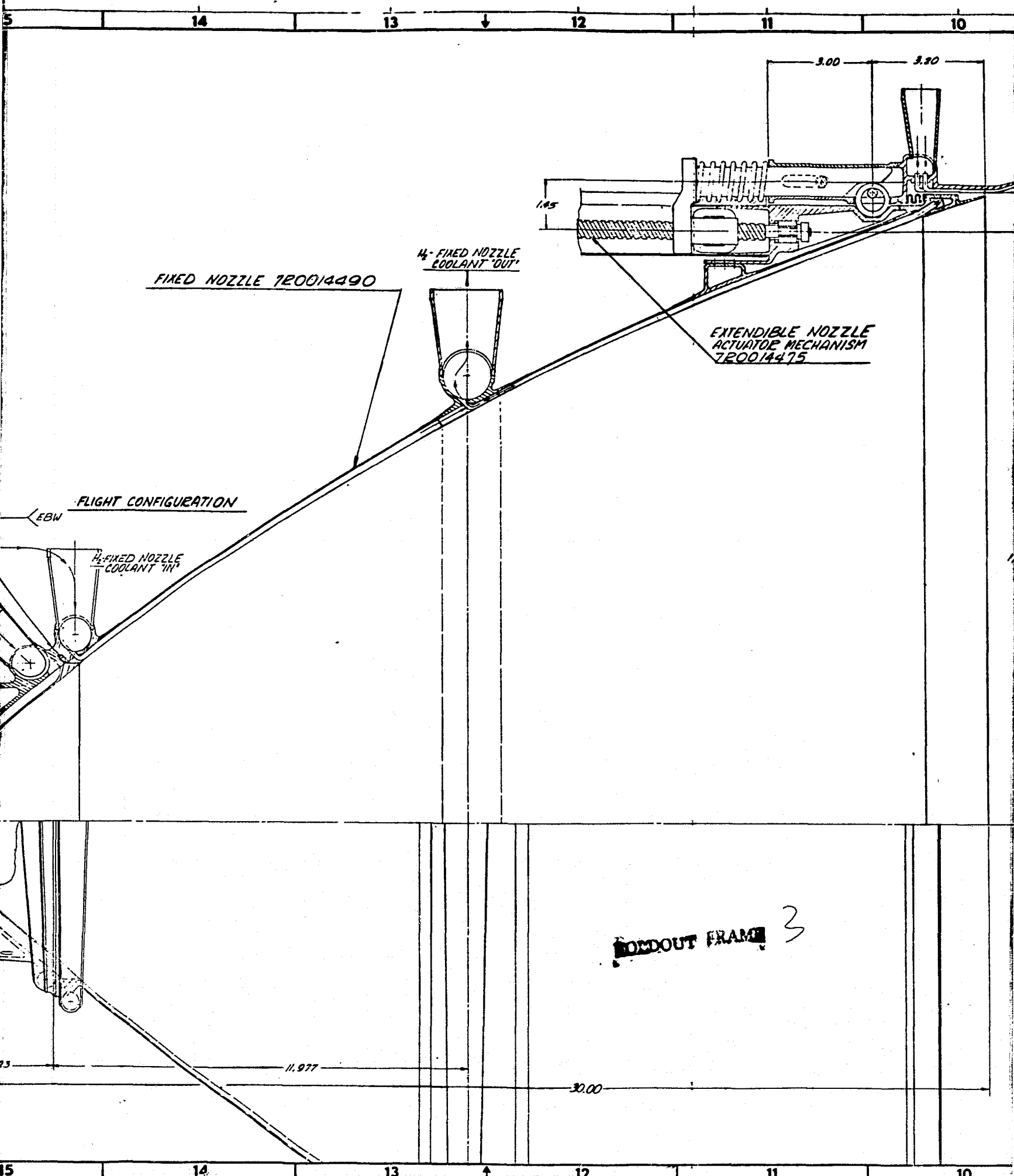

BOMDOUT FRAME 3

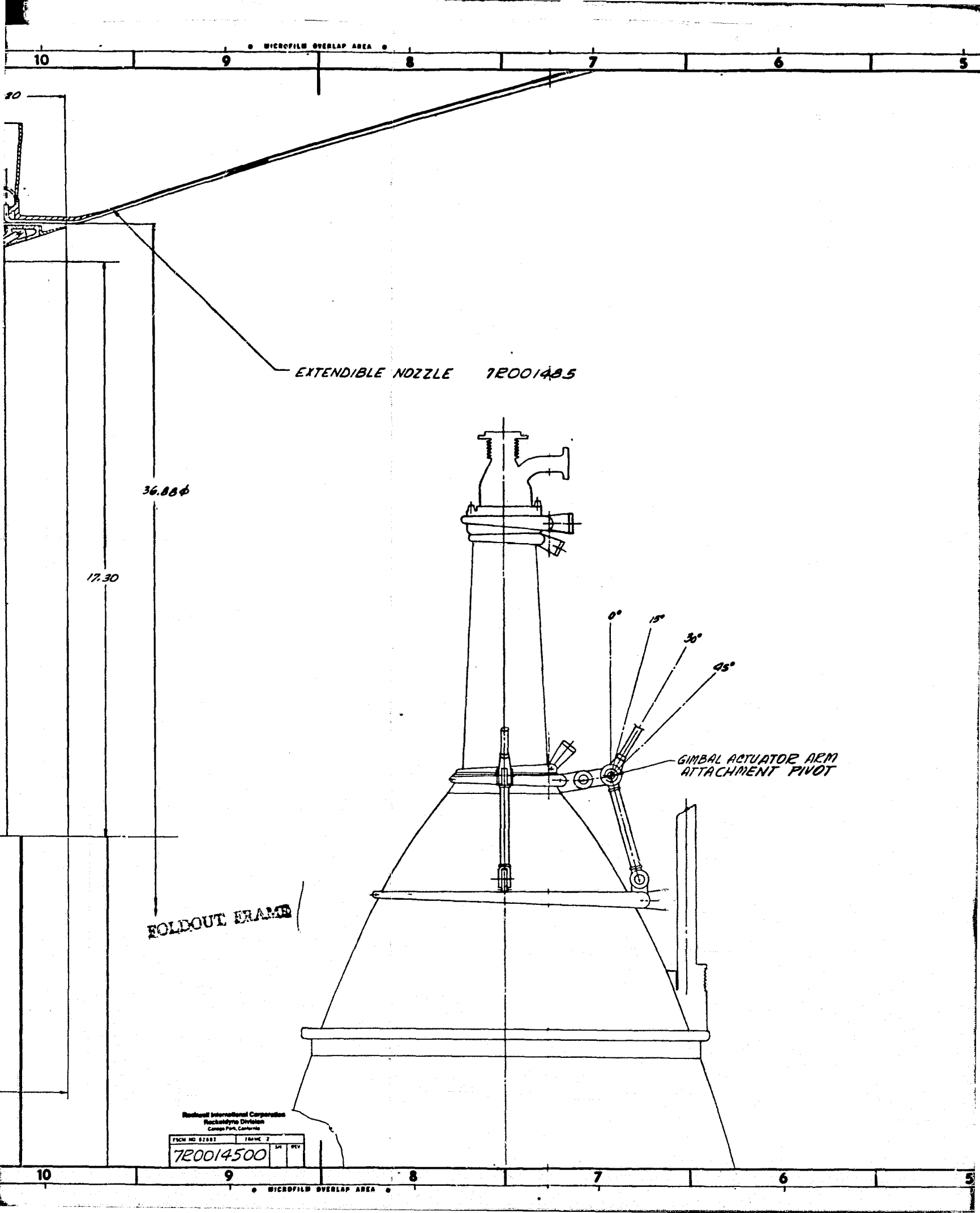
MICROFILM OVERLAP AREA
10
9
8
7
6
5
EXTENDIBLE NOZZLE 7R001485
36.88φ
17.30
0°
15°
30°
45°
GIMBAL ACTUATOR ARM
ATTACHMENT PIVOT
FOLDOUT FRAME
Rockwell International Corporation
Rocketdyne Division
Canoga Park, California
7R0014500
MICROFILM OVERLAP AREA

FOLDOUT FRAME 5

Figure 2-2

FOR INFORMATION

RI/RD80-218-2

1. ALL DIMENSIONS OF THIS DRAWING ARE REFERENCE

Rocketdyne International Corporation
Rocketdyne Division
Canoga Park, California

OTV - THRUST CHAMBER ASSY.
LAYOUT

SIZE J | FSCM NO 02602 | DWG NO 7R00014500

SCALE FULL | SHEET

7R00014500

The Advanced Expander Cycle Engine Point Design Injector incorporates many of the features from recent Rocketdyne injectors that have exhibited a high measure of success. The Space Shuttle Main Engine (SSME), the Advanced Space Engine (ASE), and the 40K SSME model injectors have all demonstrated high orders of performance and good structural integrity. The Advanced Expander Cycle thrust chamber size and operation are quite similar to the ASE operating conditions. Many of the mechanical design aspects of the SSME have been incorporated to improve maintainability, adjustability, and to increase the ease of disassembly for rework or inspection. The injector design is shown in Figure 2-4.

The basic injection pattern selected for this application is a coaxial-type injection element, oriented in a series of concentric circular locations with a Rigimesh porous metal injector faceplate. One hundred and eight elements are arranged in this pattern to provide a relatively homogeneous mass flux of injected propellants with relatively uniform radial mass distribution.

The element placement is essentially identical to the ASE pattern, and very similar in concept to the SSME. No baffle elements (such as are used on the SSME) are required in the injector design. This is based on experience with injectors of this same physical diameter. (Acoustic damping cavities are, however, included in the combustion chamber design).

The propellant flow distribution to the injector elements is well controlled to provide uniform mass distribution over the entire injector face. Maximum combustion chamber compatibility is provided in this manner by avoiding the adverse cross flowfields that can result when the combusting mass attempts to flow from

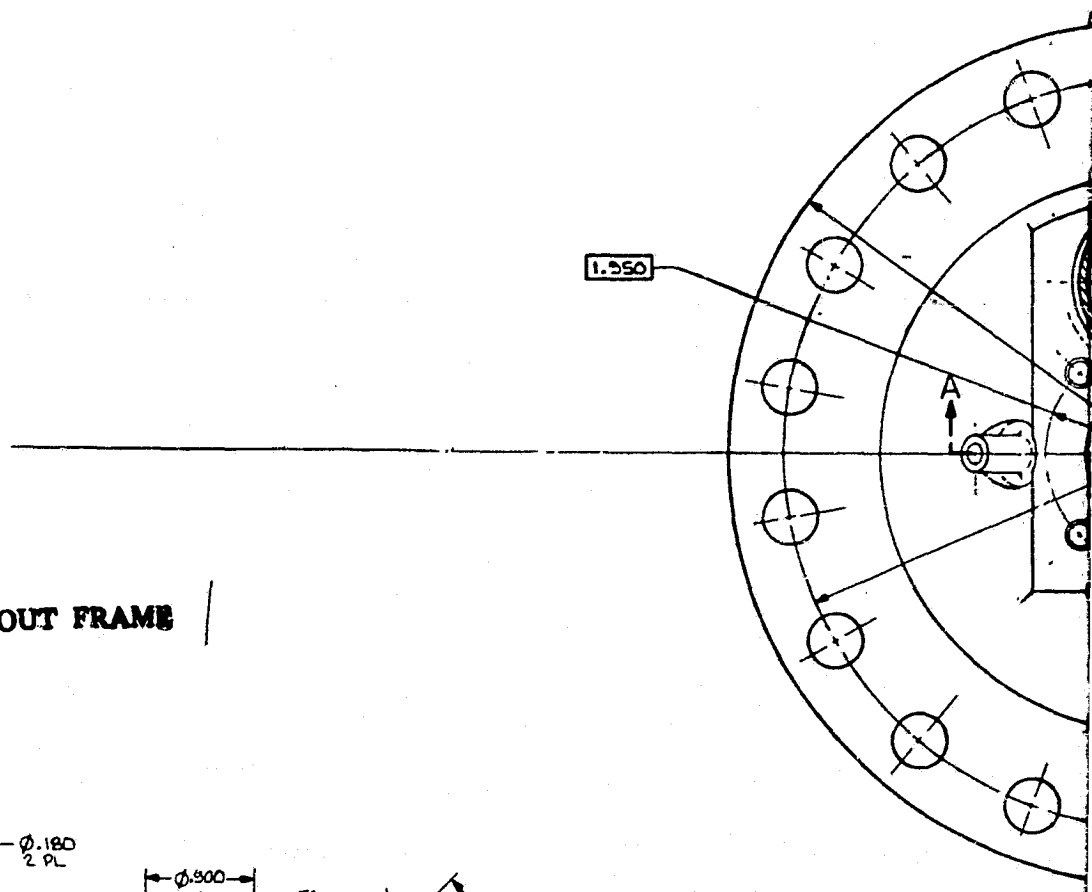

FOLDOUT FRAME 1

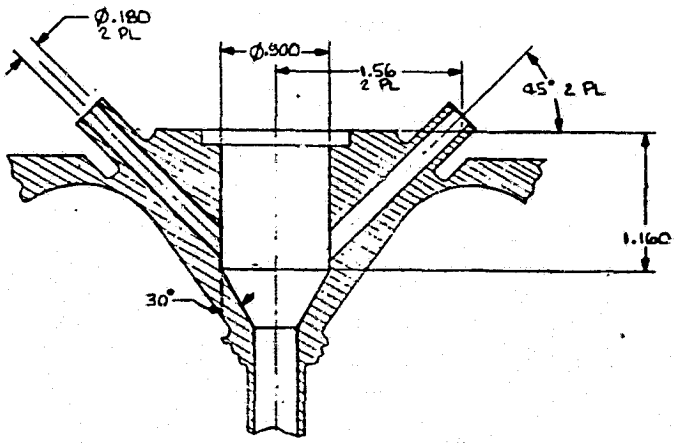

SECTION A-A 19E

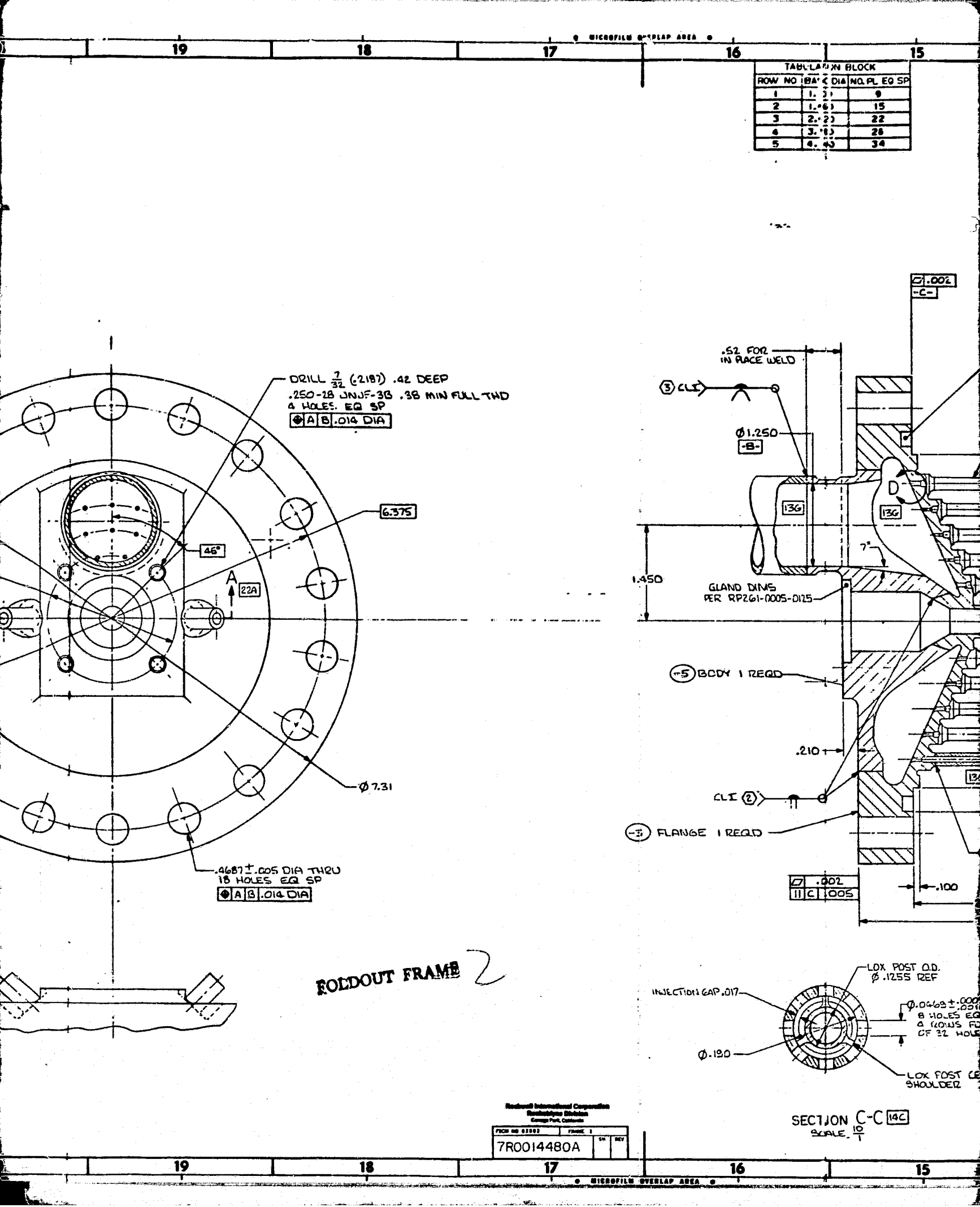

MICROFILM OVERLAP AREA
19
18
17
16
15
TABULATION BLOCK
ROW NO | BASIC DIA | NO. PL EQ SP
1 | 1.[illegible] | 9
2 | 1.[illegible] | 15
3 | 2.[illegible] | 22
4 | 3.[illegible] | 28
5 | 4.[illegible] | 34
DRILL 7/32 (.2187) .42 DEEP
.250-28 UNJF-3B .38 MIN FULL THD
4 HOLES. EQ SP
A B .014 DIA
6.375
46°
A
22A
Ø 7.31
.4687 ±.005 DIA THRU
18 HOLES EQ SP
A B .014 DIA
.002
-C-
.52 FOR
IN PLACE WELD
3 CLI
Ø1.250
-B-
13G
D
13G
7°
1.450
GLAND DIMS
PER RP261-0005-0125
-5 BODY 1 REQD
.210
CLI 2
-3 FLANGE 1 REQD
.002
C .005
.100
LOX POST O.D.
Ø .1255 REF
INJECTION GAP .017
Ø.0469 ±.000
8 HOLES EQ
4 ROWS FO
OF 32 HOLE
Ø.190
LOX POST CE
SHOULDER
SECTION C-C 14C
SCALE 10/1
FOLDOUT FRAME 2
Rockwell International Corporation
Rocketdyne Division
Canoga Park, California
FSCM NO 02602
FRAME 1
7R0014480A
SH
REV
MICROFILM OVERLAP AREA

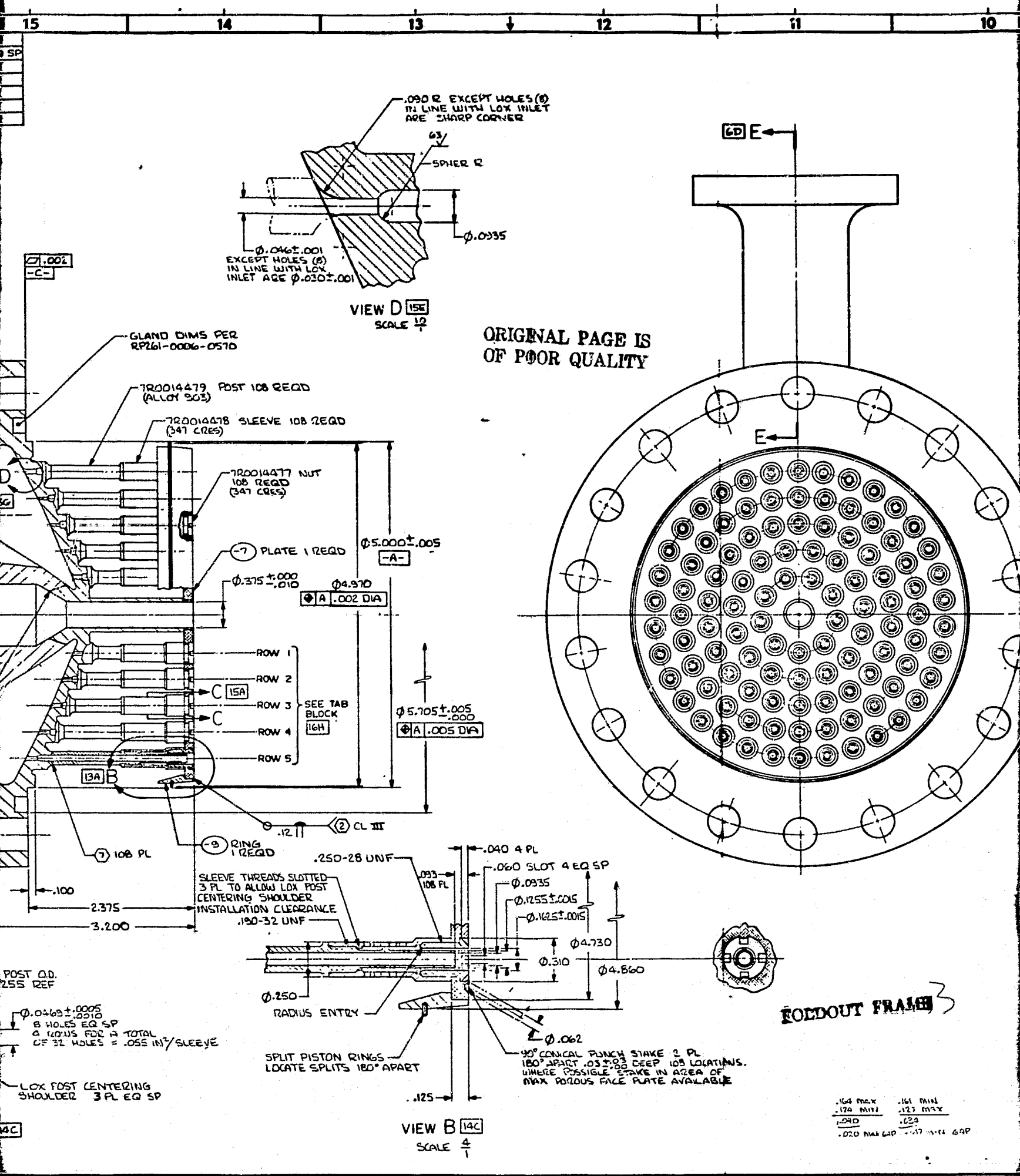

ORIGINAL PAGE IS OF POOR QUALITY

FOLDOUT FRAME 3

MICROFILM OVERLAP AREA

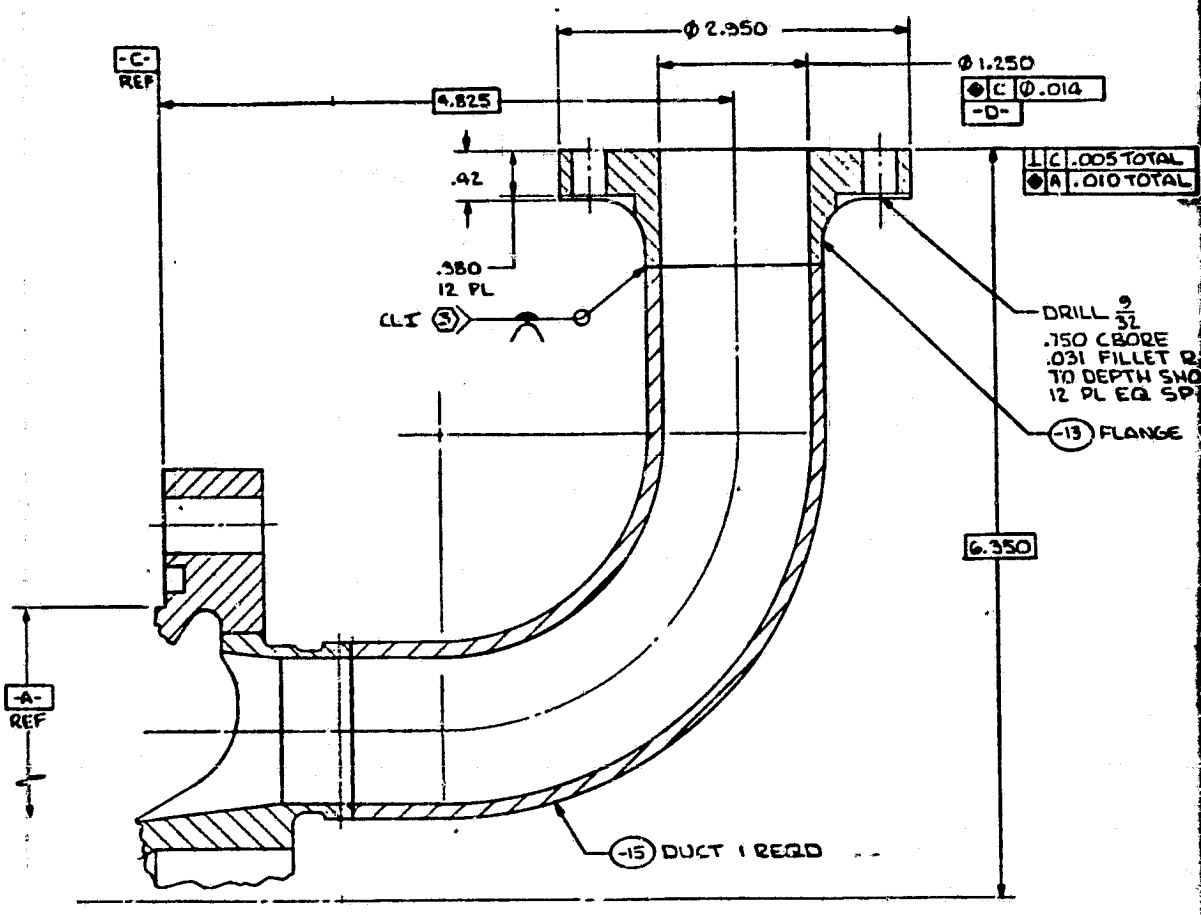

SECTION E-E

BOEDOUT FRAME 4

9 HEAT TREAT
FTU RC 38
8. CLEAN DETA
7 INERTIA WEL
IS ALLOY 30
IS PER AS1
6 ALTERNATE
5 AVERAGE PO
250 ± 25 SC
THRU WHEN
4 AIRCRAFT P
3 WELD PER
2 ELECTRON B
1. MACHINE P

Rocketdyne International Corporation
Rocketdyne Division
Canoga Park, California

FSCM NO 03502	FRAME 2		
7R0014480A		Sht	REV

MICROFILM OVERLAP AREA

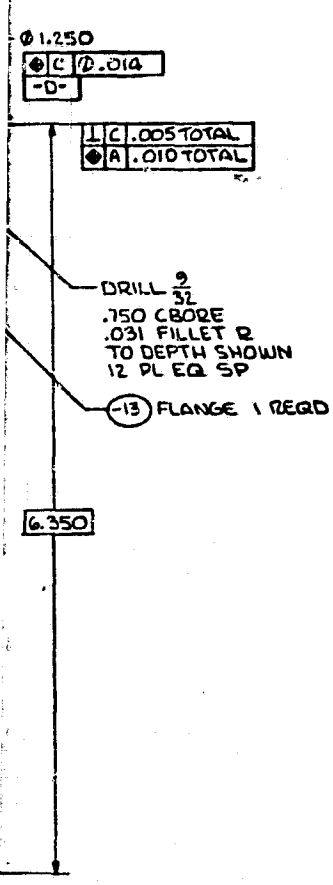

ORIGINAL PAGE IS OF POOR QUALITY

FOLDOUT FRAME 5

THIS PRINT REDUCED
THIS IS NOT A RELEASED COPY

Figure 2-4

RI/RD80-218-2

2-7

REVISED 6-2-80

(9) HEAT TREAT PER RA0111-019 TO 180,000 TO 200,000 PSI FTU RC 38-45 AFTER (7) AND PRIOR TO THDD ASSY
8. CLEAN DETAILS PER RA0110-018
(7) INERTIA WELD PER RA1607-044 EXCEPT MATERIAL IS ALLOY 903. WRENCHING ELEMENT ON LOX POST IS PER AS1159-07
(6) ALTERNATE MATERIAL: RB0170-154
(5) AVERAGE POROSITY TO BE SUCH THAT IT PERMITS 250 ± 25 SCFM/FT² OF AIR AT 70°F TO PASS THRU WHEN EXHAUSTING TO ATMOSPHERE
(4) AIRCRAFT POROUS MEDIA INC. GLEN COVE LI, N.Y.
(3) WELD PER RA0107-027
(2) ELECTRON BEAM WELD PER RA0107-042
1. MACHINE PER RA0103-016

-1
NO

NO	MATERIAL	SIZE	SPECIFICATION
-15	INCONEL 718 TUBING	1.50 O.D. x .125 W.T.	RB0170-211
-13	INCONEL 718	—	RB0170-153 (6)
-9	INCONEL 718	—	RB0170-153 (6)
-7	321 CRES SH	.125 THICK	COMML RIGIMESH (4)(5)
-5	ALLOY 903	—	RB0170-186
-3	ALLOY 903	—	RB0170-186

(9)	UNLESS OTHERWISE SPECIFIED DIMENSIONS ARE IN INCHES AND APPLY PRIOR TO FINISH. 125 MACH. SURF. ROUGHNESS	CONTR	Rocketdyne International Corporation Rocketdyne Division Canoga Park, California
FINISH NONE	TOLERANCES ON ANGLES ± 0° 30' DECIMALS .XX ± .03 .XXX ± .005 HOLES NOTED "DRILL" OVER THRU TOLERANCE	DSGN	INJECTOR, EXPANDER POINT DESIGN ENGINE LAYOUT (INERTIA WELDED)
MAT'L NOTED	NO NOT SCALE PRINT	DESIGN ACTIVITY APVD	SIZE J FSCM NO 02602 DWG NO 7R0014480A
			SCALE 2/1 SHEET

7R0014480A

high mass to lower mass injection areas. Cross velocity such as this is usually accompanied by mixture ratio striation as the fuel-rich fractions are more easily transported than the oxidizer-rich heavy fractions. The result of severe cross flow and mixture ratio striation can be streaking of the combustion chamber wall. The Advanced Expander Cycle Engine Point Design Injector described here has been designed to minimize these risks. The mixing/distribution characteristics of an injector are known to be a function of the manifold flow distribution on a microscopic scale, and the individual element mixing efficiency on a smaller scale. The manifold design of this injector provides optimized manifold distribution volumes and flow areas, consistent with other design parameters (i.e., system pressure drop, packaging, and weight). Liquid oxygen inlet velocities are moderate, and flow areas are sufficient to ensure a low cross velocity. The inlet metering orifices on the oxidizer posts provide the most consistent method of flow control with a minimum of sensitivity to external flow disturbances. The contour machined injector fuel manifolding, integral with the combustion chamber, is also designed for low inlet velocity and uniform circumferential distribution of flow. The well mixed, uniform mass distribution of the concentric flow pattern selected for this injector avoids any necessity for deliberate propellant maldistribution such as film cooling or low mixture ratio barrier zone elements sometimes required to provide the necessary thrust chamber compatibility. The use of injector film cooling on an expander cycle engine is undesirable because the reduced heat load in the forward end of the combustion chamber, by necessity, is counter productive in regard to maximizing the available turbine enthalpy.

The Expander Point Design Injector LOX posts will be inertia-welded to the injector body and machined on the injector face side to accept the threaded fuel elements. The fuel elements will also be threaded at the face end to accept the injector face retaining nuts.

The Rigimesh injector face is supported by all 108 elements, using a system of threaded sleeves, and "facenuts," similar to the SSME injector.

An outer piston ring-type seal on the faceplate allows differential thermal movements of the faceplate without inducing high stresses: the use of the facenuts in conjunction with a piston ring concept allows adjustment in cup recess (the distance from the injector face to the tip of the liquid oxygen injection central tube). This permits a fairly wide range of acceptable tolerancing and of positioning in the injection element. Replacement or reworking of the facenut also permits changes in the annular fuel gas. This provides for a possible readjustment of the fuel flow resistance and the fuel injection velocity. This adjustability allows variations of the most important coaxial injection parameters, without extensive, time-consuming, and expensive rework to the injector. Current facenut annular gap parameters are set at the predicted optimum values, as obtained through analysis; however, experimental fine tuning has been proven to be the most effective way of obtaining final optimization of the injector performance.

The injection element configuration (Fig. 2-5) includes an integral centering device on each liquid oxygen central element to keep the fuel gap concentric around the oxidizer elements. This centering device is located as close to this gap as practical, while at the same time minimizing the wake effects behind each centering devices. The wake effects are further minimized by locating the centering devices in the low-velocity region of the injector element, and accelerating the hydrogen flow in the gap immediately downstream of the centering devices.

Some large injectors used with low-density combustion gases for fuel have experienced cross flow wake-induced vibration of the oxidizer posts. With the SSME injector, where these posts are relatively long and flexible, a vortex shedding pattern of ribs was utilized to reduce these driving forces. With shorter, more rigid posts and lower manifold velocities as used in this injector, these devices are not required. These shorter, stiffer posts represent a significant reduction in fabrication costs.

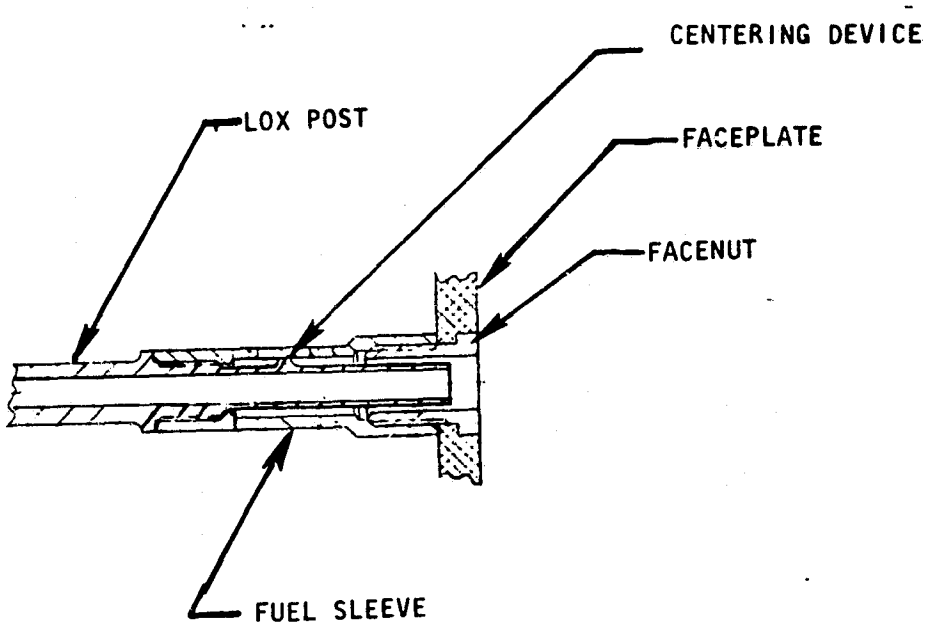

Figure 2-5. Injector Element Components

A plasma torch igniter port is provided in the center of the injection pattern for reliable multistart capability. This torch igniter has been used on the ASE program with a high degree of success, and is further described in a later section.

The fuel manifold for the Advanced Expander Cycle Engine injector utilizes a tapered cross section with appropriate length LOX posts at the different radial locations. This tapered fuel manifold cross section provides a relatively low fuel inlet velocity at the outer element row to minimize flow-driven vibrations of the oxidizer posts while the constantly decreasing flow cross section maintains a nearly constant manifold velocity across the injector body. The fuel inlet annulus around the injector body contains a removable screen/filter element (Fig. 2-2) which ensures several useful benefits. Primarily the screen filters out contamination material in the fuel flow to avoid blockage of the narrow fuel annulus gasps in the individual elements.

In either expander cycle or staged combustion cycles, this problem is known to be quite severe with the numerous potential sources of contamination in the upstream power train system and propellant tankage and ducting system. The screen element also provides a measure of flow diffusion to smooth out inlet velocity peaks that can cause oxidizer post vibration.

Locating the filter element on the perimeter of the manifold, rather than individual elements, also allows large quantities of local contamination to be trapped without seriously distorting the injector element flow distribution. With individual element screening as used on the SSME, a local mass of contamination can readily restrict individual elements, resulting in serious combustion chamber streaking problems. The single-screen element around the injector body offers advantage in cost and ease of fabrication as well.

The liquid oxygen manifold is similar in configuration to previous Rocketdyne coaxial injectors. Sufficient volume is provided to eliminate manifold velocity effects on injector propellant distribution. In addition to the volume to diffuse inlet velocity, special provision is made for the effects of inlet velocity.

Injector Material Selection

The materials selected for the Advanced Expander Cycle Engine Point Design injector are presented in Table 2-2 based on the operating environment and requirement for long life. A description of the selection criteria and tradeoffs considered are discussed in the following paragraphs.

TABLE 2-2. INJECTOR COMPONENT MATERIALS

COMPONENT	MATERIAL
INJECTOR BODY AND CLOSEOUT STRUCTURE	INCONEL 718
INJECTOR POSTS	HAYNES 188
FACEPLATE	321 CRES
RING	A286
FACEPLATE NUT	A286
INJECTOR POST SLEEVES	A286
OXIDIZING INLET ASSEMBLY	INCONEL 718
IGNITER INLET TUBES	347 CRES

Body and Closeout Materials. The weight savings provided by the high strength of Inconel 718 makes it the prime candidate material for the Injector Body and Closeout. Rocketdyne has successfully used this age-hardenable, nickel-base alloy on both the SSME and ASE injectors.

Inconel 718 alloy is suitable for service at injector operating temperatures from -423 F to 1300 F. In addition, the high fatigue strength, the excellent stress rupture properties, and good corrosion resistance make it a worthy material candidate for these components. Another outstanding characteristic of Inconel 718 is its slow response to age hardening. The slow response enables this material to be welded and annealed with no spontaneous hardness unless cooled slowly; it can also be weld repaired in the fully aged condition.

Inconel 718 is susceptible to embrittlement in the presence of high pressure hydrogen. Stress-risers, such as notches, accentuate these embrittling effects with the most pronounced degradation occurring around room temperature. Two methods have been used successfully to protect the injector face from hydrogen environment effects of strain and plastic. The first technique employs a heat shield made from a stainless steel screen. The shield serves as a thermal barrier to

reduce strains. This approach is used on the SSME injectors. The second technique utilizes copper plating. The injector face is copper plated with a barrier sufficiently thick to prevent hydrogen from contacting the Inconel 718 substrate. This approach was used on the 20K ASE injectors and is used in the Expander Point Design injector.

Injector Posts Materials. Haynes 188 alloy was selected as the prime candidate material for the injector posts because of its good low cycle fatigue life in a high pressure hydrogen environment and its excellent creep rupture strength at elevated temperatures. Haynes 188 is a cobalt-base alloy with good high temperature strength and oxidation resistance. Cryogenic temperatures do not significantly affect the ductility but strength levels are increased. Because of its good ductility, the material can be cold worked as well as forged.

Rocketdyne has fabricated injectors with Haynes 188 posts inertia welded to Inconel 718. This process and materials combination has been successfully used to manufacture both subscale and full scale SSME injectors.

Other candidate materials, such as Type 316 CRES, were eliminated because of their lower strength and lower low cycle fatigue life. Inconel 718 was not suitable for this application because of its susceptability to embrittlement from high pressure hydrogen. A286 CRES, although it possesses good strength and is resistant to HEE, has not been inertia welded and a development program would have to be conducted if this were the selected injector post material.

Faceplate Materials. The faceplate will be fabricated from Type 321 CRES. Rocketdyne has successfully used stainless-steel Rigimesh faceplates on the SSME, ASE, and 40K injectors. The Rigimesh is fabricated by weaving Type 321 CRES wire into screen, compacting layers of this screen and, finally, sintering the screens into a bonded structure. Since Type 321 CRES is a stabilized stainless steel, no detrimental carbides develop during sintering.

The Rigimesh faceplate is attached to an outside support and sealing ring by electron beam welding. Type 321 CRES has better weldability than other stabilized stainless steels. In addition to its excellent weldability, Type 321 CRES possesses good resistance to hydrogen embrittlement while exhibiting good corrosion resistance.

Oxidizer Inlet. The flange, elbow, and transition ring that comprise the oxidizer inlet will be fabricated from Inconel 718. The material properties of Inconel 718 have been discussed previously. The inlet will be fabricated as a detail and fully heat-treated prior to attaching it to the injector. The final closeout weld will be left in the as-welded condition.

Ring, Faceplate Nuts, and Injector Post Sleeves. These components will be fabricated from A286. Rocketdyne has utilized this alloy in similar applications on other injectors successfully. The material properties of A286 have been discussed previously.

Inlet Tubes for Igniter. These tubes will be fabricated from Type 316L CRES. Type 316L is a low-carbon stainless steel that possesses excellent corrosion resistance and is immune to sensitization. It was selected over stabilized grades of stainless steel because it is both weldable and brazeable. In addition, this alloy maintains excellent cryogenic properties with good retention of ductility.

Injector Performance

The mixing efficiency of the individual elements is ensured by design features based on experience with high-performance, gas-liquid coaxial element injectors. A high-velocity ratio between the gaseous fuel and the liquid oxidizer is necessary to provide the high shear forces required for droplet stripping. The element of this injector is patterned after the highly developed, hot-fire demonstrated injector elements in the SSME injector and the ASE injector. Table 2-3 shows the comparison of significant element parameters.

TABLE 2-3. INJECTOR ELEMENT DESIGN PARAMETERS

PARAMETER	ASE INJECTOR	SSME MAIN INJECTOR	ADVANCED EXPANDER CYCLE INJECTOR
SLEEVE ID, INCH	0.210	0.348	0.1625
FUEL SLEEVE GAP, INCH	0.0425	0.059	0.0185
RECESS, L, INCH	0.090	0.200	0.093
FUEL GAP VELOCITY, FT/SEC	1365	804	1487
FUEL CUP VELOCITY, FT/SEC	1096	640	903
FUEL FLOWRATE PER ELEMENT, LB/SEC	0.0873*	0.2335*	0.0357
LOX POST OD, INCH	0.125	0.230	0.125
LOX POST ID, INCH	0.093	0.188	0.093
LOX POST WALL THICKNESS, INCH	0.016	0.021	0.016
LOX POST VELOCITY, FT/SEC	87.8	101.7	72.5
LOX FLOWRATE PER ELEMENT, LB/SEC	0.292	1.466	0.247

*PREBURNER EXHAUST PRODUCTS

Injector performance characteristics are largely dictated by two parameters: mixing/distribution efficiency and vaporization reaction efficiency. The methods of performance prediction and performance analysis outlined by the JANNAF committees are based on these two parameters.

Experimental injector/chamber correlations of mixture ratio uniformity (E_m) versus a coefficient describing the primary injector design parameter were used to determine the injector mixing/distribution efficiency. The Coaxial Injection Combustion Model (CICM) was used to evaluate the injector/chamber vaporization efficiency. The product of these two efficiencies denotes the overall combustion efficiency of the injector/chamber. It was obtained in this manner for the five thrust and mixture ratio conditions indicated in Table 2-4.

TABLE 2-4. ADVANCED EXPANDER THRUST CHAMBER EFFICIENCY PARAMETERS

ENGINE THRUST, POUNDS	ENGINE MR	MIXING/DISTRIBUTION EFFICIENCY, %	VAPORIZATION EFFICIENCY, %	COMBUSTION EFFICIENCY
15,000	6	99.9	100	99.9
15,000	7	99.8	100	99.8
1,800	4	100.0	100	100.0
1,500	6	99.9	98.36	98.26
1,500(1)	6	100.0	99.3	99.3

(1) With modified injector elements

The injector/chamber combination provide combustion efficiency in excess of 99.8 at the nominal thrust operating conditions. At pump idle mode thrust, the injector provides complete combustion. A more detailed injector performance discussion appears in the section entitled Engine Data Summary.

Injector Face Heat Transfer

For preliminary design consideration, coolant flow requirements for the porous Rigimesh (CRES) were analyzed on the basis of wall heat flux data taken in water-cooled experimental chambers at the injector end location. Due to the large percentage of face area displaced by the injector elements, the face flow requirements are small (Fig.2-6). The design range requirements of 0.15 to 0.23 lb/sec will result in face temperatures of 250 to 400 F above the coolant injection temperature. Local injector element areas are to be cooled by gaseous H_2 fuel flow through the annular injection region. Combustion and mixing delay lengths result in these areas attaining a temperature equal to the main fuel injection temperature.

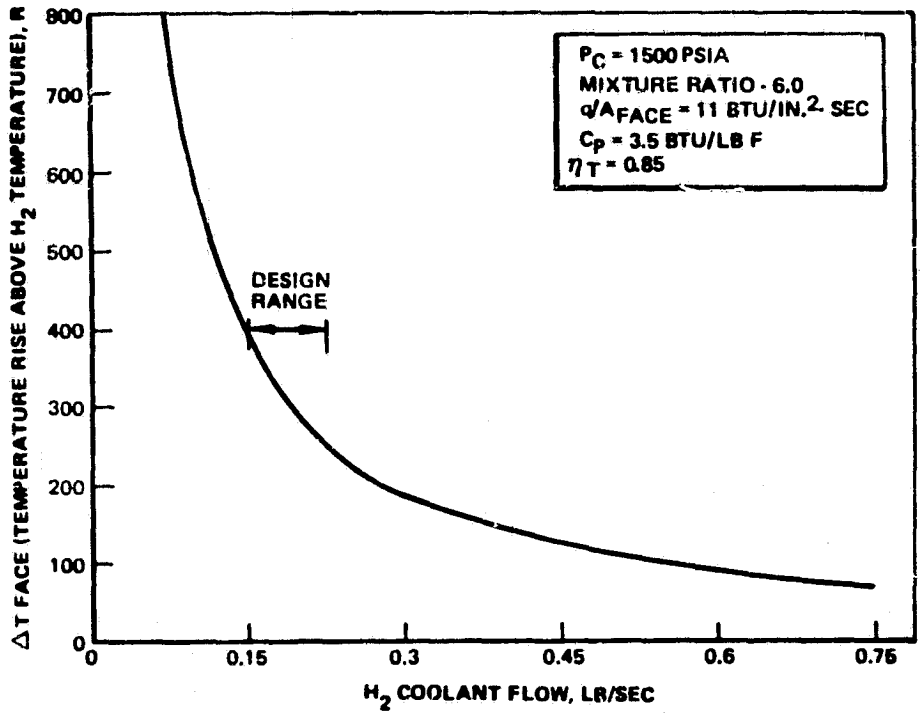

Figure 2-6. Expander Cycle Injector Rigimesh Face Temperature Rise vs H_2 Transpirant Flow

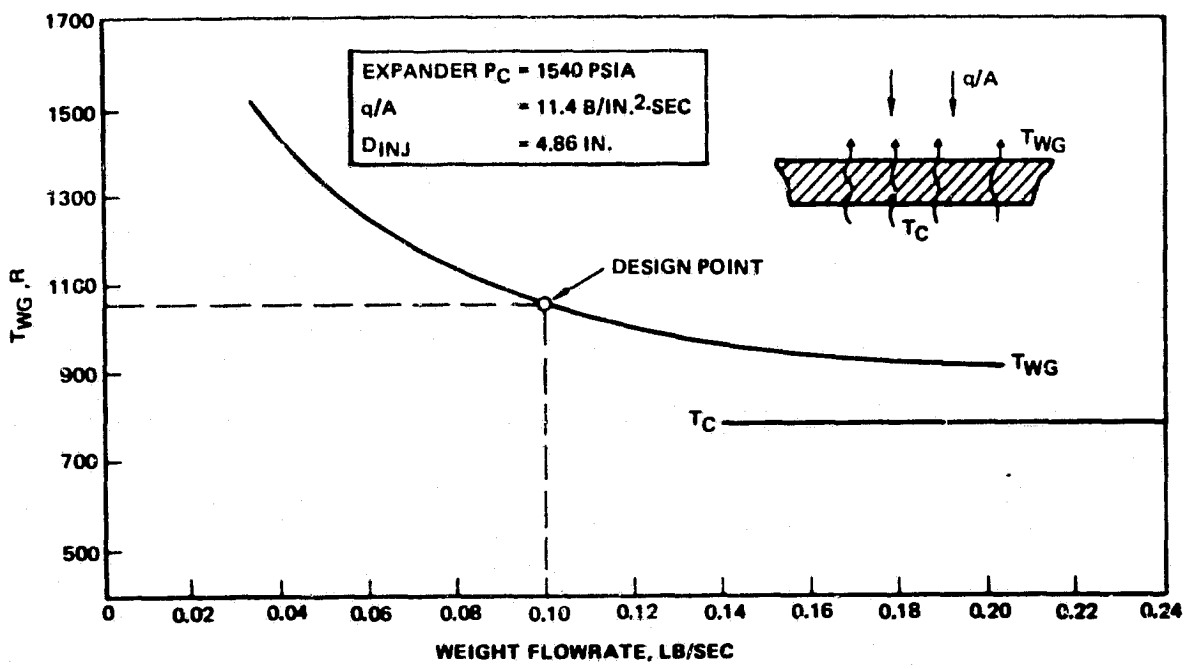

Figure 2-7. Expander Cycle Injector Rigimesh Face Temperature vs Flowrate

The cooling scheme for the Rigimesh is to supply the turbine discharge H_2 in a parallel path with 0.15 lb/sec of H_2 flow supplied to the face cooling and the remainder of the flow supplied to the fuel element annuli. The resultant face temperature will be approximately 975 R at this flow which will be well within the cyclic life capability required. Figure 2-7 illustrates the injector face temperature versus flow based on the injector end heat flux being equal to the chamber wall value at the head end location of 11.4 Btu/in.^{2}-sec.

Injector Low Thrust Operation

Operation of the Advanced Expander Point Design Thrust Chamber at 10%-12% of rated engine thrust and at engine mixture ratios of 4-6 presents a very few problems for the injector. Gas-liquid coaxial injection elements are relatively insensitive to flowrates, and they permit throttled operation with very few (if any) modifications. The gas side flow velocity remains nearly constant, and the pressure drop and inertance remain nearly in constant relationship to chamber pressure (i.e., the ΔP remains at a constant percent of chamber pressure). The incompressible liquid flow, in this case liquid oxygen, however, follows usual "square law" relationships, and the LOX ΔP will become a low percent of chamber pressure. A built-in high design thrust pressure drop value (33% of P_c) and the LOX valve pressure drop provide sufficient pressure at low thrust to result in dynamic stability. This has been ascertained in dynamic analyses performed at low thrust, and confirms that no injector modification is required on the LOX side for stable operation at low thrust.

The Coaxial Injector Combustion Model (CICM) analysis indicates no appreciable performance degradation in operation at the 10% flow and chamber pressure if kitted facenuts are used to maintain high injection velocity on the fuel side.

IGNITION SYSTEM DESIGN

Redundancy in the ignition system required for manrating engine capability is achieved through use of a dual plasma torch igniter to provide a reliable source of ignition energy at start. This type of igniter was selected because of the potential for high spark electrode durability, predictable and repeatable ignition conditions at the spark electrode, and a high temperature downstream of the igniter exit to enhance the propellant ignition in the combustion chamber. The system consists of dual exciters, harnesses and spark plugs, operating through a single combustion chamber and flame tube.

Each plasma torch igniter element consists of a small integral O_2/H_2 injector, and a combustor/nozzle for ducting the hot gas to the combustor (Figure 2-8). Oxidizer is injected from an annular manifold around the spark plug electrode. A small amount of fuel is injected into the igniter combustor/nozzle where it mixes with the oxidizer downstream of the electrode, producing an oxidizer-rich combustion (MR = 40:1). The bulk of the igniter fuel flows around the combustor and flame tube, providing necessary cooling before being discharged at the injector face. A spark plug is attached to the igniter body through a threaded joint and seal.

Three thermocouples are used to provide automatic termination of the start sequence of the engine if an igniter failure were to occur. Three thermocouples, whose junctions are spot welded to relieved sections of the igniter chamber wall, are used in the ignition detection system. A logic circuit is used to terminate the start sequence if any two of the three thermocouples fails to indicate a 110 F temperature by the time that the main fuel valve is sequenced to be activated.

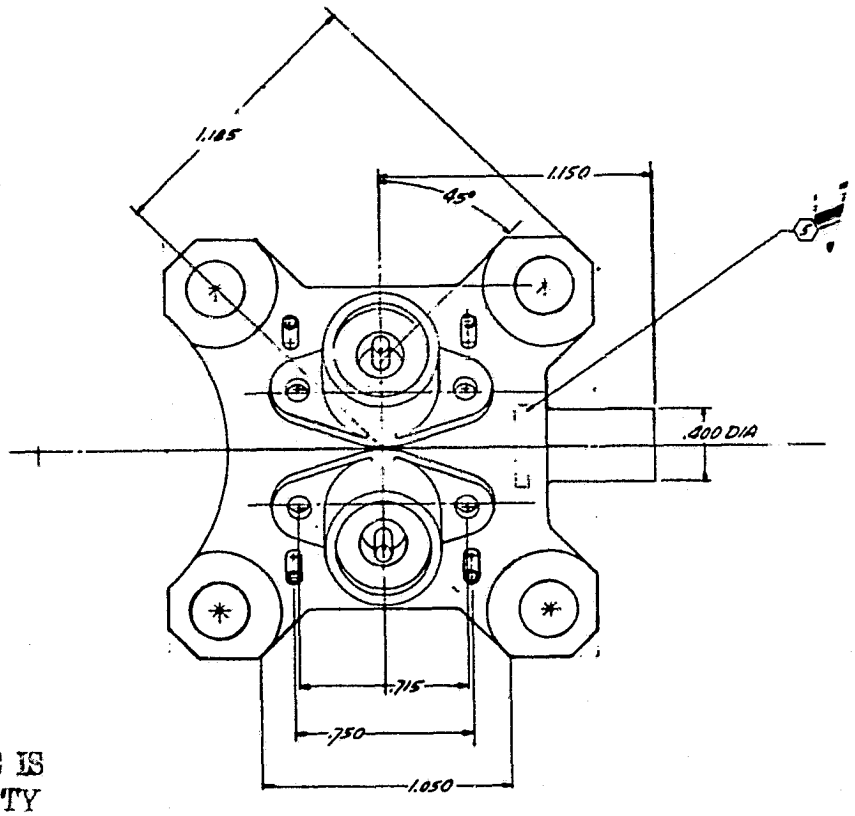

VIEW C 7c
SCALE 4/1

ORIGINAL PAGE IS
OF POOR QUALITY

FOLDOUT FRAME

MICROFILM OVERLAP AREA

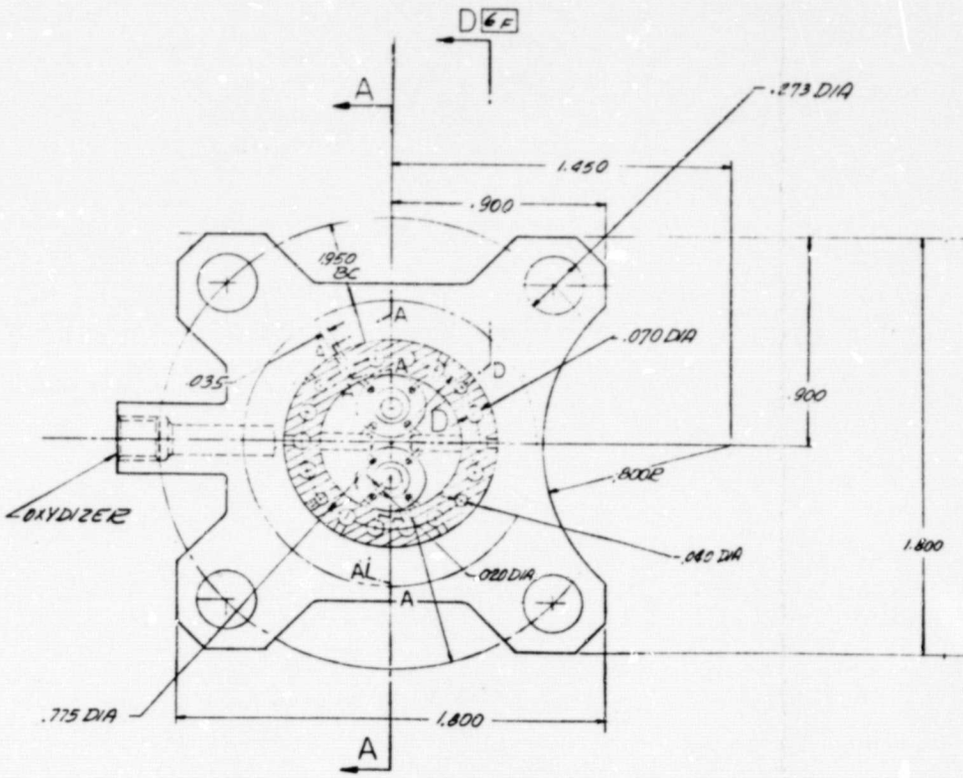

SECTION B-B 6C
SCALE 4/1

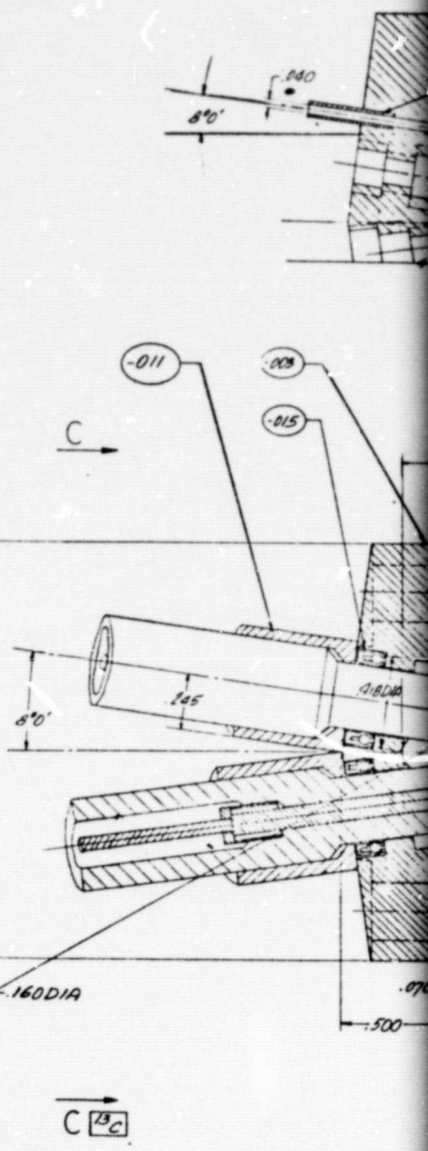

FOLDOUT FRAME 2

Rockwell International Corporation
Rocketdyne Division
Canoga Park, California

FSCM NO 67602	FRAME 1		
7R0014470		SH	REV

MICROFILM OVERLAP AREA

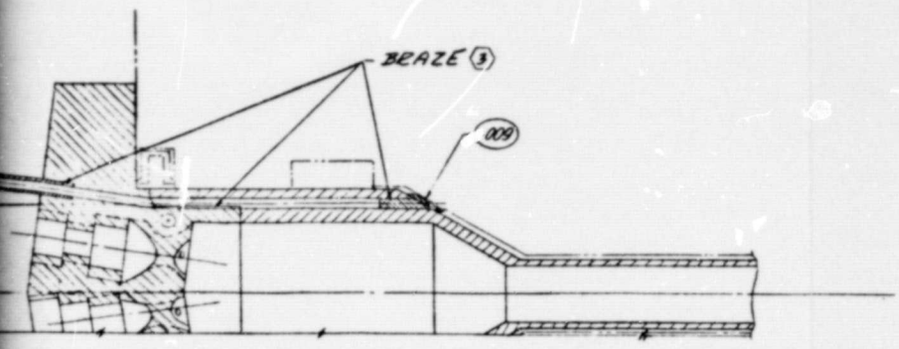

SECTION D-D [9F] (INSTRUMENTATION PASSAGE DEVELOPMENT)
SCALE 4/1 (SPARK PLUG REMOVED FOR CLARITY)

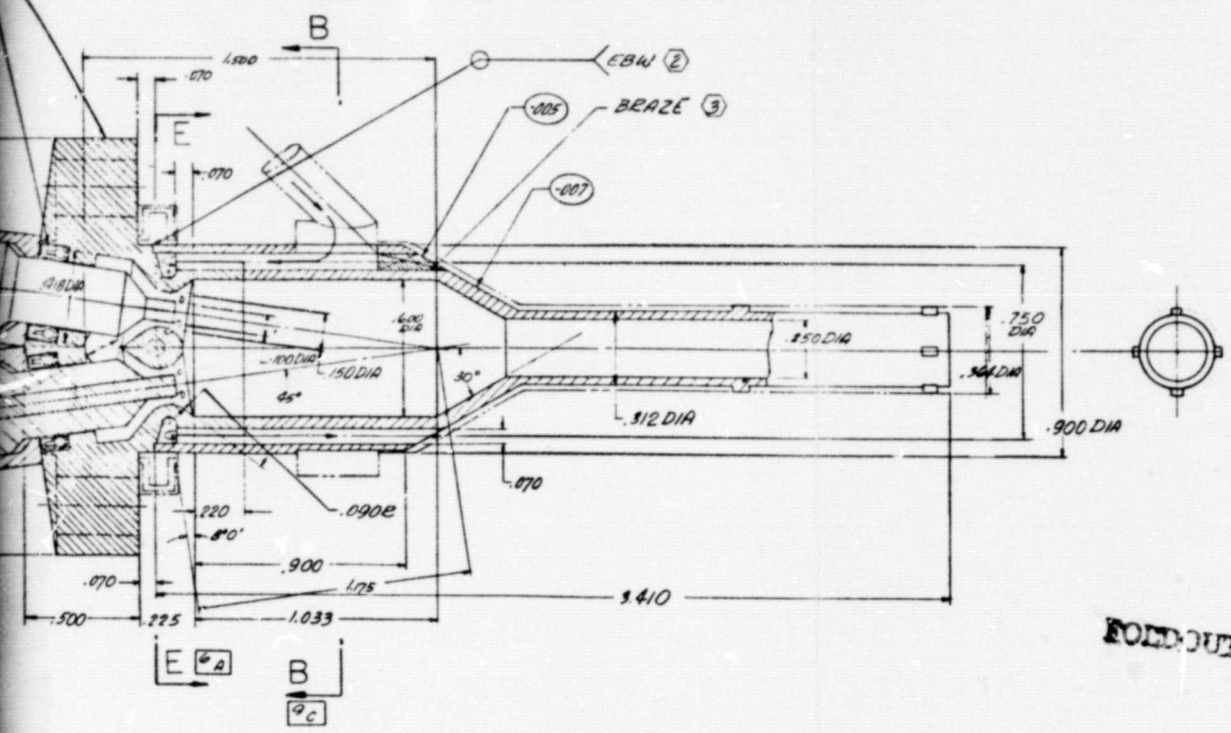

SECTION A-A (COOLANT PASSAGE DEVELOPMENT)
SCALE 4/1

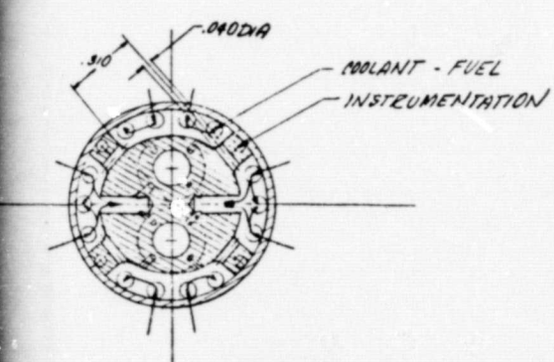

SECTION E-E [6C]
SCALE 4/1

FOLDOUT FRAME

Figure 2-

FOR INFORMA

RI/RD80-
2-2

-015	2	P/N TBD	.300 ID x .425 OD
-013			
-011	2	P/N 49876	
-009	4	Ni 200	.080 DIA x .300
-007	1	Ni 200	.900 DIA x
-005	8	Ni 200	.070 DIA x .300
-003	1	INCO 625	1.80 x 1.80 x .925
NO	#REQ	MATERIAL	SIZE

	-011
-001	
ASSY	SUBASSY

(7) HYDRODYNE DWG TBD
(6) SIMMONDS PRECISION, DWG 126961
(5) IDENTIFY PER RA0104-008, EI-CHEM ETCH
4 CLEAN PER RA0110-018
(3) FURNACE BRAZE PER M+P INSTRUCTION
(2) ELECTRON BEAM WELD PER RA0107-042
1. MACHINE PER RA0103-016
NOTE: UNLESS OTHERWISE SPECIFIED

UNLESS OTHERWISE SPECIFIED DIMENSIONS ARE IN INCHES AND APPLY PRIOR TO FINISH.
125/ MACH. SURF. ROUGHNESS
TOLERANCES ON ANGLES ± 0° 30'
DECIMALS .XX ± .03 .XXX ± .010
HOLES NOTED "DRILL"

OVER	THRU	TOLERANCE
.0000	.0400	+ .0015 — .0010
.0400	.1300	+ .0020 — .0010
.1300	.2700	+ .0045 — .0010
.2700	.5000	+ .0080 — .0010
.5000	.7500	+ .0070 — .0010
.7500	1.0000	+ .0090 — .0010
1.0000	2.0000	+ .0130 — .0010

DO NOT SCALE PRINT

CONTR
DWN
CHK
DATE
DSGN
MATL
STRUCT
DESIGN ACTIVITY APVD
DATE

IGNITER
DUAL

SIZE J
FSCM NO 0260
SCALE 4/1

FOLDOUT FRAME 8

Figure 2-8

FOR INFORMATION

RI/RD80-218-2
2-20

2	P/N TBD	.300 ID x .425 OD	(7)	
2	P/N 49876		(6)	7F
4	Ni 200	.080 DIA x .300		5G
1	Ni 200	.900 DIA x		5E
8	Ni 200	.070 DIA x .300		5E
1	INCO 625	1.80 x 1.80 x .925		7F
#REQ	MATERIAL	SIZE	SPECIFICATION	ZONE

UNLESS OTHERWISE SPECIFIED DIMENSIONS ARE IN INCHES AND APPLY PRIOR TO FINISH.
MACH. SURF. ROUGHNESS
TOLERANCES ON ANGLES ± 0° 30'
DECIMALS .XX ± .03 .XXX ± .010
HOLES NOTED "DRILL"
OVER THRU TOLERANCE
.0000 .0400 + .0015 — .0010
.0400 .1100 + .0030 — .0010
.1100 .2200 + .0045 — .0010
.2200 .5000 + .0060 — .0010
.5000 .7500 + .0070 — .0010
.7500 1.0000 + .0090 — .0010
1.0000 2.0000 + .0120 — .0010
DO NOT SCALE PRINT

CONTR
DWN [illegible] DATE
CHK DATE
DSGN [illegible]
MATL
STRUCT
DESIGN ACTIVITY APVD DATE

Rockwell International Corporation
Rocketdyne Division
Canoga Park, California

IGNITER, ASSY OF OTV DUAL

SIZE J FSCM NO 02602 DWG NO 7R0014470
SCALE 3/1 SHEET
FRAME 2

7R0014470

The igniter body is fabricated from Inconel 625, and the combustor nozzle is made of nickel and welded to the igniter body.

The torch igniter has the capability for rapid re-ignition with minimum delay in the event of a flameout during the start transition. It also provides a high mixture ratio near the electrode for reliable ignition and produces a hot core for main propellant ignition. The extremely high mixture ratio of the hot core is also advantageous for main propellant ignition because the hydrogen discharge from the coolant liner drives the hot core temperature higher through the stoichiometric point before it is totally mixed with the igniter flow. Other advantages of the torch igniter are:

1. The oxidizer flow around the electrode provides cooling for the electrode and minimizes the potential for erosion from combustion.

2. The injection technique using impinging fuel orifices below the electrode produces predictable conditions for ignition.

The igniter geometry in the region of the spark electrode, oxidizer annulus, and fuel orifices is similar to that tested under ASE contract NAS3-14348 and Rocketdyne-sponsored programs. The igniter propellant manifolds and combustor/nozzle geometry have been modified slightly to accommodate optimum packaging in the injector. A coaxial-type nozzle exit was selected for the igniter to allow mixing to take place downstream of the injector face to enhance main propellant ignition and allow the igniter to operate similarly to an injector element during mainstage.

Rocketdyne has conducted a number of contract and company in-house test programs to demonstrate the integrity of a similar ASE single element igniter and to evaluate its ability to provide proper chamber ignition (Table 2-5).

TABLE 2-5. INITIAL ASE IGNITION TEST SUMMARY

Tests Conducted:	
Preburner	14
Main Chamber	12
Duration (Maximum), Seconds	11.5
Ranges of Operation:	
Propellant Flow, lb/sec	0.084 to 0.112
Propellant Inlet Temperature, R	480 to 556
Core Mixture Ratio	13.8 to 23.4

COMBUSTION CHAMBER DESIGN

The combustion chamber (Fig. 2-9) selected for the Thrust Chamber Assembly is a single-pass, channel-wall, copper-base alloy configuration and includes a nozzle expansion section to an area ratio of 14:1. This combustion chamber concept is used successfully on the SSME and the 20K Advanced Space Engine assembly. The features of this design include a copper-alloy (NARloy-Z) slotted liner with an electroformed-nickel closeout, manifolds brazed to the liner, acoustic cavities, and injector manifold housing integral with the combustion chamber. The aft combustion chamber to nozzle interface is designed with a flanged joint for maximum ease of hardware interchangeability during engine development testing. This flange is reworkable into a lightweight welded design for flight application. The manifolding at the aft and forward ends of the combustion chamber have been designed to give a uniform flow distribution to and from the coolant passages. The combustion chamber layout is presented in Fig. 2-10.

The injector housing at the forward end of the combustion chamber incorporates a flange to allow installation and removal of the injector. The injector inlet manifolding and the housing have also been designed for uniform flow upstream of the injector manifolds to ensure even fuel distribution to the injection elements. These design features are shown in the combustion chamber configuration (Fig. 2-9).

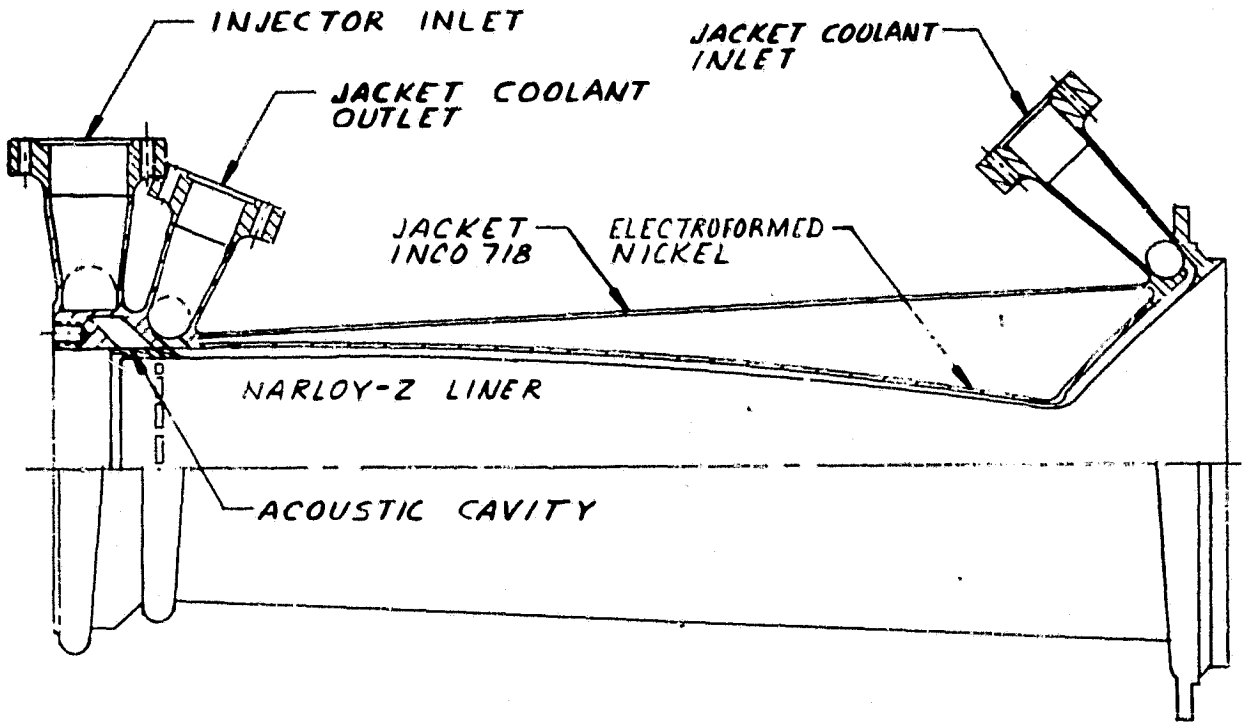

Figure 2-9. Advanced Expander Cycle Combustion Chamber

Cooling of the combustion chamber walls is accomplished by a single uppass hydrogen circuit with 4.09 lb/sec of H_2 coolant at the nominal operating point. The uppass circuit was selected because it provides the maximum capability for cooling in the high heat flux region at the throat. The cooling channel configuration has been designed with the Rocketdyne regenerative cooling analysis program which details in consecutive axial stations the wall temperature (2-dimensional) and fluid conditions along the combustion chamber length. A 0.040-inch minimum channel width has been chosen to provide a low-pressure stress within the channel and a wall temperature level consistent with achieving the required fatigue life. In the upper combustion zone and in the lower portion of the combustion chamber nozzle, the channel width is increased to 0.060 inch. A minimum wall thickness of 0.025 inch between the coolant and hot gas has been selected; this results in satisfactory thermal and structural characteristics while not compromising producibility.

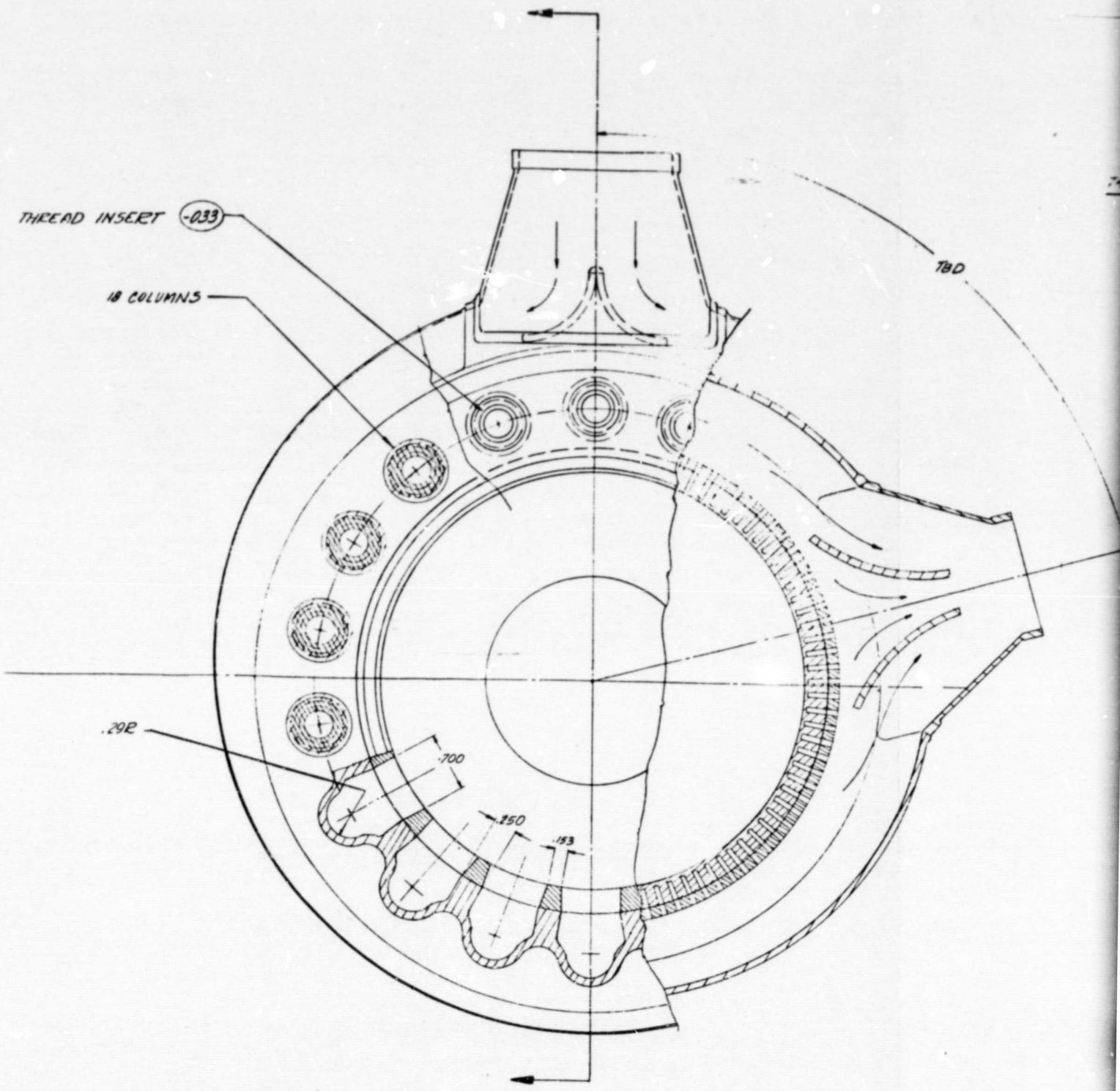

FOLDOUT FRAME

MICROFILM OVERLAP AREA

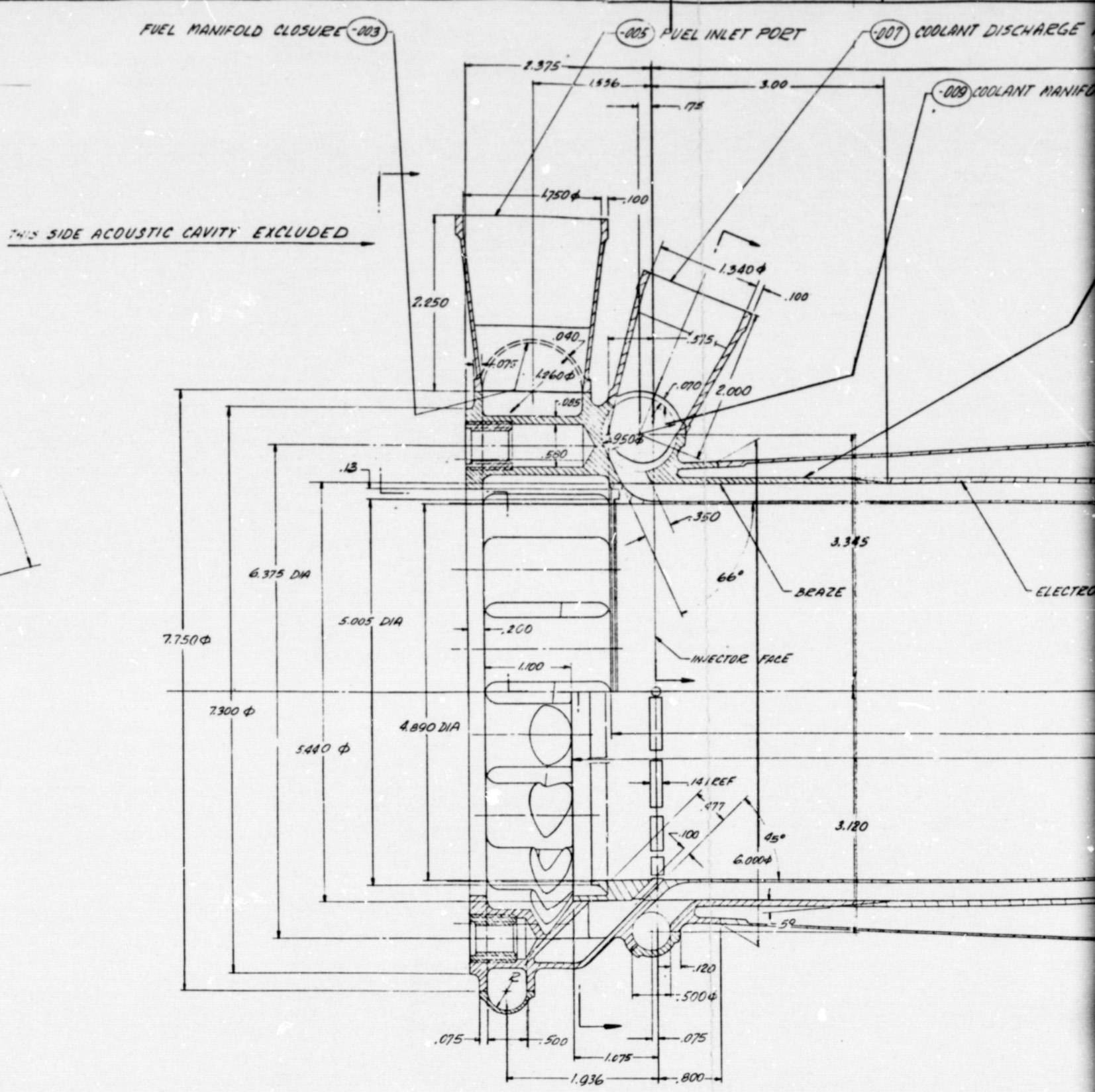

THIS SIDE ACOUSTIC CAVITY INCLUDED

FOLDOUT FRAME

ORIGINAL PAGE IS OF POOR QUALITY

Rockwell International Corporation
Rocketdyne Division
Canoga Park, California

FSCM NO 02602	FRAME 1		
7R0014495		SH	REV

MICROFILM OVERLAP AREA

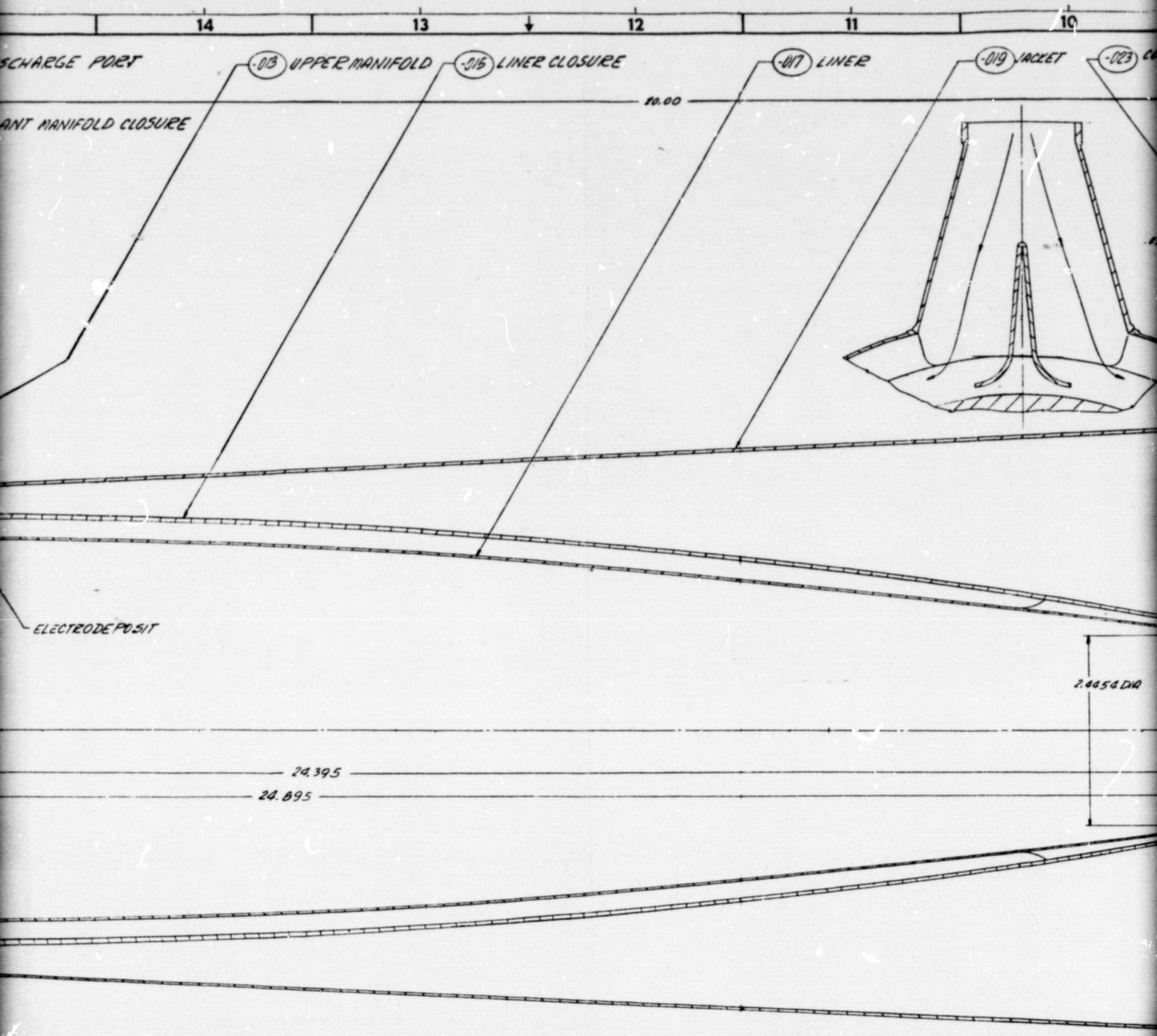

FOLDOUT FRAME 3

14
13
12
11
10

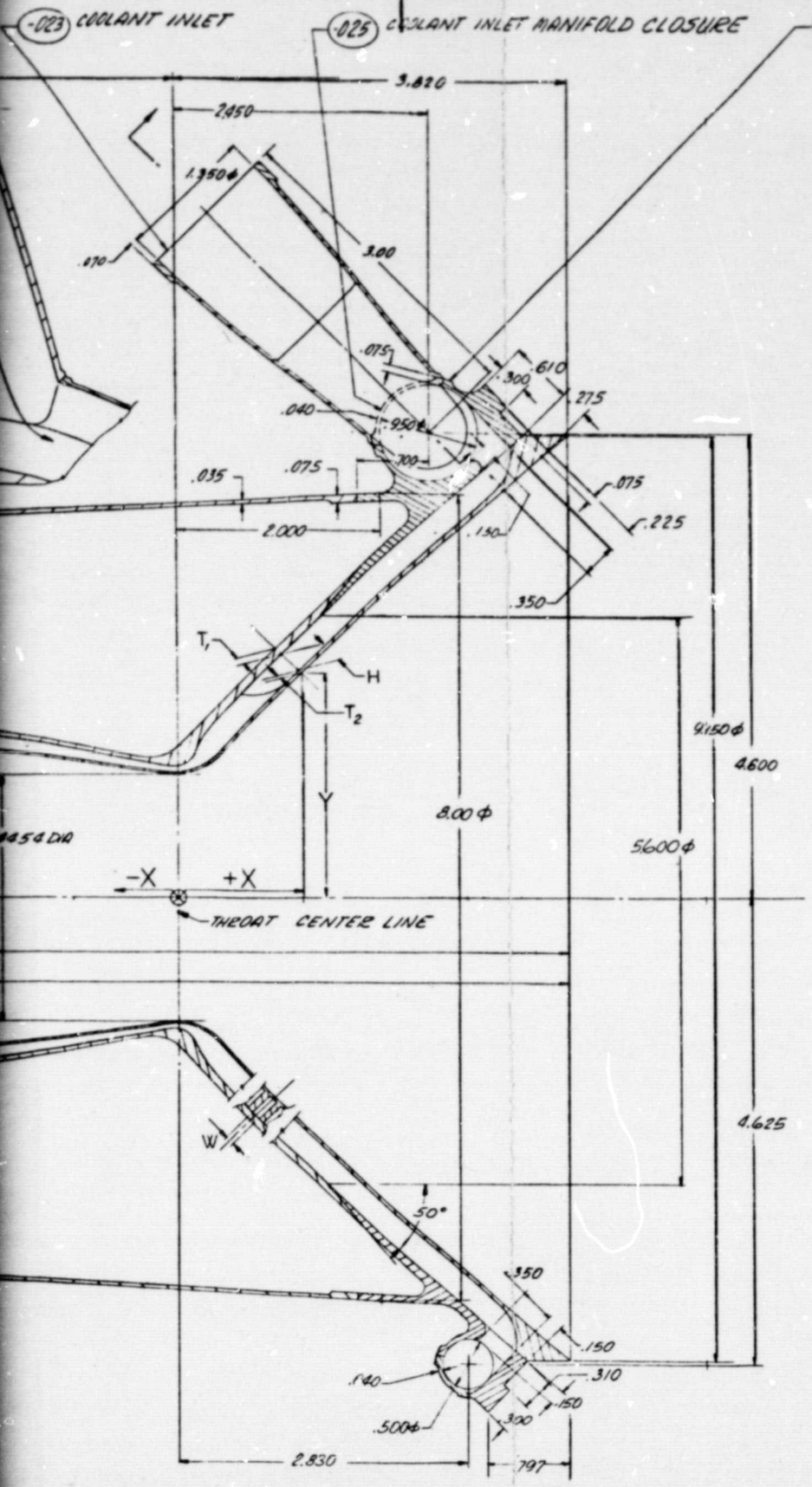

STA.	X	Y	T_1	T_2	H	W
1	-20.000	2.445		.035	.240	.060
2	-19.000	2.445			.240	.060
3	-18.000	2.445	.080		.240	.060
4	-17.000	2.445			.240	.060
5	-15.794	2.439			.240	.060
6	-14.588	2.421			.240	.060
7	-13.382	2.389			.240	.060
8	-12.177	2.346			.240	.060
9	-10.973	2.290			.240	.060
10	-9.769	2.223			.240	.060
11	-8.566	2.142			.240	.060
12	-7.363	2.049		.035	.240	.060
13	-6.162	1.945		.025	.230	.060
14	-4.962	1.827			.160	.060
15	-3.763	1.698			.160	.060
16	-2.565	1.556			.150	.040
17	-1.369	1.401			.120	
18	-.175	1.235			.060	
19	-.140	1.231			.060	
20	-.105	1.228			.070	
21	-.069	1.225			.080	
22	-.035	1.2227			.090	
23	.000	1.2227	.050		.100	
24	+.006	1.2227			.160	
25	+.017	1.2227			.160	
26	+.024	1.2227			.160	
27	+.037	1.224			.160	
28	+.044	1.225			.160	
29	+.057	1.226			.160	
30	+.065	1.228			.160	
31	+.079	1.229			.160	
32	+.087	1.230			.160	
33	+.101	1.234			.160	
34	+.116	1.237			.160	
35	+.125	1.239			.160	
36	+.141	1.243			.160	
37	+.148	1.246			.160	
38	+.164	1.251			.160	
39	+.172	1.253			.160	
40	+.188	1.261			.160	
41	+.204	1.268			.160	
42	+.213	1.272			.160	
43	+.228	1.279			.160	
44	+.236	1.283			.160	
45	+.252	1.292			.160	
46	+.268	1.302			.160	
47	+.275	1.306			.160	
48	+.291	1.318			.160	
49	+.298	1.324			.160	
50	+.313	1.336			.160	
51	+.320	1.343			.160	
52	+.334	1.355			.160	
53	+.341	1.362			.160	
54	+.352	1.372			.160	
55	+.381	1.402			.160	
56	+.511	1.536			.160	
57	+.643	1.670		.025	.160	
58	+.779	1.806		.035	.160	
59	+.850	1.676	.080		.160	.040
60	+.999	2.024			.240	.060
61	+1.078	2.103			.240	.060
62	+1.246	2.269			.240	.060
63	+1.334	2.352			.240	.060
64	+1.525	2.535			.240	.060
65	+1.739	2.740			.240	.060
66	+1.856	2.651			.240	.060
67	+2.109	3.684	.100		.240	.060
68	+2.250	3.213			.240	.060
69	+2.564	3.497			.240	.060
70	+2.927	3.820			.240	.060
71	+3.133	3.997			.240	.060
72	+3.590	4.382			.240	.060
73	+3.859	4.608		.035	.240	.060

TAPERING

TAPERING

TAPERING

FOLDOUT FRAME 4

ORIGINAL PAGE IS
OF POOR QUALITY

Rockwell International Corporation
Rocketdyne Division
Canoga Park, California

FSCM NO 07602	FRAME 2		
7R0014495		SH	REV

FOLDOUT FRAME 5

Figure 2-10

FOR INFORMATION

RI/RD80-218-2

DASH NO	MATERIAL	SIZE	SPECIFICATION	ZONE
-033	CRES AMS 5737		MS 51831-105	23G
-029				
-027	INCO 625			7H
-025	INCO 625			9H
-023	INCO 625			10H
-019	INCO 718			10H
-017	NARLOY Z			11H
-015	Ni 200			13H
-013	INCO 625			14H
-009	INCO 625			15H
-007	INCO 625			15H
-005	INCO 625			17H
-003	INCO 625			18H

1. THIS DRAWING SUPPORTS 7R0014500.

NOTE: UNLESS OTHERWISE SPECIFIED

UNLESS OTHERWISE SPECIFIED: DIMENSIONS ARE IN INCHES AND APPLY PRIOR TO FINISH. 125/ MACH. SURF. ROUGHNESS

TOLERANCES ON: ANGLES ± 0° 30' DECIMALS .XX ± .03 .XXX ± .010

HOLES NOTED "DRILL"

OVER	THRU	TOLERANCE
.0000	.0400	+ .0015 — .0010
.0400	.1300	+ .0030 — .0010
.1300	.2700	+ .0045 — .0010
.2700	.5000	+ .0060 — .0010
.5000	.7500	+ .0070 — .0010
.7500	1.0000	+ .0090 — .0010
1.0000	2.0000	+ .0120 — .0010

DO NOT SCALE PRINT

CONTR

DWN P. ENGEL DATE

CHK DATE

MATL

STRUCT

DESIGN ACTIVITY APVD DATE

Rockwell International Corporation
Rocketdyne Division
Canoga Park, California

OTV - COMBUSTOR ASSEMBLY

SIZE J FSCM NO 02602 DWG NO 7R0014495

SCALE 2/1 SHEET

FRAME 3

7R0014495

Acoustic cavities are included in the combustor design. The results of the stability analysis and acoustic cavity design are discussed in the Combustion Stability section.

Manufacturing processes used to fabricate the combustion chamber are standard manufacturing processes at Rocketdyne. New technology is not required to manufacture the combustion chamber for the Engine Point Design Thrust Chamber Assembly. Extensive experience has been gained at Rocketdyne during the manufacture of the SSME main combustion chamber and the 40K combustion chamber model for the SSME. Additional experience on a similarly sized engine was obtained on the 20K Advanced Space Engine combustion chamber, which eliminated problems encountered on the SSME main combustion chamber. The 20K ASE combustion chamber is similar in physical size to the 15K Advanced Expander Cycle Engine Combustion Chamber. Experience with these programs is directly applicable to the proposed thrust chamber.

The fabrication sequence of the combustion chamber is shown in Fig. 2-11 The NARloy-Z liner is hot shear spun from a forged flat plate. Figure 2-11 illustrates this hot spinning process. The internal contour is machined, an internal mandrel is inscalled, and the external contour machining and channel slotting is accomplished.

Coolant manifolds are partially machined and slotted for the fuel inlet passages; then they are brazed to the NARloy-Z liner. The coolant channels are closed out with electrodeposited copper for hydrogen embrittlement protection followed by the electrodeposited nickel. Final machining of the manifold sections are completed and manifolds are welded into position. Critical interfaces are then final machined. All processes required to manufacture this combustion chamber are existing technology and are standard manufacturing procedures at Rocketdyne.

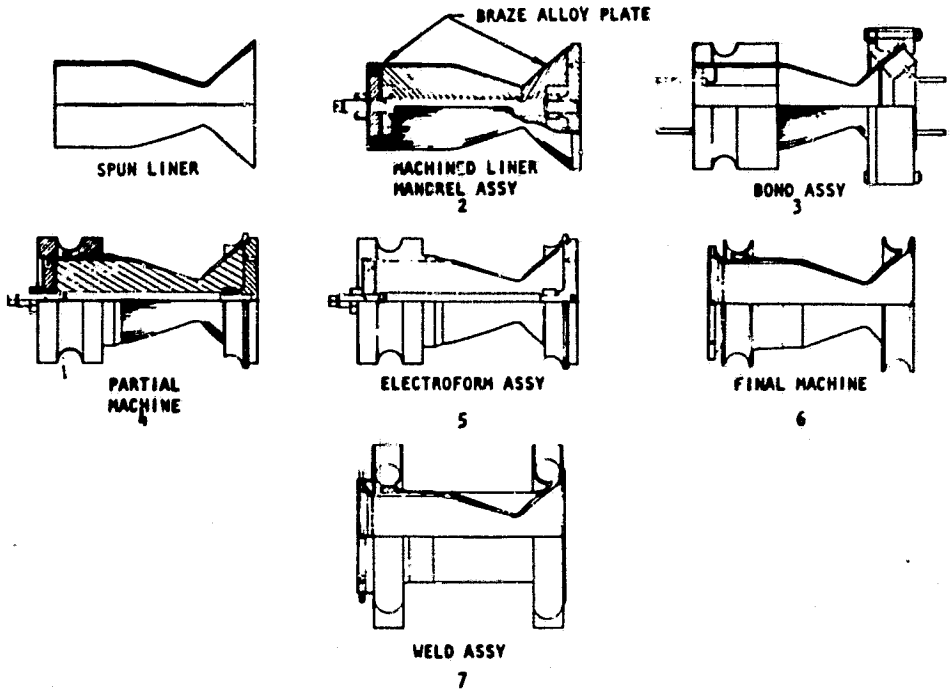

Figure 2-11. Thrust Chamber Manufacturing Flow Chart

Combustor Heat Transfer Analysis

Hydrogen cooling of the combustor is accomplished in the thrust chamber by a single uppass circuit with 4.09 lb/sec flow with an inlet at $\varepsilon = 14.0$. The high H_2 flowrate and low ε input point has been chosen to provide some residual entrance curvature and low inlet cooling effects at the throat plane, a low H_2 bulk temperature at the throat peak flux and a low H_2 bulk temperature in the cylindrical wall region to ensure a good thermal life characteristic.

The four combustor contours analyzed for the Expander Engine Point Design thrust chamber are illustrated in Fig. 2-12. Rocketdyne's boundary layer computer program was run for each contour. The results of the boundary layer program indicated that the hot-gas-side heat transfer coefficient was greatest for the tapered contour combustor. Because the engine requirements for a high heat input to the coolant can be best met by the tapered contour combustor, it was selected as the point design configuration.

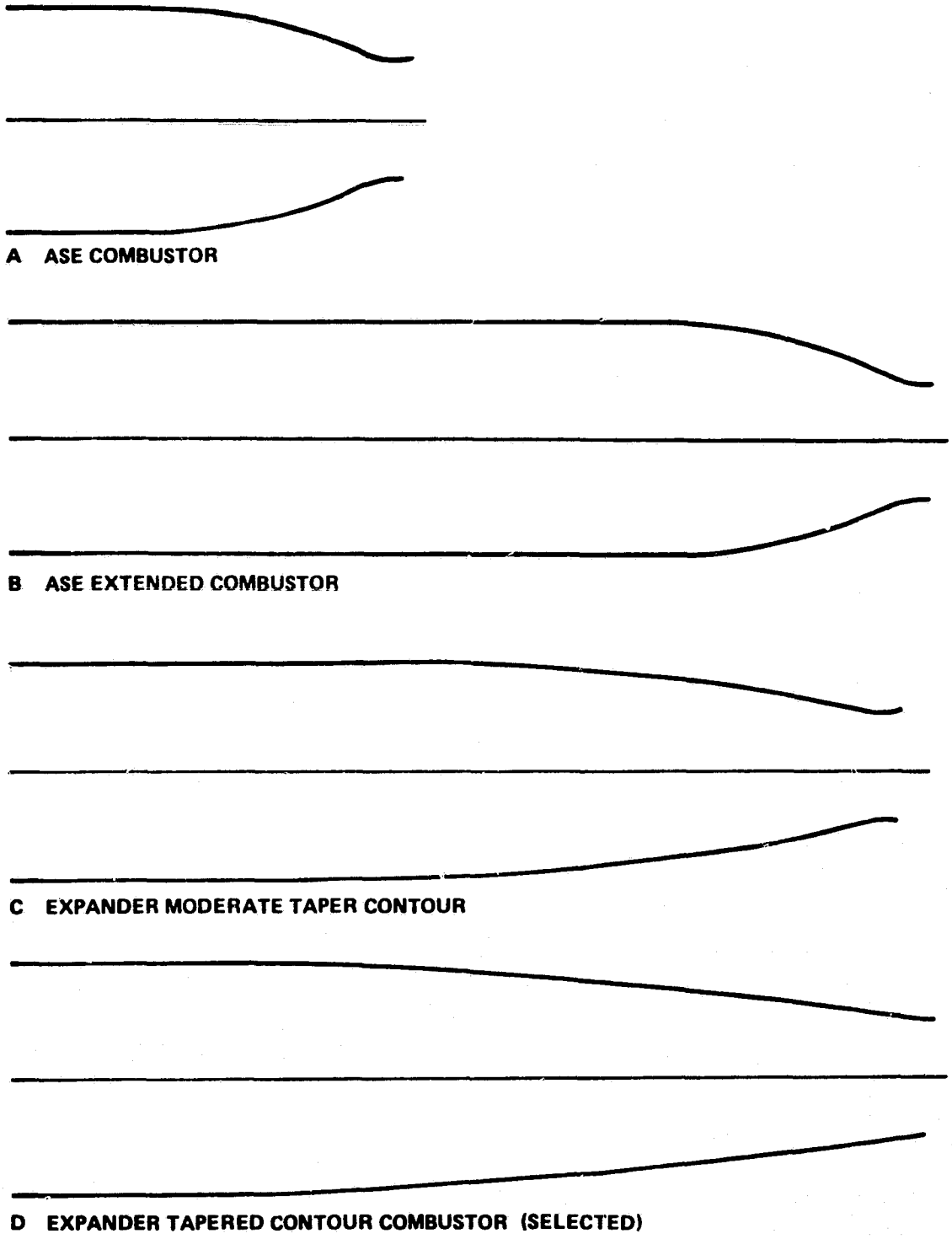

Figure 2-12. Candidate Combustor Contours

Several combustor lengths were thermally analyzed to determine the length necessary to provide the required heat input. Figure 2-13 provides a comparison of the total heat input to the coolant for various combustor lengths. The 20-inch length was selected because it provides the necessary heat input required by the expander cycle power requirements within a length that is compatible with projected engine system envelope restrictions.

The cooling channel configuration has been carefully designed with Rocketdyne's regenerative cooling analysis program (REGEN) which details in consecutive axial stations the wall temperature (2-D) and fluid conditions along the combustion chamber length.

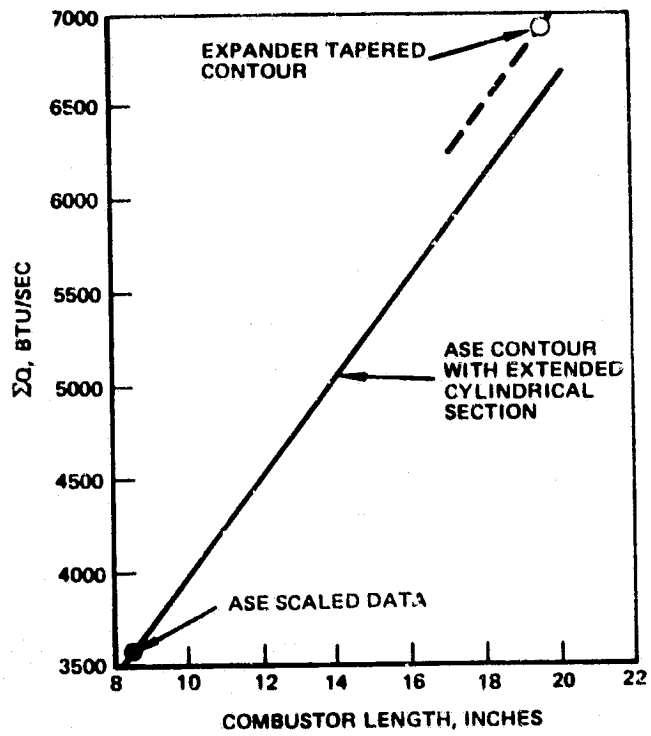

Figure 2-13. Comparison of Total Heat Input to Coolant for Various Combustor Lengths

The combustor design gas-side heat transfer film coefficient profile used for the design chamber pressure (1540 psia) is presented in Fig. 2-14. This was based on extrapolation of comprehensive (lower chamber pressure water-cooled chamber) data for nearly identical geometrical configurations (Fig. 2-15). The portion of the heat transfer coefficient profile in the supersonic section of the combustion chamber (axial distances greater than zero) was derived analytically using the Rocketdyne boundary layer program. Figure 2-16 illustrates the comparison of the design with regard to peak heat flux, injector region heat flux, and combustor integrated heat input to available thermal data. Test data obtained from the 3K cyclic life thrust chamber are presented on these curves. For the localized throat region a 20% margin of peak heat flux is shown. This has been used for conservatism in the life prediction. Therefore, the resulting thrust chamber design will ensure satisfactory cooling, and a cycle life in excess of the 1200 cycles required by the design specification. No adjustment to the test data has been made for total heat load value except for the actual 20-inch combustion length correction (Fig. 2-14).

Figure 2-17 provides the design point channel geometry for the expander cycle combustor as a function of length. The details of the channel geometry were obtained with the aid of the regenerative-cooling analysis computer program and was based on wall temperature, cycle life, stress levels and fluid conditions. Combustor wall temperature profiles and the coolant temperature are shown in Fig. 2-18.

Acoustic Absorber Cooling

The acoustic absorber cooling details are presented in Fig. 2-19. The cavity is heated by the cyclic flow of combustion gases entering the cavity. Cooling is accomplished by intimate contact with the injector fuel supply duct and the chamber coolant outlet manifold in addition to cooling obtained from flow through the injector. To determine the temperatures of the acoustic absorber during operation, a two-dimensional thermal mathematical model was developed for use in conducting a thermal analysis with the aid of a computer program.

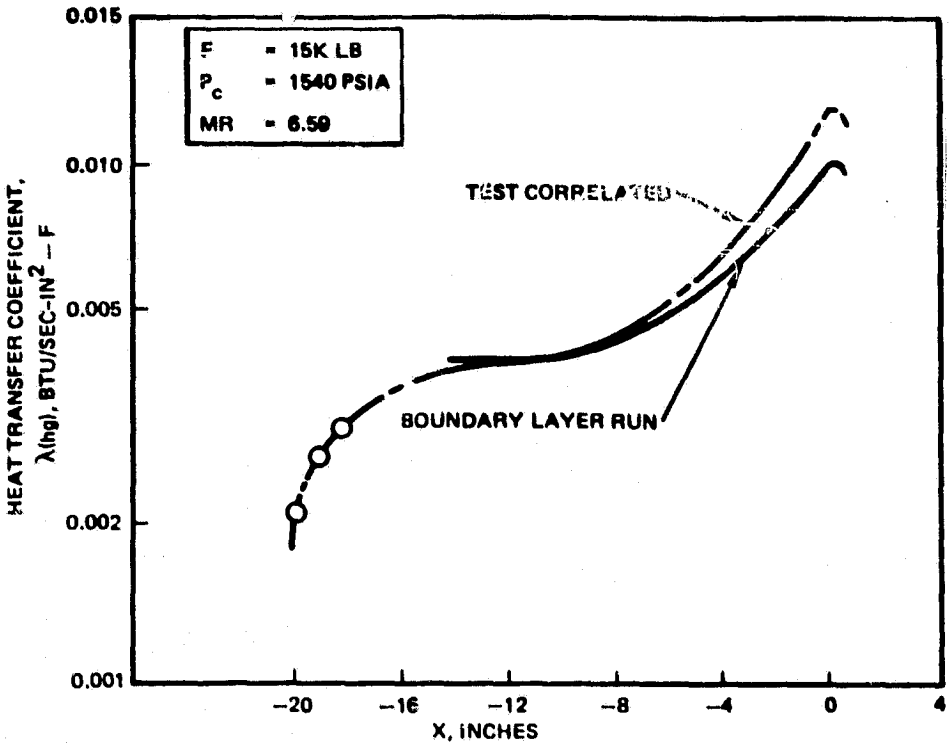

Figure 2-14. LO_2/H_2 Expander (Tapered Contour) Combustor Heat Transfer Coefficient Test Data Correlation

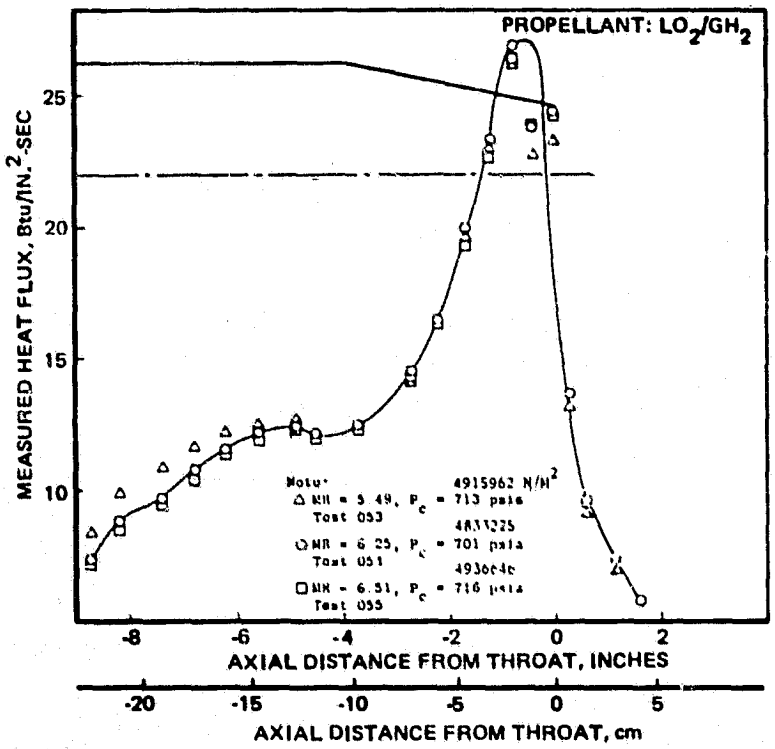

Figure 2-15. Cylindrical Chamber Wall Heat Flux Distribution, Mixture Ratio Influence, LO_2/GH_2

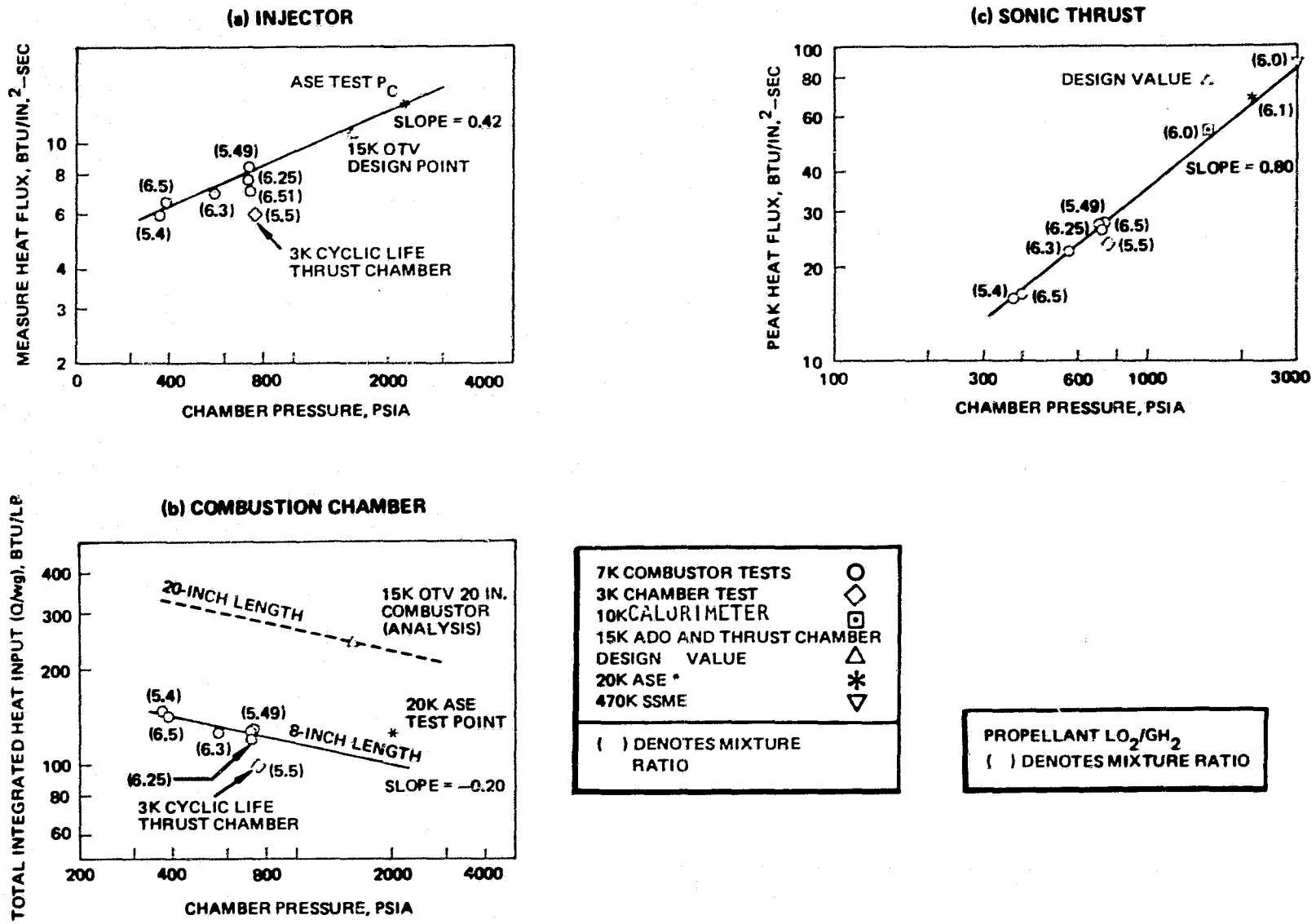

Figure 2-16. Comparison of Design With Regard to Peak Heat Flux, Injector Region Heat Flux, and Combustor Integrated Heat Flux

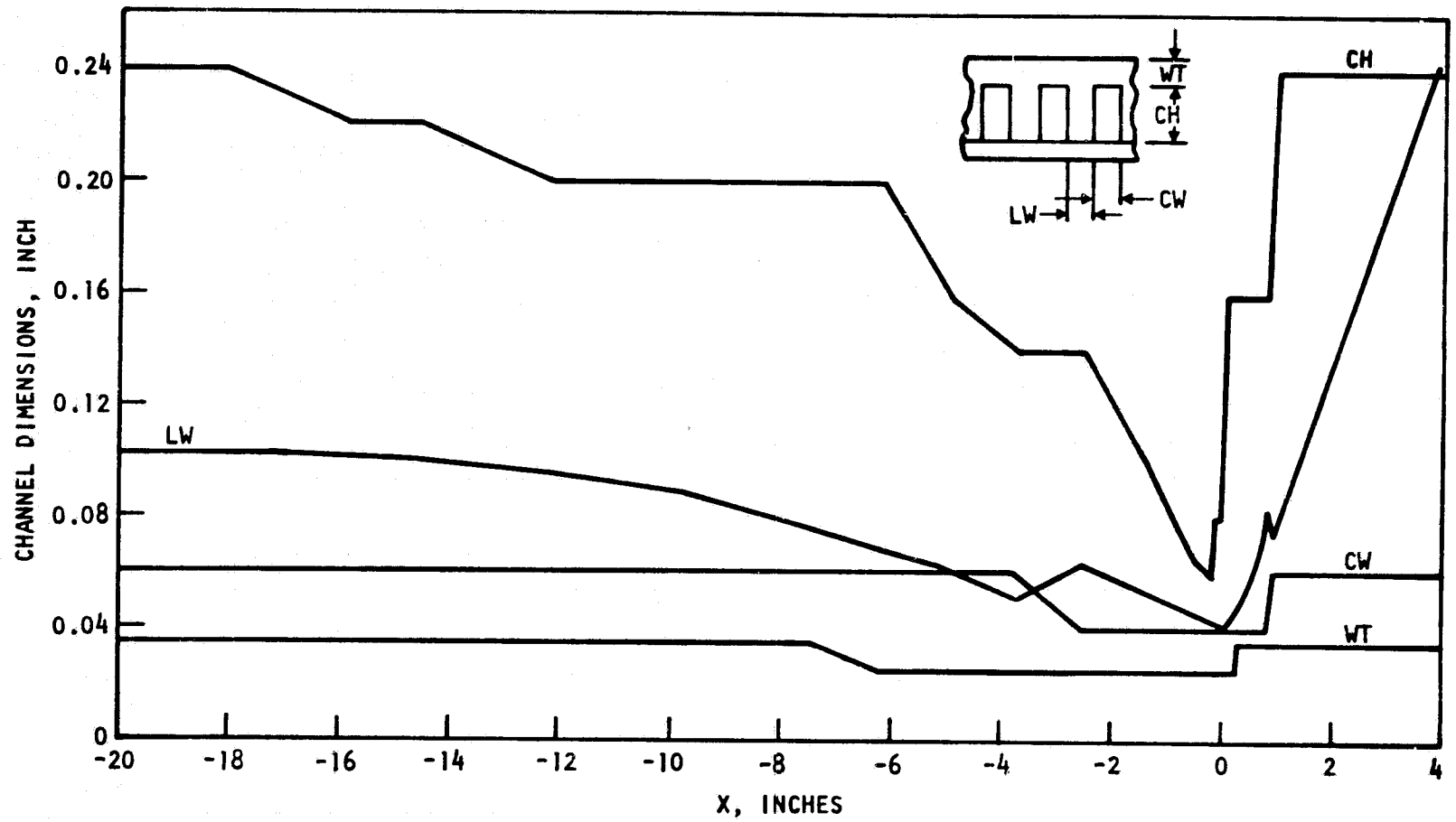

Figure 2-17. LO_2/H_2 Advanced Expander Cycle Engine Tapered Contour Combustion Channel Geometry

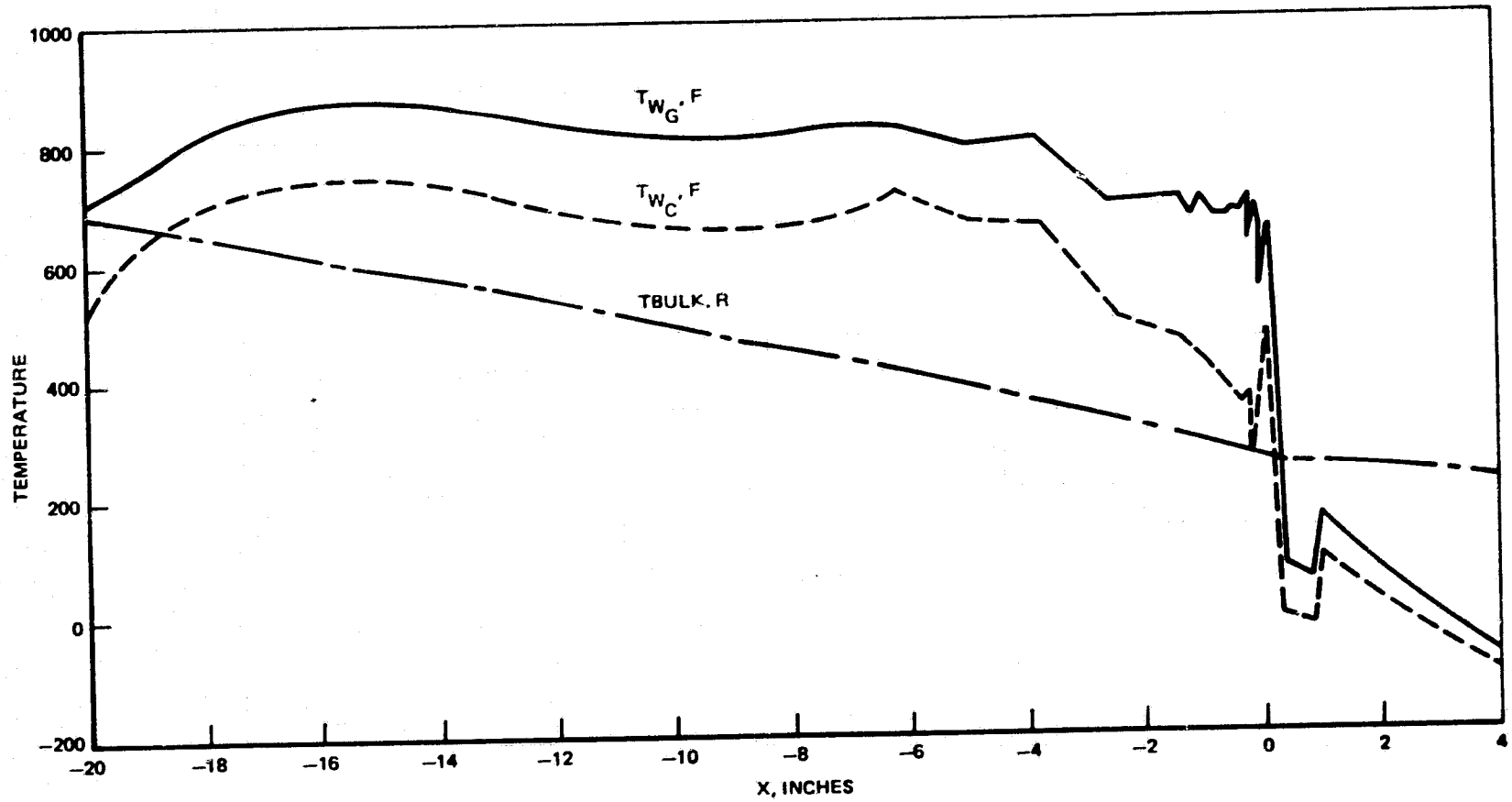

Figure 2-18. Advanced Expander Cycle Engine Combustor Temperature Profiles

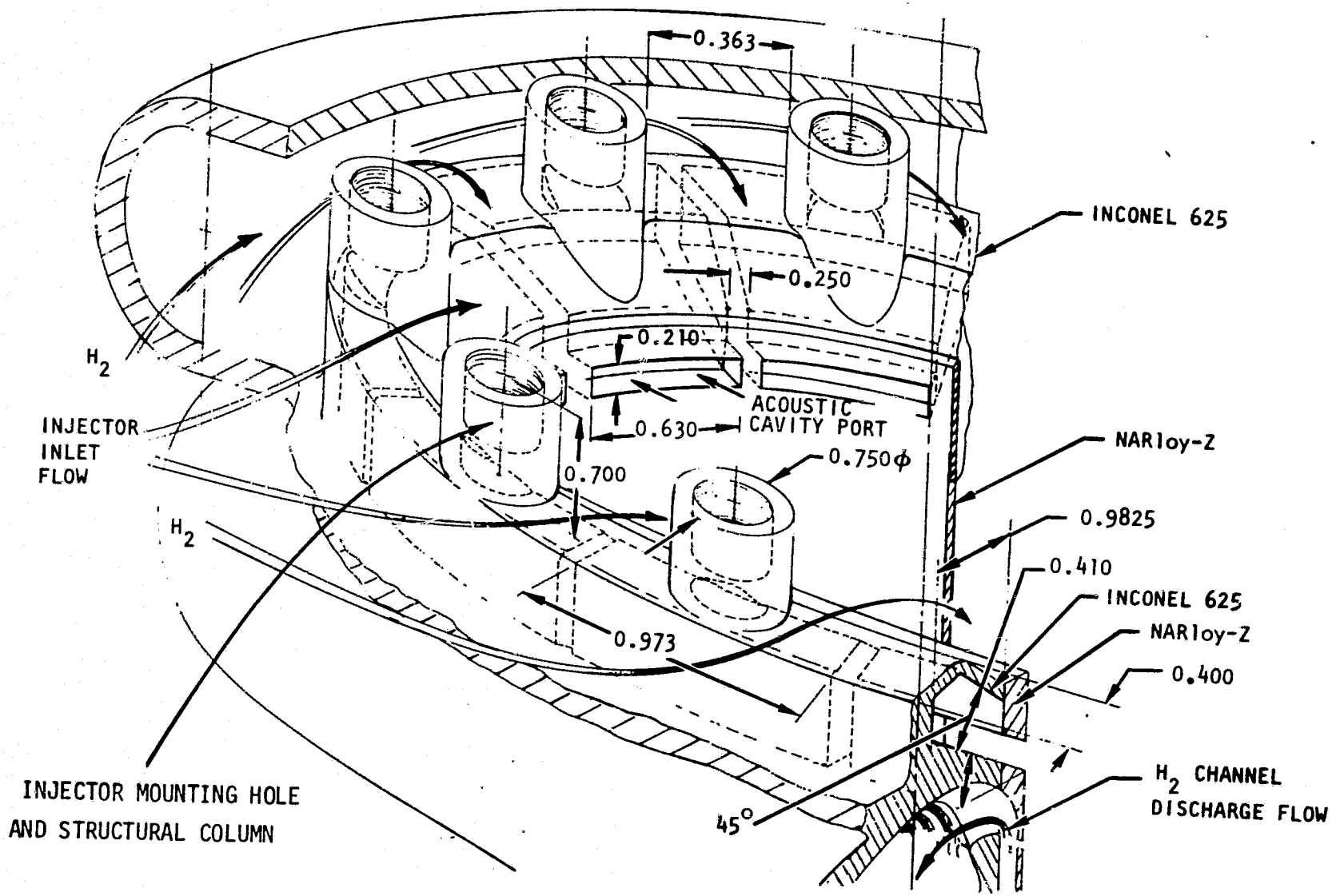

Figure 2-19. Acoustic Cavity Cooling Detail

The results of the thermal analysis of the acoustic absorber are presented in Fig. 2-20 . An injector wall h_c equal to 0.008 Btu/sec-in.^{2}, the absorber inlet h_g of 20% of the main chamber h_g, and the cavity h_g of 10% of the main chamber h_g were used for this analysis. The resulting temperatures are within acceptable limits for the acoustic absorber materials. No film cooling appears to be required at the acoustic absorber cavity.

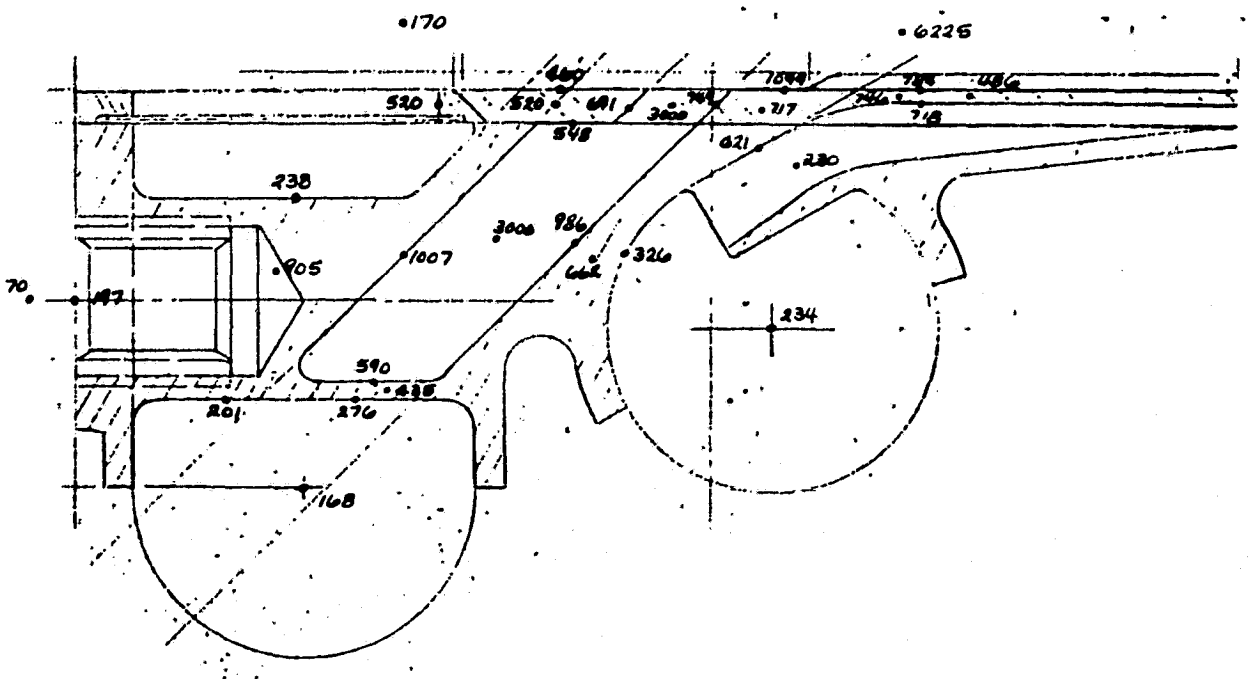

Figure 2-20. Acoustic Absorber Temperature Profile

Combustion Chamber Liner Materials

The basic characteristics required of a regeneratively cooled combustion chamber liner alloy are:

1. High thermal conductivity - to promote efficient heat transfer from the hot-gas side of the wall to the coolant fluid

2. Good creep-rupture strength - particularly important if the hot-gas wall temperature exceeds 1000 F

3. Adequate thermal fatigue life - to withstand cyclic thermal strains induced by high heat flux across the wall

4. Demonstrated performance - a successful history of service under engine hot-firing conditions

5. Demonstrated quality - the alloy must be produced via processes demonstrated to provide a product free from oxide inclusions

The ideal material for a regeneratively cooled combustion chamber liner would be one of high thermal conductivity (for effective cooling of the hot-gas wall) and high thermal fatigue resistance and creep strength.

Table 2-6 is a compilation of available information on candidate materials that have been considered for the liner. Conductivity requirements necessitate that they all be copper base. Nickel 200 (pure nickel) is shown because it is one of the highest conductivity materials available outside the copper group. Even so, the low thermal conductivity eliminates it from realistic consideration. It will be noted that certain classes of alloys (e.g., ODS materials, RSR alloys, and composites) are not yet considered state of the art, and for this reason are not included as candidates in Table 2-6 . From the group of alloys listed, candidates having adequate conductivity are NARloy-Z, zirconium-copper, PD-135 (chrome-cadium copper), CDA 194 copper-iron alloy, AMAX MZC (magnesium-zirconium-chromium copper), and OFHC copper.

TABLE 2-6. ROOM TEMPERATURE PROPERTIES FOR CANDIDATE ALLOYS

ALLOY	CONDUCTIVITY, PERCENT OFHC	STRENGTH KSI	DUCTILITY, % ELONGATION	CLEANLINESS
NARloy-Z	90	24	40 (50 AT 1000 F)	GOOD
ZIRCONIUM COPPER	86	17	40	FAIR
BERYLLIUM COPPER	60	80	15	GOOD
PD-135	92	35	4 (AT 1000 F)	GOOD
CDA-194	65	37	27	FAIR
AMAX - MZC	85	66	10	FAIR
CHROMIUM COPPER	78	43	6 (AT 1000 F)	GOOD
NICKEL 200	15	20	50	EXCELLENT
OFHC COPPER	100	6	45	EXCELLENT

Thermal fatigue is the common cause of a failure in components subject to cyclic thermal gradients sufficiently high to generate cyclic plastic strain. Since the key words are "plastic strain", a first indicator of ability to withstand thermal fatigue may be found in the ductility of an alloy. Materials of modest or low ductility (e.g., beryllium copper, PD-35, AMAX-MZC, and chromium copper) cannot therefore be considered as prime candidates. OFHC copper must also be ruled out because of its poor creep strength at elevated temperatures, leaving zirconium copper and NARloy-Z as the surviving serious candidates. Low-cycle isothermal fatigue tests, during which a specimen is cycled mechanically rather than thermally, is often used as a first laboratory approximation of thermal fatigue behavior. It is extremely important that the term "failure" be very carefully defined during such tests, otherwise a poor choice of materials or a bad design decision can result. For example, failure in a combustion chamber liner can occur when cracks in the wall have progressed to the point of significant loss of coolant. For a typical liner wall thickness of 0.030 inch, and assuming a crack aspect ratio of 3:1, cracks over 0.1 inch in length could thus be considered as prelude to eventual failure during laboratory fatigue tests. By contrast, it is common practice to define failure in laboratory fatigue tests as the onset of tensile load drop rather than the onset of gross cracking. This can lead to errors in materials selection when two alloys of dissimilar fatigue behavior patterns are compared. As a case in point, consider the divergent behavior of NARloy-Z and 1/2-hard zirconium copper ("AMZIRC"). Rocketdyne has conducted low-cycle fatigue tests on the two materials at 1000 F under a total strain range of 3%. It is obvious that zirconium copper (AMZIRC) and NARloy-Z have very different load loss characteristics during cycling at elevated temperature as indicated by the load versus cycle plots for these two materials (Fig. 2-21a). The cyclic softening characteristic of zirconium copper makes it impossible to determine when the onset of rapid tensile load drop occurs. Because of this problem, a failure criterion was used involving the onset of gross cracking. The 1/2-hard Zr-Cu lost approximately 50% of its load-bearing ability after 112 cycles, and showed visible signs of cracks after another 112 cycles.

(a) LOW CYCLE FATIGUE

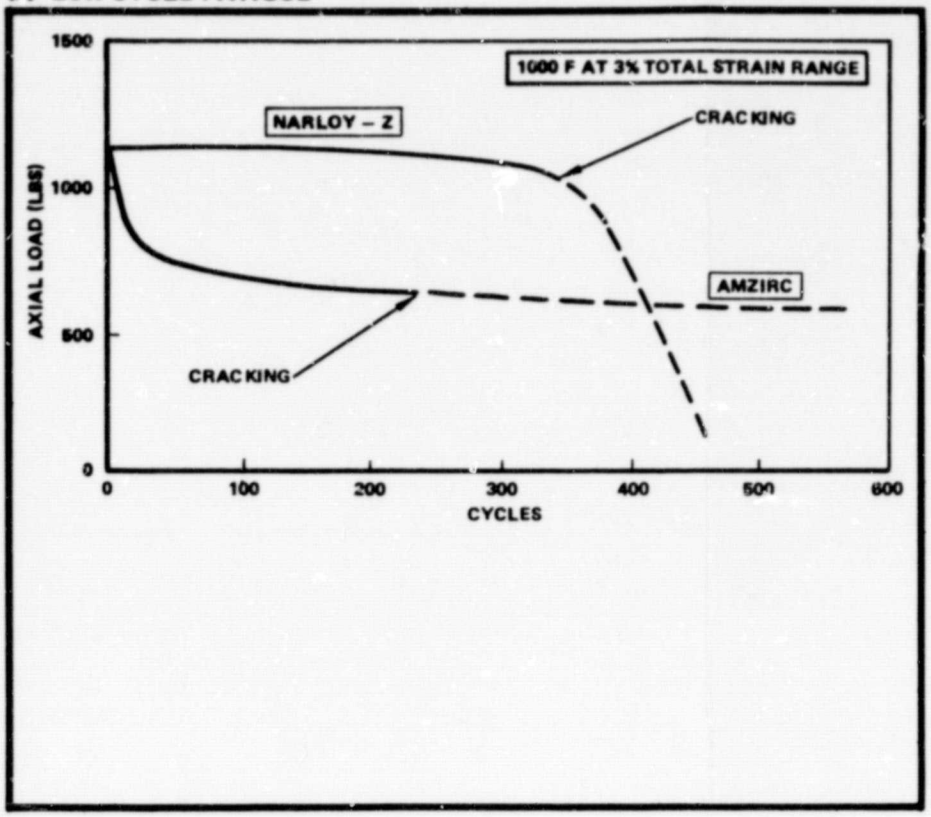

(b) SUMMARY OF CRACK INITIATION AND GRO

NARLOY-Z

CRACK	615 CYCLES ☆	○	□	C	H	T	CRACK LENGTH	654 ☆	○	□
A	X	X	X			X	0.195	X	X	X
B	X	X	X			X	0.185	X	X	X
C		X		?			0.040		X	
D		X		?			0.050		X	
E	X	X	X			X	0.185	X	X	X
F										X
G		X		?			0.085		X	
H	X	X	X			X	0.275	X	X	X
I			X		X		0.025			X
J			X		X		0.025	X	X	X

☆ DYE INJECTOR
○ X-RAY
□ SURFACE DYE-CHEK
C COOLANT SIDE
H HOT GAS SIDE
T THROUGH CRACK

(c) LOW-CYCLE FATIGUE BEHAVIOR

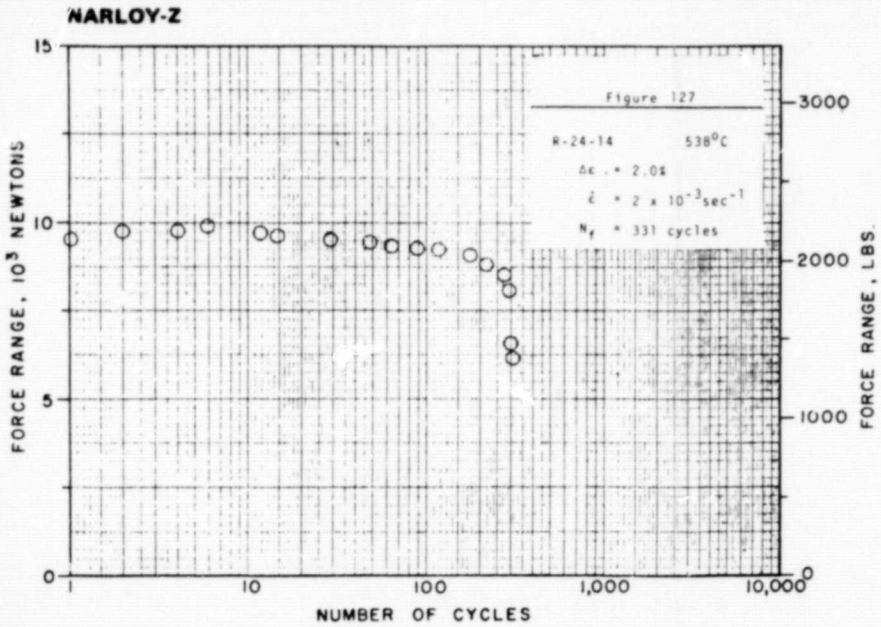

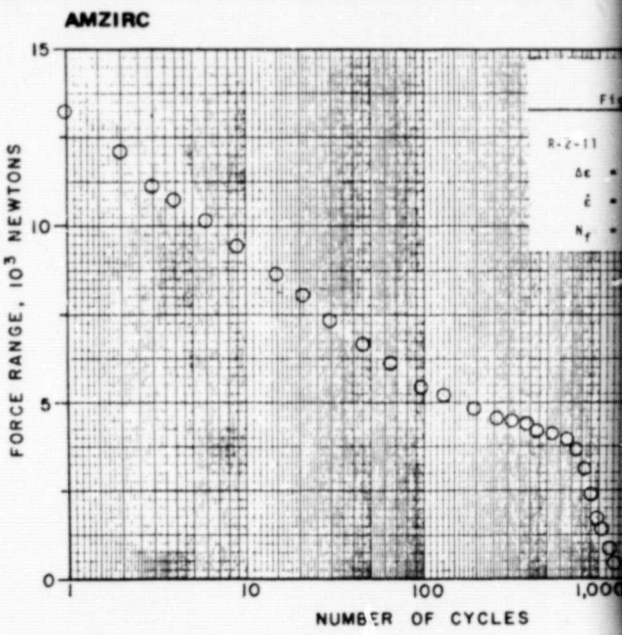

FOLDOUT FRAME

ORIGINAL PAGE IS
OF POOR QUALITY

654 CYCLES						
☆	○	□	C	H	T	CRACK LENGTH
X	X	X			X	0.225
X	X	X			X	0.225
	X		T			0.050
	X		T			0.050
X	X	X			X	0.185
		X		X		0.040
	X		T			0.085
X	X	X		X		0.300
		X				OBSCURED BY INJ. RESIDUE
X	X	X			X	0.063

AMZIRC

CRACK	529 CYCLES							587 CYCLES						
	☆	○	□	C	H	T	CRACK LENGTH	☆	○	□	C	H	T	CRACK LENGTH
A	X	X	X			X	0.075	X	X	X			X	0.075
B_1	X	X					0.2[illegible]	X	X	X			X	0.350
B_2		X		T			0.100		X		T			0.100
C									X		T			0.300
D									X		T			0.125
E_1								X	X	X			X	0.125
E_2								X	X	X			X	0.125
F_1		X					0.050		X		T			0.050
F_2									X		T			0.100
G									X		T			0.080
H		X		T			0.075	X	X	X			X	0.100
I_1	X	X	X			X	0.175	X	X	X			X	0.500
I_2									X		T			0.300
J_1								X	X	X			X	0.125
J_2		X		T			0.100	X	X	X			X	0.110
J_3	X	X	X			X	0.100	X	X	X			X	0.130
K_1	X		X			X		X	X	X			X	0.175
K_2											T			0.040
L_1		X		T			0.025		X		T			0.040
L_2	X	X	X			X	0.100	X	X	X			X	0.190
M_1		X		T			0.050	X	X	X			X	0.050
M_2											T			0.125
M_3		X		T			0.100	X	X	X			X	0.100
M_4		X		T			0.075		X		T			0.110
N	X	X	X			X	0.075	X	X	X			X	0.075 (AFSO LATRAPPED DENSE MATERIAL)
O	X		X			X	0.050	X	X	X			X	0.063
P	X	X	X			X	0.150	X	X	X			X	0.150

☆ DYE INJECTION — C COOLANT SIDE
○ X-RAY — H HOT GAS SIDE
□ SURFACE DYE-CHECK — T THROUGH CRACK

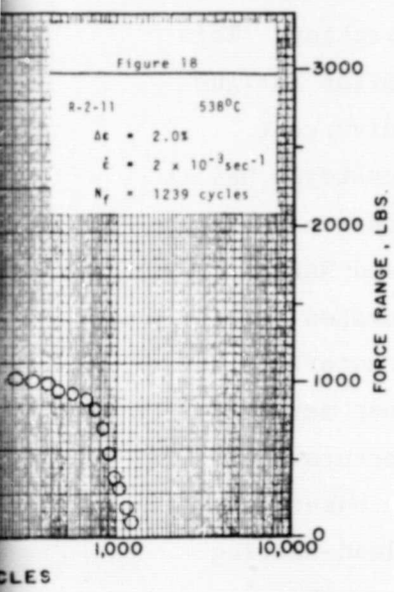

(d) TYPICAL HOT GAS WALL CRACKS

NARLOY-Z

AMZIRC

Photographs at 3X Magnification of Typical Hot Gas Wall Cracks and General Surface Condition of NARloy–Z (left) and Amzirc (right) Thermal Fatigue Chambers. Axis of Chambers is From Top to Bottom.

Figure 2-21. Thrust Chamber Thermal Fatigue Analysis

FOLDOUT FRAME 2

The NARloy-Z was inspected at 112, 224, 274, and 324 cycles. At 324 cycles the specimen had cracked. The conclusions drawn from these results were that NARloy-Z will exhibit a fatigue life about 40% greater than AMZIRC, together with more consistent load-bearing capability . Somewhat different conclusions might be drawn on the basis of tests on the same alloys as reported in Ref.2-1. In the latter case, the strain-softening behavior of AMZIRC was again noted, but the criterion for failure was physical fracture of the specimen. Under this definition, the AMZIRC alloy exhibited greater fatigue life, but at the expense of a 70% reduction in load-carrying ability at the onset of fracture (Fig.2-21c). Figure 2-21c shows the behavior of NARloy-Z under the same test conditions. The strain-softening characteristic of AMZIRC can lead to mechanical instability under certain conditions of strain cycling. This behavior has been noted in both low-cycle fatigue tests (Ref.2-2),where barrelling was observed, and in experimental rocket combustion chambers (Ref.2-3)where rumpling of liner walls occurred on a zirconium-copper chamber but not on a NARloy-Z chamber (Fig.2-21d).

Premature hot gas wall failures originated in early NARloy-Z and zirconium-copper chambers because of very small (0.010-inch long) zirconium-oxide inclusions. As can be seem from Fig. 2-21, however, the number and severity of cracks was much greater for the AMZIRC chamber than for the NARloy-Z. Since introduction of the vacuum centrifugal casting process, many destructive tests (metallography) and hot-fire tests have not uncovered a single oxide inclusion in vacuum centrifugal cast NARloy-Z. A superior quality product is thus now available in NARloy-Z, whereas a process would have to be developed to produce inclusion free zirconium-copper of equivalent cleanliness. Product development of this type would of necessity increase both cost and schedule requirements for a development program.

The most convincing evidence as a basis for alloy selection is data collected from hot-fired combustion chambers. NASA-LeRC has conducted extensive simulated hot-fire tests on small combustion chambers (Ref.2-4)made from OFHC copper and zirconium-copper (1/2 hard), and a limited number of tests with NARloy-Z under similar conditions. The report concluded that cylinders fabricated from NARloy-Z and aged AMZIRC had the best cyclic life. It also concluded that cyclic life rankings based on chamber tests do not agree with predictions based on uniaxial isothermal fatigue data; that is, the best evidence is hot-firing evidence.

Subscale (40K thrust) tests of the SSME engine configuration and full-scale test history showed NARloy-Z to be performing in a superior fashion. The 40K chamber accumulated 409 thermal cycles equivalent to a service life of 103 cycles for SSME. The most impressive record is that of the SSME; to date 17 SSME Main Combustion Chambers have been hot fired for a total test time of 83,808 seconds. The longest duration for a single chamber has been a total test time of 14,678 seconds, with 82 firing cycles at rated power level. This provides NARloy-Z with a significant test history which is unavailable for any other alloy.

Materials and Processing Considerations. NARloy-Z is presently produced via a vacuum-cast centrifugal process, which yields an ingot essentially free of the inclusions that can later act as nucleation sites for fatigue failures. The ingot is forged, machined and spun to final size and shape following the procedures outlined in Fig. 2-22 . NARloy-Z is strengthened by a simple heat treatment (solution treat 1700 F-Age 900 F).

Zirconium-copper, by contrast, derives strength by cold work which is quickly lost during elevated temperature strain cycling. Producing combustion chamber shapes and controlling cold work is not easily accomplished and introduces significant complexity in process control. Zirconium-copper would have to be spun as the only method for cold work control.

NARloy-Z will lend itself to both spinning and forge processing. The latter process could be a significant cost saving in a high volume mode. In addition, NARloy-Z retains a fine grain size (ASTM 4 or finer) even after high-temperature exposure. This latter characteristic is desirable from an inspection point of view in that high sensitivity to ultrasonic inspection is possible. The fine grain also will inhibit surface rumpling due to thermal strains during engine operation. Smooth surfaces on the liner are essential to maintain the insulating gas boundary layer.

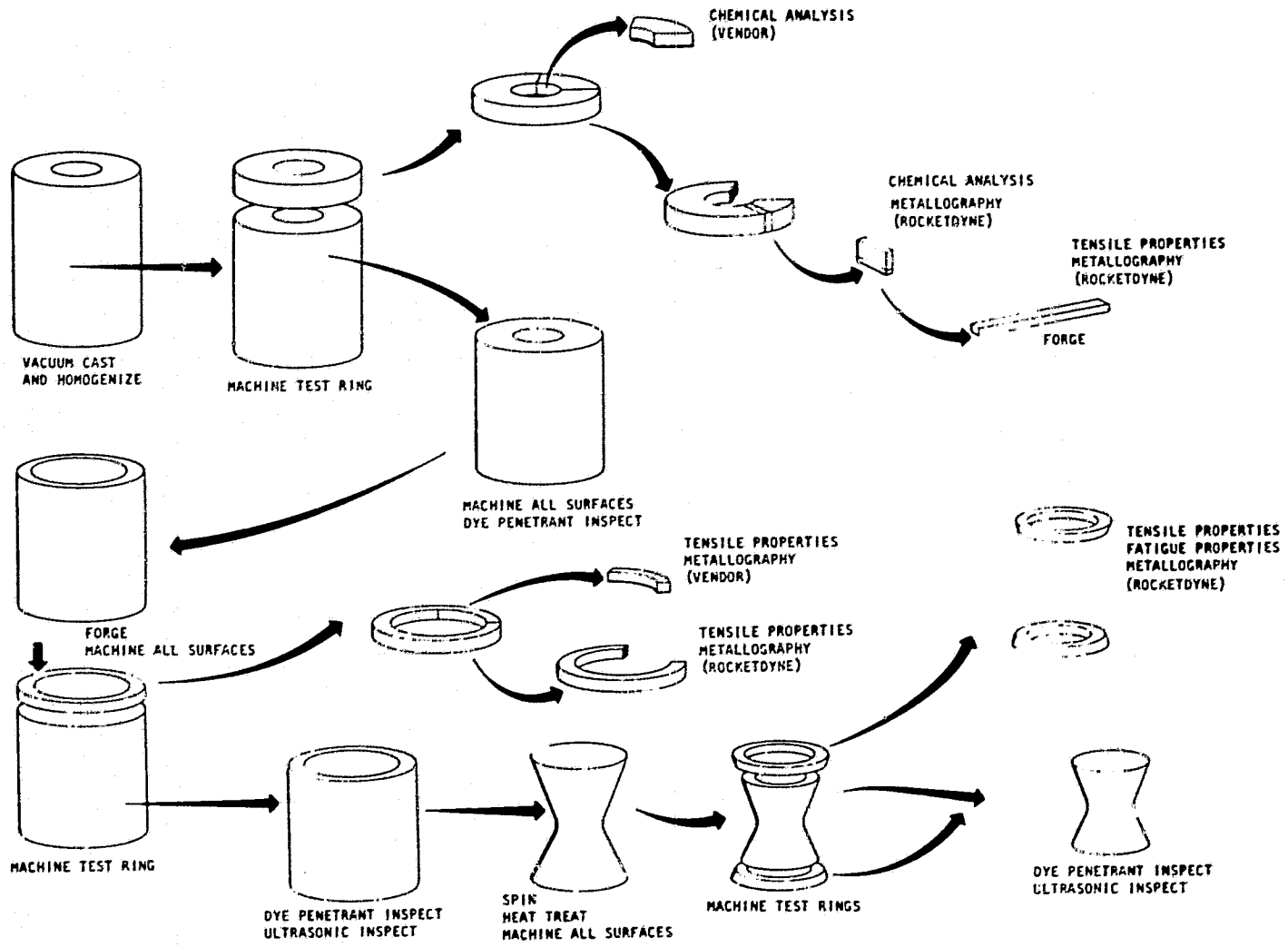

Figure 2-22. NARloy-Z Ingot Processing and Inspection

Design Characteristics. When considering combustor fabrication techniques, NARloy-Z again represents the best choice. The combustion chamber is fabricated by furnace brazing the manifold's base rings to the NARloy-Z liner. NARloy-Z can be brazed at elevated temperatures (1700 F) and still recover over 90% of its fully heat treated properties by a simple age cycle. Zirconium-copper does not affort this flexibility since it requires cold work to obtain its design strength. Because of this severe limitation, the manifolds would, of necessity, require a less satisfactory method of attachment to the liner. The usual method is a low strength weld bond between dissimilar materials.

Life Considerations. The low cycle fatigue characteristics of a material, i.e., strain range versus cycles to failure as a function of environment and temperature, provide an initial method for rating materials for life considerations. Comparing NARloy-Z (sta) and AMZIRC (sta) indicates that, depending on the magnitude of the cyclic strain range, NARloy-Z has a longer cycle life than AMZIRC (Fig. 2-21). Less significant but still a factor is that the coefficient of thermal expansion of AMZIRC is slightly larger, therefore, more strain would be generated (lower life) for the same thermal gradient.

Detailed structural analysis (discussed in the subsequent Engine Data Summary) has defined the combustor channel life as 1350 cycles (damage fraction, ϕ, = 0.89 with a factor of 4), using NARloy-Z as the channel wall material. AMZIRC would not satisfy the design requirements for the proposed combustor. In addition, previous hot fire test experience has demonstrated that crack-inducing anomalies occur from time to time, and additional life margin is highly desirable.

Comparing physical and mechanical properties at elevated temperatures show NARloy-Z to be superior in all categories. Test programs run on the two materials indicate AMZIRC strain softens in the inelastic range, which inhibits the capability of a material to redistribute stresses; an undesirable characteristic for high strain applications.

Material Experience. The most convincing argument for selection of NARloy-Z lies in its successful history as a combustion chamber liner in the SSME. As can be seen from Table 2-7, over 83000 seconds of hot-firing have been accumulated during field tests on 17 SSME chambers, with individual chambers with more than 15,000 seconds and as many as 82 firing cycles. In no case has an engine test been terminated through malfunction of a NARloy-Z combustion chamber liner. On those occasions where minor cracks were observed in liners after hot cracking, no significant effects were observed in performance, nor did any crack progress to the point where failure was imminent.

Other notable hot firing programs included chambers fabricated both from NARloy-Z and from AMZIRC. During the AFRPL thermal fatigue chamber tests, for example, NARloy-Z was superior to AMZIRC in both resistance to cracking and surface rumpling during hot firing. Thermal fatigue test chambers fired by NASA-LeRC showed similar results, with 1/2-hard AMZIRC being no better than OFHC copper.

One of the reasons for NARloy-Z's superior performance lies in the alloy's resistance to softening during extended exposure to elevated temperatures. This is clearly demonstrated in Table 2-8, where the softening resistance of NARloy-Z and AMZIRC are compared. AMZIRC must be cold worked then aged to develop full properties, but loses strength quickly if exposed to temperatures above 750 F. NARloy-Z does not require cold work, and retains its strength even after extended exposure at 1000 F or higher.

Rocketdyne's experience has demonstrated that oxide stringers or inclusions in combustion chamber liners can act as nucleation sites for fatigue cracks. This is true for either NARloy-Z or AMZIRC, and was the motivation for the early development of the vacuum centrifugal casting process used for all NARloy-Z products and illustrated in Fig. 2-22.

TABLE 2-7. COMBUSTION CHAMBER LINER EXPERIENCE

CHAMBER TYPE	CUSTOMER	MATERIAL OF CONSTRUCTION	BUILT BY	TEMPERATURE, F	LINER OPERATING CONDITIONS: DURATION, SECONDS: AT RATED POWER LEVEL	DURATION, SECONDS: TOTAL	FIRING CYCLES AT RATED POWER LEVEL	HEAT FLUX, BTU/IN.^{2}-SEC	REMARKS
SSME	NASA-MSFC	NARloy-Z	ROCKETDYNE	1080	3517	4928	11	90	NO LINER CRACKS
					8870	14212	43		THREE SMALL CRACKS IN LINER THROAT
					6291	9098	40		FOUR MODERATE CRACKS IN UPPER ZONE
					2438	3580	10		ONE SMALL CRACK IN UPPER ZONE
					1977	3239	15		THREE SMALL CRACKS IN THROAT
					2715	3839	20		THREE MINOR CRACKS; TWO IN THROAT, ONE UPPER
					467	569	2		NO CRACKS
					953	1142	3		NO CRACKS
					1005	1222	4		NO CRACKS
					424	520	1		NO CRACKS
					136	4391	32		THREE CRACKS IN UPPER ZONE
					6057	15318	53		NICKEL PLATED CHAMBER PITTED
					181	1281	18		ONE CRACK
					6879	14678	82		20 CRACKS
					278	693	5		NO CRACKS
					3035	4981	30		13 CRACKS
					811	1072	5		NO CRACKS
ASE	NASA-LeRC			870			10		WALL ROUGHENED
ASE	NASA-LeRC	AMZIRC		780			8		WALL ROUGHENED
THERMAL FATIGUE	AFRPL	NARloy-Z		700			654	25	EIGHT TOTAL CRACKS (FIVE THROUGH WALL
	AFRPL	AMZIRC		700			587	25	27 TOTAL CRACKS (16 THROUGH WALL)
	NASA-LeRC		NASA-LeRC	1000(1)		1330	381	33	PERFORMANCE EQUIVALENT TO PURE COPPER
				1440(1)		415	119		
				1500(1)		370	106		
				1040(1)		1190	340		
				730(1)		3300	944		
				900(1)		1770	505		
		AMZIRC-AGED		1500		1375	393		BETTER RESISTANCE TO FATIGUE THAN UNAGED AMZIRC
		NARloy-Z		1050		1945	556		BEST FATIGUE BEHAVIOR
		NARloy-Z		1350		2410	668		
		NARloy-Z		UNKNOWN		2375	679		

(1) CALCULATED TEMPERATURE

TABLE 2-8. RESISTANCE TO SOFTENING DURING EXPOSURE TO A TEMPERATURE OF 1000 F

MATERIAL	COLD WORKED, PERCENT	AGED, F	EXPOSURE DURATION WITHOUT APPRECIABLE SOFTENING, HOURS
AMZIRC	40	750	23
AMZIRC	40	850	36
AMZIRC	60	750	9
AMZIRC	60	860	11
NARloy-Z	0	1000	200
NARloy-Z	0	900	200
NARloy-Z	29	900	60
NARloy-Z	72	900	5

Liner Closeout

Electrodeposited nickel with an initial barrier of electrodeposited copper for hydrogen environmental protection was chosen as the method for closing out the coolant channels in the slotted liner.

Rocketdyne has utilized this approach successfully to fabricate similar non-tubular chamber closeouts on the full and subscale versions of the SSME as well as the ASE and 40K chamber. The deposited structure has excellent bonding action with the NARloy-Z liner material and makes a good structural closeout. The properties of electrodeposited nickel make it suitable for containing the coolant pressure (Table 2-9).

TABLE 2-9. PROPERTIES OF ELECTRODEPOSITED NICKEL*

TENSILE ULTIMATE STRENGTH, KSI	69
TENSILE YIELD STRENGTH, KSI	45
TENSILE ELONGATION, %	26
REDUCTION OF AREA, %	66
THERMAL CONDUCTIVITY, UNITS	34
*STRESS RELIEVED AT 650 F FOR 1 HOUR	

To prevent embrittlement from high-pressure hydrogen on the nickel closeout, a barrier of copper is first deposited between the nickel and the coolant channel. The copper barrier imparts excellent low cycle fatigue life to EDNi in the presence of high-pressure hydrogen.

Manifold Materials

All manifolding materials are Inconel 625. This nickel-base super-alloy was selected over other candidate materials for its excellent fabricability, weldability, availability, corrosion resistance, and strength. It also provides better resistance to degradation from high-pressure hydrogen than several other nickel base alloys. One other important criterion in selecting Inconel 625 is its brazeability. The manifold base rings will be brazed to the NARloy-Z liner by forming a gold-copper alloy at the interface. This technique was successfully demonstrated on the ASE thrust chamber and eliminates welding to the electroformed nickel. The braze cycle and subsequent aging of the liner do not affect the mechanical properties of Inconel 625, since it is not used in the cold work condition and derives its strength from solid solution strengthening.

Combustor Life Evaluation

The fundamental theory used in the life prediction analysis is that failure depends on the accumulation of incremental damage caused by fatigue and creep mechanisms. Where available, data obtained from material fatigue specimens and test data of actual hardware are used in life analysis. The life analysis is based on a definition of the stress-strain-time-temperature history during each operating cycle. Creep damage is evaluated from the stress-time-temperature cycle, and fatigue damage from the strain-time-temperature cycle. The life analysis logic diagram is shown in Fig. 2-23. Extensive cyclic strain analyses have been performed for the critical throat region of the channel-wall combustor using the thermal conditions given in Table 2-10. The following paragraphs present the results of these analyses.

Two finite-element structural models were used to establish the critical strain ranges of the composite channel section. An axisymmetric model of the combustor channel/wall was run to establish the varying transverse strain profile to be used for the plane strain (second model) model of a repeatable segment of the local channel cross section (Fig.2-24a). A cyclic program was used to subject the structural models to complete heatup and chilldown cycles. This was done to allow full strain hardening to occur and stabilize the strain range values at the critical locations.

The channel section analyzed was located approximately 0.18 inch forward of the geometric throat. A thermal excursion from steady-state operating temperature to a -100 F post chill was used. Coolant and hot gas pressures were used as applicable. Figure 2-24b shows the steady-state temperature profile and typical contour plots of effective strain for the heatup and cooldown cycles. Table 2-11 gives a cyclic life summary of the different materials of the coolant channel section at the critical throat region.

The results show that the minimum required life of 300 x 4 cycles is exceeded at the critical throat section of the combustor. The NARloy-Z hot-gas wall over

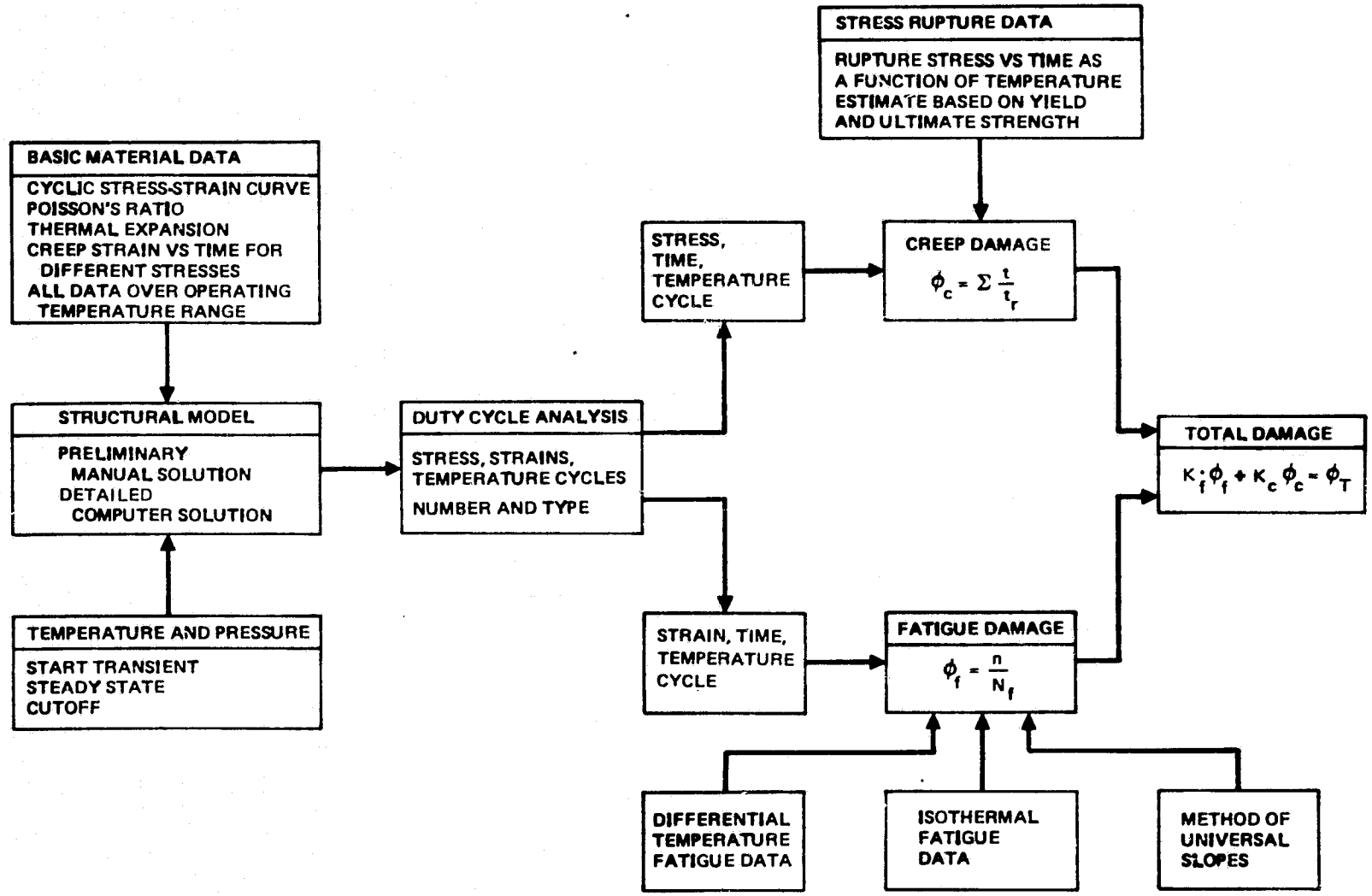

Figure 2-23. Life Analysis Logic Diagram

TABLE 2-10. THERMAL GRADIENT LOADING

Location	Maximum Temperature, F	ΔT
Combustor Hot-Gas Liner		
Throat	764	981
Chamber	771	843
Fixed Nozzle Coolant Tube	593	205
Injector Post/Shell	176	446

(a) CRITICAL THROAT REGION

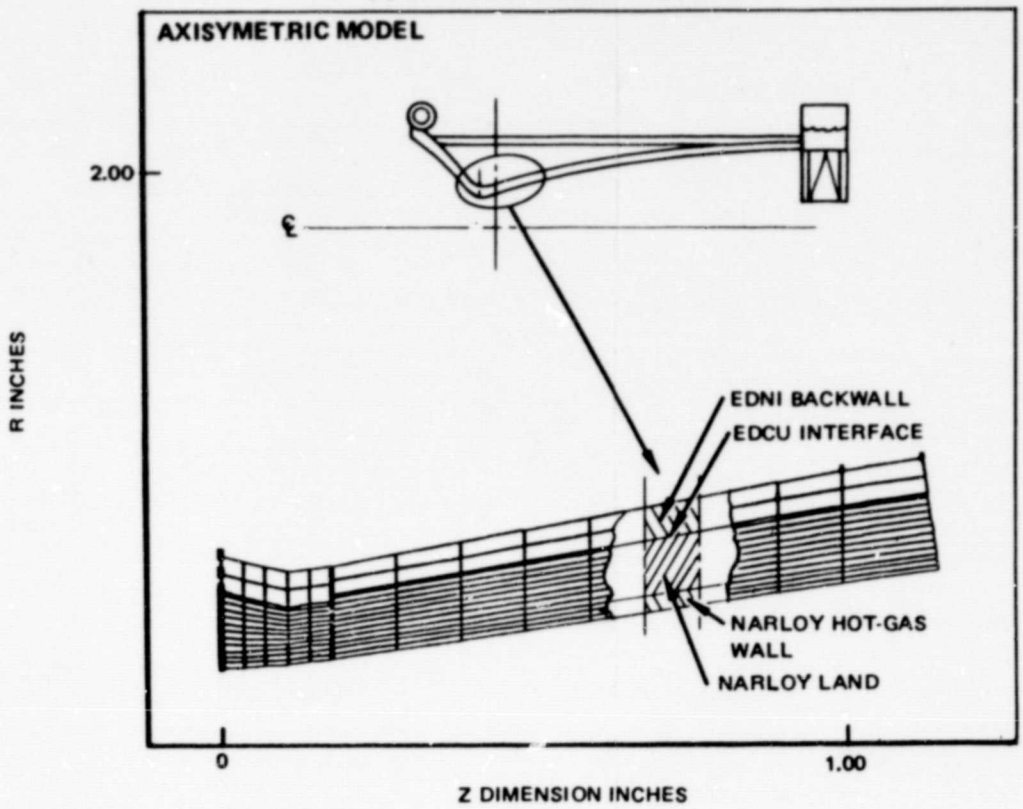

15K OTV LINER STA.180 P.S.
PLANE STRAIN ANALYSIS
UNDEFORMED STRUCTURE
TAPE ID A04688
LOAD NO. 1
PLOT NO.1

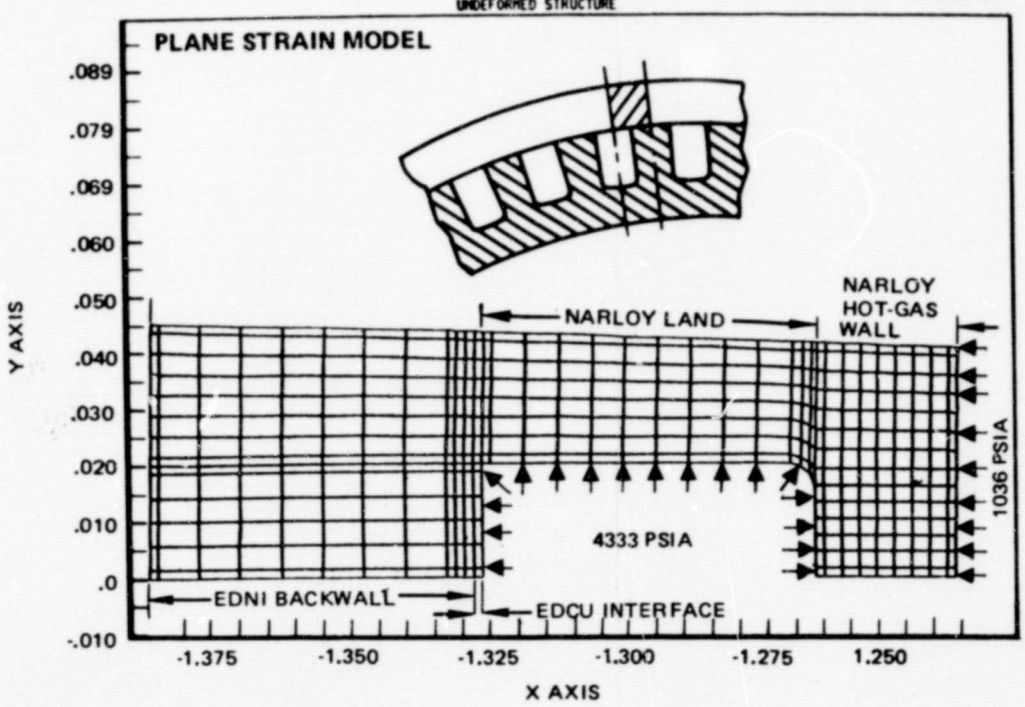

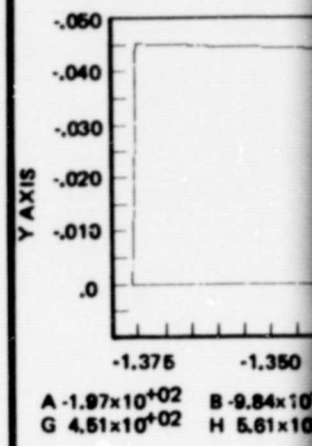

TYPICAL EFFECTI
DISTRIBUTION FO

TYPICAL EFFECTIV
STRAIN DISTRIBUT
FOR COOLDOWN C

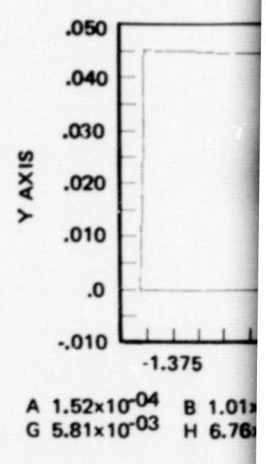

FOLDOUT FRAME

ORIGINAL PAGE IS
OF POOR QUALITY

(b) CRITICAL CHANNEL SECTION

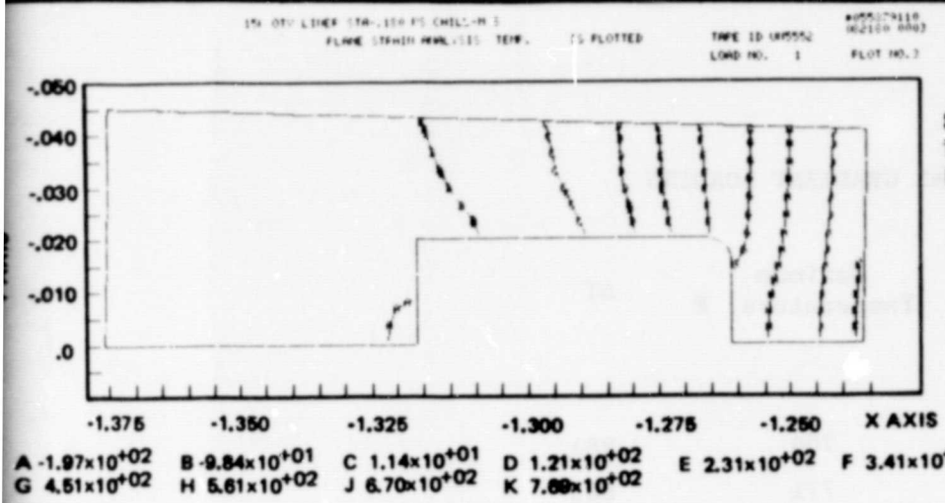

STEADY-STATE TEMPERATURE DISTRIBUTION

TYPICAL EFFECTIVE STRAIN DISTRIBUTION FOR HEAT-UP CYCLE

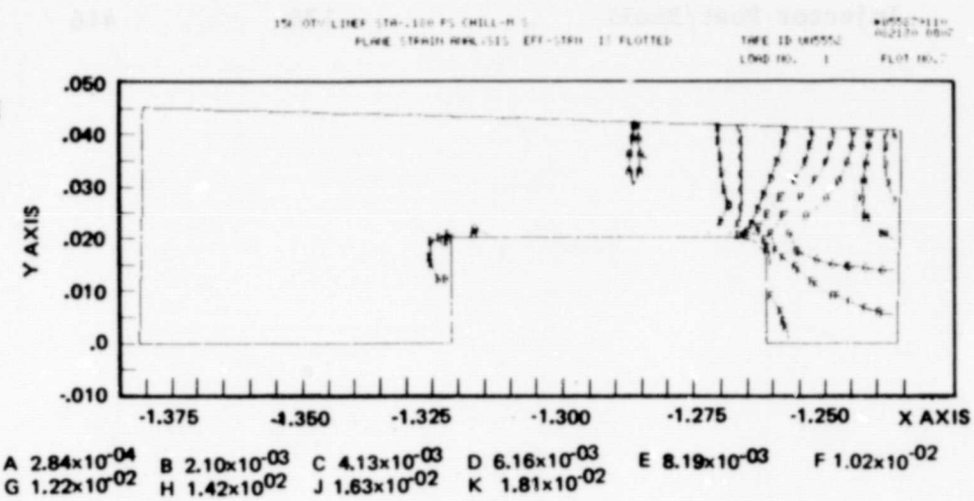

TYPICAL EFFECTIVE STRAIN DISTRIBUTION FOR COOLDOWN CYCLE

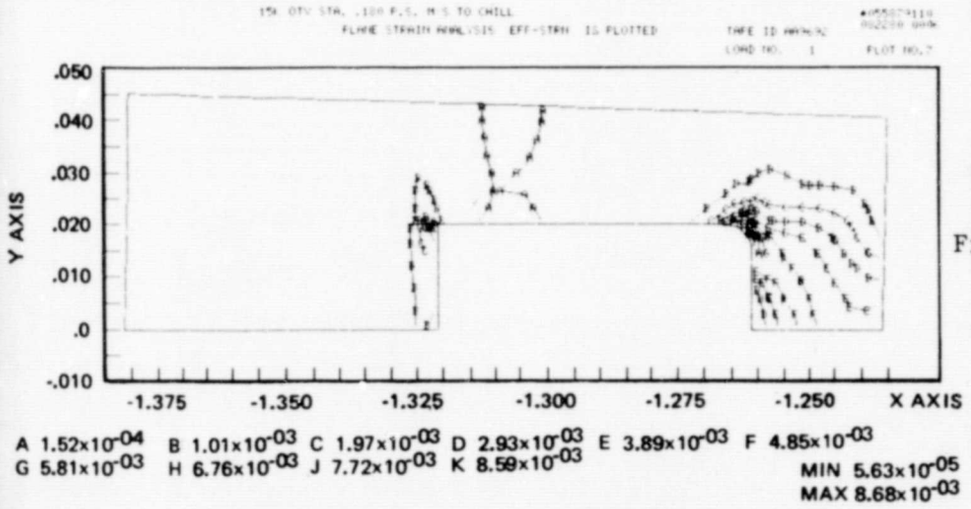

Figure 2-24. Combustor Life Cycle Analysis Models

FOLDOUT FRAME 2

TABLE 2-11. LIFE SUMMARY OF COOLANT CHANNEL SECTION AT CRITICAL THROAT REGION

LOCATION	CYCLIC STRAIN RANGE, %	LIMIT LIFE CYCLES	DAMAGE FRACTION
(A) NARloy-Z HOT GAS WALL OVER LAND	1.87	1350	0.222
(B) NARloy-Z HOT GAS WALL OVER CHANNEL	1.35	3500	0.086
(C) EDCu INTERFACE BETWEEN LAND AND BACK WALL	0.11	$\sim 10^4$	0
(D) EDNi BACK WALL	0.12	$\sim 10^4$	0

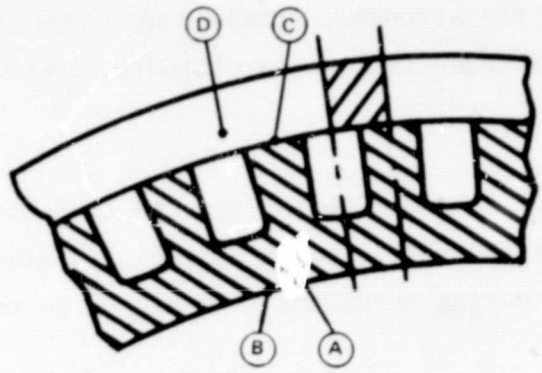

the land has the lowest life of 1350 cycles. Analysis shows no creep damage at the channel wall maximum operating temperature and stress. The cyclic strain range in the EDCu interface and the EDNi back wall are low and show no damage.

The total life criteria used are as follows:

$$\text{Life Criteria} = 4\phi_{fL} + \phi_c \leq 1.0$$

$$\text{Life Criteria} = 4\left(\frac{300}{1350}\right) + 0 = 0.89 < 1.0$$

Where:

ϕ_{fL} = low cycle fatigue damage fraction

ϕ_c = creep rupture damage fraction

4 = Safety Factor

Previous hot-fire experience with the SSME main combustion chamber and the 40K test program showed cracking occurred mid-channel as opposed to the predicted location of mid-land. Sections of the failed hardware showed thinning of the channel walls. This was attributed to a creep rupture phenomenon that was aggravated by extremely high hot-gas wall temperatures in excess of 1100 F. Later testing on SSME has verified mid-land cracking more severe than mid-channel cracking on combustion chambers that have accumulated many engine firing cycles. Since the maximum hot-gas wall temperature of this design is less than 800 F, there is no channel thinning problem expected, and this fatigue analysis is an accurate determination of the life of the combustor. The ultimate factor of safety is maintained on the stresses, strains, or loads that would cause failure, whether the failure mode is tensile ultimate, creep rupture, or instability (buckling).

All other criteria such as fatigue criteria, dynamic load criteria, and welded joints criteria are in addition to the basic criteria. Each component that experiences cyclic loading during operation is designed to the following fatigue criteria:

Low-Cycle Fatigue Limit Life = 4 X Service Life Operational Cycles

Limit life is the maximum expected usefulness of the structure expressed in time and/or cycles of loading. The service life is defined as 300 start/shutdown cycles or 10 hours of accumulated run time. The low-cycle fatigue criteria is applicable to cyclic stresses, including thermal, associated with steady-state and transient operating conditions such as an engine start/shutdown cycle. For those components experiencing low-cycle fatigue, the following generalized life equation is used to take into consideration the interaction of low-cycle fatigue and creep damage:

$$\text{Life Criteria} = 4\phi_{fL} + 4\phi_c \leq 1.0$$

Structural Design Criteria and Requirements

The following basic structural criteria were furnished in the SOW as guidelines for the stress analysis of engine components. These requirements are discussed in the combustor section but have applicability throughout.

$$\text{Yield Factor of Safety} = \frac{\text{Yield Load}}{\text{Limit Load}} \geq 1.1$$

$$\text{Ultimate Factor of Safety} = \frac{\text{Ultimate Load}}{\text{Limit Load}} \geq 1.4 \text{ (Combined Load)}$$

$$\text{Ultimate Factor of Safety} = \frac{\text{Ultimate Load}}{\text{Limit Load}} \geq 1.5 \text{ (Pressure Only)}$$

These safety factors govern the stresses induced by all operating loads and are based on minimum guaranteed material properties that include the effects of the component environment throughout the service life. Limit load represents the critical load or combination of loads for which the component is designed to operate. The limit loads include vibration, start, and shutdown transients and steady operation. The yield safety factor applies to primary stresses only. Gross total net section yielding or yielding causing detrimental deflections are not allowed. Yielding due to secondary stresses caused by bending, thermal gradients, or other deflection limited loads are governed by the ultimate load safety factor.

Low-cycle fatigue damage is evaluated by a linear damage accumulation,

$$\phi_f = \sum \frac{n_i}{N_{f_i}}$$

where n_i is the actual number of cycles at a particular stress or strain amplitude and N_{f_i} is the cycles to failure at the same amplitude (Miner's Rule).

A linear damage accumulation relationship is used to evaluate creep rupture damage,

$$\phi_c = \sum \frac{t_i}{T_{r_i}}$$

where t_i is the actual time at a particular stress and T_{r_i} is the time to rupture at that same stress. Lower bound fatigue property data are used to evaluate life.

Dynamic loads are calculated using closed-form, finite-element, and/or model analysis techniques for all major structures and for all other vibration-sensitive structures critical to the performance of the engine. Structures that incorporate inherent nonlinear stiffness, mass, and/or damping properties are analytically modeled using incremental linear analysis or by analog simulation techniques.

All components subjected to high-cycle fatigue loading are designed to operate below the endurance limits of their respective materials. This eliminates any life concerns involving high-cycle fatigue.

The criteria for welds includes a weld material factor and a weld efficiency factor in addition to the basic safety factor criteria. The weld joint efficiency factor is a function of the weld quality requirements, designated by the weld classification (Class I, II, or III), and the weld inspection requirements and/or capabilities. These factors are applied to the minimum guaranteed material properties of each weldment.

Tables 2-12 and 2-13 summarize the class of weld, weld joint efficiency factor, and minimum inspection requirements for fusion welds and electron beam welds, respectively.

TABLE 2-12. FUSION WELD JOINT EFFICIENCY FACTORS

FACTORS		CLASS OF WELD(1)			
		I	II	II	III
WELD JOINT EFFICIENCY FACTOR, %		100	80	60	40
MINIMUM INSPECTION REQUIREMENTS FOR 100 PERCENT OF JOINT LENGTH USING METHODS INDICATED	VISUAL	X	X	X	X
	DIMENSIONAL	X	X	X	X
	MAGNETIC PARTICLE OR PENETRANT	X	X	X	
	RADIOGRAPHY	X	X		
	INSPECTION AS INDICATED BY DRAWING		(2)		

(1) SPECIFIED ON DRAWING. REFERENCE APPLICABLE WELD SPECIFICATION DESIGNATED ON DRAWING FOR WELD QUALITY REQUIREMENTS

(2) RADIOGRAPHY OR PROOF TESTING REQUIRED

TABLE 2-13. ELECTRON BEAM WELD JOINT EFFICIENCY FACTORS

FACTORS	CLASS OF WELD(1)			
	III	Ia	Ib	II
WELD JOINT EFFICIENCY FACTOR, %	100	90	80	60
DIMENSIONAL (EXTERNAL)	X	X	X	X
PENETRANT OR MAGNETIC PARTICLE	X	X	X	X
ULTRASONIC INSPECTION FOR THE ENTIRE DEPTH AND LENGTH OF WELD OR RADIOGRAPHIC INSPECTION OF ENTIRE WELD SUPPLEMENTED BY VERIFICATION OF ROOT FUSION	X			
ULTRASONIC INSPECTION OF WELD ROOT (LOWER 10% OF JOINT) FOR THE ENTIRE LENGTH OF WELD		X		
ULTRASONIC INSPECTION OF WELD ROOT (LOWER 10% OF JOINT) FOR THE MINIMUM EXTENT SPECIFIED BY THE WELD SPECIFICATION			X	
FUSION ZONE GEOMETRY AS DETERMINED BY EXAMINATION OF TEST SAMPLES				X

(1) SPECIFIED ON THE DRAWING. REFERENCE APPLICABLE WELD SPECIFICATION DESIGNATED ON DRAWING FOR WELD QUALITY REQUIREMENTS.

Components that contain pressure are proof-pressure tested in accordance with one of the following criteria with a minimum time at proof pressure of 30 seconds, repeated for a total of 5 cycles:

The design temperature:

$$\text{Proof pressure} \geq 1.2 \times \text{limit pressure}$$

A nominal temperature that is different from the design temperature, with a material correction factor:

$$\text{Proof pressure} \geq 1.2 \times \frac{F_t \text{ (at proof temperature)}}{F_t \text{ (at design temperature)}} \times \text{limit pressure}$$

The material correction factor will be based on yield or ultimate, whichever gives the largest ratio. In all cases, regardless of the temperature correction factor, the minimum proof pressure will be $\geq 1.05 \times$ limit pressure.

Combustion Stability Analysis and Design

The Priem method has been applied to analyze the inherent stability of the combustion zone with respect to transverse mode acoustic instabilities. The results of these analyses show that even without stability aids this thrust chamber would be more stable than a J-2 or J-2X, while operating at nominal thrust at a mixture ratio of 6.0, a mixture ratio of 7.0, or during operation at 10% thrust.

To ensure against the possibility of an unstable operating point being encountered during the off-design operating points which constitute the start and cutoff transients, 18 Helmholtz cavity acoustic absorbers have been incorporated at the junction of the injector face and combustion chamber. The absorbers are tuned to resonate at the frequency of the first tangential mode of the chamber, but also have considerable effectiveness against higher frequency acoustic modes. The acoustic absorber throat area is 6.5 times the stability correlation threshold value, and this very conservative value, plus the results of Priem analysis for the stabilized chamber insure that no acoustic mode instability will be

encountered with the Advanced Expander Cycle Engine Point Design Thrust Chamber. Since the chamber has been intentionally overdesigned for combustion stability, the acoustic absorbers have been situated so that they can be easily removed from future versions of the engine if operational experience proves they are not required.

Priem Analysis of Acoustic Instability. The acoustic instability model used at Rocketdyne was originally developed by Dr. R. J. Priem at NASA and was later further expanded and elaborated at Rocketdyne. This model calculates the perturbations in combustion rate that result from an initial pressure perturbation of an arbitrary size, and determines the threshold value for perturbation that is required to initiate a sustained instability. This threshold perturbation is expressed as a fraction of the steady-state chamber pressure, and is referred to as the stability parameter or A_p. Thus, the magnitude of A_p is a measure of the stability of the engine (i.e., the larger the value of pressure perturbation that is required to trigger the engine into instability, the more inherently stable is the engine). The most important combustor parameters determining the value of A_p are the burning rate parameter L, the relative gas-liquid velocity term $\Delta V'$, and the unburned propellant fraction term MAP.

Fig. 2-25 illustrates the relationship between the stability parameters L, $\Delta V'$, and MAP. Multiple interpolations are required to obtain an A_p at particular values of L, $\Delta V'$, and MAP. Since these parameters vary with the axial location in the combustor, the Coaxial Injector Combustion Model (CICM) interpolates for values of A_p from internally curve-fitted maps of the three stability parameters.

Figure 2-26 compares the stability curves calculated for the Advanced Expander Thrust Chamber with similar curves previously calculated for other engines whose stability characteristics are experimentally well known. The curves express the inherent stability of the combustion zone for the first 1.5 inches downstream of the injector. Since a high value for A_p indicates a stable region in the combustion zone, and low value for A_p indicates a less stable region, a curve having a

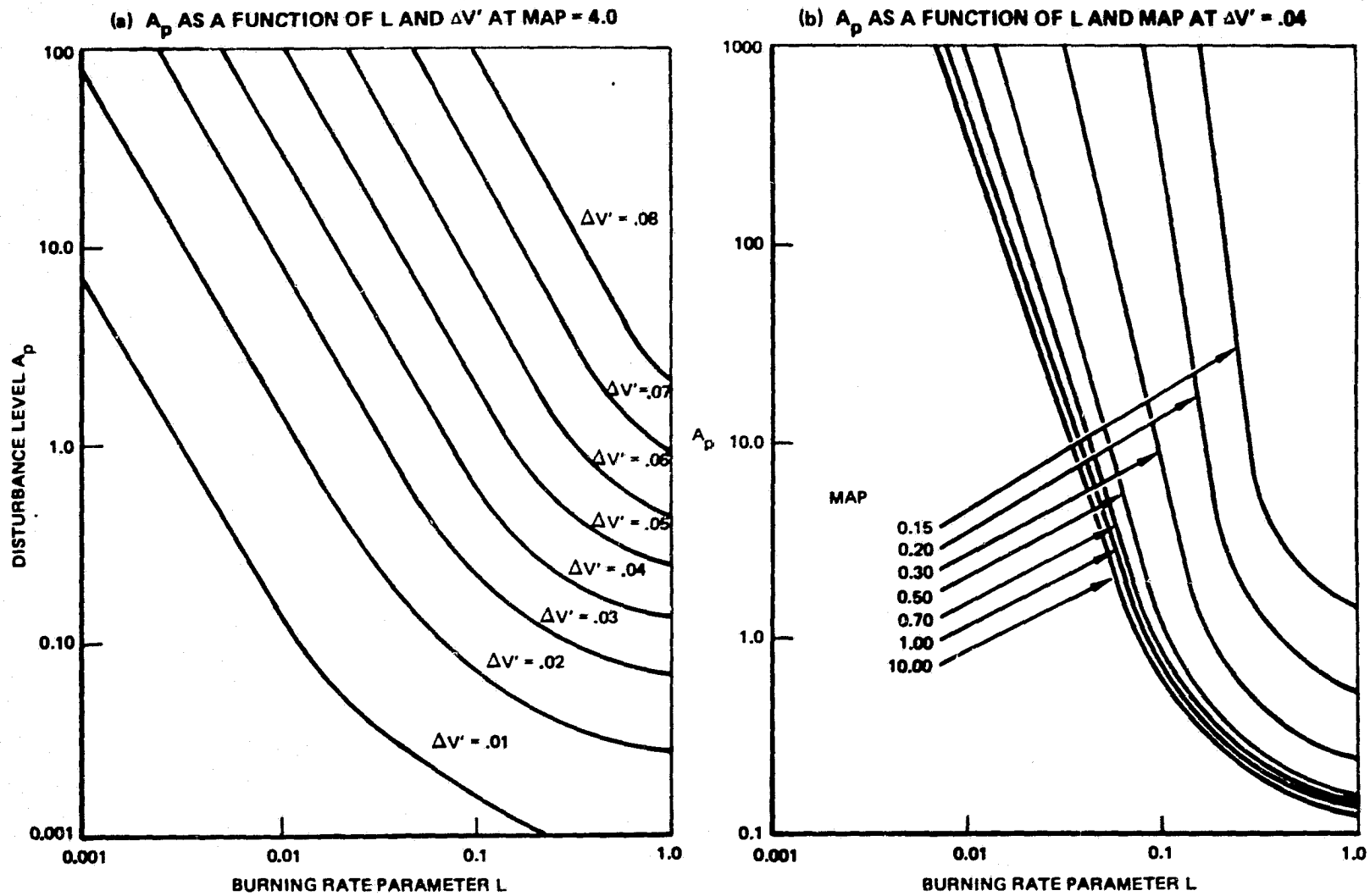

Figure 2-25. Stability Parameter (A_p) Analysis

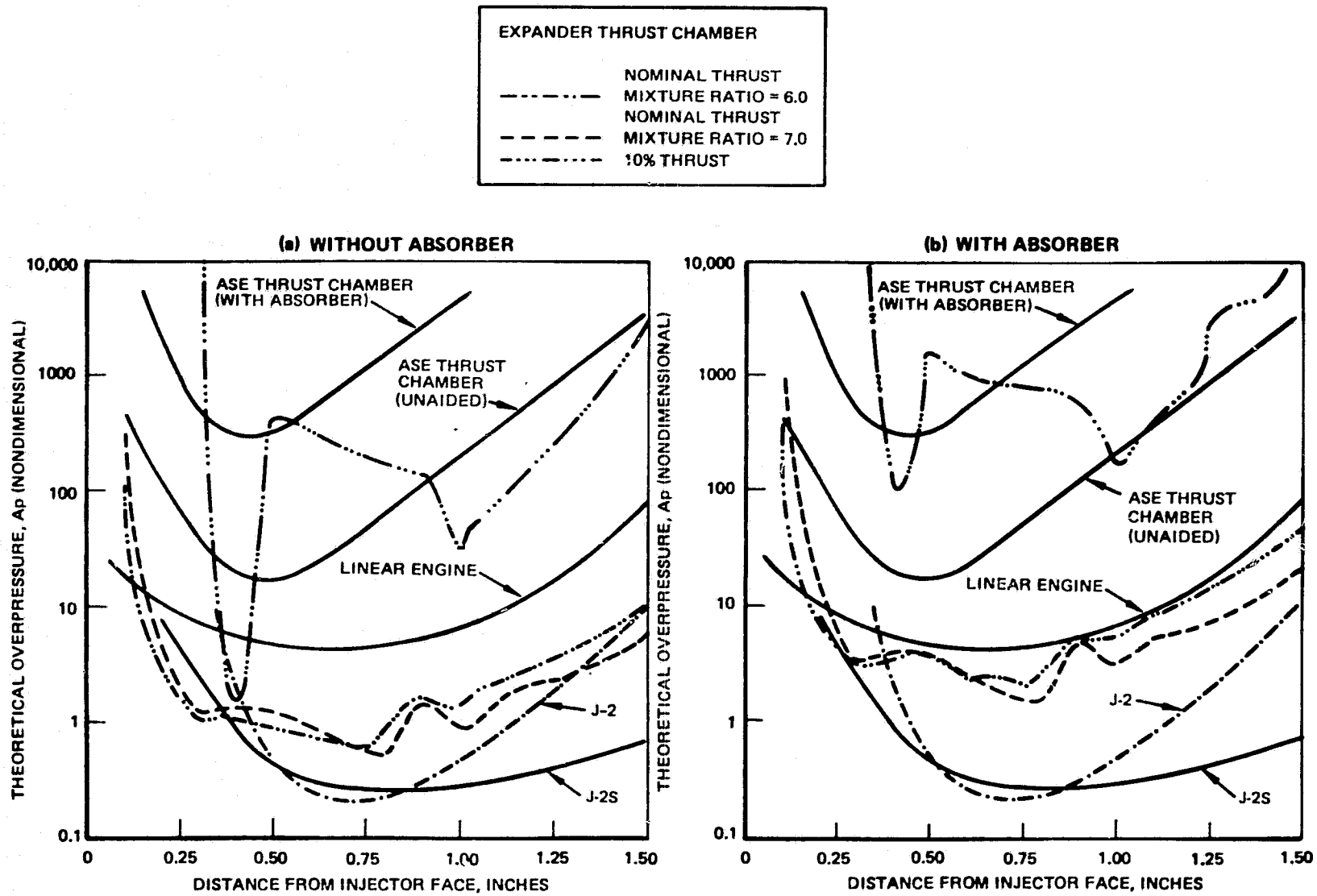

Figure 2-26. Priem Analysis of Advanced Expander Thrust Chamber

low minimum value indicates a less stable engine than a curve which has a higher minimum value. It may be seen from Fig. 2-26 that even without stability aids the Advanced Expander Engine Thrust Chamber has more inherent stability than either the J-2 or J-2S. Figure 2-26 shows that, with acoustic absorbers suppressing the first tangential mode, the Advanced Expander Engine Thrust Chamber has a stability level similar to the Rocketdyne Linear Engine.

This level of stability should ensure freedom from any acoustic stability problems with the proposed thrust chamber, since the J-2 and J-2S could only be bombed unstable during off-nominal start transients when cold hydrogen was being flowed, and the linear engine even had the capability to recover from an instability initiated during the transient.

Stability Aids Design. For acoustic modes, the primary stability aids are baffles and acoustic absorbers. Baffles are generally used in large engines with low acoustic frequencies. Absorbers have very successfully provided stability in small-diameter engines with high frequencies. With very large engines, the acoustic mode frequencies are so low as to make damping with an absorber impractical. Thus, a large engine will often be designed to include both baffles (designed to preclude low-frequency modes) and absorbers (designed to preclude high-frequency and/or baffle compartment modes).

The use of baffles has the inherent disadvantages of distorting the injector element pattern, causing heat transfer problems, decreasing flow uniformity, and hence, impairing the attainment of high performance. The use of baffles is not regarded as necessary or desirable in the expander cycle thrust chamber, which has a chamber diameter of only 4.8 inches, and relatively high natural acoustic resonant frequencies.

The resonant frequencies of the advanced expander thrust chamber are:

First Tangential Mode	7,226 Hz
Second Tangential Mode	11,986 Hz
Third Tangential Mode	16,524 Hz
First Radial Mode	15,044 Hz

Rocketdyne's history has shown baffles to be desirable on combustors whose primary acoustic frequency is less than 3500 Hz, and that acoustic absorbers are particularly effective in damping oscillations in the range of 4000 Hz and higher.

Acoustic Absorber Effectiveness. The effectiveness of acoustic absorbers for a wide variety of engine types and sizes is illustrated in Fig. 2-27. Although there is a considerable variation between engines using different propellants and injector element types, the strongest trend indicated is the increasing effectiveness of acoustic absorbers at high frequency and the increasing effectiveness when the absorber open area is increased.

Figure 2-28 illustrates the same data as Fig. 2-27 but with stability threshold lines fitted to separate the stable and unstable operating regions. The "best fit" line for the threshold has the equation $Af^2 = 1$, where A is absorber aperature open area expressed as a fraction of the chamber cross-sectional area, and f is the frequency in kilohertz . Since there is considerable variation in engine behavior, the "best fit" stability threshold line has some unstable points to its right, and some stable points to its left. To obtain a design criterion for absorber open area which will be sufficient to statistically insure the absence of instability, lines may be drawn parallel to the threshold line but displaced into the stable region. Several such lines, which have equations of the form, $A_f^2 = K$, are illustrated in Fig.2-28 . It appears that if K has a value of three or larger, the probability of unstable operation will be very small.

The acoustic absorbers used in the Advanced Expander Thrust Chamber are designed with a K value of 6.5, which is well into the stable region. A point illustrating the design has been drawn into Fig.

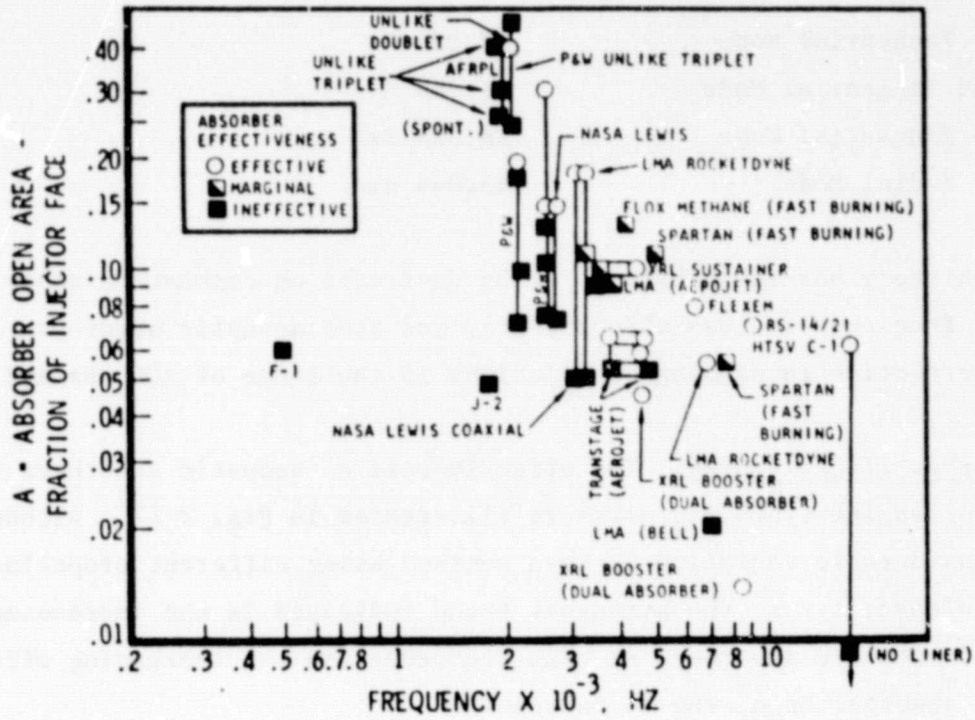

Figure 2-27. Acoustic Absorber Effectiveness

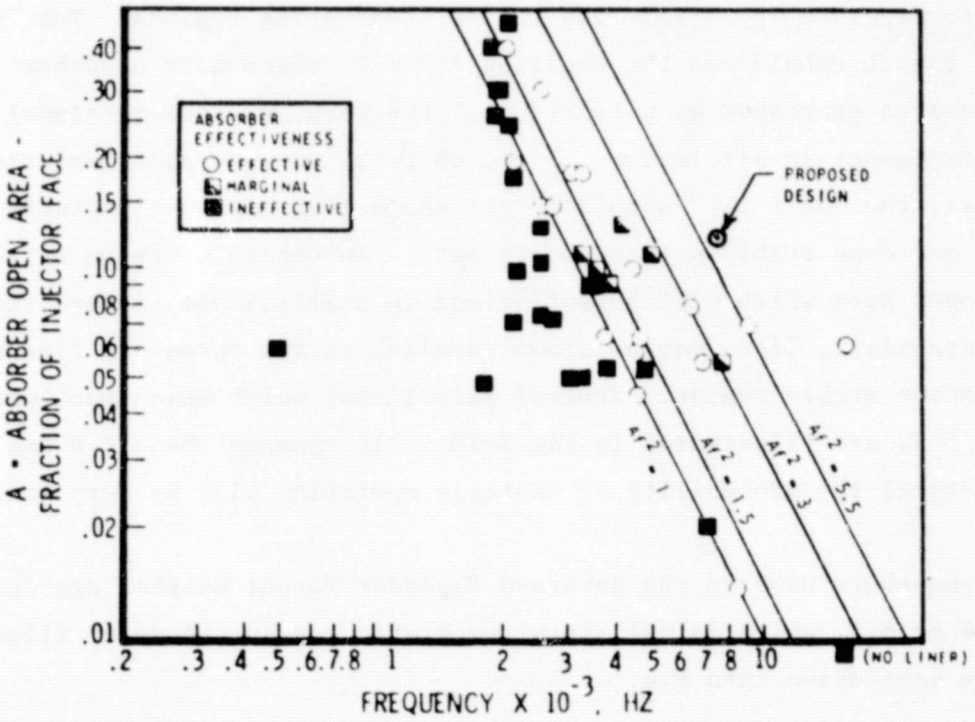

Figure 2-28. Stability Threshold Correlations and Design Point

FIXED NOZZLE DESIGN, 1-1/2 PASS

A fixed nozzle design using a 1-1/2 pass cooling circuit geometry similar to the J-2 nozzle was optimized for light-weight type hardware (Figure 2-29). The 1-1/2 pass design is interchangeable with a 1-3/4 pass test-verification nozzle and offers a design which permits a reduced assembly weight. By increasing the number of tubes to 560 at the aft end of the nozzle while maintaining the identical contour, the effective coolant tube OD can be reduced. This permits a reduction in the stress-limited wall thickness.

The 1-1/2 pass nozzle also differs from the 1-3/4 pass design in that a channel wall transition section is not required at the upstream end of the nozzle. Because the entrance end of the nozzle is formed from only 280 tubes, the reduced number of tubes can be fitted directly into the coolant manifold, thereby eliminating the channel wall transition segment.

The coolant tube configuration for the 1-1/2 pass nozzle is relatively more complex than the tube configuration for the 1-3/4 pass nozzle. Whereas the round cross-section of the 1-3/4 pass tubes lend themselves to a simple taper draw and assembly booking procedure to assure fitup, the 1-1/2 pass tubes with the midpoint transition results in increased first-unit cost. The 1-1/2 pass tubes are drawn, then pressure-formed to the very tight tolerance required to assure fit-up of the bundle. This process requires the additional pressure form tooling for each tube configuration and transition element when compared to the 1-3/4 pass design.

The 1-1/2 pass nozzle offers a weight advantage, 62.6 lb versus 67.9 lb, and extracts a lower coolant pressure loss. Materials and fabrication procedures are very similar for the 1-1/2 pass and 1-3/4 pass nozzles. They are discussed in detail for the 1-3/4 pass nozzle. This nozzle is similar to the experimental ASE nozzle and is recommended for test-verification hardware.

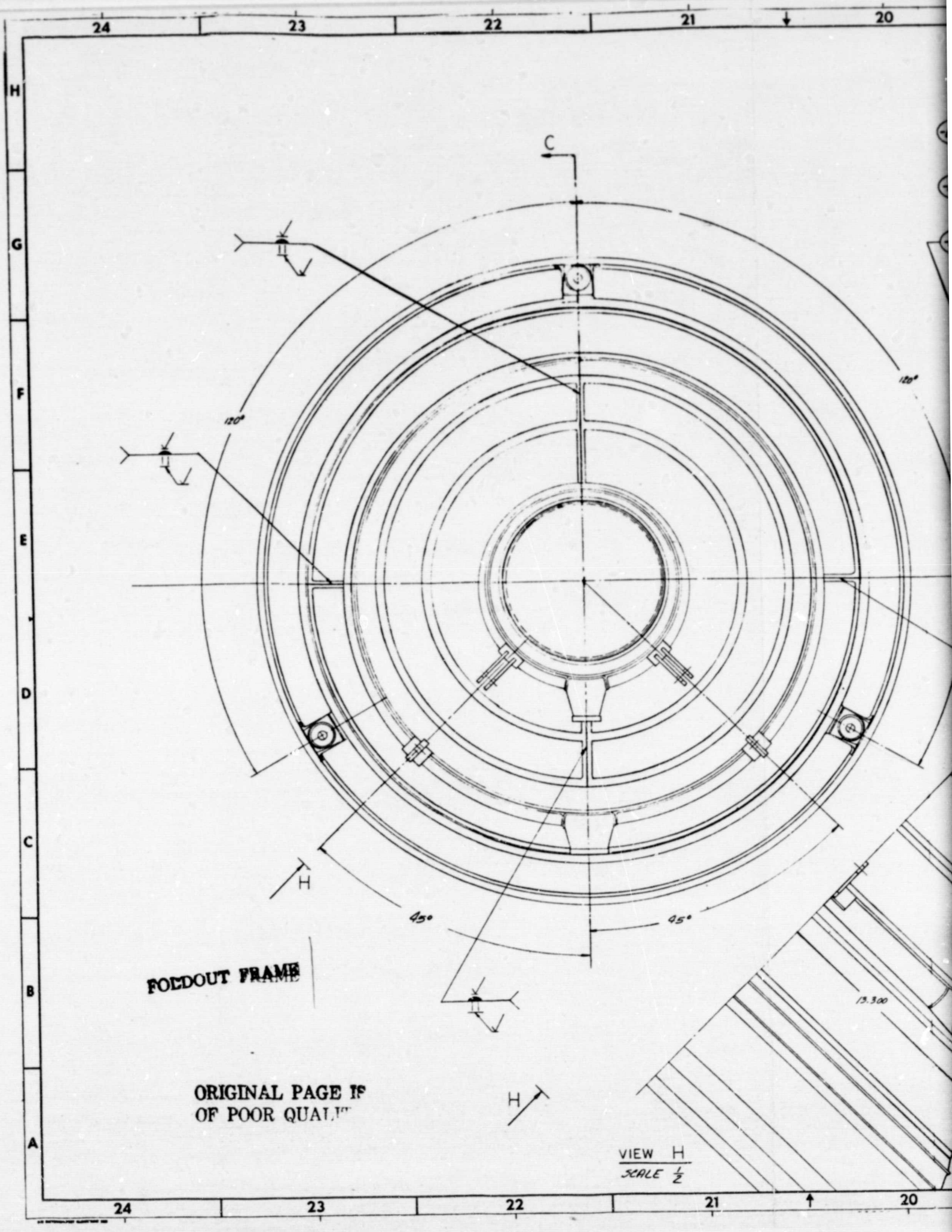

FOLDOUT FRAME

ORIGINAL PAGE IS
OF POOR QUALITY

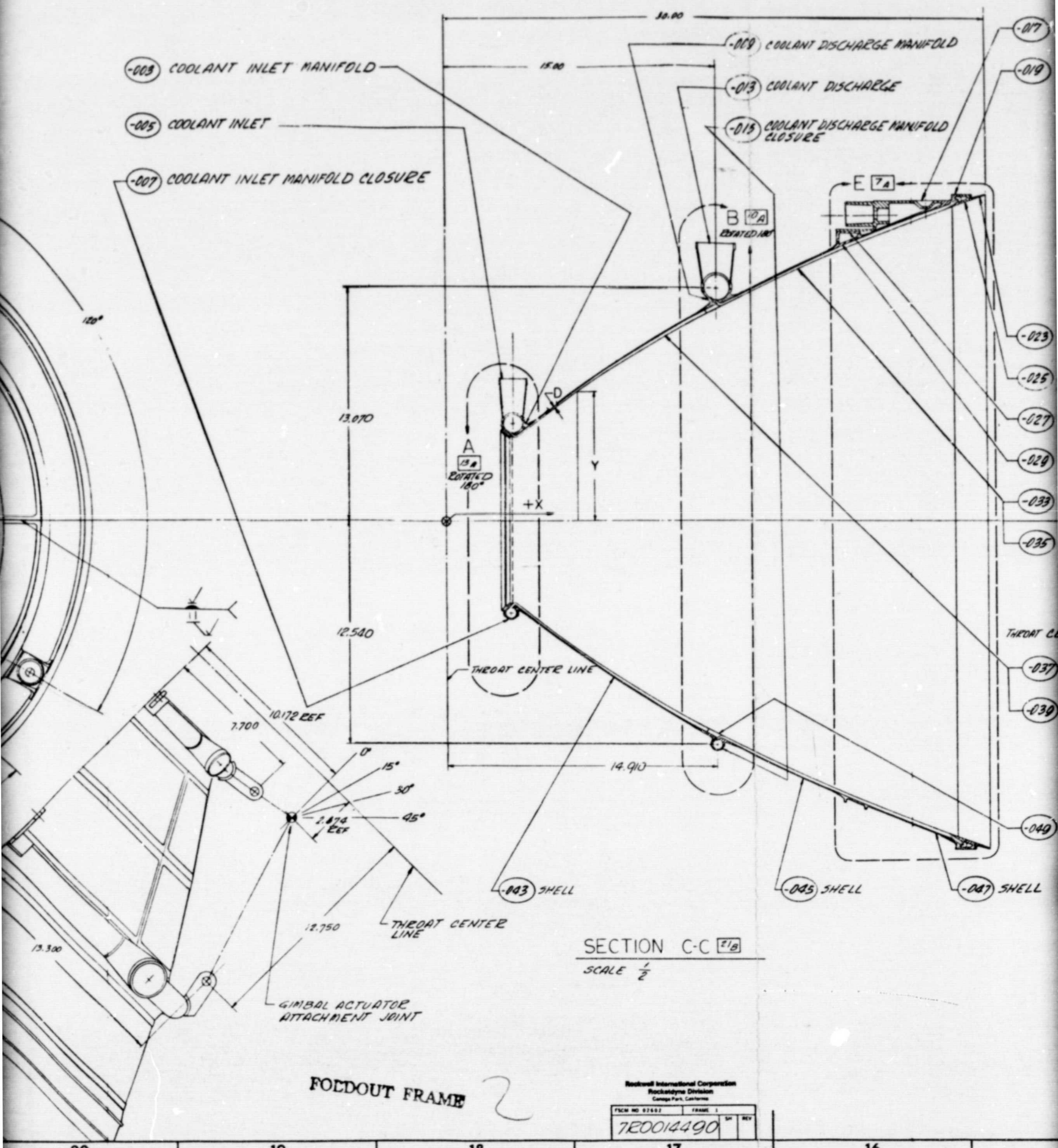

SECTION C-C 21B

SCALE 1/2

FOLDOUT FRAME 2

Rockwell International Corporation
Rocketdyne Division
Canoga Park, California

FSCM NO 07602	FRAME 1		
7R0014490		SH	REV

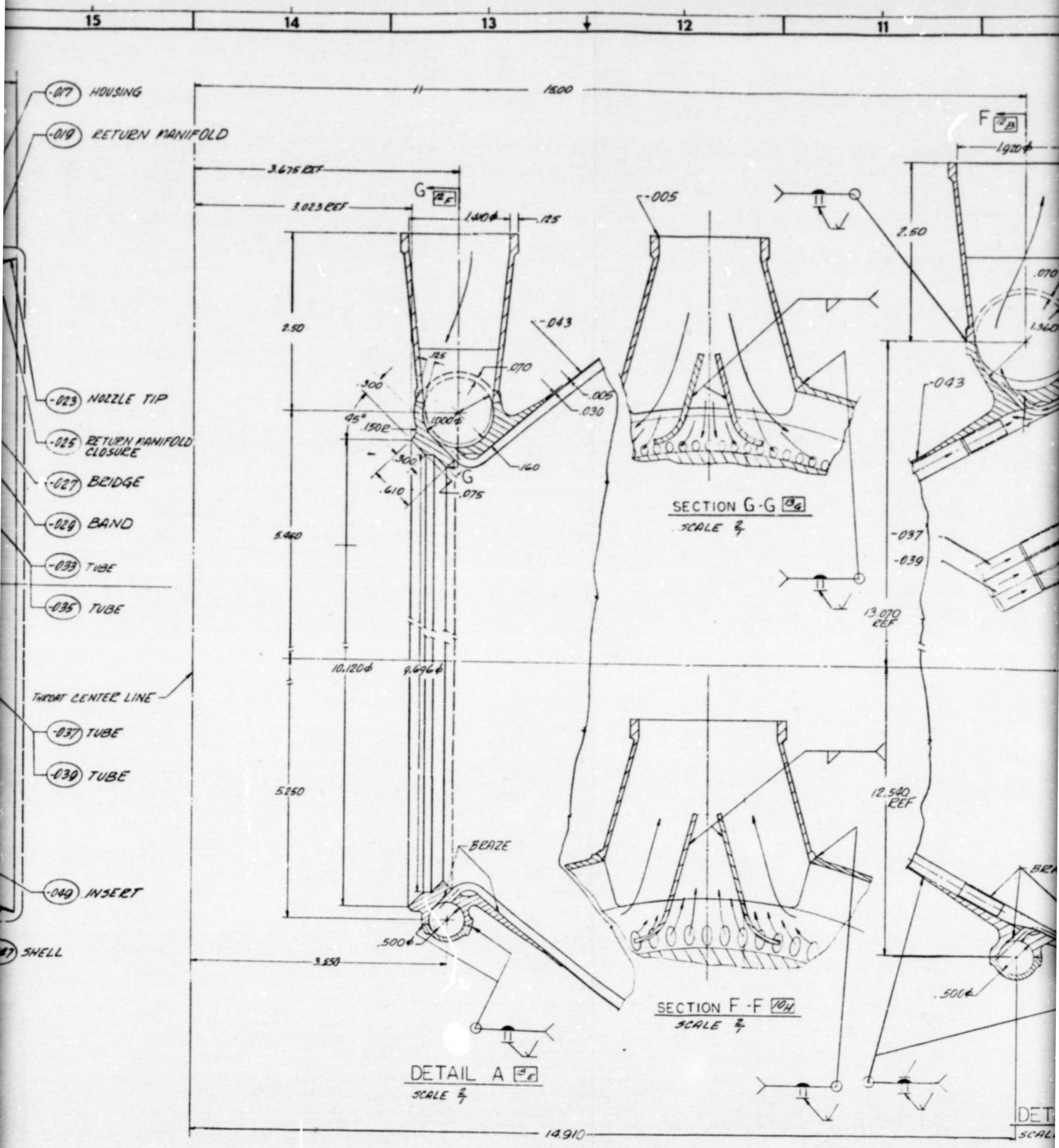

FOLDOUT FRAME 3

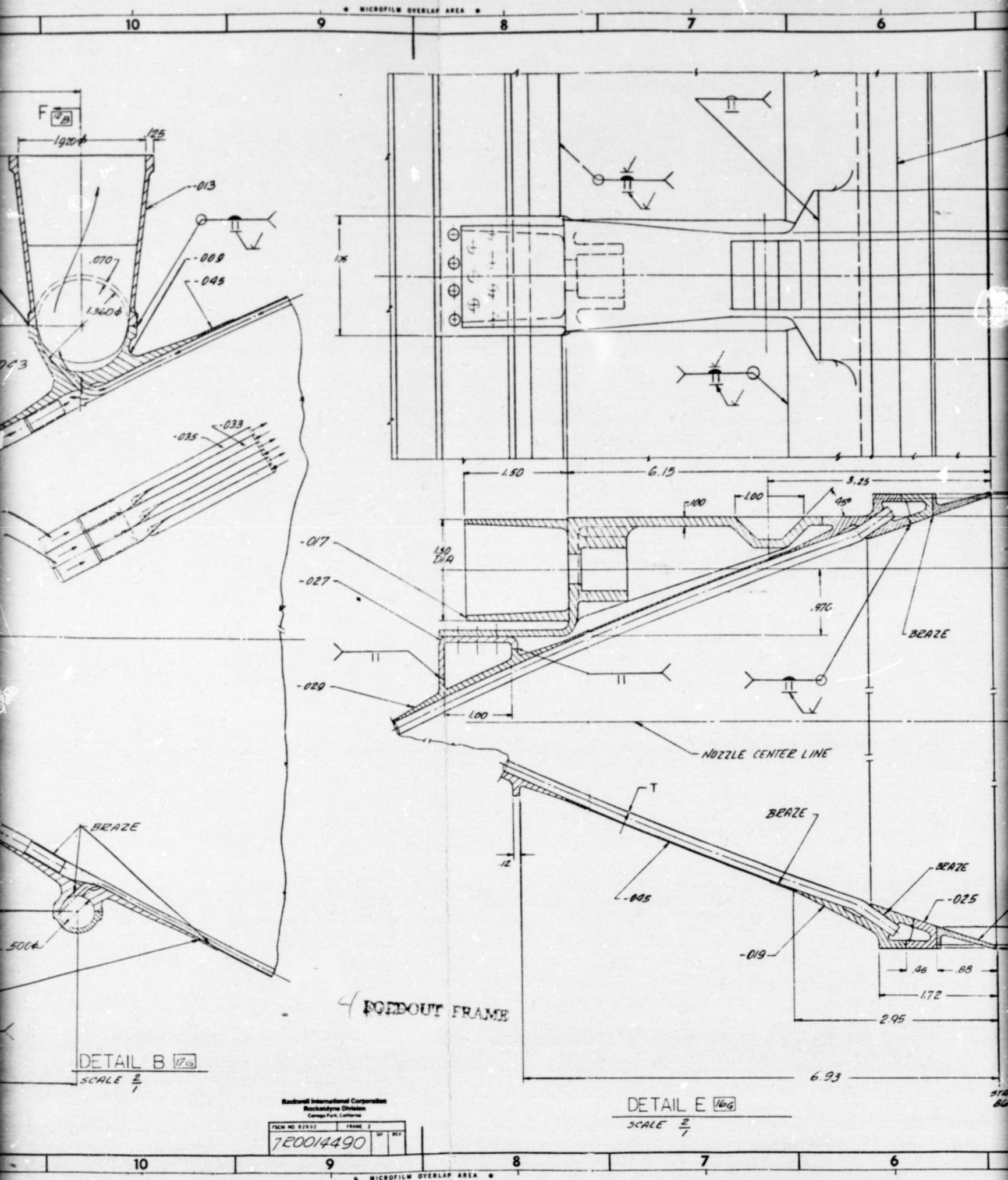

FOLDOUT FRAME

STA.	X	Y	OD TUBE	TUBE WALL THKNS	
73	3.859	4.648	.1063	.005	
74	4.484	5.123	.1160		
75	4.883	5.407	.1224		
76	6.198	6.402	.1459		
77	7.165	7.183	.1618		
78	9.360	8.628	.1955		
79	11.599	9.609	.2132		
80	13.431	11.061	.2507		
81	15.052	11.937	.1346		
82	18.776	13.790	.1555		
83	20.916	14.760	.1665		
84	25.839	16.806	.1896		
85	28.668	17.872	.2016		
86	30.000	18.339	.2069		
87	28.668	17.872	.2016		
88	25.839	16.806	.1896		
89	20.916	13.760	.1665		
90	18.776	13.790	.1555		
91	15.052	11.937	.1346	.005	

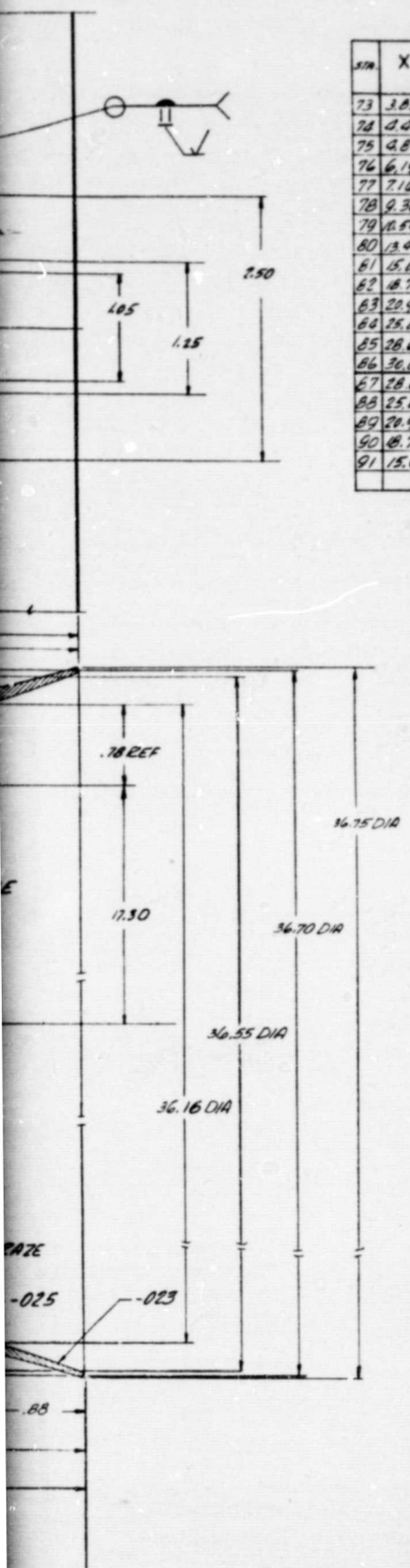

NONDOUT FRAME 5

1. THIS DRAWING SUPPORTS 720014500

NOTE: UNLESS OTHERWISE SPECIFIED

Figure 2-29

FOR INFORMATION

RI/RD80-218-2

CASW NO	MATERIAL	SIZE	SPECIFICATION	ZONE
-059				
-057				
-055				
-053				
-049				15C
-047	CRES 347	.030 THK		15B
-045	CRES 347	.030 THK		16B
-043	CRES 347	.030 THK		18B
-039	A 286	.005 WALL THK		15C
-037	A 286	.005 WALL THK		15D
-035	A 286	.005 WALL THK		15E
-033	A 286	.005 WALL THK		15E
-029	INCO 718			15E
-027	INCO 718			15E
-025	INCO 625			15F
-023	NARLOY Z			15F
-019	INCO 625			15H
-017	INCO 718			15H
-015	INCO 625			17G
-013	INCO 625			17G
-009	INCO 625			17H
-007	INCO 625			20G
-005	INCO 625			20G
-003	INCO 625			20H

HEAT TREAT
FINISH
MATL

UNLESS OTHERWISE SPECIFIED DIMENSIONS ARE IN INCHES AND APPLY PRIOR TO FINISH.
125/ MACH SURF ROUGHNESS
TOLERANCES ON ANGLES - 0° 30'
DECIMALS .XX ± .03 .XXX ± .010
HOLES NOTED "DRILL"

OVER	THRU	TOLERANCE
.0000	.0400	+ .0015 — .0010
.0400	.1300	+ .0020 — .0010
.1300	.2700	+ .0045 — .0010
.2700	.5000	+ .0060 — .0010
.5000	.7500	+ .0070 — .0010
.7500	1.0000	+ .0090 — .0010
1.0000	3.0000	+ .0120 — .0010

DO NOT SCALE PRINT

CONTR
DWN J. ENRICE DATE
CHK DATE
GROUP
MATL
STRUCT
DESIGN ACTIVITY APVD DATE

Rockwell International Corporation
Rocketdyne Division
Canoga Park, California

OTV - FIXED NOZZLE ASSEMBLY 1 1/2-PASS

SIZE J | FSCM NO 02602 | DWG NO 720014490

SCALE 4/1 | SHEET | FRAME 1

FORM NO. R1B-B-6 REV. 3-77

FIXED NOZZLE DESIGN, 1 3/4 - PASS

The test verification design selected for the Advanced Expander Point Design Thrust Chamber is a 1-3/4 coolant pass unit that attaches to the combustion chamber nozzle at $\varepsilon =$ 14.1 and extends to $\varepsilon =$ 225 (Figure 2-29).

The internozzle fairing used to attach an extension enlarges the expansion ratio to 225:1. The nozzle design is a regeneratively cooled tubular nozzle using a 1-3/4 pass coolant circuit which flows coolant hydrogen from the forward end ($\varepsilon =$ 14:1) through the return manifold located at the aft end ($\varepsilon =$ 222:1) to a final collection manifold located at the forward end.

The nozzle design selected represents a design that has been optimized for minimized cost, ease of fabrication, and of the heat load and pressure loss of an optimized expander system. The aft termination point, $\varepsilon =$ 225, is compatible with an optimized flight engine which has a limited overall package length of 60 inches. Three hundred sixty A286 round and tapered tubes of 0.010 wall were selected to form the contoured regeneratively cooled expansion nozzle. The configuration calculated heat load and pressure drop are shown in Table 2-14.

Selection of $\varepsilon =$ 14:1 for the combustion chamber to nozzle split line was based on fabrication and cooling considerations. To optimize the overall thrust chamber design, the split line between the combustion chamber and the nozzle was considered from the total system aspect.

Because the throat section contained in the channel wall combustion chamber is the area of highest heat flux and is life-limiting, it is desirable to introduce the liquid hydrogen coolant as close as possible to this region and still establish good flow characteristics prior to its entering the critical throat areas. This dictates that the entrance manifold, and subsequently, the split line, should be a relatively short distance downstream of the throat.

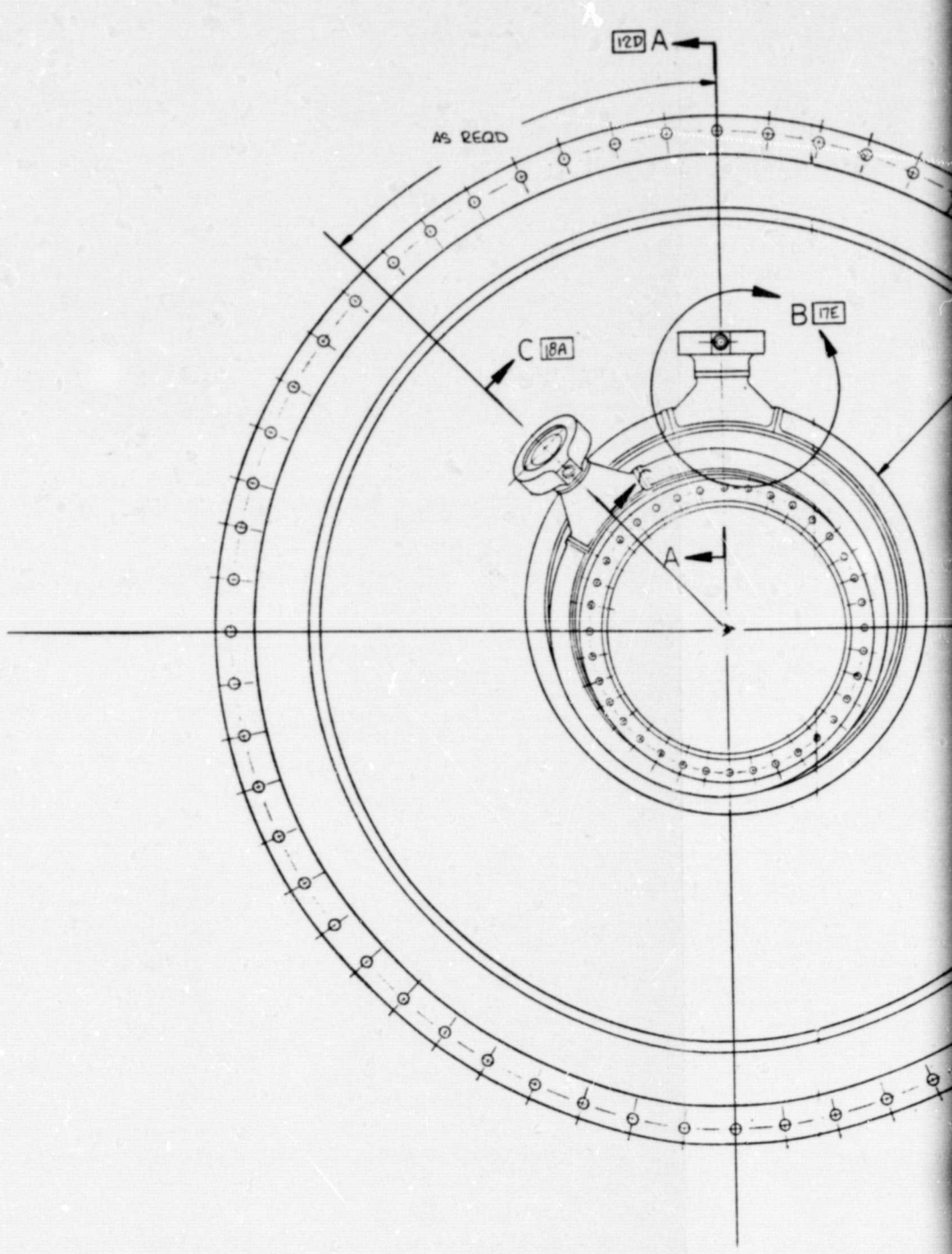

ORIGINAL PAGE IS
OF POOR QUALITY

FOLDOUT FRAME

TABULATION BLO

STATION	X DIM	Y DIM	TUB THIC
1	3.858	4.608	
2	4.843	5.407	
3	6.198	6.402	
4	7.165	7.193	
5	9.360	8.629	
6	10.599	9.409	
7	13.431	11.061	
8	15.052	11.937	
9	18.774	13.790	
10	20.906	14.760	
11	25.839	17.806	
12	28.668	17.872	
13	30.000	18.339	

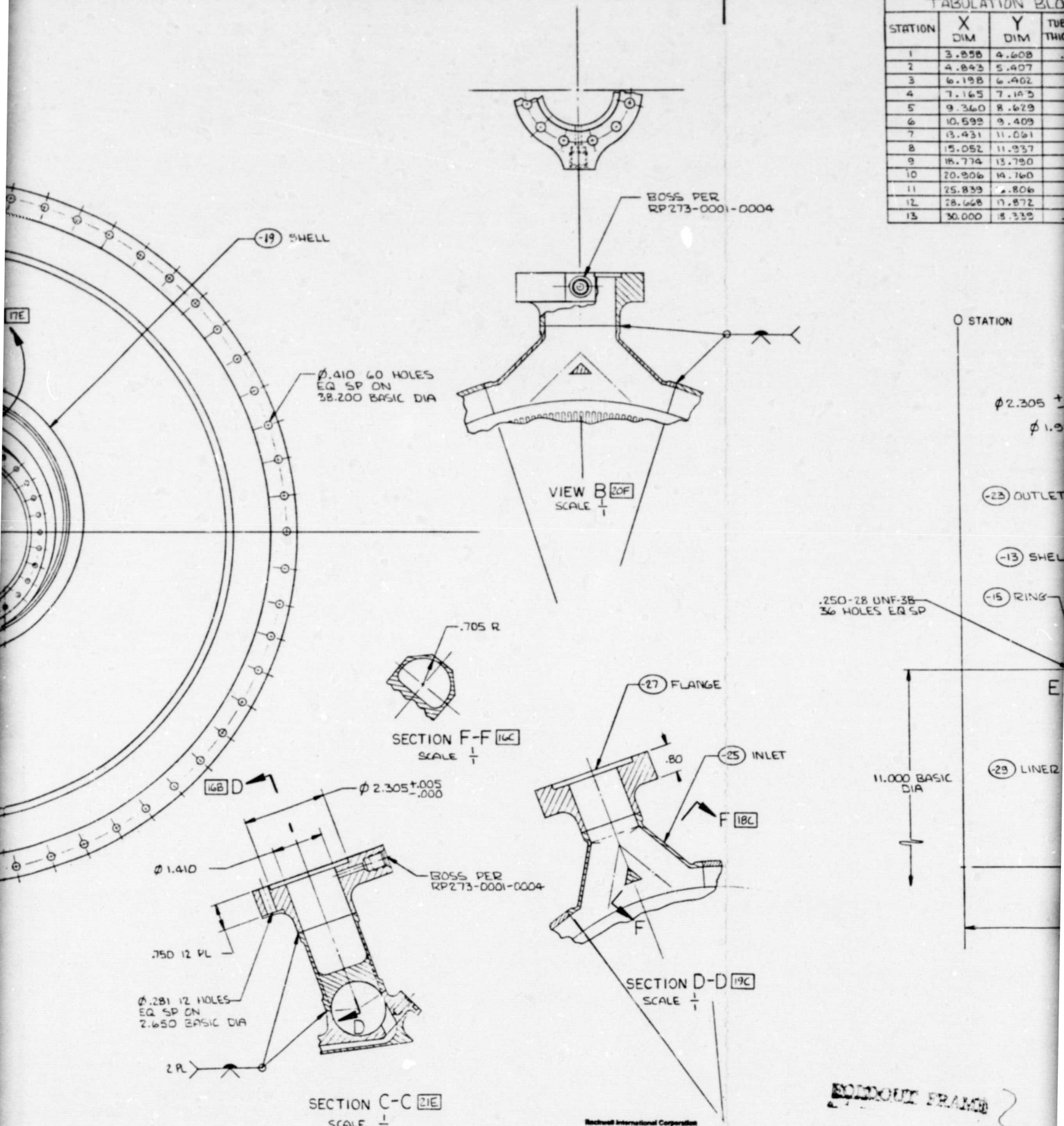

Rockwell International Corporation
Rocketdyne Division
Canoga Park, California

FSCM NO 02602	FRAME 1		
7RJ014448		SH	REV

Y M	TUBE WALL THICKNESS	D DIA
08	.010	.0810
07		.0950
02		.1132
43		.1256
29		.1517
09		.1654
061		.1945
337		.2100
90		.2426
760		.2536
306		.2557
372		.3145
339	.010	.3227

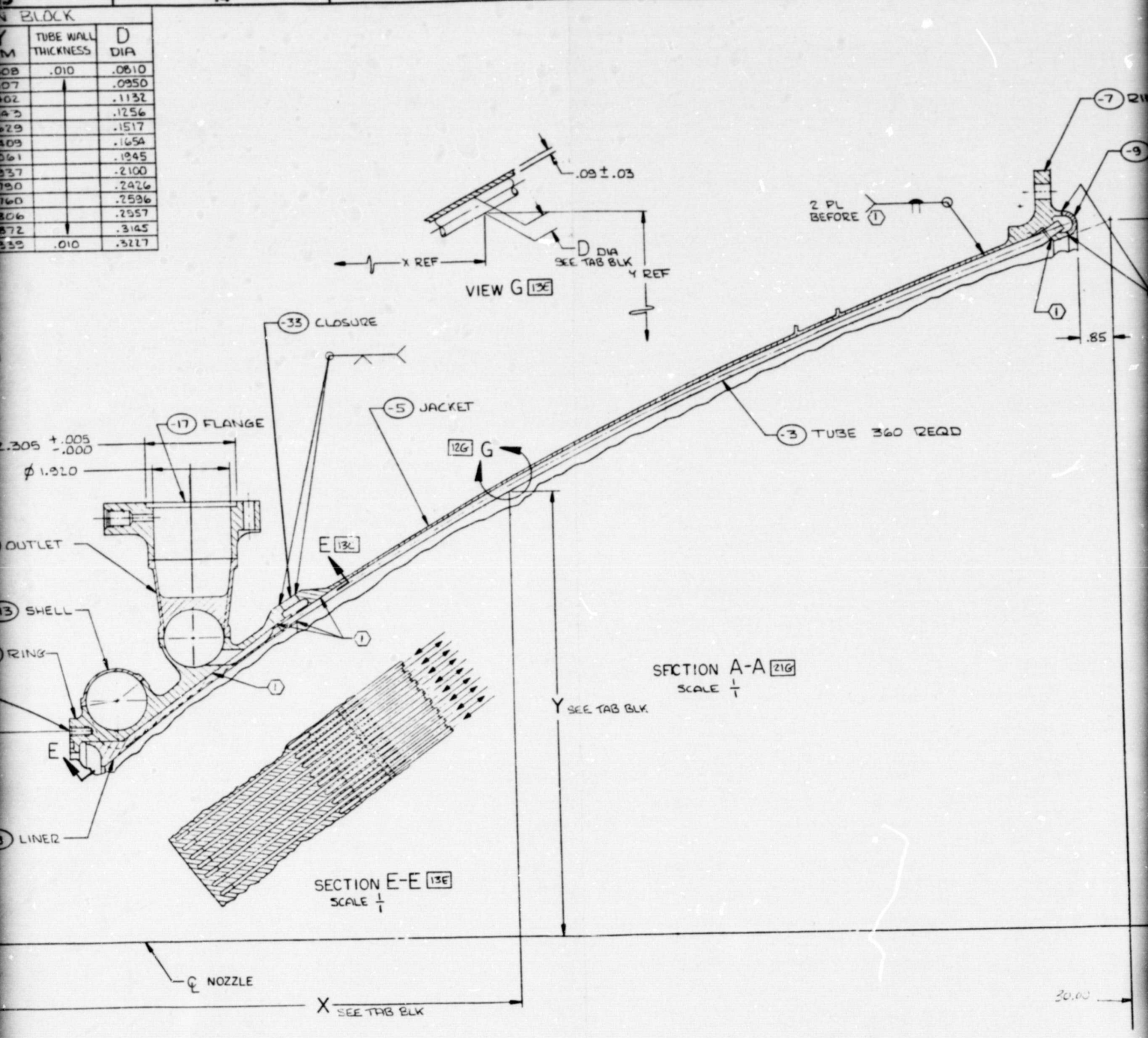

NOZZOUT FRAME 3

• MICROFILM OVERLAP AREA •

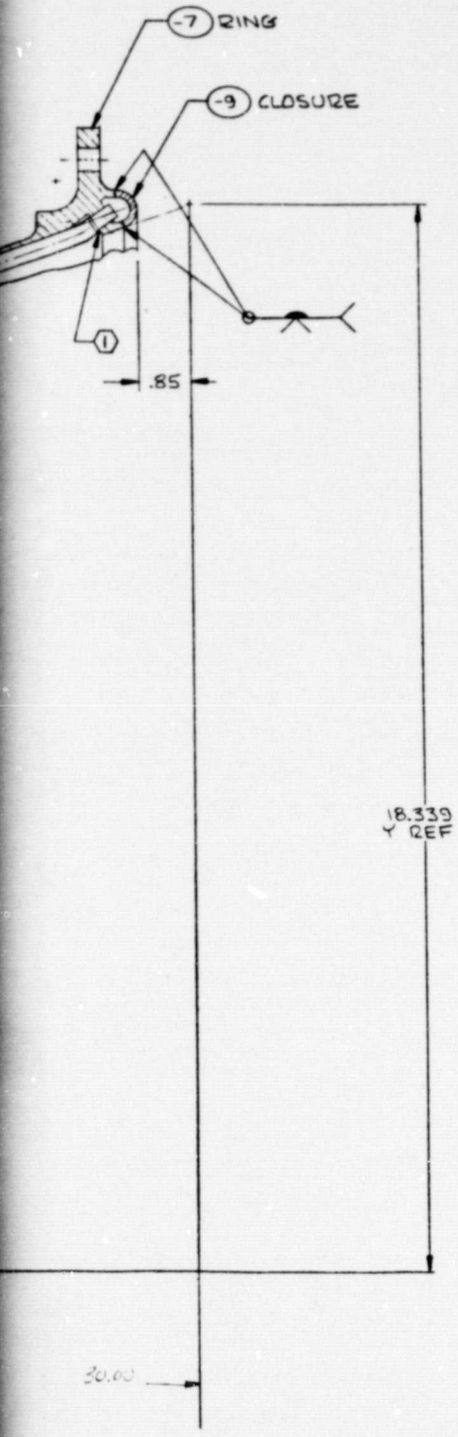

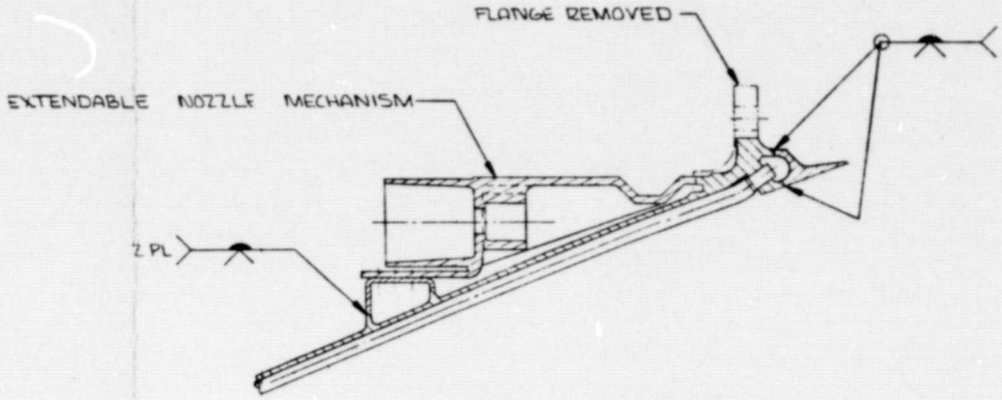

EXIT END REWORKED TO
ACCOMODATE EXTENDIBLE NOZZLE

ORIGINAL PAGE IS
OF POOR QUALITY

DOCUMENT FRAME 4

Rockwell International Corporation
Rocketdyne Division
Canoga Park, California

FSCM NO 07607	FRAME 2		
7R0014448		SH	REV

• MICROFILM OVERLAP AREA •

Figure 2-30

FOLDOUT FRAME 5

THIS IS NOT A RELEASED COPY

RI/RD80-218-2
2-66

-33	INCONEL 625	—	AMS5666	14F
-29	OFHC COPPER	—	QQ-C-576	15C
-27	INCONEL 625	—	AMS5666	17D
-25	↑	—	↑	16C
-23		—		15E
-19		—		15G
-17		—		14E
-15		—		15D
-13		—		15E
-9	↓	—	↓	16G
-7	INCONEL 625	—	AMS5666	10H
-5	INCONEL 718	—	RA0170-154	13F
-3	AVG CRES TUBE	TAPERED	RA0169-747	11E
NO	MATERIAL	SIZE	SPECIFICATION	ZONE

(4) FURNACE AGE PER M&P INSTRUCTIONS
3. WELD PER RA0103-027
2. MACHINE PER RA0103-016
(1) FURNACE BRAZE TUBES TO JACKET AND MANIFOLD PER M&P INSTRUCTIONS

NOTE: UNLESS OTHERWISE SPECIFIED

NOTED

Rockwell International Corporation
Rocketdyne Division
Canoga Park, California

NOZZLE, EXPANDER CYCLE, 1 3/4 PASS ASSY OF

J 02602 7RC014448

TABLE 2-14

EXPANDER CYCLE FIXED NOZZLE PARAMETERS,

ITEM	DESIGN PARAMETERS
ΣQ, BTU/SEC	2548
ΔP, PSI	68.0
CYCLE LIFE	12201
EXIT ε	225:1
F = 15K	
P_c = 1540 PSIA	

A split-line expansion ratio of 14:1 places the combustion chamber coolant inlet 2.45 inches aft of the throat,ensuring proper coolant flow characteristics. Additionally, the nozzle ID at ε = 14:1 is 9.17 inches in diameter, which permits use of a relatively small coolant manifold on the nozzle, keeping weight minimized, and reducing manufacturing costs. The geometric considerations of the nozzle component assembly were also addressed. The channel wall distribution segment at the forward end contains 180 channels 0.080-inch wide with tapered separating lands. This interfaces with 0.080-inch nominal diameter tubes, which package well and are easily fabricated, using existing tube tapering tooling. This design approach is similar to that used successfully on the previous ASE nozzle.

Because of cost consideration, it is desirable to fabricate the tubular wall segment of the nozzle from a single-tube configuration. This eliminates the need for the additional tooling required for multiple tube configurations. The tube configuration selected is a 0.323 to 0.080-inch OD tapered tube employing

a constant 0.010 wall. This single tube configuration serves for both up-pass and downpass applications, with the routing to separate manifolds taking place in the short channel wall sector.

Manifold Design

In the design, two coolant manifolds are integrated into the forward manifold attach ring, as shown in Figure 2-31. The coolant inlet manifold is positioned forward of the coolant exit manifold. The inlet manifold receives the warmed hydrogen from the combustion chamber and distributes it evenly among the 180 down tubes.

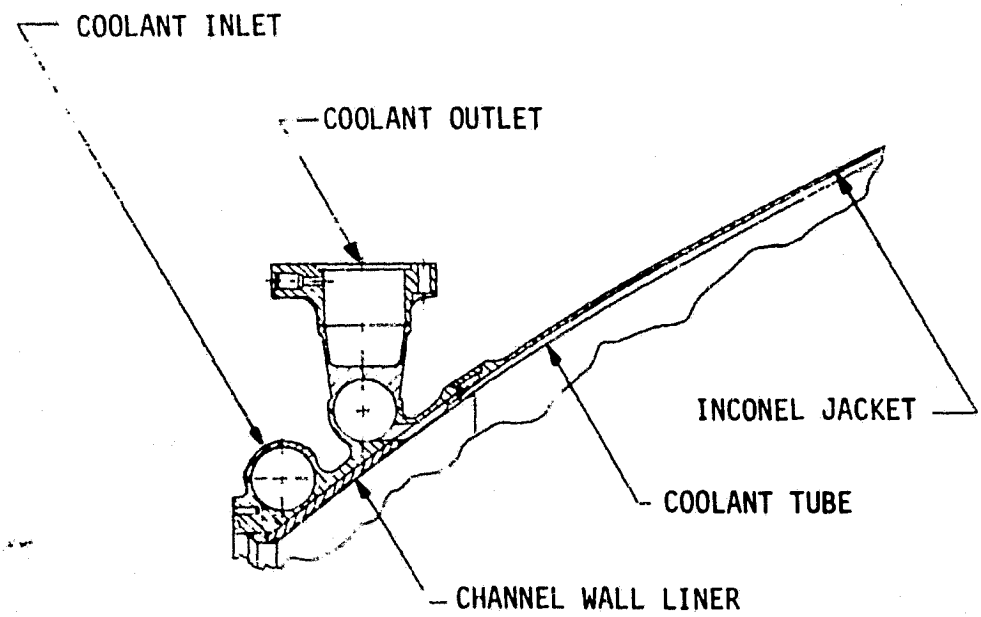

FIGURE 2-31. Nozzle Coolant Manifold Arrangement

The coolant exit manifold is located immediately aft of the inlet manifold; it collects the heated coolant from the up tubes and ducts it from the nozzle to the turbines. Both manifolds are sized for minimum pressure losses and proper flow distribution.

Coolant flow from and into these manifolds is conducted through a channel wall adaptor which features a copper liner with milled coolant channels. This liner is attached to the Inconel manifold section by a furnace braze operation. The channels in this segment have been shaped and sized to minimize pressure losses and to provide long liner life. Because the heat flux is greatly reduced at the liner's aft end (by a factor of four relative to the throat area), the coolant channel geometry can be a constant width throughout the liner length. This constant channel width results in a land width, which varies from a 0.080 inch at the forward end to approximately 0.176 inch at the aft end.

The turnaround manifold at the exit end of the nozzle (Figure 2-32) has a base ring that is machined and drilled for coolant tube insertion and brazing. All manifolds in the nozzle are closed out after the furnace braze operations with welded circumferential shells.

A flight-type extendible nozzle is attached to the aft end of the fixed nozzle to complete the full expansion area ratio of 625 (Figure 2-2). The latch and extension mechanism adapter is indicated in the figure.

Nozzle Jacket

The nozzle's jacket structure borrows from the highly successful SSME design concept which provides for enclosure of the tube bundle in a one piece thin wall jacket. This configuration provides for simplified manufacturing tooling requirements, highly reliable braze processing, lightly loaded tube members, and virtually eliminates the thermal strain problems induced when hat bands or flat bands are used. Additionally, the concept eliminates need for a critical tube-to-tube braze to effect a hot-gas seal. Instead, a simple tube-to-jacket braze is made and the external jacket prevents hot gas leakage. During final assembly operations, the jacket-to-manifold ring joints are not close out welded until after completion of the tube-to-jacket braze cycle. Only by keeping both sides of the tube braze connection accessible for inspection and leak check can the integrity of the braze operation be verified. A simple temporary bridging strip will be used to locate the jacket to manifolds during the braze cycle.

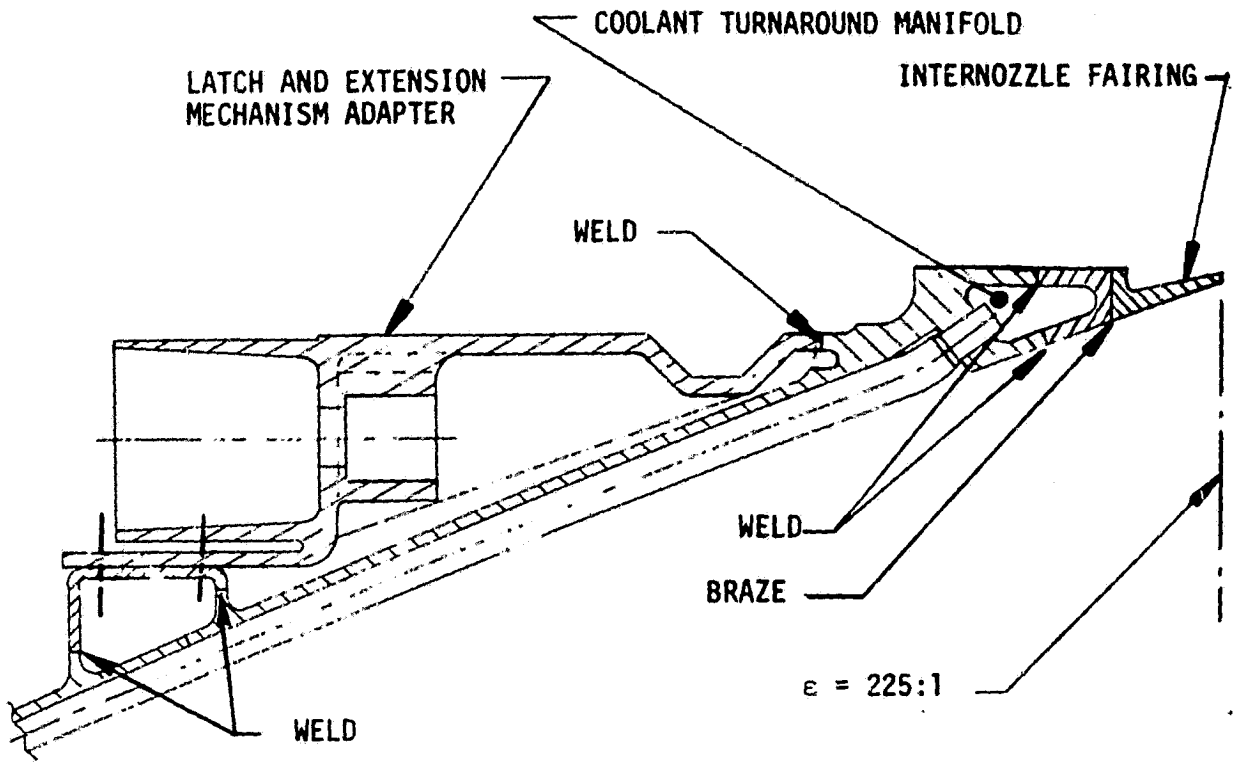

Figure 2-32. Nozzle Turnaround Manifold and Nozzle Extension Mechanism Interface

Recommended Nozzle Materials

The recommended nozzle materials are listed in Table 2-15 and discussed in the following paragraphs.

TABLE 2-15. RECOMMENDED NOZZLE MATERIALS

COMPONENT	MATERIAL
TUBES	A286
JACKET	INCONEL 718
FORWARD MANIFOLD	INCONEL 625
AFT TURNAROUND MANIFOLD	INCONEL 625
CHANNEL WALL LINER	OHFC COPPER

Nozzle Tubes. Material moderate strength and excellent resistance to high-pressure hydrogen are the primary reasons for the selection of A286 over other candidate materials. Corrosion resistance of the alloy is excellent and is far superior to that of 18-8 stainless steels such as Type 347.

Table 2-16 presents some typical mechanical properties data on A286 and 347 CRES.

TABLE 2-16 . MECHANICAL PROPERTIES OF A286 AND TYPE 347 CRES

	PROPERTIES			
	F_{tu}, KSI	F_{ty}, KSI	EL, %	RA, %
ROOM TEMPERATURE				
A286*	140	95	15	20
TYPE 347	75	30	40	50
1000 F				
A286*	115	87	15	20
TYPE 347	54	23	23	48

*HEAT TREATMENT - FURNACE BRAZE - 2 CYCLES

1. 1950 to 2000 F
2. 1900 to 1950 F + HGE 1400 F F.C. to 1200 F - 20 HOURS

A286 is formable and brazeable when plated with 0.0012 to 0.0016 inch of nickel, as demonstrated on the SSME nozzle. After the high-temperature braze cycle(s), full properties are developed with a 1400 to 1200F step age cycle. These characteristics make A286 an excellent choice for nozzle tubes.

Nozzle Jacket - Materials. The nozzle jacket will be fabricated with Inconel 718. Inconel 718 was selected over other candidate materials primarily because of availability and inherent weight savings provided by its high strength. Rocketdyne has used Inconel 718 successfully in identical application on the SSME nozzle.

Forward Manifolds - Materials. Four candidate materials were considered for the manifolds. These were: Inconel 625, Inconel 718, Incoloy 903, and Type 321 stainless steel. Type 321 CRES has excellent corrosion resistance and resistance to degradation from high pressure hydrogen effects, but because of its relatively low strength, the nozzle would suffer a weight penalty. On the other hand, Inconel 718 provides a weight savings because of its high strength, but it is subject to degradation from high pressure hydrogen. Copper plating would be required if this alloy were selected.

Incoloy 903 also offers a weight savings because of its high strength, and it is not embrittled by high pressure hydrogen; however, Incoloy 903 has poor corrosion resistance, its availability is questionable, and problems have been experienced in welding.

Inconel 625 was the best compromise of the candidate materials. It has higher strength than the 18-8 stainless steels, has excellent corrosion resistance, has better resistance to high-pressure hydrogen than Inconel 718, and also has superior weldability.

Table 2-17 shows some typical properties for the candidate materials. The Inconel 625 and Inconel 718 data is for the material in 3000 psia hydrogen. As can be seen, the yield strength of Inconel 625 is nearly twice that of Type 321 CRES.

TABLE 2-17. CANDIDATE MATERIALS FOR NOZZLE MANIFOLDS (ROOM TEMPERATURE)

	PROPERTIES			
	F_{tu}, KSI	F_{ty}, KSI	EL, %	RA, %
INCONEL 625*	96	55	30	17
INCONEL 718*	175	150	-	9
INCOLOY 903	180	150	11	15
TYPE 321	75	30	40	50

*IN 3000 PSI HYDROGEN

Channel Wall Nozzle Liner - Material. OFHC copper has been selected for the nozzle channel wall liner. The prime reason for selecting OFHC copper over other candidate materials for the expander cycle 1-3/4 pass nozzle transition ring is that it possesses good thermal conductivity and is brazeable. It is brazed to both the nickel-plated A286 tubes and the Inconel 625 manifold base ring in the temperature range of 1900 to 1950F. This braze temperature is dictated because it simultaneously serves as a solution treatment for the A286 tubes and the Inconel 718 jacket. It should be noted that there are two braze cycles: the first is to braze the Inconel 625 base ring to the copper transition ring, and the second is to braze the A286 tubes to the copper transition ring.

These brazing temperatures preclude the selection of copper-base alloys, such as NARloy-Z or AMZIRC, because they would melt prior to reaching the braze temperature. Other alloys, such as Nickel 200, which are brazeable in these temperature ranges, do not have the desirably high thermal conductivity of copper.

FIXED NOZZLE COOLING ANALYSIS AND CIRCUIT SELECTION

Selection of a full coolant flow circuit over a split flow coolant circuit was made for the Advanced Expander Cycle nozzle assembly to maximize the heat load while maintaining cooling of the critical high heat flux combustion chamber section.

Various nozzle cooling circuits, including 1-pass, 1-1/2 pass, 1-3/4 pass, and 2-pass have been compared. The lowest cooling pressure drop is a single down-pass system since the coldest, high-pressure fluid is used as coolant at the lowest area ratio (high q/A). The coolant discharge at the high ε location, however, requires a large discharge manifold at this point that would preclude the use of a translating nozzle extension. The requirement then is that of moving the manifold to a lower area ratio (also provides reduced manifold weight) to allow clearance for the extendible nozzle.

The use of a 1-1/2 pass nozzle (down-up) brings the discharge manifold to a lowered area and reduced manifold weight. Also, for minimum wall thickness, stress limited nozzle tubes, the 1-1/2 pass allows a beneficial 2:1 diameter reduction at the exit plane. The pressure drop, however, is higher.

The use of a full 2-pass cooling system allows the benefits of the lowest manifold and feed line weight in the design, and eliminates the manufacturing difficulty caused by the complex tube configuration at the discharge manifold. This difficulty remains in the 1-1/2 pass design. However, the coolant pressure drop becomes several times greater than a single pass design because the flow passes through the high heat flux region two times and the coolant is discharged at a higher velocity head level.

The 1-3/4 coolant pass (down full pass -- up 3/4 pass) circuit selected is one which has a low pressure drop, a single low cost die formed tube, and minimum manifold weights. The approach uses an OFHC copper milled channel manifold section, which provides the inlet and outlet manifolds and a single downpass

section between the two manifolds. The single downpass is run through the OFHC copper manifold section to the down tube entry plane and the up tube (3/4 pass) is connected into the transition section base to the outlet manifold.

This transition approach has been successfully used on the 20K ASE nozzle and has the advantage of a lowered ΔP in this critical region as a result of the two-dimensional fin conduction effect of the OFHC copper channel. This effect is not present for a low conductivity tube design.

The integrated transition section approach thus allows for the 1-3/4 pass approach to be used with the manifold weight advantage of the full two-pass, the tube ΔP of the 1-1/2 pass circuit and the cooling benefit of the single downpass at the attach point.

In the selection of the 1-3/4 pass tubular nozzle section, a parametric analysis of several tube configurations was conducted. Figure 2-33 presents the results of the parametric analysis. A configuration containing 180 down and 180 up tubes was selected as the design point on the basis that it provided the greatest heat input to the coolant, required for engine system operation, within acceptable coolant pressure drop limitations.

The design point channel geometry for the transition section of the nozzle is presented in Figure 2-34. Nozzle transition wall temperature profiles and the coolant temperatures are provided in Figure 2-35. Details of the channel and tube geometry were obtained using a computer program, basing the selection on acceptable wall temperatures, cycle life, stress levels and fluid conditions. The geometry of the tubular section of the nozzle is given in Figure 2-36. Tube temperature profile and coolant temperatures are presented in Figure 2-37.

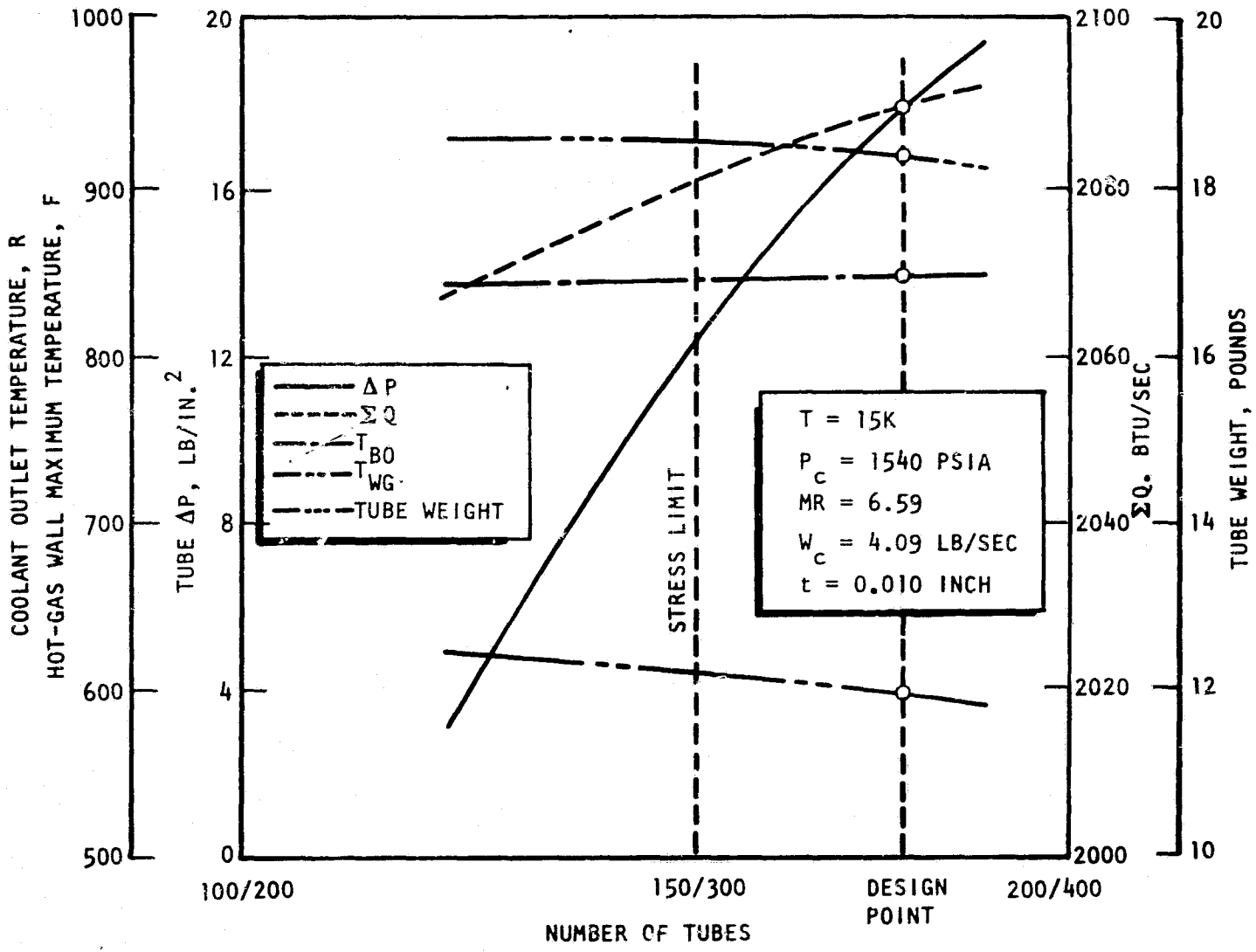

Figure 2-33. Advanced Expander Cycle 1-3/4-Pass Fixed Nozzle Parametric Results

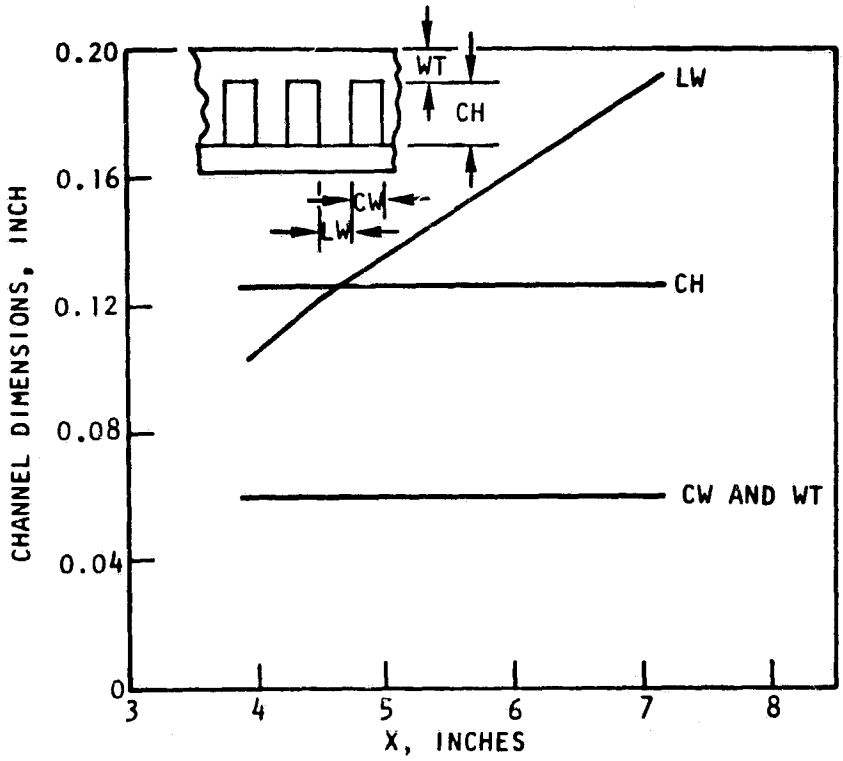

Figure 2-34. Advanced Expander Cycle Nozzle Transition Channel Geometry

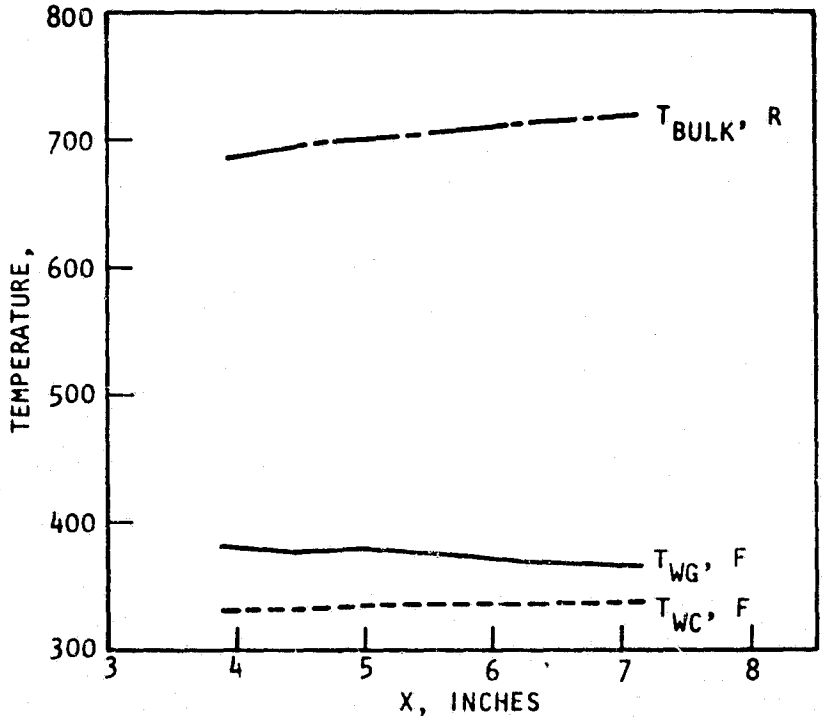

Figure 2-35. Advanced Expander Cycle Nozzle Transition Temperature Profiles

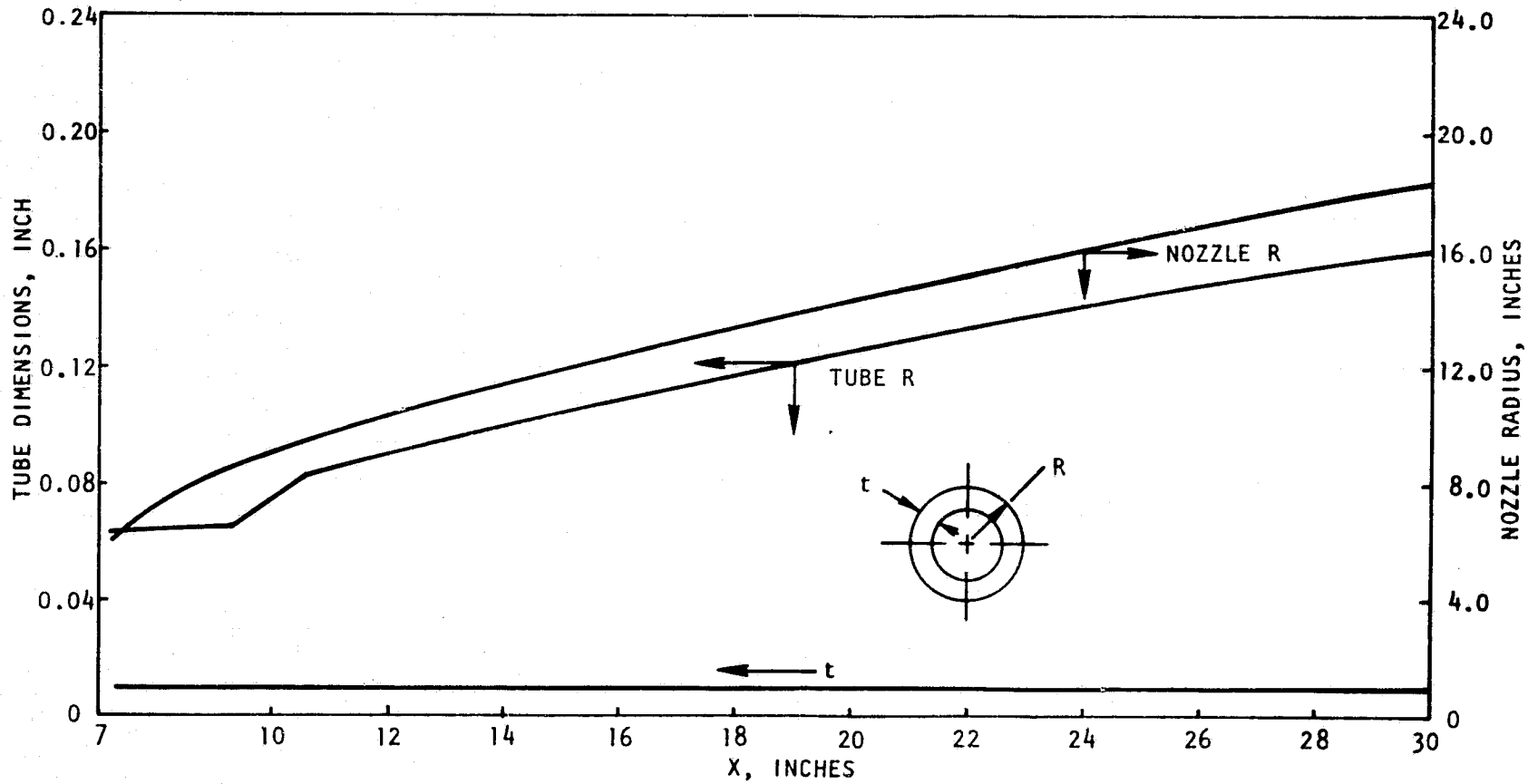

Figure 2-36. Advanced Expander Cycle Nozzle Tube Geometry

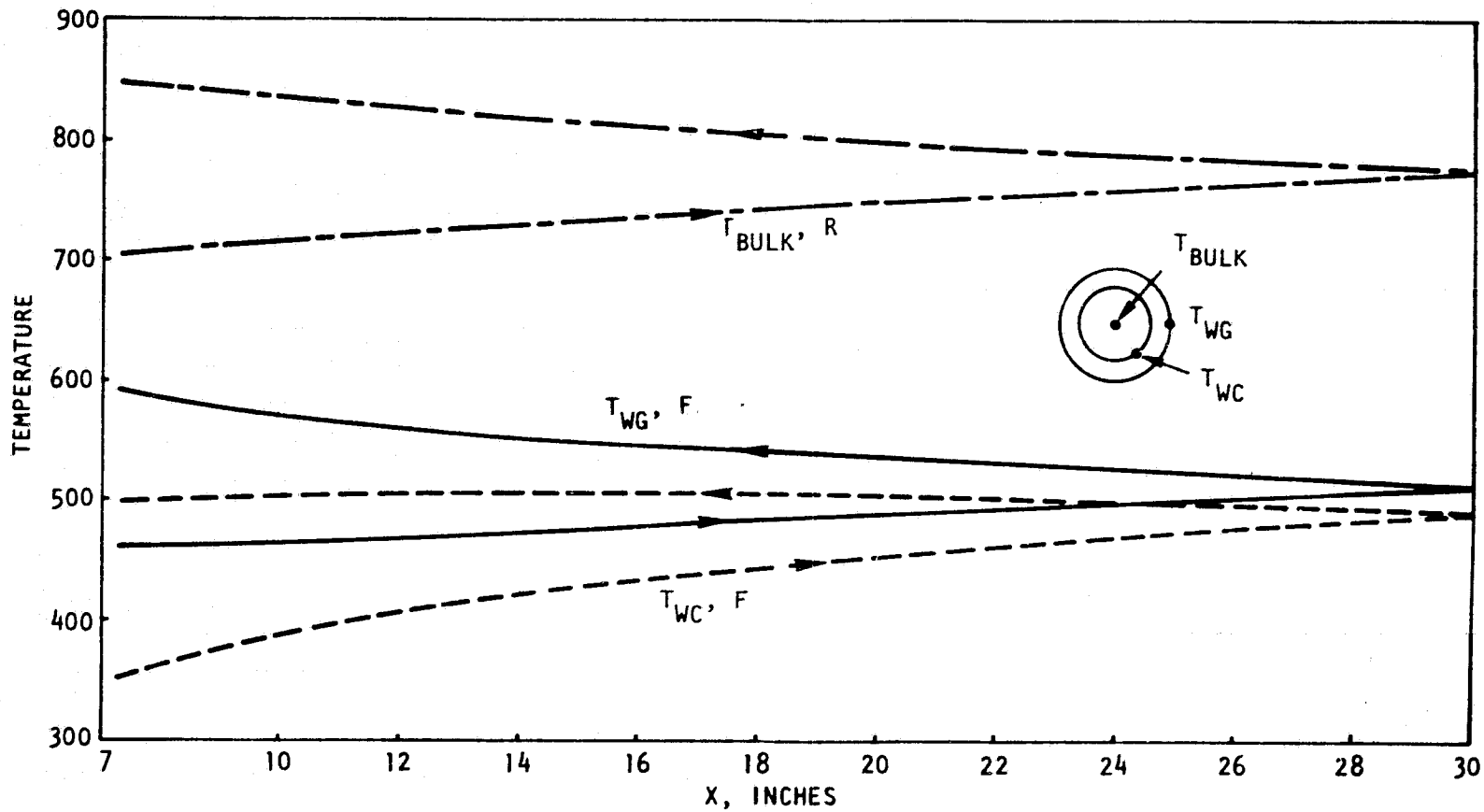

Figure 2-37. Advanced Expander Cycle Nozzle Tube Temperature Profiles

A summary of total heat load and the respective combustor and nozzle contributions are shown in Table 2-18 for the 1-3/4 pass nozzle. The combustor represents approximately 74% of the total heat load and the nozzle 26% of the heat load value. The heat load values were obtained using hot-gas heat transfer coefficients correlated to test data of configurations such as the 40K chamber, the ASE, and SSME combustors and nozzle hardware. The heat loads in Table 2-18 are sufficient to attain a chamber pressure of 1540 PSIA with the aid of a turbine gas regenerator.

TABLE 2-18. ADVANCED EXPANDER CYCLE THRUST CHAMBER, 1-3/4 PASS NOZZLE PARAMETERS, F = 15K THRUST, P_c = 1540 PSIA

PARAMETERS	COMBUSTOR	NOZZLE TRANSITION	NOZZLE	TOTAL
ΣQ, BTU/SEC	7414	458	2090	9962
ΔP, PSI	344	22	20	386
ΔT, R	464	32	145	641
$T_{wg_{MAX}}$, F	878	381	593	--
$N_{f_{MIN}}$,	1365	27966	12201	--
$\dot{w}_c$, LBM/SEC	4.09	4.09	4.09	--
ε	INJ-14	14-34	34-225	--
N	96	180	180/180	--
PASSES	1 UP	1 DOWN	1-3/4 DOWN -UP	--

A similar summary of total heat loads and combustor and nozzle breakdowns is presented in Table 2-19 for the 1-1/2 pass nozzle. Total heat loads are nearly identical between the two nozzle types. Attainable chamber pressure for the 1-3/4 pass nozzle is also 1540 PSIA.

TABLE 2-19. ADVANCED EXPANDER CYCLE THRUST CHAMBER PARAMETERS, F = 15K THRUST, P_c = 1540 PSIA 1 1/2 PASS CIRCUIT

PARAMETERS	COMBUSTOR	NOZZLE	TOTAL
ΣQ, BTU/SEC	7414	2494	9908
ΔP, PSI	344	24	368
ΔT, R	464	175	639
$T_{wg_{MAX}}$, F	878	718	--
$N_{f_{MIN}}$,	1365	9930	--
$\dot{w}_c$, LBM/SEC	4.09	4.09	--
ε	INJ-14	14-225-95	--
N	96	280/280	--
PASSES	1 UP	1 DOWN 1/2 UP	--

NOZZLE FLOW ANALYSIS AND WALL CONTOUR SELECTION

The initial step in Rocketdyne's nozzle wall contour design is to perform an analysis of the transonic flow in the region of the combustion chamber throat. Since the highest heat flux levels in the thrust chamber occur in the region of the throat, the throat geometry is generally selected to minimize surface area and enhance cooling in this region. This geometry is defined by a radius upstream and downstream of the throat. The transonic flowfield is primarily a function of the wall radius upstream of the throat (Figure 2-38) and the gas properties.

Rocketdyne computer program (9R-323) was developed to define this portion of the flow. Given the upstream wall radius, throat radius, and specific heat ratio (γ), this code computes the flow properties in the region extending from Mach No. 0.8 to 1.2. The program approximates the parabolic partial difference equations for transonic flow using a 33-term power series expansion, the coefficients of which are computed using an iterative numerical method.

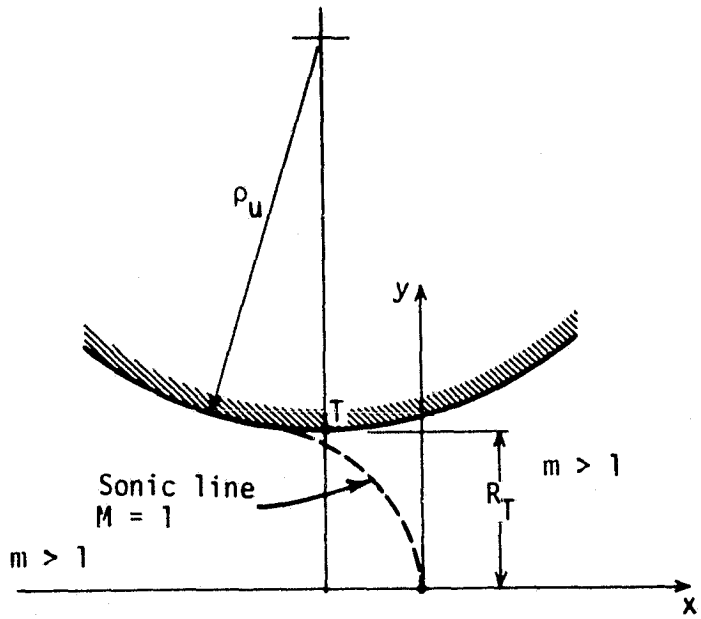

Figure 2-38. Throat Geometry for Transonic Flow Analysis

The program computes and prints iso-Mach lines including the sonic line and streamlines in the transonic region, as well as a right characteristic line from the wall at the geometric throat to the nozzle centerline to serve as starting conditions for supersonic calculations.

Due to the finite radius of wall curvature upstream of the throat, the flow at the geometric throat is nonuniform, resulting in a discharge coefficient less than unity. The potential flow discharge coefficient, C_D, is determined by computing the mass flow across the right characteristic from the vertex of the

throat of the nozzle to the exit and comparing this mass flow to the one-dimensional value.

The transonic flowfield for the Advanced Expander Cycle thrust chamber is shown in Figure 2-39. The gas accelerates to a Mach number of 0.38 in this region. This design produces a rapid expansion through the throat and minimizes wall area in the highest heat flux region of the nozzle.

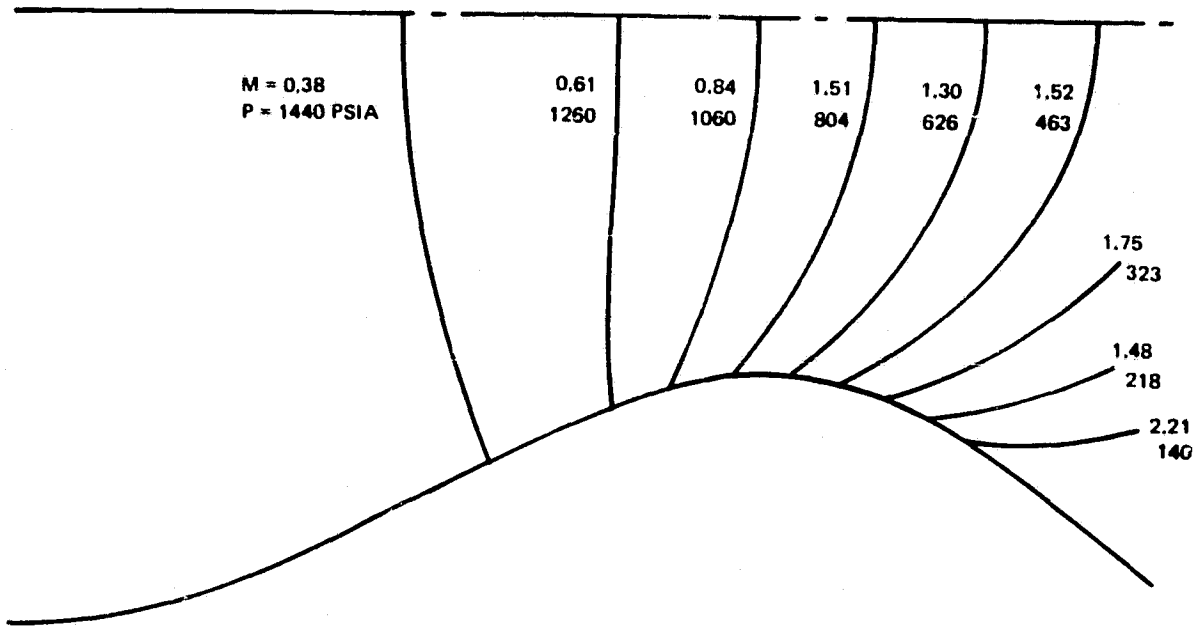

Figure 2-39. Transonic Flowfield Solution for Advanced Expander Cycle

Supersonic Contour Design

Several techniques are available for the design and analysis of the supersonic portion of the nozzle. These include the ideal nozzle, the optimum thrust nozzle (Rao nozzle), and the canted parabolic nozzle. Each of these nozzles has its advantages for specific applications and are readily analyzed using similar analysis techniques. Optimum thrust nozzles and canted parabolic nozzles were considered for the design.

Optimum Thrust Nozzle. The nozzle contour that will produce maximum thrust for selected values of nozzle length can be generated with the aid of Rocketdyne's Rocket Nozzle Design computer program (9R-313). The program is based on the theory presented by G. V. R. Rao in Ref. 2-5. Using the calculus of variations, the flow parameters at the nozzle exit that produce maximum thrust are obtained:

$$V \frac{\cos(\theta - \alpha)}{\cos \alpha} = \text{Constant},$$

where V, θ, and α are the velocity, flow direction, and Mach angle along the last left Mach line, e-f, in the nozzle flow (Figure 2-40). The changes in velocity and flow direction along the left Mach line must satisfy the following differential equation:

$$d\theta - \frac{dV}{V} \cos \alpha + \frac{\sin \alpha \sin \theta}{\sin(\theta - \alpha)} \frac{dR}{R} = 0$$

where R is the radial coordinate of the point along e-f.

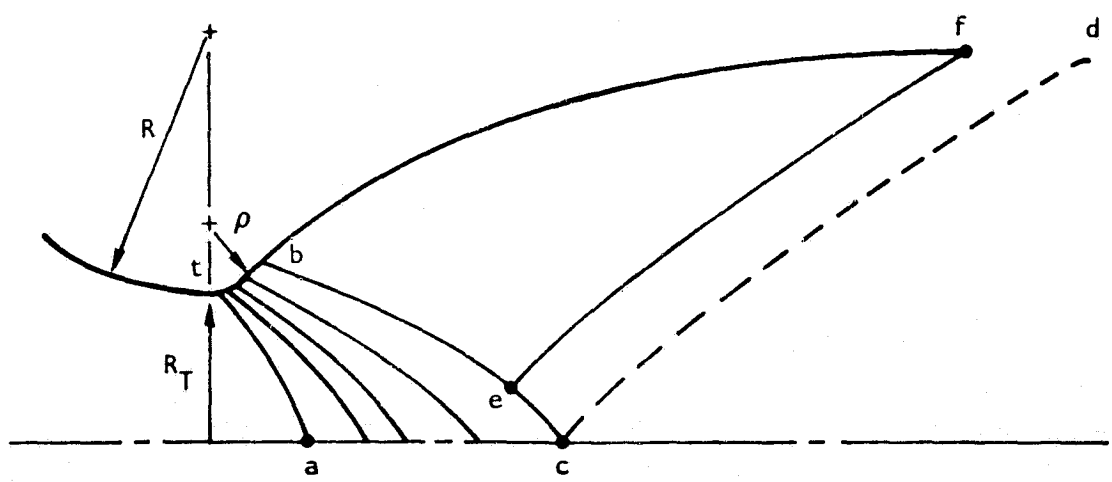

Figure 2-40. Nozzle Design Method

Starting from point e, the line e-f and the flow parameters along the line can be described by simultaneous solution of the two preceding equations. The mass

flow crossing line b-e must be equal to the mass flow crossing line e-f. The Method of Characteristics is used to calculate the flow properties within the two lines, b-e and e-f. With the flowfield in this region known, the streamline passing through b and f is known. This streamline forms the optimum contour for the given nozzle length.

Parabolic Nozzle. Rocketdyne's parabolic nozzle design code 9R-105 generates a canted parabola with performance nearly equal to a similar optimum thrust nozzle. The downstream radius ratio ρ_d/R_T, the maximum expansion angle, θ_{max}, the wall exit angle, θ_e, the area ratio ε, and the nozzle length are specified.

The maximum wall angle and exit angle are based on parametric solutions of the optimum nozzle design code. The nozzle is then analyzed using a method of characteristics analysis program. This design procedure is used to generate nozzle contours which are shorter for a specified area ratio than those that can be generated using the optimum thrust method.

Nozzle Contour Selection

An extensive parametric study of high area ratio nozzles was made to determine the optimum area ratio and nozzle contour for the expander thrust chamber. Both the nozzle design procedures discussed previously were used to develop a wide range of nozzles for study. Typical performance results in terms of area ratio versus specific impulse and OTV payload are shown in Figures 2-41 and 2-42. In these studies, performance was determined as a function of nozzle area ratio, length, and contour. The effects of divergence losses, kinetic losses, and boundary layer drag were included. The drag losses were particularly important for the high area ratio nozzles considered for the OTV. As shown in Figure 2-41, nozzles with area ratios from 600 to 800 produce maximum specific impulse for the OTV with 15K thrust. The effects of nozzle weight as a function of area ratio and length on the total system performance were also considered and, as indicated in Figure 2-42, an area ratio of 625 results in near maximum payload. As a result, this nozzle geometry was selected

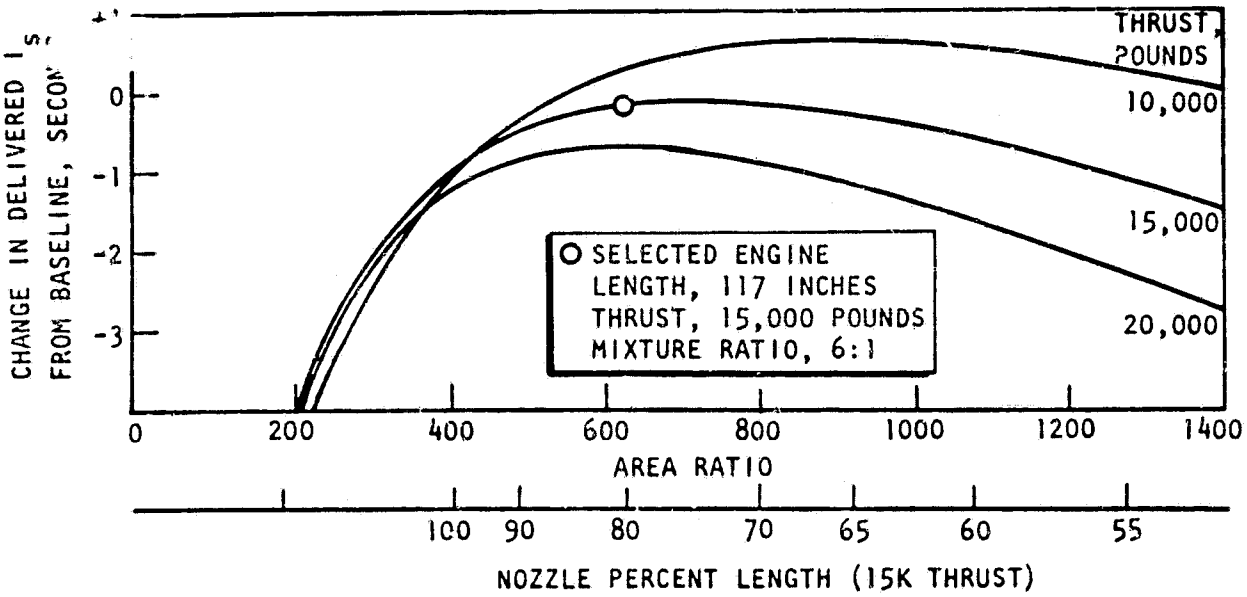

Figure 2-41. Advanced Cycle Engine Specific Impulse vs Area Ratio

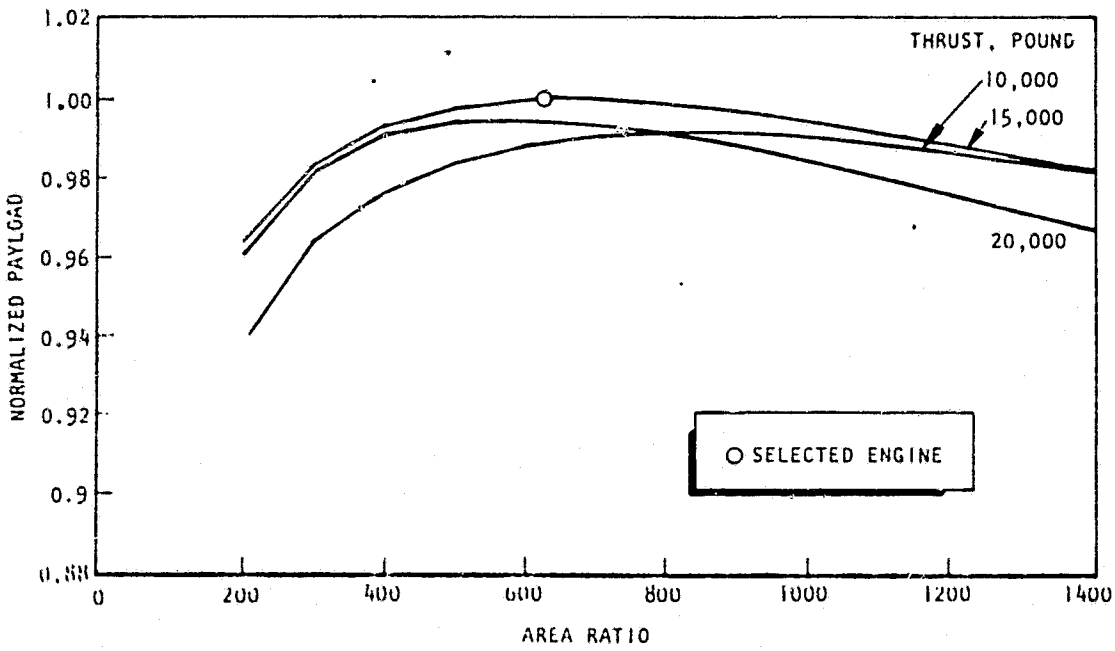

Figure 2-42. Normalized OTV Payload for 6:1 Mixture Ratio

for detailed analysis and design.

The selected $\epsilon = 625$ nozzle, was 79.40 percent length nozzle (based on an equivalent 15-degree 1/2-angle cone); this percent length met the overall length constraints of the engine. Since this is a relatively short nozzle, the parabolic design procedure was used to determine the contour. Optimum values of the maximum (θ_m) and exit (θ_a) wall angles were determined by evaluating a range of parabolic contours with the selected area ratio of 625 and percent length of 79.4. Results of this optimization are shown in Table 2-20 . The different nozzle contours evaluated are defined in Table 2-20 by the nozzle exit angle and maximum wall angle. The parabolic wall contour with $\theta_m = 46$ and $\theta_a = 7.2$ was selected for the thrust chamber nozzle. After examining data scatter inherent in the analysis (Table 2-20), the maximum wall angle and exit angle conditions were selected as representative of the highest nozzle thrust coefficient and nozzle efficiency.

This contour (shown in Figure 2-43) produces near maximum payload within OTV constraints. The wall radius ratio ρ_u/R_T, upstream of the throat is 1.0, and ρ_d/R_T, downstream of the throat is 0.4. These radius values provide a small wall area in the transonic flow region and are the same as those used for the Rocketdyne ASE and SSME designs.

TABLE 2-20. PERFORMANCE OF PARABOLIC NOZZLE CONTOURS FOR FIXED LENGTH AND AREA RATIO

%L = 79.4 ε = 625

EXIT ANGLE, DEGREES	MAXIMUM WALL ANGLE, DEGREES	EFFICIENCY	THRUST COEFFICIENT
5	44	0.989492	2.078926
6	48	0.989739	2.079444
	46	0.989798	2.079568
	44	0.989945	2.079878
	42	0.989863	2.079671
	40	0.989846	2.079636
6.8	45	0.990031	2.080058
7.2*	49	0.989803	2.079814
	48	0.989798	2.079802
	47	0.989824	2.079856
	46	0.990198	2.080619
*	45	0.990112	2.080497
	44	0.990007	2.080277
7.35	46	0.990081	2.080058
7.5	46	0.989931	2.079806
7.8	46	0.990036	2.080130
8.15	46	0.990024	2.080043
8.5	48	0.990149	2.080305
	46	0.990277	2.080575
	44	0.989984	2.079961
8.75	46	0.989921	2.079828
10	46	0.989378	2.078686
12	46	0.987729	2.075222
14	46	0.984357	2.068137

*HIGHEST THRUST CONTOUR

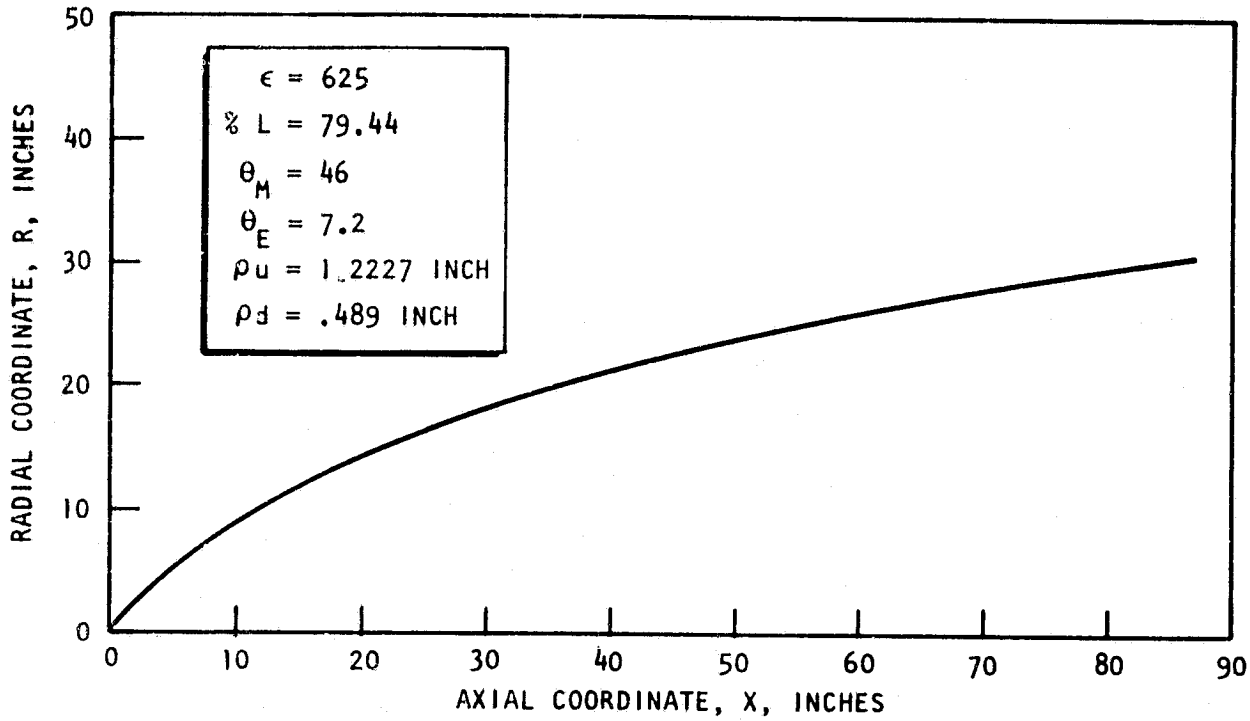

Figure 2-43. Expander Nozzle Contour

EXTENDIBLE NOZZLE DESIGN

The dump cooled, tube wall extendible nozzle selected for the OTV Point Design extends from an expansion ratio of $\varepsilon =$ 225:1 to $\varepsilon =$ 625:1 (Figure 2-44). The upstream end of the nozzle is designed to interface with the extension/retraction transport mechanism and is designed to effect a hot gas seal between the fixed and extendible nozzle when extended. The nozzle construction consists of 1080 thin wall (.005 t) 347 CRES tubes furnaced-brazed to the thin external structural shell. The tube and shell type construction is a proven concept in use on the SSME nozzle. In addition, attachment of the transport mechanism to the upstream end of the extendible nozzle includes an inlet and distribution manifold for the coolant hydrogen. At the exit end of the nozzle, (ε = 625:1), the single pass tubes include a small preformed nozzle through which the heated hydrogen coolant is accelerated and expanded to obtain additional impulse from this propellant without benefit of the combustion process. In that the coolant tube exit nozzle is configured to include a throat of .040 inch diameter. Plugging of the throat by debris is not anticipated to be a problem. If system contamination is found to present a nozzle plugging problem during testing, a filter will be included in the propellant supply line immediately downstream of the extendible nozzle coolant shutoff valve. This filter will be sized to trap all particles which could possibly plug the coolant exit nozzles.

An external thin wall shell provides the basic structure around which the extendible nozzle is constructed. This shell is formed from thin wall sheets which are butt-welded and then hydroformed to the appropriate contour. Prior to forming, the shell is butt-welded to the coolant inlet and distribution manifold. Assembly of the nozzle tube bundle consists of stacking the 1080 individual tubes into the shell structure, which doubles as the braze tooling fixture, installing the vacuum braze tooling, and vacuum-furnace-brazing the tubes to the external shell. The full length jacket provides a hot gas seal, so that there is no requirement to effect a perfect tube-to-tube braze. Instead, only a tube-to-jacket braze is necessary, eliminating the likelihood of expensive rebraze cycles.

X	Y RAD	TUBE OD	TUBE WALL t
30.000	18.339	—	—
35.187	20.077	.1171	.0045
38.949	21.215	.1238	↑
43.090	22.373	.1305	
47.679	23.553	.1374	
52.739	24.740	.1443	
58.397	25.497	.1514	
64.585	27.139	.1583	
71.546	28.340	.1653	
79.290	29.522	.1722	↓
86.996	30.560	.1783	.0045

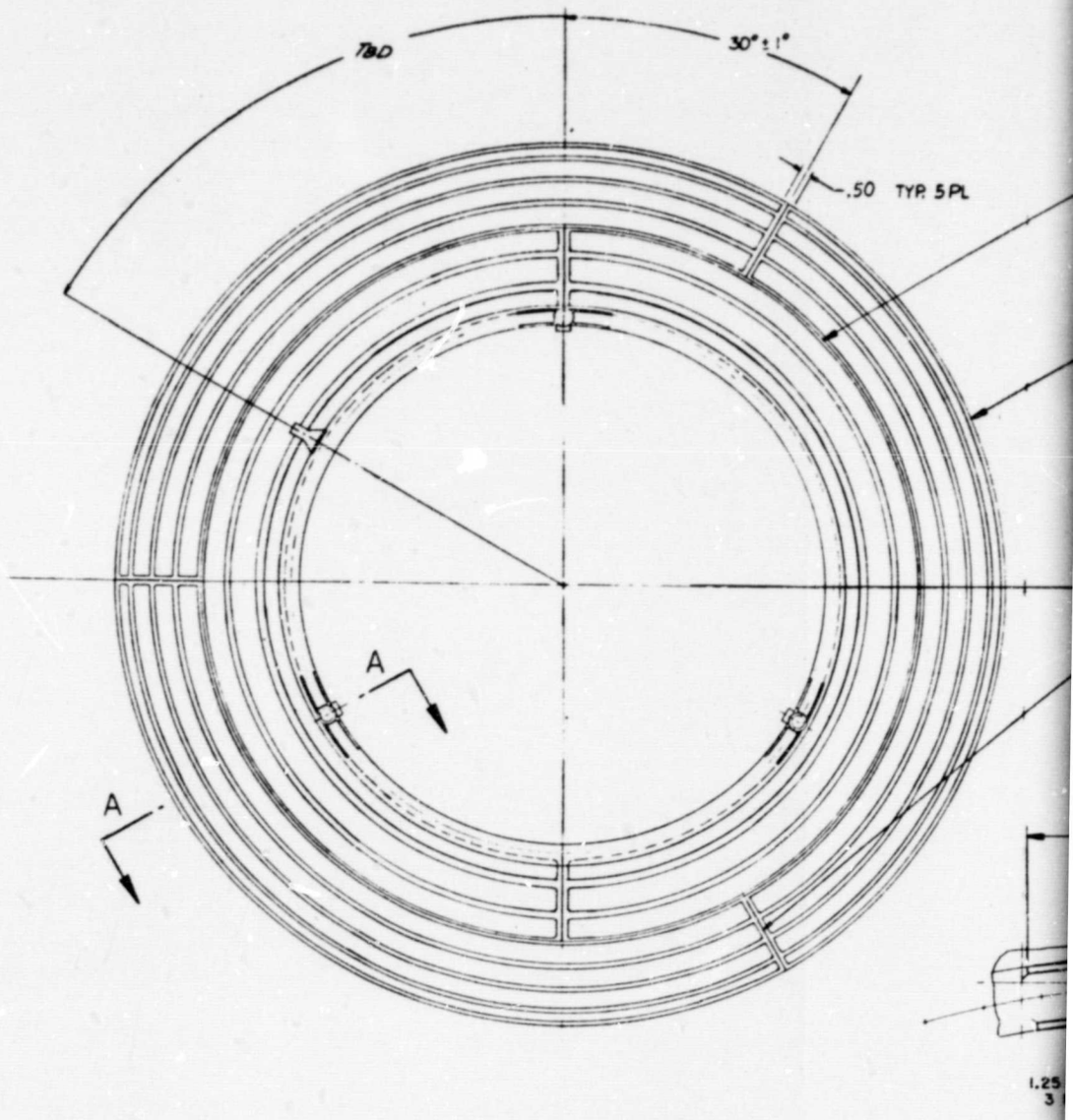

FOLDOUT FRAME

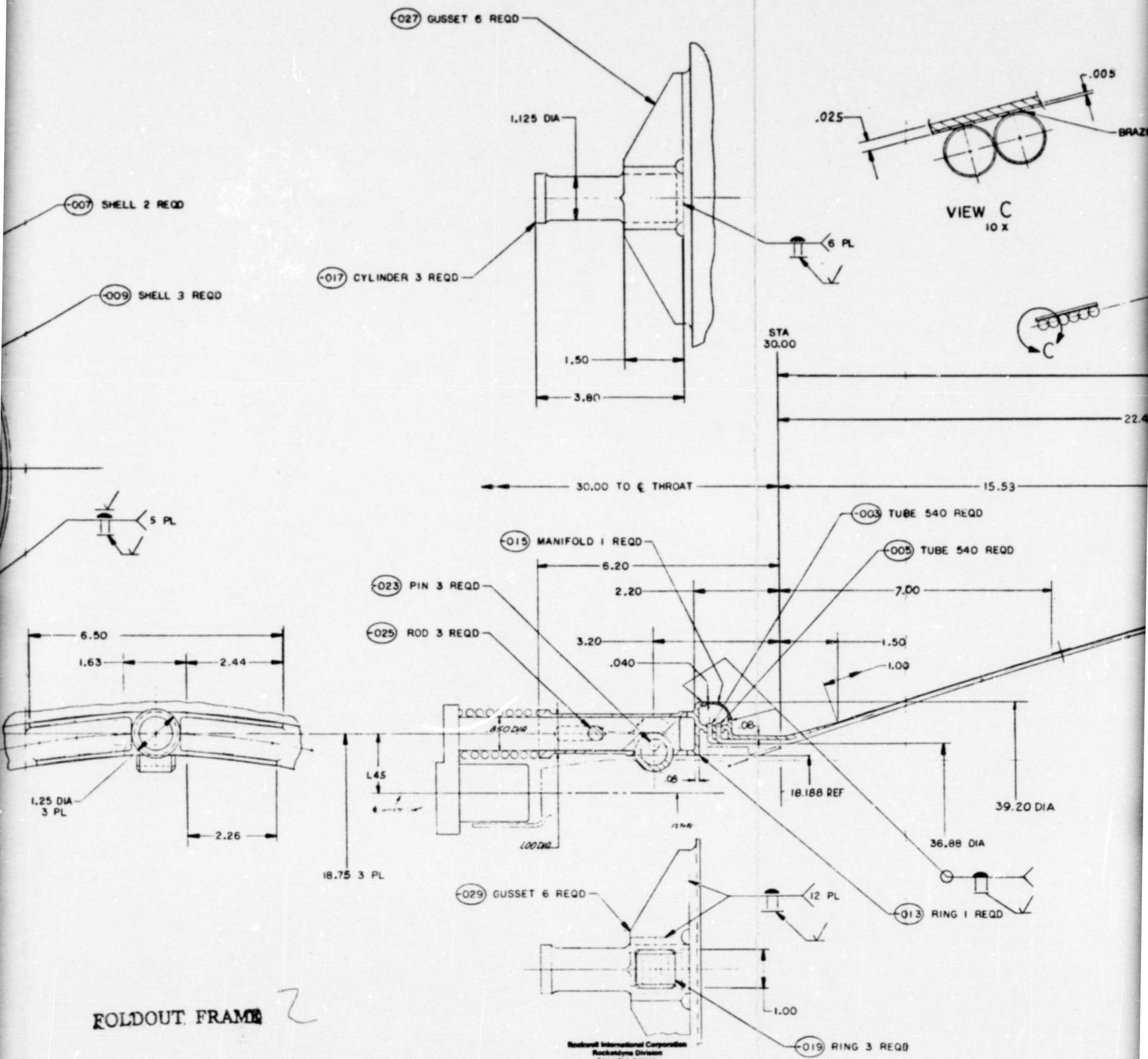

FOLDOUT FRAME 2

Rockwell International Corporation
Rocketdyne Division
Canoga Park, California

FSCM NO 02697	FRAME 1		
7R001485		SH	REV

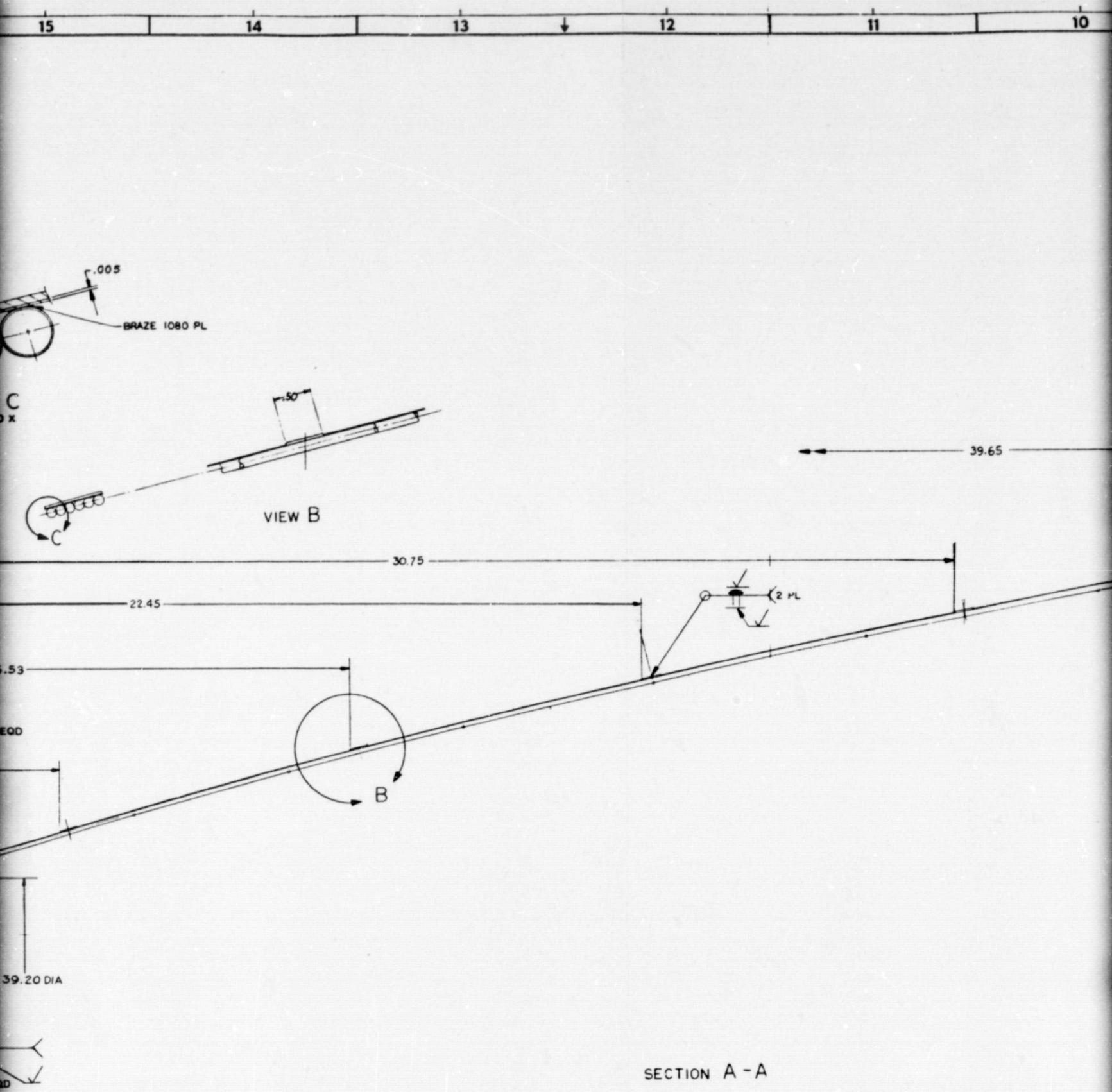

FOLDOUT FRAME 3

• MICROFILM OVERLAP AREA •

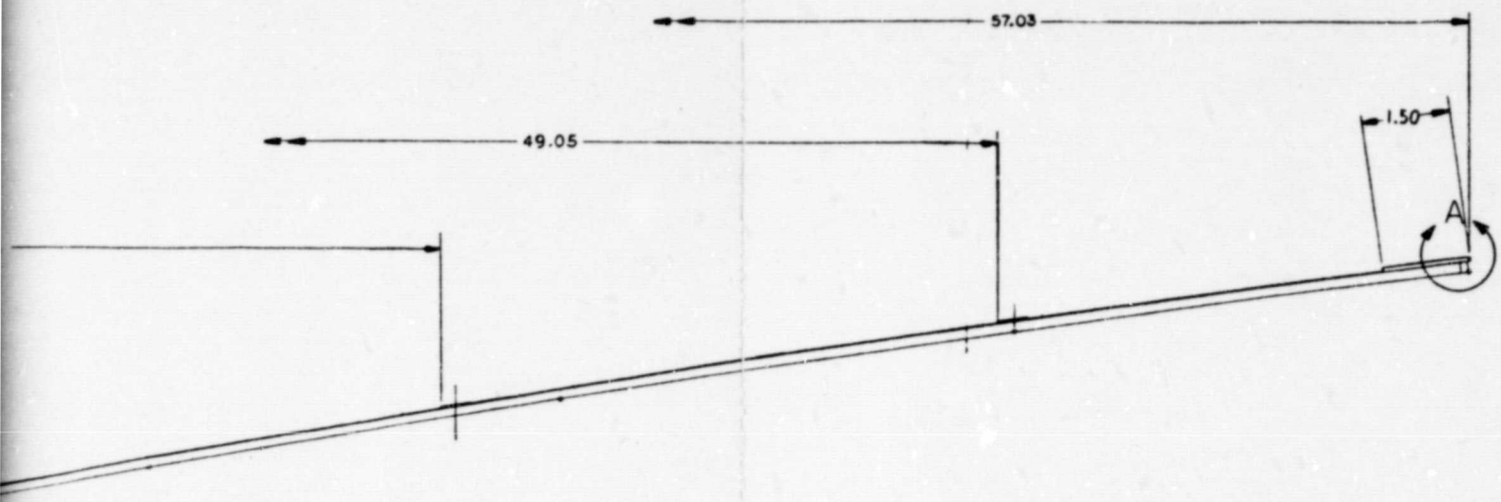

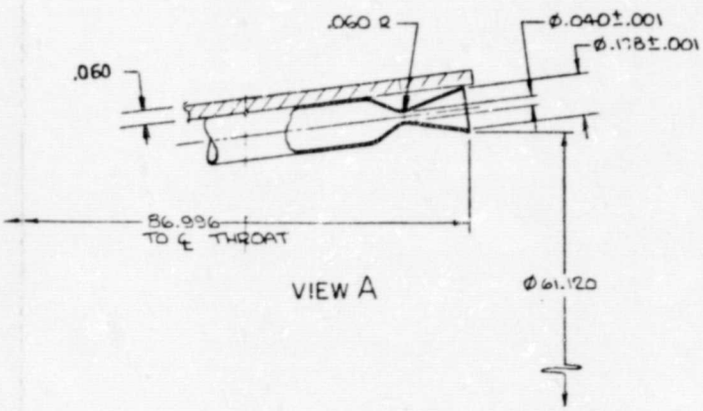

VIEW A

FOLDOUT FRAME 4

Rockwell International Corporation
Rocketdyne Division
Canoga Park, California

PSCN NO 67667	FRAME 2		
7R001485		SH	REV

• MICROFILM OVERLAP AREA •

FOLDOUT FRAME 5

Figure 2-44

FOR INFORMATION

RI/RD80-218-2

2-91

1. ALL MATL 347 ST ST

NOTE: UNLESS OTHERWISE SPECIFIED

Rockwell International Corporation
Rocketdyne Division
Canoga Park, California

NOZZLE, ASSY OF - OTV EXTENDABLE

SIZE J | FSCM NO 02602 | DWG NO 7R001485

SCALE 1/4 | SHEET

Dump-Cooled Nozzle Thermal Analysis

Based on the consideration of the 60-inch retracted length and the nozzle area ratio (625) and length (87 inches) chosen for high performance, the dump-cooled extendible nozzle would begin at an area ratio of 225 and terminate at the ε = 625 point. The thermal design is based on minimization of the coolant flow to provide both a maximum fluid temperature and thrust of the dumped flow and to minimize the shift in main chamber mixture ratio. The dump coolant flow required 0.36 lb/sec.

The design is based on a tubular nozzle design which has 1080 CRES tubes of 0.0045-inch wall thickness. The tube bundle (alone) weight is only 36.7 lbs. The wall thickness is held constant and the design has a circular tube construction all along the dump-cooled nozzle length.

Coolant flow enters in a downpass from the ε = 225 inlet and traverses to the exit. The inlet temperature and pressure are 38.5R and 35 psia, respectively. Coolant temperature rise is 2036R and the pressure drop is small at 4.1 psi, resulting in a maximum pressure (31 psia) for the dump element thrust component. Maximum surface wall temperature occurs at the nozzle exit at 1616F on a one-dimensional basis.

Tube stress levels (645 psi) are very low due to small tube pressures and small diameters, and tube fatigue life should be good due to the closeness of the fluid bulk and wall temperature along the length. The effect of transient heating of the outside hatband structure is outlined in a subsequent section on stress.

An alternate dump-cooled nozzle coolant supply pressure of 74 psia was also considered. Table 2-21 presents a comparison of the pertinent dump-cooled nozzle parameters for the two pressures considered for the engine point design configuration.

TABLE 2-21

ADVANCED EXPANDER CYCLE ENGINE POINT DESIGN

DUMP-COOLED NOZZLE PARAMETERS

$F = 15K\ lb_f$

$P_c = 1540$ psia

P_{in}, psia	35.0	73.8
P_{out}, psia	30.9	72.1
ΔP, psi	4.1	1.7
T_{in}, °R	38.6	38.6
T_{out}, °R	2074.5	1968.2
ΔT, °R	2035.9	1929.6
TWG_{max}, °R	1617	1665
$\dot{W}_c$, lbm/sec	0.36	0.36
ΣQ, Btu/sec	2555	2418
$N_f min$	11369	4328

A parametric analysis of a dump-cooled extension nozzle was conducted. The parameters varied were the coolant flowrate from 0.10 to 0.25 lb/sec, tube wall thickness from 0.0045 to 0.0065-inch, and the number of tubes from 600 to 2,000. Figure 2-45 presents the results of varying flowrates and number of tubes for a tube wall thickness of 0.0045-inch. Figures 2-46 and 2-47 present the results for tube wall thicknesses of 0.005 and 0.0065-inch, respectively. In general, for a given tube wall thickness, the heat flow to the tubes and the coolant flow pressure drop increases as the number of tubes and the coolant flowrate increases. The coolant outlet bulk temperature drops with increasing coolant flowrate and rises as the number of tubes increase, whereas the hot gas wall maximum temperature decreases with both increasing coolant flowrate and number of tubes.

Increasing the tube wall thickness will cause moderate changes in the design factors. It increases the heat flux to the coolant, the coolant flow pressure drop and the coolant outlet bulk temperature, and decreases the hot gas wall maximum temperature. The total tube weight decreases with increasing number of tubes and increases as the tube wall thickness is increased. The coolant flowrate has no effect on the total tube weight.

Nozzle Flow Balance. Consideration has been given to the flow, temperature rise and pressure imbalance in the circumferential direction which could occur as a result of non-uniform heating caused by non-uniform single-tube flow conditions. For the dump-nozzle, the nozzle supply pressure at 35 psia is reduced only slightly by the cooling. The total pressure loss is, consequently, taken by the dump-cooled nozzlette assembly at the exit.

In a scenario where the individual tube heating is higher, the added heat load will raise the wall temperature and bulk temperature simultaneously. The rise in bulk temperature will increase the flow resistance in the nozzlette throat, resulting in a successive further starvation of the tube and higher bulk temperature.

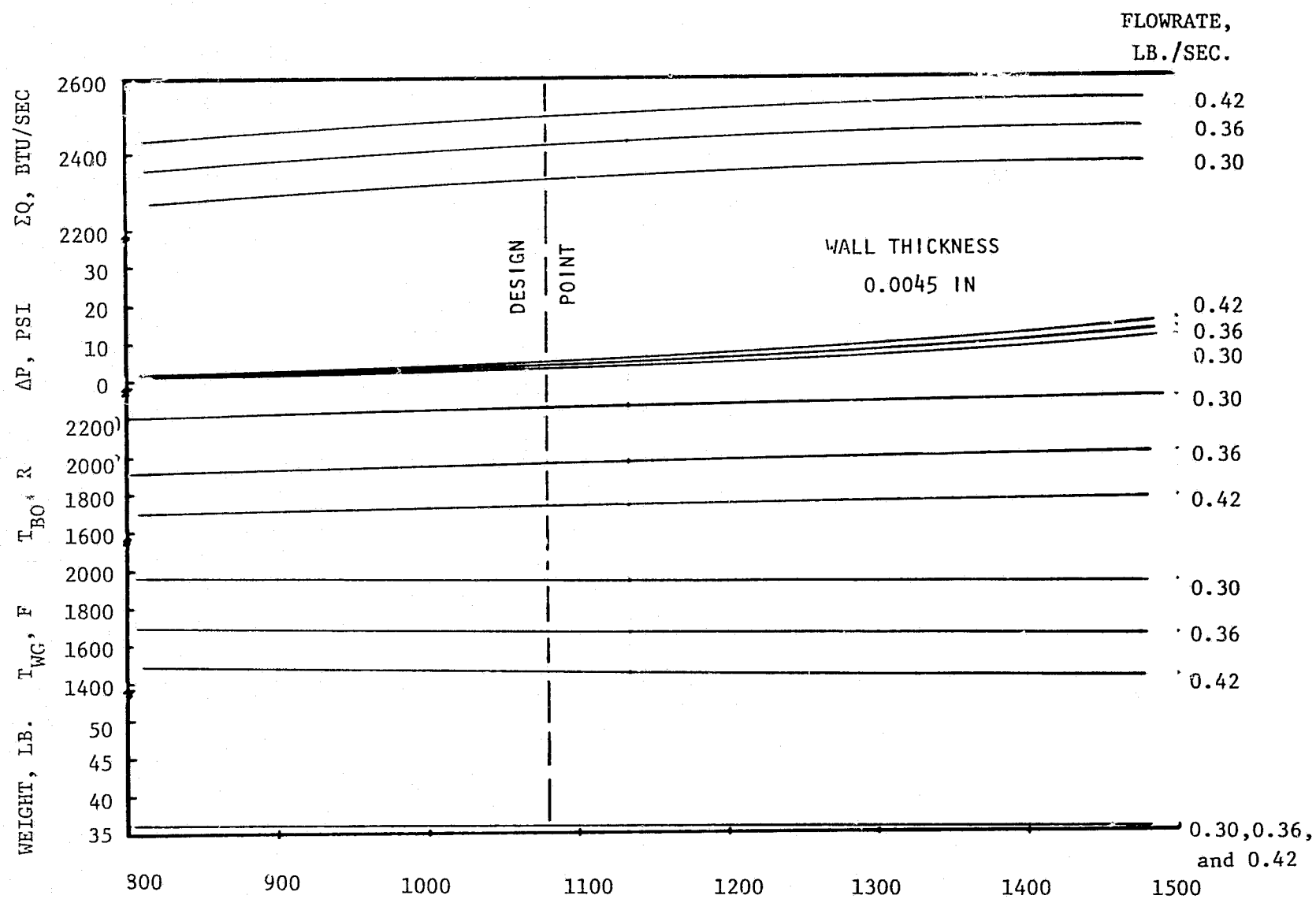

Figure 2-45. Expander Thrust Chamber Dump-Cooled Nozzle Parametrics, Wall Thickness, 0.0045 In.

C-3

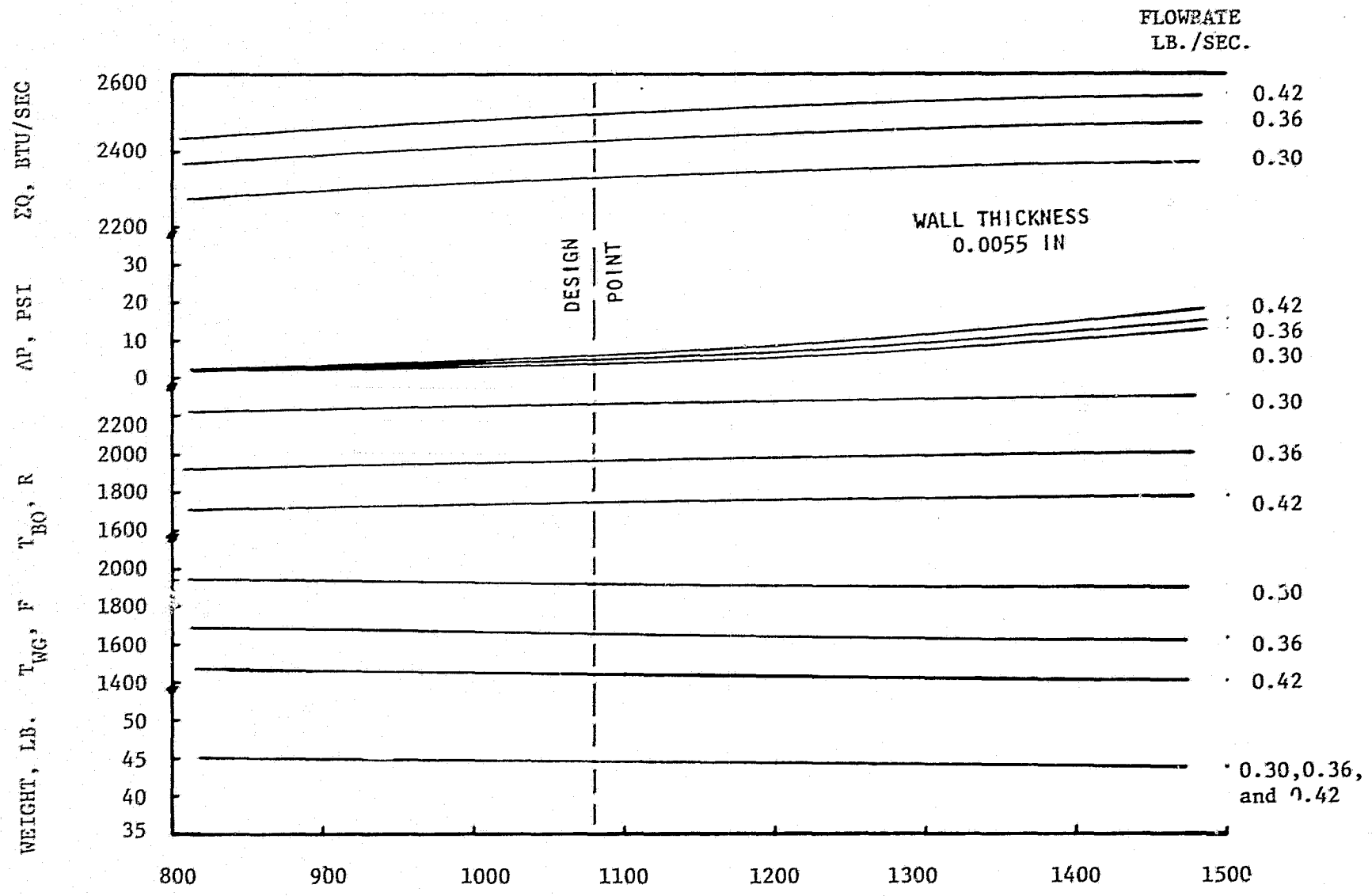

Figure 2-46. Expander Cycle Thrust Chamber Dump-Cooled Nozzle Parametrics
Wall Thickness, 0.0055 In.

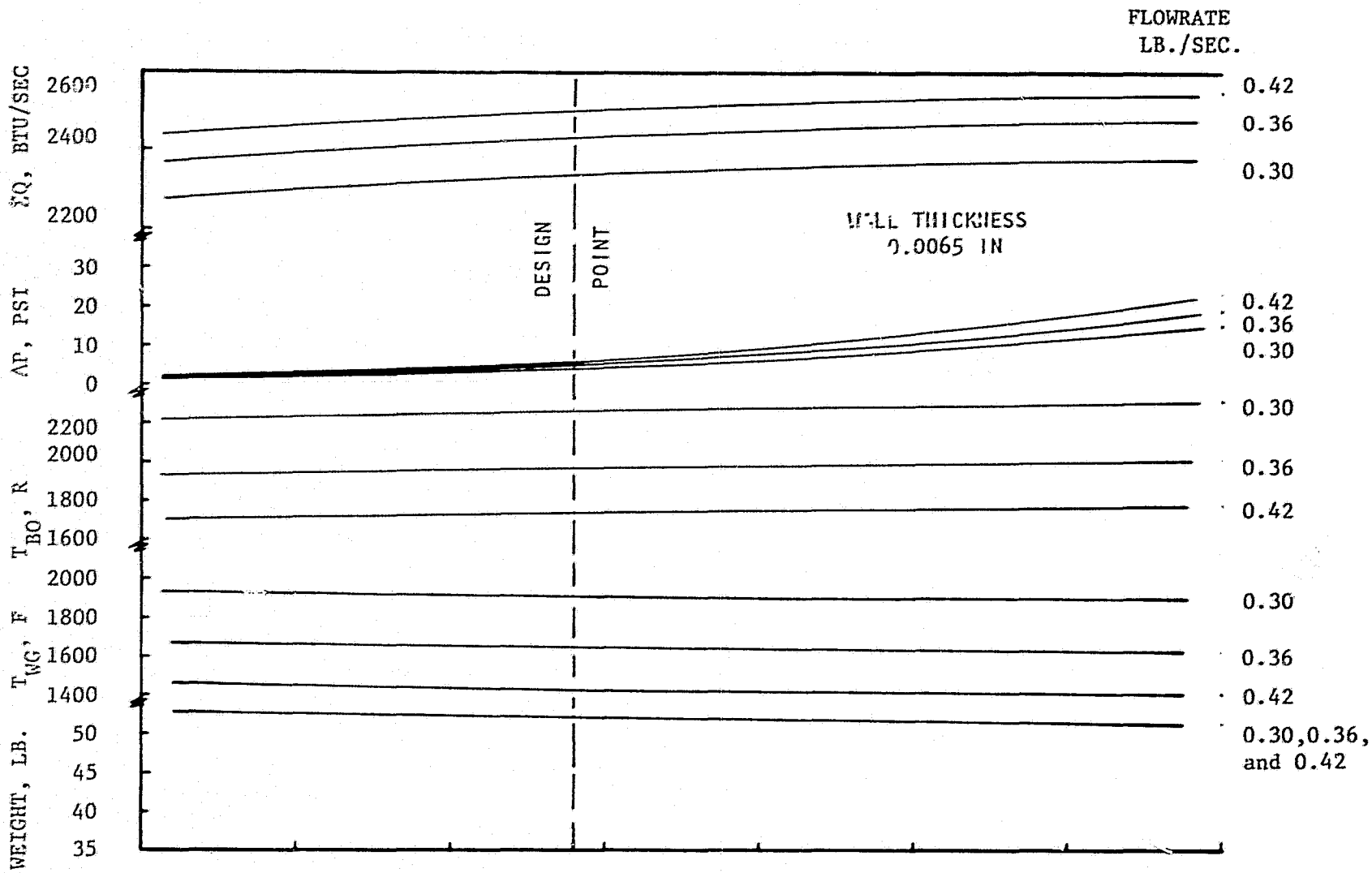

Figure 2-47. Expander Cycle Thrust Chamber Dump-Cooled Nozzle Parametrics, Wall Thickness, 0.0065 In.

The limiting effects are the tube re-radiation at the higher wall temperature and the reduced driving temperature between the gas and the wall. Methods of eliminating this parallel resistance imbalance on the OTV dump-cooled nozzle are as follows:

1. Uniform injector heat flux pattern.
2. Communicative tube exit flows.
3. Oversupply of coolant flow.
4. Controlled emissivity tube surfaces (inside and outside).

Single nozzles installed in each tube as indicated in Figure 2-44a are relatively simple and inexpensive to manufacture, and have been selected for the initial design. However, potential problems with coolant tube flow distribution result. If one tube has a smaller coolant flowrate, the temperature rise in the tube becomes greater and the higher temperature further reduces the flowrate through the choked nozzle at the tube exit. The end result of this potentiality could be a burned out tube. One method of eliminating this potential problem is to have the tubes exhaust to a single nozzle supply manifold. The manifold can then feed a series of small nozzles or a single annular nozzle.

Dump Nozzle Drag and Heat Retention. Heat lost to the dump-cooled nozzle wall is traded with the added friction on the wall. If the heat is rejected to the environment without accruing thrust, then the drag loss of successively higher area ratios will cause a partial negation of the added inviscid thrust. Consequently, any radiation nozzle designs would be the lowest performing unless running at nearly adiabatic gas temperature. The Rocketdyne approaches used to minimize the drag loss and heat loss to the nozzle are the following:

1. Low surface ripple factor - small diameter tubes, nearly flat surface (to submerge ripple well into boundary layer).

2. High surface wall temperatures - minimization of coolant flow, low drag, and nozzlette high specific impulse values.

3. **Internal and external plating of the aft 60% of the dump nozzle surface to reduce inner wall and outer wall radiation by a factor of 15.**

Alternate Dump Nozzle Wall Construction Approaches

The basic tubular nozzle offers the lightest total tube weight since the gage limit of 0.0045-inch would be used. Since the tubes are not directly manifolded into an upper end ring, individual tolerances are not critical (i.e., 1082 or 1078 tubes would be an acceptable design).

Alternate nozzle constructions would appear not to compete with the tubular nozzle because of one or more of the following reasons:

- Weight
- Unproven history of manufacturing technology
- Weld seam failure mode
- Thermal stress limitations

Some of the dump cooled nozzle design concepts considered for the base point design can be seen in Figure 2-45.

Alternate Extendible Nozzle Concepts

Three different nozzle construction techniques offered reasonable methods of obtaining the desired contour within reasonable cost, weight, and developmental risks. These configurations are presented briefly below and are discussed in terms of their state-of-the-art, service life, manufacturing and handling, safety and reliability, cost, maintainability and weight.

Regeneratively Cooled Nozzle Extension. An alternative method to low pressure dump cooling of the nozzle extension is the use of the cold high-pressure pump discharge H_2 flow in a circuit where the cooling flow is recovered to the main

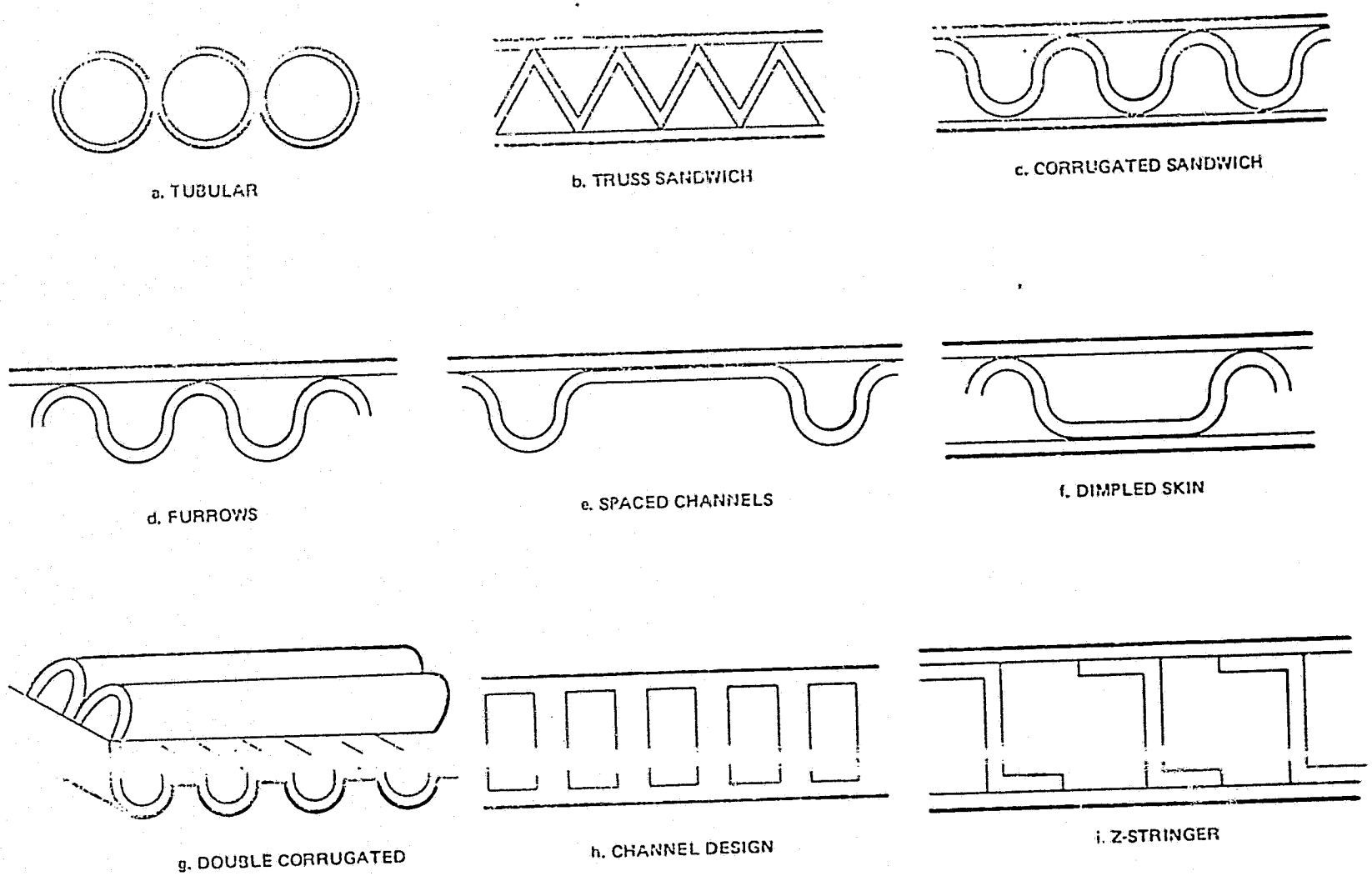

Figure 2-45. Examples of Dump-Cooled Nozzle Wall Design Concept Considered

propellant flow system and burns with the rest of the fuel coolant system, providing a more optimum performance combustion chamber mixture ratio. The principal disadvantage of the regeneratively cooled retractible nozzle has been the requirement of the extendible high-pressure inlet and return lines for the coolant flow.

The heat transferred to the coolant in the regenerative cycle represents a significant additional energy fraction (20%) to the turbine drive cycle. This can translate directly to a higher pressure, higher area ratio design of higher specific impulse performance.

Current techniques of construction would be utilized. The nozzle walls could be constructed from thin wall nickel tubing swaged to the appropriate cross-section and brazed together to form the exit nozzle. The tubing temperature would be maintained at acceptable limits through use of a double pass cooling loop. That is, hydrogen enters the tube pack through an inlet manifold and travels aft through alternating tubes to a collection manifold located at the nozzle exit. This exit manifold provides for redistribution of the collected cooling hydrogen to the alternate "up" tubes. After passage of the hydrogen through the "up" tubes, it is collected again in a manifold and then ducted into the engine system for use in driving the pump turbines.

Carbon-Carbon Nozzle. This nozzle configuration is an adaptation of a common nozzle construction technique taken from solid propellant rocket engines. In that solid propellant engines did not have a cooling propellant, materials have been developed which can withstand the extreme environment of a rocket engine exhaust gas stream. The nozzle envisioned for the OTV application consists of a thin wall carbon-carbon shell contoured to the appropriate dimensions with additional structure attached to the upstream diameter. This structure would provide the necessary ruggedness required of the unit as well as providing attachment points for the extension/retraction transport mechanism.

State-of-the-Art. Comparison of the three separate construction techniques

considered indicate the following variations in state-of-the-art. The tube wall unit (both regeneratively and dump cooled designs) is currently in use on most liquid rocket engines built within the last 25 years. This configuration can be manufactured in-house. The carbon-carbon refractory nozzle is currently used on solid rocket motors such as MX, OMS, and Minuteman. This technology dates back 7-10 years. For OTV application, the carbon-carbon nozzle must operate in a high temperature steam atmosphere, where it will be subject to erosion and conversion to methane and other products. Surface diffused coatings are required to reduce rates of erosion. This constitutes advanced technology.

Service Life. A service life comparison of three construction techniques was prepared for engine mixture ratios of 6 and 7. In that there is real data for the tube wall construction technique and only estimates of the remainder, the comparisons are quite subjective. However, at MR of 6, the tube wall units have an estimated life of 16 hours, while the carbon-carbon unit should be unlimited if the oxidation protection is effective in the H_2/O_2 hot gas environment. At MR 7, the estimated life of a tube wall unit is reduced to 10 hours while the carbon-carbon unit life is unaffected.

Manufacturing and Handling. The manufacturing process for a tube wall nozzle consists of properly bundling varying cross-section swaged tubes and brazing the assembly to form a rigid structure integral with the manifolds and reinforcing members. The special handling and tooling techniques are well developed at Rocketdyne and there is little process risk as this type of manufacture is now practiced.

The carbon-carbon configuration is a composite material made from charred rayon fabric with deposited carbon filler. This process is also a current one, although it is one which must be procured from a specialty house. The finished unit is a sturdy one and would require no handling procedures other than normal ones used for such a high value item.

Safety and Reliability. The three nozzle construction techniques considered

present significant differences in likely failure modes. The tube wall risks include tube cracks and a possible loss of coolant supply without shutoff provision and the resulting LOX rich shutdown.

The major safety threat to the carbon-carbon configuration is the risk of oxidation. It is believed that overall a carbon-carbon design would offer the most simple design and the maximum reliability.

Cost to Manufacture. Because the different configurations require significant variations in recurring and non-recurring costs, a reasonable production run should be considered to distribute the recurring cost. If 20 units are considered, the preliminary figures indicate that if even only one is to be built, the carbon-carbon unit is the least expensive. The savings increase as production volume increases.

Maintainability. In that extensive experience exists with only the tube-wall concept, evaluation of maintainability is of necessity favorable to that concept. The common tube split type failure is known to be repairable by reforming the split and brazing a saddle patch in place, or by removing the damaged tube half and replacing it with a new section. Maintenance procedures for the remaining configurations have not yet been developed.

Weight Comparisons. The estimated weights of the configurations vary from 65 to 95 pounds; the lightest being the carbon-carbon unit, while the honeycomb and radiation-cooled nozzles are expected to weigh nearly 95 pounds. Tube wall configurations are expected to weigh approximately 85 pounds.

Recommended Configuration. Because of the overwhelming advantage of the carbon-carbon nozzle in every area except the unknown risk of oxidation, it presents a strong argument to be selected as the recommended configuration. However, in that the OTV Point Design is to be based upon 1980 state-of-the-art, and because there remains significant unknowns that require developmental effort, the carbon-carbon configuration must be passed over in favor of the more

conventional tube wall techniques. It becomes apparent, however, that this developmental work to establish material compatibility data, life cycle data, and fabrication parameters will be a high priority task for liquid rocket engine technology during the near future.

The dump cooled tube wall nozzle was selected over the regeneratively cooled tube wall nozzle because it offers a performance advantage at reduced weight and overall engine complexity. The dump cooled nozzle operates at lower pressures, thereby permitting utilization of an extremely thin wall design. Additionally, the dump cooled nozzle eliminates the system complexity required to handle the coolant outflow in a regeneratively cooled design.

TURBOMACHINERY DESIGN AND PERFORMANCE (TASKS 2 AND 3)

The preliminary sizing and conceptual designs which were generated during the expander cycle turbomachinery selection phase were used as the baseline criteria to optimize the design of the individual turbopumps. From this point and after specific engine system operating parameters were updated, a more accurate performance and design analysis was accomplished. Figure 3-1 presents a schematic of the expander cycle engine system which governed the analysis and design guidelines of the turbopumps. Table 3-1 contains a summary of important features of the selected turbomachinery.

TURBOMACHINERY DESCRIPTION SUMMARY

The LOX boost pump design is an axial flow inducer driven by a Francis-type straight vane radial in-flow hydraulic turbine. The turbine straight vane design was conceived so that the fluid (LOX) entering the turbine at the outside diameter was rotating at the wheel speed, which results in a zero incident angle with the radial blades. The turbine blades are shrouded, front and rear, with bearing coolant flow tapped off at the blade tip area. Bearing coolant flow of about 5 gpm is controlled by a series of labyrinth seals downstream of the front bearing where the coolant is routed back into the boost pump discharge manifold. A duplex set of 55 mm extra light bearings was selected to accommodate the resultant unbalanced axial load toward the inducer.

The front bearing is a 17-mm extra light type. Pump speed of 6475 rpm results in a bearing DN value of 356,125 for the 55-mm set and 110,075 for the 17 mm. No problems are anticipated in achieving the 10-hour-life requirement. The projected weight of the turbopump is approximately 19 pounds and the design concept integrates the discharge housing with the inlet housing of the high pressure pump. This arrangement referred to as the "Tee mount" (Fig. 3-2) provides a lightweight, compact, and

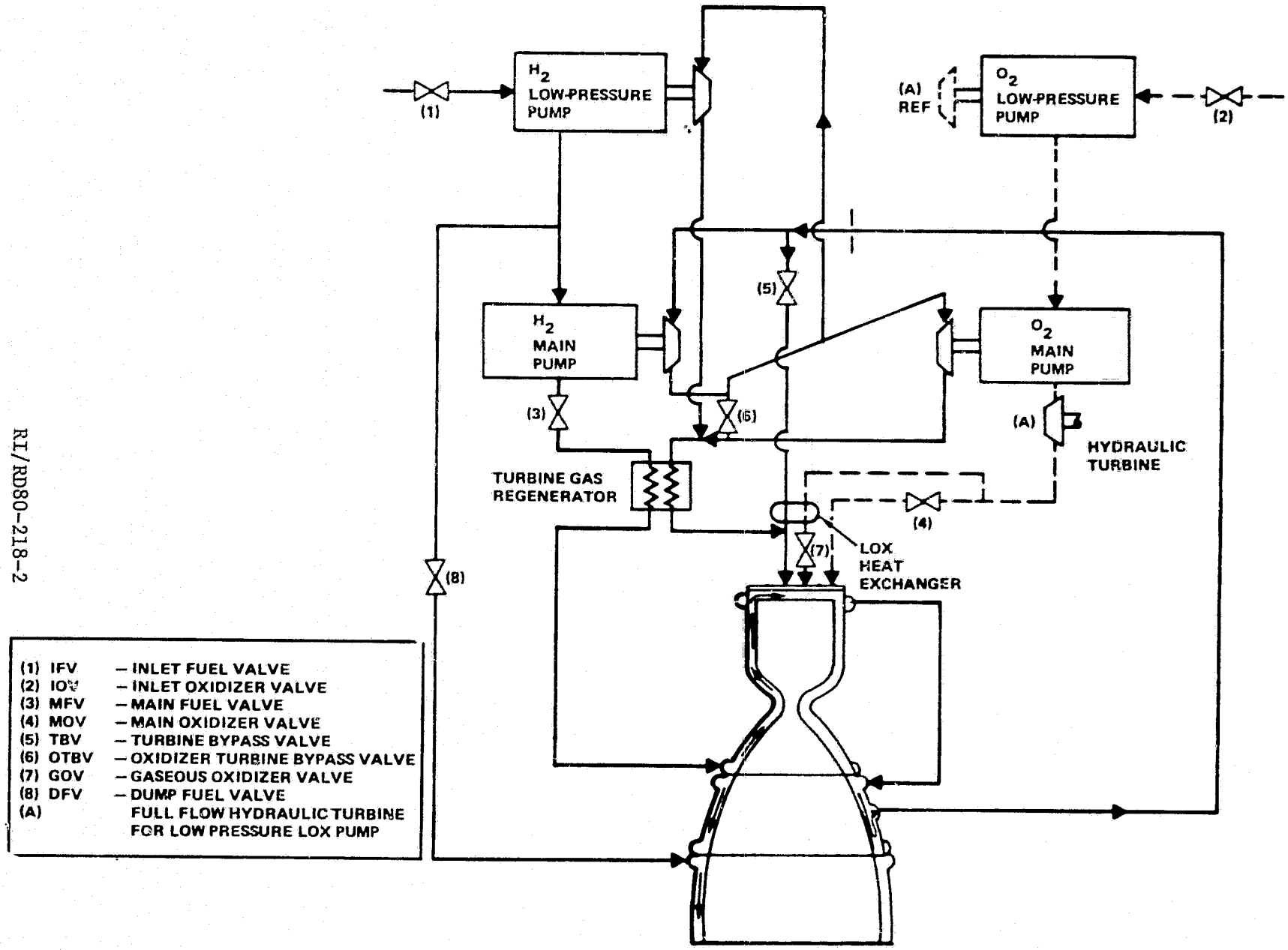

Figure 3-1. Expander Cycle Engine Schematic

TABLE 3-1

EXPANDER CYCLE TURBOMACHINERY DESCRIPTION SUMMARY

System	Turbopump Description	Turbine Description	Speed, rpm	Overall Weight, lb
LOX HP Turbopump	Single-Stage Centrifugal Preceded by Inducer, Direct Turbine Drive	Single-Stage Partial Admission (24.5 percent)	53,000	39.6
LOX LP Turbopump*	Two-Row Axial Inducer, Direct Turbine Drive	Single-Stage Francis Radial In-flow Hydraulic Turbine	6,475	18.8
Fuel HP Turbopump	Three-Stage Centrifugal Preceded by Inducer, Direct Turbine Drive	Two-Stage Partial Admission (33, 41 percent)	110,000	37.3
Fuel LP Turbopump*	Single-Row Axial Inducer, Direct Turbine Drive	Single-Stage Partial Admission (2.4 percent)	28,486	13.8

*"Tee-mounted" to applicable high pressure pump

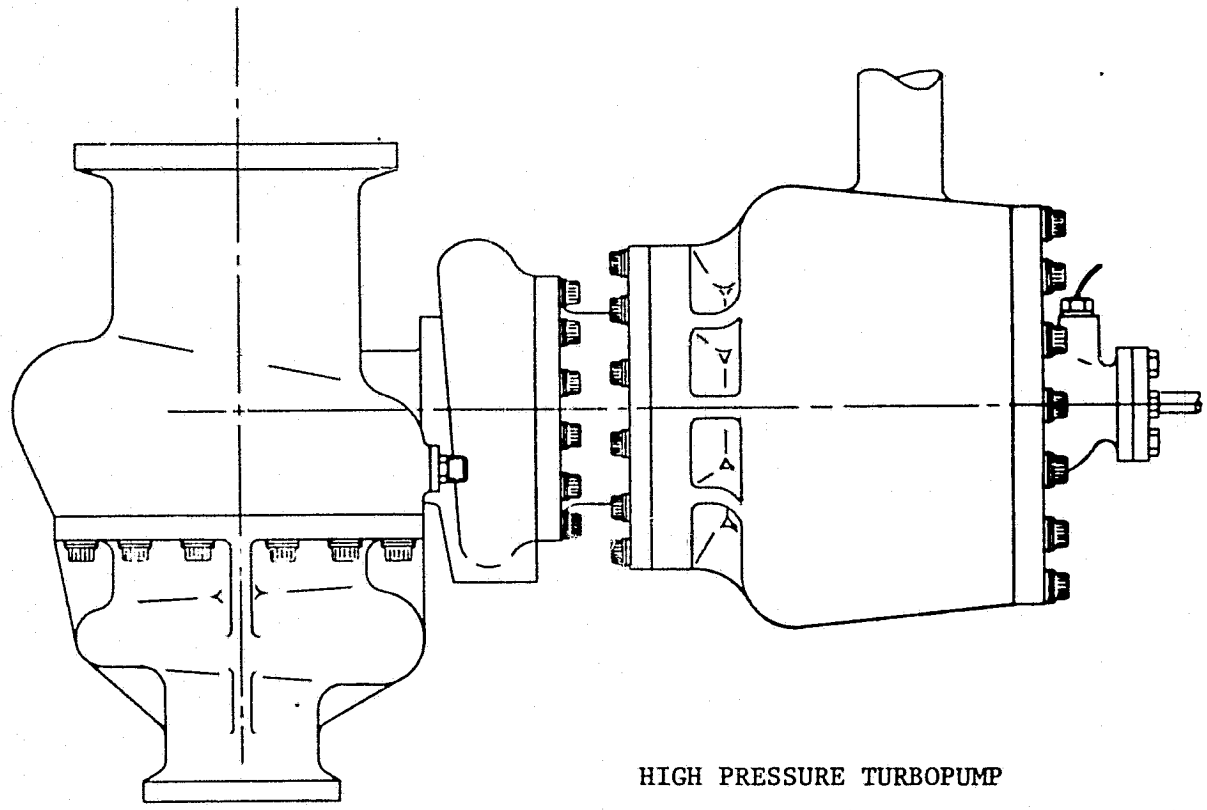

Figure 3-2. Expander Cycle Liquid Oxygen Turbomachinery "T" Mount

high efficiency pump system. The boost pump uses no bipropellant seals, purges, or dumped fluid flow.

The high pressure oxidizer turbopump is a single stage centrifugal pump preceded by an inducer. The pump is driven by a partial admission single stage impulse turbine operating with warm gaseous hydrogen. In all respects, the internal fluid passages and seal packages are identical to the Advanced Space Engine MK48 oxidizer turbopump. Two duplex sets of 20 mm angular contact bearings operate at a bearing DN of about 1.06×10^6. The front bearing set is cooled with liquid oxygen while the rear bearings are cooled with liquid hydrogen. The rear bearing coolant is supplied by the high pressure hydrogen turbopump which is injected into a collector cavity at the turbine end of the LOX turbopump. The hydrogen coolant is routed through the bearing pack, past a controlled gap shaft riding seal and then dumped into the downstream portion of the turbine exhaust nozzle. Three sets of controlled gap duplex interpropellant carbon seals are employed. The main LOX seals are separated from the warm gaseous hydrogen seals by an intermediate seal package. Primary LOX and warm hydrogen seal drain lines dump any leakage overboard, while a helium purge is injected between the intermediate seal pack to provide a protective barrier purge to aid in the separation of the two propellants. Helium purge flow nominally splits equally and is combined to flow overboard with the respective seal drain line. The weight of the turbopump is projected to be about 40 pounds but possible additional weight savings of up to 15 pounds (pump weight 25 pounds) is possible by reducing the bearing spans with detailed analysis. As mentioned earlier, the "Tee-mounted" LOX turbomachinery represents an optimized approach to achieving a compact, lightweight, and highly efficient system.

The hydrogen boost turbopump is an axial flow single stage inducer driven by a partial admission single stage warm gaseous hydrogen impulse turbine. The rotor is supported by two 35-mm bearings operating at a bearing DN of about 997,000. The bearings are cooled with liquid hydrogen supplied at about 2000 psi from the high pressure fuel turbopump. The high pressure hydrogen is collected at an inner chamber and then routed to the bearings at about 5 gpm per bearing. The

front bearing flow is redirected into the boost pump discharge after flowing past two ring controlled gap seals to reduce the pressure. The rear bearing flow is routed through similar shaft-riding controlled gap carbon seals and then into the upstream side of the turbine wheel downstream of the partial admission nozzle. The turbopump is also "Tee-mounted" (Figure 3-3) to the high pressure turbopump providing a compact low weight, and efficient system. The projected weight of the turbopump is about 14 pounds. The fuel boost pump design represents excellent state-of-the-art experience and is expected to meet the 10-hour life requirement with no problems.

The high pressure fuel turbopump is a three-stage centrifugal pump using shrouded impellers preceded by an inducer. Liquid hydrogen is supplied through an axial inlet with a centerbody housing the front duplex set of bearings. The pump discharge flow is routed through a scroll shaped outlet. The rotor is driven by a two-stage partial admission gaseous hydrogen driven turbine. The rotor is supported by two duplex sets of 17 mm bearings cooled with liquid hydrogen at about 5 gpm per bearing set. The bearings are operating at a DN of 1.9×10^6. The bearing housings have been designed with the capability of using the advanced hybrid hydrostatic/ball bearings with either a 17 or 20 mm angular contact ball design. Use of the hybrid hydrostatic/ball bearings will depend on the results of current NASA and Rocketdyne MK48F testing, but appears to have excellent potential for achieving long life at high pump speeds. Pump development could be achieved with the readily available MK48F-designed 20 mm bearings. The turbopump employs many features of the Advanced Space Engine MK48F turbopump, but a major change was incorporated with the use of a two stage partial admission turbine. The turbine design was chosen to achieve a peak efficiency for its stage velocity ratio with the two stages optimized for blade height, diameter, and admission ratio for the expander cycle operation. A "Tee-mounted" design was also used for the hydrogen turbomachinery. The high pressure fuel turbopump weighs about 37 pounds with weight-saving schemes such as flange scalloping and use of lightweight materials employed where possible.

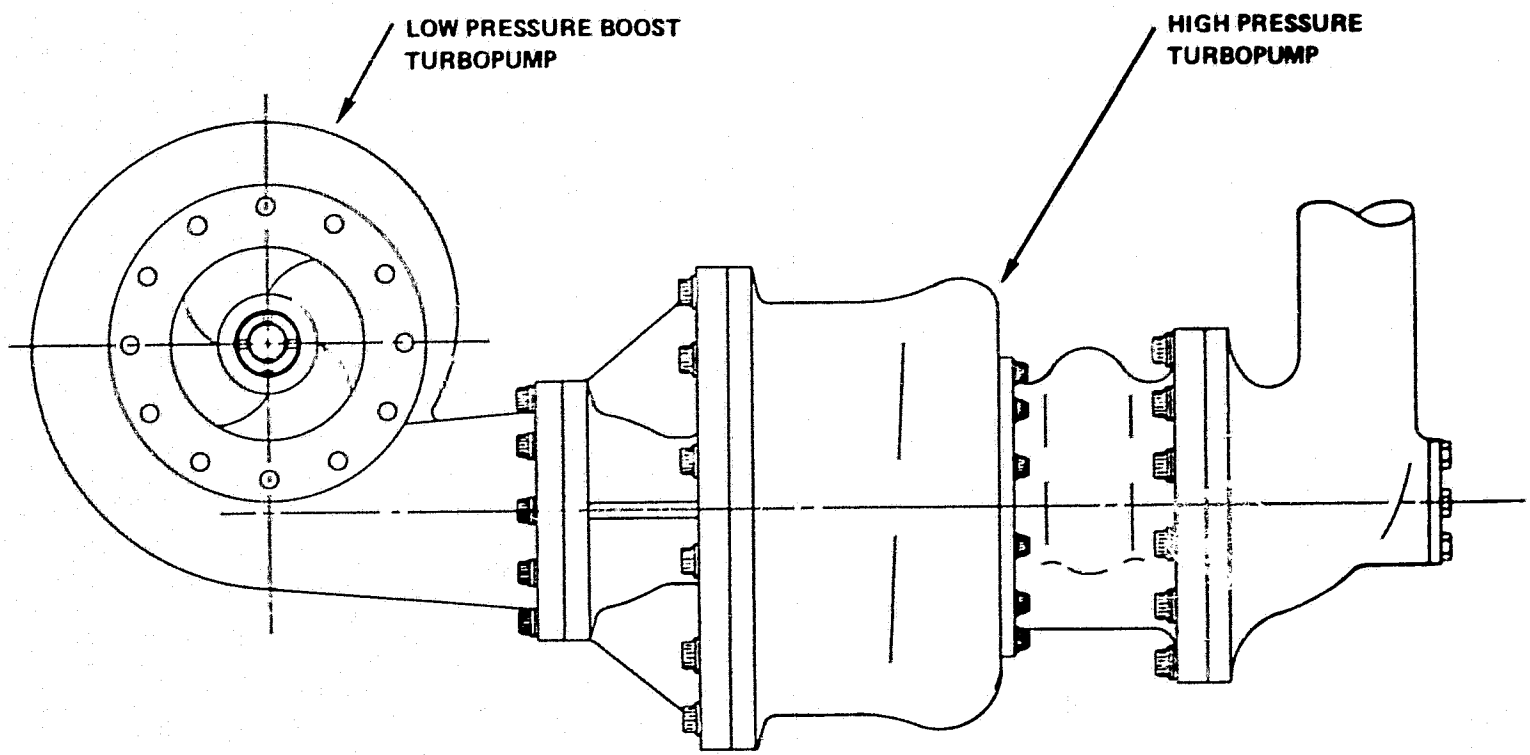

Figure 3-3. Expander Cycle Hydrogen Turbomachinery
"T" Mount

TURBOMACHINERY DESIGN SELECTION SUMMARY

An assessment of viable turbomachinery options was accomplished for both the high and the low (boost) pressure turbopumps to ascertain the most optimized system for the expander cycle engine. Included in the assessment were factors such as performance influences, the degree of development risk, the projected reliability and life of the choice, the state-of-the-art of the design and its impact on actually producing the item, flexibility of the design for improvements derived from empirical test results, and lastly, the likelihood of the performance and operating goals meeting the analytical projections.

Turbomachinery options considered are indicated in Table 3-2, listed in the order in which they were ranked upon completion of assessment studies. Tables 3-3 through 3-5 present a compilation of the major advantages and disadvantages for the various turbopump systems. A discussion of the results of the assessment performed (Tables 3-3 through 3-6) and the rankings obtained for the systems (Table 3-2) follows.

High Pressure Oxygen Turbopump

As shown in Table 3-2, the highest ranking achieved for the high pressure oxygen pump was a modified version of the ASE-designed MK48ϕ. Table 3-3 lists the advantages and disadvantages of the systems considered. The only modification required was a change to reduce the percent of the turbine arc of admission. Otherwise, the hydrodynamic passages fulfill the expander cycle flow requirements. A major factor in eliminating gear driven systems is the inability of pre-set gear ratios to meet all off-design requirements without sacrificing performance by bypassing flow from either high pressure pump. In addition, the ability of gear driven system cooled by either liquid oxygen or liquid hydrogen to meet the life requirement of 10 hours is doubtful. Cryogenically cooled gear drive systems probably will require extensive development effort and the ability of gears to meet long term operational life (10 hours) has not been proven. Thus, only two options ranked high: a new design which can incorporate

TABLE 3-2. PRELIMINARY TURBOMACHINERY SELECTION RANKINGS

High Pressure Fuel	Low Pressure Fuel	High Pressure Lox	Low Pressure Lox
1. MK 48 F (Modified)	1. Gas Turbine	1. MK 48 Ø (Modified)	1. Hydraulic
2. New Design	2. LH_2 Cooled Gears	2. New Design	2. Gas Turbine
3. No Boost Pump	3. Hydraulic	3. Synchro Gear	3. LH_2 Cooled Gears
		4. No Boost Pump	
		5. HPOTP Geared From HPFTP	

TABLE 3-3.

EXPANDER CYCLE HIGH PRESSURE
OXYGEN TURBOPUMP TRADE STUDY

OPTION	PERFORMANCE	DEVELOPMENT RISK	LIFE AND RELIABILITY	TECHNICAL FEASIBILITY	DEVELOPMENT FEASIBILITY	ANALYTICAL CORRELATION
NEW DESIGN • NEW PUMP • NEW TURBINE • BOOST PUMP	• LIKELY TO HAVE HIGHEST PUMP EFFI-	• ANALYSIS BASED ON ASE EXPERIENCE AND LIKELY TO BE COMPARABLE	• NEW HARDWARE • NOT DEMONSTRATED • LIKELY TO MEET ASE GOAL OR BETTER	• LOW WEIGHT • MINIMUM IMPACT ON SYSTEM • TYPE OF BOOST PUMP WILL INFLUENCE DESIGN • MODERATE COST	• STATE-OF-THE-ART, NO NEW PROBLEM ANTICIPATED	• NOT DEMONSTRATED, NEW DESIGN • PROBABLY WILL MATCH BASED ON UPDATED ASE RESULTS
MK-488 (MODIFIED) • INCREASED TURBINE ARE OF ADMISSION • BOOST PUMP	• PUMP PERFORMANCE MEETS EXPANDER CYCLE REQUIREMENT	• EXISTING HARDWARE • TEST DATA BASE	• DESIGN CHANGE DOES NOT AFFECT LIFE • RELIABILITY BASE ESTABLISHED	• BOOST PUMP DRIVE MAY REQUIRE REDESIGN • MINIMUM IMPACT ON SYSTEM • MINIMUM COST	• PROVEN CONCEPT • STATE-OF-THE-ART • MINOR MODIFICATION IN DESIGN CONCEPT	• DEMONSTRATED PERFORMANCE • CONFIDENT DESIGN
HPOTP GEARED FROM HPFTP	• PRECISE SPEED AND POWER RATIOS • LIMITED MIXTURE RATIO EXCURSIONS	• INDEPENDENT PUMP DEVELOPMENT DIFFICULT • MIXTURE RATIO EXCURSIONS REQUIRE ADDITIONAL CONTROL COMPLEXITY	• PITCH LINE VELOCITY LIMITED • NO DIRECT EXPERIENCE • LIFE CAPABILITY DOUBTFUL • BI PROPELLANT SEAL PACKAGE	• POOR MAINTAINABILITY • MODERATE COST	• SYSTEM DESIGN STATE-OF-THE-ART BUT DEMONSTRATION OF LONG LIFE AND PACKAGING UNTRIED	• ACTUAL POWER RATIO INFLUENCE AND BALANCE UNCERTAIN • PUMP PERFORMANCE PROBABLY WILL MATCH BASED ON ASE RESULTS • NOT DEMONSTRATED
SYNCHRO GEAR (HPOTP TO HPFTP) • SERIES TURBINES	• PRECISE SPEED AND POWER RATIOS • LIMITED MIXTURE RATIO EXCURSIONS	• INDEPENDENT PUMP DEVELOPMENT DIFFICULT • MIXTURE RATIO EXCURSIONS REQUIRES ADDITIONAL CONTROL COMPLEXITY	• LOW PITCH LINE VELOCITIES WITH IDLER GEAR • LIFE CAPABILITY DOUBTFUL • BI PROPELLANT SEAL PACKAGE	• SYNCHRO GEAR INFLUENCES NEEDS ANALYSIS • POOR MAINTAINABILITY • POOR PACKAGING FLEXIBILITY • MODERATE COST	• SEAL PACKAGE AND INDEPENDENT PERFORMANCE TESTING, DIFFICULT TO DEVELOP	• SYNCHRO GEAR INFLUENCE ON PERFORMANCE NOT DEMONSTRATED • PUMP PERFORMANCE PROBABLY WILL MATCH BASED ON ASE RESULTS
NO BOOST PUMP (NEW DESIGN)	• LOWER PERFORMANCE DUE TO LOWER SPEED	• LOWER SPEED SOURCES RISK	• EXISTING ROTATING PARTS, SEALS, BEARINGS DESIGN SHOULD MEET LIFE • LOWER SPEED ENHANCES DESIGN-TO-LIFE	• LOWER SPEED • LARGER AND HEAVIER • LIMITED PACKAGING FLEXIBILITY • MODERATE COST	• ACHIEVING THE MINIMUM NPSH MAY BE DIFFICULT AND REQUIRE EXTENSIVE TESTING	• NOT DEMONSTRATED, NEW DESIGN

optimized features empirically derived from related test experience, or the modified (turbine) MK48Ø which provides proven design concepts with minimum expected design iterations.

Additional parametric studies were then accomplished to evaluate the performance sensitivity of these choices to the type of boost pump drive, weight, size, NPSH requirement, shaft torque versus shaft (bearing) size, bearing DN, and the expected bearing cryogenic fatigue life. Included in the study was the use of an alternate and passive (no rotating parts) jet boost pump. Fig. 3-4 presents the results of the parametric study conducted on the high pressure oxidizer pump. The jet pump was eliminated as a possible boost pump due to its low performance and higher required NPSH. Certain critical observations of the oxidizer pump parametric studies are evident in Figure 3-4.

1. Pump speed and selected boost pump drive option affects efficiency.

   a. Recirculating hydraulic hub turbine efficiency maximum of 66 percent at 60,000 rpm

   b. Full flow Francis-type hydraulic turbine efficiency maximum of 70 percent at 75,000 rpm

2. Francis hydraulic turbine used with the MK48Ø turbopump results in a two-percentage point penalty over a new design because of the projected speed. No hydrodynamic changes would be required in a new pump in which the MK48Ø hydrodynamic concept was used.

3. Higher speeds result in lower weight, larger impeller tip widths (machineable)but increase required NPSH.

4. MK48Ø 20-mm bearings are projected to have longer cryogenic fatigue life over the 15 or 17-mm bearings up to about 82,000 rpm.

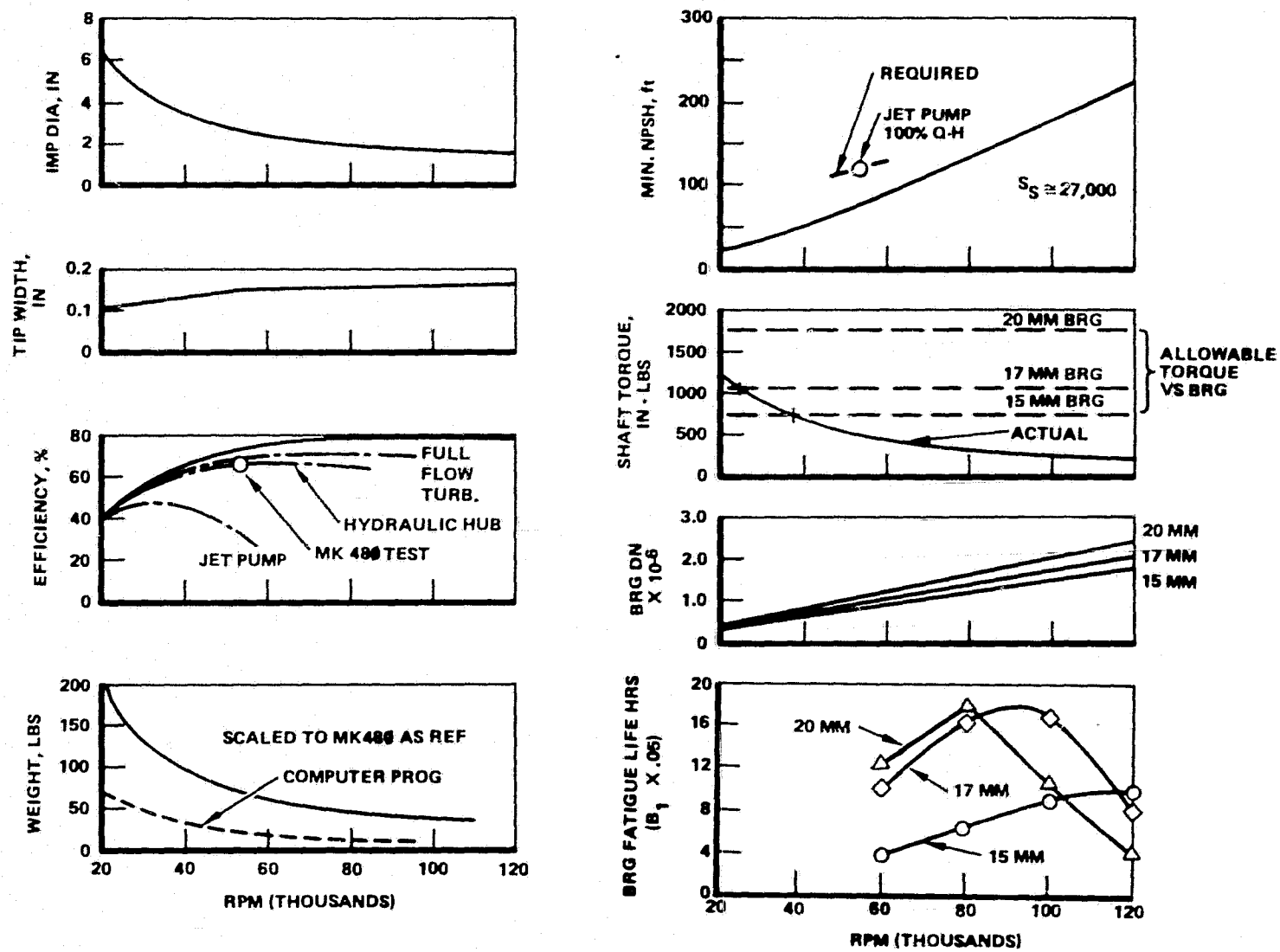

Figure 3-4. Expander Cycle LOX Pump Study

Thus, the most optimized high pressure oxidizer turbopump for the expander cycle is a combination of the MK48Ø hydrodynamic design concept with a smaller overall envelope to reduce weight. The smaller envelope satisfies the minimum weight penalty requirement yet accommodates the new arc of admission design. The inlet and discharge volutes can be designed as an integral package with the low pressure oxidizer (boost) pump to provide a compact, lightweight system.

High Pressure Fuel Turbopump

The advantages and disadvantages of the high pressure fuel turbomachinery system options considered are indicated in Table 3-4. As shown in Table 3-2, only two options ranked high in the selection: a new design and the modified (diffuser discharge area and arc of admission change) Advanced Space Engine MK48F. Gear drives, although not listed in the High Pressure Fuel Turbopump rankings, were ranked in the High Pressure Oxidizer Turbopump section and were eliminated for reasons discussed in that section. No boost pump option (that is, a main turbopump which by design can operate throughout a wide range of NPSH) could be incorporated but with major sacrifices in performance and weight penalties which is not consistent with the attempt to optimize the system. Additional screening of the high pressure pump options were accomplished by performing a trade study similar to the main oxidizer turbopump study discussed earlier. Those factors and results are shown in Fig. 3-4 . Certain observations as a result of the high pressure hydrogen turbopump trade study are evident from Fig. 3-4.

1. Higher speeds result in higher pump efficiency, lower weight, larger impeller tip widths (machineable) but increases the required NPSH.

2. Boost pump is required but the type (geared, gas turbine, or hydraulic) would not appreciably affect the high pressure pump performance. The selection of the particular boost pump option is discussed later.

TABLE 3-4

EXPANDER CYCLE HIGH PRESSURE
FUEL TURBOPUMP TRADE STUDY

OPTION	PERFORMANCE	DEVELOPMENT RISK	LIFE AND RELIABILITY	TECHNICAL FEASIBILITY	DEVELOPMENT FEASIBILITY	ANALYTICAL CORRELATION
NEW DESIGN • NEW PUMP (HYDRO) • NEW TURBINE • BOOST PUMP	• HIGHEST PREDICTED EFFICIENCY (64.5%) • NEGATIVE H-Q SLOPE ASSURED	• ANALYSIS BASED ON ASE EXPERIENCE AND LIKELY TO BE COMPARABLE	• NEW HARDWARE • NOT DEMONSTRATED • LIKELY TO MEET ASE REQUIREMENTS OR BETTER	• TYPE OF BOOST PUMP WILL INFLUENCE DESIGN • MINIMUM IMPACT ON SYSTEM • MODERATE COST	• STATE-OF-THE-ART • HIGH SPEEDS LIMIT BEARING CHOICE FOR LONG LIFE	• NOT DEMONSTRATED, NEW DESIGN • PROBABLY WILL MATCH BASED ON UPDATED ASE RESULTS
MK-48F (MODIFIED) • DIFFUSER AREA DECREASE • NEW TURBINE • BOOST PUMP	• PROJECTED MODS ALLOW PUMP TO MEET EXPANDER CYCLE OPERATION • PUMP PERFORMANCE LOWER THAN NEW DESIGN (η = 61%)	• EXISTING HARDWARE • TEST DATA BASE	• DESIGN CHANGES DO NOT AFFECT LIFE • RELIABILITY BASE ESTABLISHED	• TYPE OF BOOST PUMP WILL INFLUENCE DESIGN • MINIMUM IMPACT ON SYSTEM • MINIMUM COST	• PROVEN CONCEPT • MODIFICATION MAY REQUIRE RETEST (DIFFUSER AREA)	• DEMONSTRATED PERFORMANCE • CONFIDENT DESIGN
NO BOOST PUMP (NEW DESIGN)	• LOWER PERFORMANCE DUE TO LOWER SPEED • POSSIBLE BOIL-OUT-STALL PROBLEM	• LOWER SPEED REDUCES RISK	• EXISTING ROTATING PARTS, SEALS, BEARINGS DESIGN SHOULD MEET LIFE • LOWER SPEED ENHANCES DESIGN-TO-LIFE	• LOWER SPEED • LARGER AND HEAVIER • MODERATE COST	• ACHIEVING THE MINIMUM NPSH MAY BE DIFFICULT AND REQUIRE EXTENSIVE TESTING	• NOT DEMONSTRATED, NEW DESIGN

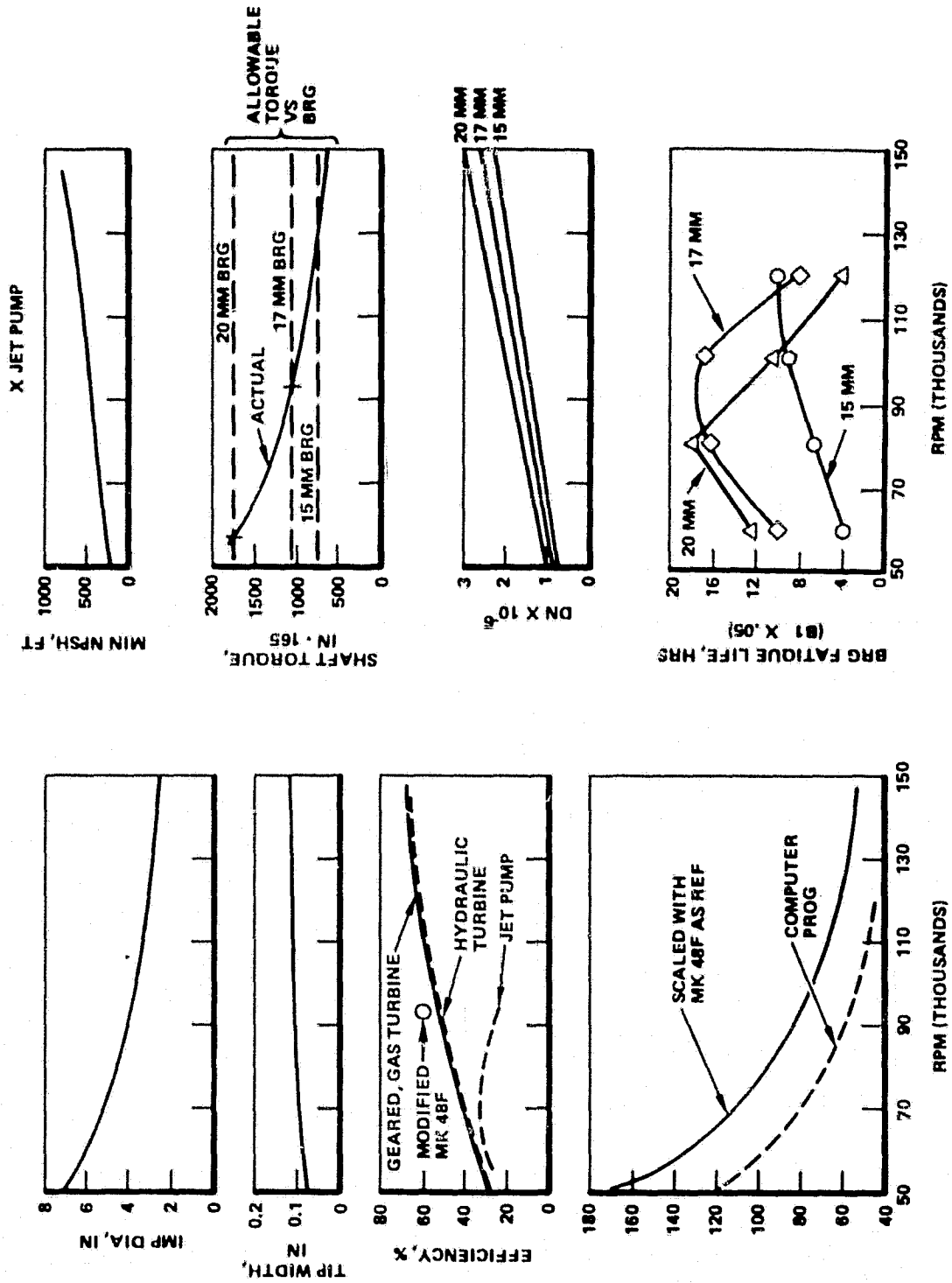

Figure 3-5. Expander Cycle Fuel Pump Study

3. Maximum operating speed is limited by allowable shaft torque, shaft size, and bearing size

   a. 20 mm bearing limits speed at constant horsepower to 80,000 rpm

   b. 17 mm bearing limits minimum speed at constant horsepower, to 93,000 rpm by allowable shaft torque

   c. 15 mm bearing limits minimum speed at constant horsepower to 130,000 rpm

From the bearing study alone, the 17-mm bearing offers the highest confidence of obtaining the life requirement and highest performance. However, for development and validation of the pump and turbine system, the readily available MK48Ø 20-mm bearings can be included as an off-shelf workhorse hardware easily adapted to the turbopump design. Also, the evaluation of a passive jet pump boost system failed to meet minimum requirements. After reviewing the advantages and disadvantages, and the trade study, the best candidate for the expander cycle fuel high pressure turbopump is a new design, lightweight, high performance concept incorporating many design features of the MK48F. Three major hydrodynamic goals were set: (1) design the hydrodynamic passages to achieve highest efficiency and ensure a negative H/Q slope at the operating point, (2) design sufficient rotor and pump operating margins to permit operation at the idle mode level, or 12 percent thrust, and (3) assure that sufficient detailed analysis and testing are accomplished on the two-stage partial admission turbine, a critical required design feature for the expander cycle operation.

Low Pressure (Boost) Oxidizer Turbopump

Table 3-5 presents the advantages and disadvantages of the candidate low pressure oxidizer turbopump systems. As indicated in Table 3-2 , the hydraulic turbine

TABLE 3-5. EXPANDER CYCLE LOW PRESSURE OXYGEN BOOST PUMP DRIVE TRADE STUDY

DRIVE OPTION	PERFORMANCE	DEVELOPMENT RISK (FLEXIBILITY)	LIFE AND RELIABILITY	TECHNICAL FEASIBILITY	DEVELOPMENT FEASIBILITY	ANALYTICAL CORRELATION
GAS DRIVEN TURBINE	• PERFORMANCE IMPACT LOW • PARALLEL TURBINE DRIVE SENSITIVE TO FLOW CHANGES • WIDE RANGE OF PERFORMANCE CONTROLS	• STATE-OF-THE-ART • GOOD ANALYTICAL BASE • AXIAL THRUST CONTROLS • OVERSPEED POSSIBLE • COMPLEX CONTROL SYSTEM • BIPROPELLANT SEAL PACKAGE	• LONG LIFE PROJECTED • CHILLDOWN ACCOMPLISHED EASILY - REPEATABLE STARTS • BIPROPELLANT SEALS • NPSH MARGIN	• FABRICATION STATE-OF-ART • COST TO PRODUCE MODERATE • PACKAGING FLEXIBILITY • MODERATE WEIGHT DUE TO GH_2 DRIVE SYSTEM AND CONTROLS • MAINTENANCE INDEPENDENT OF HP PUMPS • COMPLEX TURBINE WHEELS WITH LONG LEAD FABRICATION TIME • COMPLEX GH_2 DRIVE SYSTEM • BIPROPELLANT SEAL PACKAGE	• INDEPENDENT DEVELOPMENT TESTING • FACILITY ADAPTION STATE-OF-ART • REDESIGN RESULTS IN LONG FABRICATION TO TEST TIME • GH_2 DRIVE CONTROL AND SUPPLY SYSTEM • HAZARDOUS GAS SUPPLY (GH_2)	• EXCELLENT EXPERIENCE FOR DRIVE SYSTEM
LH_2 COOLED GEAR DRIVE	• KNOWN SPEED RATIOS • INDEPENDENT PERFORMANCE CONTROL NOT POSSIBLE	• SIMPLIFIED CONTROL SYSTEM • MINIMUM AXIAL THRUST PROBLEMS • NO LONG TERM EXPERIENCE • GEAR MATERIAL DEVELOPMENT • INDEPENDENT DEVELOPMENT NOT EASILY ACCOMPLISHED • BIPROPELLANT SEAL PACKAGE	• HIGH DRIVE EFFICIENCY • DIRECT HIGH PRESSURE TO LOW PRESSURE SPEED RATIOS • LONG LIFE NOT DEMONSTRATED • SYSTEM CHILLDOWN SLOW • BIPROPELLANT SEALS	• RELATIVELY LOW OVERALL WEIGHT • FABRICATION STATE-OF-ART OVERALL • COST TO PRODUCT MODERATE • MAINTENANCE ABILITY POOR-COMPLEXITY OF GEAR BOX ASSOCIATED WITH HP PUMP • MOUNTED AT ENGINE/HP PUMP ONLY • SMALL GEARS FOR LOW PITCH LINE VELOCITIES REQUIRE MORE FAB TIME • LIMITED LOCATION PREFERENCE WITH RESPECT TO HP PUMP	• KNOWN POWER/SPEED RATIOS • NO INDEPENDENT TESTING OF FINAL DESIGN-MAIN PUMPS ALSO REQUIRED • GEARS AND HOUSING DESIGN DIFFICULT TO CHANGE/FABRICATE/RETEST • GEAR INSPECTION PERIODS REQUIRE TEST DOWNTIME	• NO DIRECT LONG TERM EXPERIENCE
HYDRAULIC DRIVEN	• PERFORMANCE IMPACT LOW • EFFICIENCY DEPENDENT ON HIGH PRESSURE PUMP • INDEPENDENT PERFORMANCE CONTROL DIFFICULT	• LOW AXIAL THRUST • NO BIPROPELLANT SEALS • REDESIGN IMPACTS HIGH PRESSURE PUMP • INTERNAL THERMOPHYSICAL PROPERTIES NOT EASILY EVALUATED	• NO MECHANICAL DRIVE TO MAIN PUMP • LONG LIFE PROJECTED • NO BIPROPELLANT SEALS • LONG AND PROBABLY NOT REPEATABLE STARTS	• MINIMUM WEIGHT PENALTY • MINIMUM COST • FABRICATION STATE-OF-ART • NON-FLEXIBLE MOUNTING WHICH MUST CONFORM TO MAIN PUMP INLET	• SIMPLIFIED SYSTEM • NO INDEPENDENT TESTING OF FINAL DESIGN-MAIN PUMPS ALSO REQUIRED • REDESIGN CAUSES COMPLETE TEST DOWNTIME	• INTERNAL THERMOPHYSICAL INFLUENCE NOT WELL DEFINED
ELECTRIC MOTOR DRIVEN	• HIGHEST PROJECTED PERFORMANCE • EXCELLENT CONTROL OF SPEEDS • INDEPENDENT OF MAIN PUMPS • ADDED WEIGHT PENALIZES PERFORMANCE GAINS	• MINIMUM CONTROL COMPLEXITY • PERFORMANCE LIMITS EASILY EXPLORED • NO BIPROPELLANT SEALS • WIRE BUNDLES • POWER GENERATION SYSTEM REQUIRED • SHAFT SEALS TO ATMOSPHERE	• SYSTEM CHILLDOWN EASY REPEATABLE STARTS • NO BIPROPELLANT SEALS • NPSH MARGIN • LONG LIFE PROJECTED • HIGH DRIVE EFFICIENCY • INCREASED CHILLDOWN MASS (WEIGHT)	• REPLACEABLE, OFF-SHELF MOTORS • INDEPENDENT VEHICLE LOCATIONS • EASY MAINTENANCE • PUMP FABRICATION STATE-OF-ART • HIGH WEIGHT PENALTY DUE TO MOTOR AND POWER GENERATION SYSTEM • HIGH COST	• INTERCHANGEABLE MOTORS FOR DRIVE • PUMP ONLY DESIGN • INDEPENDENT DEVELOPMENT TESTING • POWER GENERATION SYSTEM DEVELOPMENT MAY NOT PARALLEL PUMP DEVELOPMENT. VERIFICATION TESTING SCHEDULE DELAYS	• EXCELLENT MOTOR DRIVE EXPERIENCE, LIMITED DIRECT EXPERIENCE

ORIGINAL PAGE IS OF POOR QUALITY

driven boost pump yielded the highest rank over the nearest candidate (gas turbine). The major reason was the extremely low projected efficiency of the gas turbine (~ 10 percent) and its sensitivity to flow changes in a parallel gas drive system. Gear drive systems were eliminated for basically the same reasons as discussed earlier (high pressure oxidizer pump) while the electric motor drive systems were eliminated prior to point awards because of the high weight penalty of the power generator system. Power requirement for the electrically driven pumps would be greater than the projected entire power system for the vehicle.

The oxidizer boost pump system selected is the Francis type radial in-flow turbine. The turbine is driven by the entire high pressure oxidizer pump discharge flow. A promising high-low pump integration scheme mounts the low pressure pump/turbine in a "Tee mount." In this arrangement, the high and low pressure pump shafts are perpendicular to each other with the low pressure boost pump mounted ahead of the high pressure pump. Major design considerations for the oxidizer boost pump are: (1) high pressure turbine inlet pressure (~ 2600 psi), (2) pump/turbine labyrinth seal design to limit the recirculation flows, and (3) fabrication details of the integral volute designs.

Low Pressure (Boost) Fuel Turbopump

Options considered and results of the overall assessment appear in Table 3-6. The preliminary ranking of the fuel boost pump drive options showed (Table 3-2) that the gas turbine and LH_2 cooled gear drive rate equally well as turbine drive option. Two major factors finally drove the choice of the fuel boost pump drive to the warm gas turbine drive. First, the experience of gas turbines at Rocketdyne is extensive and no problems are foreseen in developing a reliable, long-life turbopump using moderately low temperature gaseous hydrogen as the turbine drive media. Cryogenically cooled geared drives, although having been tested at Rocketdyne and other aerospace companies, do not have the extensive long life test experience. The expander cycle life requirement is 10 hours without overhaul. The maximum life experience of cryogenically

TABLE 3-6. EXPANDER CYCLE LOW PRESSURE FUEL BOOST PUMP DRIVE TRADE STUDY

DRIVE OPTION	PERFORMANCE	DEVELOPMENT RISK	LIFE AND RELIABILITY	TECHNICAL FEASIBILITY	DEVELOPMENT FEASIBILITY	ANALYTICAL CORRELATION
GAS DRIVEN TURBINE	•OVERALL PERFORMANCE IMPACT LOW •PARALLEL TURBINE DRIVE SENSITIVE FLOW FLUCTUATIONS •PARALLEL - HIGH SENSITIVITY •SERIES - LOW SENSITIVITY	•STATE-OF-THE-ART •ANALYTICAL TO EMPIRICAL PROJECTIONS •AXIAL THRUST CONTROLS •OVERSPEED POSSIBLE •COMPLEX CONTROL SYSTEM	•LONG LIFE PROJECTED •STATE-OF-ART •CHILLDOWN ACCOMPLISHED EASILY AND INDEPENDENT OF HP PUMP OPERATION •NPSH MARGIN	•FABRICATION STATE-OF-ART •COST TO PRODUCE MODERATE •PACKAGING FLEXIBILITY •MODERATE WEIGHT DUE TO GH_2 DRIVE SYSTEM AND CONTROLS •MAINTENANCE INDEPENDENT OF HP PUMPS •COMPLEX TURBINE WHEELS WITH LONG LEAD FABRICATION TIME •COMPLEX GH_2 DRIVE SYSTEM	•INDEPENDENT DEVELOPMENT TESTING •FACILITY ADAPTION STATE-OF-ART •REDESIGN RESULTS IN LONG FABRICATION TO TEST TIME •GH_2 DRIVE CONTROL AND SUPPLY SYSTEM •HAZARDOUS GAS SUPPLY (GH_2)	•EXCELLENT EXPERIENCE
LH_2 COOLED GEAR DRIVEN	•KNOWN PERFORMANCE/SPEED RATIOS •INDEPENDENT PERFORMANCE CONTROL NOT POSSIBLE	•SIMPLIFIED CONTROL SYSTEMS •OTHER DEVELOPMENT DRIVE SYSTEMS AVAILABLE FOR INTERIM TESTING •NO AXIAL THRUST PROBLEMS •NO DIRECT LONG TERM EXPERIENCE •HIGH PITCH LINE VELOCITIES •POTENTIAL ROTORDYNAMICS PROBLEMS •GEAR MATERIAL/COATING DEVELOPMENT •INDEPENDENT DEVELOPMENT NOT EASILY RELATED TO SYSTEM OPERATION	•HIGH DRIVE EFFICIENCY •DIRECT HP TO LP SPEED RATIOS •LONG LIFE DEMONSTRATION REQUIRED •SYSTEM CHILLDOWN DEPENDS ON HP PUMP START-LONG START TRANSIENTS	•RELATIVELY LOW OVERALL WEIGHT •FABRICATION STATE-OF-ART OVERALL •COST TO PRODUCE MODERATE •MAINTENANCE ABILITY POOR-COMPLEXITY OF GEAR BOX ASSOCIATED WITH HP PUMP •MOUNTED AT ENGINE/HP PUMP ONLY •SMALL GEARS FOR LOW PITCH LINE VELOCITIES REQUIRE MORE FAB TIME •LIMITED LOCATION PREFERENCE WITH RESPECT TO HP PUMP	•KNOWN POWER/SPEED RATIOS •NO INDEPENDENT TESTING OF FINAL DESIGN-MAIN PUMPS ALSO REQUIRED •GEARS AND HOUSING DESIGN DIFFICULT TO CHANGE/FABRICATE/RETEST •GEAR INSPECTION PERIODS REQUIRE TEST DOWNTIME	•NO DIRECT LONG TERM EXPERIENCE
HYDRAULICALLY DRIVEN	•OVERALL PERFORMANCE IMPACT LOW •EFFICIENCY DEPENDENT ON PERFORMANCE OF MAIN PUMP •INDEPENDENT PERFORMANCE CONTROL NOT POSSIBLE	•LOW AXIAL THRUST •INTERNAL THERMOPHYSICAL PROPERTIES OF DESIGN NOT EASILY PROJECTED •REDESIGN IMPACTS HIPRESSURE PUMP	•NO DIRECT CONNECTION WITH HP PUMP •LONG LIFE PROJECTED •SYSTEM CHILLDOWN DEPENDS ON HP PUMP START-LONG START TRANSIENTS	•MINIMUM WEIGHT PENALTY •MINIMUM COST •FABRICATION STATE-OF-ART •NON-FLEXIBLE MOUNTING WHICH MUST CONFORM TO MAIN PUMP INLET	•SIMPLIFIED SYSTEM •NO INDEPENDENT TESTING OF FINAL DESIGN-MAIN PUMPS ALSO REQUIRED •REDESIGN CAUSES COMPLETE TEST DOWNTIME	•INTERNAL THERMOPHYSICAL INFLUENCES NOT WELL DEFINED
ELECTRIC MOTOR DRIVEN	•HIGH PERFORMANCE •ABILITY TO CONTROL SPEEDS/PERFORMANCE •INDEPENDENT OF MAIN SYSTEM •ADDED WEIGHT PENALTY DETRACTS FROM OVERALL PERFORMANCE	•MOTORS AVAILABLE •MINIMUM CONTROL COMPLEXITY •PUMP PERFORMANCE LIMITS EASILY EXPLORED •WIRE BUNDLES •POWER GENERATION SYSTEM AN ADDITIONAL DEVELOPMENT PROGRAM •SHAFT SEALS TO ATMOSPHERE	•SYSTEM CHILLDOWN INDEPENDENT OF HP PUMP OPERATION •HIGH DRIVE EFFICIENCY •LONG LIFE PROJECTED •NPSH MARGIN •INCREASED CHILLDOWN MASS	•REPLACEABLE, OFF-SHELF MOTORS •INDEPENDENT VEHICLE LOCATIONS •EASY MAINTENANCE •PUMP FABRICATION STATE-OF-ART •HIGH WEIGHT PENALTY DUE TO MOTOR AND POWER GENERATION SYSTEM •HIGH COST	•INTERCHANGEABLE MOTORS FOR DRIVE •PUMP ONLY DESIGN •INDEPENDENT DEVELOPMENT TESTING •POWER GENERATION SYSTEM DEVELOPMENT MAY NOT PARALLEL PUMP DEVELOPMENT. VERIFICATION TESTING SCHEDULE DELAYS	•EXCELLENT MOTOR DRIVE EXPERIENCE, LIMITED DIRECT EXPERIENCE

cooled gear drive at Rocketdyne is about one hour. Gear drive systems if designed offer little versatility in packaging, development flexibility, or off-design operation. Second, for vehicle applications, the gas driven turbine boost pump offers fast chilldown and ramp to operating levels whereas the geared system represents a slow chilldown and start transient operation. Only the electrically driven boost pump offers better control of chilldown and start transient but as discussed earlier, the prohibitively high weight penalty precludes use of the electrically driven boost pump. The expander cycle engine will derive higher benefits if the gas turbine drive boost pump is used. The selected design of the fuel boost turbopump is a single stage axial flow inducer driven by a single stage partial admission turbine. The low pressure pump will be "Tee-mounted" to the main high pressure turbopump to provide a compact, low weight system.

HYDROGEN TURBOMACHINERY - DETAILED DESIGN

In this section a detailed description of the hydrogen turbomachinery is presented which includes the mechanical design description, pump performance analysis, turbine performance analysis, rotordynamic analysis, and technology and development issues. A summary of the turbomachinery operating parameters as determined from the expander engine cycle optimization program is presented in Table 3-7. These parameters were used to size the turbomachinery components. Analysis of these components then led to establishment of their design-point efficiencies. These efficiencies were then input into the cycle optimizer program to update the engine balance and turbomachinery operating parameters. This iterative process was carried out a number of times until acceptable differences existed between initial and updated values. Table 3-7 represents values obtained in the last stage of the iteration process.

Low Pressure Fuel Boost Turbopump

The turbopump is an axial flow single stage inducer driven by a partial admission gaseous hydrogen impulse turbine. Figures 3-6 through 3-8 present the

TABLE 3-7. EXPANDER CYCLE ENGINE POINT-DESIGN TURBOMACHINERY, OPERATING PARAMETERS

Parameter	High Pressure Fuel	Low Pressure Fuel	High Pressure LOX	Low Pressure LOX
Turbine Inlet Pressure, psia	3787	2186	2186	2649
Turbine Discharge Pressure, psia	2202	1809	1809	2522
Pressure Ratio	1.72	1.21	1.21	1.05
Turbine Inlet Temperature, R	875	797	797	LOX NBP
Turbine Flowrate, lb/sec	3.65	0.29	2.99	26.88
Pump NPSH Available, ft	-	15.0	-	2.0
Pump Inlet Pressure, psia	64	18.82	71	16.33
Pump Inlet Temperature, R	-	37.8	-	162.7
Pump Flowrate, lb/sec	4.12	4.48	26.88	26.88
Pump Discharge Pressure, psia	4671	74	2649	86
Speed, rpm	110,000	28,486	52837	6475

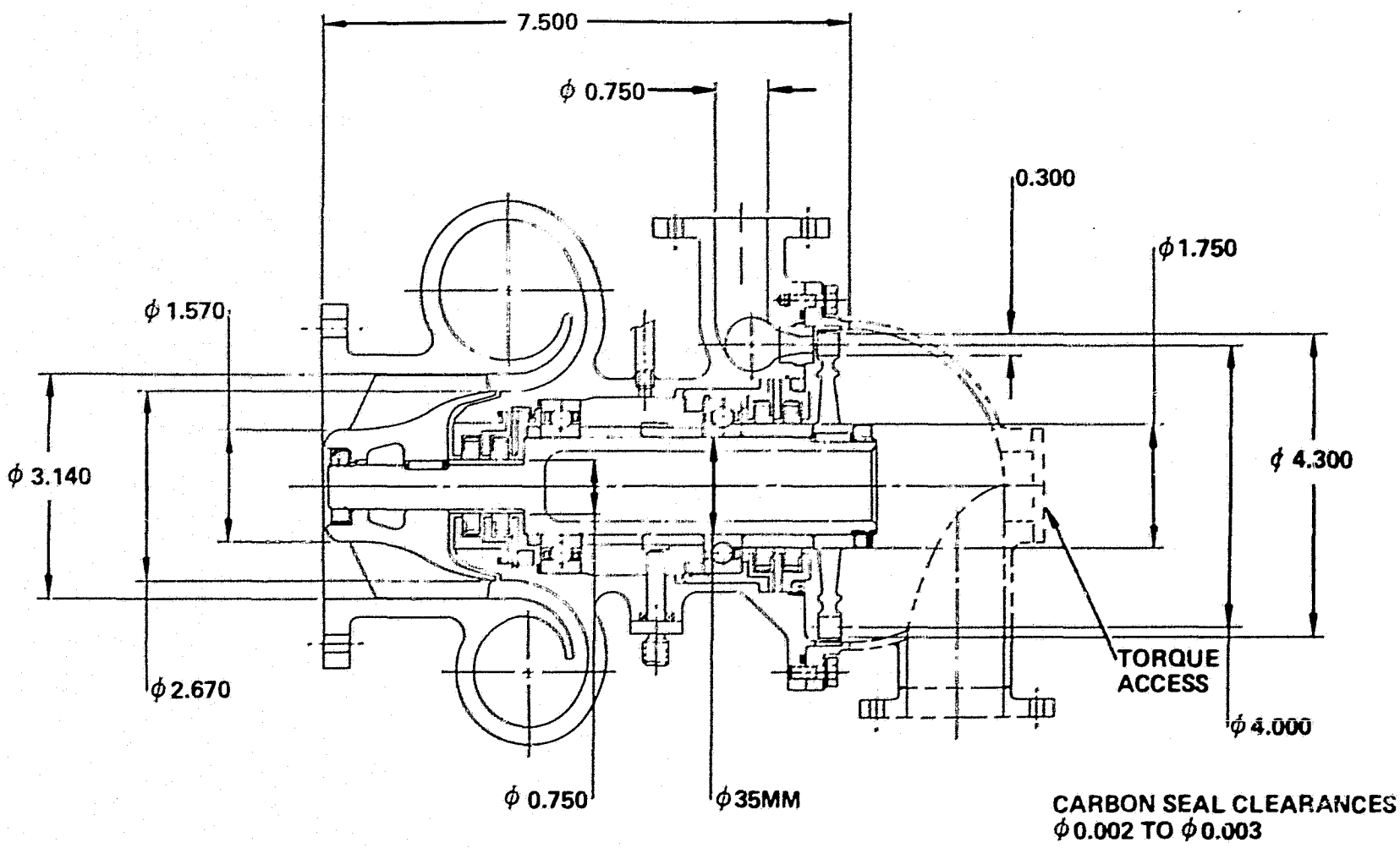

Figure 3-6. Fuel Low Pressure Pump

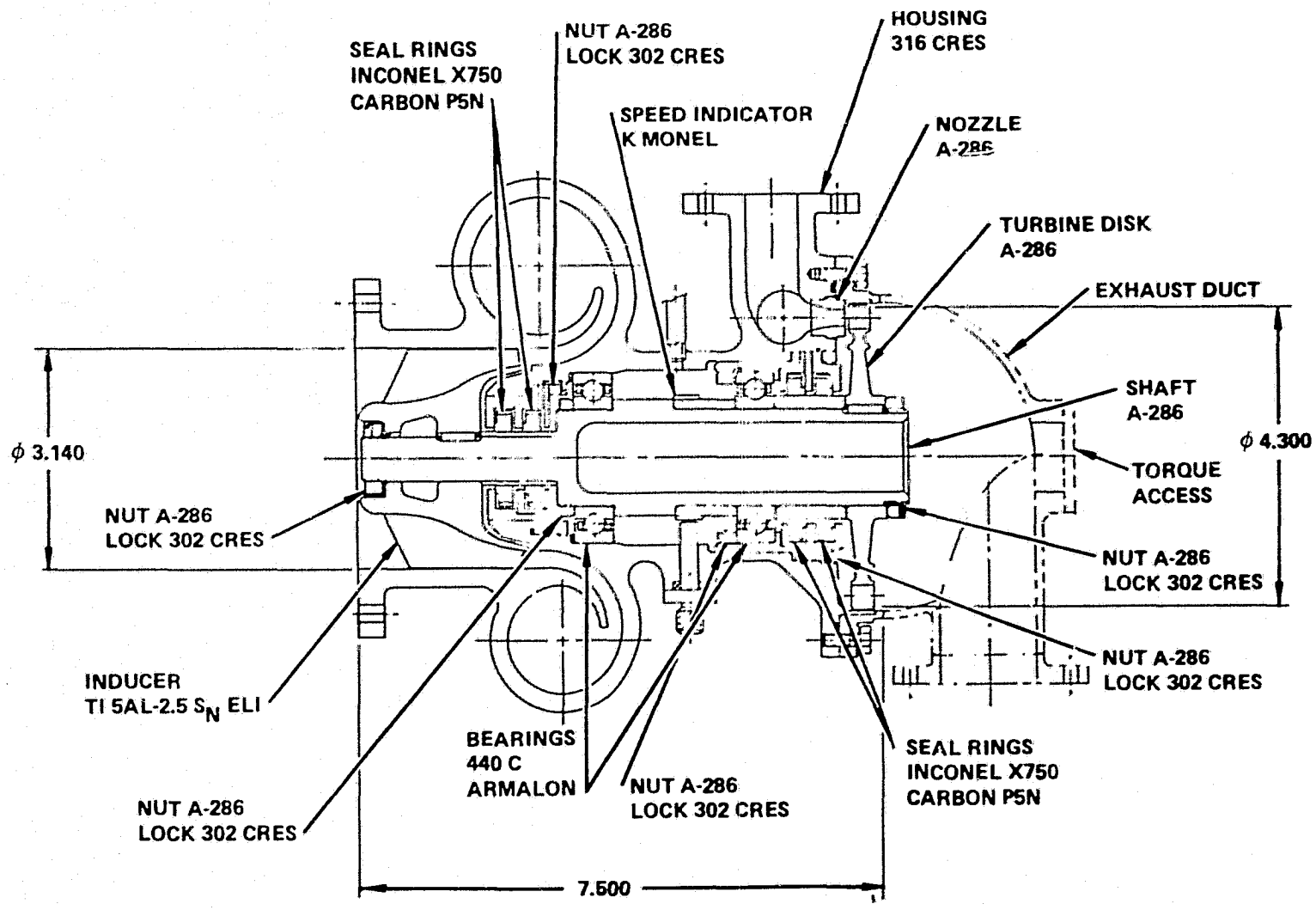

Figure 3-7. Fuel Low Pressure Turbopump Material Selection

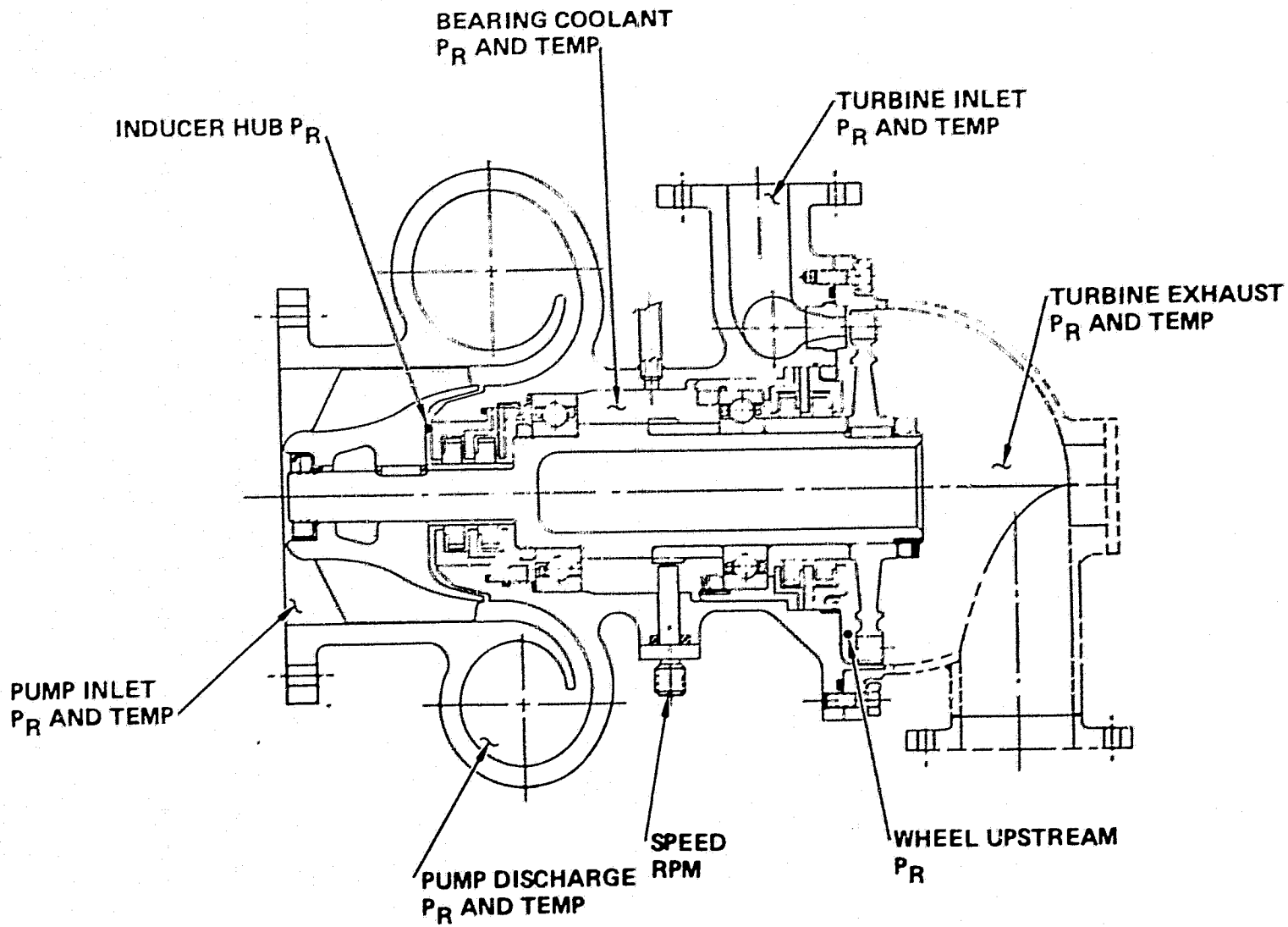

Figure 3-8. Fuel Low Pressure Turbopump Development Instrumentation Selection

turbopump layouts showing respectively, (1) principal dimensions, (2) hardware and materials identification and (3) development instrumentation selections.

The pump design consists of an inducer, a vaneless radial diffuser and a volute. The rotor is supported by two 35-mm-diameter bearings, operating at a DN value of 1.0×10^6. Bearing coolant is provided by high pressure liquid hydrogen supplied from the high pressure pump. Bearing flow control is maintained by a floating ring controlled gap seal at each bearing location. Coolant flow is introduced into a cavity between the pump and turbine end bearings. Pump end bearing coolant flow (~ 5 gpm) is routed into the discharge of the inducer while turbine end bearing coolant flow (~ 5 gpm) is directed into the turbine wheel cavity which is downstream of the partial admission turbine nozzle but upstream of the wheel.

In order to minimize system hydraulic resistance and to provide for a compact installation, the fuel boost turbopump is "Tee-mounted," similar to the oxidizer boost turbopump, to the high pressure fuel turbopump. Figure 3-3 shows an envelope drawing of the fuel turbomachinery system. The boost turbopump shaft is parallel to the direction of vehicle flight, while the high pressure fuel turbopump shaft is perpendicular to the boost pump shaft.

The total estimated weight of the low pressure fuel turbopump, based on individual component geometry and material, is about 13.8 pounds.

Pump Performance. The low pressure fuel pump is required to operate with a minimum supplied NPSH of 15 feet of liquid hydrogen at a design flow of 4.48 lb/sec. If necessary, the pump must be able to operate with an entrance two-phase flow mixture of vapor and liquid. The pressure rise through the pump must be sufficient to insure that there will be no head loss resulting from cavitation on the high pressure fuel pump inducer. On the other hand, it is desirable to keep the boost pump design head coefficient $\psi_{design} = g\ H/U_T^2$ as low as possible

to minimize the blade loading. Ideally, the blade loading can be kept low enough that a simple inducer can be used. The tip blade speed U_T, however, should not be allowed to become so large that the design inlet flow coefficient $\phi_{design} = Q/A_{IN}\ U_T$ becomes too small. Low inlet flow coefficients result in manufacturing difficulty and inducer friction losses large enough to seriously degrade the boost pump efficiency. The overall pump size should be kept as small as is possible.

The pump design consists of an inducer, a vaneless radial diffuser and a volute. The simple inducer operates at a design inlet flow coefficient, $\phi_{design} = 0.065$. Rocketdyne has developed several inducer designs that operate with good performance to well below a 0.06 flow coefficient. The inducer only head coefficient is 0.295, which is low enough that a simple four-blade inducer may be used. At design, the adjusted suction specific speed S_S^* is 92,467 which is high but well within liquid hydrogen experience. The discharge hub diameter of the inducer was obtained by maximizing the static hub pressure so as to minimize the possibility of cavitation on static elements following the inducer.

The inducer is followed by a vaneless diffuser which significantly reduces both meridional and tangential components of the flow leaving the inducer. The vaneless diffuser is followed by a volute, which has a discharge diameter of 1.96 inches with a centerline diameter from the pump axis of 5.0 inches.

Table 3-8shows the basic design parameters for the low pressure fuel pump. The pump operates with a predicted design head rise of 1309 feet and an efficiency of 73.1 percent. This corresponds to a head coefficient of 0.277. The minimum available discharge NPSH is 1296.4 feet. Predicted pump ψ vs ϕ and efficiency η vs ϕ curves are shown in Fig. 3-9. As can be seen, the pump design point occurs at maximum efficiency. The limiting value of suction specific speed S_S before head falloff due to cavitation occurs is plotted in Figure 3-10 as a function of flow coefficient. The design point was chosen to correspond to a $\frac{NPSH}{Cm_1^2/2g}$ value of 1.5 which is sufficient margin to prevent cavitation. The maximum value of the suction specific speed that can be attained without

significant head loss was assumed to correspond to a minimum $\frac{NPSH}{C_{m_1}^2/2g}$ value of 1.0 at the pump inlet.

TABLE 3-8. LOW PRESSURE FUEL PUMP DESIGN

OPERATING CONDITION	
Speed, rpm	28486
Design Weight Flow, lb/sec	4.48
Density, lb/ft^3	4.36
Design Flow, gpm	459.1
Inlet Total Pressure, psia	18.8
Inlet Temperature, R	37.8
Minimum Inlet NPSH, ft	15.0
Pump ΔH, ft	1309
Design Efficiency, Overall	0.731
Suction Specific Speed, S_S	80,079
Corrected for Hub-Tip Size	92,467
$NPSH/(C_{m_1}^2/2g)$	1.5
PUMP DISCHARGE CONDITIONS	
Discharge Total Pressure, psia	58.45
Discharge Temperature, R	38.3
Discharge NPSH, ft	1296
Vaneless Diffuser Discharge Diameter, in.	4.78
Vaneless Diffuser Discharge Width, in.	0.202
Volute Discharge Passage Diameter, in.	1.960
Volute Discharge C.L. Diameter, in. (from pump centerline)	5.00
Pump Head Coefficient	0.377

TABLE 3-8. LOW PRESSURE FUEL PUMP DESIGN (CONT'D)

INDUCER

Inducer Inlet Tip Diameter, in.	3.14
Inducer Inlet Hub Diameter, in.	1.57
Inducer Discharge Tip Diameter, in.	3.14
Inducer Discharge Hub Diameter, in.	2.67
Inducer Inlet Flow Coefficient	0.065
Inducer Only Head Coefficient	0.295
Design Efficiency	0.780

BALANCE

Rotor Bearing Axial Force, lb	175.5 (toward inducer)

This is typical for liquid hydrogen. The shape of the curve and the value of ϕ where the maximum value of S_S occurs were both obtained from Rocketdyne test experience.

If the design head coefficient is allowed to increase somewhat, more NPSH can be supplied to the high pressure fuel pump. In this event, an additional blade row would be required to compensate for the extra loading. As an alternate, the pump speed could be decreased, along with a corresponding increase in ϕ_{design} and a decrease in S_S design. The friction losses will drop somewhat at the lower speed and the inducer cavitation margin will increase. At lower pump speeds, a stator may be necessary to take out the additional inducer exit whirl, but the pump will stay the same size. The lower speed would increase the drive torque requirement.

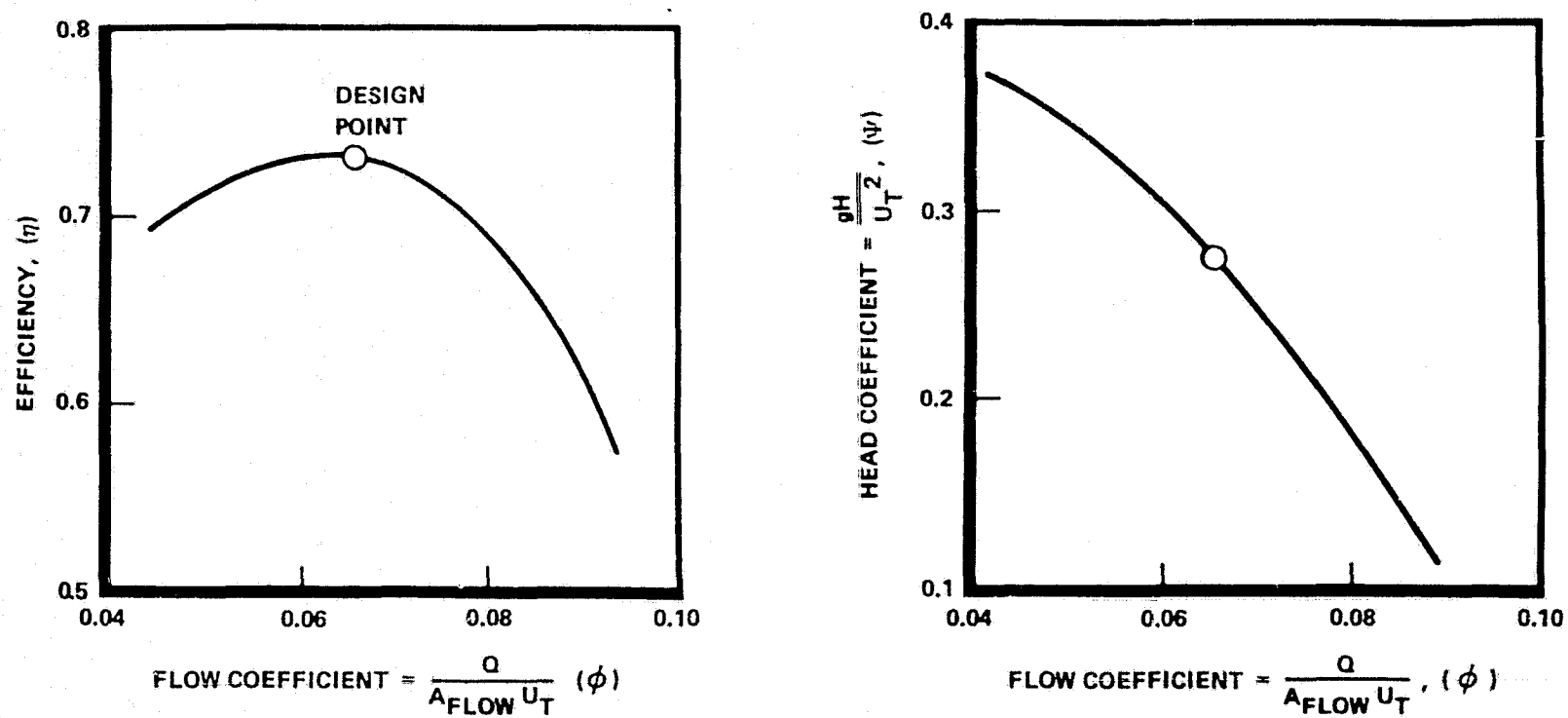

Figure 3-9. Low Pressure Fuel Pump Efficiency and Head Coefficient

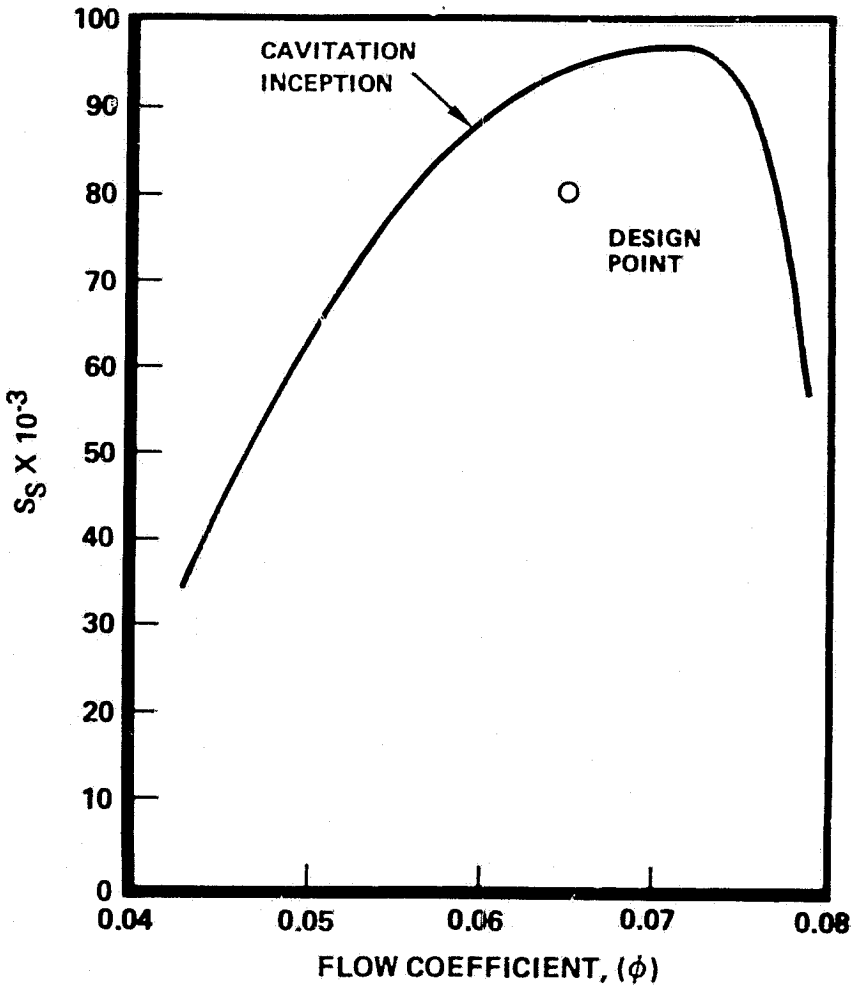

Figure 3-10. Fuel Boost Pump Suction Performance

The wide flow range head ratio and efficiency versus flow ratio characteristics are presented in Fig. 3-11. The efficiency curve shows the influence of the low head rise at 20 percent of the design flow/speed ratio.

LPFTP Turbine Analysis. The low pressure fuel turbine will drive the liquid hydrogen boost pump with GH_2 drive, in parallel with the high pressure oxidizer turbine. The required turbine power and speed were derived from the pump design, while the turbine inlet conditions and pressure ratio were established from the engine balance, which included a heat exchanger to increase turbine inlet gaseous hydrogen temperature. Turbine flowrate was set to provide the required power for the turbine design efficiency and available energy.

The turbine design was optimized for the performance and was conducted utilizing Rocketdyne's partial admission, gaseous hydrogen turbine analys s computer program. The program includes all gas path losses due to friction, turning, tip clearance losses and partial admission losses.

A tabulation of principal turbine design parameters is presented in Table 3-9 . Turbine inlet flow, inlet total pressure, and inlet total temperature are specified at the turbine inlet flange which is in the turbine inlet just upstream of the turbine inlet manifold. Turbine exit total pressure and temperature are specified in the turbine outlet pipe just downstream of the turbine outlet collector. Pressure drop between the turbine inlet and nozzle inlet is 25 psi.

Turbine geometry parameters were optimized for high performance and minimum weight. The selected turbine mean diameter of 4.0 inches is shown in Fig. 3-12 for optimized blade height and angle. On the expanded efficiency scale, the selected diameter of 4.0 inches is within 0.012 points of the peak efficiency of 0.3205, as shown in Fig. 3-12. The selected diameter is 6.3 percent smaller that the diameter at the maximum efficiency, but results in performance very close to the peak efficiency and minimizes turbopump weight.

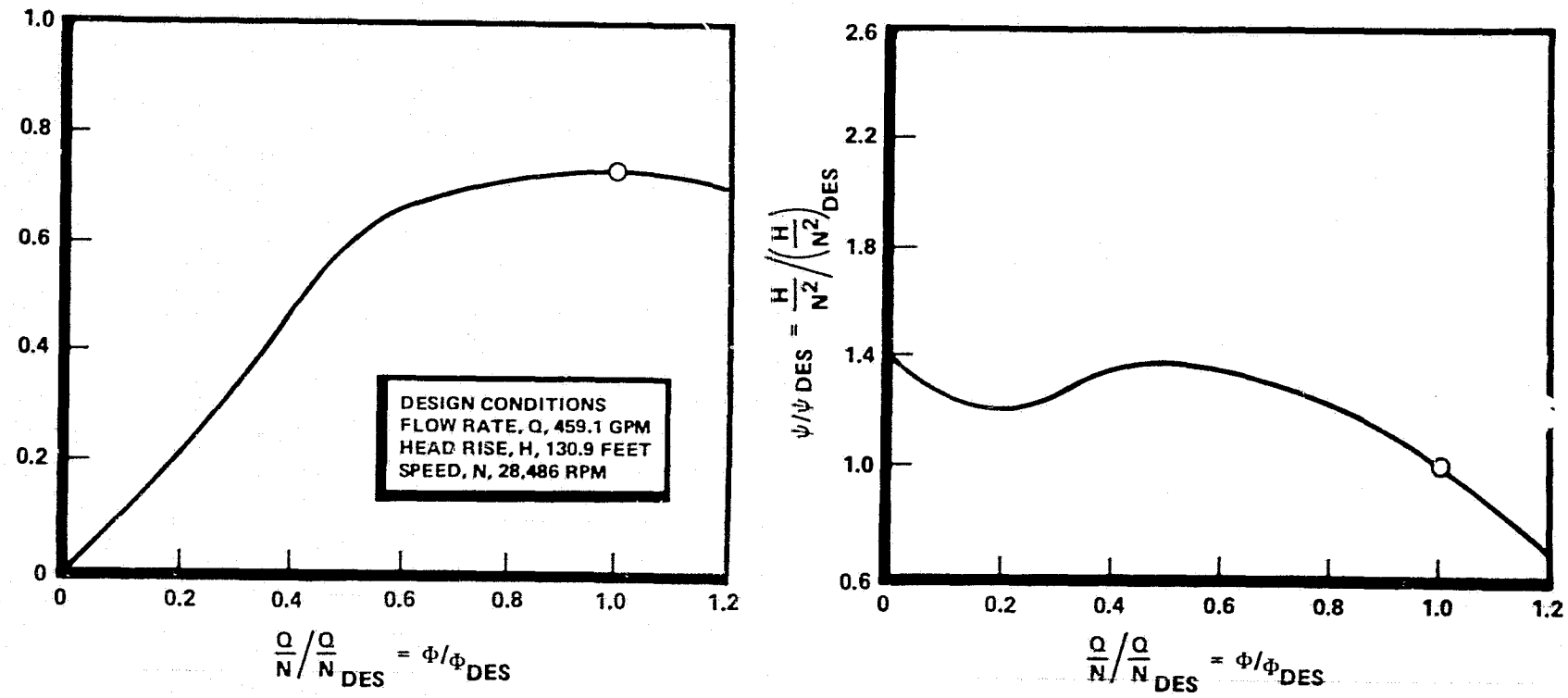

Figure 3-11. Low Pressure Fuel Pump Normalized Performance

TABLE 3-9. LOW PRESSURE FUEL TURBOPUMP TURBINE PERFORMANCE PARAMETERS

Working Fluid	GH_2
Output Power, HP	21.505
Speed, RPM	28486
Inlet Flowrate, LB/SEC	0.29
Inlet Total Temperature, °R	797
Inlet Total Pressure, PSIAT	2186
Outlet Total Pressure, PSIAT	1809
Pressure Ratio, Total-to-Total	1.209
Available Energy, BTU/LB	164.2
Isentropic Velocity, FT/SEC	2867.8
Mean Diameter, INCH	4.0
Mean Blade Speed, FT/SEC	497.2
Overall Velocity Ratio	0.1734
Efficiency, Total-to-Total	0.319

The turbine predicted power losses are tabulated in Table 3-10. Primary losses are the gas path element wall friction and turbulence losses established from the expansion and kinetic energy coefficients, which are a function of the blade deflecting angle and blade size. Additional losses include the turbine inlet manifold loss, disk friction loss, and partial admission losses.

The velocity vectors shown in Fig. 3-13 include flow path friction and turning losses but not losses due to shaft seal leakage, disk friction, size effects, and partial admission. The rotor outlet angle of 25 degrees was selected for this work output to provide a design with proper match of rotor and nozzle. The rotor blade inlet angle was set for zero incidence.

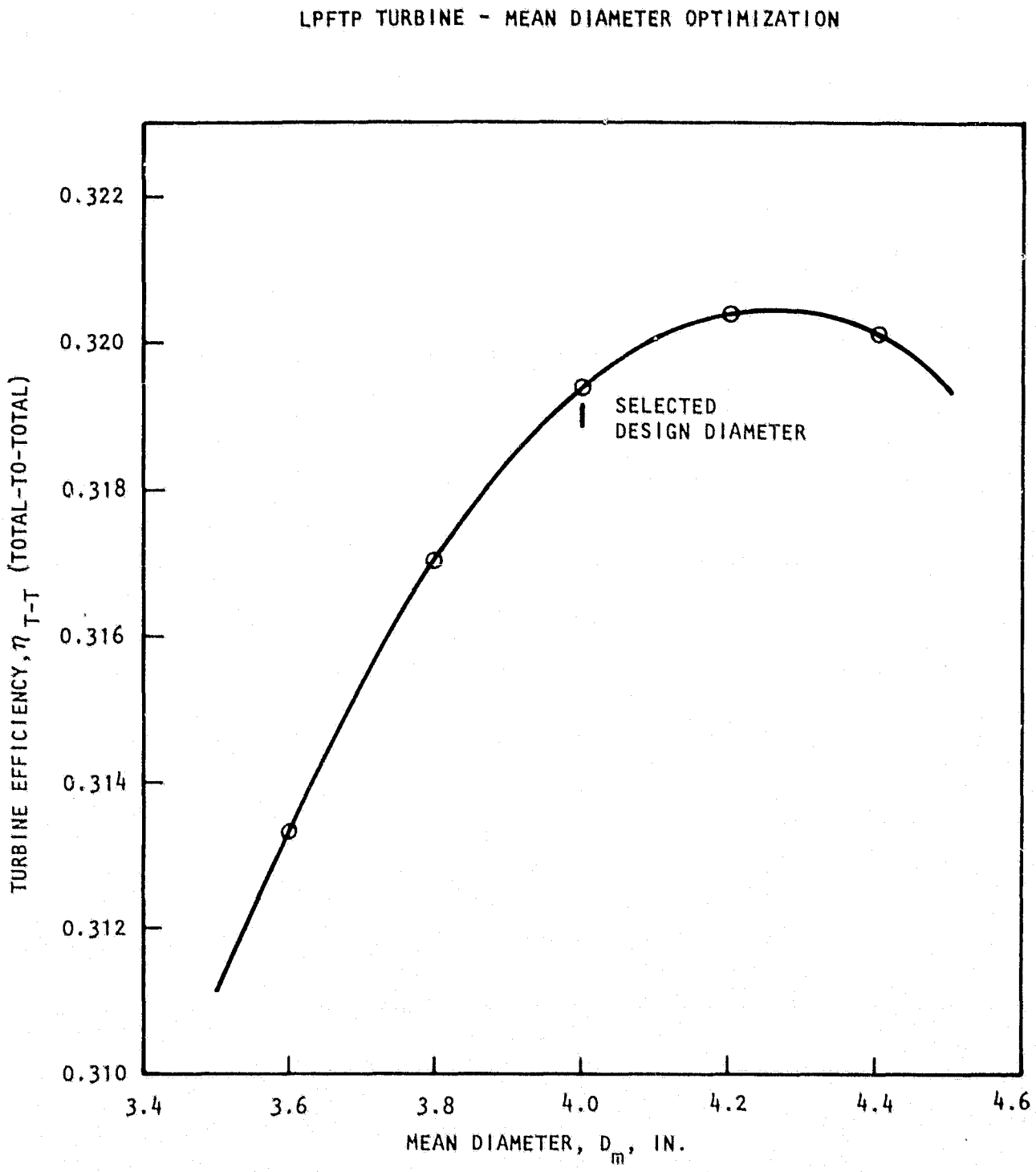

Figure 3-12. Low Pressure Fuel Turbopump Turbine Mean Diameter Optimization

TABLE 3-10. LOW PRESSURE FUEL TURBOPUMP TURBINE, FLANGE-TO-FLANGE EFFICIENCY AND PERFORMANCE

	Flowrate Lb/Sec	Enthalpy Btu/Lb	Power Loss HP
1. Power Losses			
Inlet Manifold	.290	7.5261	3.087
1-N Inlet Incidence	.290	.0000	.0000
1-N Inlet Kinetic Energy	.290	.0000	.0000
1-N Expansion Energy	.290	12.2575	5.0272
1-R U/S Shaft Seal	.0336	71.4754	3.3964
1-R Inlet Incidence	.2564	.0000	.0000
1-R Expansion Energy	.2564	41.7172	15.1270
1-R Windage			1.6294
1-R End Sector Mixing			2.6813
1-R Rim Friction			.2403
1-R Disk Frcition			.3144
1-R End Clearance*	.2564	0.0	0.0
S-1 Diagram Factor Adjustment	.2564	7.7824	2.8220
1-R Leaving Energy	.2564	31.7377	11.5083
TOTAL POWER LOSSES			45.8332
*Included in Diagram Factor Adjustment			
2. Available Power			
WDOT Inlet Flange, Lb/Sec	.290		
DHA T-T F-F, Btu/Lb	164.1900		
HP Available T-T F-F	67.3386		
3. Shaft Power, Etc. Overall			
HP Available T-T F-F	67.3386		
Total Power Losses	45.8332		
Shaft BHP	21.505		
Overall Efficiency T-T F-F	.3194		
Overall UM/CO T-T	.1734		

The total and static pressures and temperature in the blade path are listed in Table 3-11.The entire pressure drop occurs across the nozzle for the partial admission, impulse design. All of the expansion and acceleration of the flow occurs across the nozzle at the design condition.

Turbine sizing is shown in Table 3-12 The mean diameter is 4.0 inches for each element. The nozzle outlet height is 0.25 inch and the rotor blade height overlaps the nozzle outlet height by 20 percent. The rotor axial width was selected to be 0.31 inch. The axial space between the nozzle and rotor is 0.05 inch. The arc of admission is 2.4 percent, which represents a single nozzle. The low partial admission provides a higher efficiency than a reduced blade height with higher arc of admission.

Table 3-13 presents the turbine blade path geometry assumptions. The rotor is shrouded to improve efficiency. The radial tip clearance of 0.005 inch was selected and resulted in a clearance/blade height ratio of 0.017.

The design and off-design predicted performance are shown in Figures 3-14 and 3-15. The predicted turbine efficiency as a function of mean velocity ratio is shown in Figure 3-14. A design point efficiency of 0.319 is achieved at a design mean velocity ratio of 0.1734. The flow parameter as defined in Figure 3-15 is a function of turbine pressure ratio and turbine speed parameter. The flow parameters were calculated from an interactive computer program matching flow element areas with turbine operating conditions.

Technology and Development Issues. The fuel boost pump represents a nominally low risk development item. One concern is the coolant scheme of the bearings, particularly at the front end bearing. The turbopump operates with a very high differential pressure between the pump discharge (~ 58 psia) and the turbine discharge (~ 1850 psia). Coolant of the rear (turbine) bearing cannot be achieved with the low pressure available at the pump discharge. Control of the turbine end labyrinth seals to meet differential pressure of about 200 psia are possible with either a labyrinth seal (shown) or shaft riding carbon seals. However, the high differential pressure across the front labyrinth seal (~ 1950

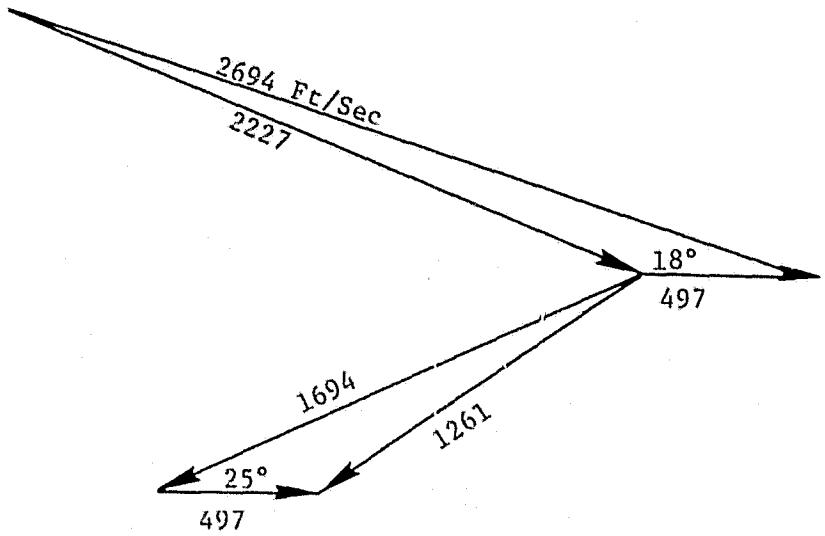

$N = 28486$ RPM

$P_{t_1} = 2186$ PSIA

$P_{N_1} = 2161$ PSIA

$P_{s_2} = 1809$ PSIA

$T_{t_1} = 797$ °R

$\dot{W} = 0.29$ LB/SEC

$D_m = 4.0$ IN.

Shaft HP = 21.505

$\eta_{T-T} = 0.319$

Figure 3-13. Low Pressure Fuel Turbine, Velocity Vector Diagram

TABLE 3-11. LOW PRESSURE FUEL TURBOPUMP TURBINE, BLADE PATH STATE CONDITIONS

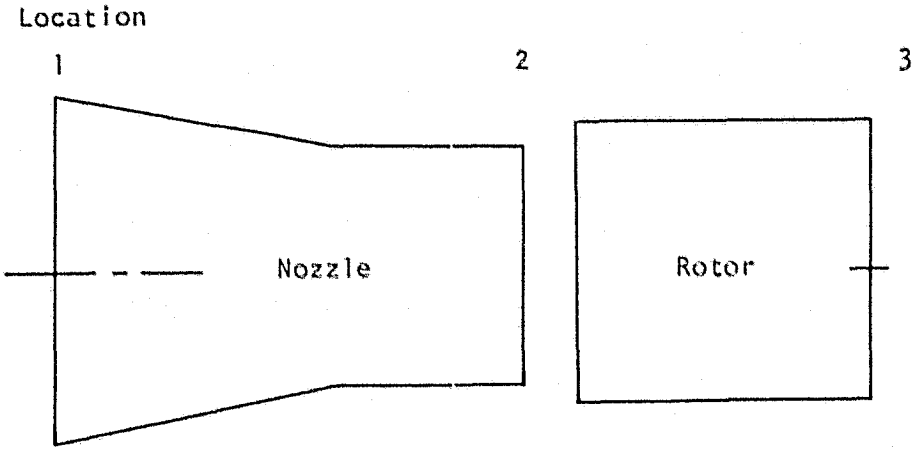

Location	1	2	3
Pressure, psia			
Total	2186		
Static		1809	1809
Temperature, °R			
Total	797		
Static			786

TABLE 3-12. LOW PRESSURE FUEL TURBOPUMP TURBINE, PRELIMINARY TURBINE BLADE PATH DATA

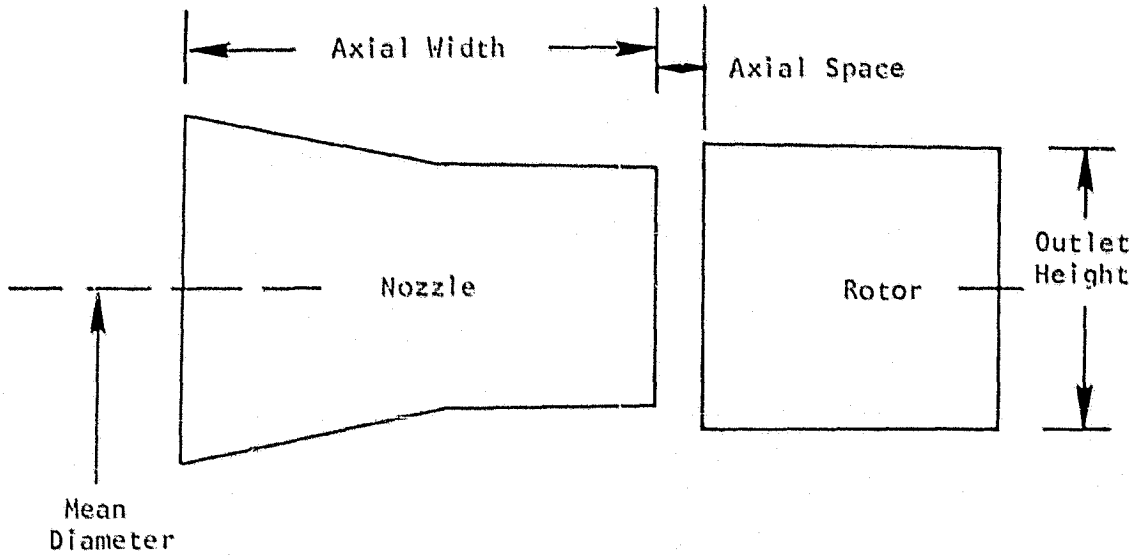

Element	Nozzle		Rotor
Mean Diameter, Inch	4.0		4.0
Outlet Height, Inch	0.25		0.30
Inlet Height, Inch	0.37		0.30
Axial Width, Inch	0.50		0.31
Axial Space, Inch		.050	
Percent Admission, %	2.4		
Admission Sectors	1		

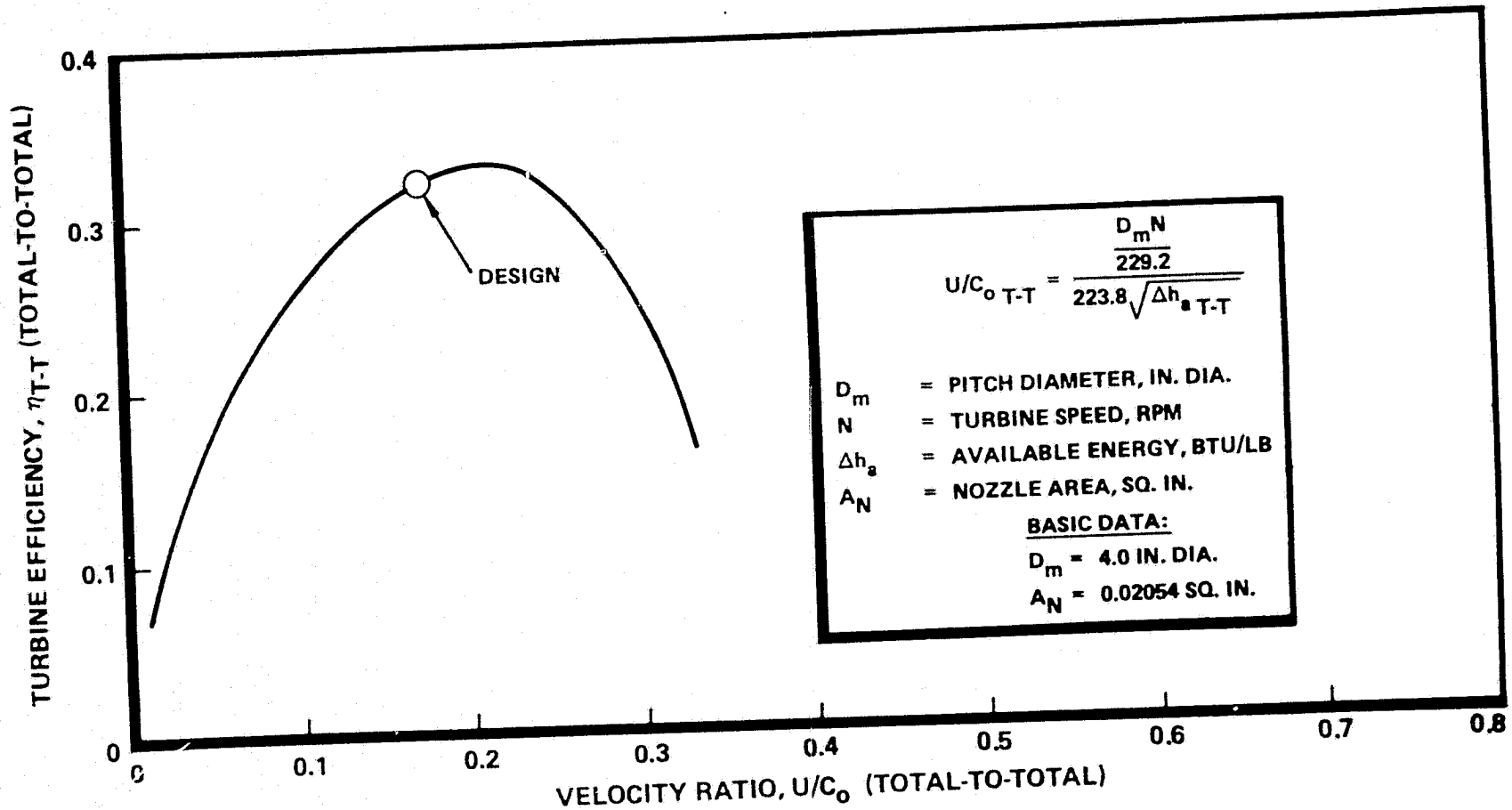

Figure 3-14. Low Pressure Fuel Turbopump Turbine Performance

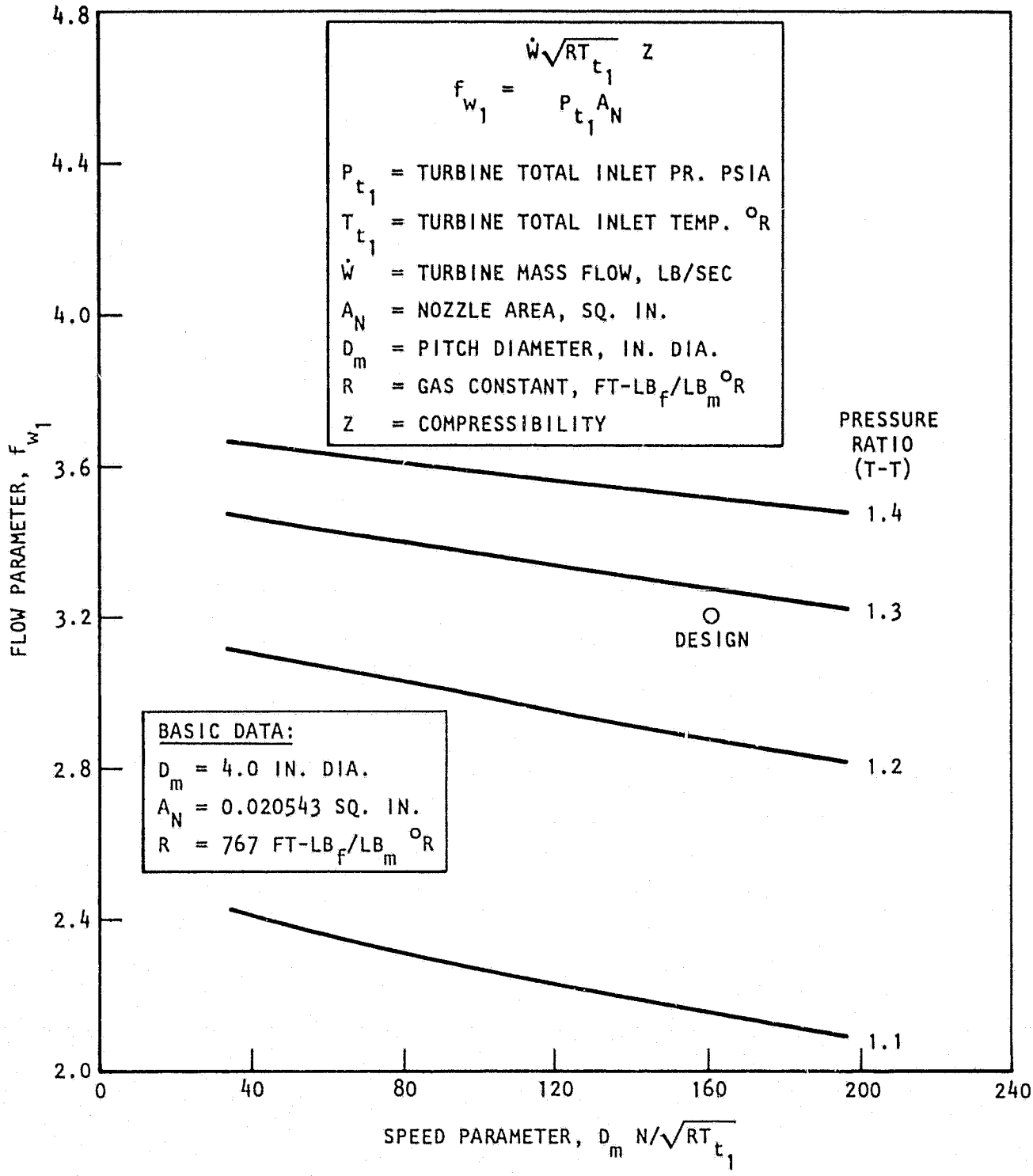

Figure 3-15. Low Pressure Fuel Turbopump Turbine Off-Design Performance

TABLE 3-13. LOW PRESSURE FUEL TURBOPUMP TURBINE, BLADE PATH GEOMETRY ASSUMPTIONS

Shrouded Rotor

Rotor Radial Tip Clearance = 0.0005 Inch

Rotor Upstream Shaft Seal

Diameter	= 0.55 Inch
Radial Clearance	= 0.002 Inch
Discharge Coefficient	= 0.65
Sonic Flow	

psia) at a bearing coolant flow of about 5 GPM will require development effort.

Rotordynamic Analysis. The low pressure fuel turbopump (LPFTP) will operate at 28,500 RPM which is below its calculated first critical speed of 35,180 RPM. The critical speed and mode shape analysis was based on a minimum bearing radial stiffness of 250,000 lb/in. The modal lumped mass group locations are shown on Figure 3-16. The critical speed plots and mode shapes are presented in Figures 3-17 and 3-18. No rotordynamic problems are anticipated.

High Pressure Fuel Turbopump

The pumping elements consist of three centrifugal impellers containing vanes, radial diffusers after each impeller, and an internal crossover passage following the first and second stage diffusers. Liquid hydrogen is introduced to the pump through an axial inlet with a centerbody housing the front bearing duplex pack and discharged through a scroll shaped outlet. The turbine assembly is a two stage partial admission design utilizing warm (860 R) gaseous hydrogen as the drive media. Turbopump speed for the expander cycle operation has been sized at approximately 110,000 RPM.

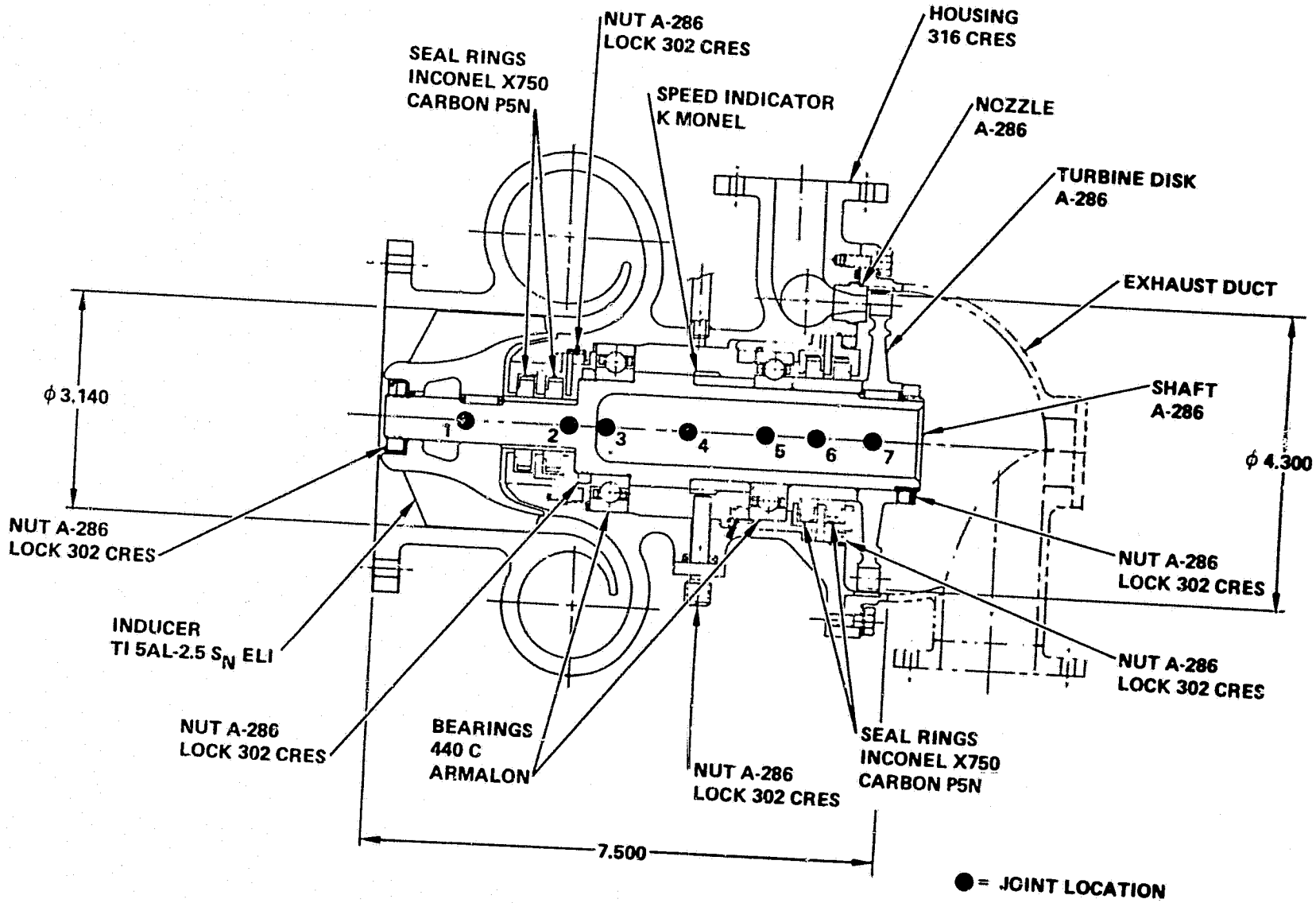

Figure 3-16. Fuel Low Pressure Turbopump

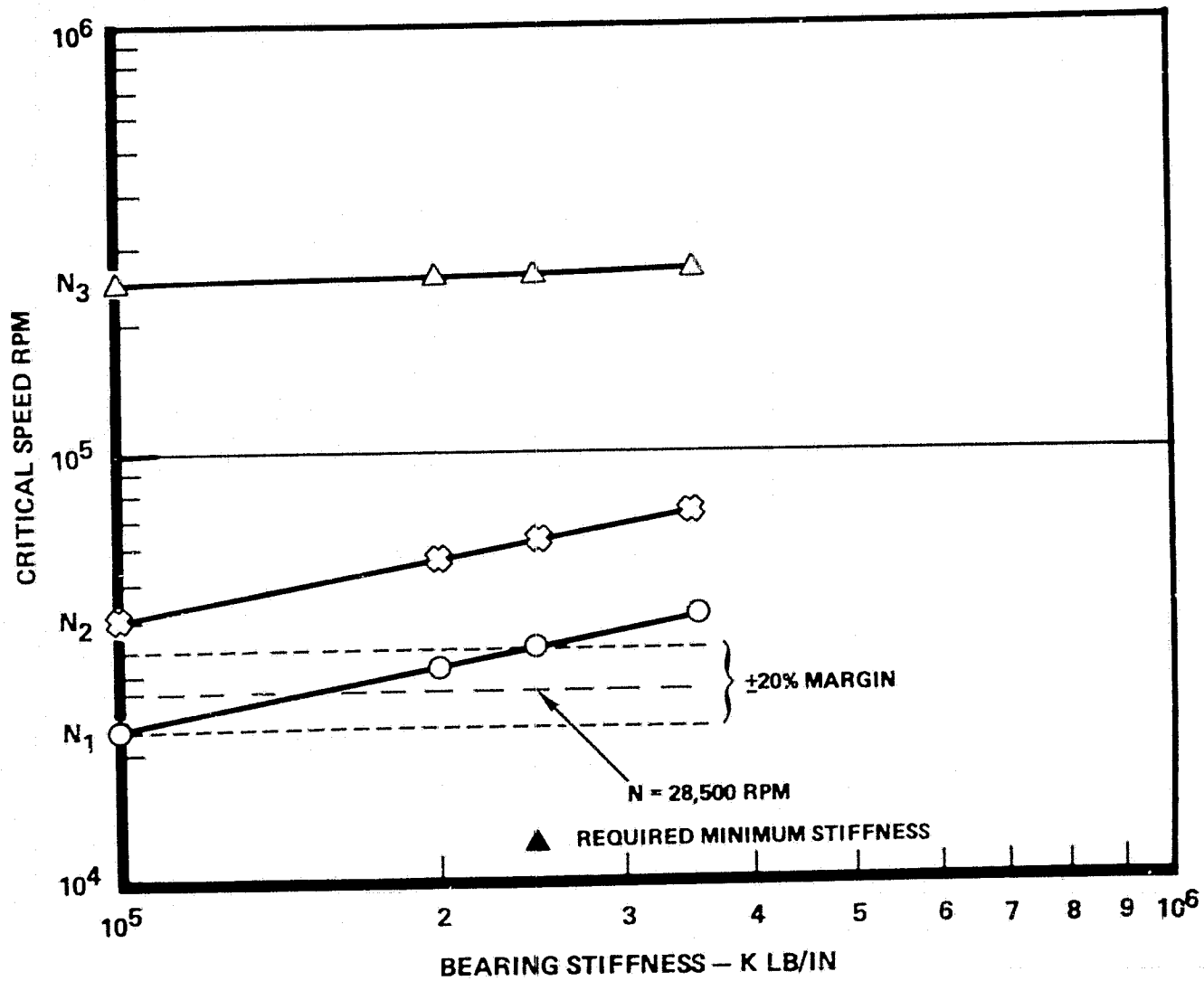

Figure 3-17. Critical Speed Vs. Bearing Stiffness

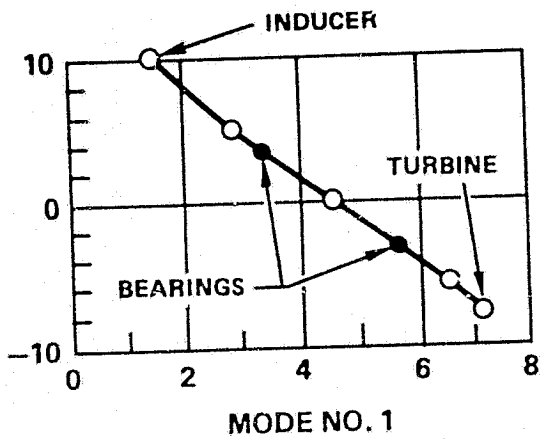

MODE NO. 1

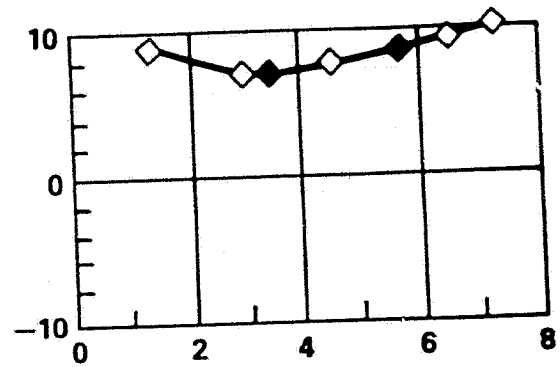

MODE NO. 3

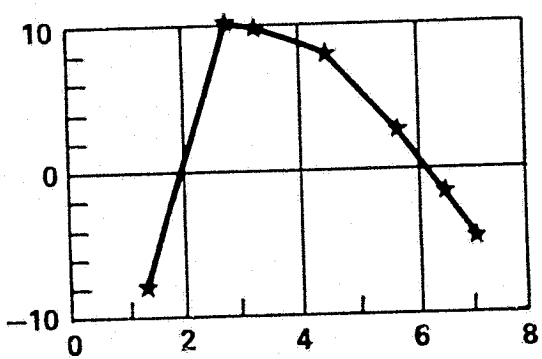

MODE NO. 2

MODE	HZ	RPM
1	586.320	35179.
2	1045.700	62743.
3	4296.100	257770.

K1 = 250000. LB/IN
K2 = 250000. LB/IN

MODE SHAPES

Figure 3-18. Low Pressure Fuel Turbopump Critical Speeds

Figure 3-19 shows the major dimensions of the turbopump, while Figures 3-20 and 3-21 show layouts of the turbopump assembly indicating the hardware description, material and development instrumentation selections.

Bearing design consists of two sets of 17 mm duplex bearings cooled with liquid hydrogen at a flow of about 5 GPM, each duplex pair.

The front (pump) end bearings are cooled by liquid hydrogen tapped off downstream of the inducer then re-directed immediately upstream of the inducer. Rear (turbine) bearing coolant is tapped off the pump discharge volute and directed into the aft side of the bearing pack into the balance piston sump where it joins the balance piston flow. The combination of both flowrates is then re-directed back to the eye of the second stage impeller.

The estimated total weight of the high pressure fuel turbopump, based on individual component geometry and material is about 37.3 pounds. Weight saving schemes include the use of bolt flange scalloping and the use of lightweight TENS-50 aluminum for the inlet housing and crossovers.

Pump Performance. The pump is required to deliver liquid hydrogen at a pressure of 4669 psia in the expander cycle. To develop the required pressure, a boost pump is used to increase the pressure at the high pressure pump inlet to a sufficient level to avoid cavitation. The high pressure pump then raises the pressure to the engine system requirement.

The thermodynamic analysis produced the flows, pressures, specific weights, and temperatures shown in Figures 3-22 and 3-24. These are based on hydrogen properties traceable to the National Bureau of Standards. A schematic diagram of the pump showing the flow paths is presented in Figure 3-22. The flow (4.12 #/sec) from the boost pump enters on the left and goes through the inducer into the first impeller eye.

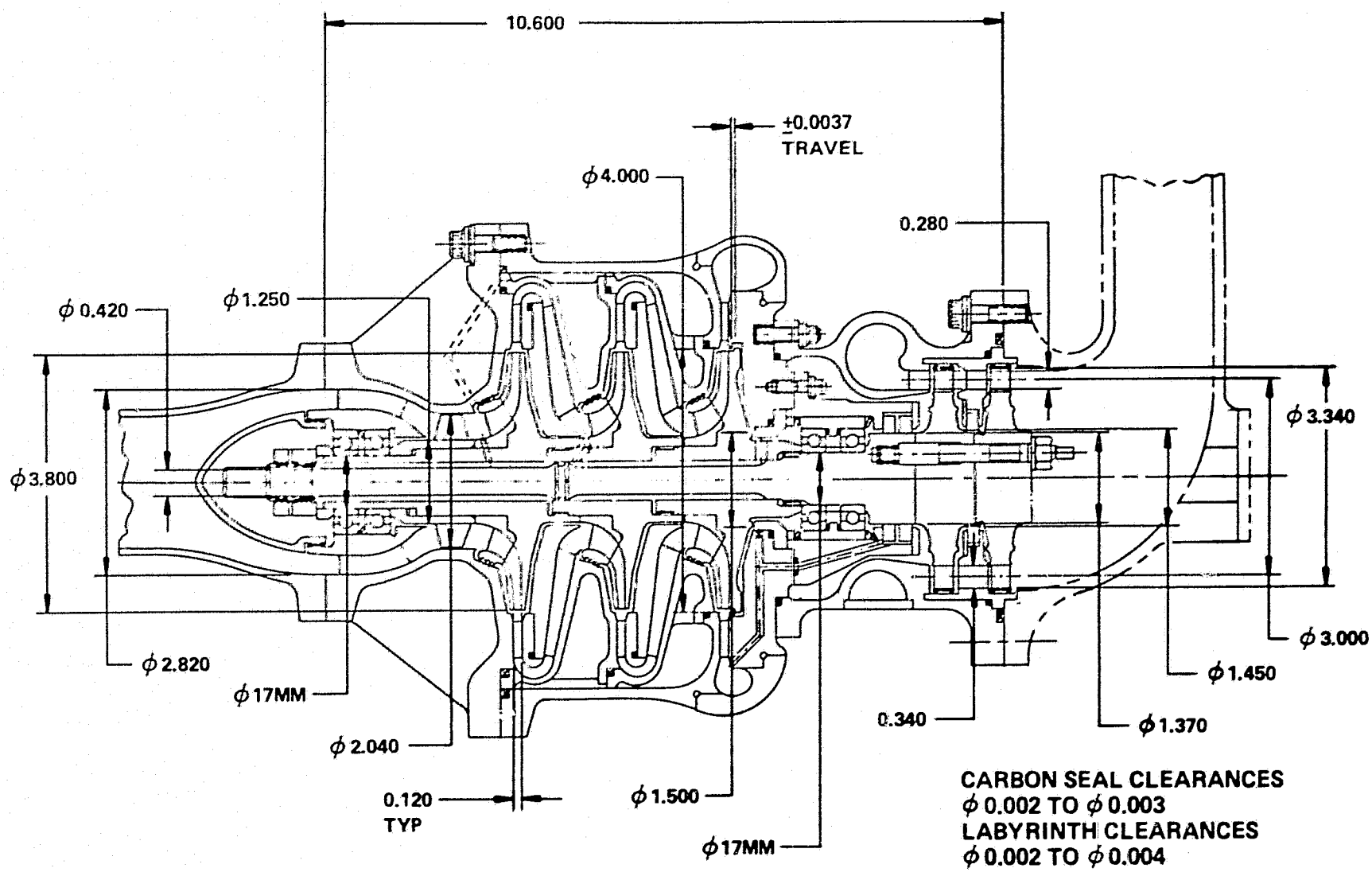

Figure 3-19. Fuel - High Pressure Turbopump

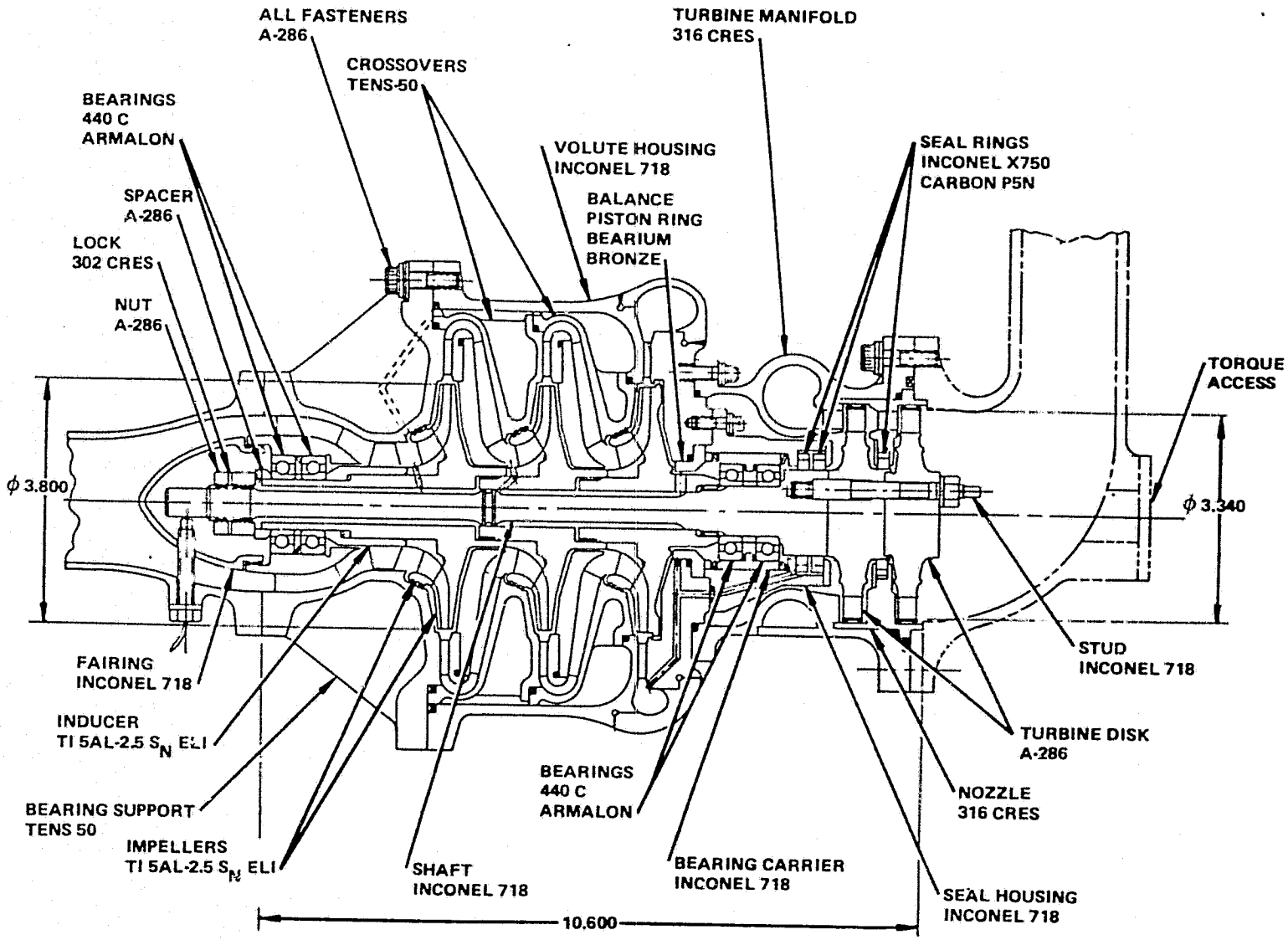

Figure 3-20. Fuel - High Pressure Turbopump Material Selection

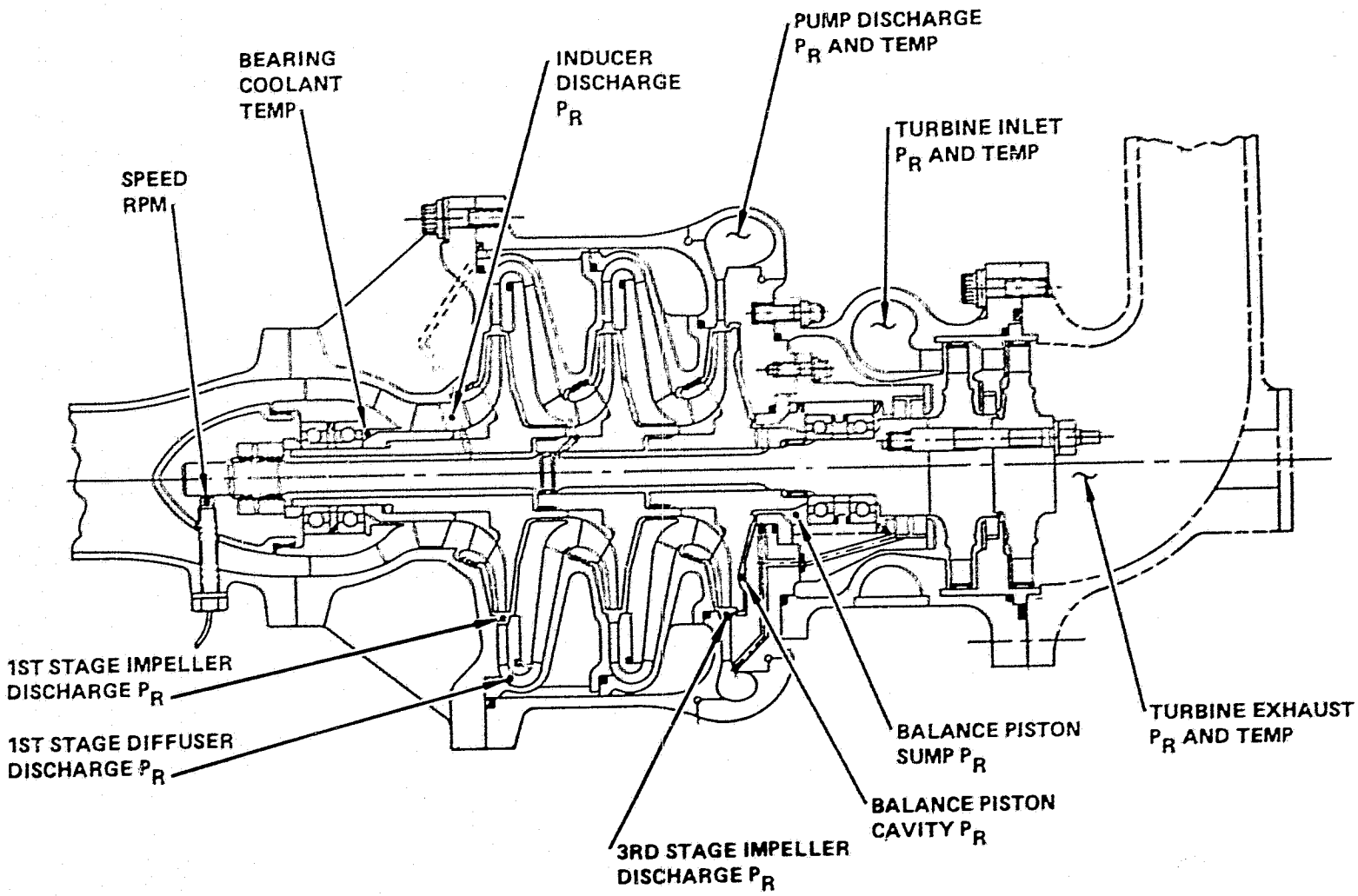

Figure 3-21. Fuel - High Pressure Turbopump
Development Instrumentation Selection

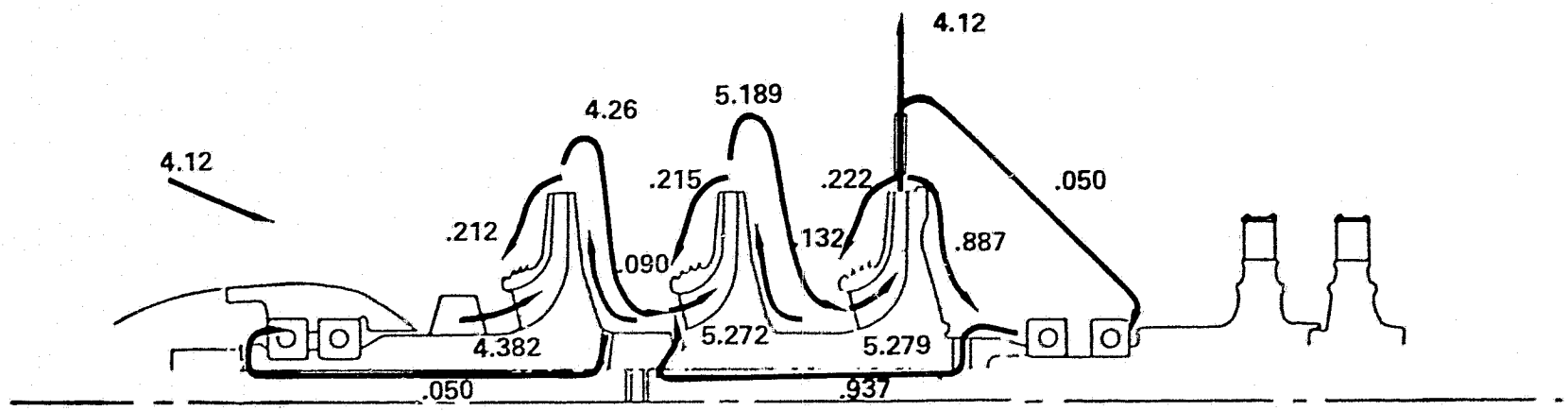

110,000 RPM
EXPANDER CYCLE
HIGH PRESSURE FUEL PUMP
FLOWS – LBS. PER SEC.

Figure 3-22. Flowrate Profiles in High Pressure Fuel Pump

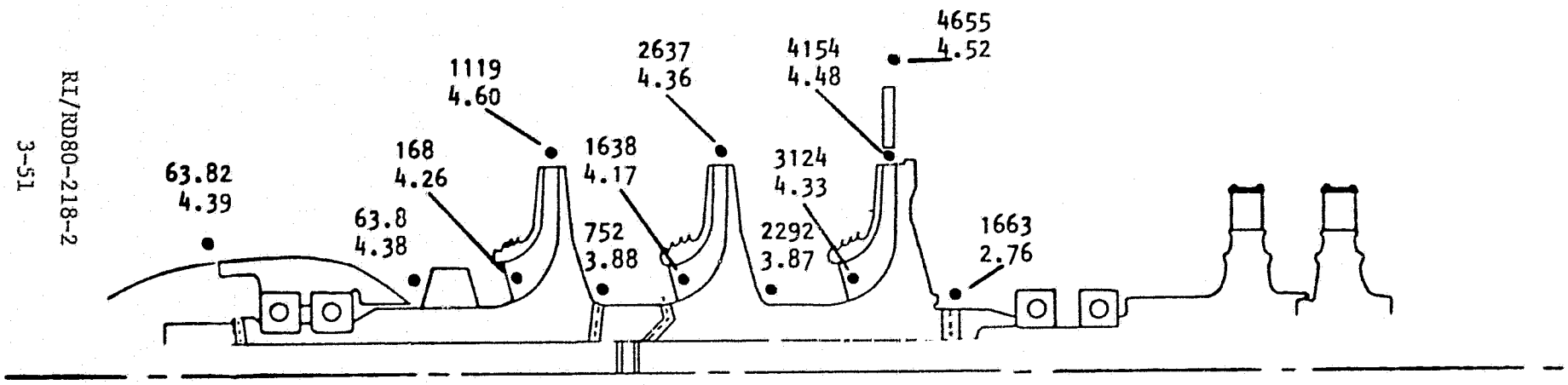

110,000 RPM

EXPANDER CYCLE

HIGH PRESSURE FUEL PUMP

PRESSURES - PSIA

SPECIFIC WTS. - LB. PER CU. FT.

Figure 3-23. Pressure and Density Profiles in High Pressure Fuel Pump

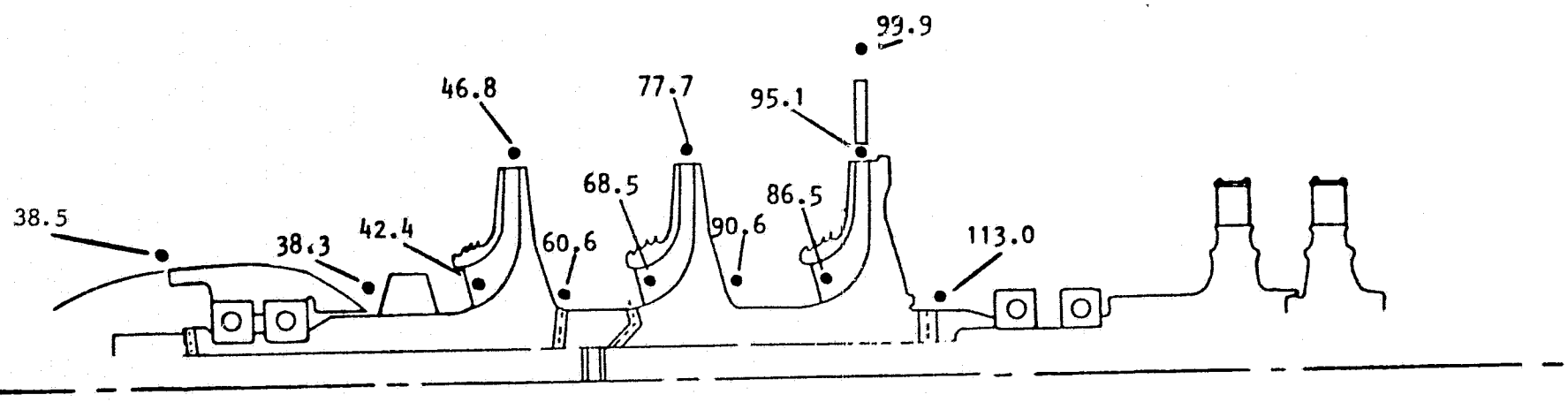

110,000 RPM

EXPANDER CYCLE

HIGH PRESSURE FUEL PUMP

TEMPERATURES - DEG. R.

Figure 3-24. Temperature Profiles in High Pressure Fuel Pump

It was assumed that the entering pressure is 10 psi lower than the boost pump discharge pressure. The front wearing ring flows of the impellers enter their respective impeller inlets. The first and second impeller rear shroud flows enter at the impeller discharge. Flow is removed from the first stage discharge to cool the front bearings. It is then returned to the pump inlet.

The balance piston flow returns to the second stage impeller eye. This produces a greater balance piston range than would be obtained if it were returned to the third stage impeller eye. The rear bearing (turbine end) is cooled by flow removed from the volute or diffuser discharge (Figure 3-22).

In this analysis, the bearing flowrates were assumed to be .05 pounds per second. The wearing ring clearances were assumed to be 0.002 inches radial. This is about as small as can realistically be fabricated. The first and second stage impeller rear wearing rings (MK48F design) were replaced by interstage seals at a smaller diameter which resulted in an efficiency of 63.5 percent. This improvement is more than would be expected in itself since only two of the five wearing rings were involved. However, these changes can effect changes in other areas such as in the balance piston flow. This influence is strong because the balance piston flow is about four times that of one wearing ring or interstage seal. The turbine thrust influence on balance piston flow has been included. The rear and front wearing ring discharge coefficients were assumed to be 0.6 and 0.5, respectively. The balance piston travel is 0.0073 inches.

The pump design parameter summary is presented in Table 3-14. The net pumped flow 4.12 lb/sec (Figure 3-22) leaves the pump third stage at a discharge pressure of 4655 psia (Figure 3-23) and a temperature of 95.1 R (Figure 3-24).

A head-capacity and efficiency capacity curve is presented in Figure 3-25. These are based on Mark 48 fuel pump data modified for the narrower impeller widths and resized volute.

TABLE 3-14. EXPANDER CYCLE HIGH PRESSURE FUEL PUMP AT 110,000 RPM

Operating Conditions:	
Speed, rpm	110,000
Flow, lb/sec	4.12
Inlet Pressure, psia	63.82
Inlet Temperature, Deg. R	38.5
Isentropic Head, ft.	134,635
Overall Efficiency, percent	63.6
Suct. Sp., Speed at Min. Available NPSH	16,400
Stage Conditions:	
Number of Stages	3
Stage Head, ft.	50,886
Stage Efficiency, pct.	72
Stage Specific Speed	657
Inducer:	
Tip Diameter, in.	2.04
Hub Diameter, in.	1.25
Head, ft.	2,953
Impeller:	
Tip Diameter, in.	3.8
Eye Diameter, in.	2.05
Hub Diameter, in.	1.3
Front Wearing Ring Diameter, in.	2.3
Interstage Seal Diameter, in.	1.3
Tip Speed, fps.	1,824
Tip Width, in.	0.120
Balance Piston:	
Total Travel, in.	0.0073
High Pressure Pad Diameter, in.	4.0
Low Pressure Pad Diameter, in.	1.5
Diffuser and Volute:	
Diffuser I. D., in.	4.10
Diffuser O. D., in.	5.25
Volute Maximum Area, sq. in.	0.550

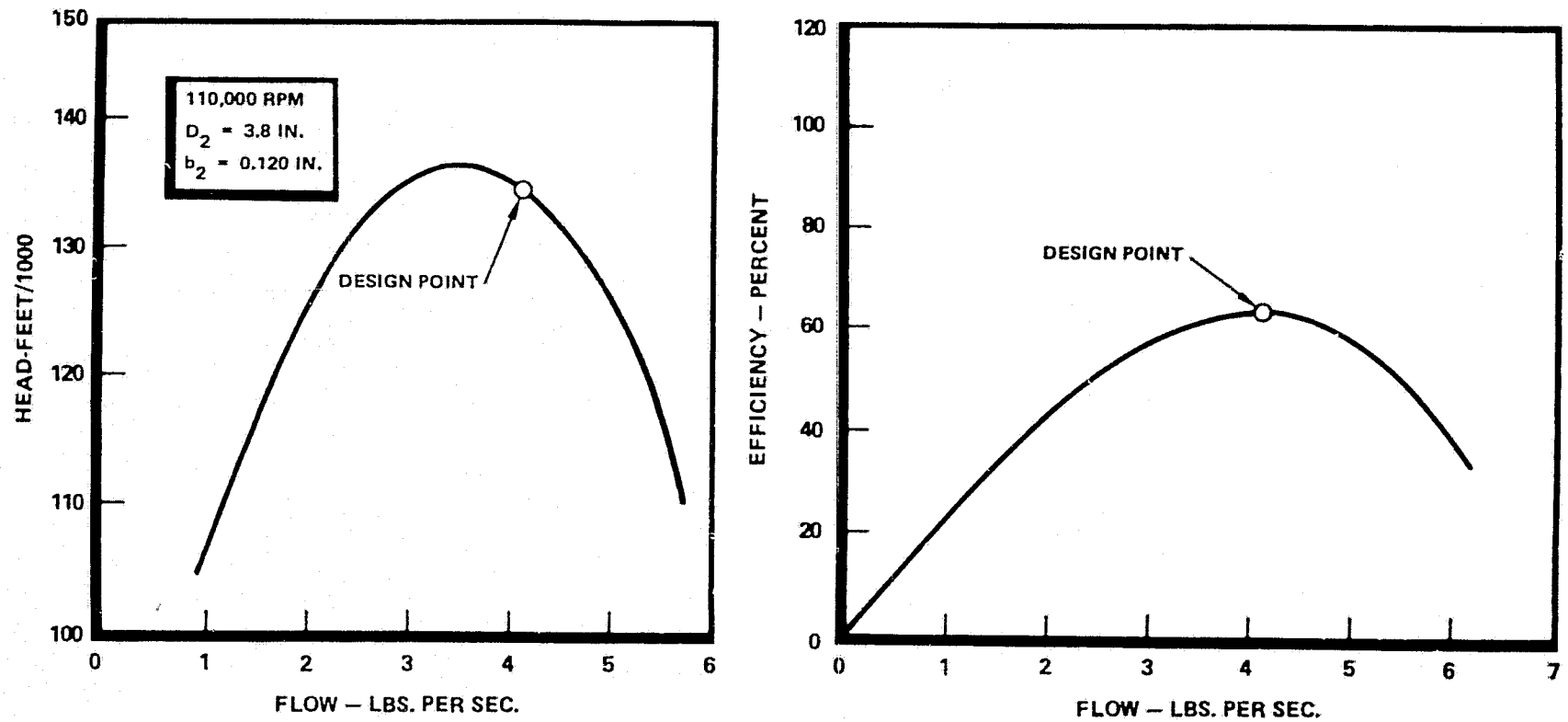

Figure 3-25. Head and Efficiency Vs. Capacity, High Pressure Fuel Pump

The minimum available NPSH results in a maximum suction specific speed for the high pressure pump of 15,000, which dictates incorporating an inducer before the first stage impeller. Based on conservative estimates from Rocketdyne data on pump suction performance, the inducer will have a suction specific speed capability of 25,300, which provides a large margin.

The radial load of the pump is predicted to be 100 pounds acting over the third impeller discharge. To determine this value, the SSME-HPFP value was scaled to this size and a small pad added to allow for exaggerated manufacturing variations as a result of the smaller size.

The net axial thrust of the pump is 26,266 pounds toward the turbine. The balance piston flowrate and capability are shown in Figure 3-26. Without the turbine, the pump would operate at 21 percent of the force range and with the orifice open to 35 percent of the total travel. When the turbine thrust is added, the balance point is at 55 percent of the force range and with the top orifice 31 percent open.

HPFTP Turbine Analysis. The HPFTP turbine design for the expander engine is similar in size and operating conditions to the Mark 48-F turbine for the Advanced Space Engine Fuel turbopump. However, the Mark 48-F was a two-stage full admission design, whereas the expander turbine is partial admission. The partial admission losses for this design have been conservatively estimated, and the confidence of meeting the predicted turbine performance is high.

The turbine was designed for optimum performance and minimum weight. The analysis was performed using Rocketdyne's Partial Admission Gaseous Hydrogen Turbine Analysis Computer Program. The program includes all gas path losses due to friction, turning, and secondary flows as well as partial admission losses due to blade pumping and windage, end sector losses, and staging losses, as well as a size effect based on experimental test results.

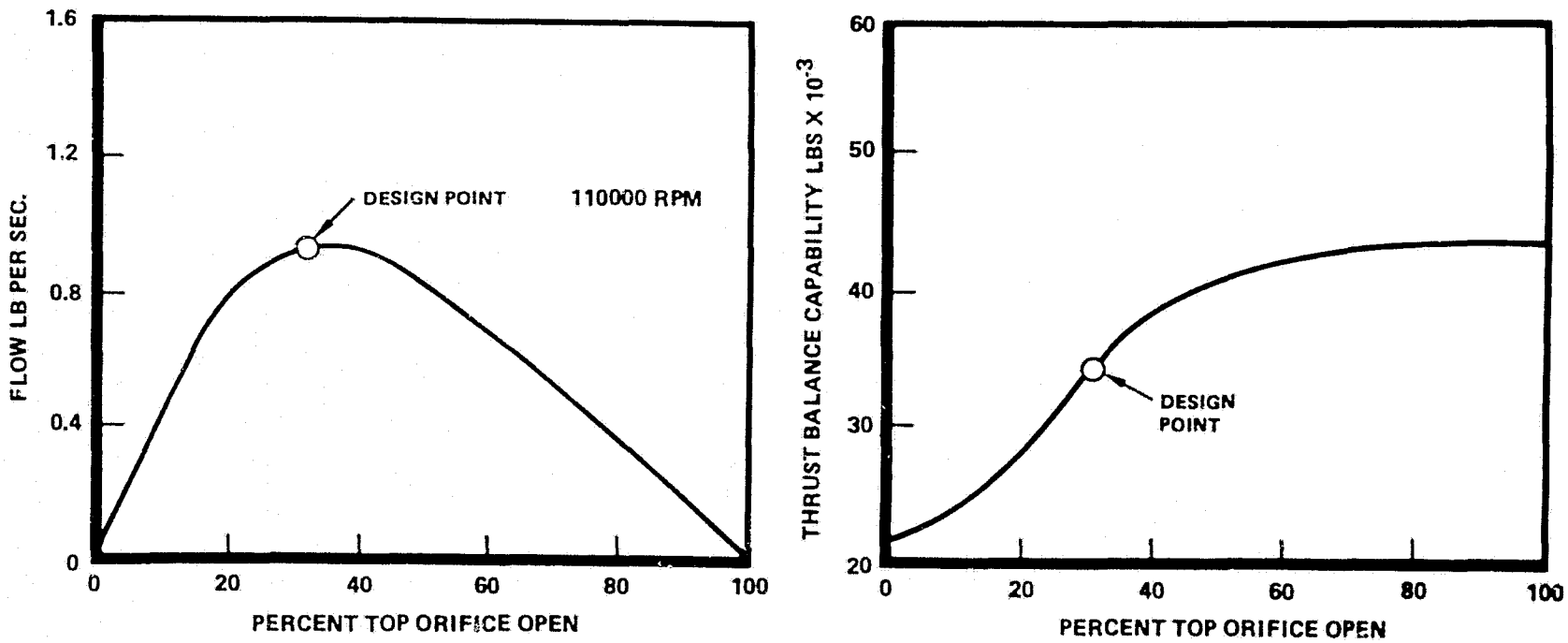

Figure 3-26. Balance Piston Flow and Performance, High Pressure Fuel Pump

Turbine design parameters are listed in Table 3-15. Turbine power and speed were from the pump design. Turbine flow, inlet pressure and temperature, and pressure ratio were taken from the engine computer balance. Inlet conditions were considered specified at the turbine inlet flange which is in the turbine inlet pipe just upstream of the turbine inlet manifold. Turbine outlet total pressure and temperature are specified in the turbine outlet pipe just downstream of the turbine outlet collector.

Turbine geometry parameters were optimized for high performance and minimum weight. The selected turbine mean diameter is shown in Fig. 3-27 for optimized blade heights and angles. On the greatly expanded relative efficiency scale, the selected diameter of 3.0 inches is shown to be within .03 points of the peak efficiency, but is 7 percent smaller than the diameter at peak efficiency. The selected diameter results in performance very close to peak efficiency but with a smaller size resulting in a lower weight of the turbine high pressure housings and rotors.

The turbine predicted power losses are tabulated in Table 3-16. Primary losses are due to friction and turning in the nozzle and rotor profiles as shown by the expansion and kinetic energy losses. The inlet manifold loss was for a manifold with a radial inlet on a bifurcated torus to each sector of axial inlet nozzles. The velocity out of the first stage was assumed not available to the second partial admission stage. The velocity out of the second stage was also assumed lost in the outlet manifold, and the total pressure at the turbine outlet flange was assumed to be equal to the static pressure at the second rotor outlet. Partial admission losses and disk friction losses are also shown for each stage.

The velocity vector diagrams are shown in Fig. 3-28 for the design condition. Velocities out of each element include losses due to friction and turning but not losses due to disk friction, size effect or partial admission. Nozzle outlet mach numbers are less than 0.65. It was conservatively assumed that all of the absolute kinetic energy out of the first rotor (the energy equivalent for the 815 feet per second velocity) was lost and not available to the second stage, partial admission nozzle. The turbine was designed for equal power from each stage.

TABLE 3-15. HIGH PRESSURE FUEL TURBOPUMP TURBINE, PERFORMANCE PARAMETERS

Working Fluid	-	Gaseous Hydrogen
Output Power	HP	1550
Speed	RPM	110,000
Inlet Flowrate	Lb/Sec	3.64
Inlet Total Temperature	°R	861
Inlet Total Pressure	PSIAT	3787
Outlet Total Pressure	PSIAT	2202
Pressure Ratio, Total-To-Total	-	1.7193
Available Energy	BTU/LB	473.7
Isentropic Velocity	FT/SEC	4894
Mean Diameter	INCH	3.000
Mean Blade Speed	FT/SEC	1440
Overall Velocity Ratio	-	0.294
Equivalent Stage Velocity Ratio	-	0.416
Efficiency, Total-To-Total	-	0.636

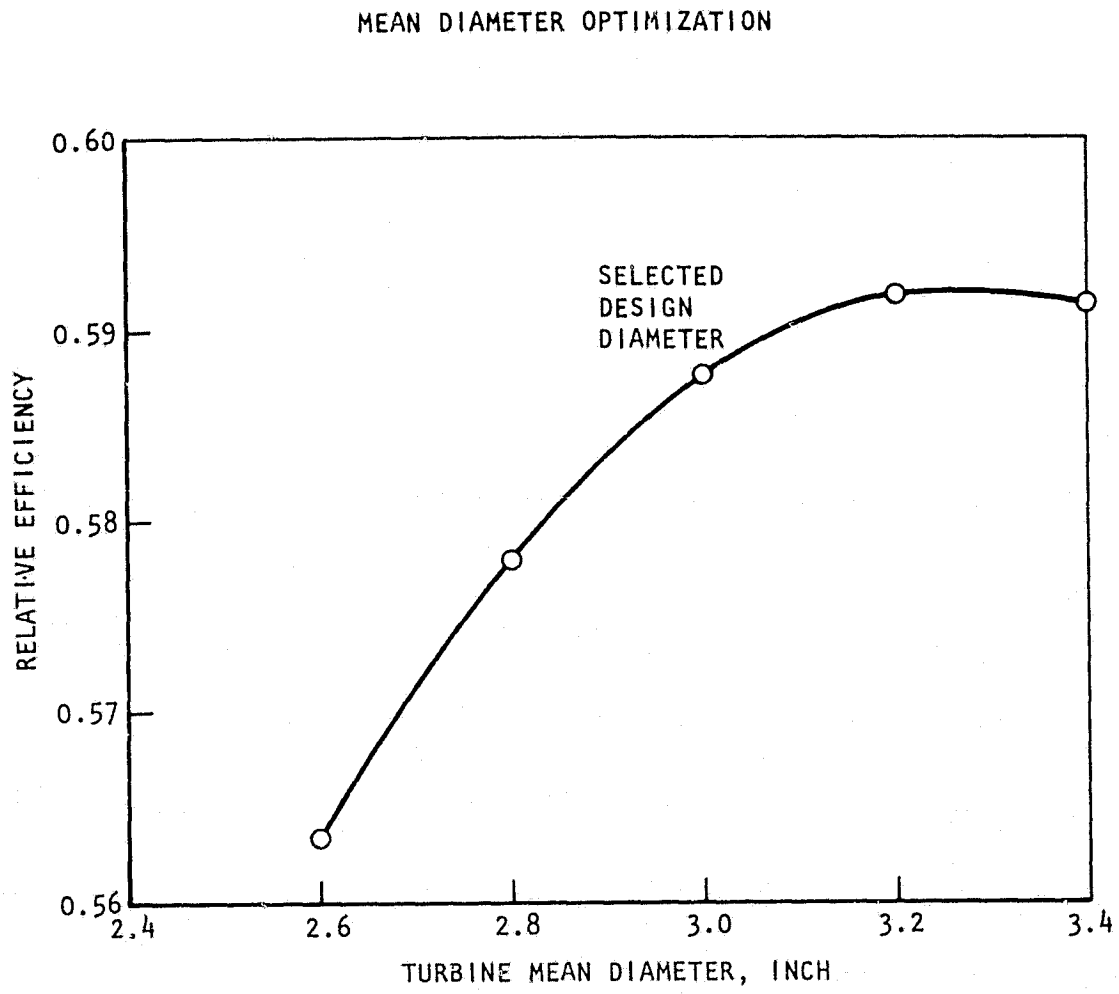

Figure 3-27. Mean Diameter Optimization, High Pressure Fuel Turbopump Turbine

TABLE 3-16. HIGH PRESSURE FUEL TURBOPUMP TURBINE, FLANGE TO FLANGE EFFICIENCY AND PERFORMANCE

	Flowrate Lb/Sec	Enthalpy Btu/Lb	Power Loss HP
1. Power Losses			
Inlet Manifold	3.6400	16.8909	86.9984
1-N Inlet Incidence	3.6400	.0000	.0000
1-N Inlet Kinetic Energy	3.6400	.0000	.0000
1-N Expansion Energy	3.6400	20.3717	104.9265
1-R U/S Shaft Seal	.0000	356.3101	.0000
1-R Inlet Incidence	3.6400	.0000	.0000
1-R Inlet Kinetic Energy	3.6400	26.8572	138.3305
1-R Expansion Energy	3.6400	.0000	.0000
1-R Windage			27.3922
1-R End Sector Mixing			16.7441
1-R Rim Friction			5.3291
1-R Disk Friction			3.3545
1-R End Clearance	3.6400	.0000	.0000
S-1 Diagram Factor Adjustment	3.6400	7.5921	38.1152
2-N Shaft Seal	.1326	176.5299	33.1171
2-N Inlet Incidence	3.5074	.0000	.0000
2-N Inlet Kinetic Energy	3.5074	13.2570	65.7941
2-N Expansion Energy	3.5074	18.2142	90.3969
2-R Inlet Incidence	3.5074	.0000	.0000
2-R Inlet Kinetic Energy	3.5074	25.8631	128.3585
2-R Expansion Energy	3.5074	.0000	.0000
2-R Windage			20.1080
2-R End Sector Mixing			12.9287
2-R Rim Friction			4.3981
2-R Disk Friction			2.7685
2-R End Clearance*	3.5074	.0000	.0000
S-2 Diagram Factor Adjustment	3.5074	7.4550	36.0242
2-R Leaving Energy	3.6400	12.8647	66.2611
TOTAL POWER LOSSES			881.3457
*Include in Diagram Factor Adjustment			
2. Available Power			
WDOT Inlet Flange	3.6400		
DHA T-T F-F **	473.6620		
HP Available T-T F-F	2439.6436		
3. Shaft Power, Etc., Overhaul			
HP Available T-T F-F	2439.6436		
Total Power Losses	881.3457		
Shaft BHP	1558.2979		
Overall Efficiency T-T F-F	0.6387		
Overall UM/CO T-T	.2956		
Overall UM/CO T-T SQRT (2)	.4181		

**T-T F-F: Total-to-Total, Flange-to-Flange

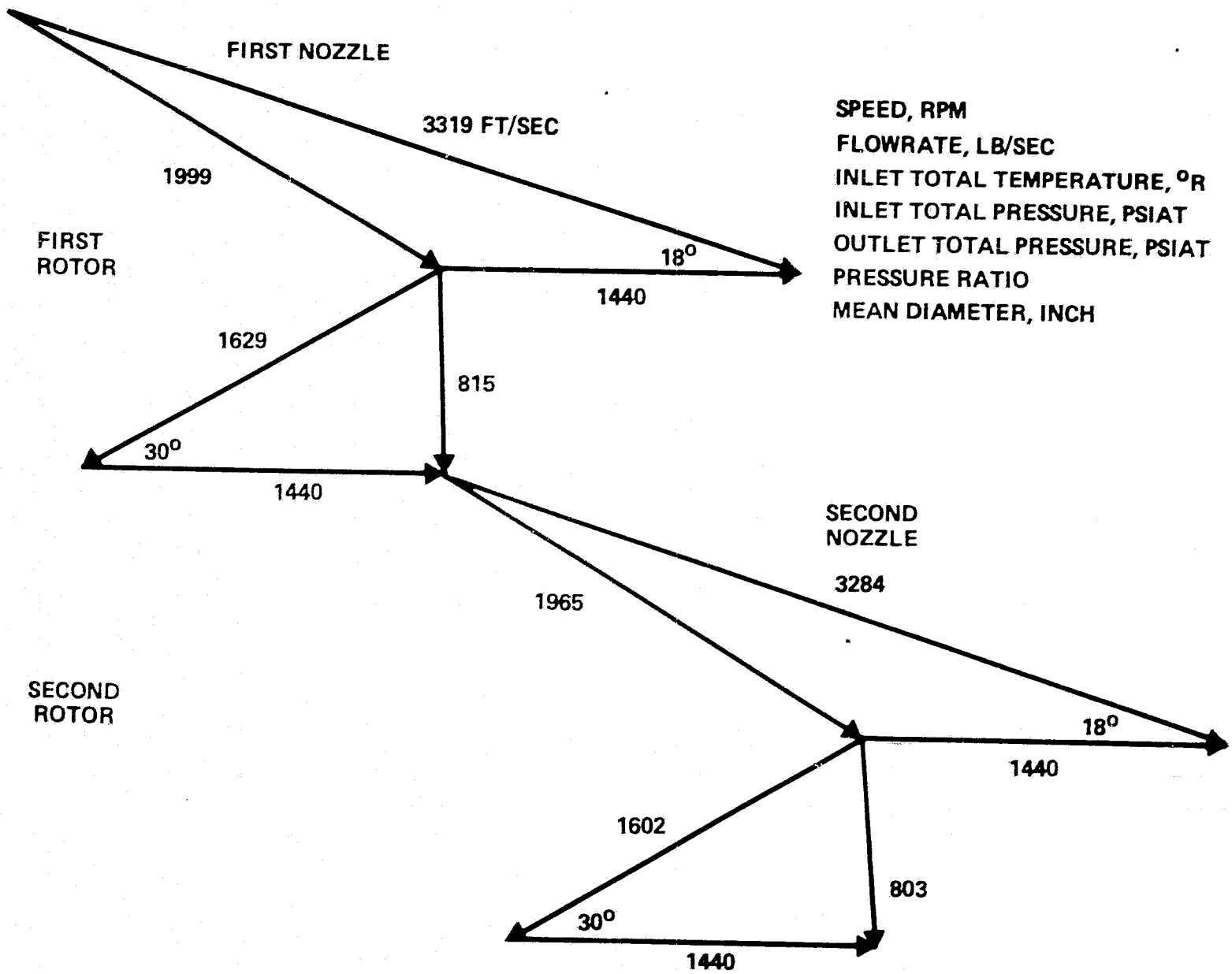

SPEED, RPM	110,000
FLOWRATE, LB/SEC	3.64
INLET TOTAL TEMPERATURE, °R	875
INLET TOTAL PRESSURE, PSIAT	3787
OUTLET TOTAL PRESSURE, PSIAT	2202
PRESSURE RATIO	1.72
MEAN DIAMETER, INCH	3.0

Figure 3-28. Velocity Vector Diagrams, High Pressure Fuel Turbopump Turbine

The total and static pressures and temperatures in the blade path are shown in Fig. 3-29. The constant static pressure across the first and second stage rotors are for the impulse design and to minimize pumping losses in the inactive rotor blades with partial admission. All the expansion and acceleration of the flow occurs across the nozzles at the design condition. Since each rotor is pressure balanced, there will be no rotor axial thrust component at the design condition. Axial thrust will be generated from the second rotor outlet pressure applied over the area inside the turbine interstage seal diameter.

Turbine sizing is shown in Fig. 3-30 with a mean diameter of 3.0 inches for each element. Nozzle heights and widths were the same for both stages to minimize costs by using the same profile for both stages. The arc of admission was varied to achieve the required flow areas. Rotor heights and widths were also the same for both stages. The axial spaces between the nozzles and rotors should be minimum to reduce spillage loss at the ends of the arcs of admission. A large space equal to two-thirds of the rotor width was provided between the first rotor and the second nozzle. The large space provides room for the gas to flow into the second stage nozzle after the partial admission first stage. Two nozzle sectors (groups) were assumed for each nozzle to provide structural and dynamic symmetry. Using a single sector of nozzles would improve turbine performance by approximately 2-3 percent.

The blade path assumptions are listed in Table 3-17. The rotor blades were shrouded for improved performance with a radial tip clearance of 0.005 inch. The leakage past the first rotor upstream side shaft seal was into the blading. This leakage was assumed to do no work in the turbine. Flow area sizing will include the leakage. The leakage through the second nozzle shaft seal, by-passing the second nozzle was assumed to do no work in the second stage.

Design and off-design predicted performance is shown in Figures 3-31 and 3-32. Turbine flowrate in Fig. 3-31 varies with speed, turbine inlet conditions, and turbine pressure ratio. Turbine efficiency for the subsonic design varies with turbine velocity ratio in Figure 3-38.

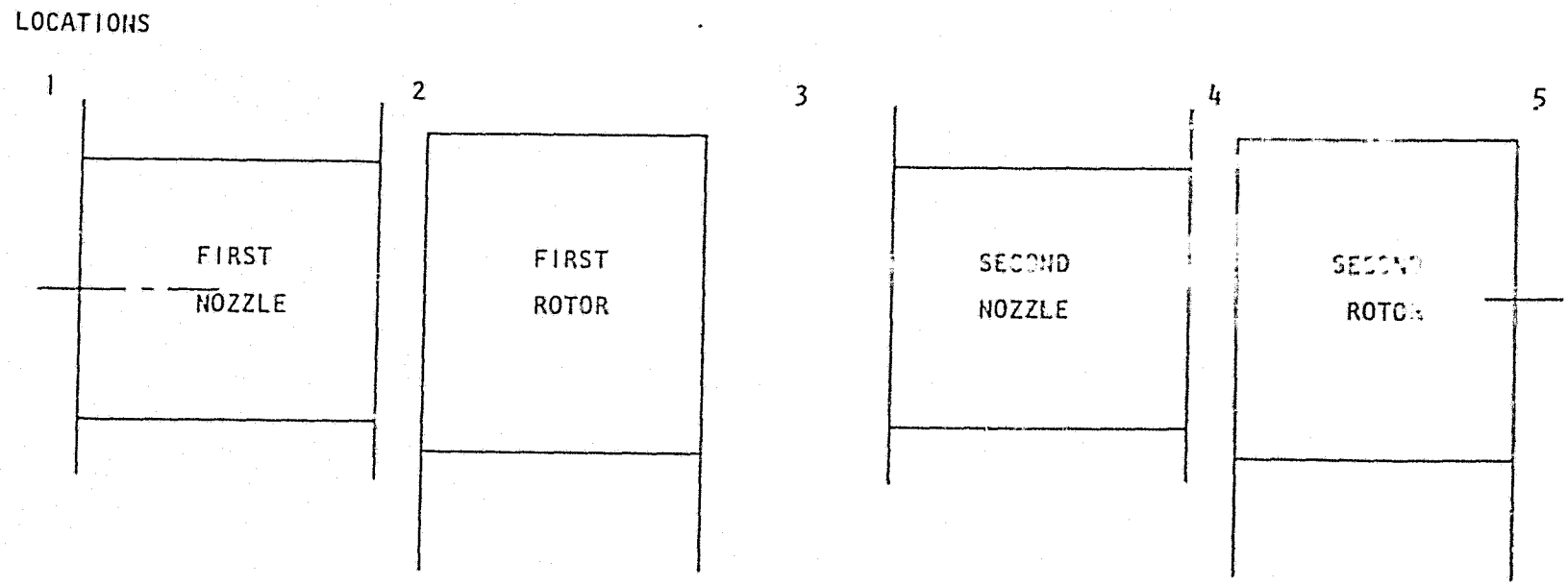

LOCATION	1	2	3	4	5
PRESSURES, PSIA					
TOTAL	3787	-	-	-	-
STATIC	-	2887	2887	2202	2202
TEMPERATURES, ^{o}R					
TOTAL	875	-	-	-	-
STATIC	-	826	834	808	797

Figure 3-29. HPFTP Turbine - Expander Engine Blade Path State Conditions

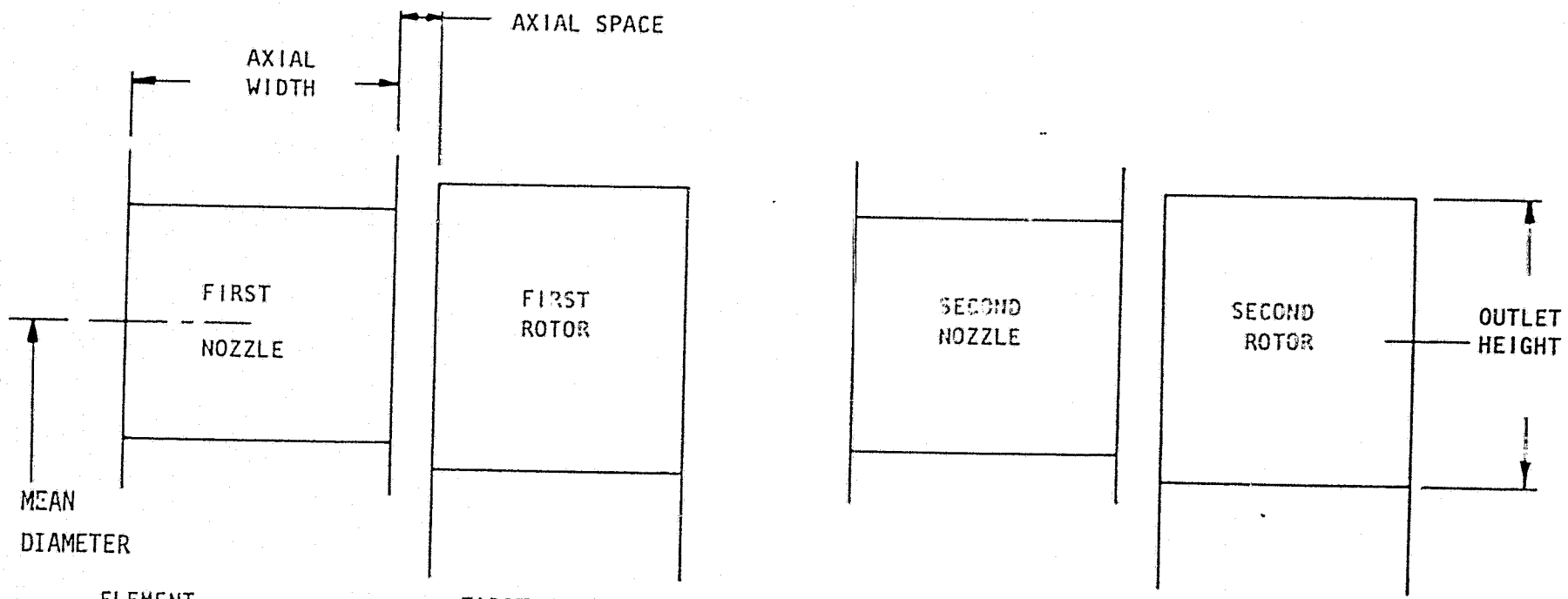

ELEMENT	FIRST NOZZLE		FIRST ROTOR		SECOND NOZZLE		SECOND ROTOR
MEAN DIAMETER, INCH	3.0		3.0		3.0		3.0
OUTLET HEIGHT, INCH	0.28		0.34		0.28		0.34
AXIAL WIDTH, INCH	0.32		0.30		0.32		0.30
AXIAL SPACE, INCH		0.05		0.20		0.05	
PERCENT ADMISSION, %	33				41		
ADMISSION SECTORS	2				2		

Figure 3-30. HPFTP Turbine Preliminary Turbine Blade Path Data

TABLE 3-17. HIGH PRESSURE FUEL TURBOPUMP TURBINE, BLADE PATH GEOMETRY ASSUMPTIONS

Shrouded Rotors	
Rotor Radial Tip Clearance	= 0.005 Inch
First Rotor Upstream Shaft Seal	
Leakage into Blade Path	
No Work Done by Leakage	
Flow Areas Sized to Include Leakage	
Second Nozzle Seal	
Diameter	= 2.00 Inch
Radial Clearance	= 0.0025 Inch
Discharge Coefficient	= 0.65

High Pressure Fuel Turbopump Rotordynamics Analysis. A preliminary analysis of the original design concept indicated the turbopump could operate at approximately 100,000 RPM between the second and third critical speeds. Recommended design changes increased the third critical speed to 129,000 RPM. However, iterative design changes for this revised analysis have an operational speed of 110,000 RPM, an inducer on the shaft and increased length between the third stage impeller and the turbine bearings. The increase in speed alone violates the 20 percent critical speed design margin practice based on the original analysis. The additional inducer weight and increased flexibility with the additional length in a shaft section with a significant effect on the location of the third critical are both changes in an undesirable direction. Modal lumped mass group locations used in this analysis are shown in Figure 3-33.

For the current design a radial bearing stiffness of 150,000 lb/in is required to provide an equivalent bearing pair radial stiffness of 300,000 lb/in and raise the third critical speed above 148,500 RPM. This bearing spring rate sets the

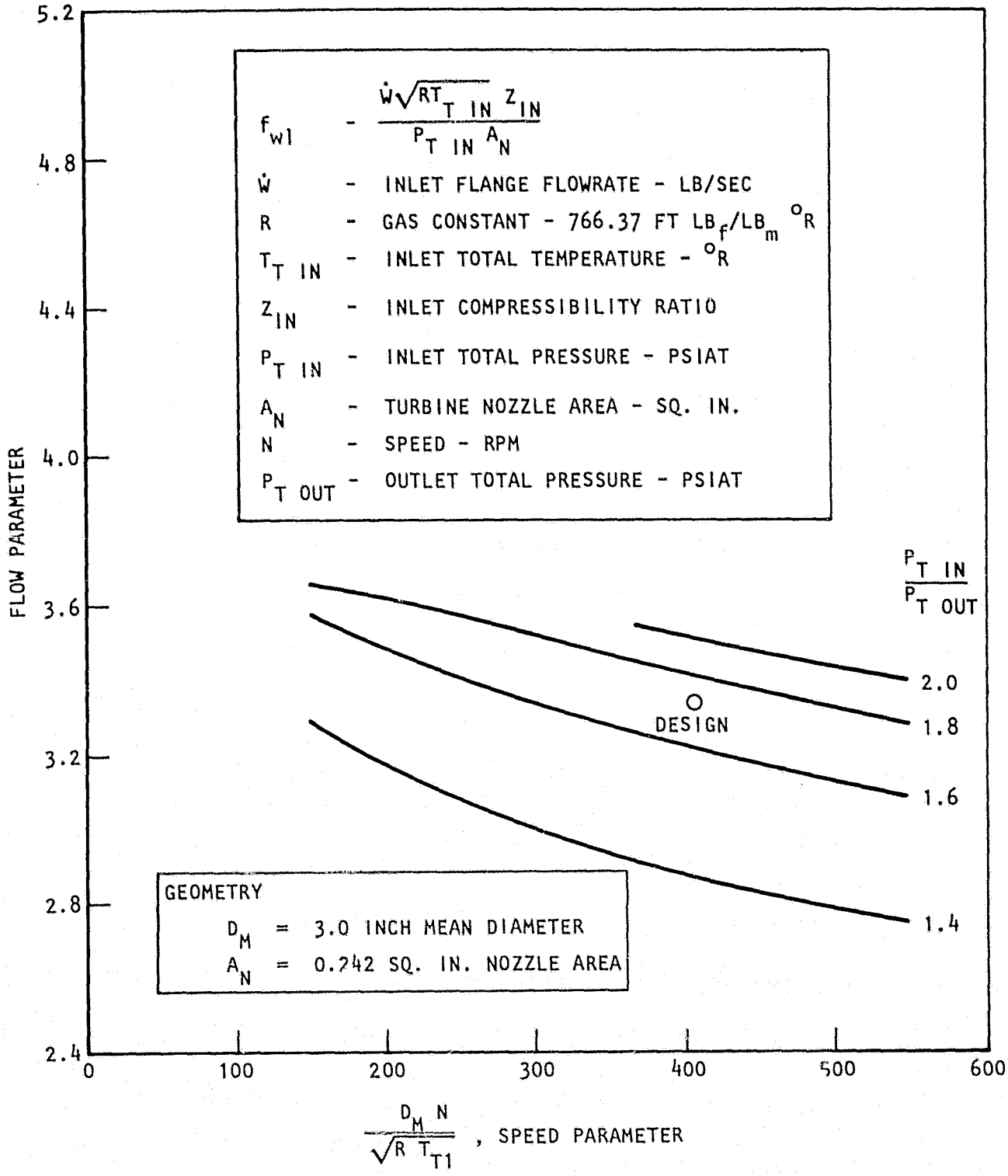

Figure 3-31. Off-Design Performance, High Pressure Fuel Turbopump Performance

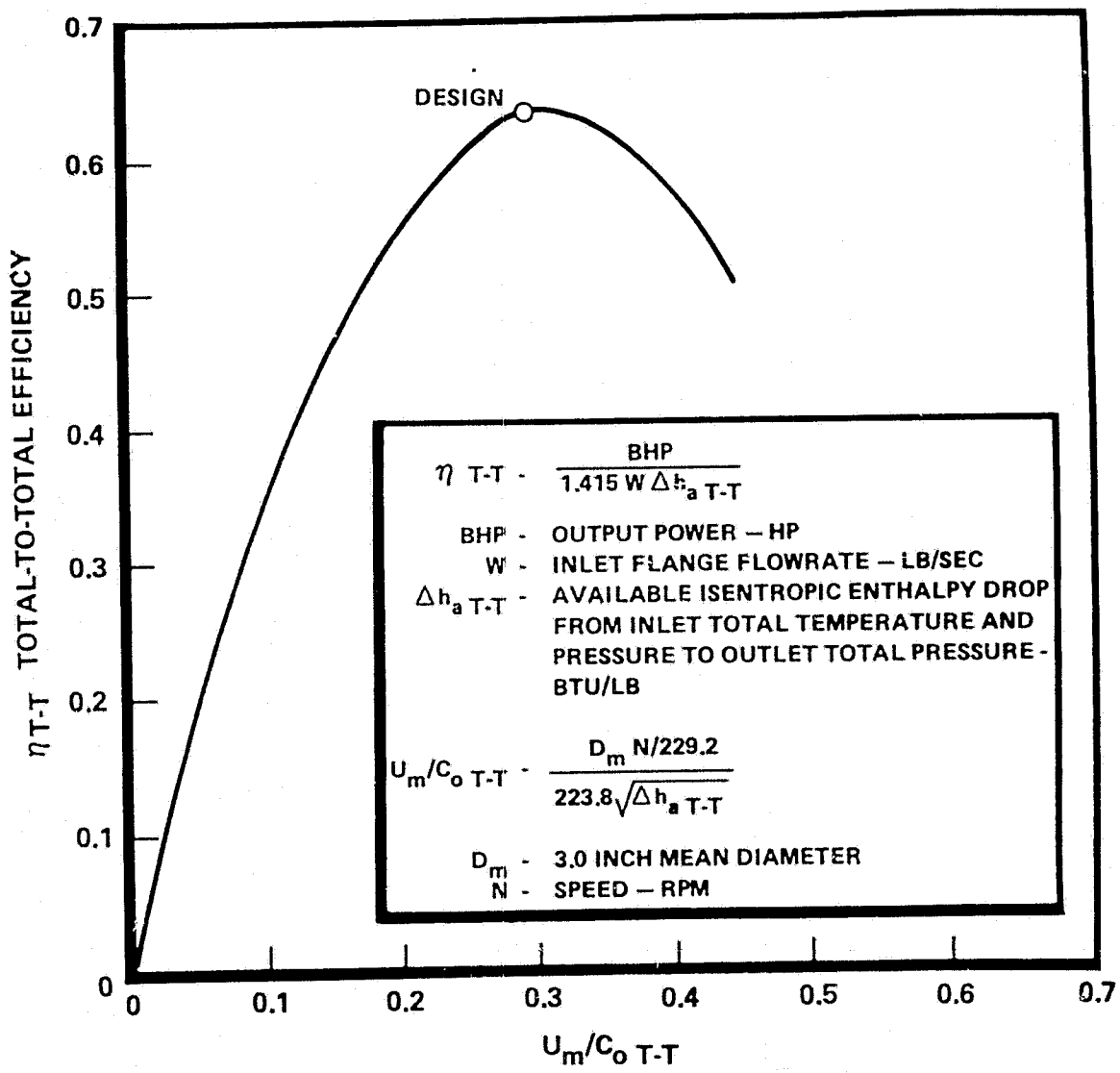

Figure 3-32. Predicted Efficiency, High Pressure Fuel Turbopump Turbine

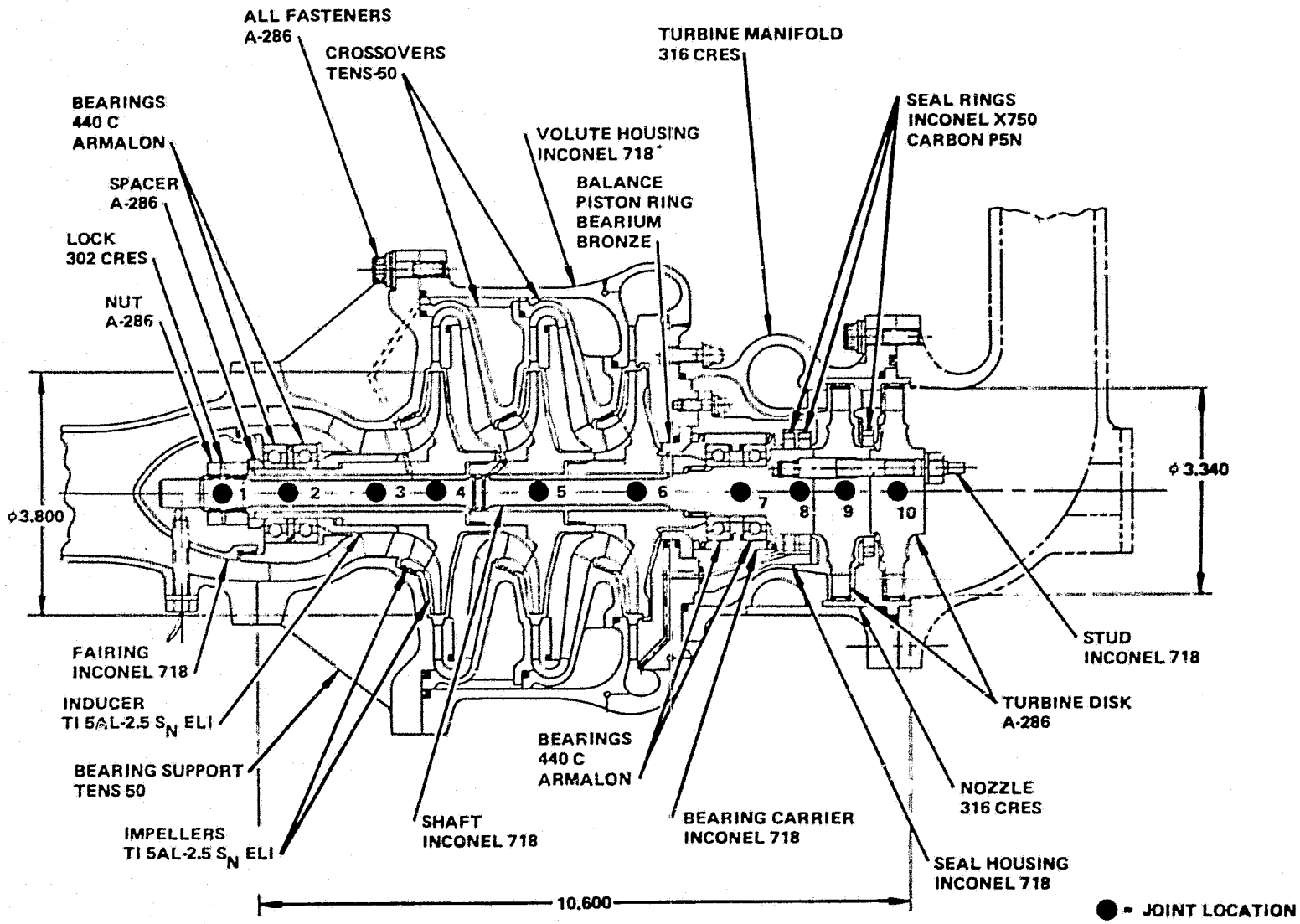

Figure 3-33. Fuel - High Pressure Turbopump

operating speed between the second and third critical speed with 35 percent margin for the third critical (Fig. 3-34). This radial bearing stiffness is achievable by adjusting the bearing preload value with minimal effect on bearing life. The first three critical speeds and mode shapes are shown in Figure 3-35. Since the operational speed greatly exceeds the first and second critical speeds, rotor stability becomes an important consideration. A more detailed finite element analysis will be required when the design has matured to insure no rotor-dynamic problems are present. This preliminary analysis does not include the seals stiffness and damping effects and the turbine aerodynamic cross-coupling forces.

The results of this analysis also indicated critical speed interference at the 12 percent power level. The pumped idle mode (12 percent power level) speed is about 40,000 RPM with a calculated first critical speed at 38,966 RPM.

The HPFTP design was then re-evaluated to determine what could be done to raise the first critical speed to 50,000 RPM, having 20 percent design margin on the 40,000 RPM idle mode speed. When the radial stiffness that the hydrodynamic seals provide between the impeller disks is included, the first critical speed is approximately 44,000 RPM. This is based on a feasible estimation of at least a 500,000 lb/in per bearing pair radial support stiffness and a calculated 35,000 lb/in hydrodynamic seal radial stiffness. This provides only a 10 percent margin and further redesign is required to reach the 50,000 RPM goal. To accomplish this, the distance between the third stage impeller and turbine bearing can be decreased by angling the radial balance cavity drain holes under the third stage impeller. This would shorten this section by approximately 0.25" and stiffen the rotor. Also, the turbine overhung mass and length must be reduced as much as possible to increase the first critical speed. It is believed these changes could provide the required additional 6,000 RPM increase in first critical speed.

No redesign analysis effort was completed to determine exactly how much weight and length decrease would be required to raise the first critical speed above

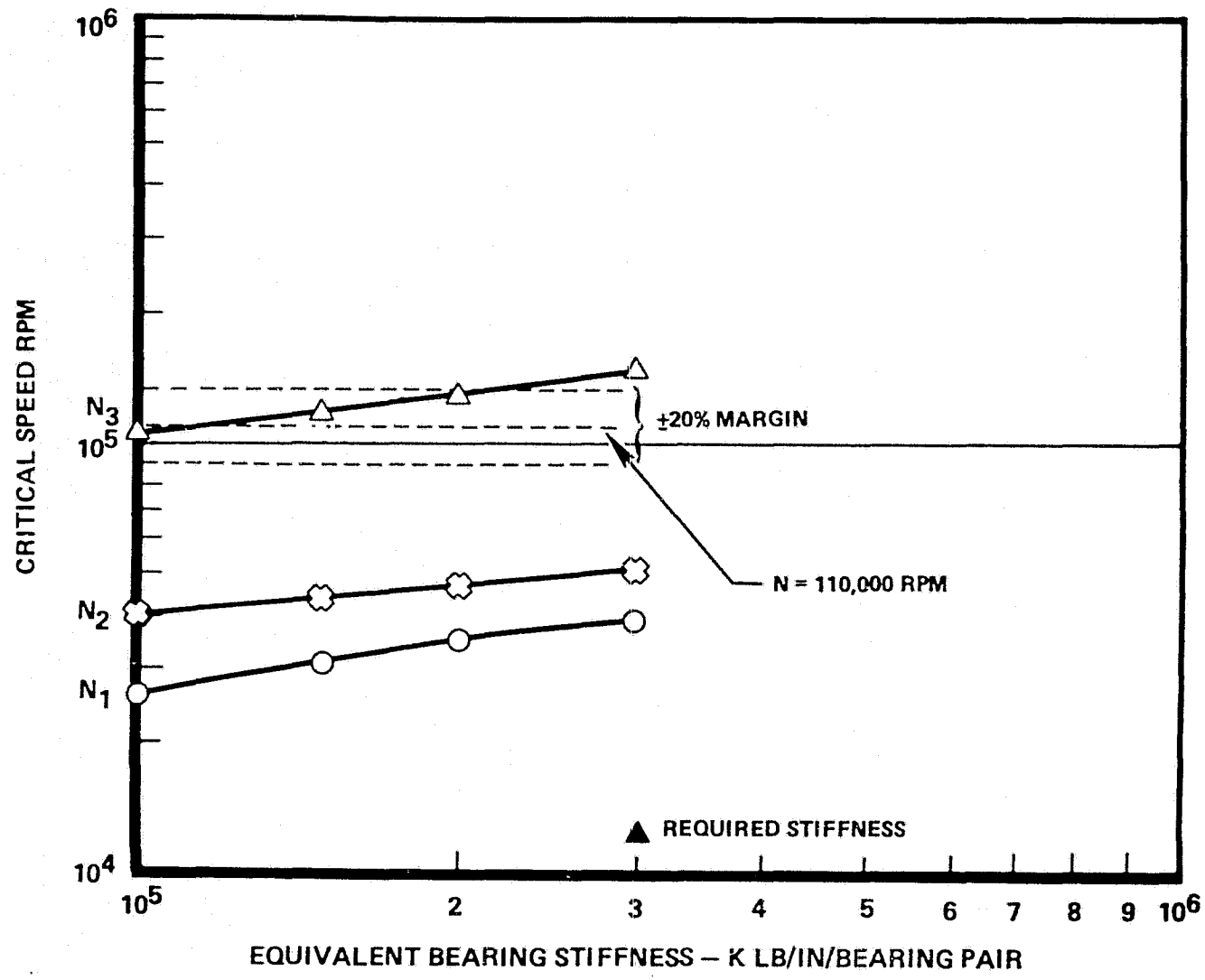

Figure 3-34. Critical Speeds vs. Bearing Stiffness
High Pressure Fuel Turbopump

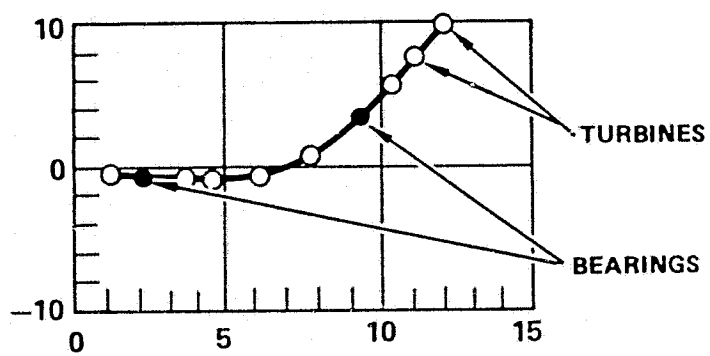

MODE NO. 1

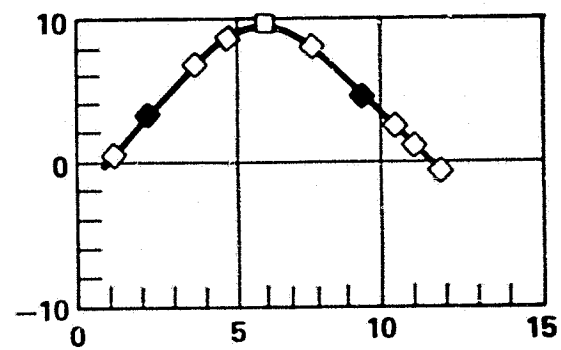

MODE NO. 2

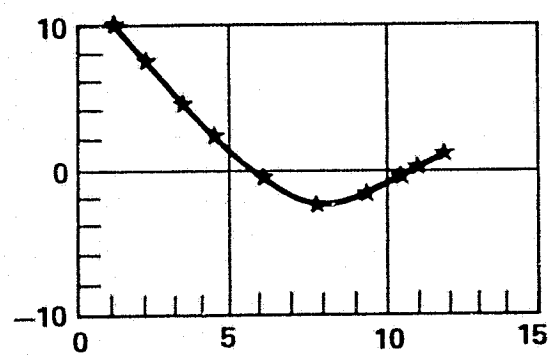

MODE NO. 3

MODE	HZ	FPM
1	649.430	38966.
2	852.320	51139.
3	2475.300	148500.

K1 = 300000. LB/IN
K2 = 300000. LB/IN

MODE SHAPES

Figure 3-35. Critical Speeds and Mode Shapes
High Pressure Fuel Turbopump

50,000 RPM. The critical speeds will have to be recalculated when the redesigned configuration drawings are available. The above recommendations are in the rigi[illegible]ction and if implemented, the turbopump stands a good chance of operating below its first critical speed during pumped idle mode operation. In addition, a slight decrease in overall turbopump weight may be achieved with the recommended design changes. Also, preliminary analysis indicated these changes affect the second and third critical speeds, but the rotor would still operate at 110,000 RPM between the second and third critical speeds with 20% design margin.

High Pressure Fuel Turbopump, Off-Design Operation and Performance. The expander cycle is also required to operate at 12 percent of the nominal thrust level. It was necessary to determine the required operating speed and state conditions in the high pressure fuel pump to determine its ability to operate satisfactorily at this condition.

The analysis was accomplished by adjusting the pump speed until the desired discharge pressure, as required by the engine balance, was obtained. The speed was found to be 40,000 RPM with a ratio of flow coefficient to design flow coefficient of 0.51.

The suction specific speed is 3900 which is adequate for this operating condition.

The flow entering the pump inlet from the front bearing pair is two phase, but if it has time to mix, there is no adverse effect. The state conditions entering the inducer in Figures 3-36 and 3-37 assume complete mixing. This fluid quality could be improved with a higher front bearing flowrate. The turbine-end bearing flow is liquid because of the higher pressure.

The state point conditions at several places in the pump are shown in Figures 3-36 to 3-37. These are based on National Bureau of Standards properties. The desired pump flowrate is 0.71 lbs. per second at a discharge pressure of 616 psia.

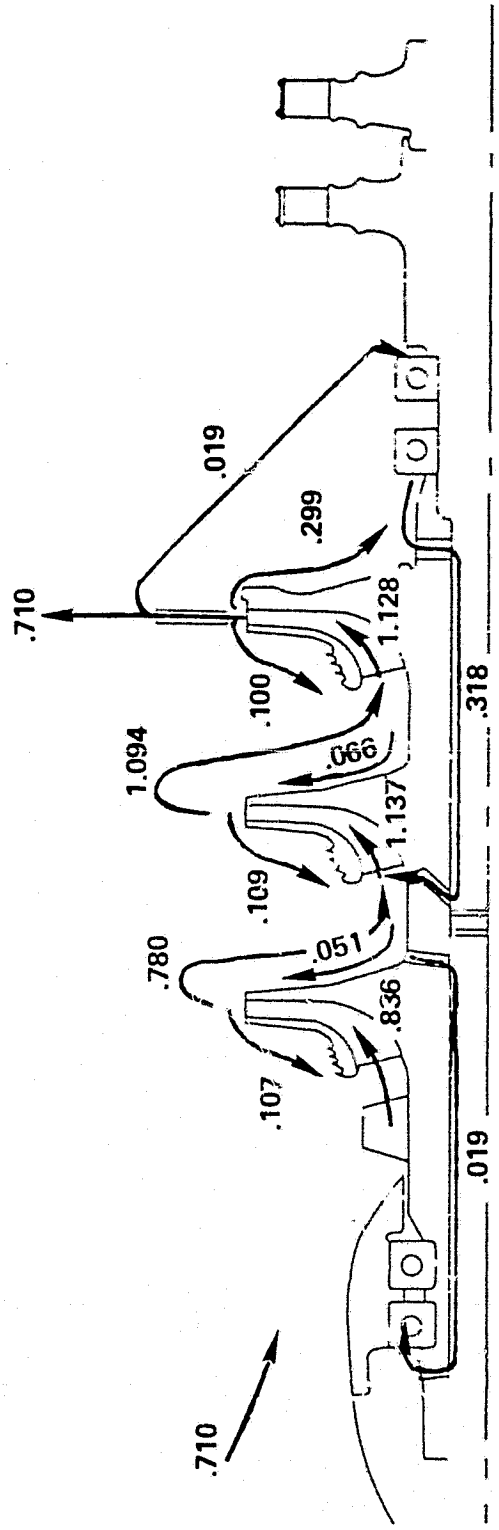

Figure 3-36. Off-Design Pump Flow Profiles

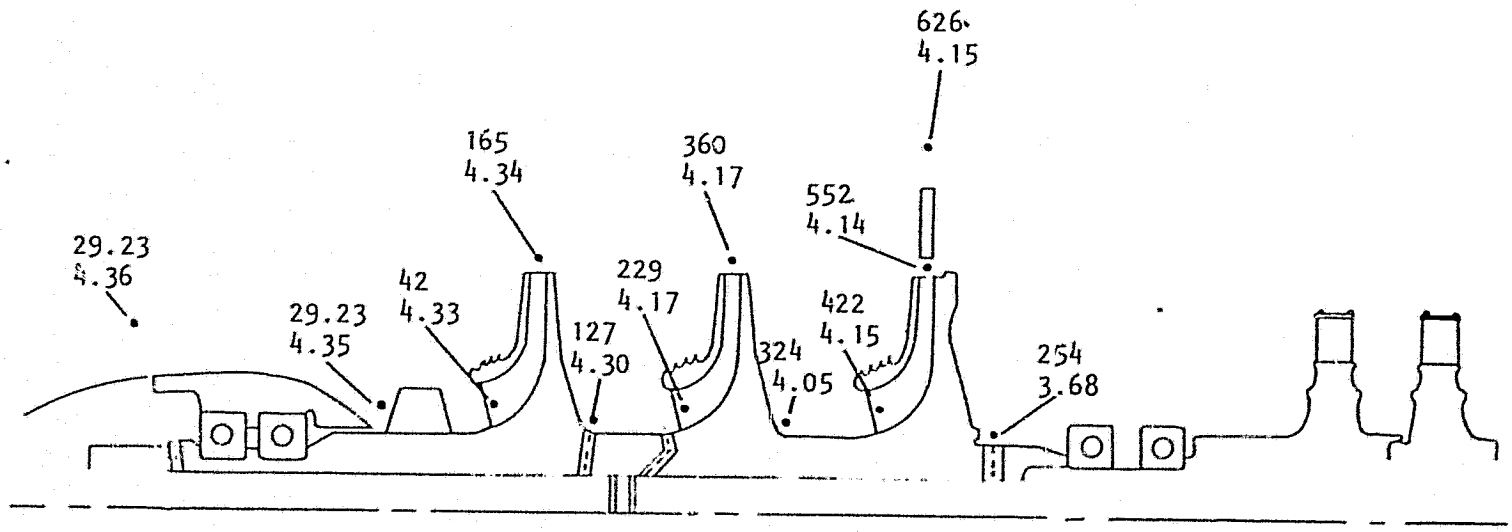

Figure 3-37. Off-Design Pump Pressure, Density Profiles

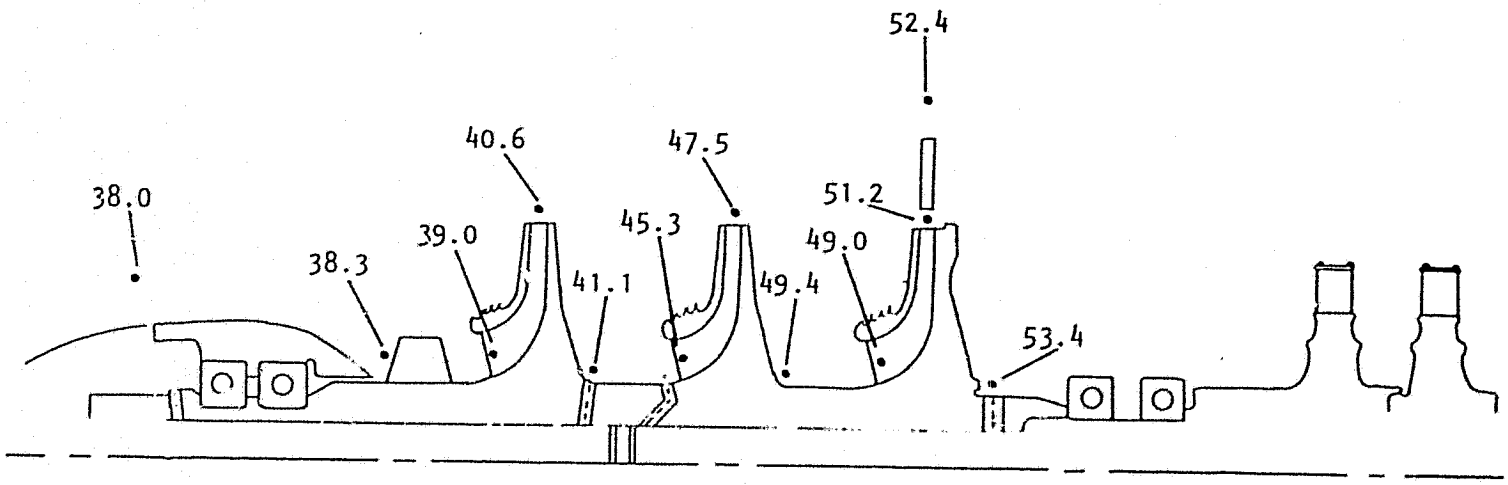

Figure 3-38. Off-Design Pump Temperature Profiles

The discharge pressure in Figure 3-37 is 625.7 psia. A value closer to 616 can be obtained but at the expense of additional iterations. 625.7 psi results in acceptably close temperatures and forces. At these conditions, the overall pump efficiency is 46 percent. Table 3-18 presents the operating conditions at this point.

The high pressure fuel pump performance characteristics at idle mode are presented in Figure 3-39. The peak efficiency occurs at the design flow/speed ratio. The maximum head rise occurs at 90 percent of the design flow/speed ratio. The lower head rise at lower flowrates results from the fluid heating influence and is influenced by speed. A much more detailed analysis would be required to present the influence of speed upon the normalized characteristics. A general statement may be made that lower efficiency and normalized head values occur at higher speeds.

The resultant axial thrust of the turbopump is 5555 pounds toward the turbine. The maximum capability of the balance piston is 4924 pounds. Therefore, the bearing must absorb 631 pounds. This is excessive because the bearings can probably absorb 300 or 400 pounds for a short period of time. Some of this imbalance could be removed by increasing the interstage seal and front wearing ring diameters. If the diameters were increased sufficiently to eliminate this imbalance completely, the balance would be destroyed at the 100 percent thrust design point. One other possibility is to increase the pump through flow and bypass the difference back in upstream. However, this could increase the required power and increase fluid heating. Draining the balance piston flow to the inlet of the pump instead of the second stage is not a solution. The lower end of the balance piston range would be reduced substantially and the higher would be reduced slightly. A solution requires; increased higher end trust capability, decreased turbopump axial thrust, increase in the minimum engine thrust level.

A secondary problem also surfaced, in that operation at the pumped idle mode speed (40,000 RPM) caused interference with the first critical speed (38,966 RPM). As discussed earlier, the critical speed problem can be solved by in-

TABLE 3-18 EXPANDER CYCLE HIGH PRESSURE FUEL PUMP

Operating Conditions:	
Speed, rpm	40,000
Flow, lb/sec	0.71
Inlet Pressure, psia	29.23
Inlet Temperature, Deg. R	38.02
Isentropic Head, ft.	19,272
Suction Specific Speed Available, ft.	3900
Overall Efficiency, pct.	46
Stage Conditions:	
Stage Head, ft.	6745
Stage Efficiency, pct.	48.3

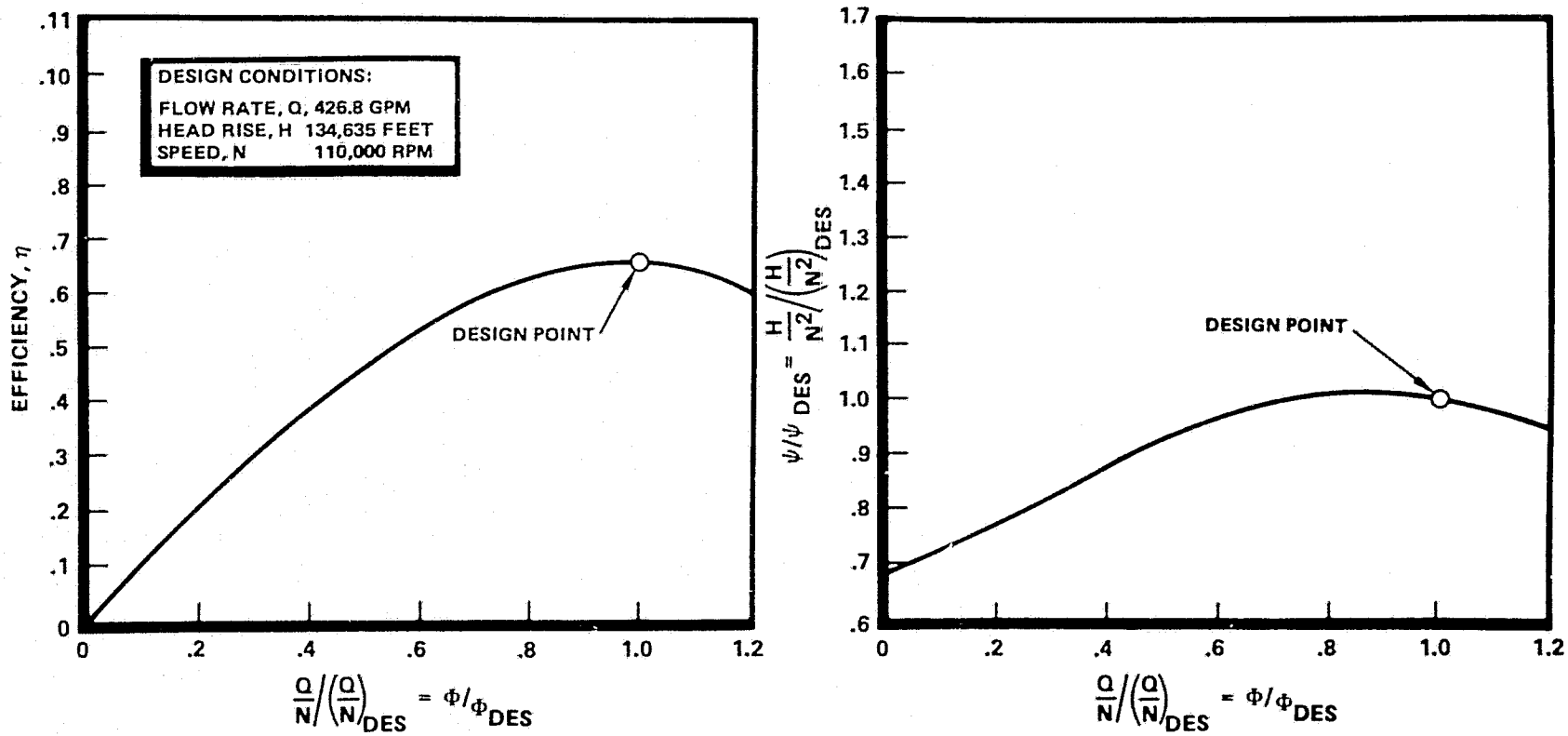

Figure 3-39. Pump Performance Characteristics at Pumped-Idle

creasing the bearing support stiffness and reducing the turbine overhung mass. Although preliminary analysis indicates a probable resolution of these concerns, detailed analysis must be performed to solve the critical speed and axial thrust capability problems.

Technology Requirements. The high pressure fuel turbopump employs many of the design features used in the ASE MK48F concept. Since the expander cycle turbine gases are much cooler (860R versus 1860R) than the MK48F, a turbine design change to a two stage partial admission concept was required. Analytical to empirical test verification for two stage partial admission turbines is limited throughout industry. Of major concern is the performance sensitivity of the arc of admission, circumferential alignment of the two partial admission nozzles, and speed effects. The design chosen represents the most optimum for the expander cycle but analytical to empirical test verification program will be required to optimize the particular design.

Bearing size selection was another critical area. To operate satisfactorily at 110,000 RPM yet achieve long life with expected operational loads presents a major concern. The design as selected (Figure 3-3) employs 17 mm duplex bearings at the pump and turbine end giving a DN of 1.87×10^6 for each bearing. The extrapolation of B_{10} bearing life to cryogenic conditions is somewhat limited and depends largely on the quality and cleanness of the coolant. Provisions have been made within the turbopump concept to adapt to the relatively new concept of a hybrid bearing design of either 20 mm or 17 mm size. Future test results of the hybrid bearing (20 mm) is expected to provide guidelines for final design of the expander cycle fuel turbopump bearing choice. Bearing type selection in either case may require the addition of bearing coolant filtration to assure the cleanliness level of the coolant. The bearing coolant filtration scheme must be considered not only for the fuel high pressure pump, but for each of the boost turbopumps as well as the LOX high pressure turbopump.

OXYGEN TURBOMACHINERY DETAIL DESIGN

The principal design parameters for the oxygen turbomachinery were presented in Table 3-7 . These parameters resulted from the last iteration performed between the engine balance with the cycle eptimizer program and the detail oxygen turbomachinery component design and analysis effort. This latter effort produced the turbomachinery component geometry and performance required to deliver the 15K thrust at a chamber pressure of 1540 PSIA. In this section the results of the detailed pump and turbine component analysis is presented.

Low Pressure LOX Boost Turbopump

The turbopump consists of an axial flow inducer driven by a Francis type radial inflow hydraulic turbine. Fig. 3-40presents the major dimensions of the turbopump. Materials and proposed instrumentations for development are shown in Fig. 3-41 and 3-42. Turbine drive media is the entire LOX discharge flow from the main oxidizer turbopump. In order to minimize system hydraulic resistance and to provide for a compact installation, the LOX boost turbopump is "T" mounted in close proximity to the main LOX turbopump. Fig. 3-2 depicts the arrangement with the LOX boost turbopump shaft parallel to the direction of vehicle flight with the main LOX turbopump shaft perpendicular to the boost pump shaft.

The bearings for the boost pump were chosen to carry the maximum expected axial loads (~1400 pounds toward the inducer) with sufficient load margin, and to meet the expander cycle life requirement of 10 hours. The front bearing (pump end) is a 17 mm extra light type while the rear bearings are a duplex set of 55 mm extra light type. Bearing coolant (LOX) is directed past the turbine runner tip into the duplex bearings then toward the front bearing. A labyrinth seal package just downstream of the front bearing lowers the coolant pressure (~2500 psid) before being directed into the rear shroud of the inducer and then into the boost pump discharge (~88 psia). Bearing coolant flow of about 5 GPM or about 3 percent of the total flowrate is required to cool the bearings.

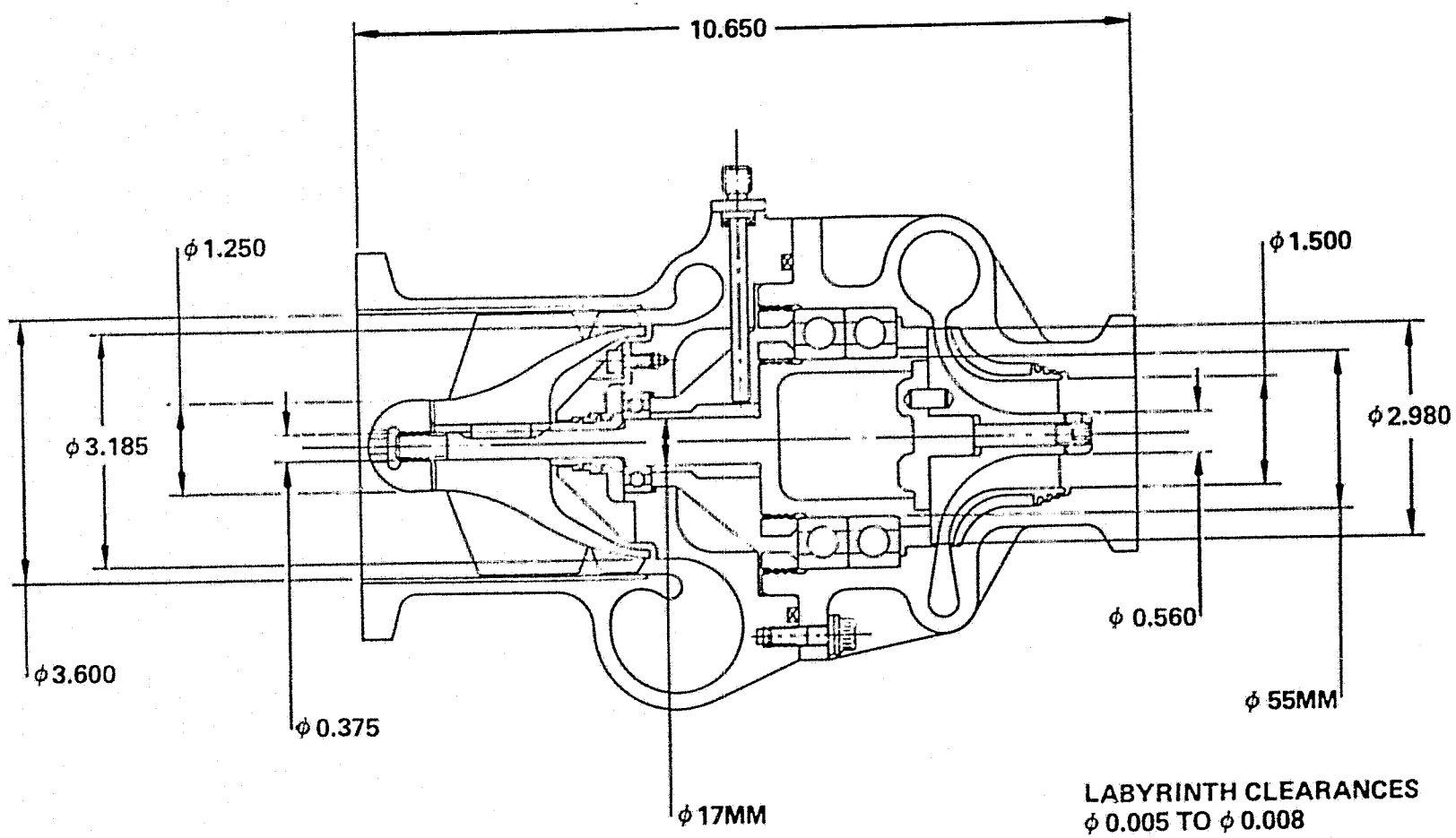

Figure 3-40. Oxidizer - Low Pressure Turbopump

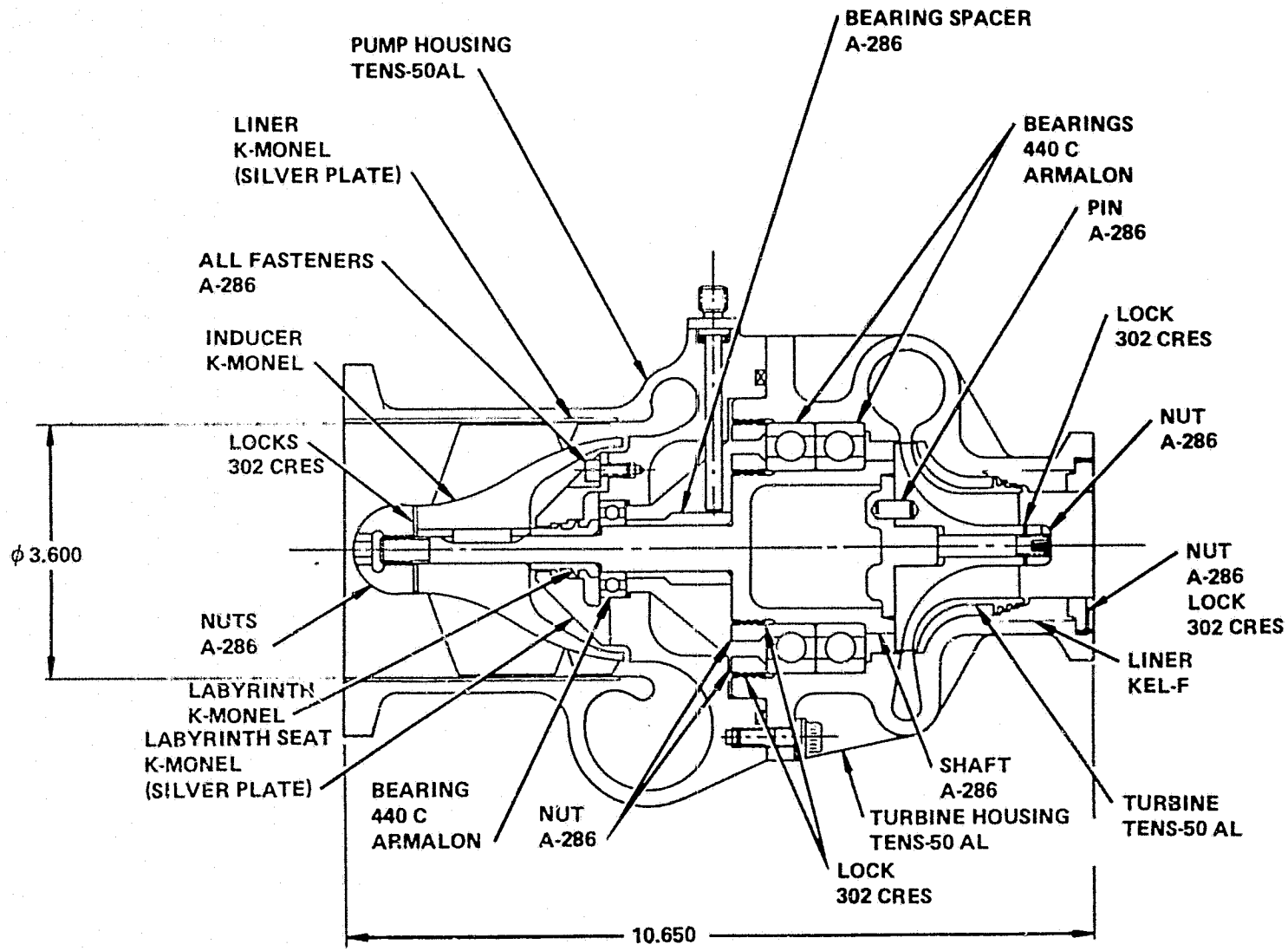

Figure 3-41. Oxidizer Low Pressure Turbopump Material Selection

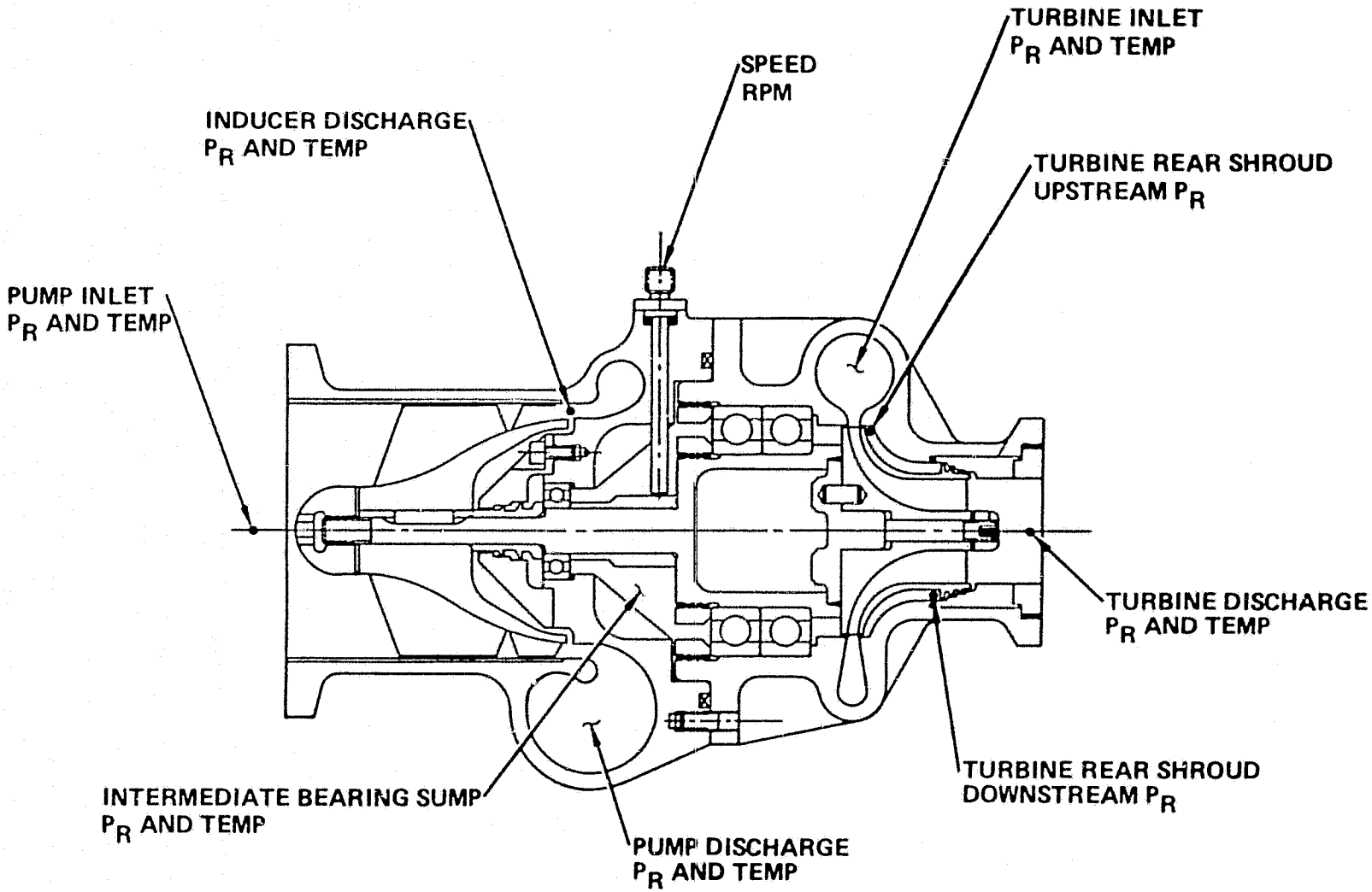

Figure 3-42. Oxidizer Low Pressure Turbopump Development Instrumentation Selection

The overall weight of the turbopump is projected to be about 18.8 pounds. The weight was calculated based on each individual part's geometry and material designation. Minor weight savings schemes, such as flange scalloping around bolt holes and increased number of smaller bolts to reduce the mass of the flanges were considered in the design.

Pump Performance Analysis. The basic design requirements information was taken from the expander cycle balance computer output.

Weight Flow, #/SEC	26.88
Inlet Pressure, PSIA	16.3
Discharge Pressure, PSIA	71.3
Minimum Available NPSH, FT	2.0
Inlet Temperature, °R	162.7

The inducer minimum available NPSH establishes the axial velocity using a criteria $c_m^2/2g = 3.3$ for NPSH margin. The resulting axial velocity is 6.65 fps with an inlet flow coefficient set at 0.064. The result in a tip speed of 101.7 fps with an inlet hub diameter of 1.25 inches.

The inducer is driven by a radial inflow hydraulic turbine (discussed later). This arrangement requires the inducer exit flow to discharge through a volute. Because of high inducer head coefficient, a tandem blade design was used with a 4-blade front row of solidity 1.8 followed by 8 kicker blades as a second row with a 1.5 solidity. The inducer discharges the fluid to a vaneless diffuser and volute combination. The volute has a maximum area of 2.138 square inches. To provide the inducer with some two-phase pumping capability, the tip in incidence angle was set at 3.43° and blade angle, 6.86°. Table 3-19 lists the turbopump inducer design data. Figures 3-43 and 3-44 show the overall head, efficiency and velocity vectors calculated by INDANA program, while Figure 3-45 is the suction performance.

TABLE 3-19. LOX BOOST PUMP INDUCER DESIGN

Operating Conditions:

Speed, RPM	6475
Flow, #/sec	26.88
Inlet Pressure, psia	16.3
Inlet Temperature, °F	162.7
Overall Efficiency, percent	69.2
Suction Specific Speed at Min. Available NPSH	49,977
Overall Head Coefficient	0.454

Stage Conditons:

Number of Blades - First Row	4
Number of Kicker Blades	8
Radial Tip Clearance, in.	0.006

	Tip		Hub
Inlet Diameter, in.	3.60		1.25
Exit Diameter, in.	3.60		3.185
Inlet Tip-Hub Ratio		0.347	
Exit Tip-Hub Ratio		0.885	
Tip Speed, Ft/Sec		101.7	
Inducer Head Coefficient		0.56	

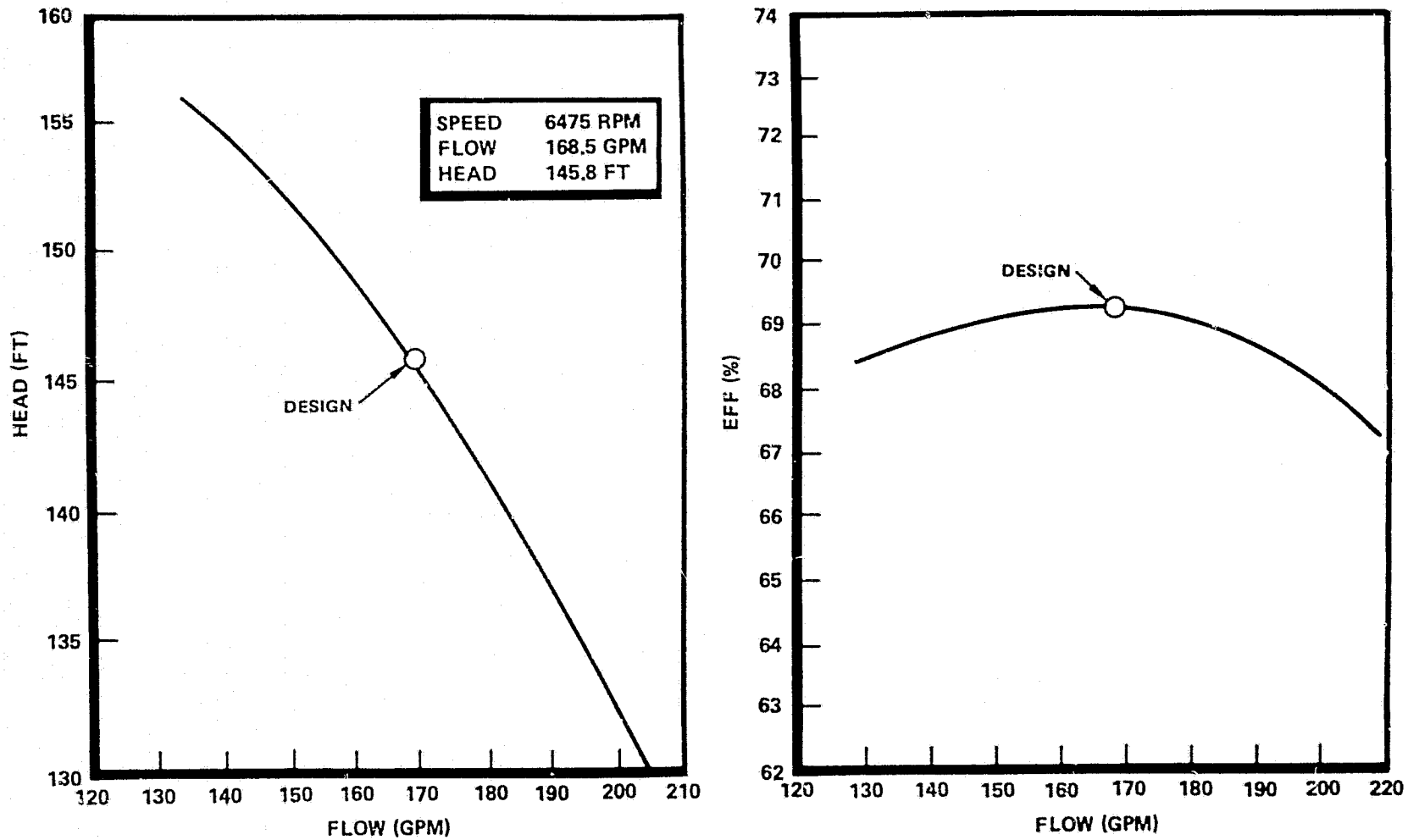

Figure 3-43. Overall Head and Efficiency, Low Pressure Pump

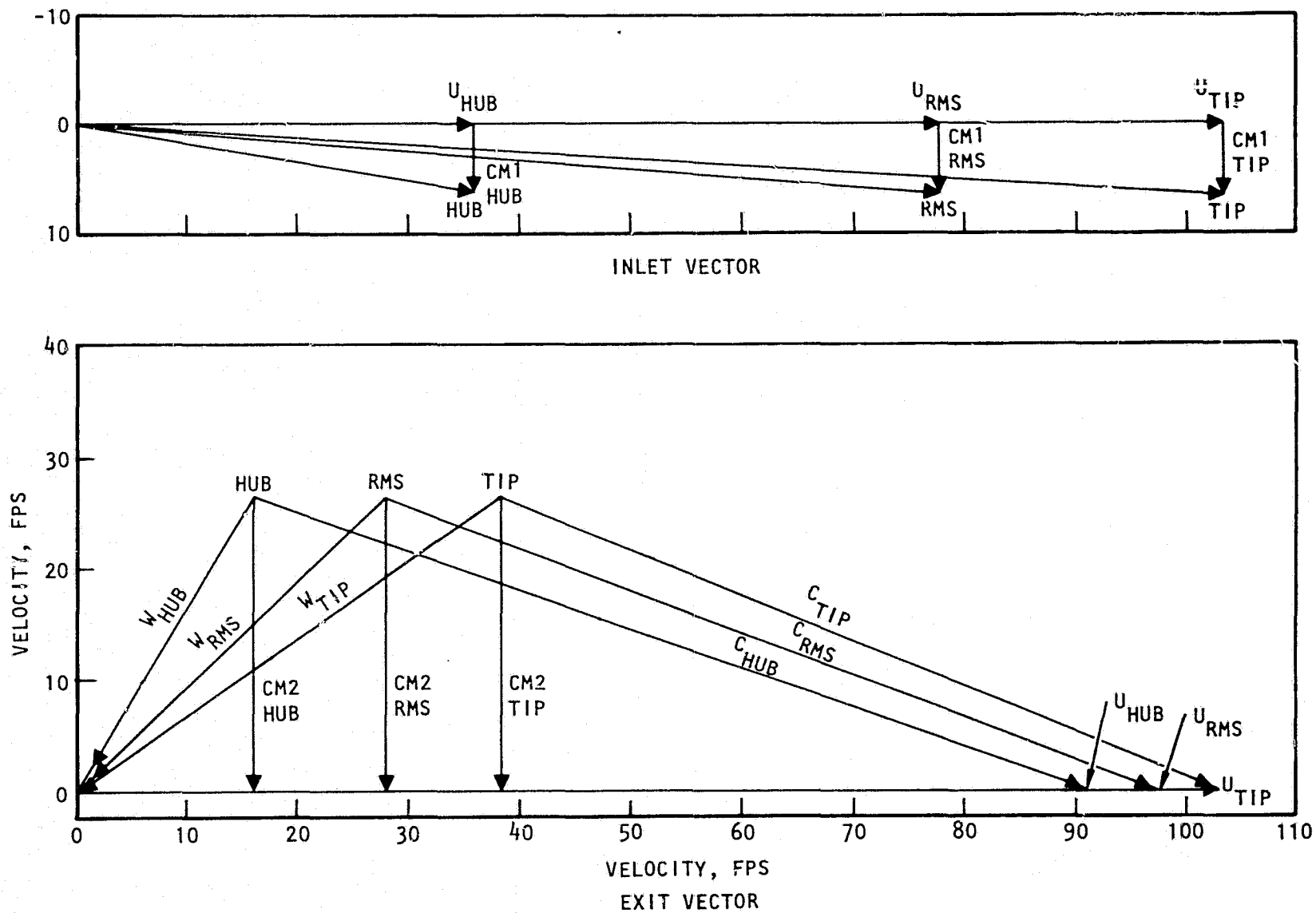

Figure 3-44. Velocity Vector, Low Pressure LOX Pump

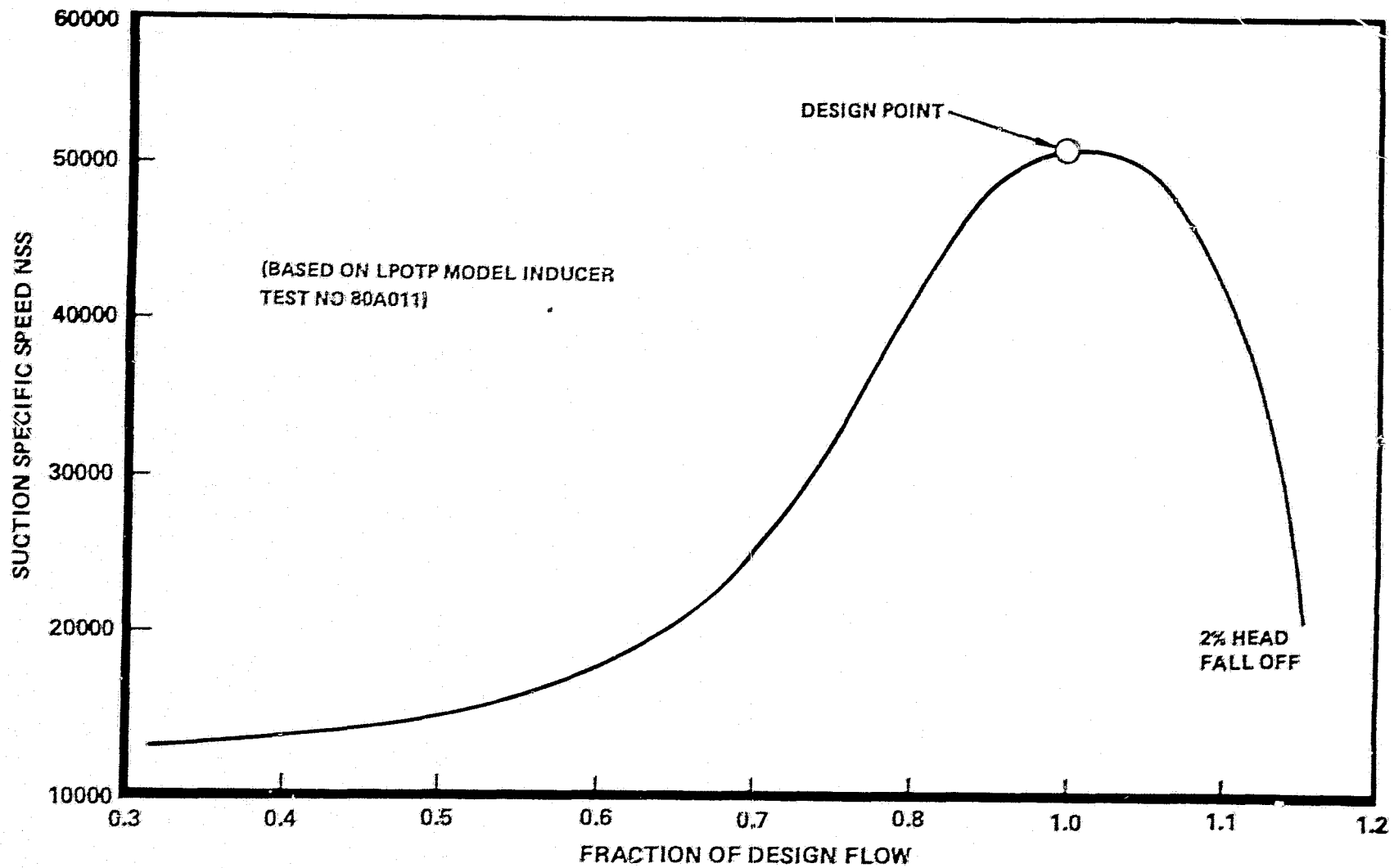

Figure 3-45. Suction Performance, Low Pressure LOX Pump

Low Pressure LOX Turbopump Turbine Design and Performance Analysis. The LOX boost turbopump is driven by a single stage Francis type full radial inflow turbine using the entire discharge flow from the main LOX high pressure turbopump. The vanes are radially straight and utilize the rotation of the fluid (LOX) entering the turbine at the outside diameter which rotates at wheel speed. This provides a zero incidence angle with the radial blades. The turbine blades are radial down to the exducer. The exducer will then turn through an angle of 60° with a circular-arc meanline at the tip with a straight line extension. The blades are a helical design with a variable lead. The design requirements for the turbine were as follows:

FLUID	LIQUID OXYGEN
Inlet Temperature, $^{\circ}F$	174.9
Inlet Pressure, PSIA	2648.9
Density, lb per cu ft	71.56
Weight Flow, lb per sec	26.88
Speed, rpm	6475
Horsepower	10.3

Preliminary calculations were made to size the turbine, shaft, bearings and seals. Calculations were then made of the leakage through the seals on the turbine exducer and the seals on the shaft between the bearings. The weight flow of this leakage was subtracted from the total weight flow and the turbine rotor was resized. It was desirable that the turbine discharge into a 1.5-inch pipe, and this proved to be convenient as it provided for an exducer hub diameter of 0.560 in., a hub to eye diameter ratio of 0.373 and an exducer blade angle at the tip of 30° with the tangent. Allowing for deviation, this will result in a flow angle of 39.5° with no rotation left in the fluid.

The tip speed at the exducer exit will be 42.38 ft. per sec. and the leaving axial velocity 34.93 ft. per sec. If this resultant velocity head were considered lost, it would amount to only 18.97 ft.; this velocity, however, is necessary for the system so the turbine efficiency should be on a total-to-total basis.

The turbine was designed so that the fluid entering the turbine at the outside.

The Euler head necessary to produce the desired horsepower was calculated to be 220.38 ft.; this resulted in a turbine tip speed of 84.20 ft. per sec. and a tip diameter of 2.980 in. The ratio of eye diameter to tip diameter is 0.49 which is considered an efficient proportion.

The area perpendicular to meridional velocity was held constant through the rotor. This will produce a meridional velocity that is nearly constant being affected only by the variation in blade blockage; it resulted in a tip passage width of 0.159 in. The radial velocity in the vaneless space at the impeller entrance will be 35.99 ft. per sec. (flow includes leakage). With a flow rotational velocity of 84.20 ft. per sec., this gives a flow angle of 23.1^{o} with the tangent. This is in the accepted range for good design.

It is planned that the radial turbine and exducer will have 12 blades, but this will depend somewhat on Stress and Manufacturing. Another possibility is 12 radial turbine blades and 6 exducer blades. This would result in an exducer that is twice as long as the one shown, but there is ample room for it (Figure 3-40).

Preliminary calculations indicated that nozzle vanes would not be necessary. The velocity in the 1-inch pipe leaving the main pump is 68.41 ft/sec. If the diameter of this pipe is gradually increased to 1.108 in., and then connected to a scroll with a constant centerline diameter of 4.5 in., the momentum of the free vortex entering the turbine will provide the necessary rotational velocity at the turbine entrance.

The leakage through the front labyrinth seal was calculated to be 1.35 gpm while that through the bearings and rear seal was 4.14 gpm which is sufficient to cool the bearings.

The static pressure drop across the turbine is only 82 psi. As a result, there is a fairly large force on the discharge side of the turbine wheel. The leakage

flow through the bearings enters the low pressure pump at the point where the pressure is only 64 psia. The resultant large pressure drop in combination with the seal diameter produces less force on the rear of the impeller than on the front. The resultant force when added to the inducer thrust (300 lb.) produces a total force of approximately 1390 lb. toward the inducer end of the turbopump.

The specific speed of the turbine is 1507 (71 in CFS units), the leakage loss is only 3 percent of the throughflow and the U/C ratio of the turbine is 0.707 at the peak of the theoretical efficiency curves for radia-inflow turbines. The efficiency should, therefore, be about 80 percent. Figure 3-46 is a curve showing the estimated efficiency of the turbine as a function of u/c.

Rotordynamic Analysis. An analysis of the low pressure LOX boost pump rotor system indicates no rotordynamic problem. The turbopump will operate at 6475 RPM or well below the calculated first critical speed of approximately 19,000 RPM. The critical speeds were based partly on a minimum inducer end bearing stiffness of 100,000 lb/in. The first three critical speed plots are shown on Figure 3-47 while the mode shapes corresponding to those critical speeds are shown on Figure 3-48. Nodal locations used in the analysis are shown in Figure 3-49.

Turbopump Off-Design Operation and Performance. The wide flow range (off-design) head ratio and efficiency versus flow ratio characteristics is presented in Figure 3-50.

Technology Requirements. The LOX boost pump design represents a compact system which does not employ any unproven technology. All technical issues of the design represent a low development risk.

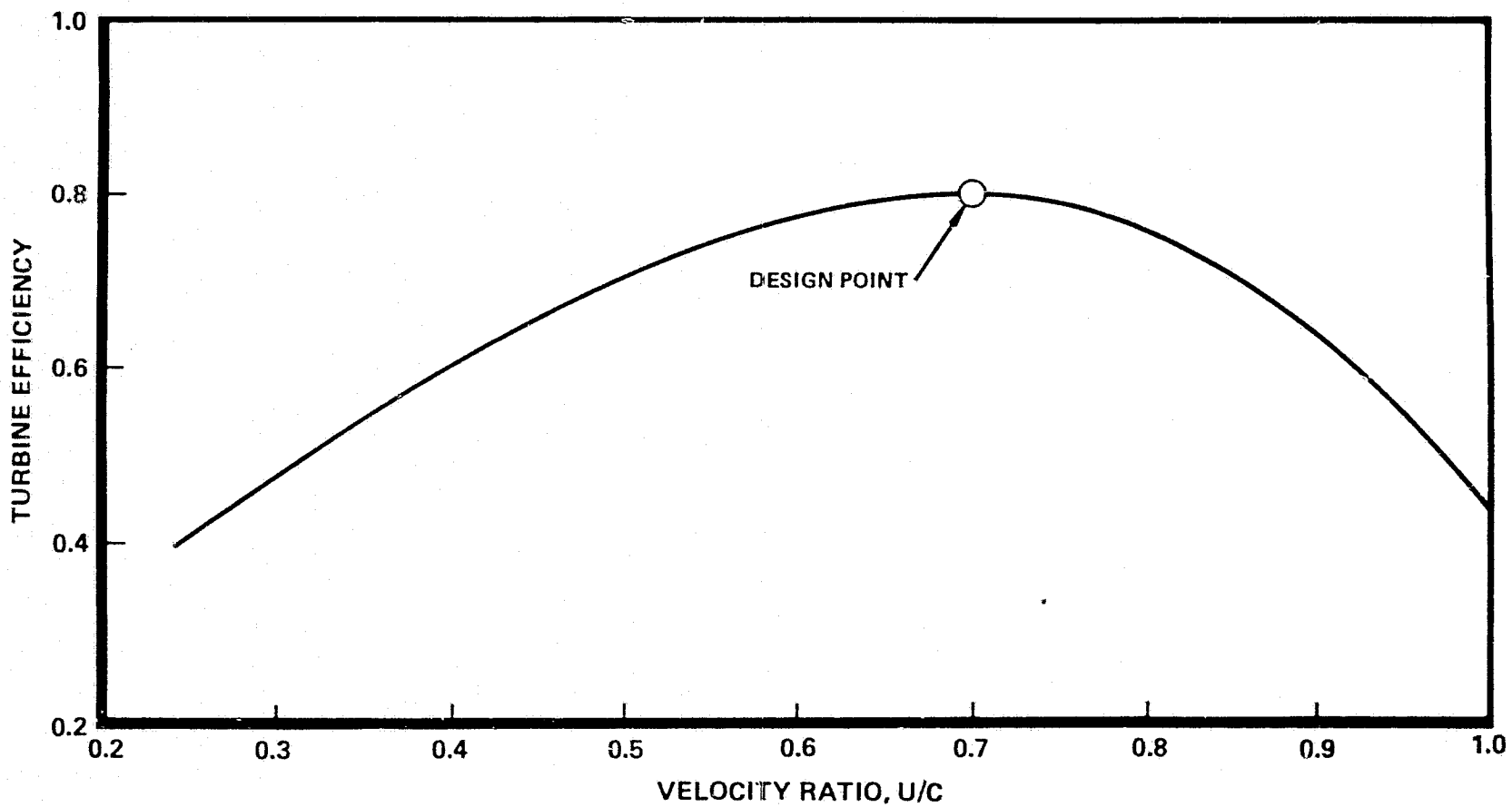

Figure 3-46. Turbine Efficiency, Low Pressure LOX Turbopump Turbine

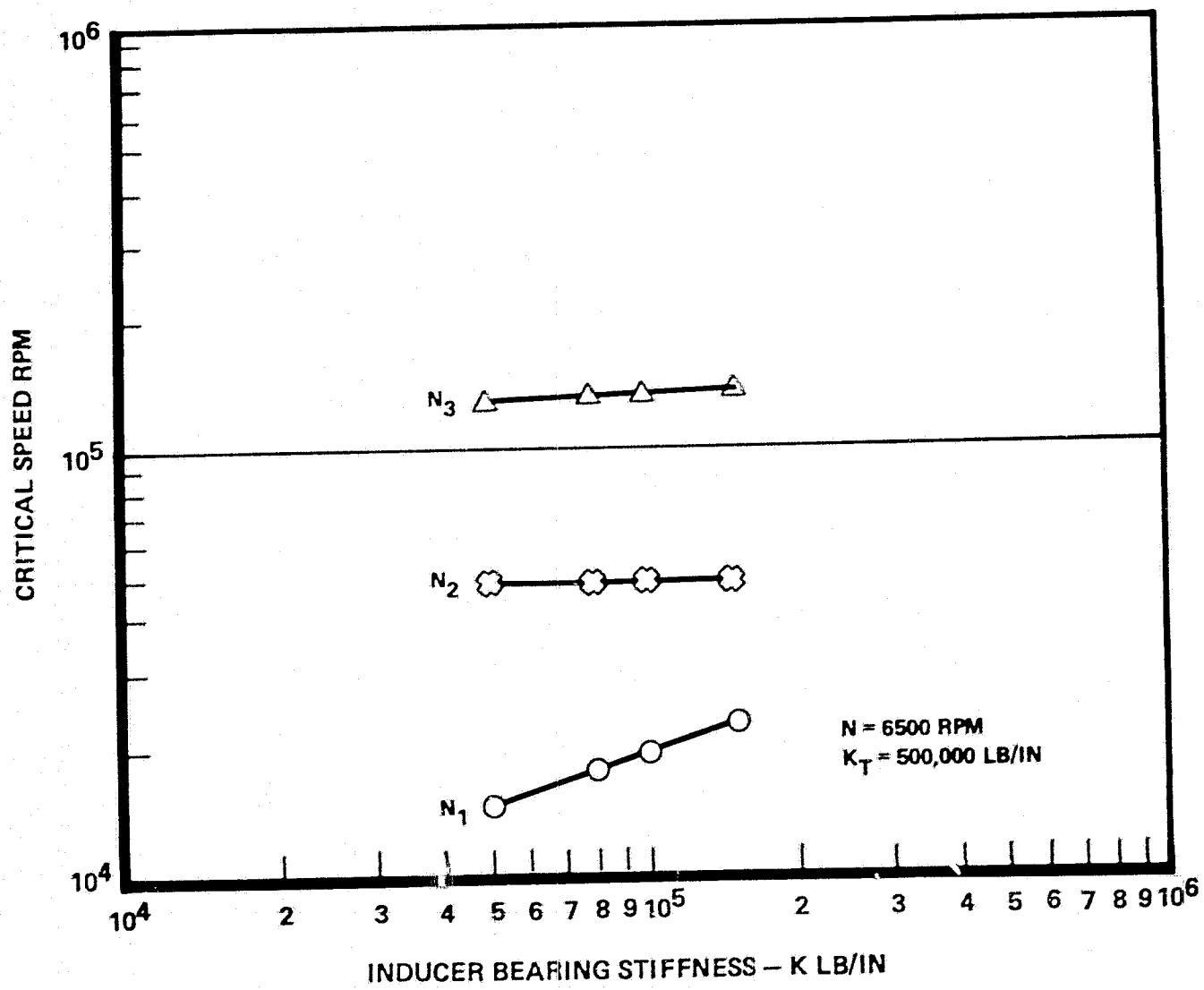

Figure 3-47. Critical Speeds vs. Bearing Stiffness
Low Pressure LOX Turbopump

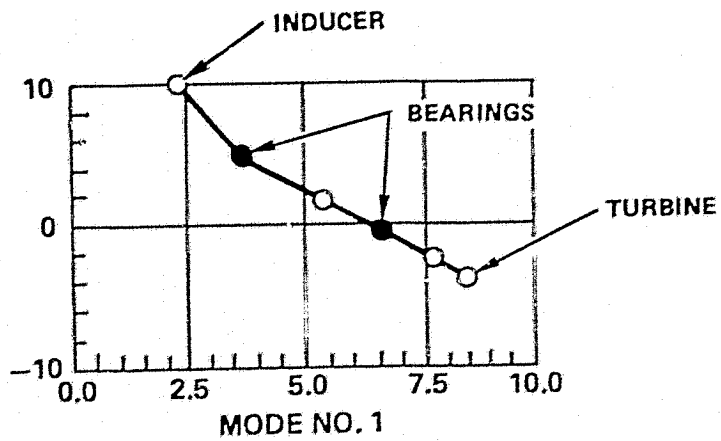

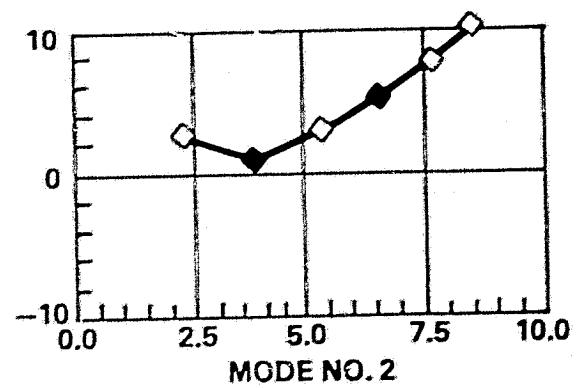

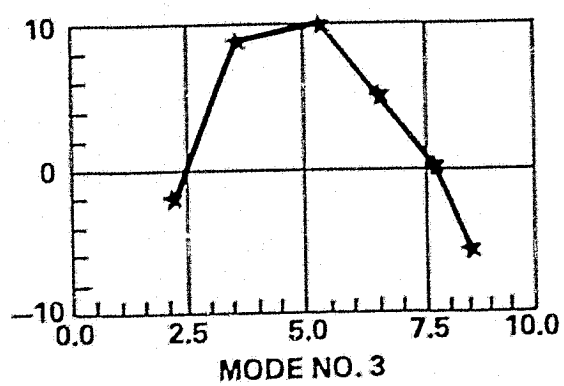

MODE	HZ	RPM
1	318.730	19124.
2	797.450	47847.
3	2187.200	131230.

K1 = 100000. LB/IN
K2 = 500000. LB/IN

MODE SHAPES

Figure 3-48. Critical Speeds and Mode Shapes, Low Pressure LOX Turbopump

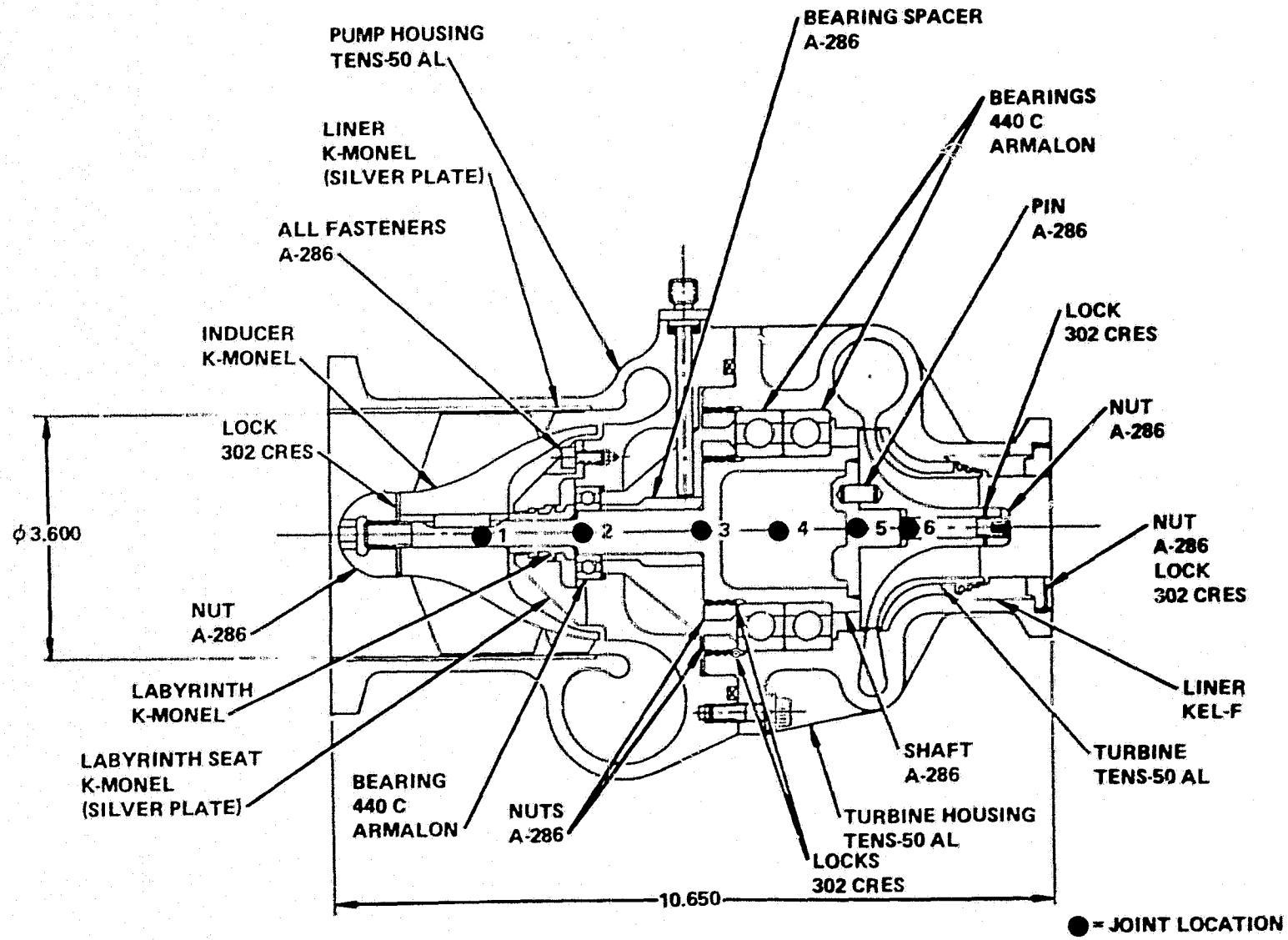

Figure 3-49. Nodal Point Locations, Critical Speeds Study, Low Pressure LOX Turbopump

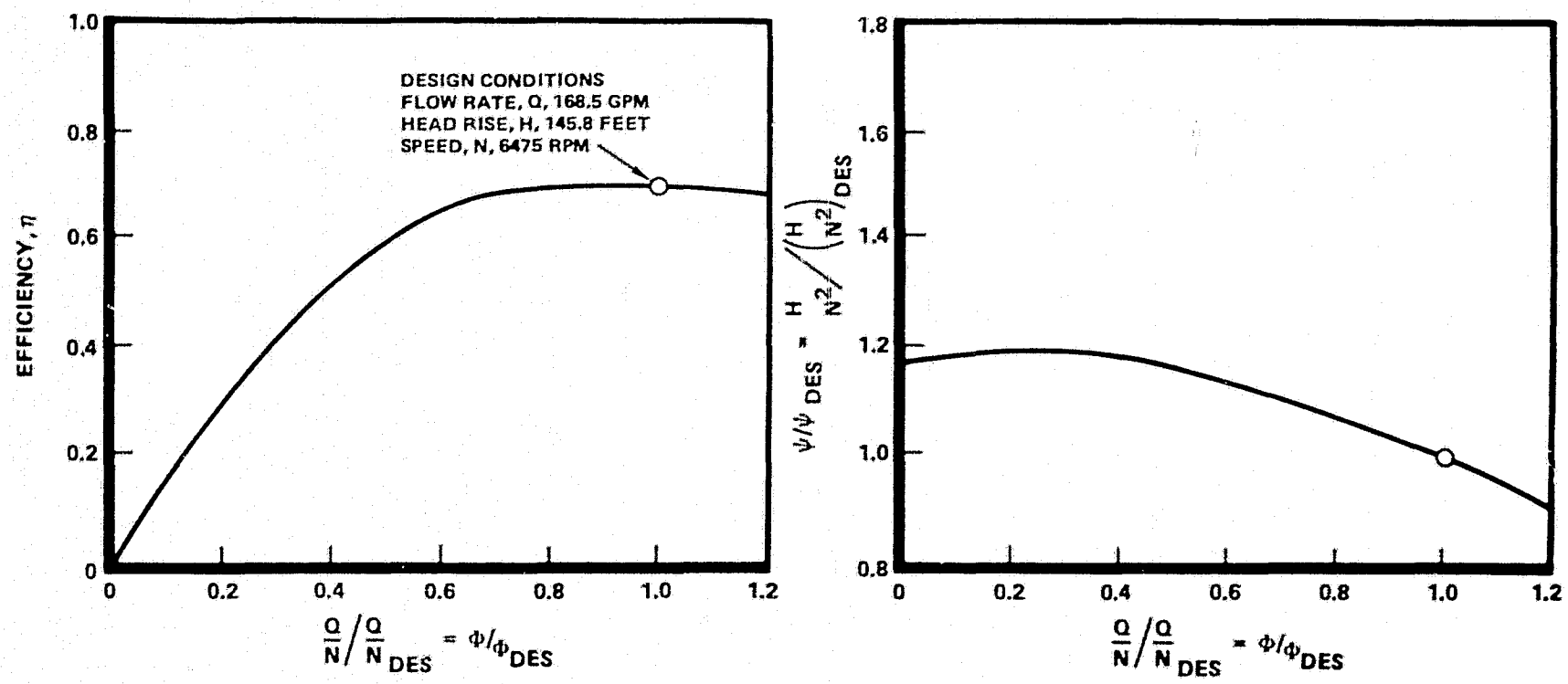

Figure 3-50. Off-Design Performance, Low Pressure LOX Turbopump

High Pressure LOX Turbopump

The high pressure LOX pump rotor and hydraulic passages are nearly identical to the MK480 turbopump. The turbopump employs a single stage centrifugal pump preceded by an inducer. The turbine is a partial admission single stage impulse type. Turbopump speed for the expander cycle operation has been sized at approximately 53,000 RPM. The external envelope (of the MK480 concept) has been reduced to minimize weight and envelope size to a flight type configuration. Figure 3-51 is a layout of the pump indicating principal dimensions. Figures 3-52 and 3-53 present layouts of the turbopump showing the overall description, material and development instrumentation selections.

Front bearing (pump end) coolant and balance piston flow passages have been integrated into the volute housing. The rear bearing (turbine end) coolant is liquid hydrogen which is supplied from the high pressure fuel turbopump to the aft port of the turbine housing. Bearing flow proceeds through the bearing, past a controlled gap shaft riding seal and into the turbine discharge cavity. Front and rear bearings are 20 mm angular contact duplex sets running at a DN (bearing internal diameter X speed) of about 1.07×10^6.

The overall weight of the turbopump has been calculated, on a part by part basis, to be approximately 39.6 pounds. Included in the weight saving scheme is the addition of casting scalloping, where feasible, along with bolt hole flange scalloping, where feasible, along with bolt hole flange scalloping. The projected weight (39.6 pounds) represents the current design as shown in Figure 3-52. As discussed later in the rotordynamic analysis, additional weight savings of about 12-15 pounds could be achieved by reducing bearing spans. A complete design analysis must be accomplished to verify the projected design change.

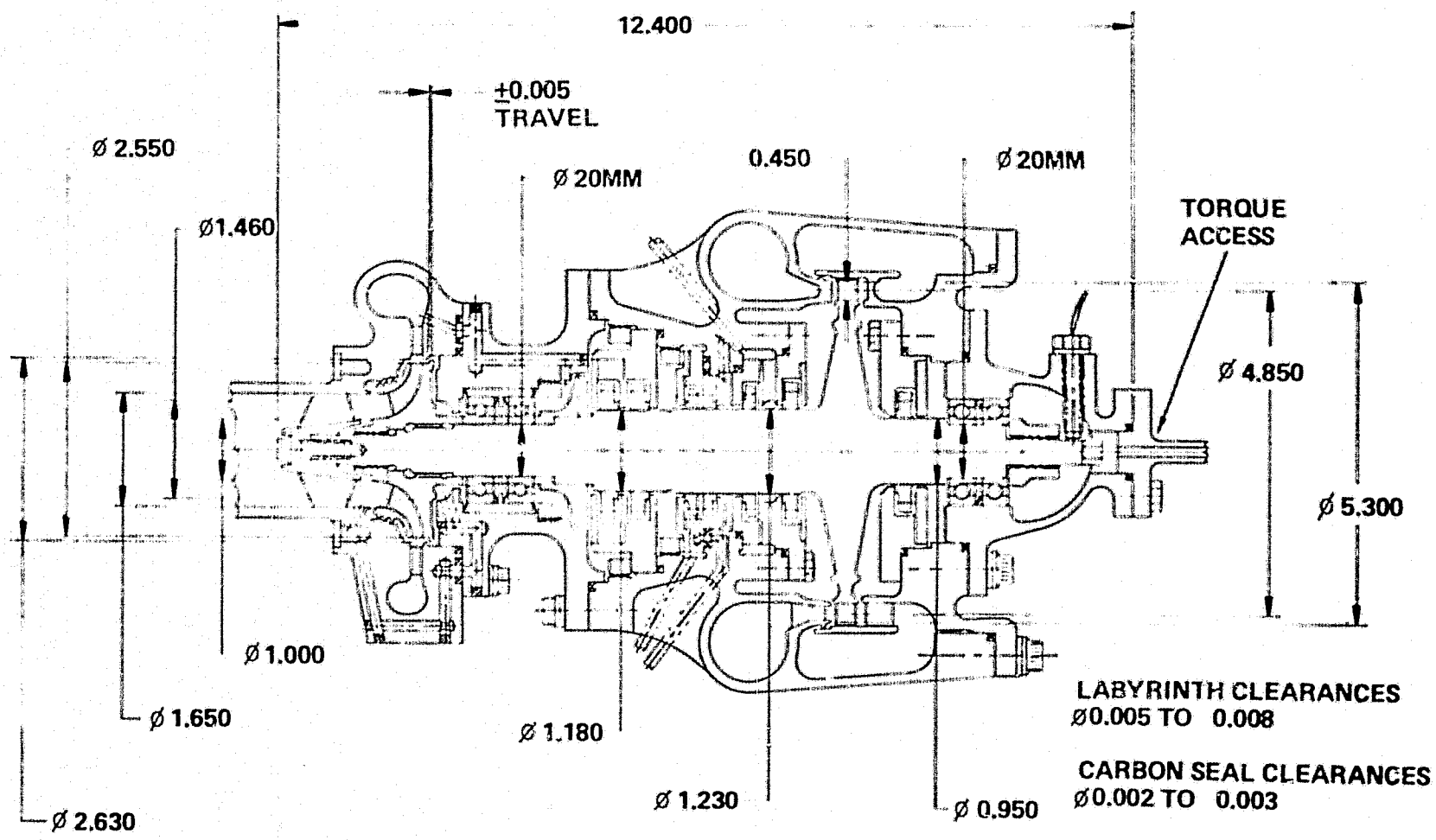

Figure 3-51. Oxidizer - High Pressure Turbopump

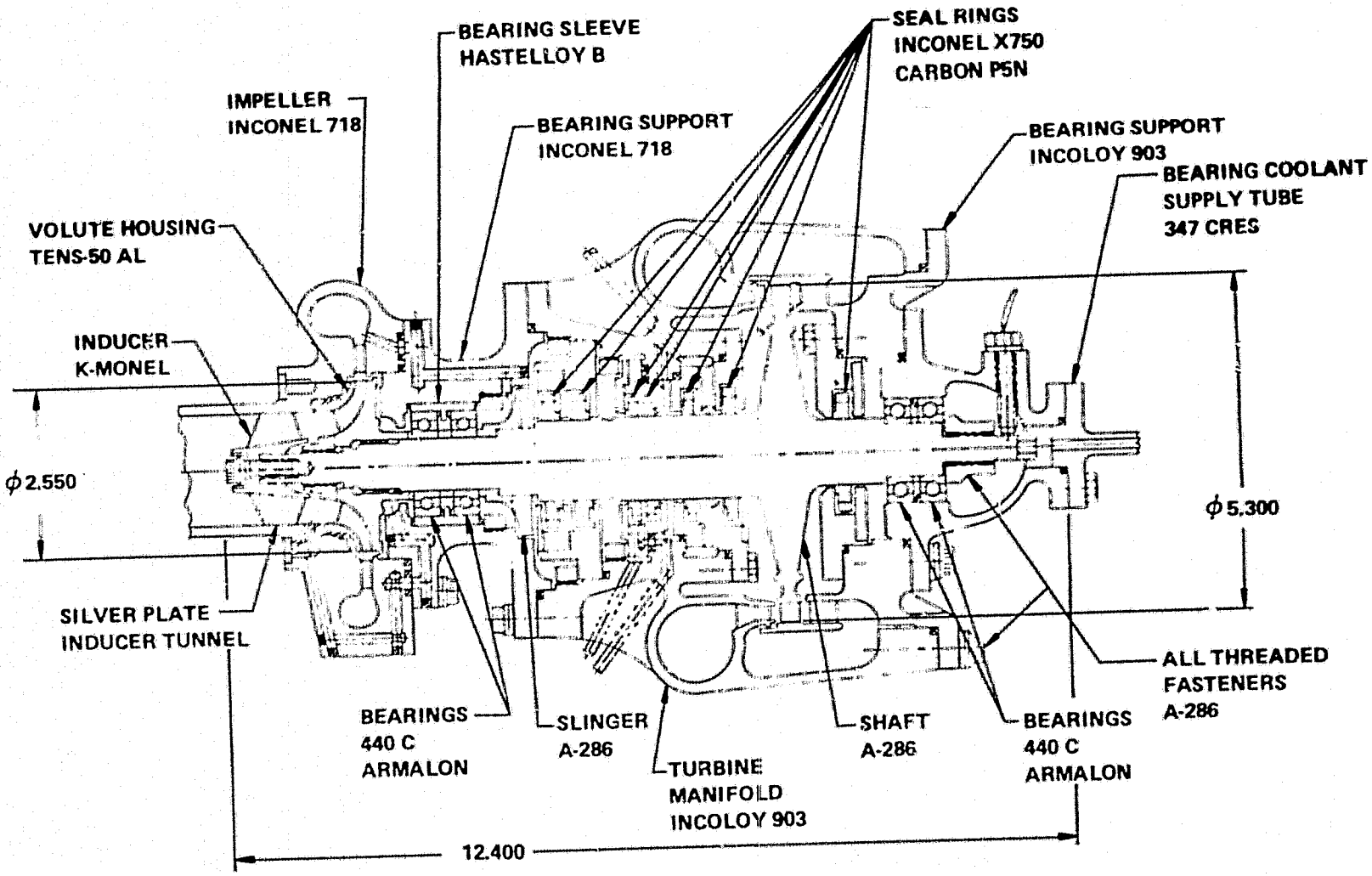

Figure 3-52. Oxidizer - High Pressure Turbopump Material Selection

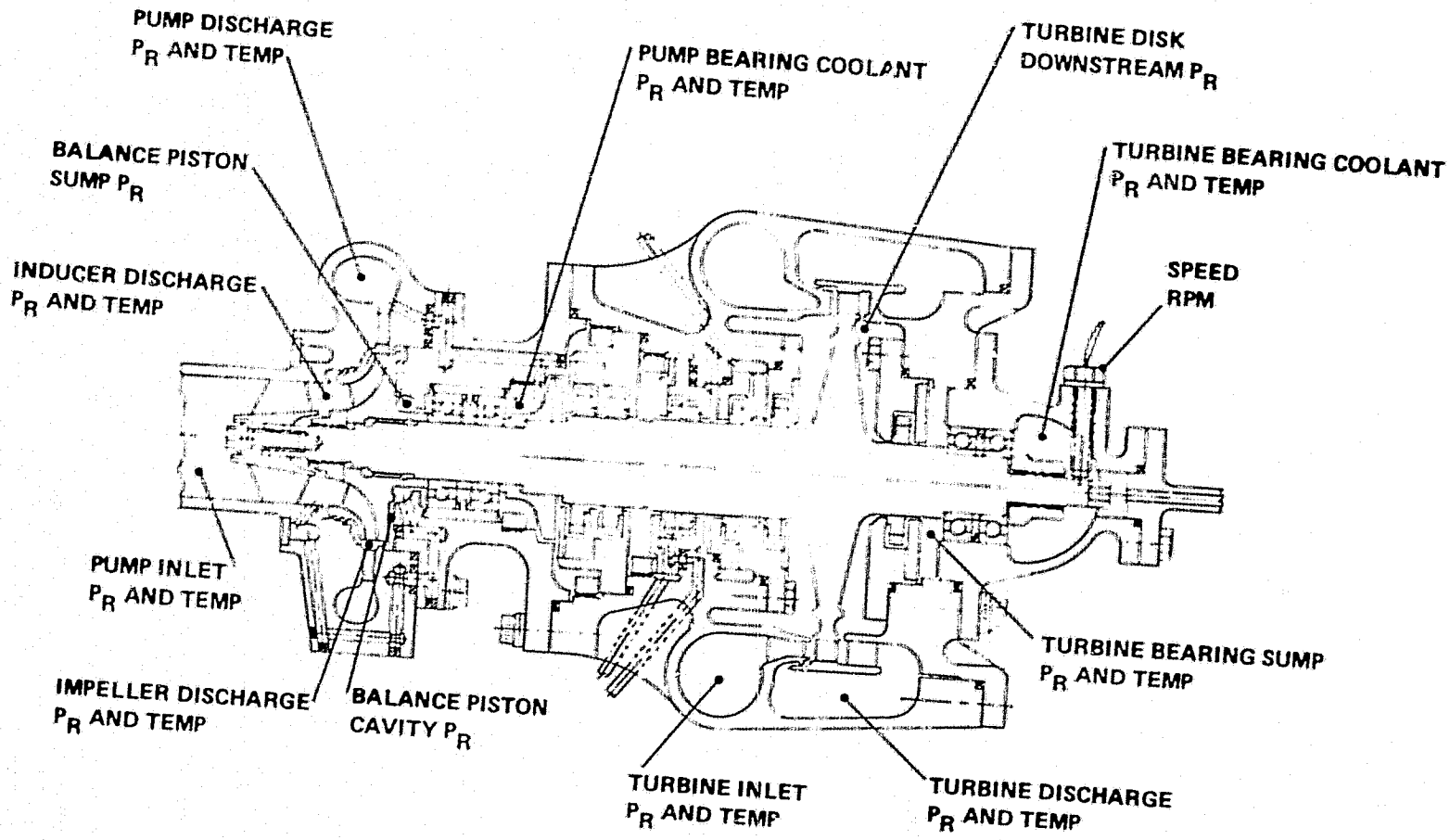

Figure 3-53. Oxidizer - High Pressure Turbopump Development Instrumentation Selection

Pump Performance. The high pressure oxidizer pump is required to operate with a flow of 26.88 lb/sec of liquid oxygen. The inlet flow to the pump is provided by the discharge flow from the low pressure oxidizer pump. Sufficient NPSH is provided that cavitation problems are not expected in the high pressure pump. A discharge pressure from the high pressure oxidizer pump of at least 2648 psia is required, giving a pump head rise of about 5206 ft. As high an efficiency as possible is, of course, to be provided by the HPOP. In addition, geometric dimensions of the pump are to be kept as small as possible. Because of the high head rise and relatively low flow, a centrifugal impeller was selected as a likely pump candidate. The high speed necessary for such a pump made incorporation of an inducer necessary to prevent cavitation on the impeller.

The number of centrifugal pumps which have been designed and tested at Rocketdyne over the years were reviewed. It has turned out that the dimensionless characteristics of the Mark 480 oxidizer pump closely match the design point requirements for the Expander Cycle HPOP being considered. Plots of dimensionless head rise H/N^2 and efficiency (η) vs dimensionless flow Q/N for this pump are shown in Fig. 3-51. The Mark 480 is an inducer-single stage centrifugal impeller pump designed for a flow of 232 gpm at a speed N of 70,000 rpm and a head rise of about 9,000 ft pumping liquid oxygen. Without changing in any way the size or basic hydrodynamic design of the pump, the flow, speed and head defined by the Mark 480 characteristics in Fig. 3-54 were scaled until the necessary design point of the Expander Cycle HPOP was obtained. The necessary head rise and flow for the HPOP were obtained at a speed of 52,827 rpm on the Mark 480. The original design value of Q/N on the operating point only 4 percent below the old design Q/N. The new design efficiency is 66.6 percent. Basic design parameters of the Expander Cycle HPOP are shown in Table 3-20.

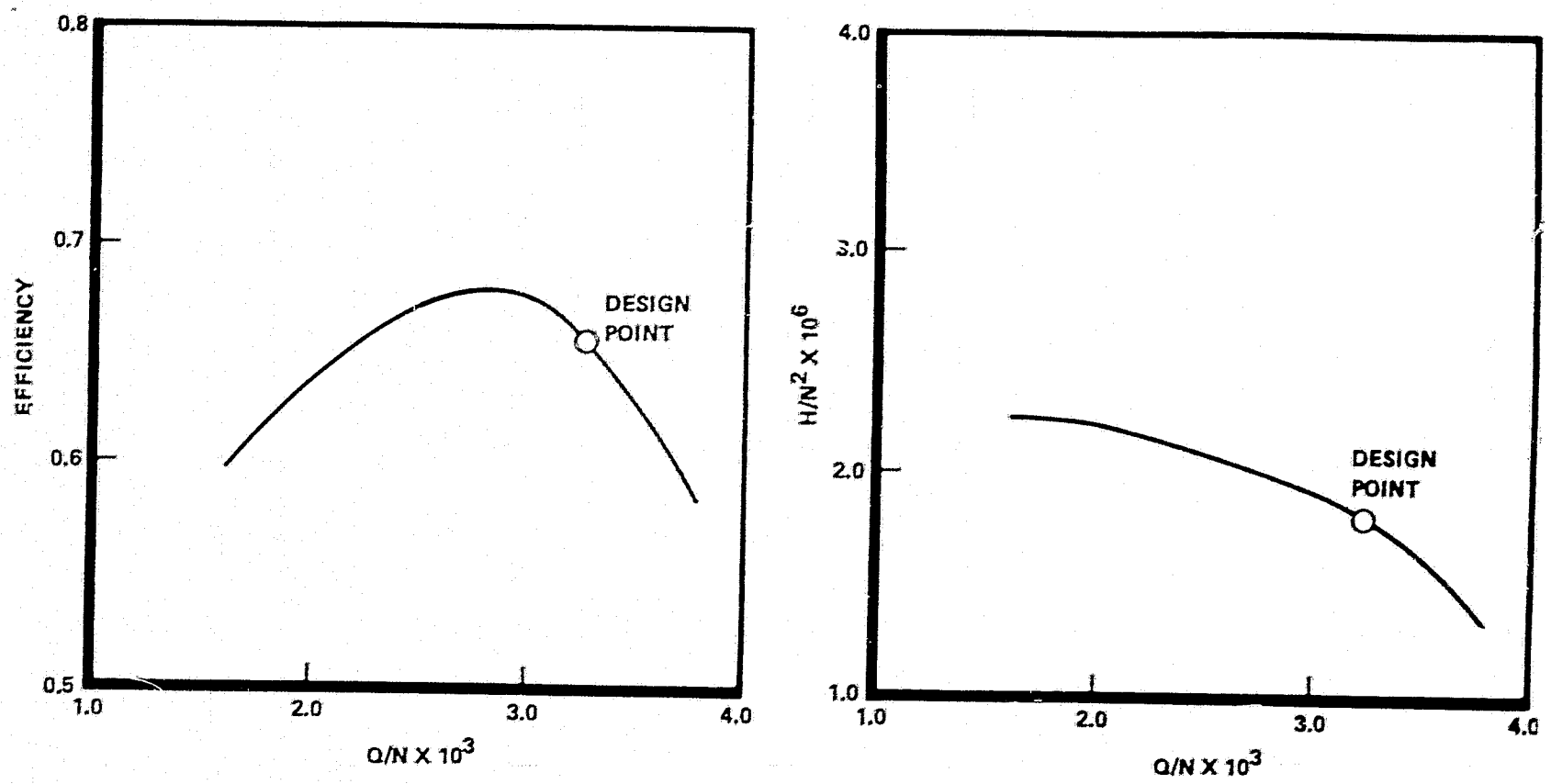

Figure 3-54. Efficiency and Dimensionless Headrise, High Pressure Oxidizer Pump

TABLE 3-20. EXPANDER CYCLE HIGH PRESSURE OXIDIZER PUMP

Operating Conditions:	
Speed, rpm	53,000
Flow, lb/sec	26.88
Inlet Pressure, psia	71.33
Inlet Temperature, Deg. r	163.40
Head Rise, ft.	5,206
Overall Efficiency, percent	66.6
Suction Specific Speed at Min. Available NPSH	19,960
Stage Conditions:	
Number of Stages	1
Specific Speed	1,122
Inducer:	
Tip Diameter, in.	1.65
Hub Diameter, in.	0.70
Head, ft.	229
Impeller:	
Tip Diameter, in.	2.55
Eye Diameter, in.	1.65
Hub Diameter, inc.	1.00
Front Wearing Ring Diameter, in.	2.05
Tip Speed, fps	590
Tip Width, in.	0.151
Balance Piston:	
Total travel, in.	0.010
High Pressure Pad Diameter, in.	2.63
Low Pressure Pad Diameter, in.	1.46
Diffuser and Volutes:	
Diffuser I.D., in.	2.75
Diffuser O.D., in.	3.65
Volute Maximum Area, sq. in.	0.54

The hydrodynamic passage design is identical with that of the Mark 48 oxidizer pump.

At design, the suction specific speed of the HPOP inducer is 16,171. The cavitation limit line (break point suction specific speed S_S vs. Q/N) is shown in Figure 3-55. The shape and magnitude of the line and the point of best cavitation performance of the inducer were obtained from Rocketdyne inducer test experience. As can be seen, the HPOP inducer is operating safely within the break point line with no head loss at design.

The centrifugal impeller allows recirculating flow through the inlet wear ring and the balance piston behind the impeller, and through the pump bearings and seals. The position of the rotor varies axially to seek an axial thrust balance. The pressure forces on the front and back of the impeller, along with all other pump pressure and momentum forces were evaluated and both plotted in Figure 3-55 as a function of the fraction of the impeller tip orifice open at design Q/N. If the turbine thrust is also known, the position of the balance piston when all forces are balanced can be obtained.

Depending on how the bearing flow is dumped (overboard, upstream of the inducer), the pump characteristics can be affected. Dumping of the flow upstream of the inducer can slightly degrade head rise performance and design efficiency. Break point suction specific speed will be lowered, but it is not anticipated that such effects will change the operating point by more than 2 percent.

<u>High Pressure Oxidizer Pump Turbine Analysis</u>. The high pressure oxidizer turbopump (HPOTP) turbine is a single-stage, partial admission, turbine similar to the Mark 48ϕ turbine. The developed power and operating speed were determined by the optimized pump design. Turbine design conditions were taken from the engine balance and includes a heat exchanger to increase the turbine inlet temperature. A partial admission design was used because the design mass flowrate is so small that a normal full admission design would give very small blade heights with an attendant low efficiency.

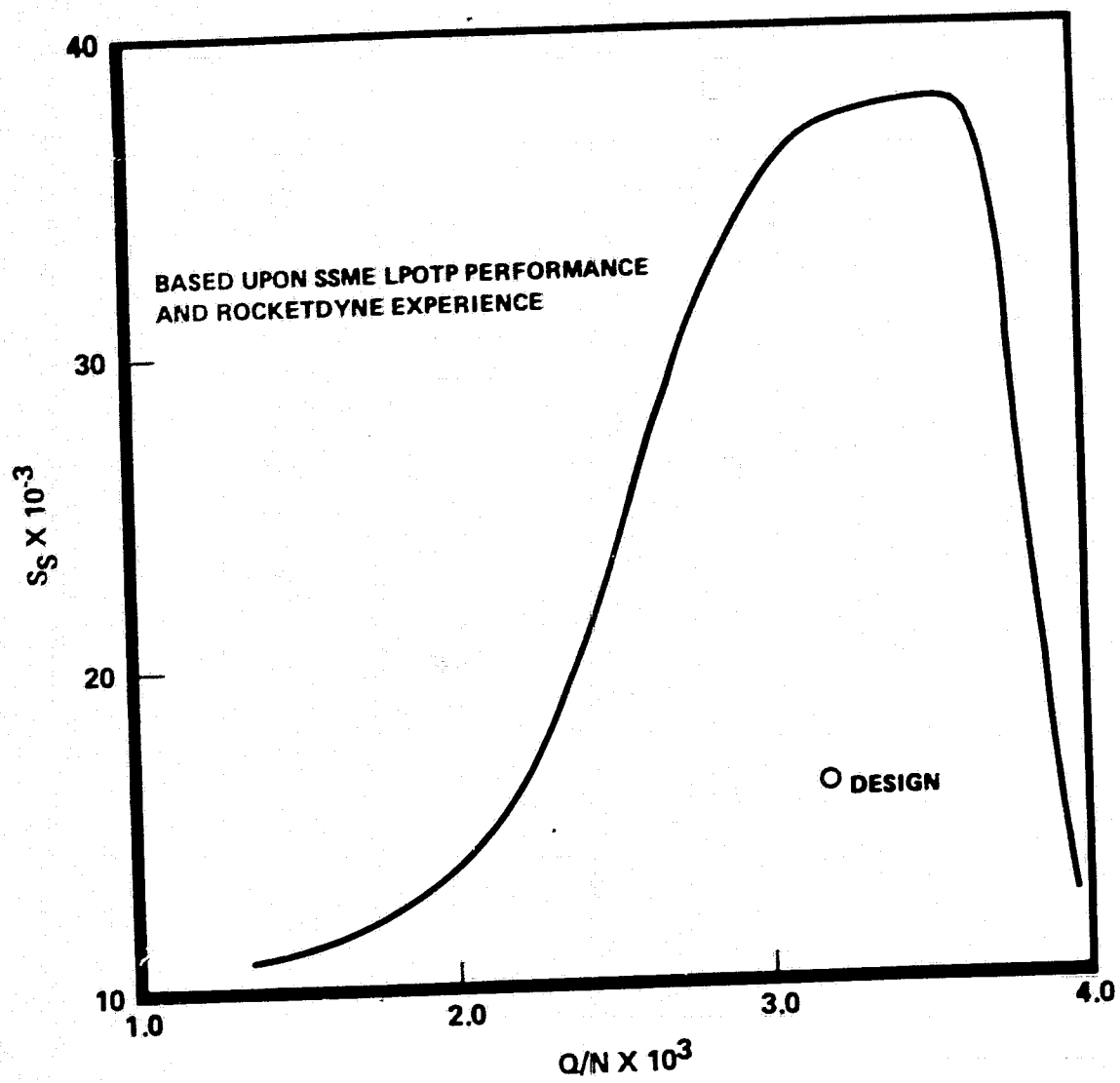

Figure 3-55. Cavitation Performance, High Pressure Oxidizer Pump

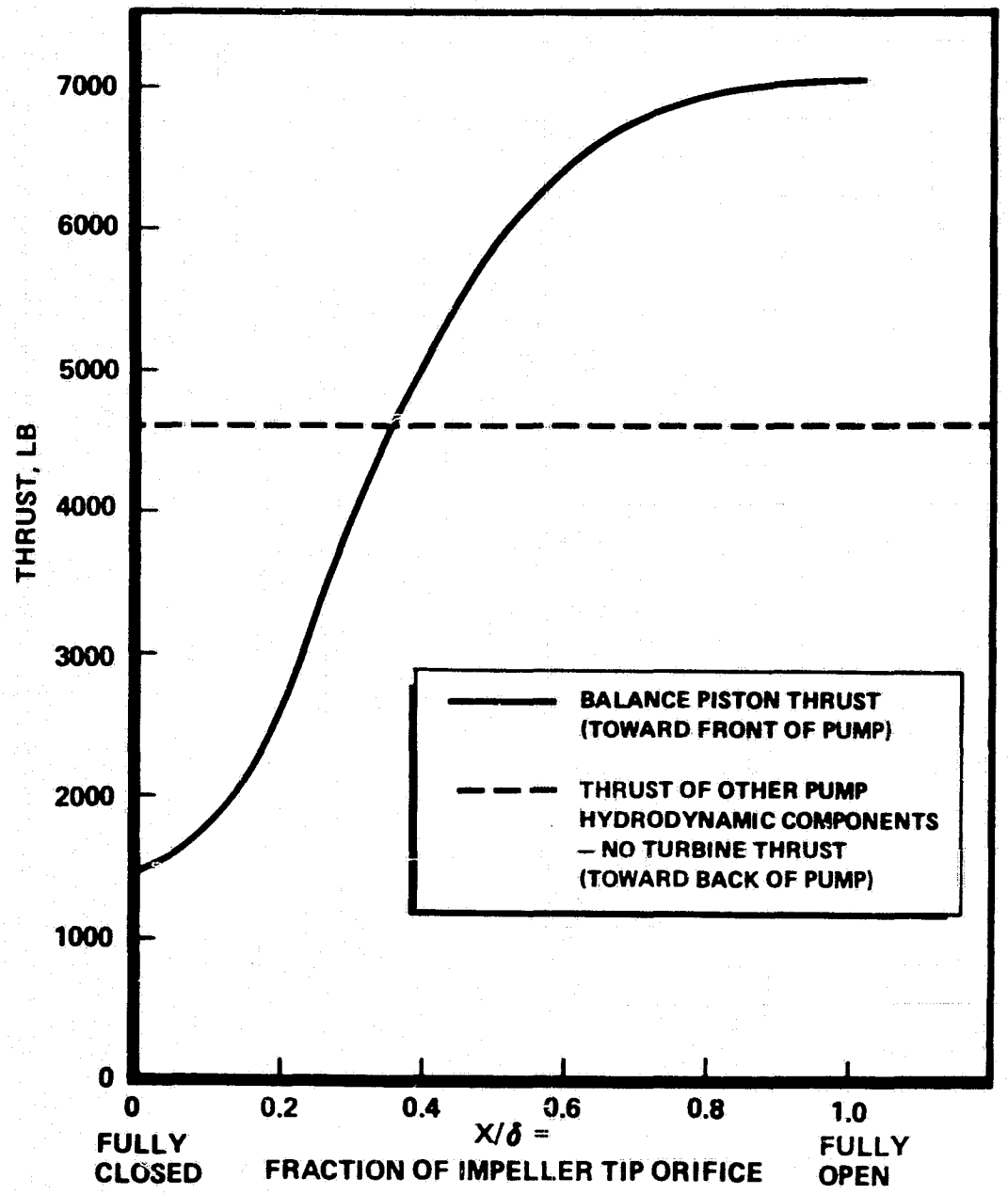

Figure 3-56. Balance Piston Thrust, High Pressure Oxidizer Pump

The design analysis was conducted utilizing Rocketdyne's gaseous hydrogen, partial admission, turbine computer program. The program accounts for the following kinds of losses: profile loss, end wall loss, tip clearance loss, and disc friction loss existing in partial admission turbines as well as in full admission turbines. Additional losses due to partial admission include: (1) entering end loss occurring at the beginning of the active arc of admission, (2) leaving end loss occurring at the end of the active arc of admission, (3) loss due to blade pumping in the inactive portion of the arc, and (4) loss due to leakage of working fluid between the rotor and stator.

Turbine design parameters are shown in Table 3-21. Turbine speed and power were from the pump design, while turbine inlet conditions and pressure ratio were taken from the engine balance. Turbine inlet flow, inlet total pressure, and inlet total temperature are specified at the turbine inlet flange which is in the turbine inlet pipe just upstream of the turbine inlet manifold. Turbine exit total pressure and temperature are specified in the turbine outlet pipe just downstream of the turbine outlet collector. The pressure drop between the turbine inlet and nozzle inlet is 26 psi. The loss is for a tangential inlet manifold and radially convergent nozzles.

Turbine geometry parameters were optimized for high performance and minimum weight. Fig. 3-57 shows turbine mean diameter versus turbine efficiency for optimized blade height and angle. The turbine mean diameter of 4.85 inches was selected near the peak efficiency on the smaller side of diameters to minimize the weight of the turbine high pressure housings.

The turbine predicted power losses are tabulated in Table 3-22. Primary losses are gas path losses due to friction, turning in the nozzle and rotor profile as shown by the expansion and kinetic energy losses. Partial admission losses and disk friction losses are listed.

The velocity vector diagram shown in Fig. 3-58 includes flow path friction and turning losses but excludes losses due to shaft seal leakage, disk friction, size effects, and partial admission. The rotor blade inlet incidence angle

TABLE 3-21. HIGH PRESSURE OXIDIZER TURBOPUMP EXPANDER TURBINE PERFORMANCE PARAMETERS

Working Fluid		GH_2
Output Power	HP	408
Speed	RPM	53000
Inlet Flowrate	Lb/Sec	2.99
Inlet Total Temperature	^oR	797
Inlet Total Pressure	PsiaT	2186
Outlet Total Pressure	PsiaT	1809
Pressure Ratio, Total-to-Total	—	1.2082
Available Energy	Btu/Lb	153.5
Isentropic Velocity	Ft/Sec	2773
Mean Diameter	Inch	4.85
Mean Blade Speed	Ft/Sec	1121
Overall Velocity Ratio	—	0.404
Efficiency, Total-to-Total	—	0.629

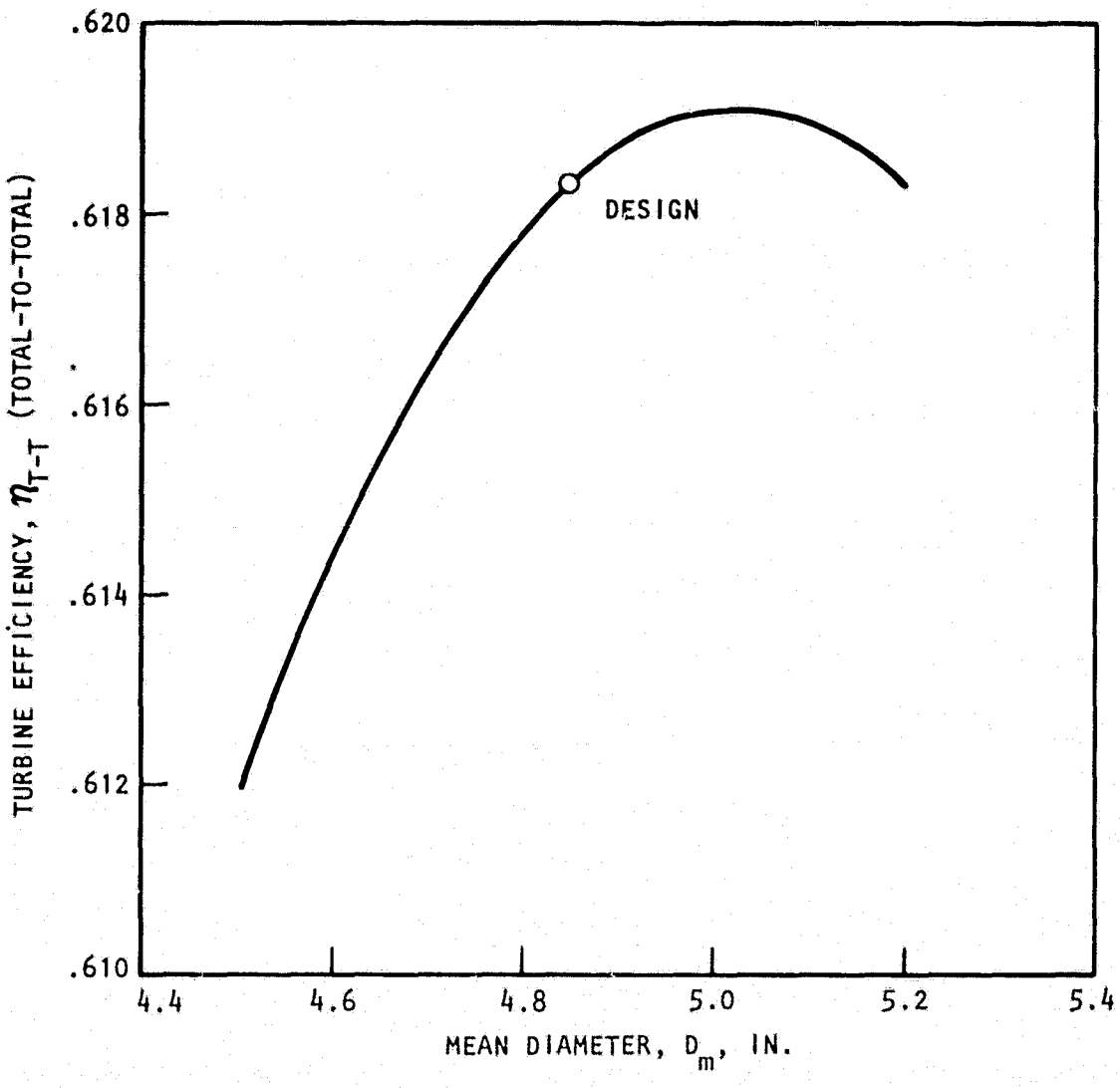

Figure 3-57. High Pressure Oxidizer Turbopump Turbine Mean Diameter Optimization

TABLE 3-22. HIGH PRESSURE OXIDIZER TURBOPUMP EXPANDER ENGINE FLANGE TO FLANGE EFFICIENCY AND PERFORMANCE

1. Power Losses

	Flowrate Lb/Sec	Enthalpy Btu/Lb	Power Loss HP
Inlet Manifold	2.99	7.2343	30.6074
1-N Inlet Incidence	2.99	.0000	.0000
1-N Inlet Kinetic Energy	2.99	.0000	.0000
1-N Expansion Energy	2.99	10.7009	45.2738
1-R U/S Shaft Seal	.0704	111.1212	11.0725
1-R Inlet Incidence	2.9196	.0000	.0000
1-R Inlet Kinetic Energy	2.9196	15.6767	64.7638
1-R Expansion Energy	2.9196	.0000	.0000
1-R Windage			16.3916
1-R End Sector Mixing			9.0459
1-R Rim Friction			2.5813
1-R Disk Friction			2.6975
1-R End Clearance*	2.9196	0.0	0.0
S-1 Diagram Factor Adjustment	2.9196	5.0356	20.8030
1-R Leaving Energy	2.9196	9.1716	37.8899
Total Power Losses			241.1267

*Included in diagram factor adjustment

2. Available Power

WDOT Inlet Flange, Lb/Sec	2.99
DHA T-T F-F, Btu/Lb	153.5396
HP Available T-T F-F	649.6028

3. Shaft Power, Etc, Overall

HP Available T-T F-F	649.6028
Total Power Losses	241.13
Shaft BHP	408.47
Overall Efficiency	.6288
Overall UM/Co T-T	.4044

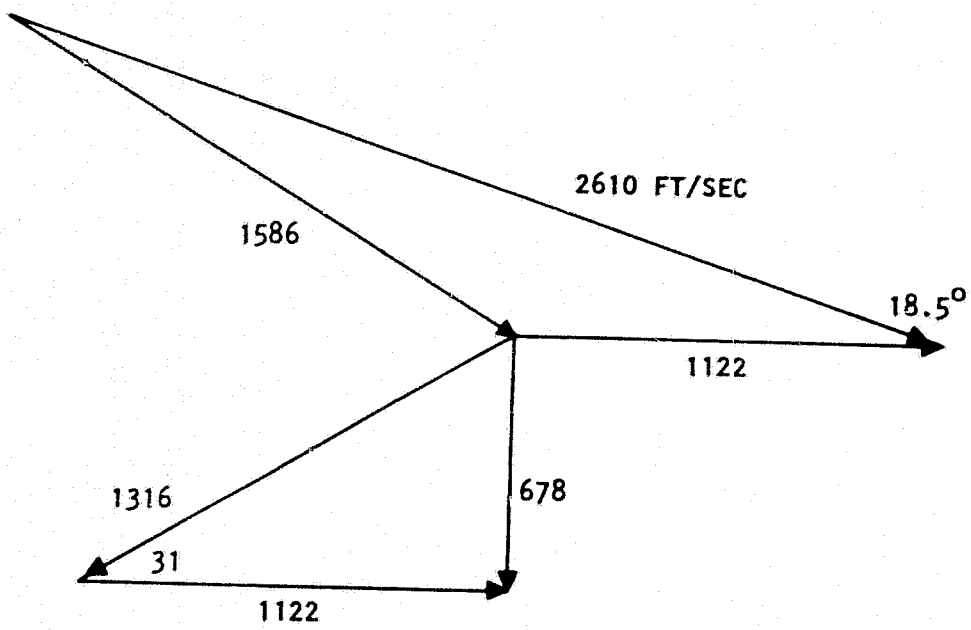

N	= 53000 RPM
P_{t_1}	= 2186 PSIA
T_{t_1}	= 797 °R
W	= 2.99 LB/SEC
D_m	= 4.85 IN.
SHAFT HP	= 408
η_{T-T}	= .629

Figure 3-58. Velocity Vector Diagram, High Pressure LOX Turbopump Turbine

was set for zero. A rotor outlet angle of 31 degrees was selected for high work output and low leaving loss.

A tabulation of the resultant turbine design pressure and temperature distribution data established with the gas path analysis appears in Table 3-23. That data indicates that there is no static pressure change across the rotor for the impulse design, because all the expansion and acceleration of the flow occurs across the nozzle at the design condition.

Turbine sizing is shown in Table 3-24. The mean diameter is 4.85 inches for each element. The nozzle outlet height is 0.37 inch and the blade outlet height was set 20 percent higher than the nozzle outlet height. The rotor outlet and inlet height are 0.45 inch. The nozzle inlet height of 0.54 inch was determined from the original MK48Ø sizing. The nozzle inlet height was selected to provide the area required to match the turbine inlet velocity, and the flow was then accelerated through the nozzle by radial acceleration. The axial widths for the nozzle and rotor are 0.65 inch and 0.40 inch, respectively. The axial space between the nozzle and rotor is a minimum, 0.05 inch, to reduce spillage loss at the ends of the arc of admission.

The blade path assumptions are listed in Table 3-25. The rotor blade is shrouded for the better performance with a radial tip clearance of 0.005 inch.

The design and off-design predicted performance are shown in Figures 3-59 and 3-60. A plot of predicted turbine efficiency for velocity ratios ranging from 0 to 0.6 is shown in Fig. 3-59; the predicted turbine efficiency at the design velocity ratio of 0.379 is 60.3 percent total-to-total.

The predicted turbine flow parameter characteristics are shown in Figure 3-60. The flow parameter as defined in Fig. 3-60 is a function of turbine pressure ratio and speed parameter. The flow parameter characteristics were determined from the gas path program matching flow element areas with turbine operating conditions.

TABLE 3-23. HIGH PRESSURE OXIDIZER TURBOPUMP TURBINE

BLADE PATH STATE CONDITIONS

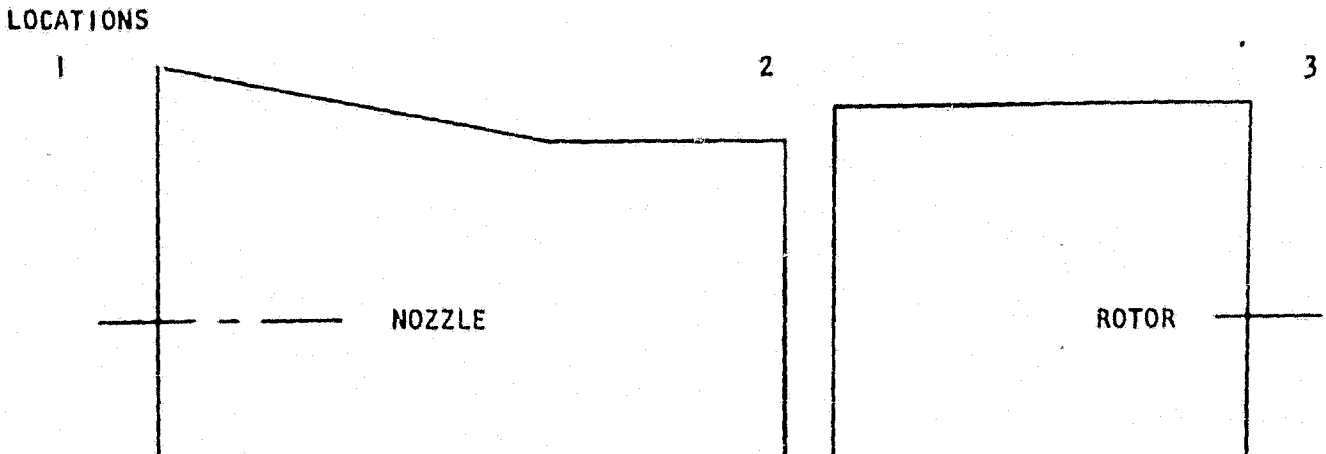

LOCATION	1	2	3
PRESSURES, PSIA			
TOTAL	2186	-	-
STATIC		1809	1809
TEMPERATURES, °R			
TOTAL	797		
STATIC		619	614

TABLE 3-24. HIGH PRESSURE OXIDIZER TURBOPUMP TURBINE - PRELIMINARY TURBINE BLADE PATH DATA

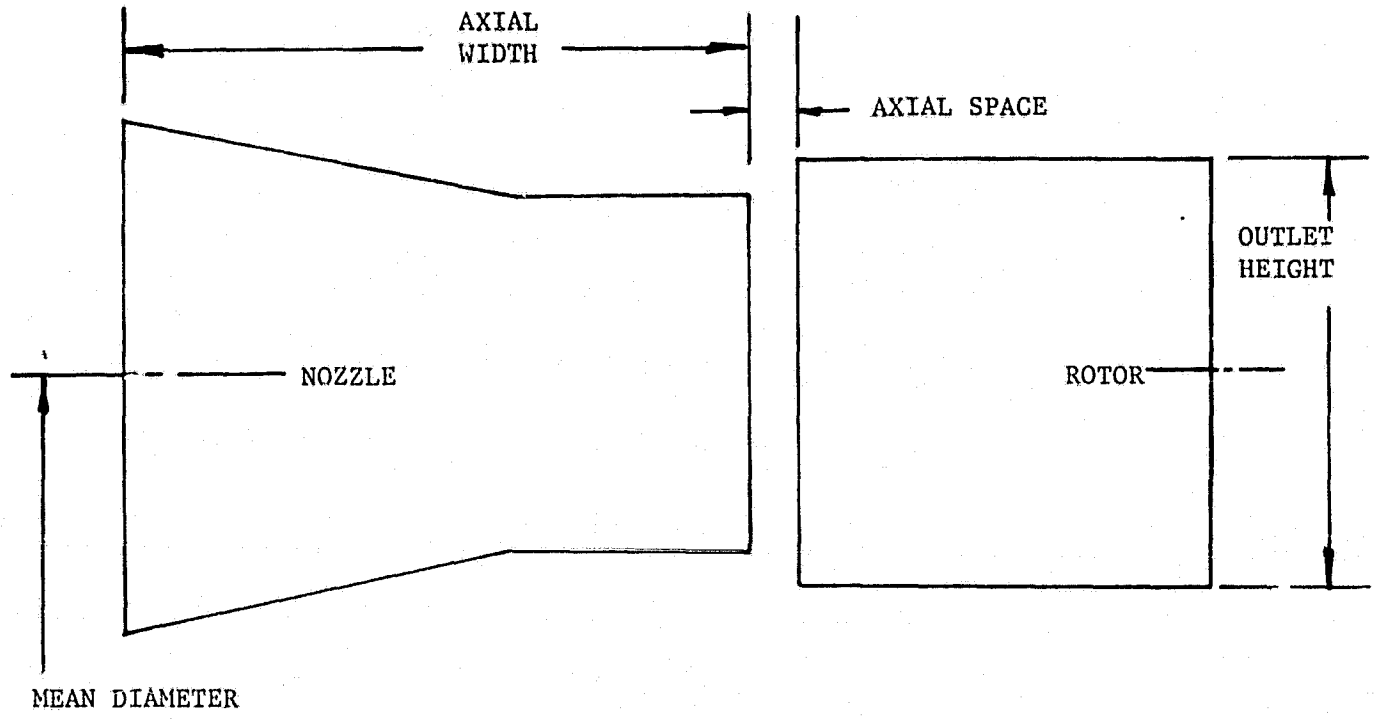

ELEMENT	NOZZLE	ROTOR
MEAN DIAMETER, INCH	4.85	4.85
OUTLET HEIGHT, INCH	0.37	0.45
INLET HEIGHT, INCH	0.54	0.45
AXIAL WIDTH, INCH	0.65	0.40
AXIAL SPACE, INCH	0.05	
PERCENT ADMISSION, %	24.5	
ADMISSION SECTORS	2	

TABLE 3-25. HIGH PRESSURE OXIDIZER TURBOPUMP — BLADE PATH GEOMETRY ASSUMPTIONS

SHROUDED	
ROTOR RADIAL TIP CLEARANCE	= 0.005 Inch
ROTOR UPSTREAM SHAFT SEAL	
DIAMETER	= 1.25 Inch
RADIAL CLEARANCE	= 0.003 Inch
SONIC FLOW	

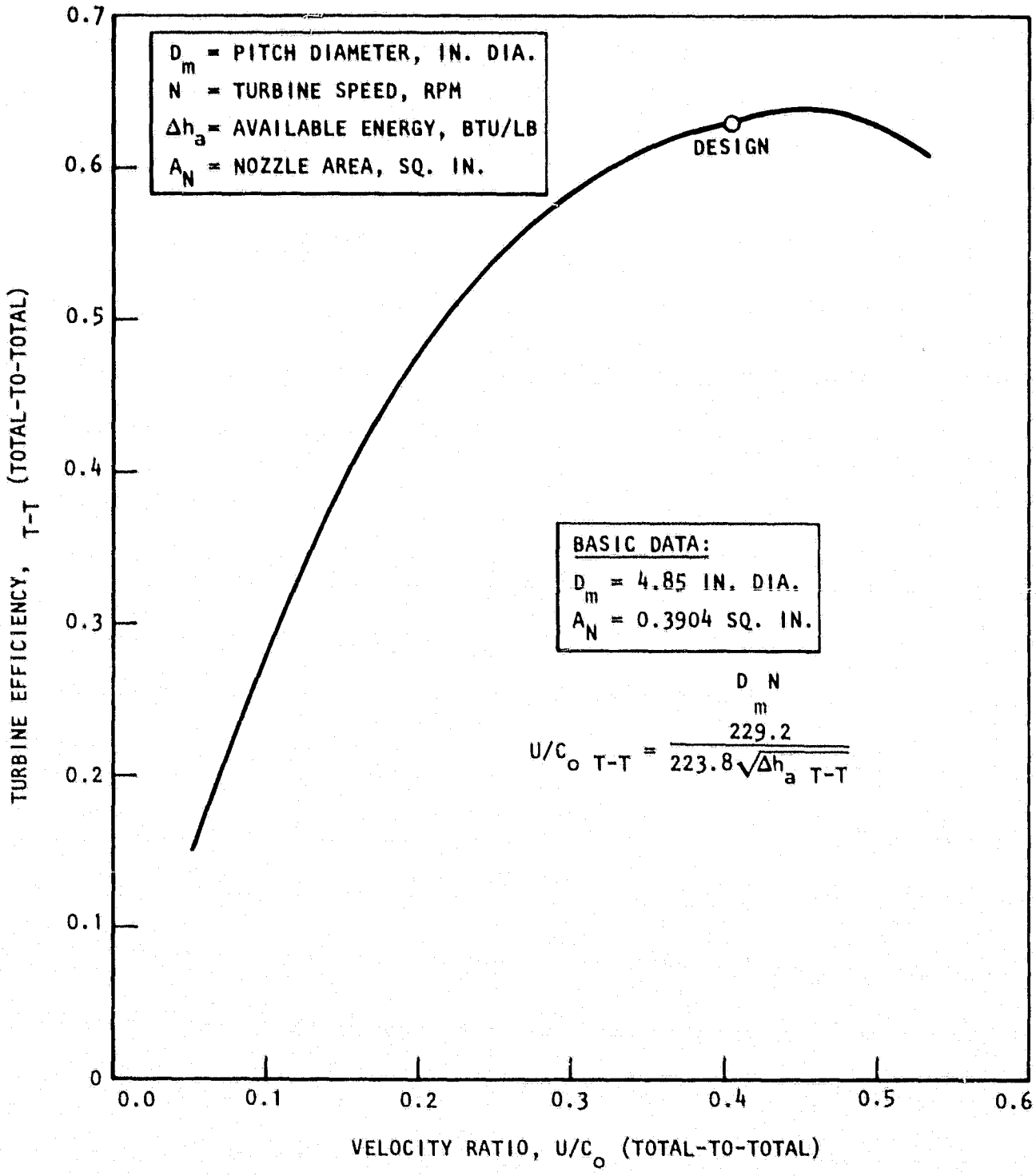

Figure 3-59. Off-Design Efficiency, High Pressure Oxidizer Turbopump Turbine

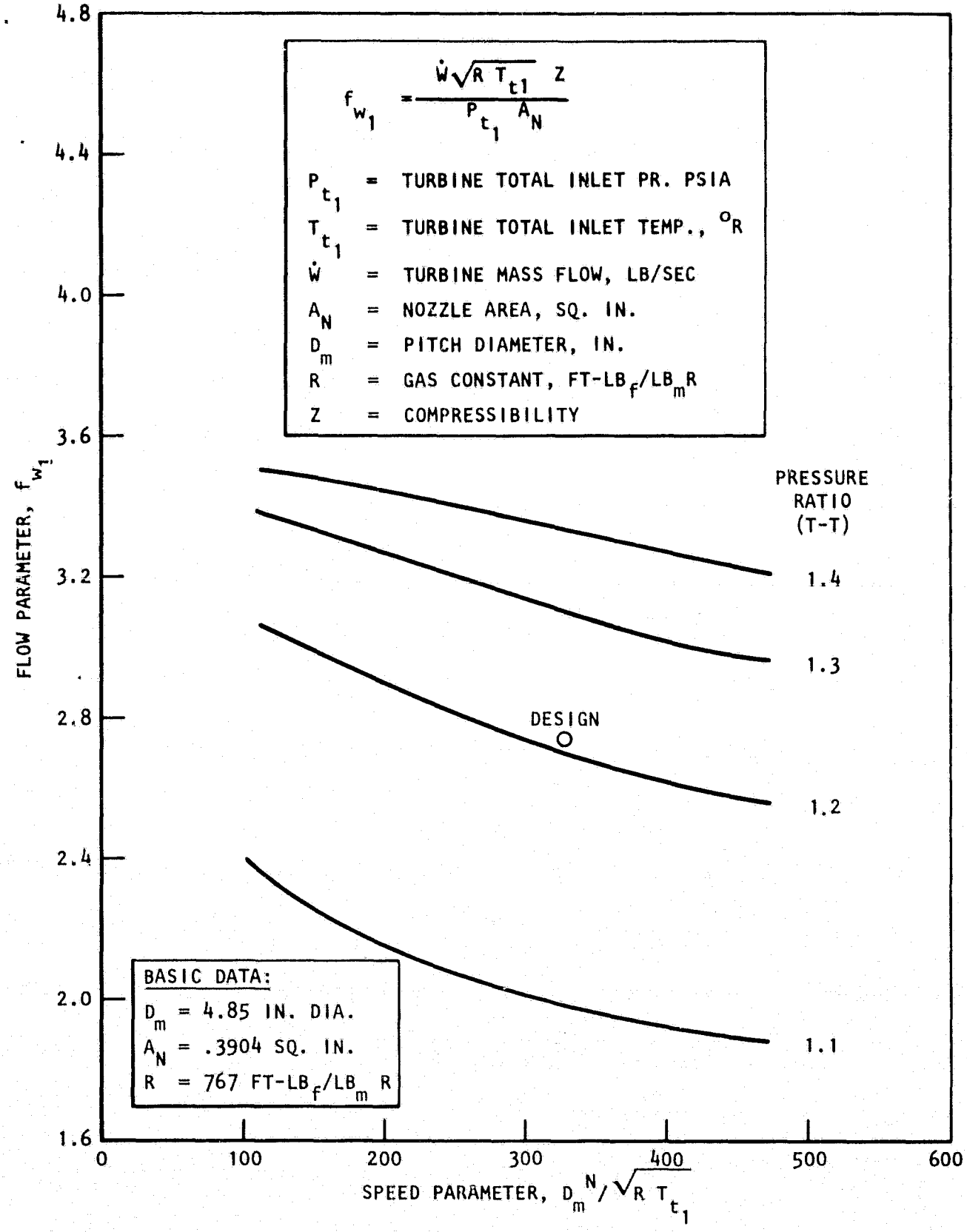

Figure 3-60. Off-Design Flow Parameter, High Pressure Oxidizer Turbopump Turbine

Rotordynamic Analysis. The high pressure oxidizer turbopump (HPOTP) rotor design is very similar to the MK48Ø which operates at approximately 70,000 RPM and has critical speeds of 44,782, 50,986 and 97,711 RPM. The expander cycle HPOTP is designed to operate at 52,837 RPM. It was therefore not surprising to find the first and second critical speed interference with the operational speed for estimated bearing stiffnesses (Fig. 3-61. The model lumped mass group locations are shown in Fig. 3-62. The resultant first three critical speeds and mode shapes are shown in Figure 3-63.

Turbopump operating speed levels within plus or minus 20% of a known critical speed is not recommended. Two design options are available which affect the level of the critical speed regions: Decreasing or increasing the bearing effective radial stiffness and shaft stiffness.

Decreasing the effective bearing radial stiffness to lower the first and second critical speeds below 42,300 RPM would require a maximum effective radial support stiffness of about 90,000 lb/in for both bearing packages. This change would require a more compliant bearing support in series with the bearing pair(s) and would result in a first critical speed of 41,400 RPM with a 22% margin (Fig. 3-64). The first three critical speeds and mode shapes for this design are shown in Fig. 3-65 and represents the minimum change in the design as shown in Figure 3-62.

Increasing the support stiffness requires a more detailed design change to the turbopump but offers the most promising method to eliminate critical speed interferences with the operating speed. In fact, the first critical speed can be increased to 20% above the maximum turbopump operating speed of 52,837 RPM. Turbopump idle mode and full thrust operation are thus below any critical speed regions - a desirable feature. A secondary benefit results in an overall turbopump weight reduction of about 12-15 pounds for a total estimated HPOTP weight of about 26 pounds.

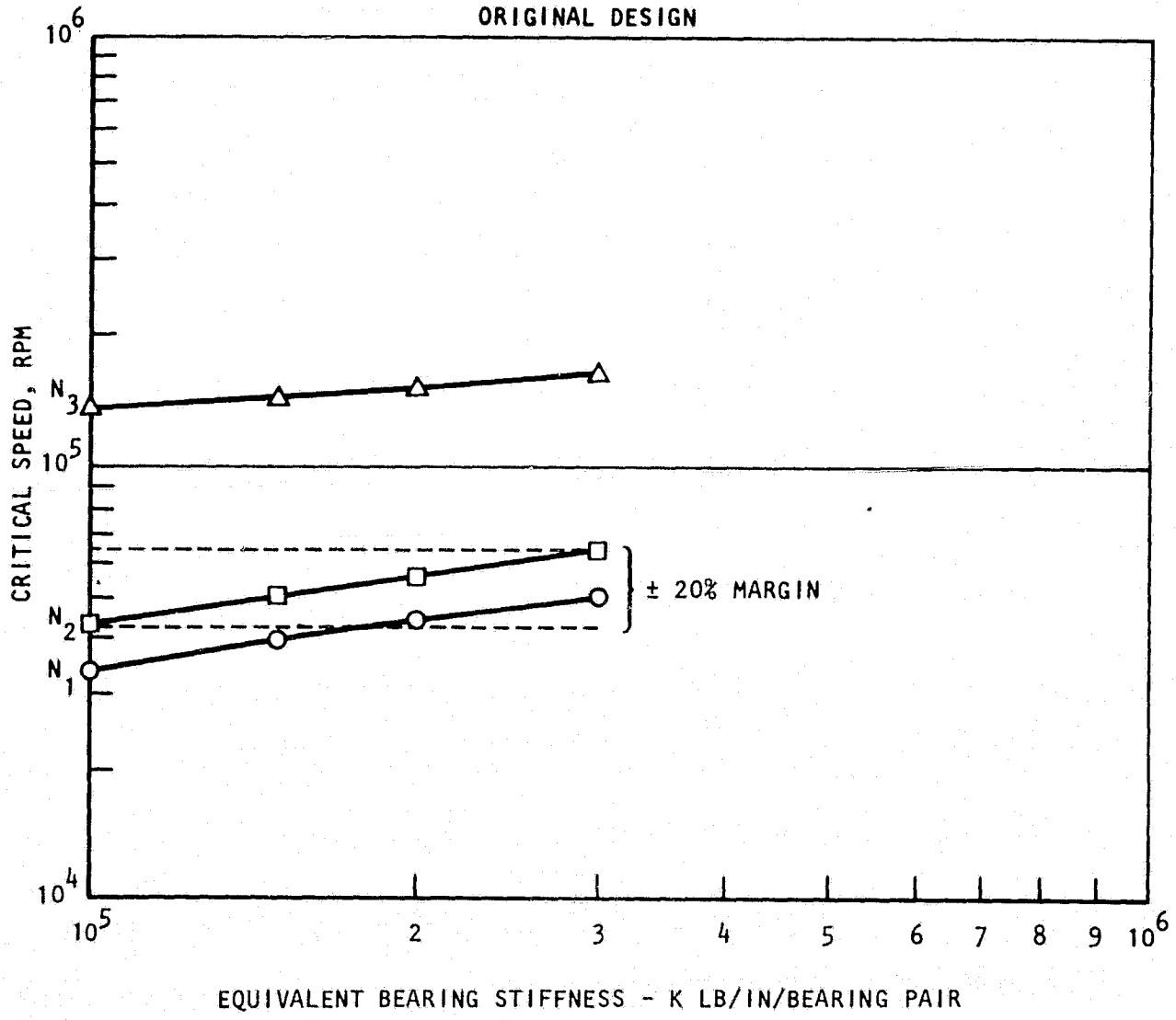

Figure 3-61. Critical Speed vs Bearing Stiffness, High Pressure Lox Turbopump

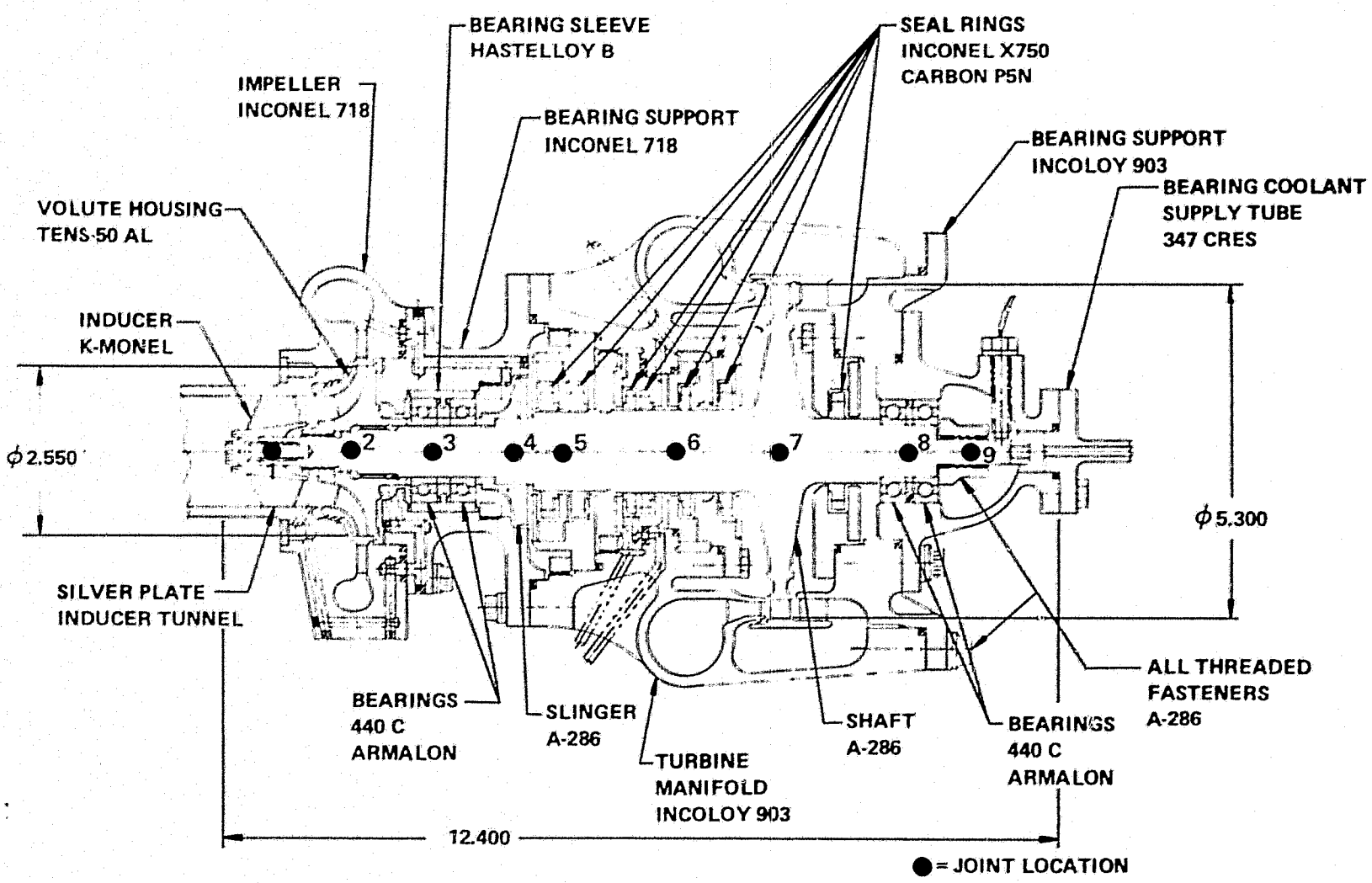

Figure 3-62. Oxidizer - High Pressure Turbopump, Critical Speed Node Locations

CRITICAL SPEEDS (ORIGINAL DESIGN)

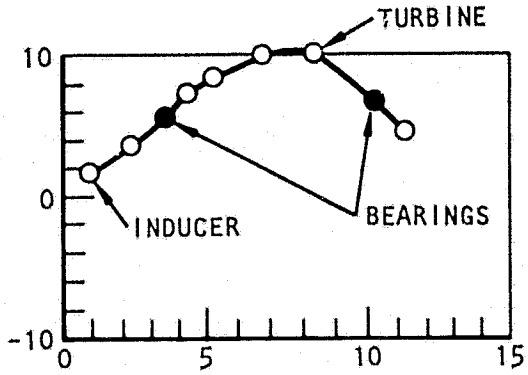

MODE #1

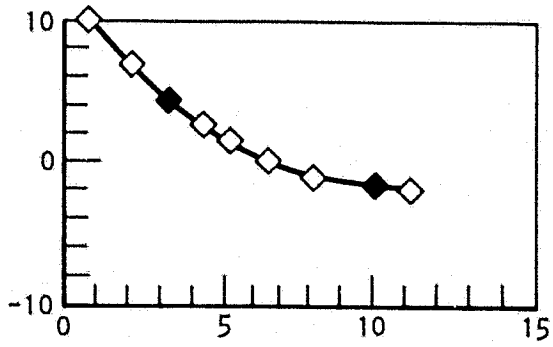

MODE #2

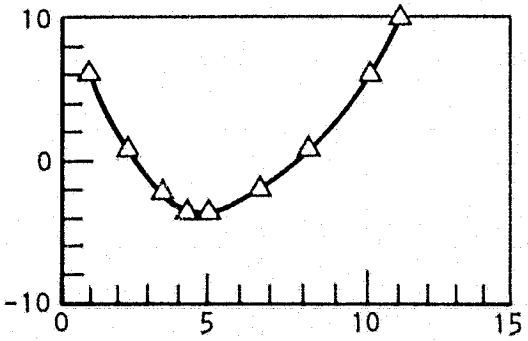

MODE #3

MODE	HZ	RPM
1	736.470	44188.
2	929.620	55777.
3	2515.200	150910.

K1 = 200000. LB/IN
K2 = 200000. LB/IN

MODE SHAPES

Figure 3-63. Critical Speeds and Mode Shapes, High Pressure Oxidizer Turbopump

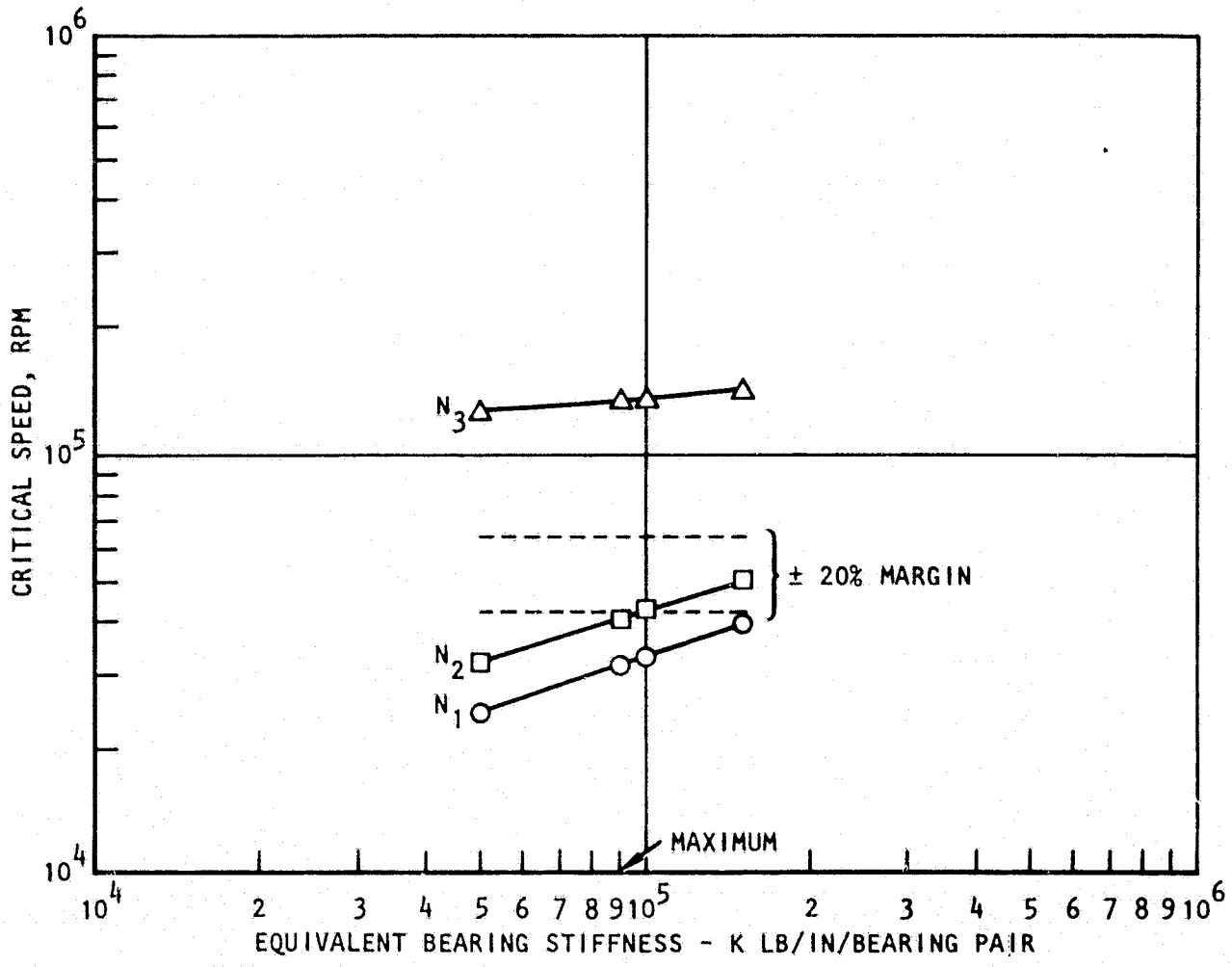

Figure 3-64. Critical Speed vs Bearing Stiffness, First Re-design High Pressure Lox Turbopump

CRITICAL SPEEDS

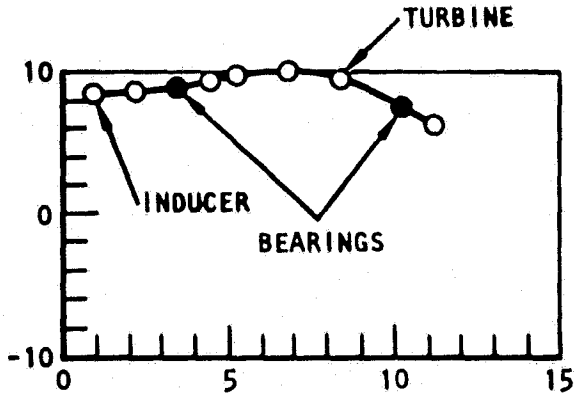

MODE #1

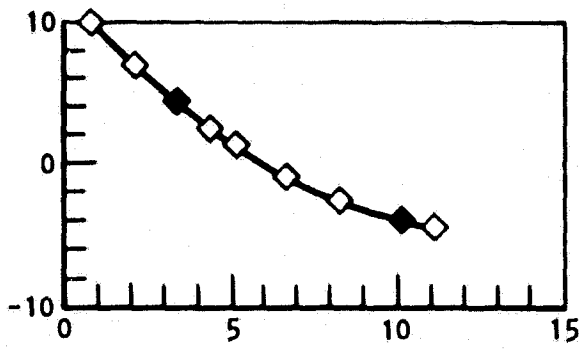

MODE #2

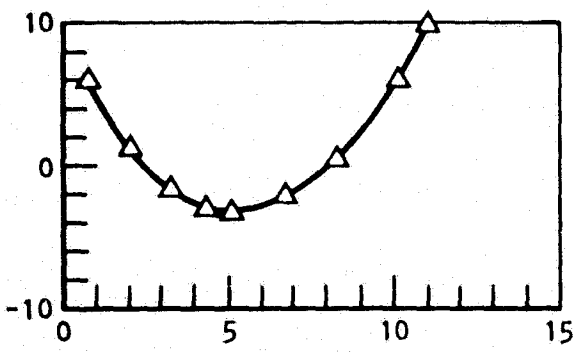

MODE #3

MODE	HZ	RPM
1	537.200	32232.
2	690.050	41403.
3	2235.500	134130.

K1 = 90000. LB/IN
K2 = 90000. LB/IN

MODE SHAPES

Figure 3-65. Critical Speeds and Mode Shapes First Redesign High Pressure Turbopump

The following design changes are feasible to raise the bearing pair radial support stiffness to at least 500,000 lb/in and thus raise the first critical speed to about 66,500 RPM.

(1) Relocate the turbine bearing package approximately 0.40" closer to the turbine disk by decreasing gap between the seal and the bearings.

(2) Resize the turbine disk thickness for 53,000 RPM and material compatibility (A286). Currently, the disk is sized for MK48ϕ operational speed of 78,000 RPM. This would decrease the disk weight and width.

(3) The front bearing slinger can be reduced to approximately 1.5" diameter and decreased approximately 0.25" in length. In addition to the associated weight savings, this will allow the pump end bearings to move the 0.25" or closer to the turbine.

(4) Approximately 0.15" in length can be removed from the floating ring seal package design.

(5) Reposition the inducer closer to the impeller to decrease the inducer/impeller overhang.

A critical speed plot and mode shapes for the above design changes are shown in Fig. 3-66 and 3-67. These calculations and design recommendations are presented as estimates of the proposed change effects. A more thorough analysis must be accomplished to verify the proposed changes.

Turbopump Off-Design Operation and Performance. The wide flow range head ratio and efficiency versus flow ratio characteristics is presented in Fig. 3-68. The peak efficiency is shown to occur at approximately 90 percent of the design flow/speed, Q/N ratio. The peak head rise occurs at approximately 50 percent of the design flow/speed ratio.

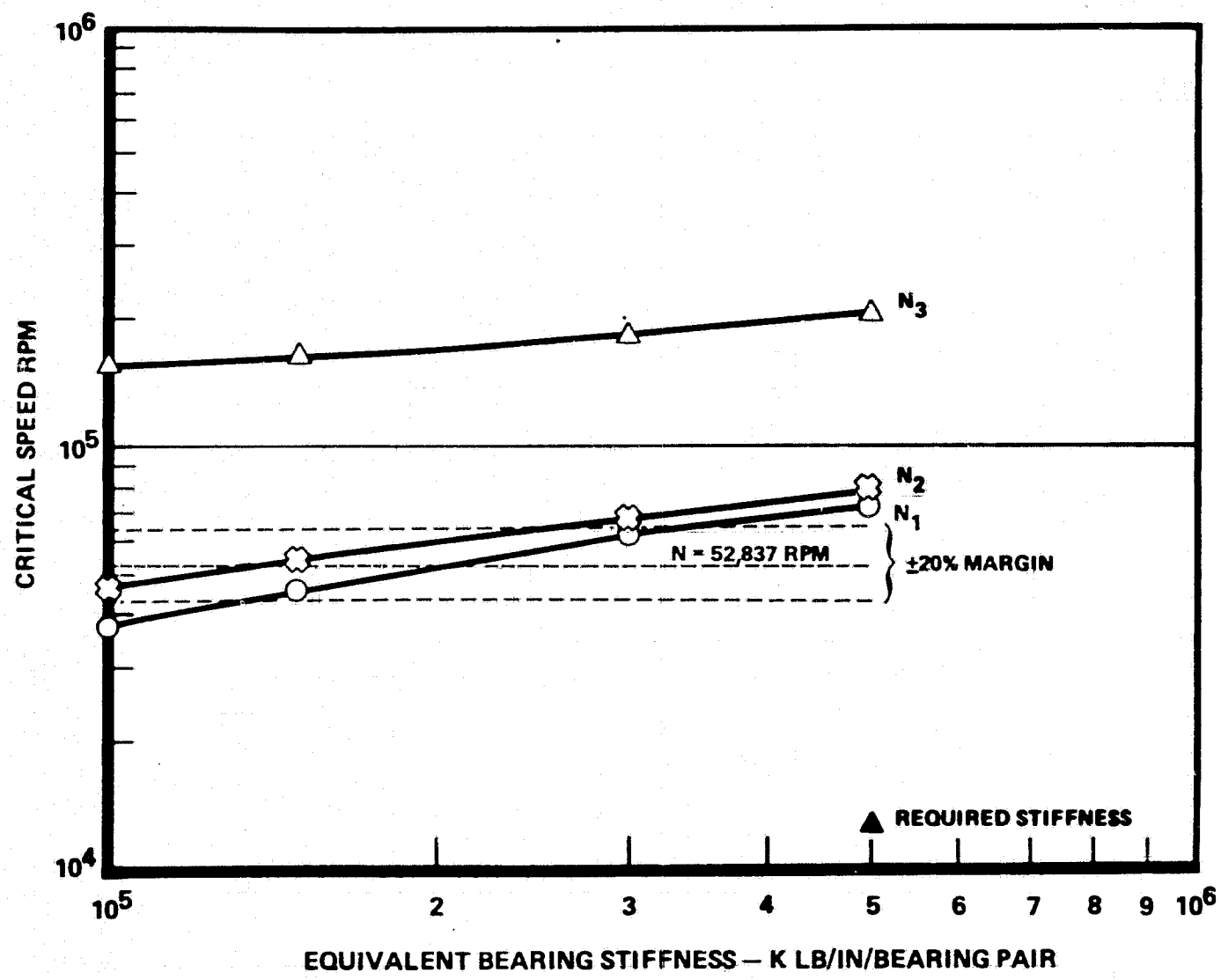

Figure 3-66. Critical Speed vs. Bearing Stiffness, Second Redesign High Pressure Oxidizer Pump

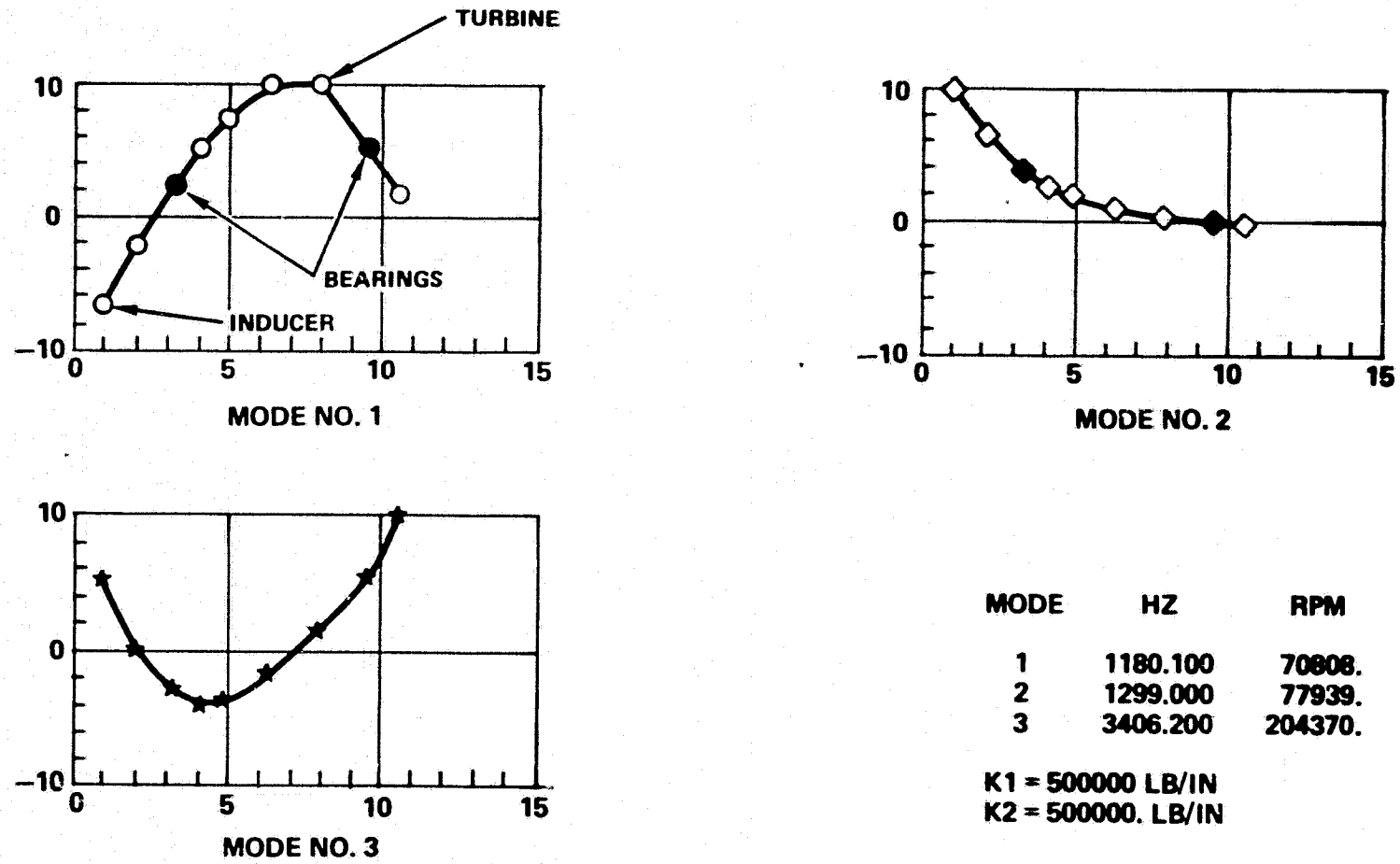

MODE	HZ	RPM
1	1180.100	70808.
2	1299.000	77939.
3	3406.200	204370.

K1 = 500000 LB/IN
K2 = 500000. LB/IN

MODE SHAPES

Figure 3-67. Critical Speed and Mode Shapes, Second Redesign, High Pressure LOX Turbopump

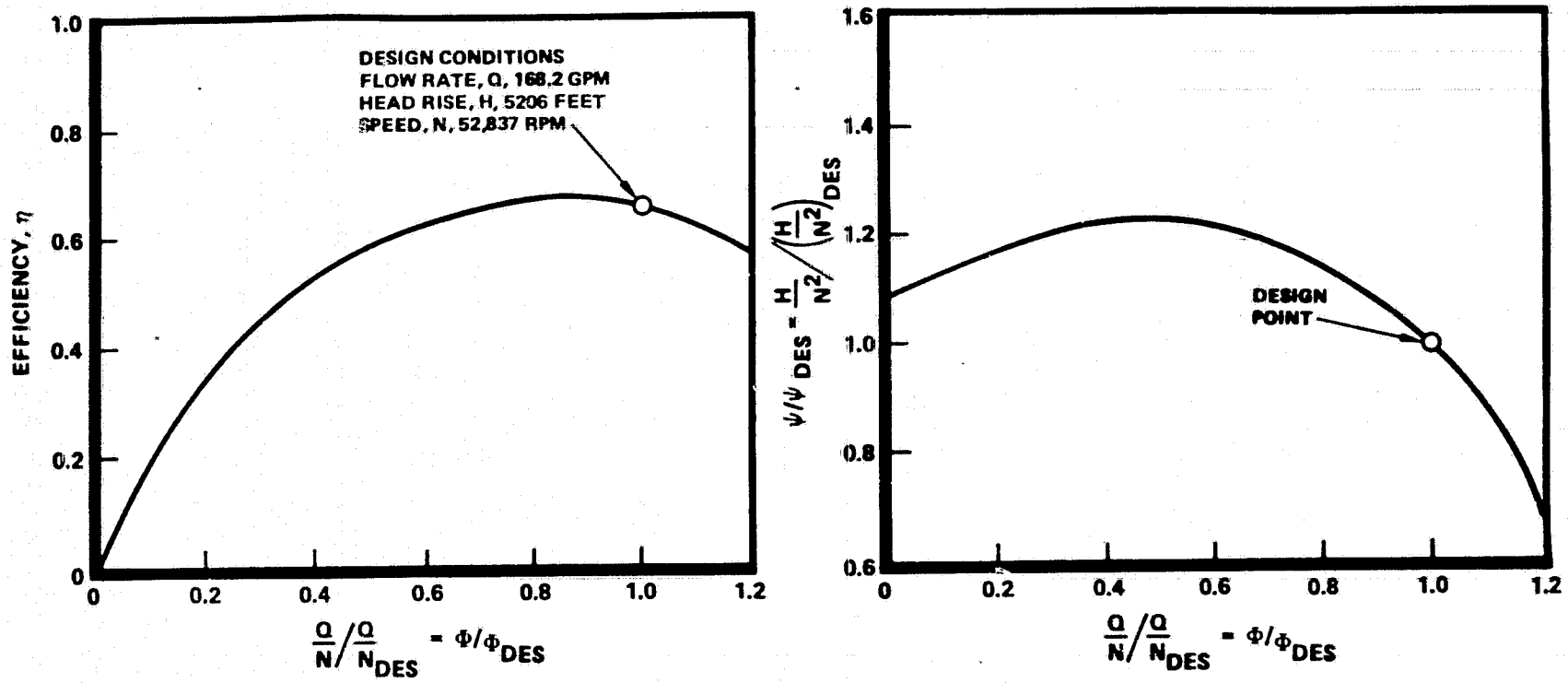

Figure 3-68. Efficiency and Head Ratio, High Pressure LOX Pump

Technology Requirements. The majority of the LOX high pressure pump design represents state-of-the-art with a low risk development effort. One operational and design change over the MK48ϕ concept is the proposed method of supplying rear bearing coolant from the aft end and the elimination of two shaft riding seals. These seals previously isolated the high pressure liquid hydrogen from the turbine. With the new scheme, additional axial load toward the pump will be introduced. With the additional loading, transient and steady state balance piston operation and margin will require development.

TURBOMACHINERY TECHNOLOGY AND DEVELOPMENT ISSUE SUMMARY

The analytical and design optimization of the expander cycle engine turbomachinery revealed only one new technology concern and several issues which will require turbopump development effort to finalize the design.

The choice of the two-stage partial admission turbine for the fuel high pressure pumps represents the only item which may be considered a technology issue. Design wise, a two-stage partial admission turbine is not new, but research and test data throughout industry is very limited. Specific areas of concern are the amount of admission alignment and separation distances of the two nozzles. Additional in-depth analysis with actual test verification is needed to optimize the two-stage partial admission for the expander cycle engine high pressure fuel turbopump.

The following issues will require additional analysis and/or development test verification.

1) Bearing Life - A ten-hour total life without bearing replacement appears to be beyond current bearing operational experience at cryogenic conditions. Specifically, the HP fuel turbopump speed (110,000 RPM) appears marginal for even the 17 mm bearing capabilities. Current testing at NASA is evaluating a hybrid bearing (20 mm) that possibly could meet the ten-hour life requirement, but more development

experience is needed. The fuel high pressure pump has been designed to accept either a 20 mm, 17 mm or a hybrid 20 mm bearing. It is proposed that the initial development effort on the HPFTP use the readily available 20 mm ASE fuel pump bearing design to baseline the operational limits of the 20 mm bearing at expander cycle fuel pump speed. At such time when the hybrid design is fully evaluated, the HPFTP bearings can be replaced with either the 17 mm or 20 mm hybrid depending on the test results.

2) "T"-mounted Turbopumps - The "T" mount offers a weight savings by deleting requirements for interconnecting fluid ducts and the attendant joint-seal problems. At the same time, a lower system overall pressure drop is realized which allows a greater pressure management throughout the active system components. Lastly, the "T"-mounts minimize engine system assembly or disassembly effort. The turbopumps evaluated for the expander cycle have been designed to incorporate flanges at the fluid inlet and discharge, and the turbine gas inlet and discharge to facilitate development testing of the first article. Turbine drive media for the HPOTP, HPFTP, and LPFTP can be easily provided with warm temperature (∿860R) gaseous hydrogen. Turbine drive media for the LPOTP can be supplied by an off stand high pressure LOX tank (3000 psig) in a blowdown mode. Following initial design verification, the applicable system turbopumps in the "T"-mount can be tested as a complete system. On concern, hydrodynamically, is the influence of the relatively short interconnecting fluid passages between the BP pump outlets and the respective high pressure pump inlets. Again, initial development testing on the individual pumps can simulate the actual flow passage geometry to optimize the design before integral castings are fabricated.

3) Pumped Idle Mode - Operation of the engine at 12% of nominal thrust areas presents certain problems or concerns for each of the turbopumps.

a) The high pressure fuel turbopump is axially force-balanced at the full thrust condition, but not at pumped idle for the current design. An unbalance force of about 600 pounds is reacted through the bearings toward the turbine. Although the projected total operational time at pump idle mode is only 1.5 hours out of a total of 10 hours, the capability of the bearings to meet the life requirement is seriously jeopardized. Several design options are possible to reduce the axial thrust unbalance but more in-depth analysis is required.

b) The fuel and oxidizer pumps are predicted to operate in the stall region at pump idle mode. The pumps can operate stabily in stall as long as the operating point is outside the stall transition zone. Figure 3-69 presents a schematic of the head-flow curve showing the relationship of the stall transition zone to the full thrust and idle mode thrust operation. The degree of stall and the efficiency for each pump can only be determined by additional detailed analysis, followed by test verification.

c) The low pressure fuel boost pump will operate at a very low Q/N but will generate sufficient head rise to satisfy the high pressure pump inlet requirement. The flow is likely to be unstable at the estimated Q/N of 41 percent.

d) The low pressure LOX boost pump will operate with a very low head rise at approximately the design value of Q/N. The head rise generated will still be sufficient to satisfy the high pressure pump inlet requirements.

e) The impact of the HPOTP re-directed turbine and bearing liquid hydrogen flow on the axial thrust balance and system performance will require additional analysis both from the engine system power balance and the turbopump operations.

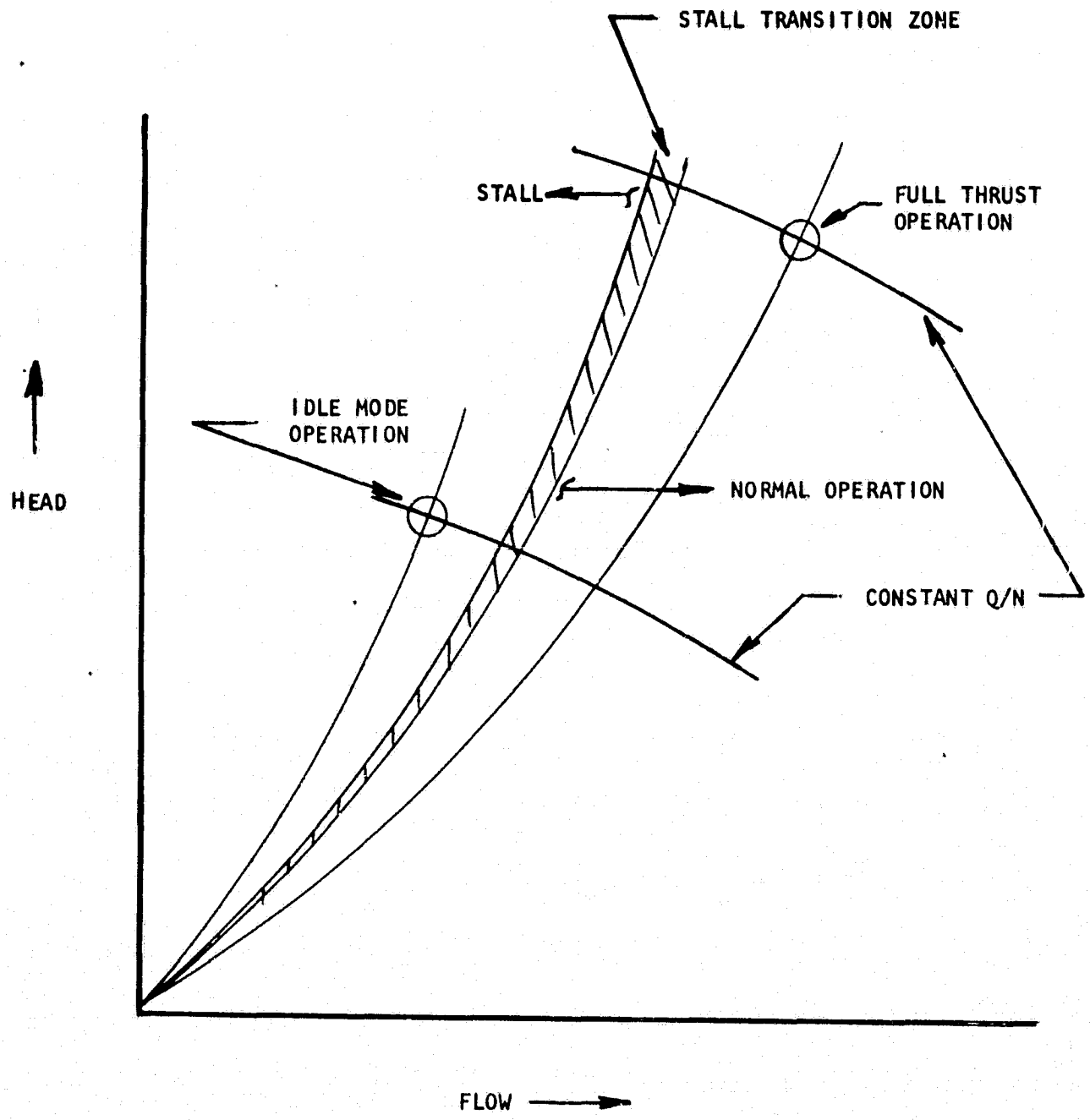

NOTE: No scale

Figure 3-69. Characteristics of Turbopump Operation

4) Additional weight savings can be achieved by changing the bearing span and shortening the inducer to impeller distance of the HPOTP. Design effort as well as detailed rotordynamic analysis will be required.

5) Performance effects of the liquid hydrogen bearing coolant flow within the low pressure fuel boost turbopump will require more analysis followed by test verification.

6) Although not shown on either of the high pressure turbopump designs within this study, some type of breaking system will be required on the high pressure turbopump rotors to prevent rotation during the tank head idle mode operation. Various schemes are possible, such as lift off face seals which must be actuated for normal pump operation.

CONCLUSION

The preliminary designs of the expander cycle turbomachinery presented herein represent the results of a series of analytical and design iterations. The turbopump layouts shown depict conceptually accurate data but are not without certain acknowledged technical concerns. Additional design and analytical effort is required to solve those technical issues and produce an optimized turbomachinery system for the 15K expander cycle engine.

ENGINE CONTROL SYSTEM (TASKS 4 and 5)

An engine transient computer model was developed in Task 4 and a User's manual documented in Rocketdyne Report RD/R180-214. This computer model of the engine was used in Task 5 to evolve the control system for the Expander Cycle Engine Point Design. The control system for this engine covers a variety of components and impacts all phases of engine operation. The optimization of that control system thus comprised a wide range of subjects and considerations. Specifically, the areas that were evaluated in Task 5 studies included: control point selection, steady state performance, starts and shutdown, redundancy issue, controller, valves, actuators and instrumentation. In performing the control systems trade study, four controls options were defined and used in each of the above areas. The control options as defined in Table 4-1. reflect control options that very from no on-board controller to mechanical pneumatic control, to full range on-board control.

CONTROL SYSTEM SELECTED

A simplified engine schematic for the series turbine engine used as a control systems baseline is depicted in Fig. 4-1, showing only the primary flow paths and potential thrust and mixture ratio control points. A full schematic of the engine is presented in Fig. 4-2. The primary control points selected are the main oxidizer valve (MOV) and the turbines bypass valve (TBV). The MFV is used for start and shutdown and the OTBV is used to achieve satisfactory operation during powered idle mode. In addition, the extended nozzle coolant control valve must have a throttled position during powered idle mode. The MOV and TBV were selected as the control points for thrust and mixture ratio.

To accomplish control of the engine, an on-board electronic controller was selected. The electronic controller has the functions of engine checkout and monitoring, redline monitoring, receiving and conditioning sensed signals, interfacing with the vehicle, electronic commands to modulate and sequence the valves and energizing the ignition system.

TABLE 4-1. ENGINE CONTROLS SYSTEM CONCEPTS DEFINITION

A. Minimum Electronic Systems

- No Controller
- Mechanical Sequencing
- Monitoring Instrumentation for Reusable Engine
- Redline Monitoring for Man-Rating
- Checkout by Off-Engine Means

B. Open Loop

- Electrical Sequence Control
- No Valve Positioning Control
- Monitoring Instrumentation and Redline Monitoring
- Checkout and Status Monitoring on Engine

C. Mainstage Trim Controls

- Electrical Sequence Control
- No Valve Positioning Control During Start and Shutdown
- Monitoring Instrumentation and Redline Monitoring
- Performance Instrumentation
- Feedback During M/S to Trim F & MR
- Checkout and Status Monitoring by Engine

D. Full Range Controls

- Controller Performing Valve Position Control
- Feedback to Control F & MR as required
- Monitoring Instrumentation and Redline Monitoring
- Performance Instrumentation
- Checkout & Status Monitoring by Engine

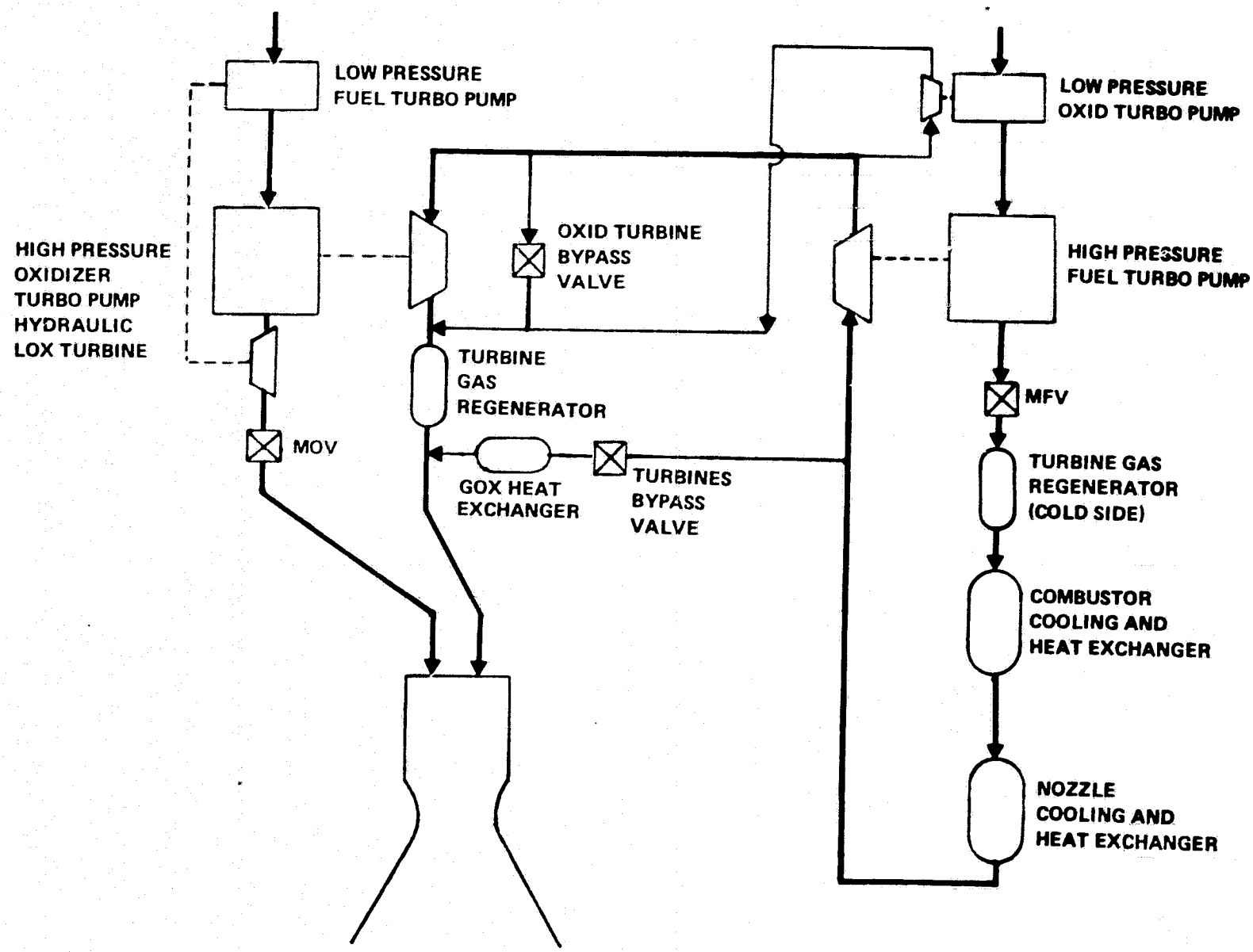

Figure 4-1. Series Turbines Baseline Engine Main Propellant Controls

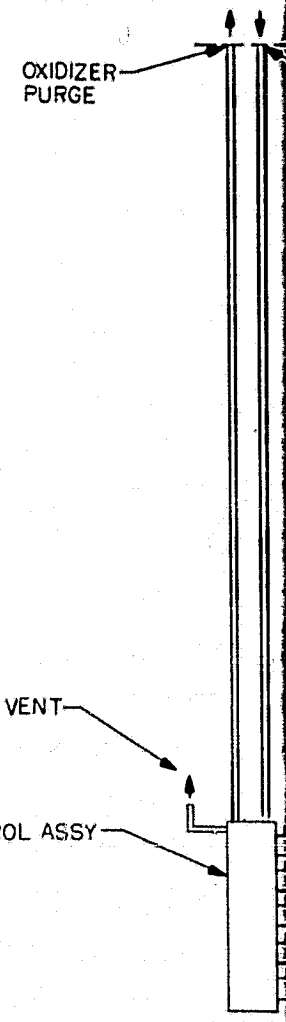

ORIGINAL PAGE IS
OF POOR QUALITY

FOLDOUT FRAME

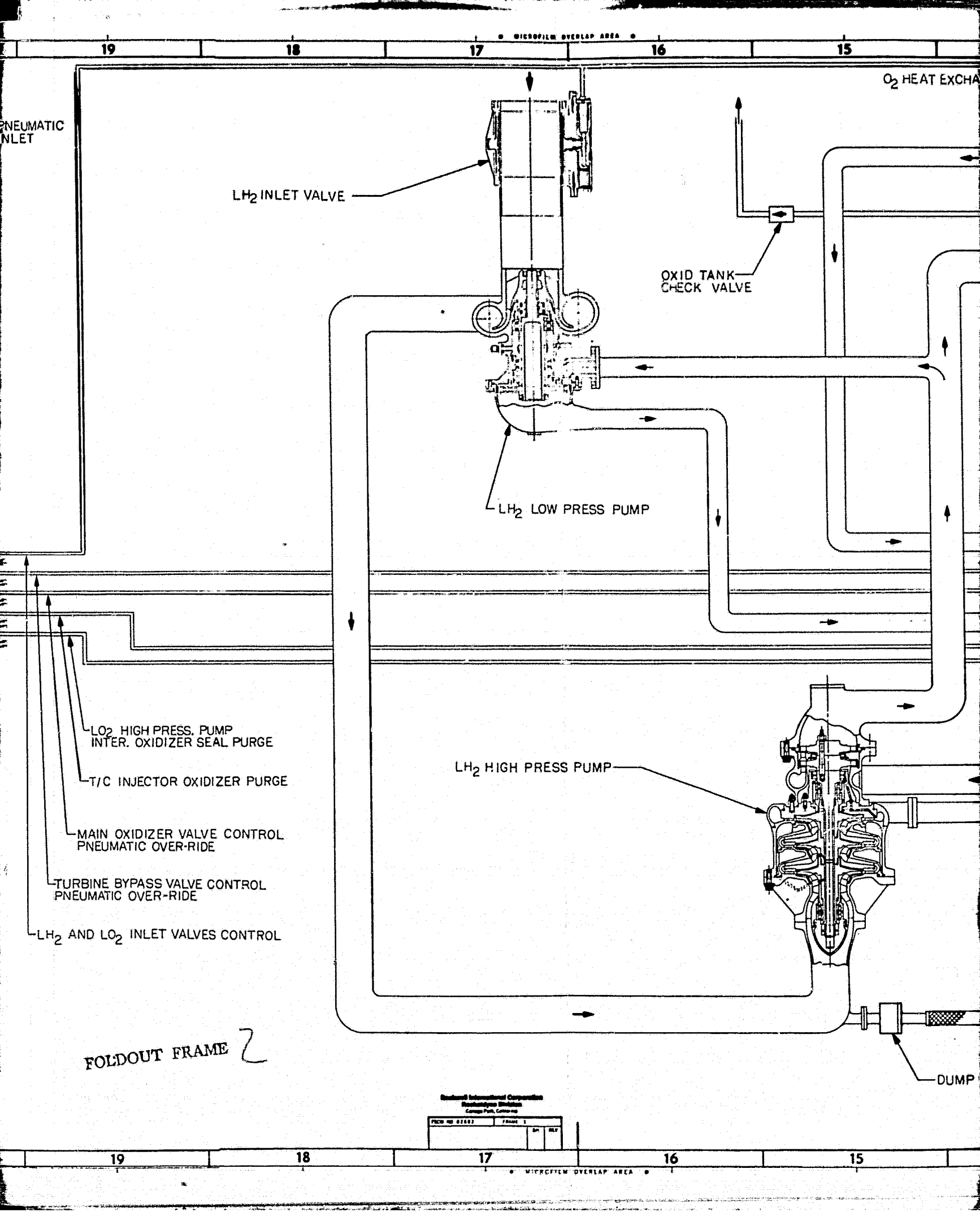

FOLDOUT FRAME 2

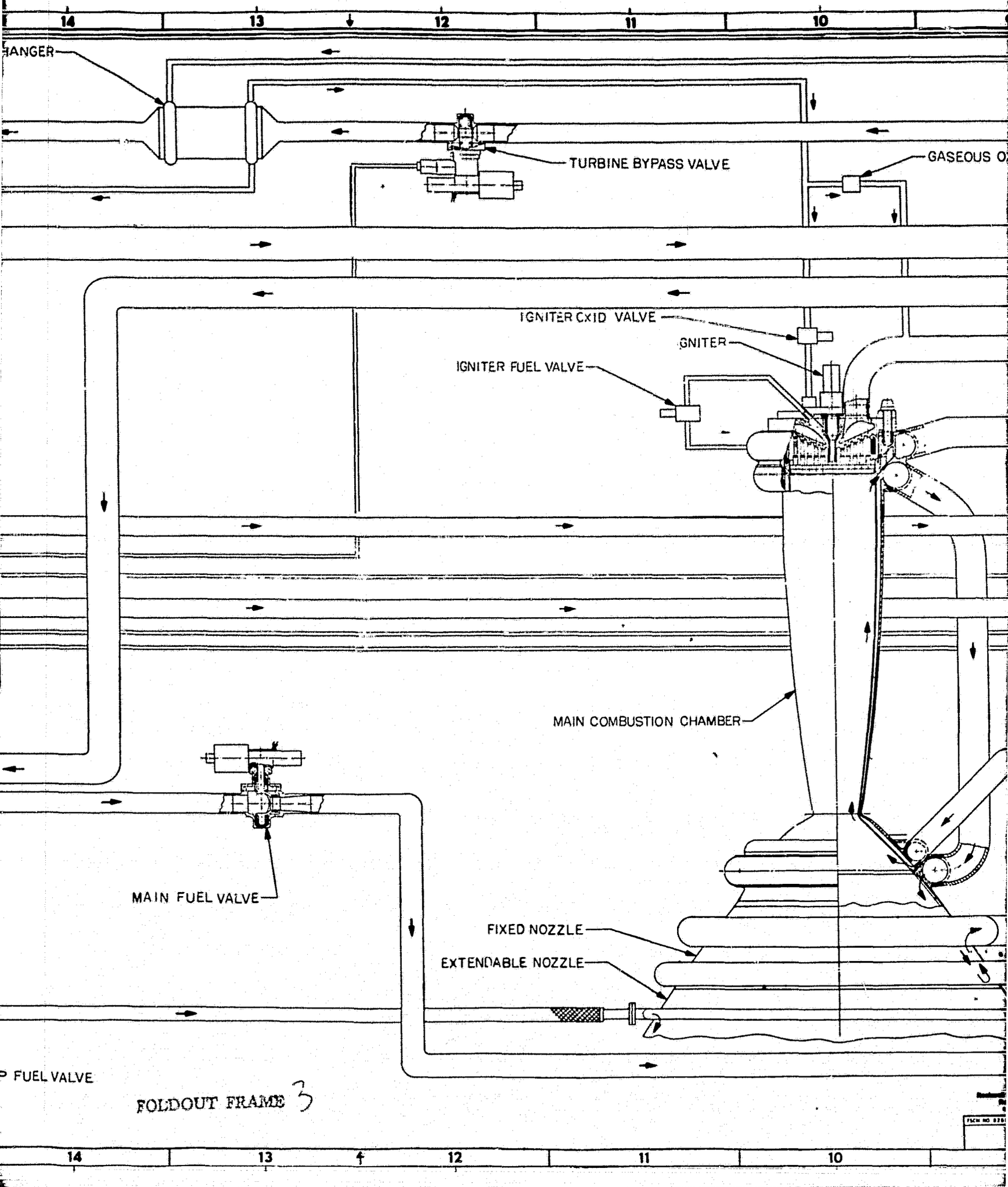

FOLDOUT FRAME 3

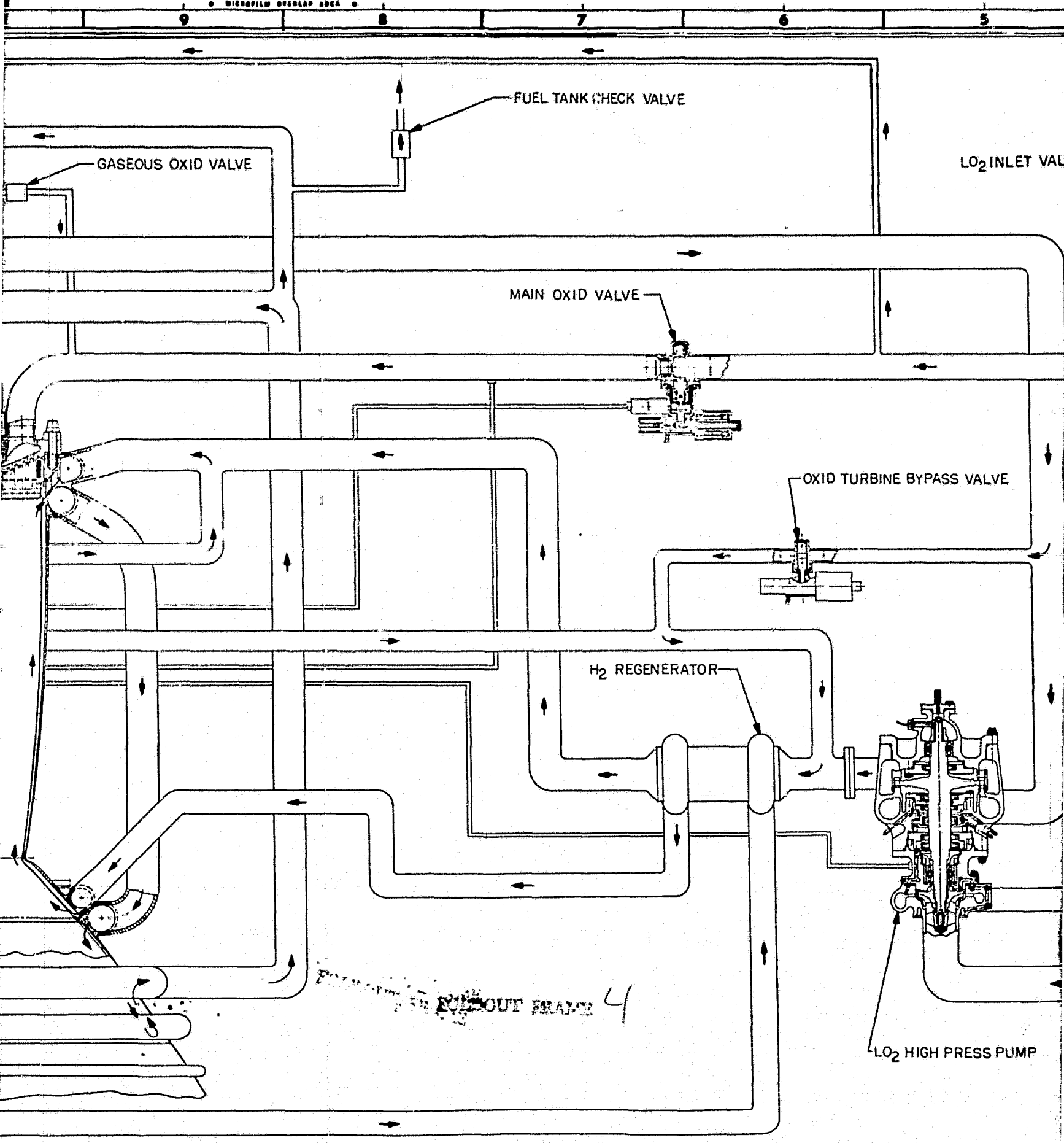

MICROFILM OVERLAP AREA
9
8
7
6
5
FUEL TANK CHECK VALVE
GASEOUS OXID VALVE
LO2 INLET VAL
MAIN OXID VALVE
OXID TURBINE BYPASS VALVE
H2 REGENERATOR
LO2 HIGH PRESS PUMP
FOLDOUT FRAME 4
Rockwell International Corporation
Rocketdyne Division
Canoga Park, California
FSCM NO 02652
FRAME 5
SH
REV

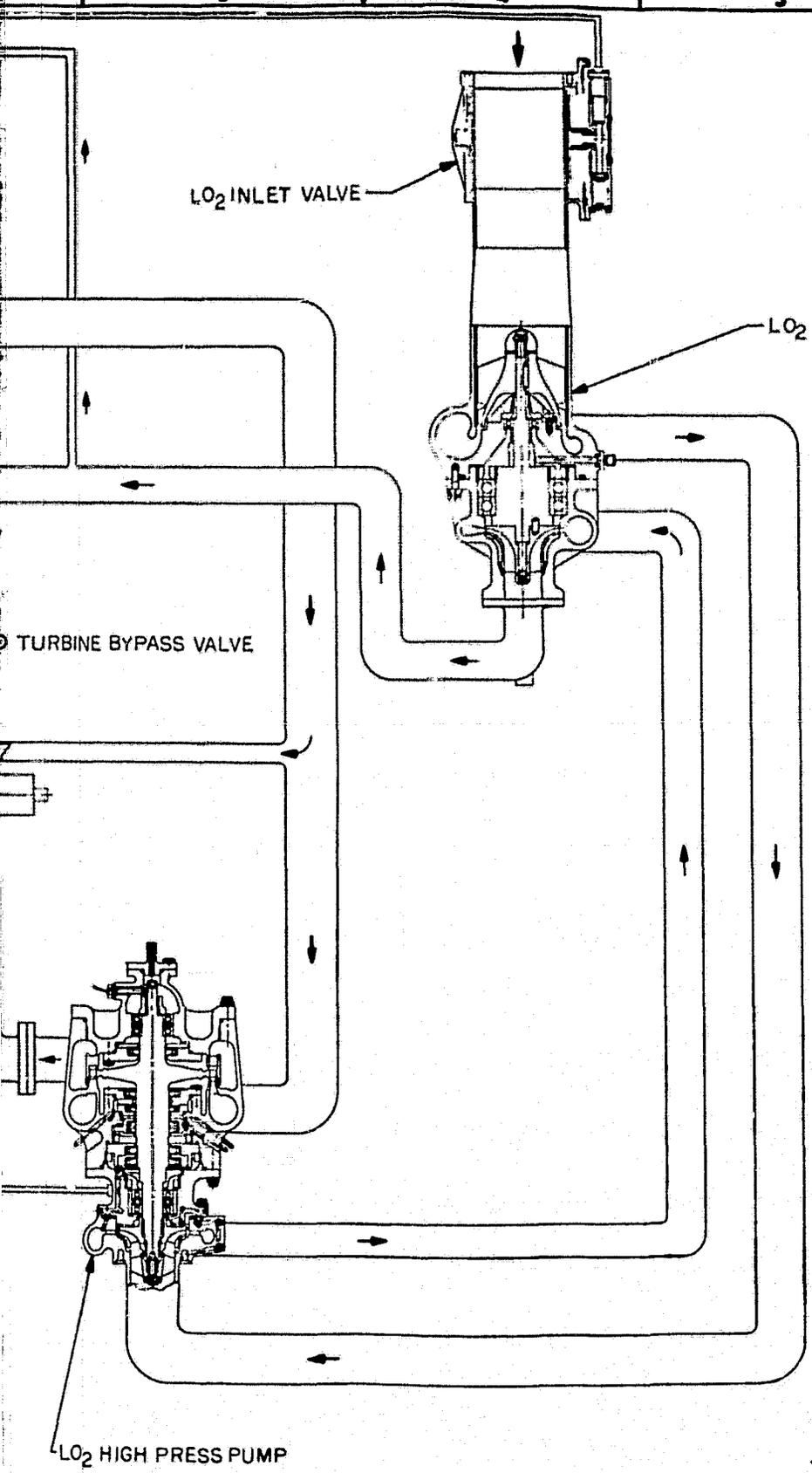

ROLLOUT FRAME 5

Figure 4-2

THIS PRINT REDUCED
THIS IS NOT A RELEASED COPY

SCHEMATIC-EXPANDER CYCLE SYSTEM (OTV)

J 02602 7RC014395

The control of the engine and its operating modes during start, mainstage and shutdown account for approximately 11 percent of the functions required of the engine controller and control system. Other major function categories comprise the following percentages of the total function; Checkout and Status Monitoring 34 percent, Input/Output Data Processing 21 percent, and Protection of Engine and Man-Rated Capability 34 percent.

Checkout and status monitoring includes those functions starting during engine preparation for flight and continuing during engine operation. They ascertain the viability of each component to operate and to continue operating during the flight. The input/output data processing includes all those listed functions for engine maintenance and performance evaluation, the processing of commands and monitoring of status, failures and initial conditions. The protection of engine and manrated capability group includes all the functions concerned with safe and reliable operation of the engine. It is believed that all of these functions must be present in the Advanced Expander Cycle Engine Point Design Control system to provide the reliability required of this reusable engine as used in the OTV manned missions. The man rating and safety requirements for the OTV cannot be met without the engine control, engine health monitoring and checkout provided by the controller.

Power for valve and actuation and controller operation was assumed to be directly available from the stage as direct DC to controller, actuators, solenoids and ignitors.

Electronic system redundancy is being addressed by a system approach using multi-level redundancy. Specifically, the electronic system chosen is illustrated in Fig. 4-3 and is a dual-dual redundant cross -strapped system. This system provides more redundancy for components that are more subject to failure and less redundancy to more reliable components.

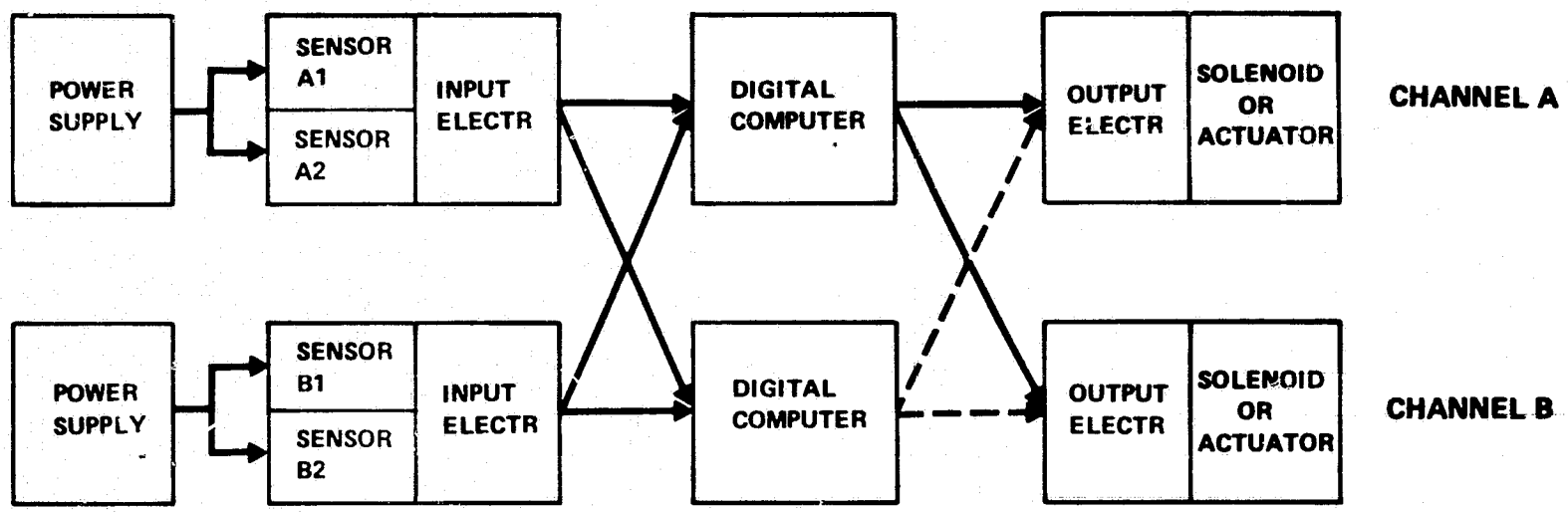

PRO

- GREATEST CHANCE OF MISSION SUCCESS
- STRENGTHENS WEAKEST LINK
- SOME EXPERIENCE ON SSME

CON

- NOT FO/FO/FS AT ALL LEVELS

Figure 4-3. Dual-Dual Redundant Cross-Strapped System (Recommended System for OTV Engine)

Design of the primary valves is based on rotary valve element configurations utilizing common electric actuator designs. Four of these valves are shown in Fig. 4-4 . Electrical fail operational function in the actuator is provided by dual electric motors and coils in the linear variable differential transformer position transducer. Fail safe engine shutdown is provided by pneumatic override pistons in the MOV and TBV actuated from separate three solenoid valves. The MOV and MFV employ a common design rotary sector ball valve closure with positive shutoff seat seal. The TBV and OTBV utilize a more simple rotary plug configuration without tight shutoff seal requirements.

Engine inlet shutoff valves (FIV and OIV) are required to isolate propellants from turbopump seals before and after firing. These two valves are similar in design to the MOV valve and provide straight through line diameters equal to pump inlet diameters to minimize pressure drop and flow disturbances upstream of pumps. The design layouts presented in the Valve Section shows a light-weight ball valve with shaft and seat seals identical with the MOV.

Secondary valves include the gaseous oxidizer valve (GOX), the dump coolant valve (DCV), the two igniter propellant valves and the two tank pressurization valves. Design details of these valves are discussed in the Valves Section.

To enable control of thrust and mixture ratio level during mainstage and start, a simple three-valve closed-loop control system has been defined. The control points selected have capability to fully control the engine thrust and mixture ratio over the full range of required engine operating conditions. The control modulates the areas of the main oxidizer valve (MOV), the turbine bypass valve (TBV), and the oxidizer turbine bypass valve (OTBV) to achieve independently the proper balance of propellant flows for independent control of thrust and mixture ratio. The main fuel valve (MFV), the fuel inlet valve (FIV), and the oxidizer inlet valve (OIV) are designed as on-off valves requiring no modulation.

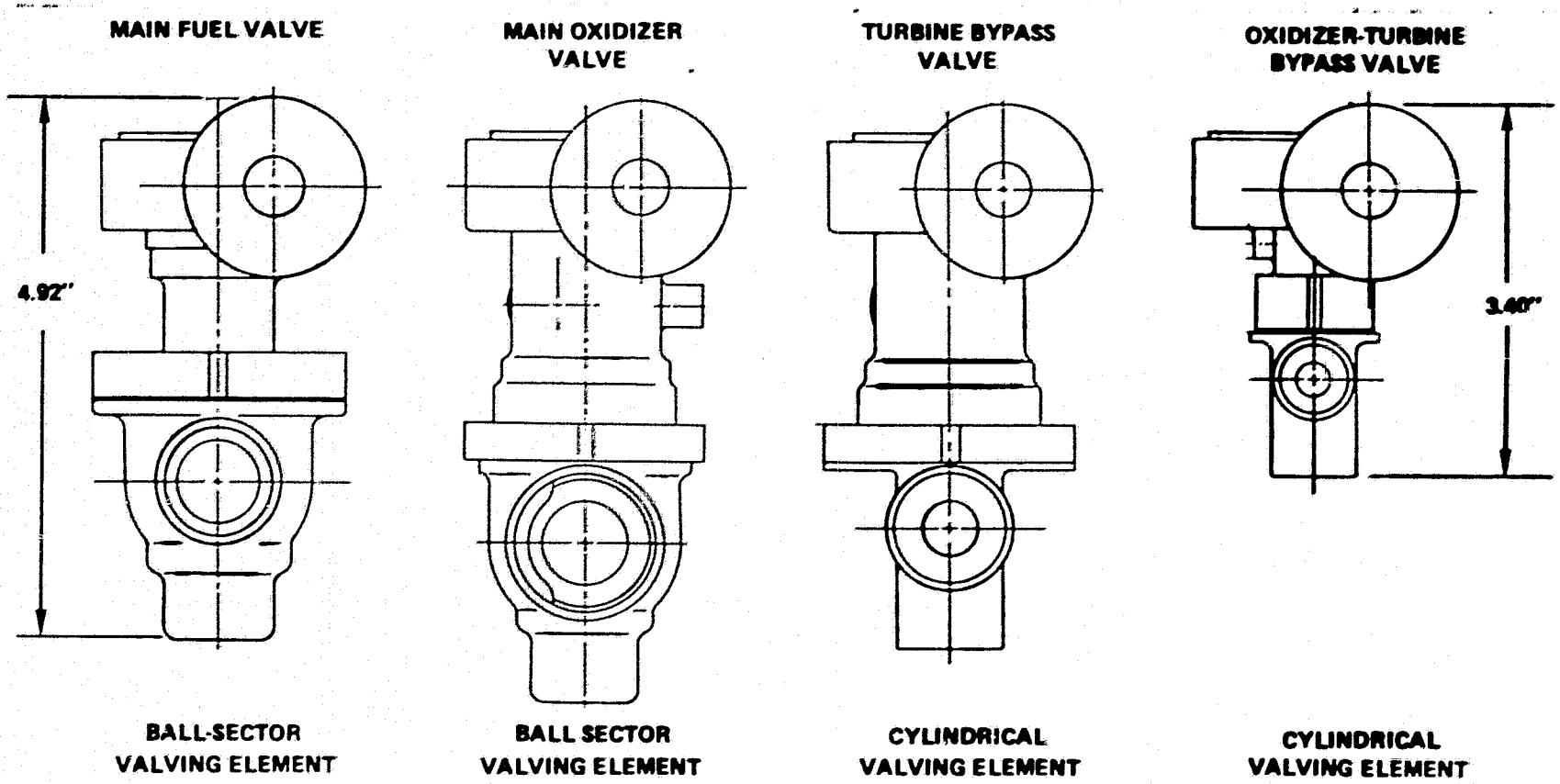

COMMON VALVE CHARACTERISTICS

VALVE ELEMENT MOVEMENT	ROTARY
VALVE ACTUATOR	ELECTRIC MOTOR
FAIL OPERATIONAL	DUAL MOTORS
FAIL SAFE	PNEUMATIC OVERRIDE

Figure 4-4. Primary Valves, Advanced Expander Cycle Engine Point-Design

In mainstage, closed loop thrust and mixture ratio control are exercised as required by the system controller and vehicle commands. The three modulated valves depicted on the schematic in Fig. 4-1 are used for control of thrust during start transients and mainstage, and for control of mixture ratio between 6:1 and 7:1. Thrust control is more sensitive to modulation of the turbine's bypass valve located in parallel arrangement with the two main turbines. Mixture ratio control is more sensitive to the main oxidizer valve situated in the liquid oxygen line downstream of the main oxidizer pump. An oxidizer turbine bypass valve increases the sensitivity of the thrust control valve during mixture ratio extremes. It performs this function by varying the flow-split between oxidizer and fuel turbines. It also extends the mixture ratio control range of the main oxidizer valve at low thrusts and allows control of mixture ratio to the levels required for stable engine operation in pump-idle mode.

CONTROL POINT SELECTION

Control point selection was based on a combination of required control points, a sensitivity analysis, simplicity, minimum weight and stability. Two valves, the MOV and MFV are required for start and shutdown to secure propellants. Two other valves, the inlet fuel valve (IFV) and inlet oxidizer valve (IOV) are required for long term coast and redundant propellant isolation. The next issue is then to determine the need for more than on-off valves for start.

An evaluation was made on thrust and mixture ratio variations that could be expected in-run and run-to-run over the life of a reusable engine. The data obtained was taken from space shuttle main engine test data. The SSME is a controlled engine, but by determining the valve position variations required to obtain constant thrust and MR and using influence coefficients relating the valve position to thrust and MR, the thrust and MR variations could be estimated. The results, as presented in Table 4-2 indicate that in-run variation of 7% on thrust and 0.3 units on MR could be expected, and that for combined in-run and run-to-run, variations of 20% in thrust and 0.8 units of MR could be expected. These variations result from factors such as thermal variations with time, component wear and/or damage, and component replacement. For

Engine Control Concept	In-Run & Run-To-Run		In-Run	
	Thrust Variation	MR Variation	Thrust Variation	MR Variation
A	20%	0.8 Units	7%	0.3 Units
B	20%	0.8 Units	7%	0.3 Units
C	2%	0.1 Units	2%	0.1 Units
D	2%	0.1 Units	2%	0.1 Units

Table 4-2. Expander Cycle Performance

space propulsion applications such as contemplated for the OTV, thrust variations of ±5% and MR variations of ±2% were assumed. To meet the above requirement some type of thrust and MR sensing and control or trim is required. To control two variables, at least two control points are required. Because the MFV and MOV are already required for start and shutdown, these become the first candidates. A control valve, as such, requires that adequate pressure loss be designed into the valve; pressure drop in the MFV is undesirable from an engine efficiency viewpoint. Other valves considered were the turbines bypass valve (TBV) and the oxidizer turbine by-pass valve (OTBV). By controlling the flow to both turbines the TBV can control thrust effectively, while the OTBV can control mixture ratio by varying the power of the oxidizer turbine. The inlet line valves cannot be used for control purposes without causing pump cavitation; they were thus rejected as control points other than for on-off.

A sensitivity study was made for each of the valves and is presented in Figure 4-5 From that data the TBV is the most desirable for thrust control and the MOV or OTBV would provide good MR control. Requirements that the MOV be able to have position control during start results in choosing the MOV. The OTBV is still required to achieve powered idle mode and maintain reasonable oxidizer pump speeds. The OTBV need only have two positions and need not seal.

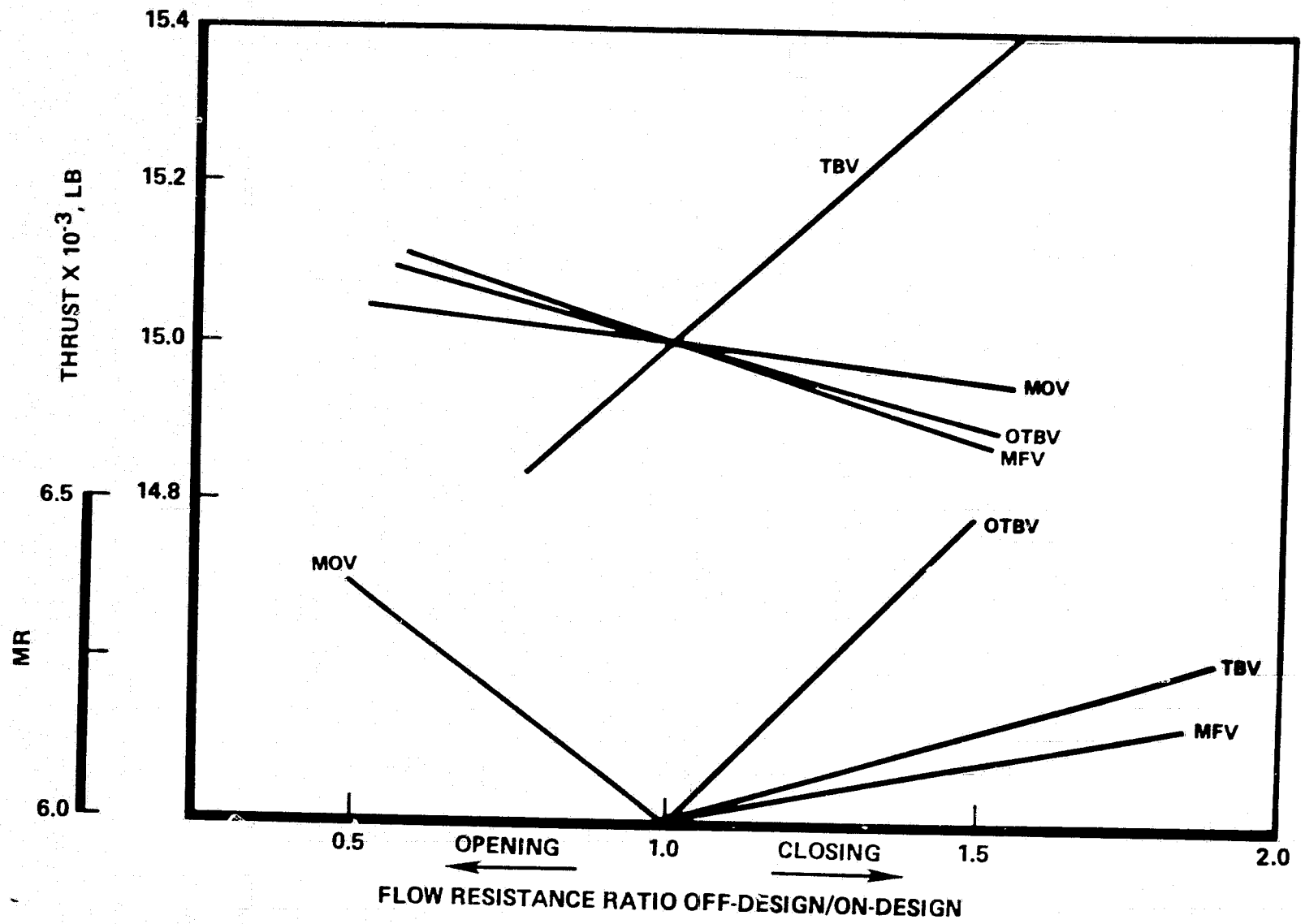

Figure 4-5. Effect on Thrust and Mixture Ratio of Varying Individual Valve Flow Areas

The remaining issue is the location of the MFV. Locating the MFV upstream of the thrust chamber regen cooling results in a smaller valve and adds stability to pump flow during idle mode. Locating the MFV downstream of the T/C cooling jacket and the TBV branch point would result in not needing a positive break on the turbopumps during tank head idle mode, but would require a larger MFV (no longer common with the MOV) and would require that the TBV have a positive seal. As a baseline the MFV upstream position was selected but the impact of the turbopump break design may cause that decision to change.

CLOSED LOOP CONTROL

The thrust and mixture ratio levels are variable upon vehicle command. The control is required to maintain engine thrust and mixture ratio, within anticipated values of ±5 percent and ±2 percent, respectively of the commanded mainstage values. This type of precision is similar to Centaur upper stage engine thrust and mixture ratio precision requirements of ±2 percent. These can be relaxed somewhat for the OTV, especially on the thrust requirement. Space Shuttle Main Engine (SSME) precision requirements are ±1.25 percent in thrust and ±2 percent in mixture ratio. A closed-loop control is required for this type of precision. As determined from SSME test data, much wider variation would be incurred if the engine is not closed-loop controlled. Large variations in mixture ratio during startup and mainstage would be detrimental to both engine performance and engine life. A sequencing type control (which is an open -loop control) does not have the precision to control variable thrust and mixture ratio without greatly relaxed precision.

Start and Shutdown

An additional issue is how the engine start and shutdown will be accomplished. Start and shutdown impose extreme operating conditions on the engine and maintaining proper relationships of pressures and temperature can be extremely important for reliability and long life of a system. Positioning and controlling the engine system valves properly can only realistically be accomplished

with an electronic controller. Some 30 valves on the engine must be sequenced to open or close at the proper times during start, mainstage and shutdown. Actuator requirements, as defined in Table 4-3, result in actuator types for engine control that cannot be purely open loop positioned; some type of position control must be employed to ramp the valves slowly, repeatable, and reliably and still have the capability to adapt as new requirements are generated or system limits or problems are encountered. The above is summarized on Table 4-4. Thus, start and shutdown requirements not only define an electronic sequence controller, but a valve position control and valve position reference command capability. Even though requiring sequence and valve position control, no closed loop operation appears to be required for start and shutdown. The implementation of valve position control allows for closed loop engine control to be implemented during any phase of engine operation where closed loop control may be required, such as for MR control during mainstage.

Controller Selection

The extent of control for an OTV engine has been strongly debated. One one extreme are the views that the engine have a simplified configuration with minimum controls and therefore fewer components for maximum reliability; on the other extreme is the concept of a highly automated engine with electronic monitors and controls to reduce failure modes and thus achieve high reliability. These two extremes in control concepts and two other variations between them are outlined in Table 4-4.

An evaluation was made of system performance, operation, reliability, and program costs and schedule impacts of the four control system concepts, Table 4-4.

The following basic conclusions resulted from the evaluation. A certain degree of closed loop control is required to maintain thrust and mixture ratio accuracy. An electronic control is the best method of achieving that control, whether the control is a trim or full authority control. Engine checkout and status monitoring cannot be eliminated but could be accomplished by ground or space operations. Remote sensing would undoubtedly be more complicated and expensive.

TABLE 4-3. ACTUATOR REQUIREMENTS

ENGINE CONTROL CONCEPT	VALVE	POSITIONING REQUIREMENTS SLEWRATE - PRECISION		
		START	CUTOFF	MAINSTAGE
A	MFV	Ramp between stops 75%/SEC±25%/SEC	Same as Start	Full Open
	MOV	20%/SEC±5%/SEC,±2 1/2% 2 intermediate positions	50%/SEC±10%/SEC ramp closed	± 1/2%
	TURB BYPASS	40%/SEC±10%/SEC,±2 1/2% 2 intermediate positions	No Req'mt	± 1/2%
	OXID TURB BYPASS	60%/SEC±40%/SEC,±2 1/2% 1 position besides open	No Req'mt	± 1/2%
B	(SAME AS "A" ENGINE FOR ALL REQUIREMENTS)			
C	MFV	START AND CUTOFF		Full Open
	MOV	HAVE SAME		0.5% resolution
	TURB BYPASS	REQUIREMENTS AS "A"		0.5% resolution
	OXID TURB BYPASS			0.5% resolution
D	MFV	(SAME AS "A" ABOVE)		Full Open
	MOV	50%/SEC with 0.5% Resolution		0.5% resolution
	TURB BYPASS	50%/SEC with 0.5% Resolution		0.5% resolution
	OXID TURB BYPASS	50%/SEC with 0.5% Resolution		0.5% resolution

Table 4-4. OTV Expander Cycle Start and Shutdown Controller Requirements

Engine Control Concept	Operational Changes	Test Variations
A	Changes Require Mechanical Parts to be Redesigned	Test-to-Test Variations Must be Accepted or Complex Mechanical Compensation Systems Designed and Developed
B	Sequence Times Can Be Programmed. Opening Rates or Area Changes of Control Points Require Mechanical Part Redesign	Test-to-Test Variations Must be Accepted or Complex Mechanical Compensation Systems Designed and Developed
C	Sequence Times Can be Programmed. Opening Rates or Area Changes of Control Points Require Mechanical Part Redesign	Test-to-Test Variations Must be Accepted or Complex Mechanical Compensation Systems Designed and Developed
D	Capable of Adapting to Large Class of Required Changes by Changes to Software	Control Can be Used to Absorbe Variations

Data monitoring during operation must be performed for maintenance trend evaluation and redline monitoring. The operation could be cabled directly to vehicle controller but cable weights are significant, complexity is just passed on to the vehicle, and this results in greatly restricted flexibility and growth potential. In general, the functions above must be performed and a programmable digital controller is the best approach. Table 4-6 defines the OTV controller compared to an SSME. Table 4-5 shows how the various functions of the controller could be shared.

Any alternate to an integrated digital controller will end up with a patchwork design with low reliability, low performance, low growth potential, and high operational and maintenance cost. Included in Table 4-6 is a comparison of controller requirements for the range of control approaches. The conclusion is that a digital controller is the most cost effective engine controls option and offers the only viable approach to achieving non-rated capability.

To clarify the differences between control concepts, schematics of those control concepts are presented in Figures 4-7 and 4-8. Figure 4-7 is a closed loop control for mainstage using trim; all primary valves for start and shutdown would be scheduled open loop. Any changes to valve opening characteristics would require hardware changes to the valve actuator assembly. Figure 4-8 shows a position feedback control on the valve actuator. The valve position command is issued from the controller. The valve positioning is relatively repeatable and reliable, but most importantly, can be modified as needed to support engine or stage development needs, or to adopt a new engine or stage requirement. Most changes in valve scheduling are merely a software change. As can also be seen in Figure 4-8, implementing full closed loop control can be accomplished whenever needed for convenience of engine operation.

REDUNDANCY

The redundancy study evaluated the basic philosophy of redundancy and then evaluated four basic configurations of redundancy for the electronic system: (a)dual

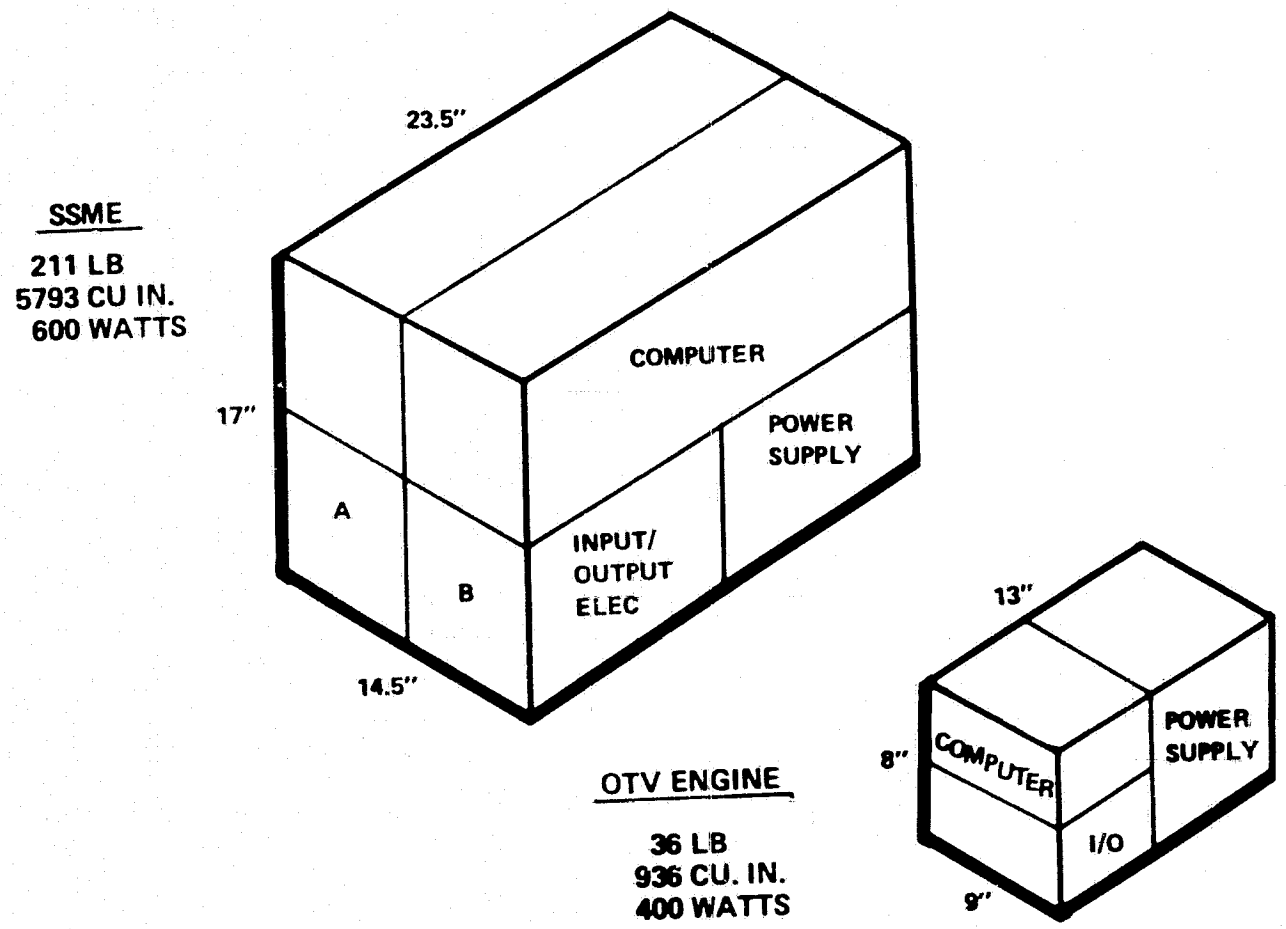

Figure 4-6. Controller Comparisons

Table 4-5. Controller Functions for Manned OTV

Control of Engine and Operating Modes (11%)

- Valve Sequencing and Control
- Closed-Loop Pc and MR Control
- Purge Sequences and Thermal Conditioning

Checkout and Status Monitoring (34%)

- Automatic Component Checkout
- Flight Readiness Test
- Controller Redundancy Verification

Input/Output Data Processing (21%)

- Data Reporting for Maintenance and Performance
- Vehicle Command Processing
- Status Reporting (Operating Mode)
- Failure Reporting
- Memory Load and Readout

Protection of Engine and Man-Rated Capability (34%)

- Redline Monitoring
- Redundancy Management and Failure Response
- Engine Ready Verification
- Emergency Abort Return
- Pogo Suppression*
- Controller Self-Test

*Requirement Currently Not Defined

Table 4-6. Controller Trade Study Summary

Engine Control Concept	Memory	Power	Weight	Cost/Unit	Dev Cost	Effect On Total Engine Cost
A	55%	110 Watts (100-200)	13 lb	$5M	$10M	$300M
B	89%	180 Watts (150-300)	26 lb	10M	18M	170M
C	95%	200 Watts (150-800)	32 lb	13M	25M	81M
D	100%	400 Watts (200-1000)	36 lb	14M	27M	86M

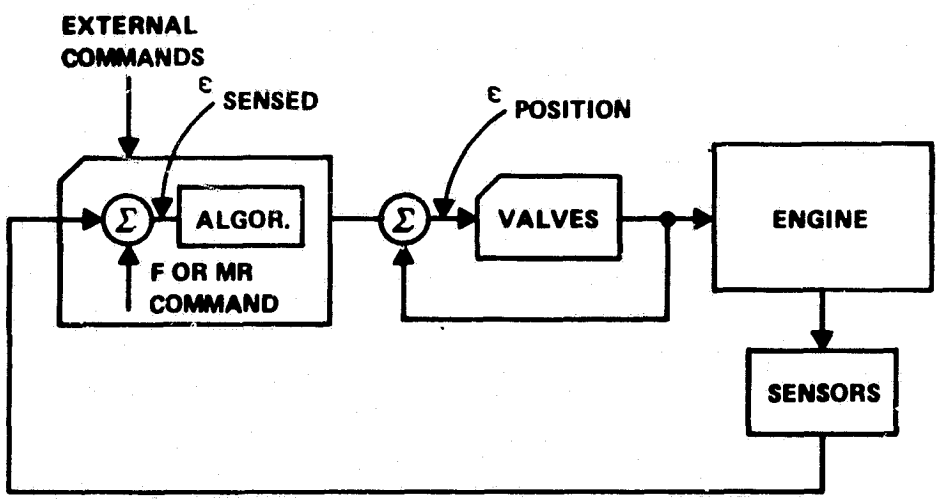

FULL-RANGE CONTROL

- SEQUENCING PROGRAMMABLE
- VALVE RATES PROGRAMMABLE
- CLOSED-LOOP CONTROL DURING MAINSTAGE
- CLOSED-LOOP CONTROL DURING START, SHUTDOWN, OR IDLE MODES IF REQUIRED

Figure 4-7. Valve Position-Feedback Closed-Loop Control System

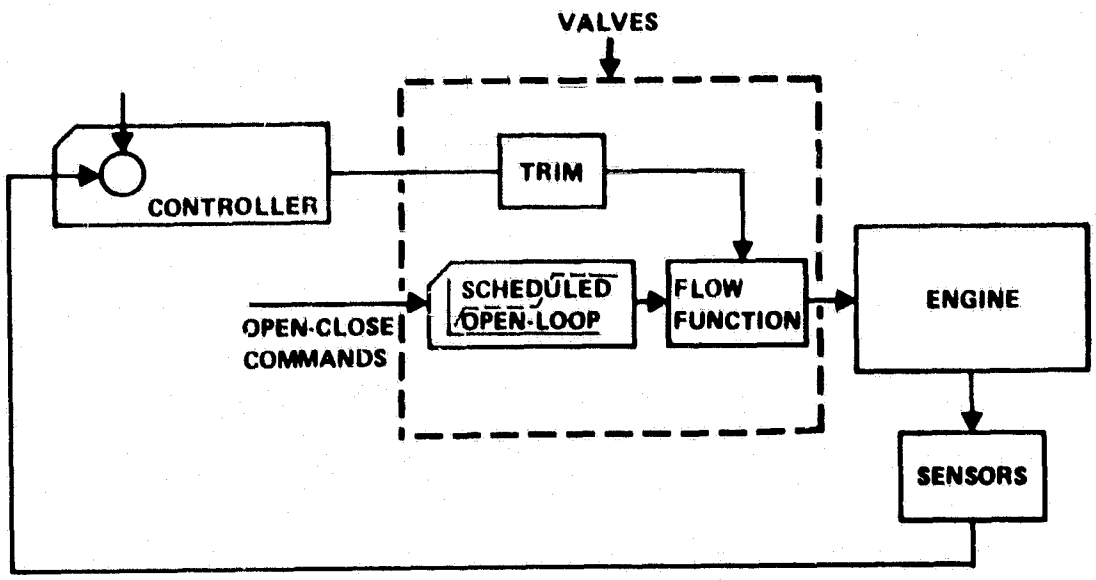

MAINSTAGE-TRIM CONTROL

- CLOSED-LOOP CONTROL DURING MAINSTAGE
- POTENTIALLY LESS COMPLICATED

Figure 4-8. Mainstage-Trim Closed-Loop Control

redundant rail system, (b) dual redundant cross-strapped systems (c) triple redundant cross strapped system and (d) dual-dual cross strapped systems. The four configurations are illustrated in Figures 4-9 through 4-12.

In evaluating the redundancy requirements, the real issue is mission success. To achieve mission success components must be reliable enough to work for the entire duty life, or redundancy must be provided for failed components. In examining the control system components the controller itself is extremely reliable and, in fact, one of the most reliable components on the engine, in spite of having to operate several hours for each hot-fire test. Even with the high level of reliability of the controller, electronics are subject to random failure, thus some kind of redundancy for the controller is still required.

On the other extreme, engine system sensors are expected to experience a relatively high rate of failure due to the severe environments associated with the sensing locations; thus, some type of additional redundancy for critical sensors is required. Reliability data from SSME was used as a guide in performing this evaluation. The dual-dual cross-strapped system was selected as the least complex, most effective approach toward achieving the highest probability of mission success.

POWER DISTRIBUTION

A tradeoff made relative to the controller was performed relative to power distribution and controller options. The power distribution method is relatively independent of other options and is discussed separately.

While controller subsystems such as the computers and input-output electronic can be greatly reduced in size by using the latest microelectronic technology, the power supply is not very amenable to miniaturization. Hence, a power distribution study was conducted to evaluate the power supply options. The distribution configurations evaluated were (a) AC/DC power conditioning by controller,

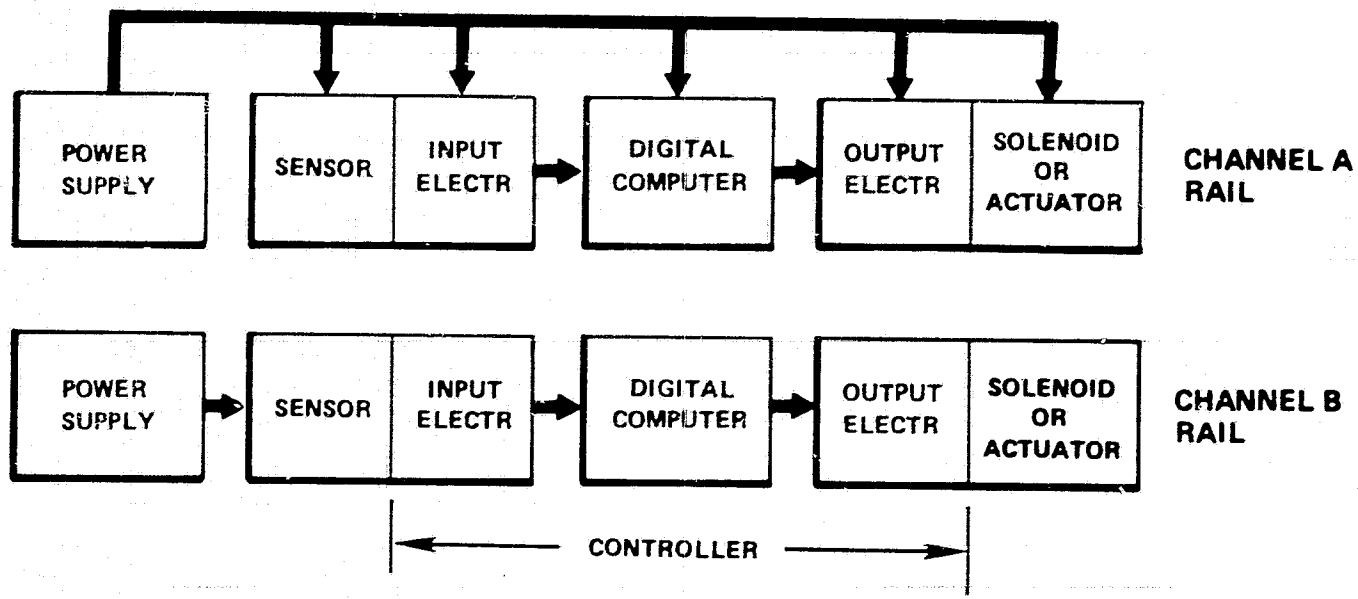

PRO

- SIMPLICITY

CON

- FAILURE IN ONE COMPONENT CAUSES DISQUALIFICATION OF AN ENTIRE CHANNEL
- LOW PROBABILITY OF MISSION SUCCESS

Figure 4-9. Dual Redundant Rail System

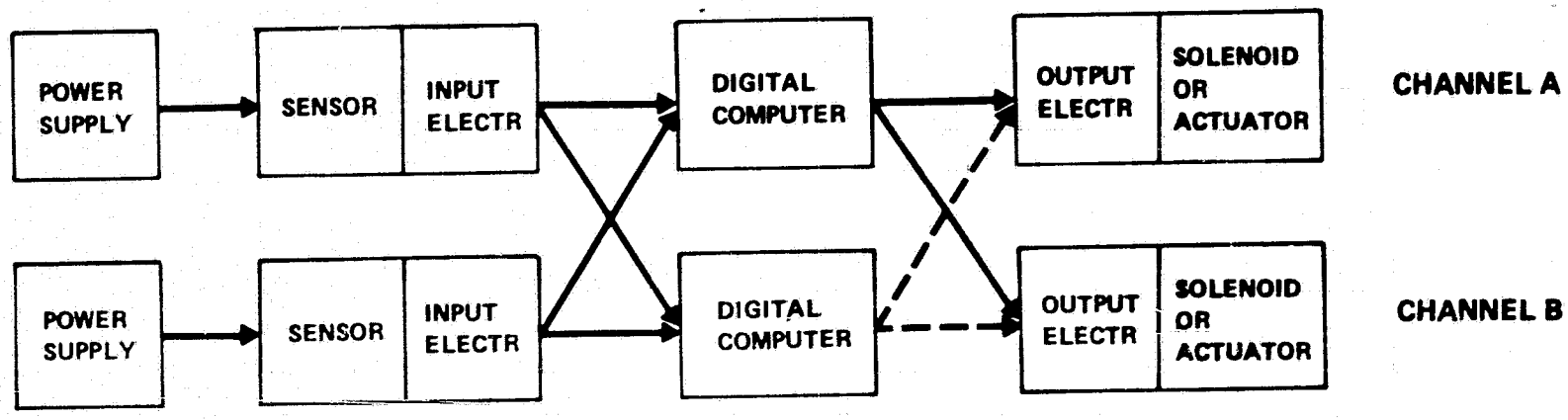

PRO

- GREATER CHANCE OF MISSION SUCCESS THAN RAIL SYSTEM
- EXPERIENCE WITH SSME

CON

- SENSORS WEAKEST LINK

Figure 4-10. Dual Redundant Cross-Strapped System (SSME Configuration)

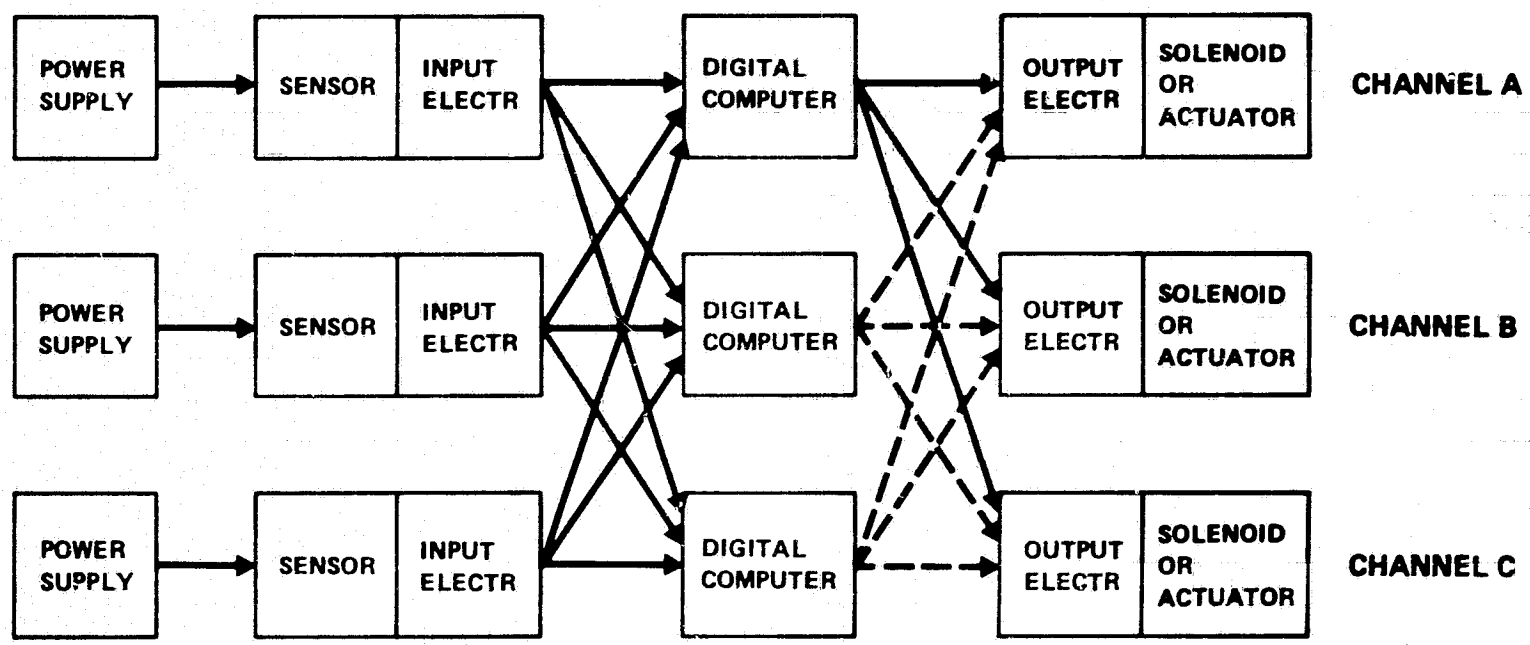

PRO

- GREATER CHANCE OF MISSION SUCCESS THAN DUAL REDUNDANT SYSTEM
- FO/FO/FS AT ALL LEVELS

CON

- REQUIRES THREE POWER SUPPLIES
- COMPLEXITY
- SYNCHRONIZATION PROBLEM
- SENSORS WEAKEST LINK
- HIGH DEVELOPMENT AND PRODUCTION COST

Figure 4-11. Triple Redundant Cross-Strapped System

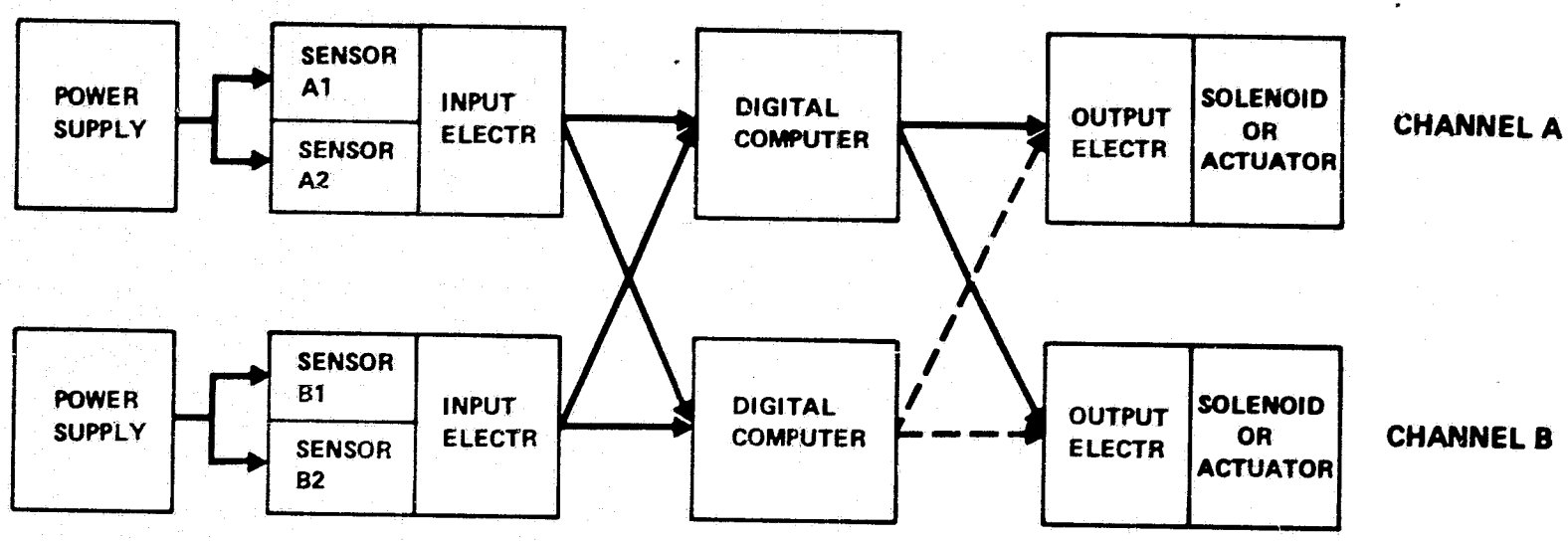

PRO

- GREATEST CHANCE OF MISSION SUCCESS
- STRENGTHENS WEAKEST LINK
- SOME EXPERIENCE ON SSME

CON

- NOT FO/FO/FS AT ALL LEVELS

Figure 4-12. Dual-Dual Redundant Cross-Strapped System (Recommended System for OTV Engine)

(b) direct DC from stage, power conditioned by controller and (c) direct DC to controller, actuators, solenoids and igniters. Configuration (c) requires the smallest power supply and is the recommended option. However, vehicle design factors, such as location of the fuel cells, must be considered before the power distribution question can be resolved.

CONCEPTUAL DESIGNS FOR CONTROL VALVES

Based on the requirements defined in the Control Valve Trade Study, above, conceptual design layouts of four primary engine control valves and one inlet valve have been prepared to support the point design engine. Design concepts are based on requirements established from analysis of engine flow requirements and a trade study of design features (Ref. 4-1). Primary design goals are minimum weight and complexity based on past Rocketdyne engine control valve experience, particularly from SSME and ASE.

Presented herein are layouts for the main oxidizer valve (MOV), main fuel valve (MFV), fuel turbine bypass valve (FTBV), oxidizer turbine bypass valve (OTBV), and inlet valve (common to oxidizer and fuel lines) and schematics for the gaseous oxygen valve and fuel dump valve. Valve specifications are presented in Appendix A.

Design of the four primary control valves (MOV, MFV, TBV and OTBV) is based on a rotary configuration utilizing a common electric actuator. Electrical fail operational function in the actuator is provided by dual electric motors and coils in the linear variable differential transformer (LVDT) position transducer. Fail safe engine shutdown is provided by pneumatic override piston on the MOV and TBV actuated from separate three way solenoid valves.

The MOV and MFV employ a common design sector ball valve closure with positive shutoff seat seal. The turbine valves utilize a more simple rotary plug configuration since tight shutoff is not required. Because of the common features of these four valves a detailed discussion of the MOV is initially presented to cover most essential details. Elemental differences of the MFV and turbine

valves follow, including discussion of the inlet valves and other subsidiary valves.

Main Oxidizer Valve

The MOV (Figure 4-13) must be capable of closed loop modulation control of oxidizer flow during full thrust and commanded position control during idle modes. The valve is sized to provide the minimum required resistance at 80% geometric area ratio. For open loop control during pumped idle, flow resistance variation is held to less than ± 10% for angular position variation of ±0.5 degree rotation. The entire valve, including the actuator, must operate at cryogenic temperatures.

Design of the MOV is based upon proven features developed for the ASE ball valves. The basic ball type rotary closure, continuous contact seat seal, and roller bearing support designs have been retained. There are no metal-to-metal sliding parts in the valve, therefore lubrication is not required. Elements and features of the valve are described as follows.

Valving Element. Significant weight saving has been obtained by minimizing flow torque, thus actuation force, through use of a sector (eyelid) type ball closure. Preliminary analysis indicates the sector design to have less than 1/3 the closing torque of a conventional ball valve of the same size. Other advantages are the simplified flow path and reduced throttle sensitivity afforded by the single orifice.

Minimum friction in the ball suspension is afforded by two roller bearings at the valve ball shaft and a roller thrust bearingto support shaft seal unbalanced area.

Seals. A continuous contact seal of DuPont Vespel polyimide is used which provides simplicity, minimal throttle sleeve overhang and proven throttle capability. This seat seal is unique to Rocketdyne valves and has been demonstrated to be capable of maintaining required leakage. The ASE MOV of similar

FOLDOUT FRAME

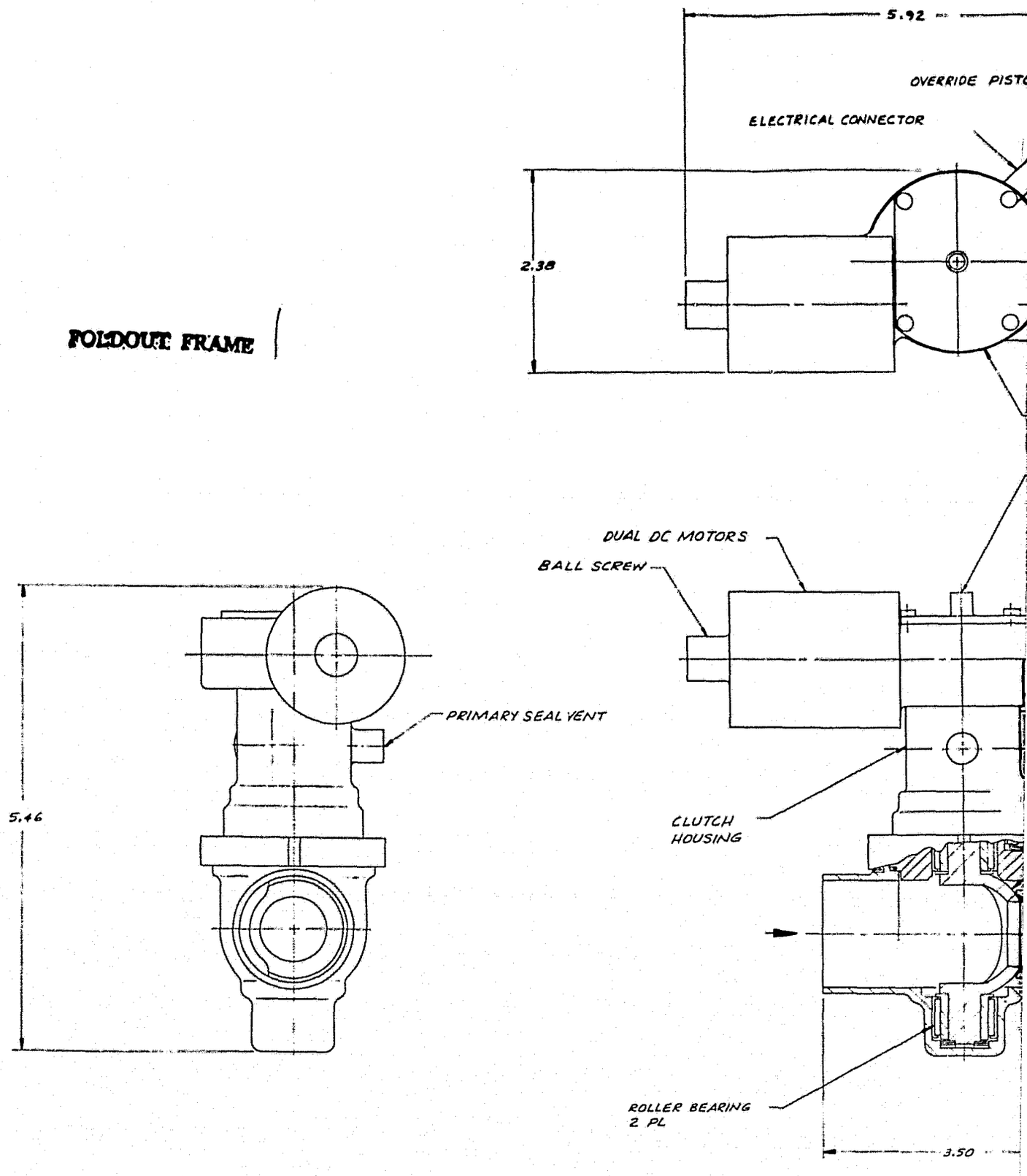

1. DESIGN REQUIREMENTS PER IL

NOTE: UNLESS OTHERWISE SPECIFIED

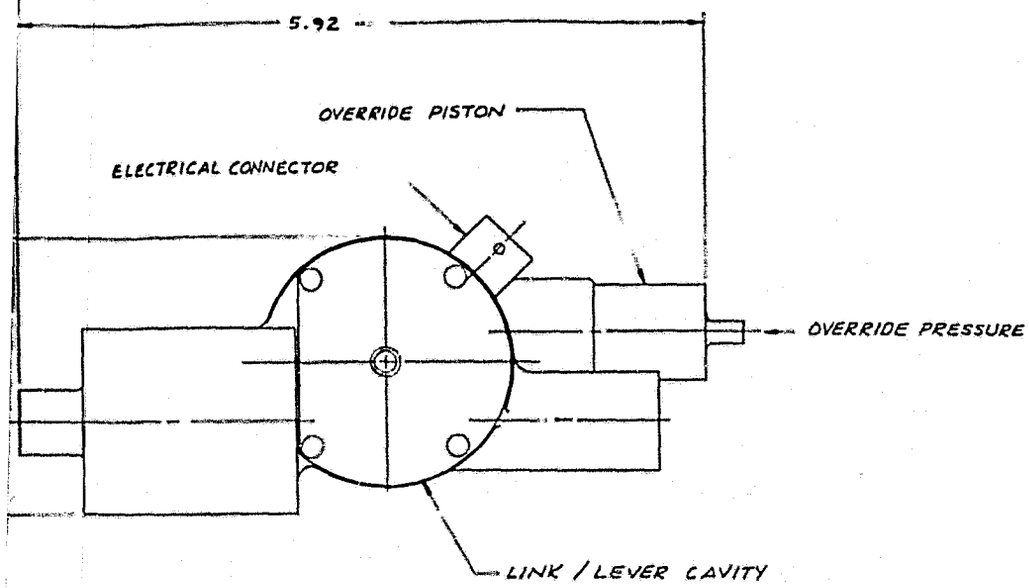

FOLDOUT FRAME 2

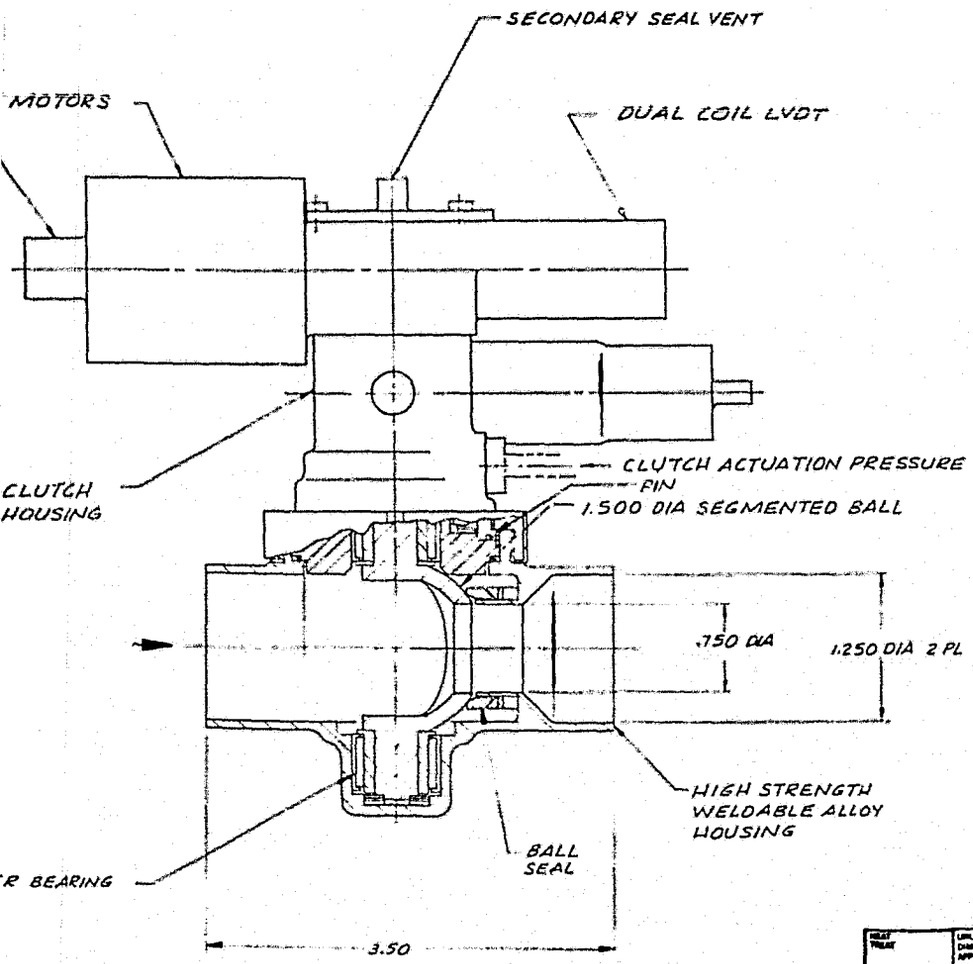

Figure 4-13

THIS IS NOT A RELEASED COPY

1. DESIGN REQUIREMENTS PER IL 141-42-8242, ITEM 1.

Rockwell International Corporation
Rocketdyne Division
Canoga Park, California

MAIN OXIDIZER VALVE-OTV

SIZE E | FSCM NO 02602 | DWG NO 7R0014583 | SCALE 2/1 | SHEET

size has sustained 33 open-close cycles of operation at pressure drop exceeding 4000 psid with liquid oxygen.

Piston seals and redundant dynamic shaft seals are triangular type of Vespel polyimide similar to the seat seal. SSME and ASE experience has demonstrated cryogenic leakage less than 10 scim helium at pressures from 0 to 8000 psid.

Static seals are the miniature K-type metal seal coated with Teflon. Leakage less than 1.0 scim helium can be achieved with these seals with adequate finish on mating surfaces.

Housing. The valve housing is designed for direct welding into the propellant line. All internal elements are line replaceable by removal of one cap nut which allows intact removal of the actuator followed by the sector ball, bearings and seat seal. The design shown in the layout avoids heavy flanges and thereby assures minimum weight.

Electric Motor Actuator. Two independent rare earth torque motors are mounted onto a ball screw suspended between spring loaded axial contact ball bearings. Linear motion from the ball screw is converted to rotary via a lever-link assembly. Drive to the ball shaft is obtained directly through a serrated clutch and flexure which allows disengagement for pneumatic override fail-safe closure.

Each contacting element in the drive train is wedge-spring-loaded to eliminate all backlash. This includes the ball bearings, ball screw, lever-link pin joints, and clutch. Valve position, thus throttle resistance, can thereby be commanded to within the resolution accuracy of the position indicator. Elasticity between the indicator and ball hole, and flow resistance/position calibration input data are secondary errors.

Fail operable redundancy in the electric drive system is provided by the two independent motors. Each motor is capable of meeting the MOV maximum torque

requirement and slewing the valve full open (or closed) within 1.0 second with less than 100 watts power input. By driving with both motors, normal maximum power demand would be less than 50 watts. Power input to hold 10 inch pounds locking torque is 7.2 watts. Either or both motors can produce double torque for a short period with input of 480 watts each. All mechanical elements in the drive train can accommodate maximum overload torque.

Pneumatic Override Piston and Clutch. For emergency fail safe shutdown, the MOV (and TBV) are equipped with a pneumatic clutch (to disengage the electric actuator) and a pneumatic piston for closure of the valve. Clutch actuation and override piston pressure (600 psig) are initiated by de-energizing a normally open 3-way solenoid valve. The clutch actuation pressure acts over an annular area to drive apart the two halves of the serrated clutch.

A permanent magnet at the retracted end of the override piston restrains the piston against the building override pressure until the clutch has disengaged. When the holding force of the magnet is overcome by pressure acting on the piston area, the piston rod is driven into a shoulder on the ball shaft to fully close the valve. The valve actuator is reactivated by positioning the ball screw to the closed position where actuation pressure is removed and the clutch is again engaged. Interference angles in the teeth of the serrated clutch eliminate backlash in the clutch. A flexure connection between the lower clutch half and the ball shaft eliminate backlash at this interface. Using the actuator to rotate the ball to the full open position returns the override piston to its normal position where the permanent magnet again holds the piston fully retracted during normal operation.

Position Indicator. An LVDT is shown directly off the ball screw shaft. Dual coils provide for electrical redundancy. Non-linearity due to short length and temperature extremes will be compensated within electronic command circuitry. As previously noted, position error is minimized by zero backlash mechanisms. Alternate means of position indication will be considered in a final design, such as absolute optical encoders which provide a precise digital position output.

Material ctuator housing is constructed of aluminum. The electric motors have permanent magnets made of the rare-earth compound, samarium-cobolt ($SmCo_5$), surrounded by copper coil windings. The ball screw, ball bearings and LVDT probe (magnetic) are made of corrosion resistance steel (CRES). The LVDT has dual copper coil windings. The link and lever mechanism of the actuator, clutch, ball shaft and valve body are all constructed of a high strength nickel base alloy. The override piston and clutch housing are made of CRES. There is one teflon washer at the base of the ball shaft and all other washers, screws, springs and thrust bearings are composed of CRES. Static seals are Teflon coated A286 alloy steel and all ball and shaft dynamic seals are made of DuPont Vespel which is compatible with both propellants.

Maintenance. No scheduled maintenance is required throughout the service life of the valve. Should service be required, however, easy access to the valve details is afforded by the threaded collar design feature. This permits the valve assembly to be removed from the engine while leaving the body welded in-line.

Main Fuel Valve

Valving elements of the MFV and MOV are identical (Figure 4-14). Line geometry and sizes differ as the MFV operates full open with requirement for minimum pressure drop. A downstream diffuser is therefore included to provide maximum pressure recovery. The electric actuator on the MFV is identical with the MOV except that the pneumatic override and clutch assemblies are omitted.

Some pressure drop through the MFV is sacrificed to allow common details with the MOV. A rounded inlet and straight-through tube could be provided to reduce pressure drop from a maximum of 25 psid now projected to less than 5.0 psid. However, this minimal saving is not warranted considering added valve complexity.

Turbines Bypass Valve

The TBV (Fig. 4-15) provides a critical throttle function in the engine by

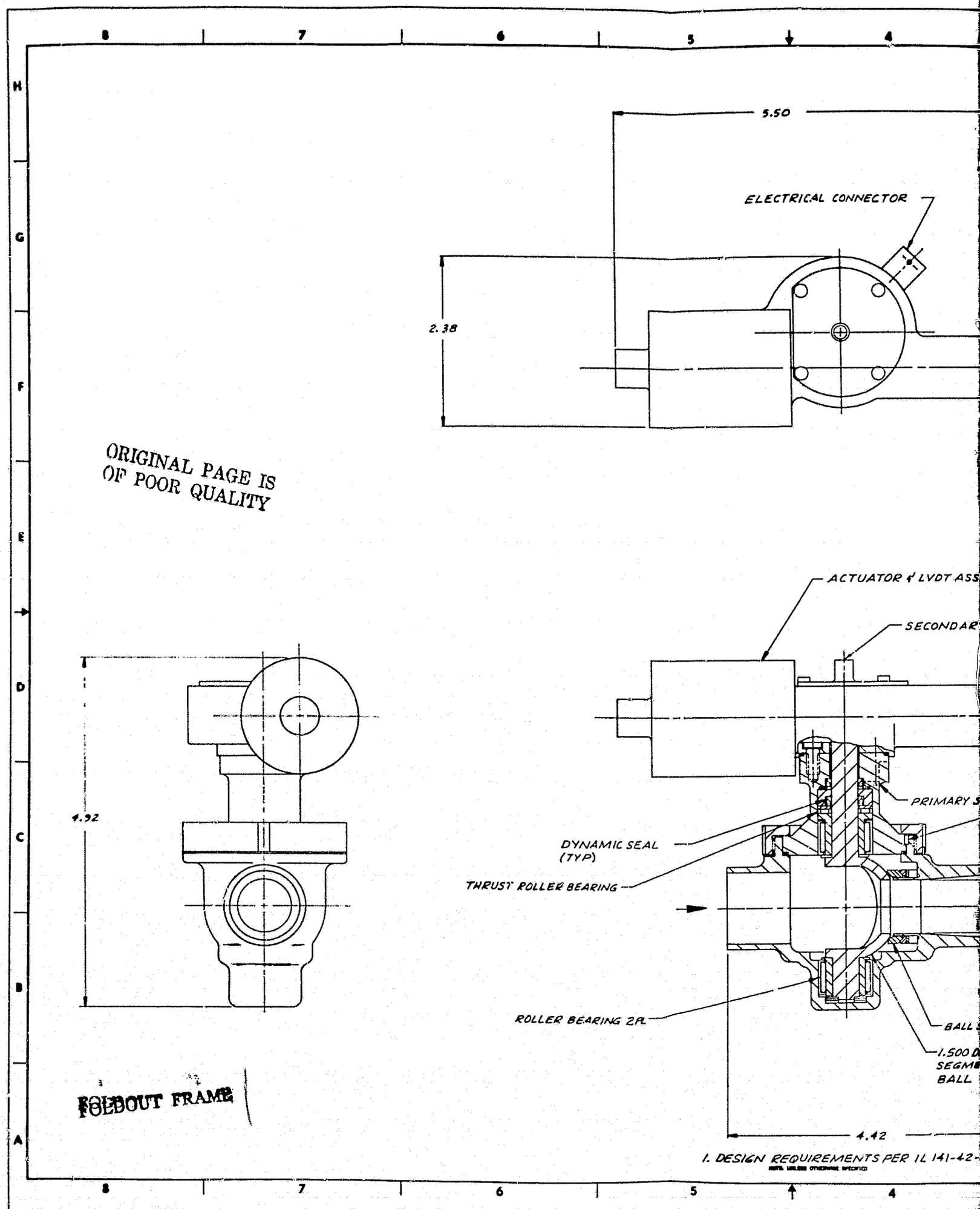

ORIGINAL PAGE IS
OF POOR QUALITY

FOLDOUT FRAME

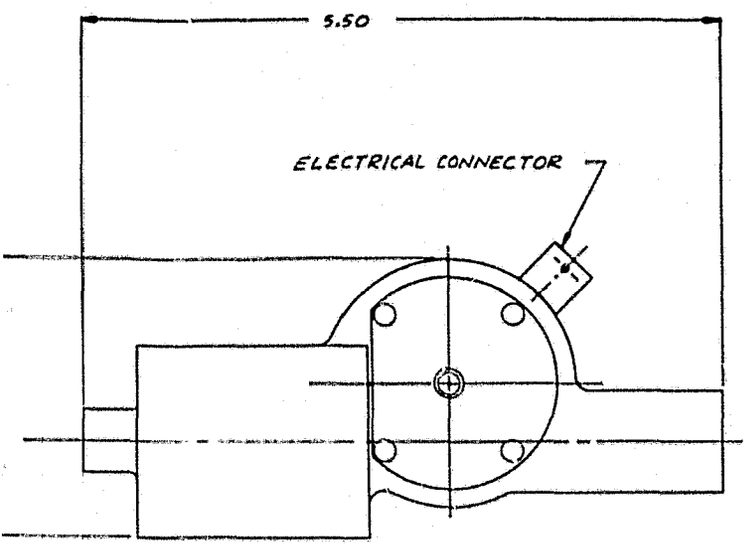

FOLDOUT FRAME 2

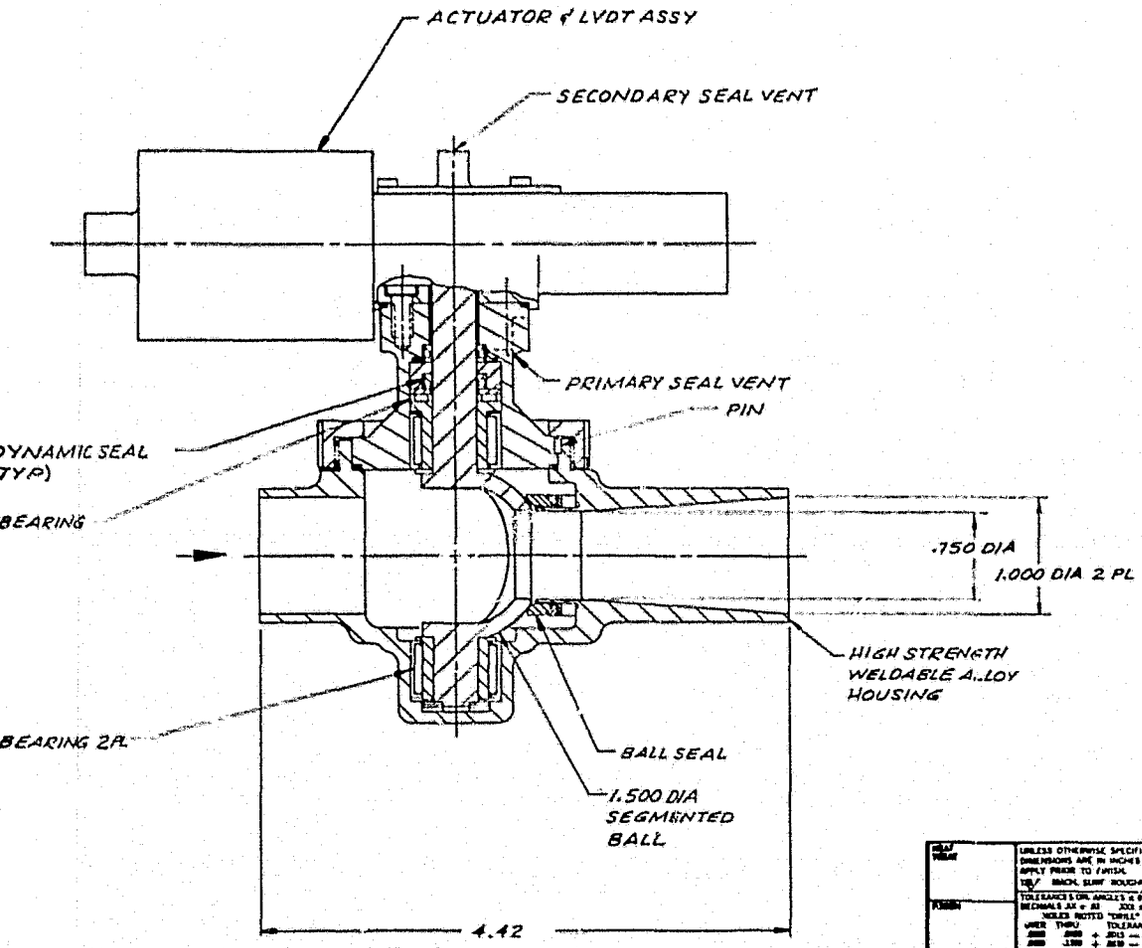

1. DESIGN REQUIREMENTS PER IL 141-42-8242, ITEM 2

Figure 4-14

THIS PRINT IS NOT A RELEASED COPY

Rockwell International Corporation
Rocketdyne Division
Canoga Park, California

MAIN FUEL VALVE-OTV

E 02602 7R0014581

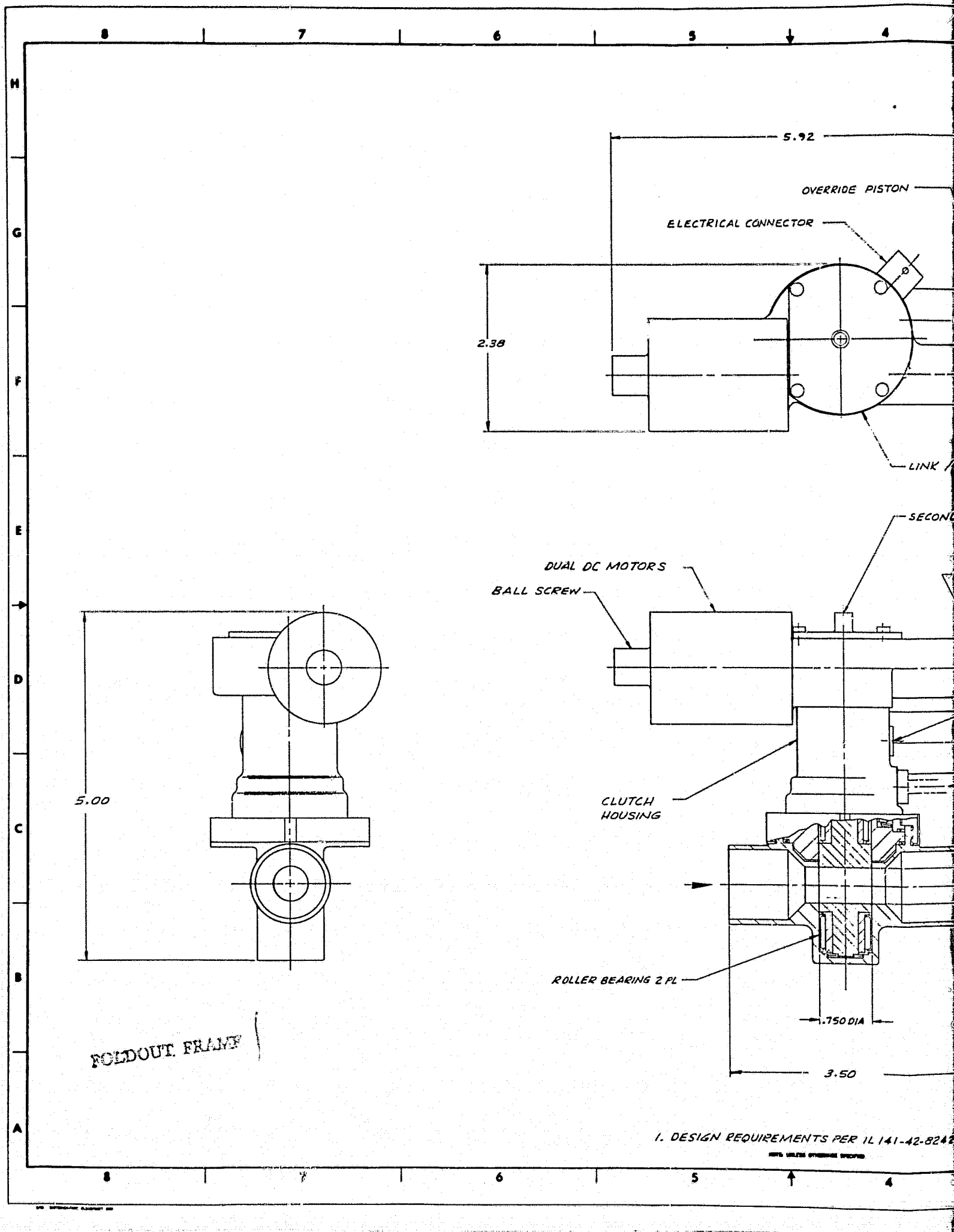
5.92
OVERRIDE PISTON
ELECTRICAL CONNECTOR
2.38
LINK
SECOND
DUAL DC MOTORS
BALL SCREW
5.00
CLUTCH HOUSING
ROLLER BEARING 2 PL
.750 DIA
3.50
FOLDOUT FRAME
1. DESIGN REQUIREMENTS PER IL 141-42-8242

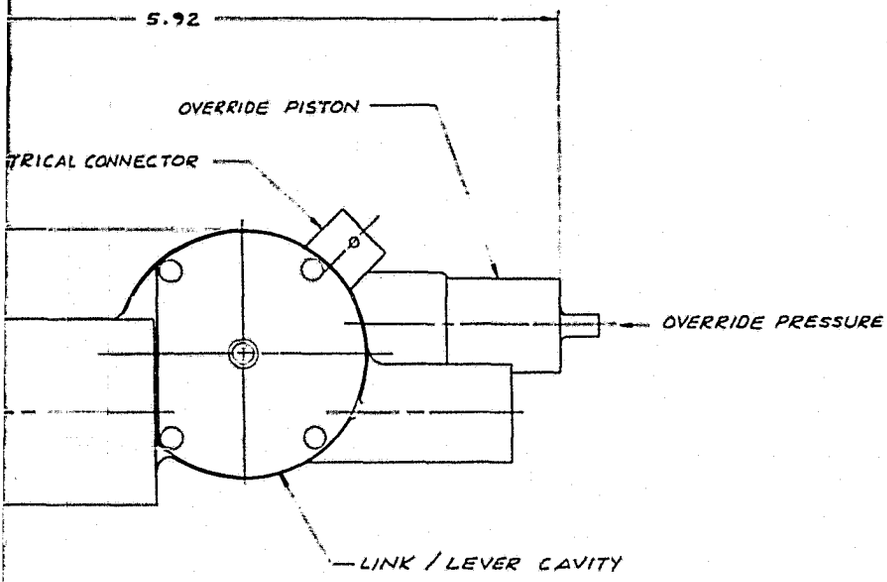

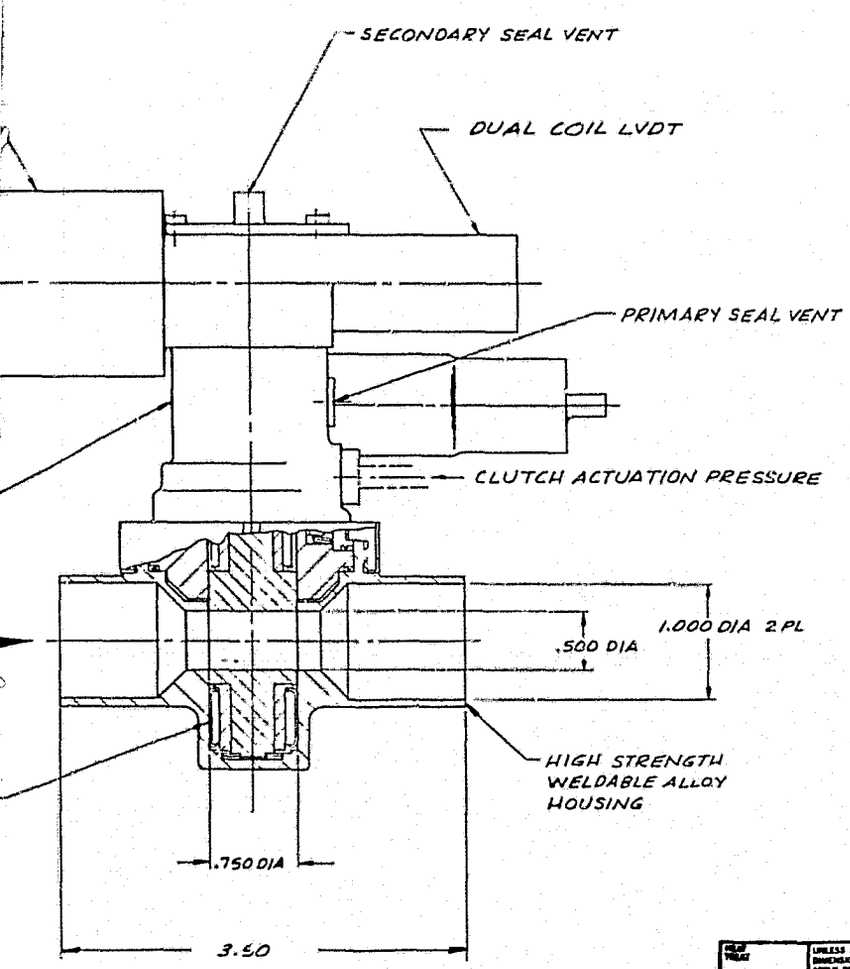

FOLDOUT FRAME 2

Figure 4-15.

THIS PRINT REDUCED
THIS IS NOT A RELEASED COPY

SIGN REQUIREMENTS PER IL 141-42-8242, ITEM 3.

Rockwell International Corporation
Rocketdyne Division
Canoga Park, California

GH_2 TURBINE BYPASS VALVE -OTV

SIZE E | FSCM NO 02602 | DWG NO 7R0014585

SCALE 2:1 | SHEET

7R0014585

controlling gaseous hydrogen flow to the two turbines and thereby engine thrust. Operating full open at tank head idle and near 80% open at pumped idle, the valve must be capable of precise position control to provide a resistance variation less than ±5% for angular rotation of ±0.5 degree. During full thrust, the valve must throttle down to an area ratio of about 10% with closed loop modulation control of thrust.

A rotary plug configuration was selected for this application because of construction simplicity and lack of tight shutoff requirement. The plug is guided by precision roller bearings similar to the MOV. Throttle control is provided by a 0.5 inch diameter hole in a 0.75 [illegible] cylinder with 0.01 inch gap between the cylinder and housing. Assembly and construction features of shaft seals and the actuator are identical with the MOV.

Oxidizer Turbine Bypass Valve

The OTBV (Figure 4-16) provides a balance of gaseous hydrogen flow between the fuel and oxidizer turbines. The valve design is similar to the TBV but reduced actuation torque permits use of polyimide bushings to simplify construction. Assembly and design features of shaft seals and the actuator are identical with the MFV (i.e., pneumatic override is omitted).

Gaseous Oxygen Valve

The GOV (Figure 4-17) is a normally open, line pressure actuated valve that is open only during start and tank head idle. Valve function is to provide gaseous oxygen flow to the combustor prior to opening of the MOV. Increased pressure during pumped idle closes the valve. A schematic of the valve is shown in Figure 4-16.

Dump Coolant Control Valve

The DCV (Figure 4-18) is a normally closed, line pressure actuated valve which

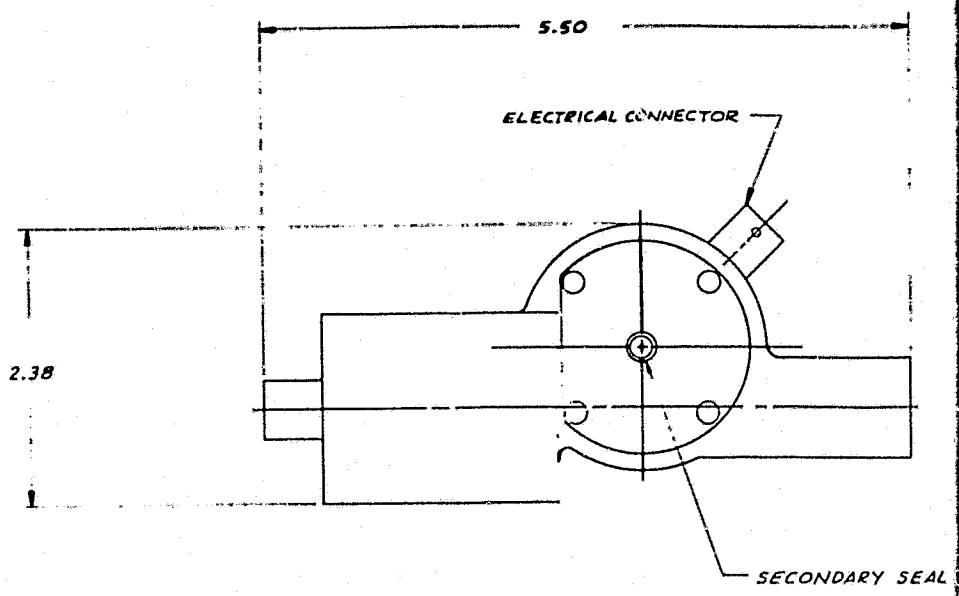

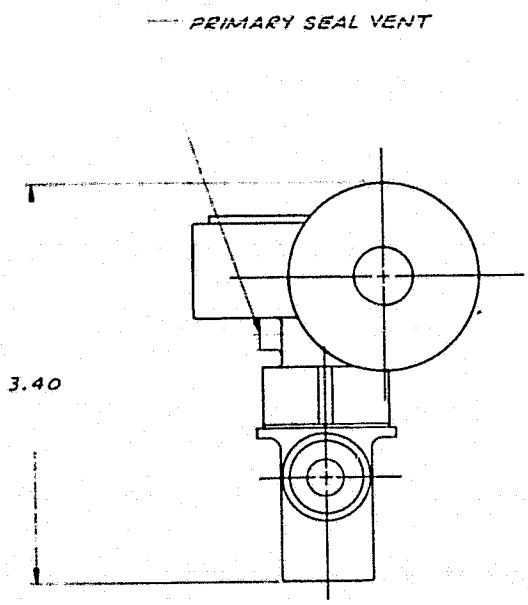

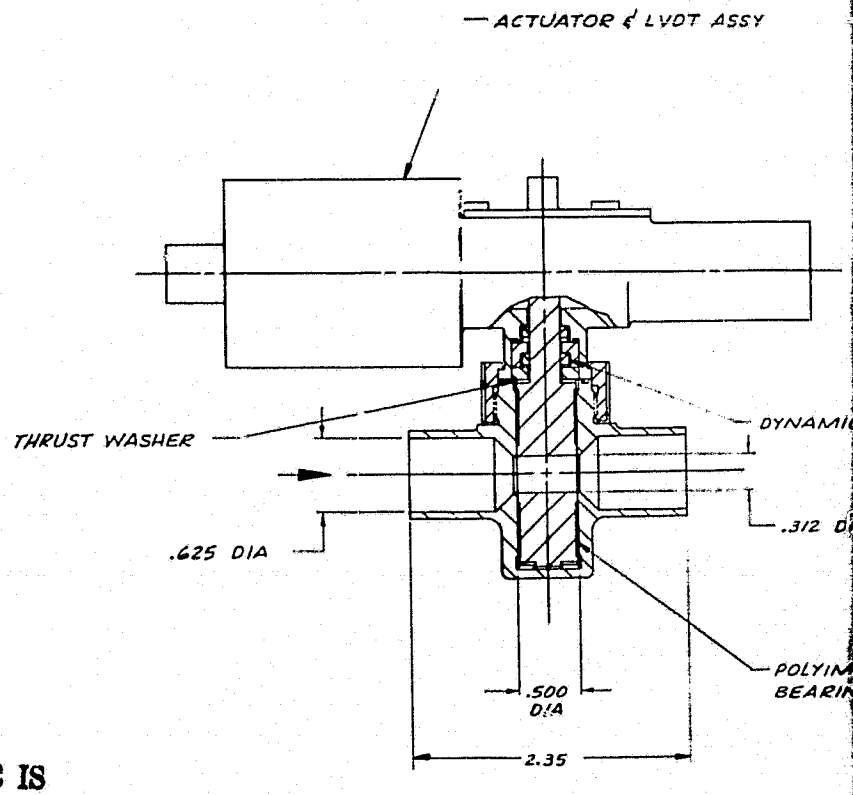

ORIGINAL PAGE IS
OF POOR QUALITY

1. DESIGN REQUIREMENTS PER IL 141-42-8242, ITEM 4

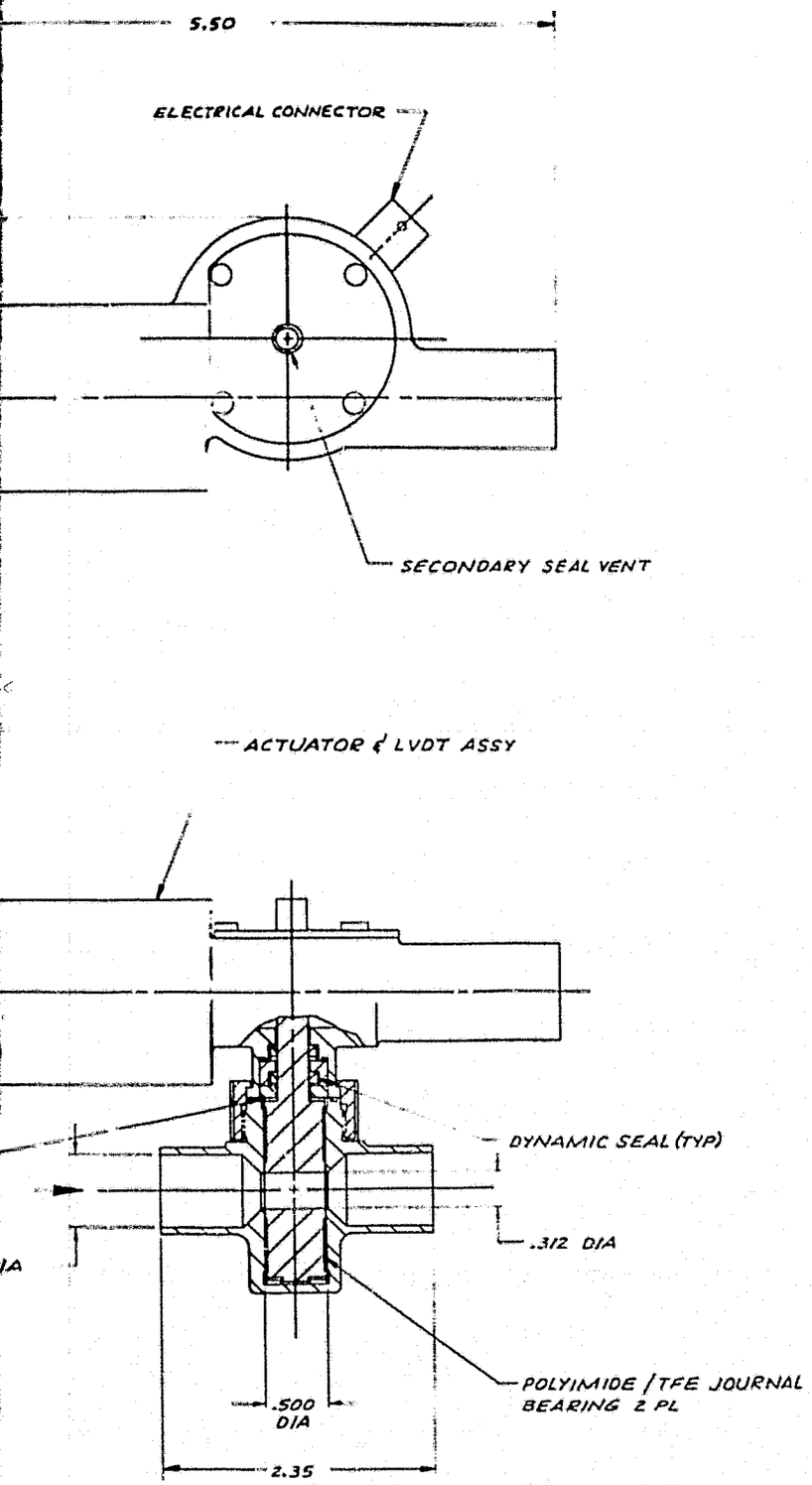

Figure 4-16

THIS PRINT REDUCED
THIS IS NOT A RELEASED COPY

1. DESIGN REQUIREMENTS PER IL 141-42-8242, ITEM 4

Rockwell International Corporation
Rocketdyne Division
Canoga Park, California

OXIDIZER TURBINE
BYPASS VALVE-OTV

SIZE E | FSCM NO 02602 | DWG NO 7R0014 584

SCALE 2/1

7R0014 584

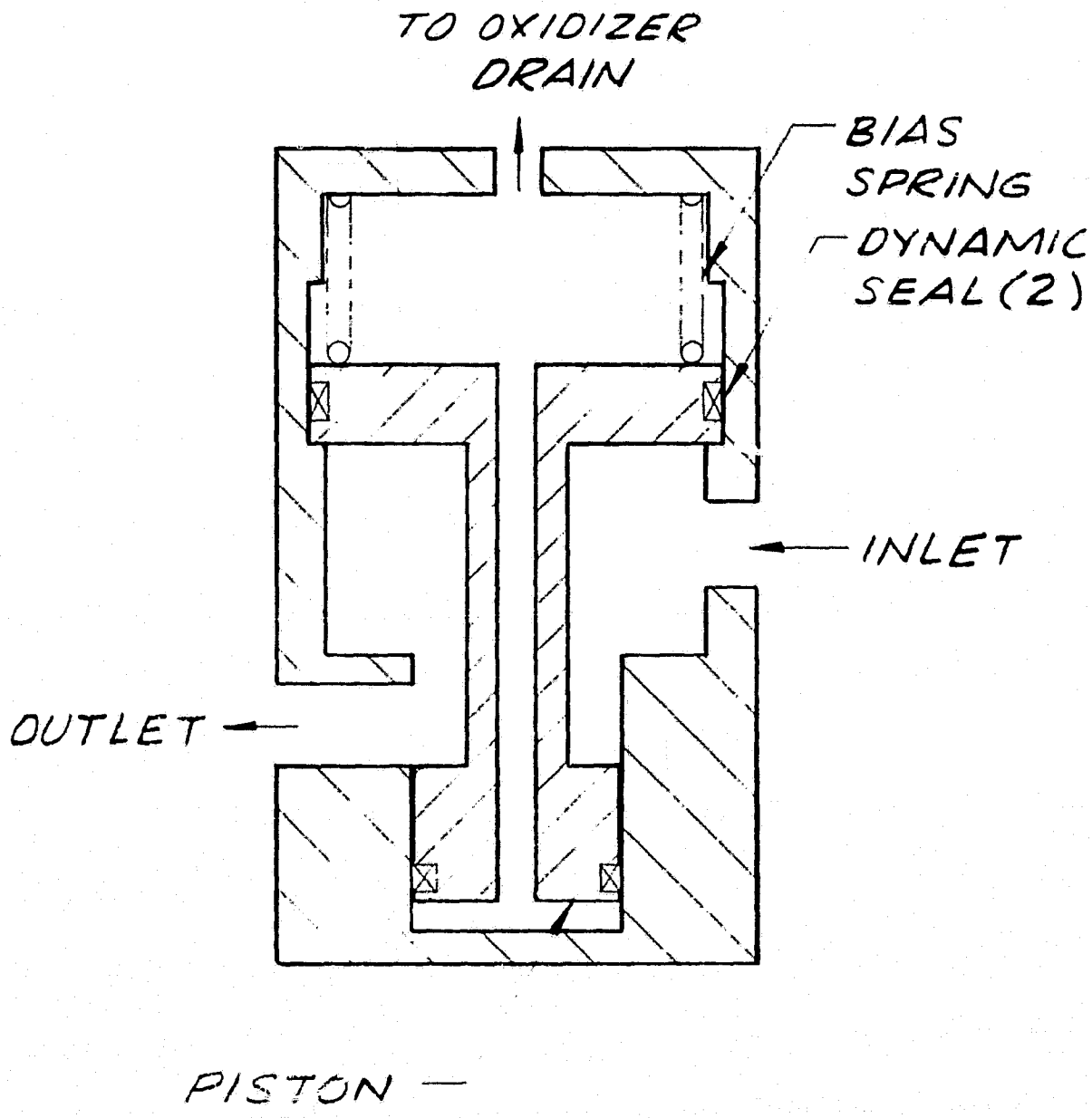

Figure 4-17. Gaseous Oxidizer Valve

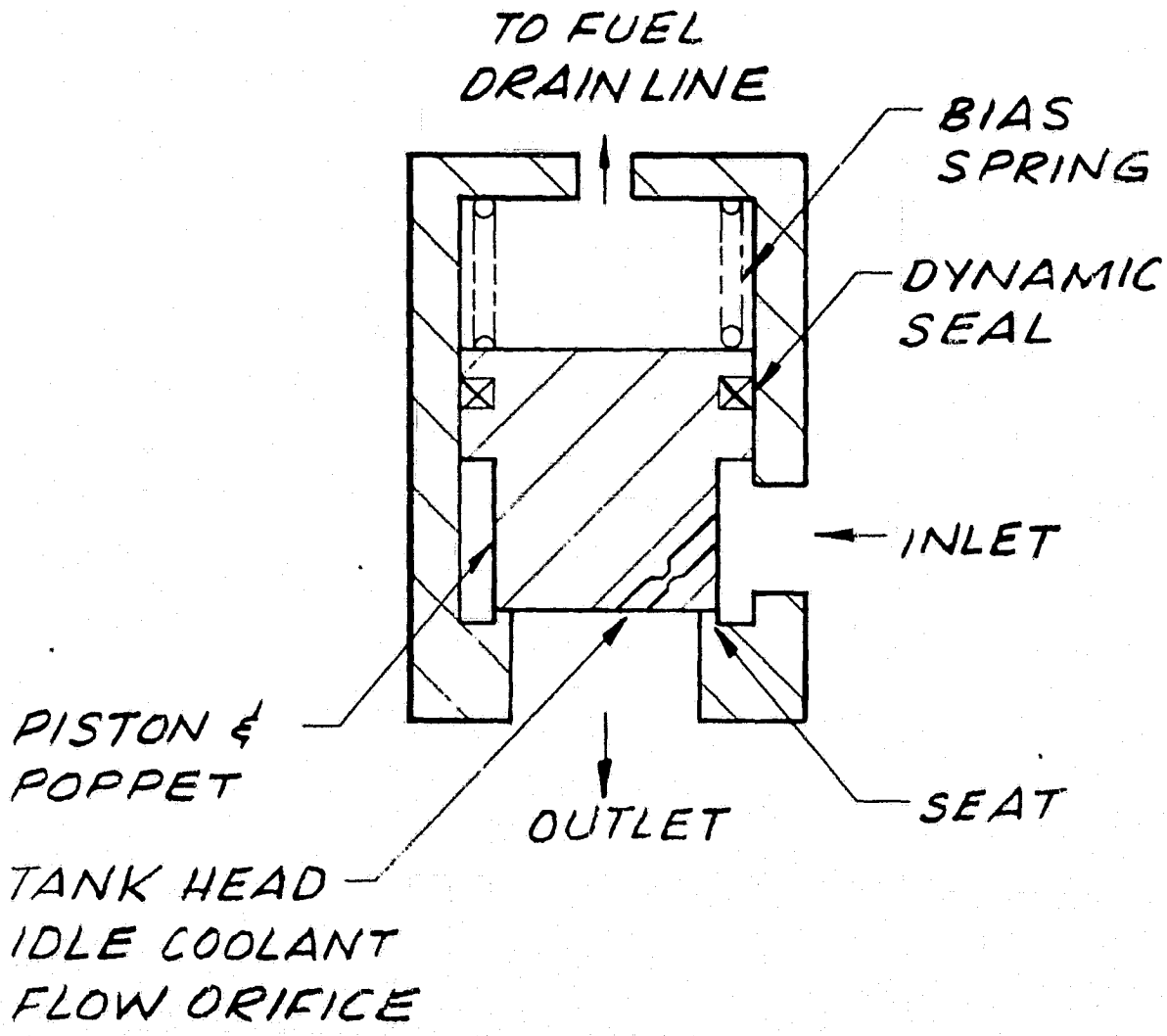

Figure 4-18. Dump-Coolant Control Valve

controls nozzle coolant flow. During tank held idle, the valve is closed and cold hydrogen gas is metered through a fixed orifice.

Pumped idle pressures force the valve open to an intermediate position with attendant increased coolant flow. The valve is full open at full thrust.

Igniter Valves

The igniter fuel and igniter oxidizer valves are small two-way, direct actuated solenoid valves providing oxidizer and fuel to the igniter during start and idle modes. They are equipped with dual coil, hermetically sealed solenoids. An axial flow configuration (similar to check valve) is anticipated with TFE seating.

Tank Pressurization Valves

Tap-off of gaseous propellants provide for tank pressurization. Spring-loaded check valves (FTPV & OTPV) serve to prevent back flow from propellant tanks and allow free flow to pressurant propellants during pumped idle and full thrust. A conventional axial valve construction is anticipated with TFE seating.

Inlet Valves

Engine inlet shutoff valves (FIV & OIV) are required to isolate propellants from turbopump seals before and after firing. A valve configuration providing uninterrupted straight through line diameters equal to the pump inlets is necessary to provide minimum pressure drop and disturbance to pump inlet flows. The design layout (Figure 4-19) shows a light-weight ball valve (LOX side) with shaft and seat seals identical with the MOV. The valve is lever-link actuated open with a pneumatic piston overcoming the normally closed spring force. Both oxidizer and fuel valves are simultaneously actuated open with a 3-way normally closed solenoid valve. Switches provide indication of open/closed positions. All aluminum construction provides minimum weight.

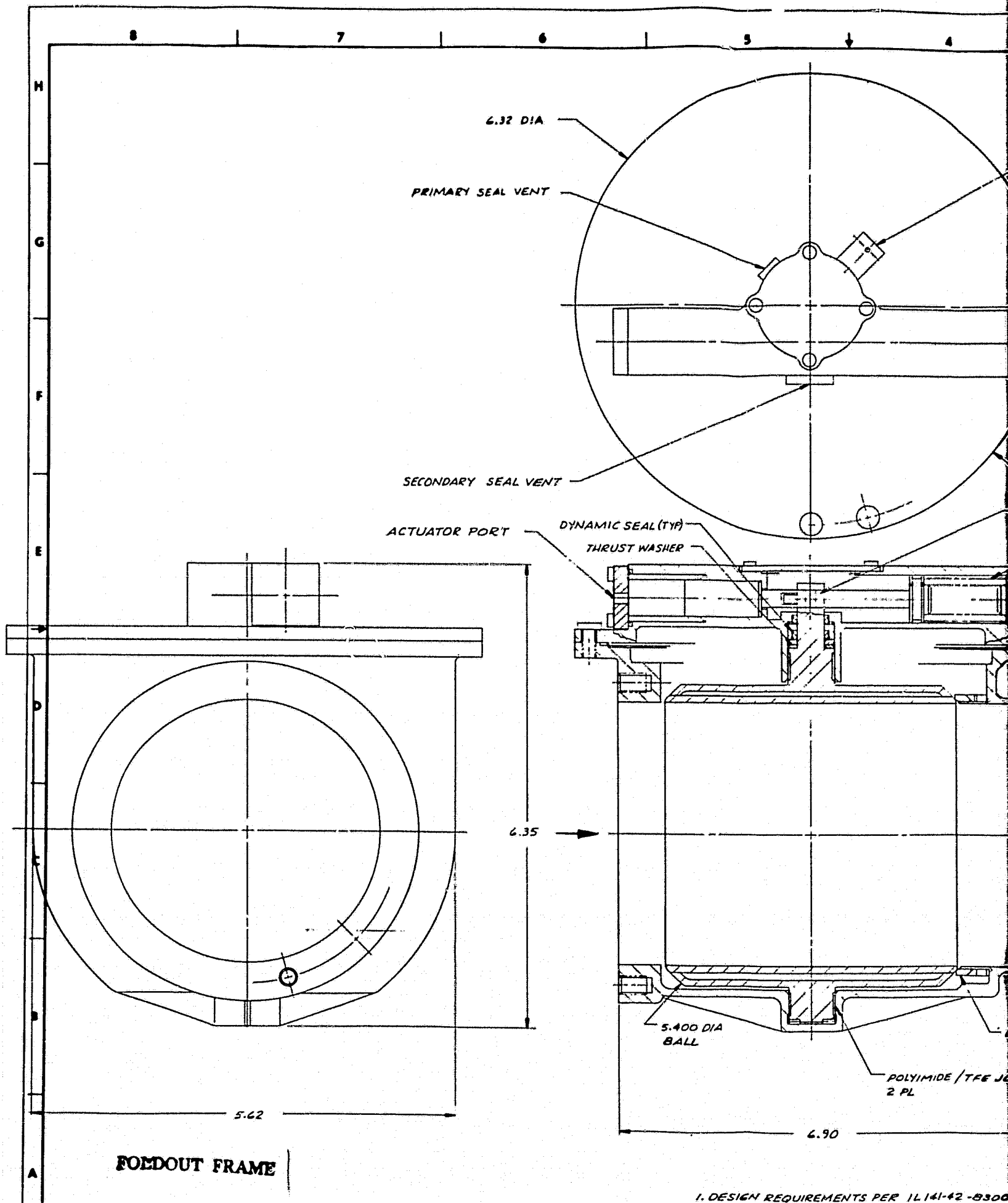

FOLDOUT FRAME

1. DESIGN REQUIREMENTS PER IL141-42-8300

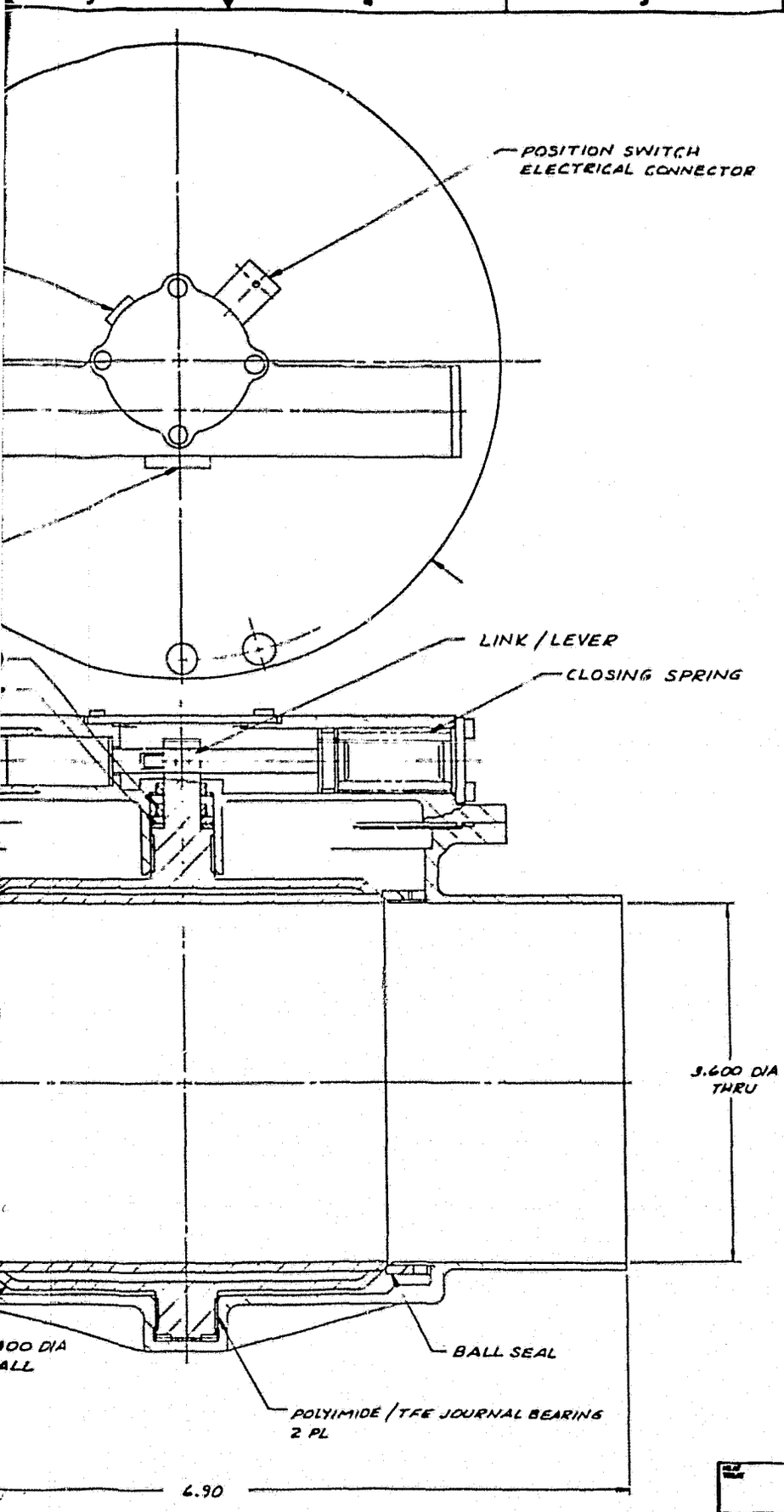

FOLDOUT FRAME 2

Figure 4-19.

THIS PRINT REDUCED
THIS IS NOT A RELEASED COPY

1. DESIGN REQUIREMENTS PER IL 141-42-8300, ITEM 13

Rockwell International Corporation
Rocketdyne Division
Canoga Park, California

LOX INLET VALVE

E 02602 7R0014582

SCALE 2/1

Low pressure operation of the valve, coupled with pneumatic actuation allows use of polyimide bushings to guide the ball.

Solenoid Control Valves

Five three-way control solenoid valves are required for the following functions:

1. MOV safe shutdown
2. TBV safe shutdown
3. Inlet valve open/close
4. LOX dome purge for shutdown
5. LOX pump seal purge

These valves are small (0.062 inch orifice), direct operated three-way valves for cryogenic operation at about 600 psig helium. The solenoids contain dual coils which individually can operate the valve. Solenoid construction is hermetic for high reliability. Internal valving is flat metal-to-metal to provide less than 1.0 scim helium leakage.

Valve Weights Summary

Weights of the four main and inlet valves have been computed based upon layout dimensions. These weights are now reflected in the Appendix specifications. Other weights are estimated. Weights of all valves, including actuators, is summarized in Table 4-7.

TABLE 4-7.

Valve Name	Symbol	Weight, Lbs.
Main Oxidizer Valve	MOV	3.5
Main Fuel Valve	MFV	3.3
Turbines Bypass Valve	TBV	3.5
Oxidizer Turbine Bypass Valve	OTBV	2.0
Gaseous Oxidizer Valve	GOV	3.0
Dump Flow Valve	DFV	1.0
Inlet Fuel Valve	IFV	1.0
Inlet Oxidizer Valve	IOV	1.0
Fuel Tank Pressurization Valve	FTPV	0.2
Oxygen Tank Pressurization Valve	OTPV	0.2
Fuel Inlet Valve	FIV	4.0
Oxidizer Inlet Valve	OIV	4.4
Solenoid	SCV	1.5 (5 each)
	Total	28.6

ENGINE START TRANSIENT SIMULATION

The engine transient simulation program developed under Task 4 of the contract was used to evaluate the effectiveness of the selected 3-valve control system in obtaining adequate engine starts to main thrust, and off-design mixture ratio operation in both the open and closed-loop control modes. Starts to main thrust occurred from a condition of thermally equilibrated hardware at the completion of pumped idle mode. This study resulted in the selection of open-loop valve schedules and valve ramping rates. It also guided the selection of control-valve and LOX vaporizer heat exchangers. For example, the size of the LOX heat exchanger and turbine bypass valve in series with it determined the level of pumped-idle thrust achievable. These components were sized to obtain 1800 lb. thrust (12% of mainstage) at steady-state pumped-idle conditions. The LOX heat exchanger resistance chosen resulted in a pressure drop of 1 psi on the hydrogen side. The gaseous oxidizer valve was in like manner sized to obtain a mixture ratio of 4:1 in pumped idle conditions. This mixture ratio was found to be the highest mixture ratio attainable by the system, at the selected 1800 lb. thrust pumped idle, without any tendency to flow and pressure instability. Pump and thrust chamber coolant jacket coupling of pressure fluctuations beyond a mixture ratio of 4:1 led to instability caused primarily by the low fuel pump flow coefficients. The oxidizer turbine bypass valve was shown to be required to achieve desired pumped-idle conditions of mixture ratio. This valve was also found effective in achieving off-design mixture ratio of 7:1 operation at full thrust.

Engine Starts from Pumped-Idle Mode

An open-loop control start to mainstage thrust is obtained from pumped idle conditions with the valve setting indicated in Figure 4-20 . Ninety percent of full chamber pressure and thrust are achieved within 3.5 seconds (Figures 4-20a and 4-20b) after full-thrust command is activated. The main fuel valve is ramped open at time 0 to achieve fully opened positons in 0.5 second. This action primes coolant jackets and provides a fuel lead thrust chamber start in tank-head idle. In pumped idle, the main oxidizer valve is ramped to tank-head-idle position at a pre-established rate that will maintain mixture ratio

C-5

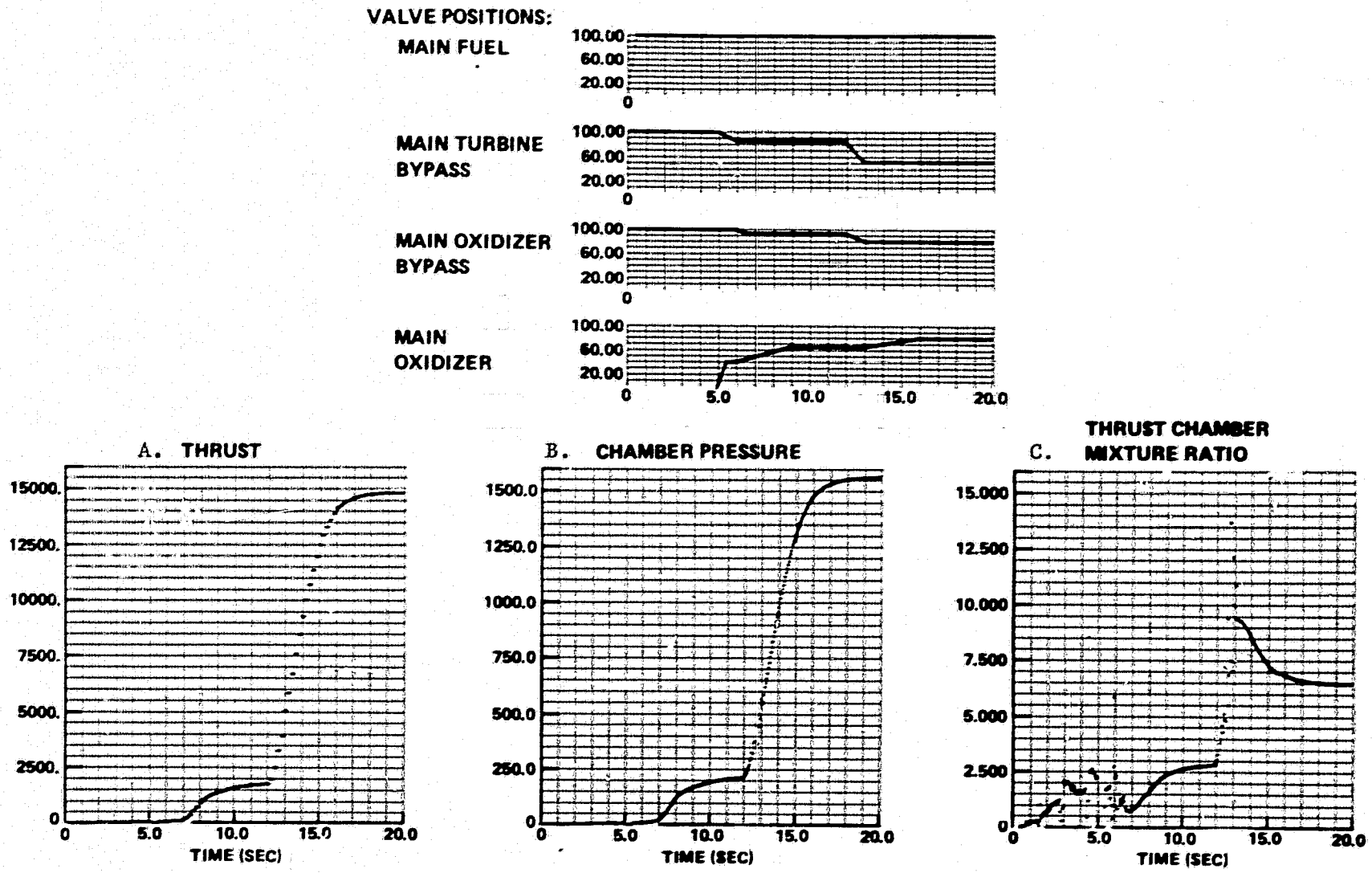

Figure 4-20. Expander Engine Start From Tank-Head Idle Mode

variations within safe limits (Figure 4-20c). Closed-loop control of chamber pressure is actuated within 2.6 seconds after full-thrust command is given to carry the engine into full thrust conditions without undue overshoots in engine thrust, thrust chamber mixture ratio, and pump speeds. Closed-loop mixture ratio control is activated as soon as the engine achieves full thrust.

Off-Design Mixture Ratio

After attaining mainstage conditions, off-design mixture ratio is obtained by the use of the main oxidizer valve (Figure 4-21). The turbine's bypass valve and oxidizer turbine bypass valve are used to maintain total power and power split at valves required for constant thrust. Chamber pressure decays slightly at mixture ratio of 7 (Figure 4-21a), but thrust remains constant at 15,000 lb. (Figure 4-21b). Closed loop control of thrust chamber mixture ratio maintains this variable to remain within safer limits during the transient to full thrust (Figure 4-21c) and during the transient to off-design mixture ratio. Mixture ratio variations during these two transients is improved over that obtained without closed-loop control (Figure 4-20c).

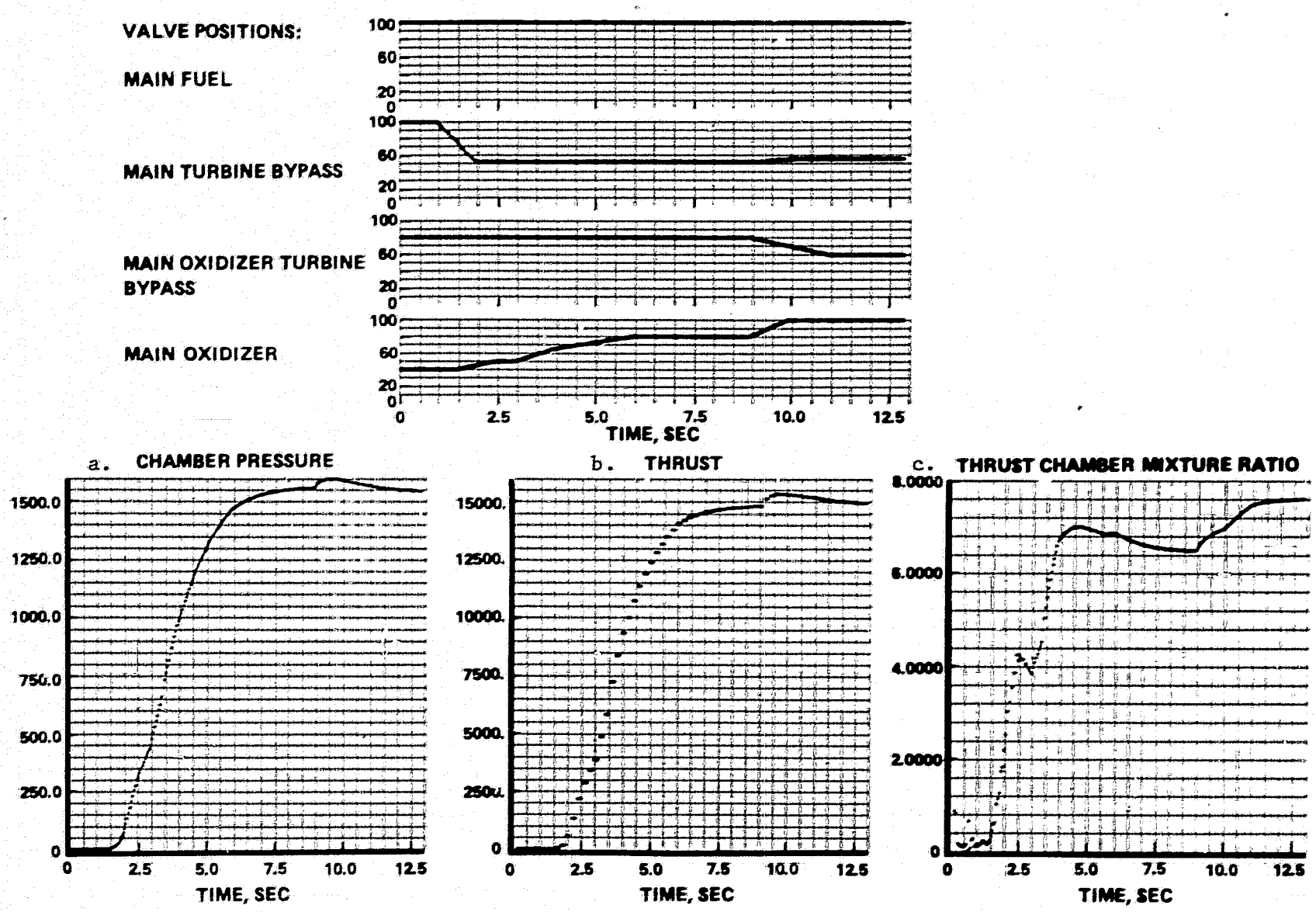

Figure 4-21. Expander Engine Closed-Loop Control of Thrust and Mixture Ratio

ENGINE POWER ACCESSORIES (TASKS 2 AND 3)

This category of components has been chosen to encompass components of the power cycle other than pump, turbines and control valves.

Included in this classification are the turbine gas regenerator and the oxygen gasifier, both of which consist of heat exchanger hardware. The oxygen gasifier furnishes an oxygen tank pressurization gas source, and in that manner provides oxygen boost pump NPSH requirements at mainstage. The oxygen gasifier heat exchanger uses hydrogen at the turbine's bypass valve for the source of thermal energy it requires. The turbine gas regenerator exchanges heat between the cold pump hydrogen and the hot turbine exhaust hydrogen to boost cycle power through augmentation of the turbine inlet temperature.

LOX HEAT EXCHANGER - REQUIREMENTS AND CANDIDATE CONFIGURATIONS

The Advanced Expander engine is designed to provide autogenous pressurization of vehicle propellant tanks. Gaseous fuel, for fuel tank pressurization, is readily available from the main chamber and nozzle coolant. However, to provide gaseous oxygen for oxidizer tank pressurization, a separate heat exchanger is required. This LOX heat exchanger also provides gaseous oxygen for the main chamber igniters during all modes of engine operation. During tank head idle, the heat exchanger also provides gaseous oxidizer to the main chamber.

Selection of LOX heat exchanger concepts and locations made use of analysis conducted for the ASE Preburner Assembly under contract NAS3-20386. The candidate exchangers identified under that effort are shown in Figure 5-1 along with their features and possible problem areas. The simplest of these options is the concentric tube approach where the oxygen flows in the center tube and the hydrogen in the annulus. Due to its relatively large hydraulic diameter, this configuration will typically be long. The coiled tube within a tube is a modification of the concentric tube approach to reduce the heat exchanger length. With a continuous inner tube, both tubular concepts do not contain an interpropellant joint. Because pressurization requirements and thrust level were

CANDIDATE OXIDIZER HEAT EXCHANGERS

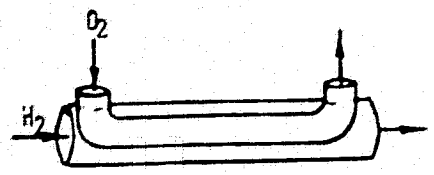

FEATURES

- SIMPLE CONCEPT
- LOW COST
- LOW ΔPS

POSSIBLE PROBLEMS

- LONG HEAT EXCHANGER

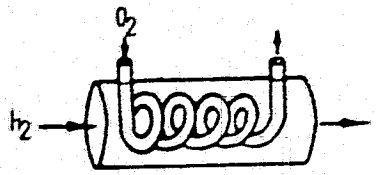

FEATURES

- SIMPLE CONCEPT
- SHORTER HEAT EXCHANGER

POSSIBLE PROBLEMS

- GEOMETRIC COMPATIBILITY

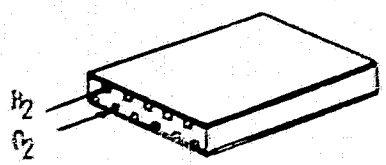

FEATURES

- SHORT HEAT EXCHANGER
- SIMPLE CONCEPT
- VARIABLE O_2H_2 FLOW AREA

POSSIBLE PROBLEMS

- FABRICATION COST
- O_2H_2 SEALING

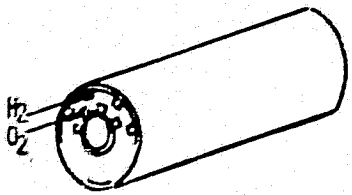

FEATURES

- SHORT HEAT EXCHANGER
- SIMPLE CONCEPT
- VARIABLE O_2H_2 FLOW AREA

POSSIBLE PROBLEMS

- FABRICATION COST
- O_2H_2 SEALING

Figure 5-1. Candidate Oxidizer Heat Exchangers

similar to those of the expander engine, the results of this work are applicable. The panel heat exchanger configuration enables a shorter heat exchanger due to its small hydraulic diameters. Also, since channels form the flow passages, the channel depth may be changed along the panel length to minimize pressure drop. The fourth configuration is merely the milled channel configuration in the form of a cylinder. In both of the panel configurations, the hydrogen and oxygen channels could be machined from one piece of material which eliminates any interpropellant joint.

Heat Exchanger Location

Two alternate locations (Figure 5-2) were examined for placement of the hydrogen side of the heat exchanger. One possible site for the gasifier is in the nozzle coolant discharge line, upstream of the main turbines. A second option is to place the hydrogen side of the heat exchanger in series with the main turbine bypass valve and downstream of the valve.

The first alternate location has the advantage that all of the mainstage hydrogen flow is available to heat the oxidizer. However, not all of the flow will be required to perform the necessary vaporization. A drawback to this location is that wide hydrogen flowrate swings will result as thrust is reduced. Only 1/8 of the flow available at mainstage will be available at pumped idle. A gasifier designed for full mainstage flowrate will therefore be operating far from its design flow at idle thrust.

The second alternate, in the bypass line, possesses the advantage that bypass valve modulations for thrust control tend to keep a steady flowrate through the bypass line. This minimizes the effect of flowrate variations on the heat exchanger and allows it to operate closer to its design point at all thrust levels. A negative aspect is the need for very low hydrogen-side pressure drop at the low-thrust operating point. This requirement, discussed below, arises from the need to bypass a relatively large fraction of the total hydrogen around the turbines during idle mode operation. Location of the heat exchanger

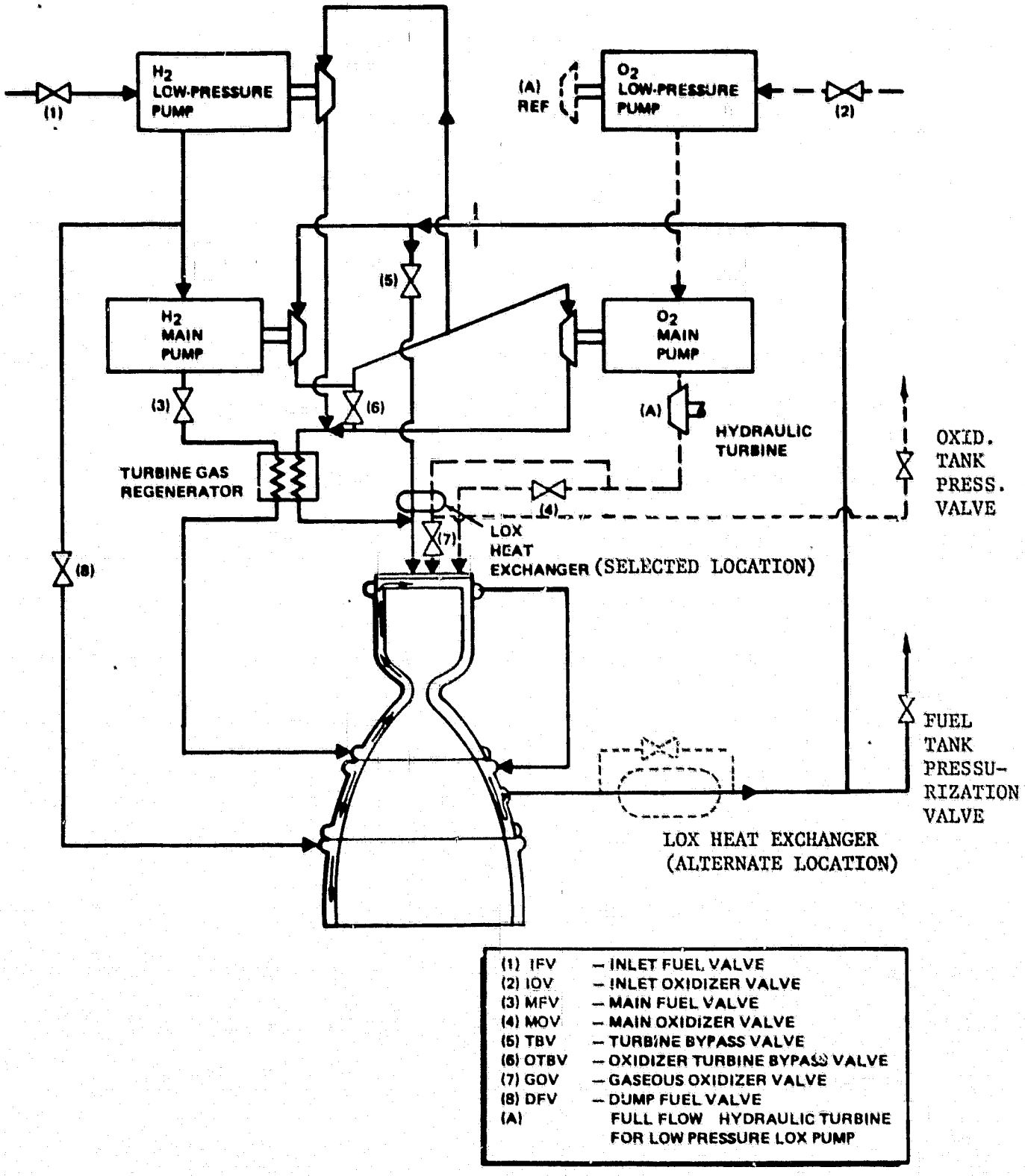

Figure 5-2. Expander Engine Schematic

in the bypass line provides approximately 0.4 lb/sec of heated hydrogen for vaporizing the oxygen. This quantity is more than adequate for this function, even though it represents about 10% of the total engine H_2 flowrate at mainstage.

The selected gasifier location is in the bypass line as shown in Figure 5-2. The selection was based upon relative merit of this placement compared with the nozzle discharge location. The latter location leads to a more complex control problem, as a bypass valve may be necessary to help control the gasifier hydrogen flow. The selected location avoids the necessity of an additional control valve. Analysis indicated that the low pressure drop requirement of this location could be met without great difficulty.

Pressurization System Requirements

The flow requirements of the LOX heat exchanger are summarized in Table 5-1 for both idle and mainstage operation. Because the selected location of the heat exchanger places it in the main turbine bypass line (Figure 5-2), it receives the full bypass hydrogen flowrate at any operating condition. Oxygen pressurization and igniter flowrates are set by valves at values required to pressurize the tanks and supply the igniters.

Table 5-1. LOX Heat Exchanger Flowrates, (lb/sec)

Propellant	Tank Idle	Pumped Idle	Mainstage
H_2	0.018	0.385	0.410
O_2	0.107	0.144 (total) 0.090 (pres) 0.054 (igniters)	0.224 (total) 0.134 (pres) 0.090 (igniters)

Temperature Requirements. Based upon the results of NAS3-20386, a design oxidizer exit temperature of 640R at mainstage was selected. This was intended to assure that an adequate temperature level will be achieved at pumped idle conditions by designing for excess temperature at mainstage. Balances conducted

during design iteration revealed, however, that oxygen outlet temperature actually increases with reduced thrust level (Table 5-1) for the expander cycle. This is caused by increasing hydrogen temperature coupled with bypass flowrates which remain relatively high (percent of total H_2 increases) as thrust is reduced. The energy available per pound of hydrogen to heat the oxygen is thus greater at pumped-idle-mode thrust than at mainstage. At tanked idle oxygen outlet temperature is reduced, but remains high enough for complete vaporization. The net result of the selected design is therefore a LOX heat exchanger with large margins at all operating conditions. The danger of failing to vaporize the oxygen at a certain operating point is thus eliminated.

Pressure-Drop Requirements. Due to the placement of the hydrogen side of the LOX heat exchanger in the line of the main turbine bypass valve, it will have an impact upon control, especially at idle-mode operating points. Successful thrust level control at tank-head and pumped idle depends upon achieving the necessary level of hydrogen bypass around the turbines. The full-open resistance of the turbine bypass valve and the line must be carefully designed to be as small as possible. A high LOX heat exchanger hydrogen-side pressure drop will therefore prevent successful low-thrust operation.

A critical parameter is therefore the hydrogen side delta-P of the LOX heat exchanger. Because hydrogen density is much lower (.06 lb/ft^3 vs. .73 lb/ft^3) at the pumped idle point than at mainstage, a very low design pressure drop is needed in order to assure acceptable delta-P at pumped idle. A design delta-P of approximately 1 psia was found necessary based upon idle mode simulations conducted with the Transient Engine Model. The LOX heat exchanger is designed to this pressure drop value.

Concentric Tube Configuration

Analysis conducted under NAS3-20386 showed that the concentric tube configuration resulted in excessive LOX heat exchanger length and weight (Figure 5-3). It was therefore not selected as a viable alternate for application to the Advanced Expander engine.

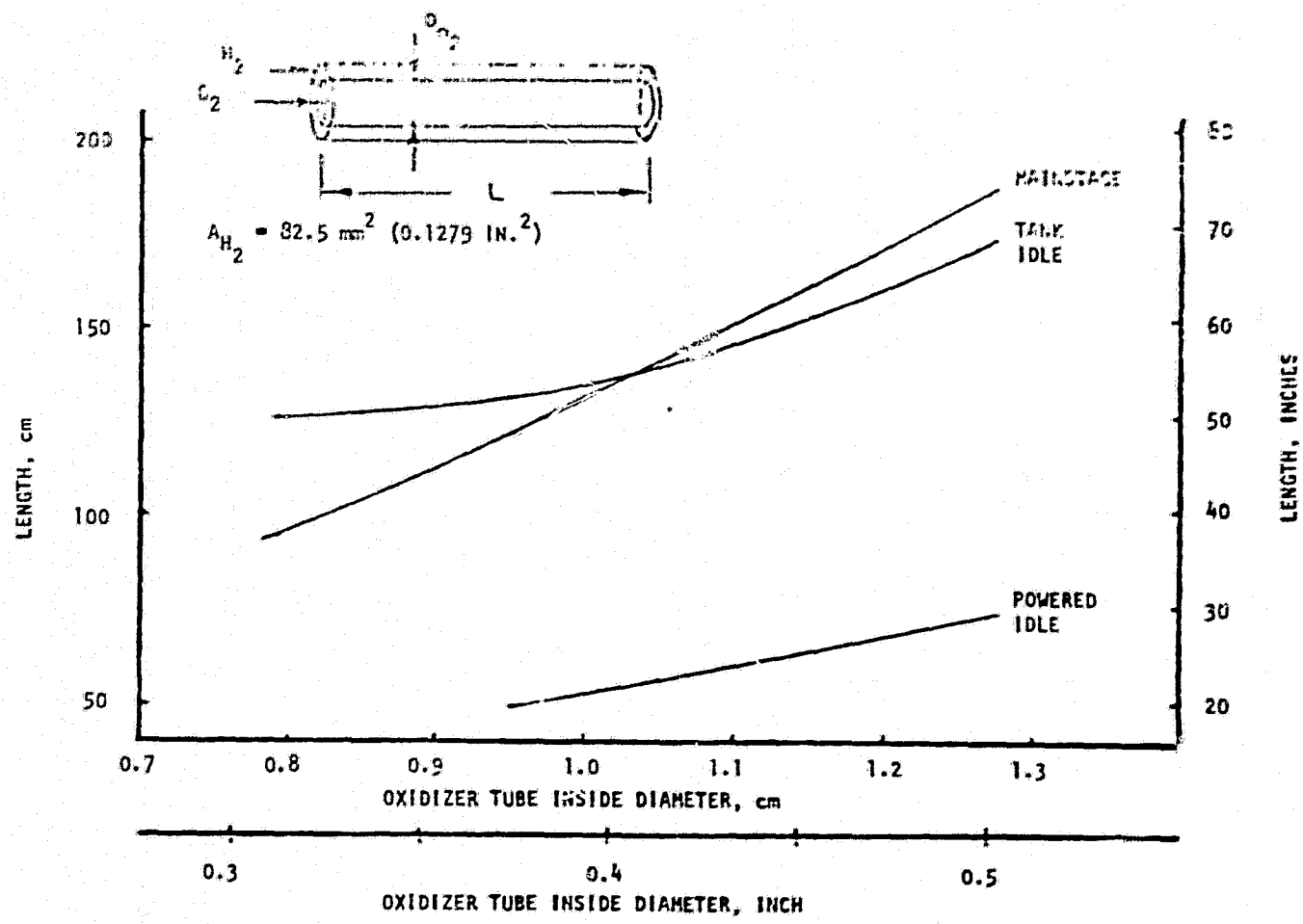

Figure 5-3. Concentric Tube Heat Exchanger Length Requirements

Plate - Stack Configuration

A plate-stack LOX heat exchanger configuration has potential for allowing significant weight and envelope reductions compared to conventional approaches. Figure 5-1 illustrates this geometry. A variant of this approach is the panel configuration, which consists of one or two pairs of hot and cold channel layers. This was the selected design concept. The selection was based upon the ability of this configuration to avoid interpropellant joints, and on weight, envelope, and packaging considerations.

Selected Liquid Oxidizer Gasifier Design

The design features simple construction, no interpropellant leak paths, high heat transfer efficiency, easy engine packaging, reliability, and low pressure drops. The gasifier is illustrated in Figure 5-4. It consists of two flat OFHC copper plates which are slotted and then brazed together. Manifolds are brazed on before nickel is electrodeposited as a channel closeout. The completed panel is then formed to its final curved shape.

There are three layers of channels, with the central layer, containing the hydrogen gas flow, sandwiched between two layers of oxygen channels, providing efficient heat transfer. This arrangement is formed by milling channels on both sides of one of the copper plates. This plate has 86 hydrogen channels 0.160 deep, 0.080 wide, and 0.040 apart on one side as well as 86 oxygen channels 0.060 wide and 0.060 apart on the opposite side. The layers are aligned with each other to provide a constant 0.025 of parent material in all thickness along each pair. The oxygen channels taper in depth from 0.020 at the inlet to 0.080 at the exit to permit expansion from liquid to gas. The second copper plate has an identical set of oxygen channels on one side with a flat surface on the other side and a wall thickness to the bottom of the channels of 0.025. After milling, the plates are furnace-brazed together so that the lands of the hydrogen channels are brazed to the flat side of the second plate. Channel geometry is summarized in Table 5-2.

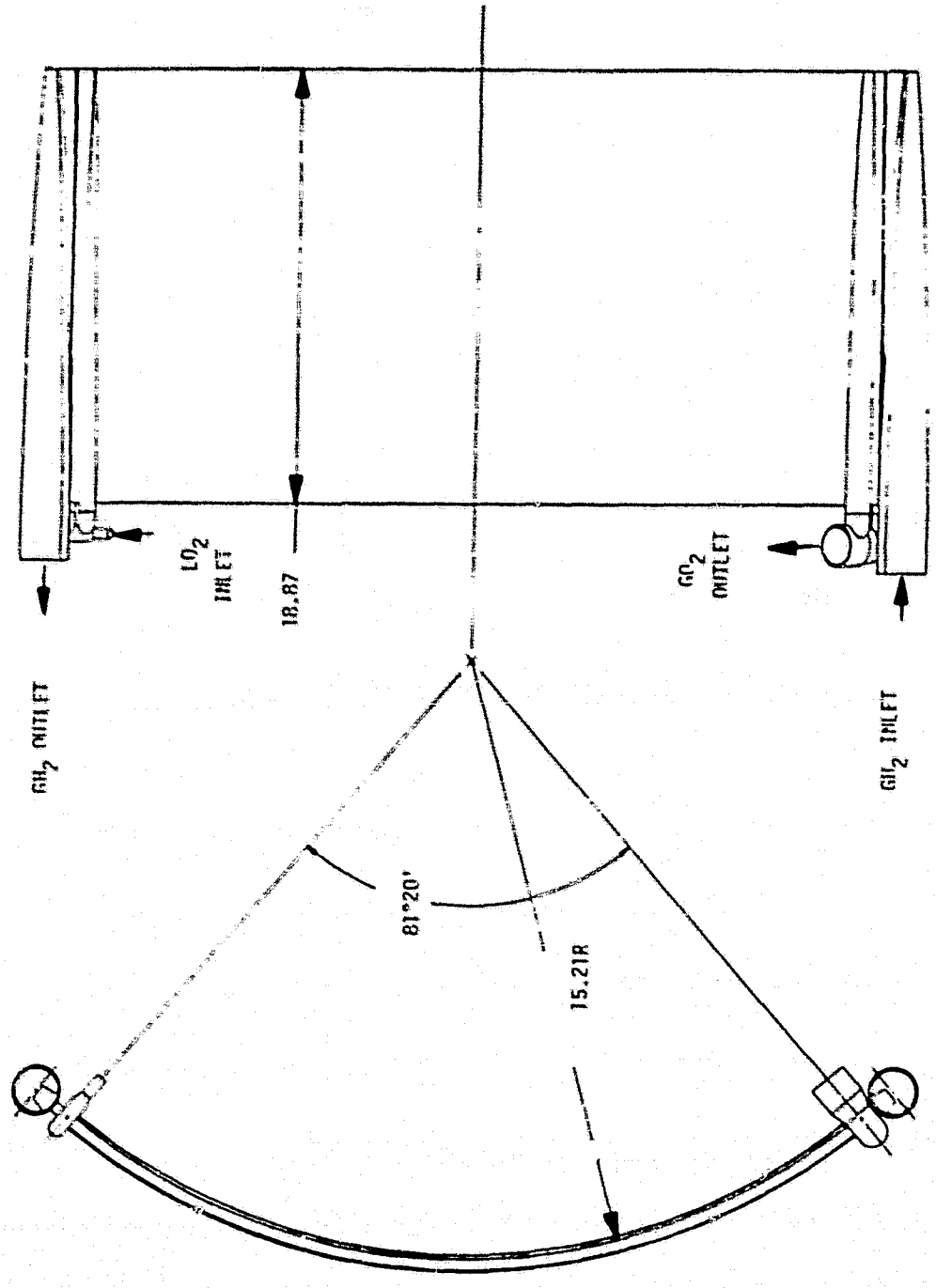

Figure 5-4. Liquid Oxygen Gasifier

Table 5-2. LOX Heat Exchanger Geometry

DIMENSION	OXYGEN CHANNELS	HYDROGEN CHANNELS
Channel Height, In.	.060	.080
Channel Width, In.	.020 (inlet) .080 (exit)	.160
Channel Length, In.	21.96	21.97
Channel Spacing, In.	.060	.040
Wall Thickness, In.	.025	.025

The manifolds are brazed to the plates in a manner which eliminates all inter-propellant joints. All are tapered so as to provide minimum pressure losses and weight. The oxygen manifolds, two at both the inlet and outlet, are each machined of a single rod of Inconel 625 and, after brazing, each pair are welded to a distribution fitting. The hydrogen manifolds, machined from Incoloy 903 bar, are of a welded two piece configuration. Their location at the ends of the hydrogen channels provide for minimum inertial losses in the flow.

After the manifolds have been brazed in place, nickel is electro-deposited on the plates to close out the oxidizer channels. The E.D. nickel also provides additional strength to the structure, especially since it may remain in the as-deposited condition. The assembly is then cold-rolled to the proper radius. Table 5-3 summarizes inlet and exit conditions for the various engine operating points.

TURBINE GAS REGENERATOR

The turbine inlet gas temperature obtained with the 20-inch combustor length is not sufficient to sustain chamber pressures higher than 1400 psia. Within the 1980 state-of-the-art technology, it is not possible to increase heat loads in a length restricted chamber through thermal enhancement schemes. With the 20-inch tapered combustor, the calculated maximum wall temperature is 810F, a

Table 5-3 LOX Heat Exchanger Requirements

Engine Operational Mode	Flowrate, Lb/Sec		Pressure Drop, PSID		Inlet Temperature R		Outlet Temperature R	
	O_2	H_2	O_2	H_2	O_2	H_2	O_2	H_2
Mainstage	0.224	0.410	<1	1.14	164	887	640	870
Pumped Idle	0.144	0.385	10.95	9.5	164	778	682	765
Tank-Head Idle	0.107	0.018	0.6	3.06	171	520	219	506

value still below the imposed limit of 1000F (Table 1-4), above which hot gas wall erosion becomes a factor.

Turbine gas regeneration can be employed to increase the turbine gas inlet temperature at the expense of increasing the wall temperature to 858R, without decreasing the thrust chamber cycle life. It was found feasible to achieve a 100 degree increase in turbine inlet temperature with only a moderate increase in wall temperatures, without a decrease in cycle life. The turbine gas regenerator thus provided a viable scheme for a significantly increased chamber pressure (1540 psia, Table 1-4) making it possible to retain the power margins previously adopted for contingencies arising during development of the engine. This design approach was selected as the baseline configuration.

Turbine gas regeneration is accomplished within a countercurrent heat exchanger. The heat exchanger's hot-side thermal capacity accumulates heat from the turbine exhaust hydrogen gases. This heat is picked up by the cold hydrogen liquid from the pump prior to entry into the coolant chamber. The heat exchanger design of low weight (16 pounds) is utilized which provides an AMOTV round trip increase of 70 pounds in payload* through the increase in chamber pressure and specific impulse (Table 1-4).

Within limits established by the chamber hot-gas wall temperature, the turbine gas regenerator design can be altered to furnish a certain amount of additional engine power margin. This would provide for unforeseen contingencies in system and component pressure drops, turbomachinery efficiencies, or combustor and nozzle heat loads.

Regenerator Location

The selected location of the regenerator is downstream of the turbines (hot side) and upstream of the cooling jacket (cold side). Figure 5-2 shows this

*Based on AMOTV defined in NASA TMX-73394.

arrangement. Other locations are possible. Several of these options were evaluated during Task 8 of the Phase A Extension (NAS8-32996). Options considered (Figure 5-5) included locating the hot side of the regenerator between the turbines (number 4 of Figure 5-5) and placing the cold side between the combustor and nozzle jackets (number 5 in Figure 5-5).

The motivation behind the first option (between turbines) is to cool the oxidizer turbine inlet gas in order to reduce the nozzle spouting velocity (C_o) in the oxidizer turbine. This has the effect of increasing U/C_o, the velocity ratio, which results in higher efficiency for this turbine. However, during engine configuration studies performed prior to selecting the baseline design, it was found that this location resulted in too low an inlet temperature for the oxidizer turbine. The available energy reduction exceeded the efficiency gain.

The second option, cold side between jackets, has the advantage of allowing nozzle exit temperatures of 1260R without adversely affecting the combustor wall temperature. However, work performed under NAS8-32996 showed that regenerators at this location became very heavy (approximately 120 lbs) when providing optimum regeneration. This was due principally to the greatly reduced cold-side density encountered at this location, which led to a large heat exchanger flow area.

The results of such studies ultimately led to placement of the regenerator downstream of all turbines, where it absorbs energy not used by the turbines and pumps it back to the inlet side of the cycle.

Regenerator Configuration Selection

The selected regenerator configuration is a compact plate-stack design. Alternate configurations, such as shell-and-tube and concentric tube designs, were considered and were found to be unsatisfactory due to excessive weight and envelope. The flow path is counterflow. This approach leads to the

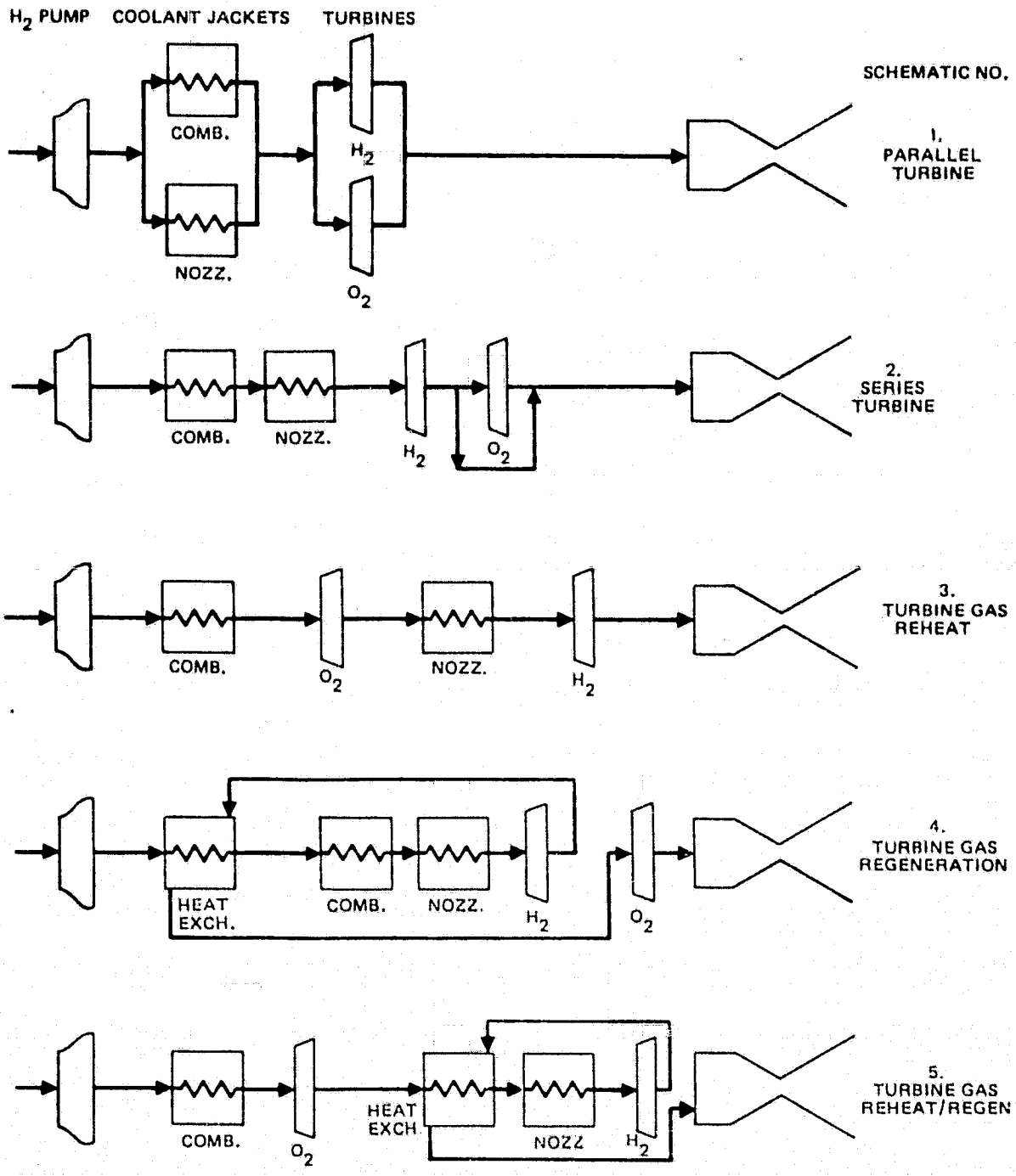

Figure 5-5. Expander Engine Schematics

smallest heat exchanger for a given quantity of heat transferred, and manifolding is relatively easy when the counterflow technique is employed with the plate-stack design.

Heat Exchanger Geometry Optimization

A digital computer model of the regenerator was written and exercised in order to optimize the geometry of the heat exchanger. The model is identical to the model contained in the Steady-State Design Code, but can be run independently. This arrangement facilitates optimization of the heat exchanger without performing costly system balances. Figure 5-6 presents a typical output of the heat exchanger model. Heat exchanger inlet flows, temperature and required heat loads are inputs. Heat exchanger geometry, pressure drops and outlet temperatures and pressures are outputs of the program as indicated in Figure 5-6.

Using this tool, exchanger channel geometry and frontal area were varied in order to define an optimum design. The goal of the optimization was to achieve minimum pressure drops along with a compact envelope. It was desired to achieve a near-cubical envelope for the exchanger (exclusive of manifolds) in the interest of minimizing packaging difficulty.

The final design point selected has a 16 in.^{2} frontal area and a length (minus manifolds) of 3.8 inches, which is very nearly cubical. The selected channel geometry for both hot-and cold-sides are identical. The unit is essentially a series of OFHC copper plates stacked in parallel, then brazed to form a rectangular shaped heat exchanger approximately 3-1/2 x 3-1/2 x 6 inches long. Incoloy 903 manifolds are brazed to provide counterflow characteristics for improved efficiency. The regenerator is mounted near the fuel pump discharge and main injector minimizing feed system ducting. The turbine gas regenerator is illustrated in Figure 5-7.

```
HEAT EXCHANGER TYPE =  COUNTERFLOW
TC2  ,DEG R                          212.800
TH2  ,DEG R                          657.620
Q    ,BTU/SEC                       1626.499
AC   ,IN**2                            4.444
AH   ,IN**2                            4.444
HC                                     0.012
HH                                     0.011
XK                                     7.855
DTA, DEG R                           565.875
LENGTH, IN                             3.815
COLD SIDE DP, PSIA                     0.634
HOT  SIDE DP, PSIA                     3.309
COLD SIDE WDOT, LB/SEC                 4.062
HOT  SIDE WDOT, LB/SEC                 3.636
WEIGHT, LB                             2.839

HOT -SIDE HYDROGEN PROPERTIES:
            PRESS      TEMP        ENTROPY ENTHALPY    DENSITY

          2359.50   784.810     11.790  2708.070      0.520
          2356.19   657.620     11.162  2260.744      0.619

COLD-SIDE HYDROGEN PROPERTIES:
        PRESS      TEMP        ENTROPY   ENTHALPY  DENSITY

          4577.50    97.880      3.360   168.460      4.550
          4576.87   212.800      6.002   568.888      2.869
```

Figure 5-6. Sample Regenerator Model Output

ORIGINAL PAGE IS
OF POOR QUALITY

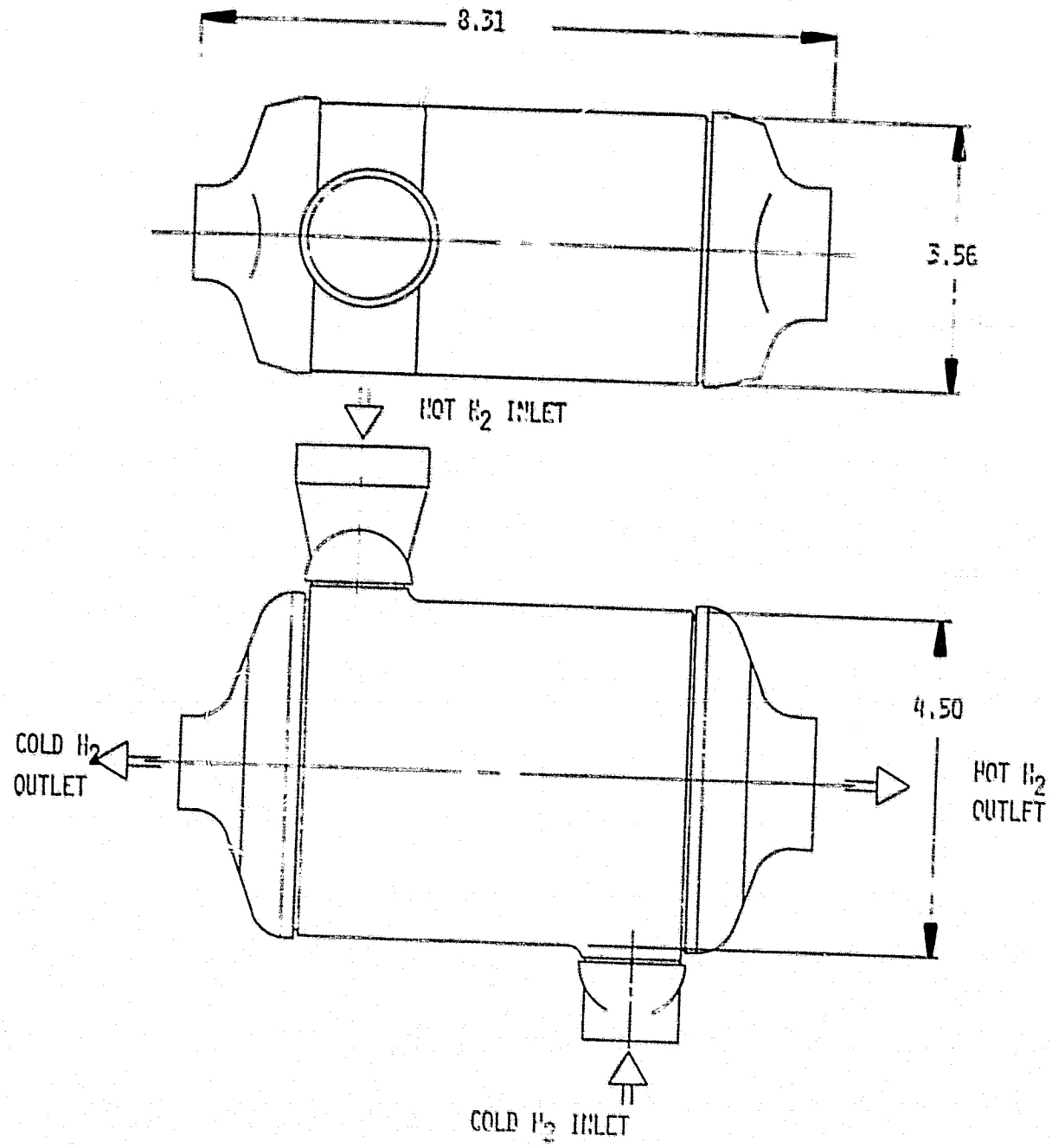

Figure 5-7. Turbine Gas Regenerator

ENGINE CONFIGURATION LAYOUT (TASK 6)

The OTV advanced expander cycle engine delivers 15,000 pounds of thrust from liquid oxygen/hydrogen propellants supplied at NPSH values of 2 and 15 feet, respectively. Major engine components include boost pumps to provide main pump NPSH and high pressure turbopumps to provide high pressure propellants to the combustion chamber/injector assembly. The thrust chamber assembly provides the heat source with which hydrogen is expanded to drive the turbopumps. Power accessories consisting of a turbine gas regenerator and a liquid oxygen vaporizer provide, respectively, a boost in turbine temperature and NPSH requirements of the oxygen boost pump. An ignition system provides combustion start-up, and a control system consisting of sensors, electronics, and valves maintains the desired engine operating conditions.

ENGINE OPERATION

Operation of the system in mainstage can be illustrated with the aid of the shaded engine layout in Figure 6-1. The engine fuel propellant flow is initiated by opening the fuel inlet valves and the main fuel valve. The inlet fuel valve is located two diameters upstream of the fuel boost turbopump and the main fuel valve ahead of the combustor coolant jacket. A small portion of the hydrogen boost pump flow is used to cool the extendible nozzle (not shown). After flowing through the main fuel valve (Figure 6-1), the high pressure hydrogen is heated as it successively picks up heat from the turbine gas regenerator (1), the combustor coolant jacket (2-3) and the fixed nozzle coolant jacket (4-5-6). Most of this hydrogen is then used to power the high pressure fuel pump turbine (8), the fuel boost pump turbine, and high pressure oxidizer pump turbine (9) before passing through the turbine gas regenerator (1) as hot hydrogen on its way into the injector (10). The fuel and oxidizer turbine flows are balanced with the oxidizer bypass valve (11). Thrust control is provided by detouring some of the heated hydrogen flow around the turbines through the turbine bypass valve (7). This bypassed fuel is also used in the oxygen gasifier (11-12) to gasify oxygen, required for tank pressurization and igniter operation.

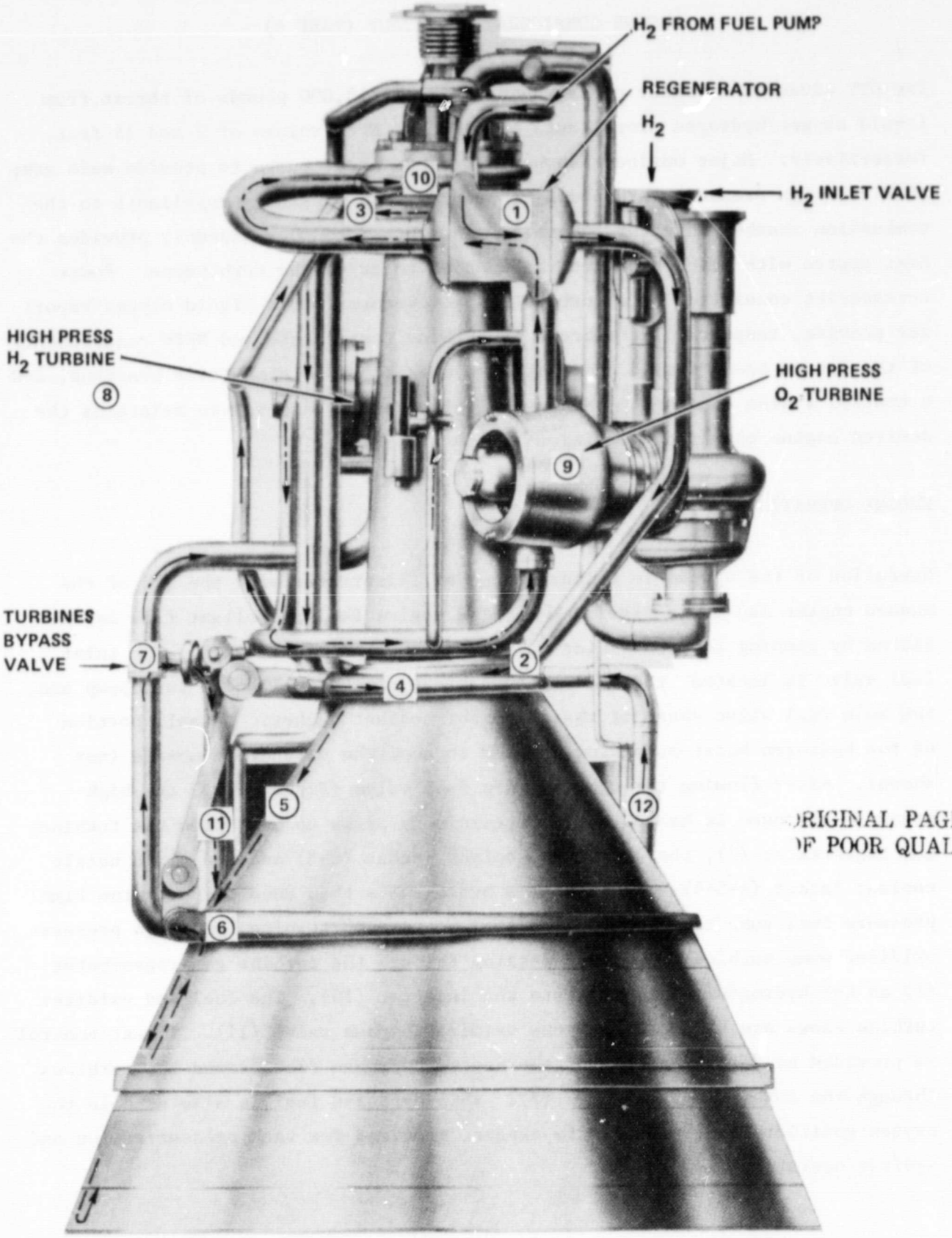

ORIGINAL PAGE IS
OF POOR QUALITY

Figure 6-1. Hydrogen Flow in Advanced Expander Engine Point Design

Liquid oxygen enters the lox boost pump (2) through the fully-opened inlet (1) oxygen valve (Figure 6-2). Boost pump flow elevated to a high pressure in the high pressure lox pump (3) enters the boost pump turbine (4) to provide required torque. Oxygen from the boost pump turbine is directed to the injector through the main and mixture ratio control valve (5). A small portion of the oxygen flow is gasified at the lox heat exchanger (6-7) and routed near the gaseous oxidizer valve (8) to the igniter and tank pressurization check valves. The injector lox and hydrogen flows are combusted at a mixture ratio of 6:1 and expanded to an area ratio of 625:1 through the two piece nozzle. The forward nozzle section is fixed to the combustion chamber, whereas the aft nozzle section is retractable to facilitate the stowing of the vehicle into the Space Shuttle cargo bay.

Ignition of the propellants in the combustion chamber is accomplished with a flame torch igniter. This device utilizes two small redundant spark plugs, each with its own, separate, exciter signal, to ignite a fuel-rich mixture of the propellant gases. Oxidizer gas is supplied from the liquid oxygen gasifier, whereas igniter fuel is bled from the combustion chamber coolant discharge manifold. Each igniter gas stream is controlled by a two position solenoid valve.

An on-board digital controller utilizes instrumentation and vehicle command data to operate the system valves as required to produce the desired engine output. Depending on the operational requirements of each valve, pneumatic solenoid, self-activating, and electric/pneumatic-overide type valve actuators are used.

Besides the nominal conditions of thrust and mixture ratio, the engine is capable through modulation of its four primary control valves of operating at: (1) full thrust with mixture ratio of 7:1; (2) pump-fed idle mode thrust of 1800 and mixture ratio of 4:1; and (3) tank-head idle thrust and mixture ratio. The oxygen heat exchanger provides gaseous oxygen propellant through the gaseous oxidizer valve (8) at tank-head idle with high enough injector pressure drop to ensure combustion stability.

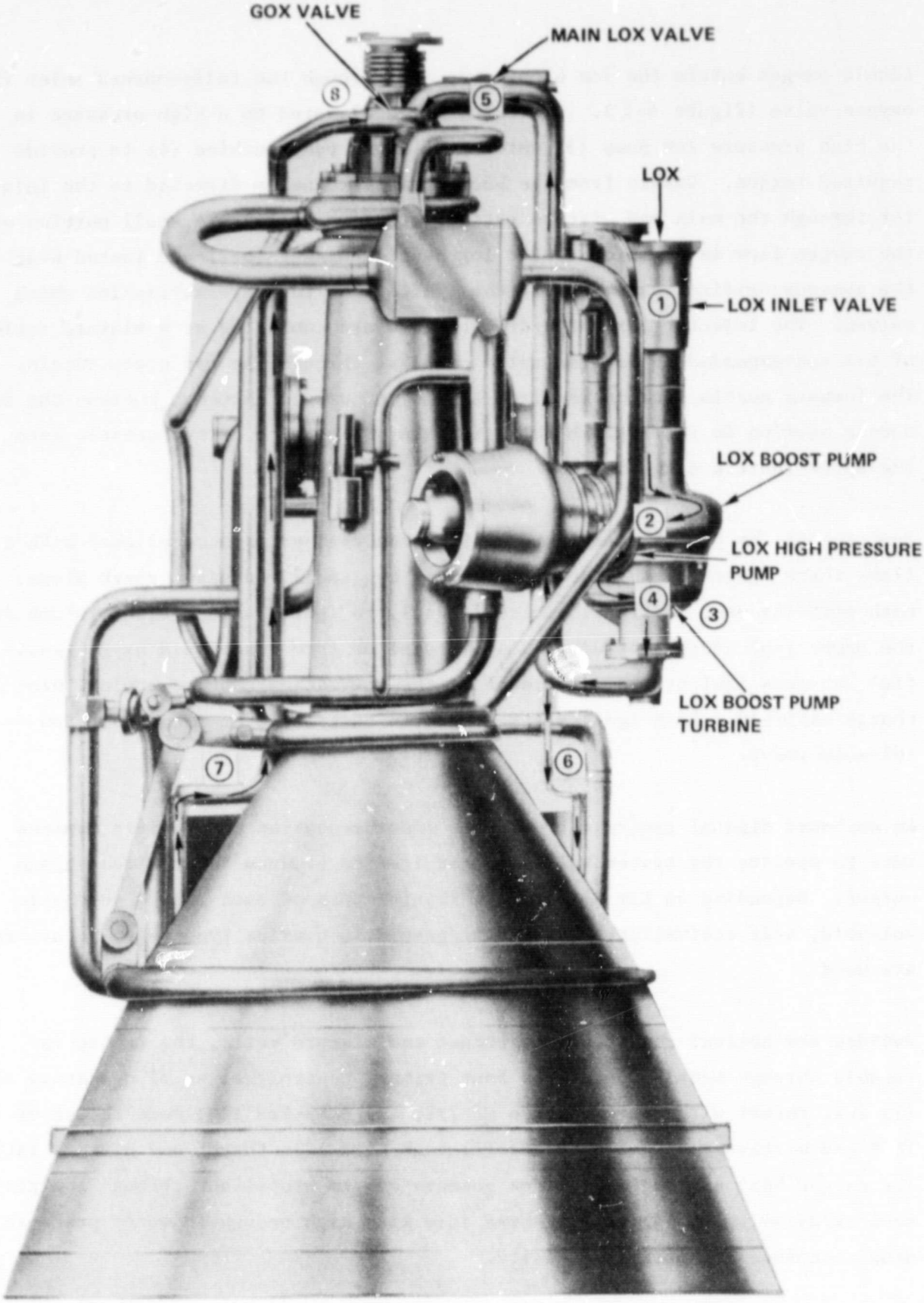

Figure 6-2. Oxygen Flow in Advanced Expander Engine Point Design

ORIGINAL PAGE IS
OF POOR QUALITY

ENGINE ASSEMBLY LAYOUT

The Engine System Assembly and Interface drawing, Figure 6-3, illustrates the component arrangement, component locations, and vehicle interfaces of the OTV expander cycle engine. This layout was developed through consideration of factors such as performance, weight, cost, reliability, and maintainability in addition to meeting all envelope and interface requirements. A prime design philosophy was to duplicate all major Centaur propulsion system fluid and mechanical interfaces, thus providing interchangeability with current LOX/Hydrogen space engines.

Special design considerations are needed for the system ducting. Besides being required to transport the propellants between engine components, most ducts also serve to support components. Large temperature differences between some components also necessitate special care to minimize thermal stresses in the interconnecting ducts. For completeness, the final design must include a dynamic stress analysis of the entire system which will include these factors. Preliminary design of the major propellant ducting is shown in Table 6-1. The ducting was sized to be of minimum weight and size while still maintaining acceptable velocities and pressure drops under all engine operating modes. Material selection is based on factors such as high strength, weldability, and hydrogen embrittlement resistance.

The propellant inlet valve forward flanges constitute the engine/vehicle propellant interface plane. These valves are required to shut off all propellant flow to the engine when not in operation. Although not included as part of the engine layout in Figure 6-3, propellant feed ducting compatible with the inlet and gimbaling requirements has been designed and is discussed in a separate section. It is highly desirable to include the propellant feed ducting with the engine because the feed system must also satisfy pump inlet loading and flow directional requirements. For example, turning vanes in the elbows just upstream of the inlet valves are often required to improve pump inducer performance.

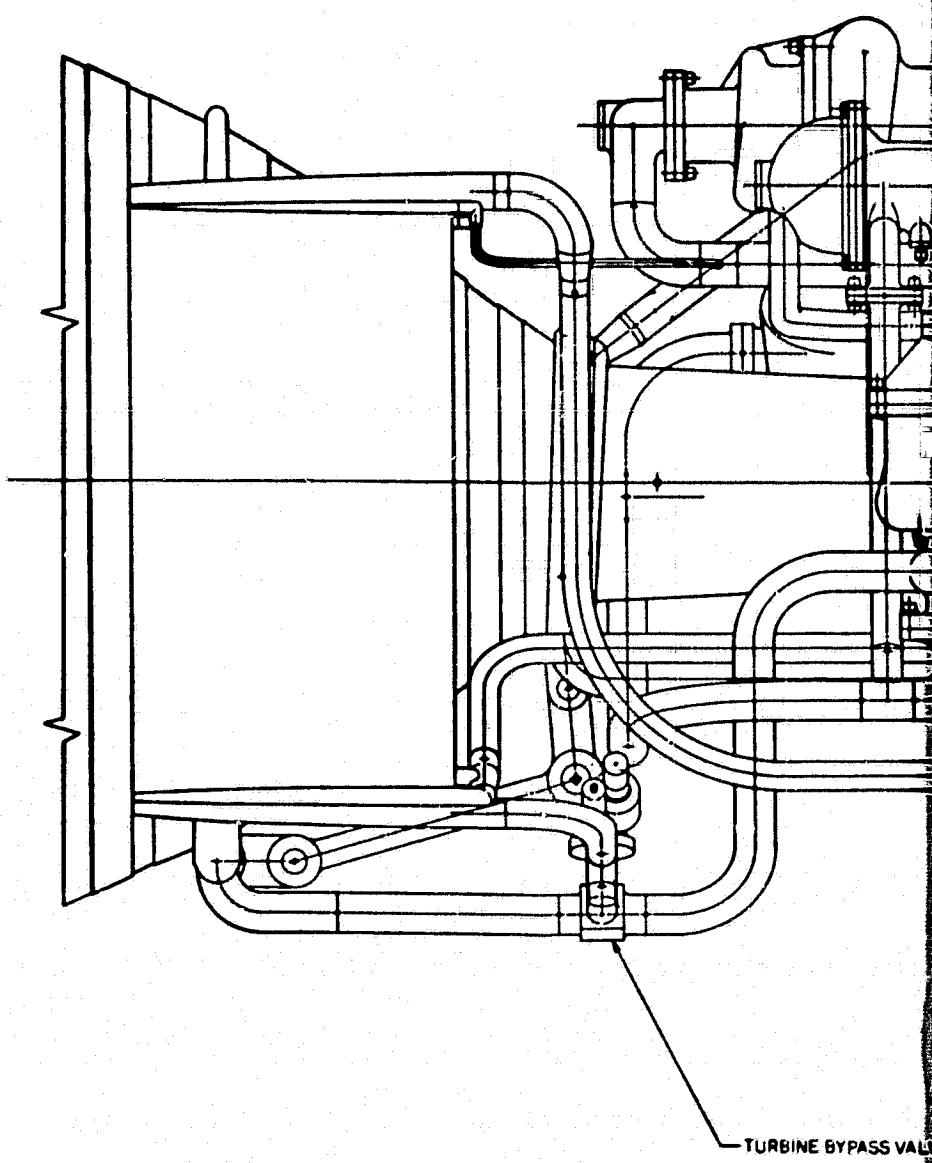

ORIGINAL PAGE IS
OF POOR QUALITY

FOLDOUT FRAME

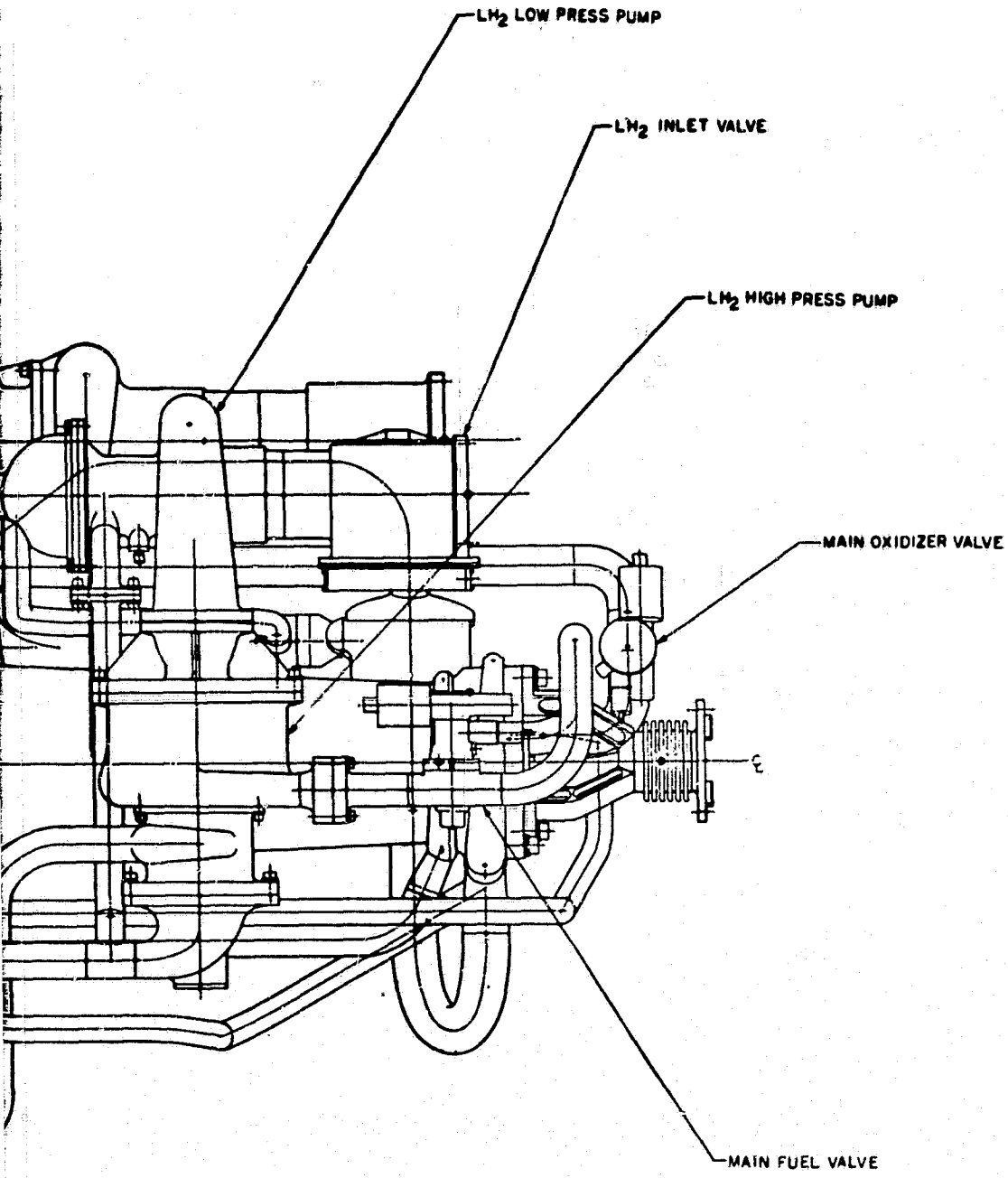

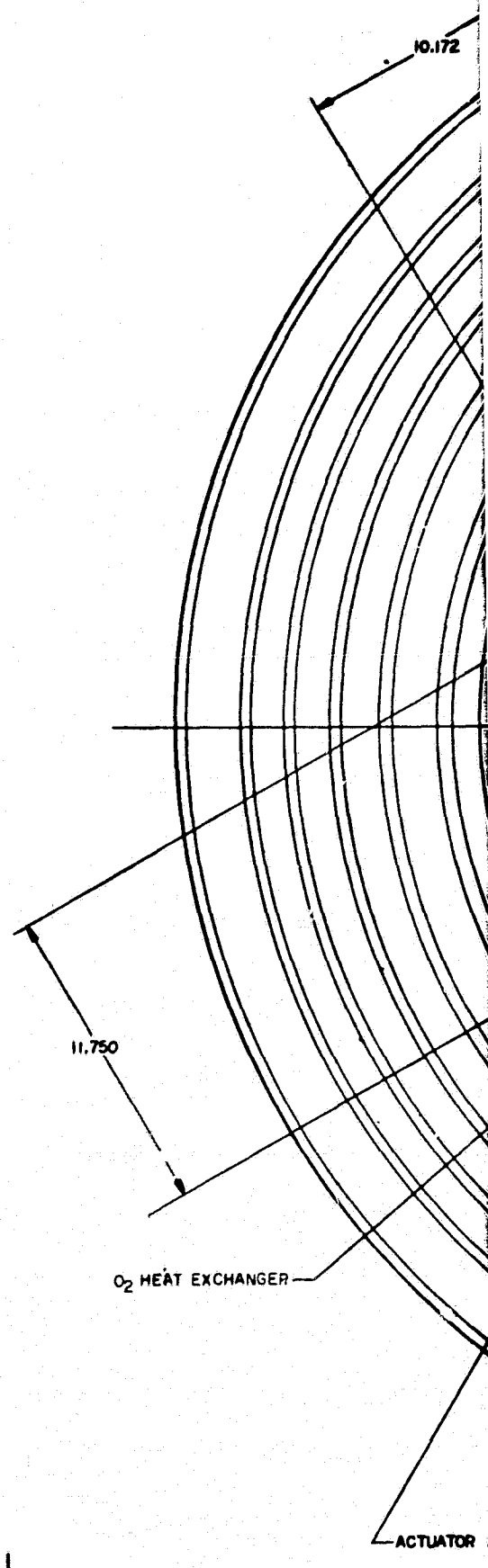

RBINE BYPASS VALVE

FOLDOUT FRAME 2

7R0014400

MICROFILM OVERLAP

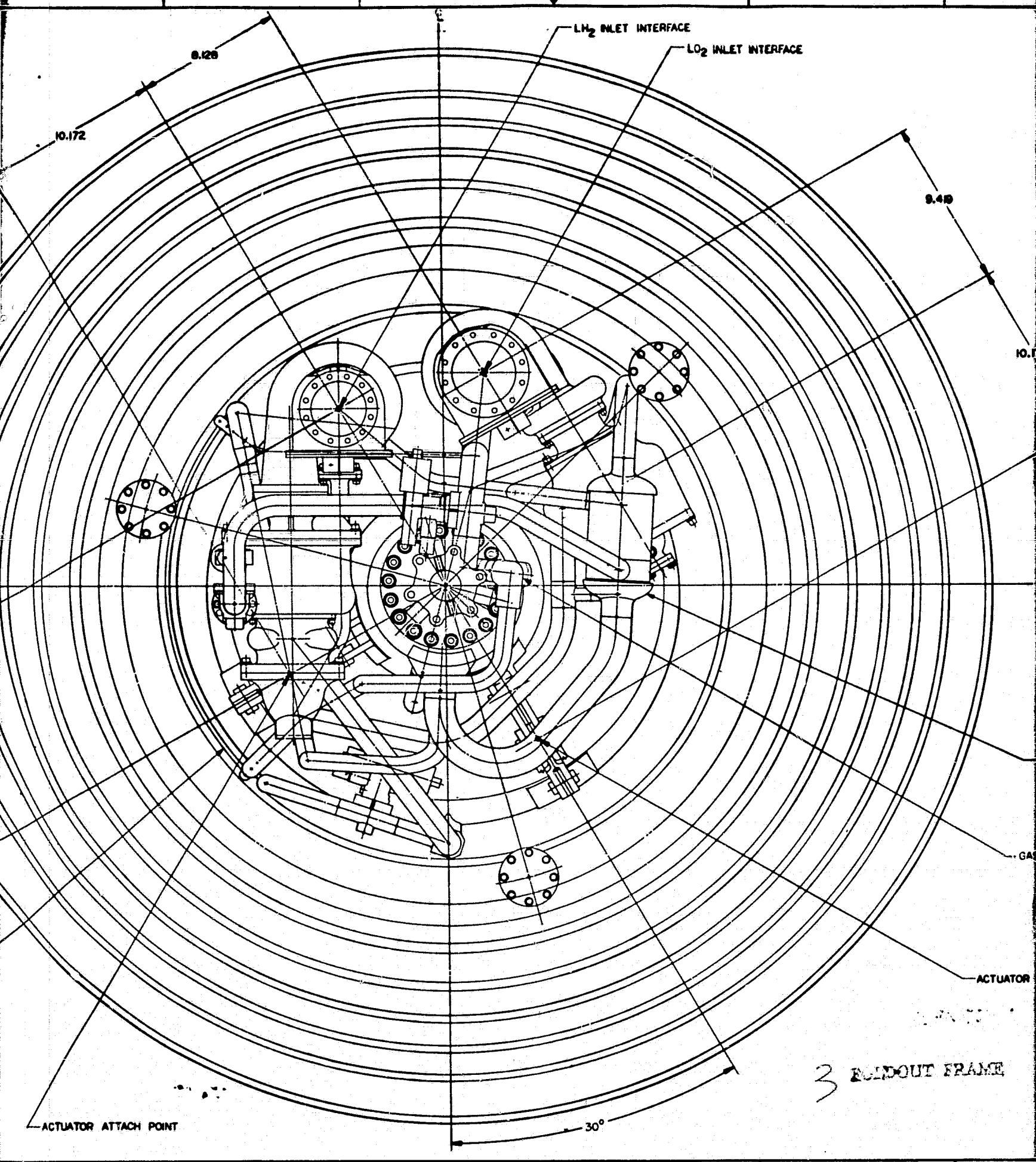

3 FOLDOUT FRAME

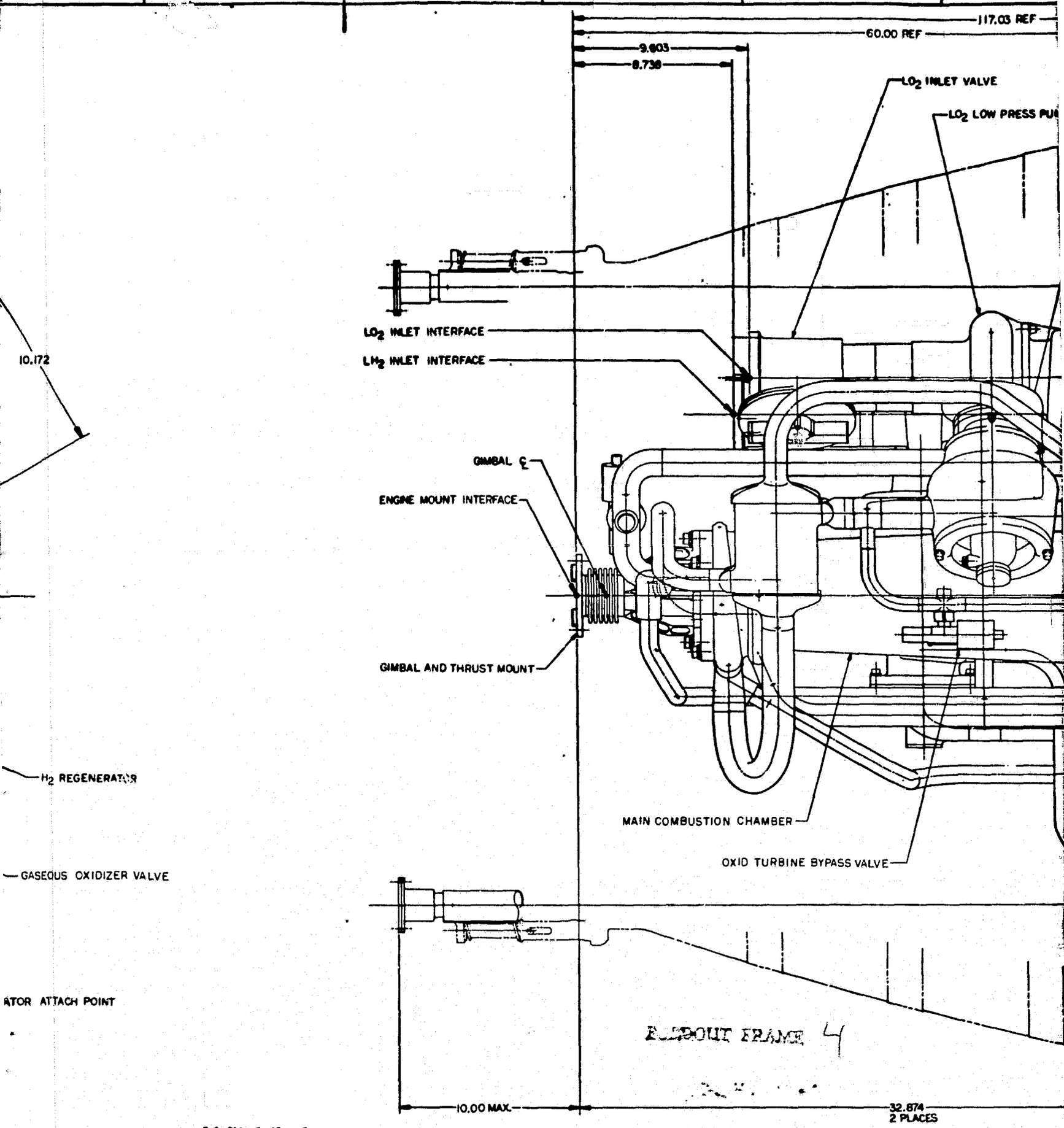

FOLDOUT FRAME 4

Rockwell International Corporation
Rocketdyne Division
Canoga Park, California

FORM NO 02662	FRAME 1		
7R0014400		SH —	REV

MICROFILM OVERLAP AREA

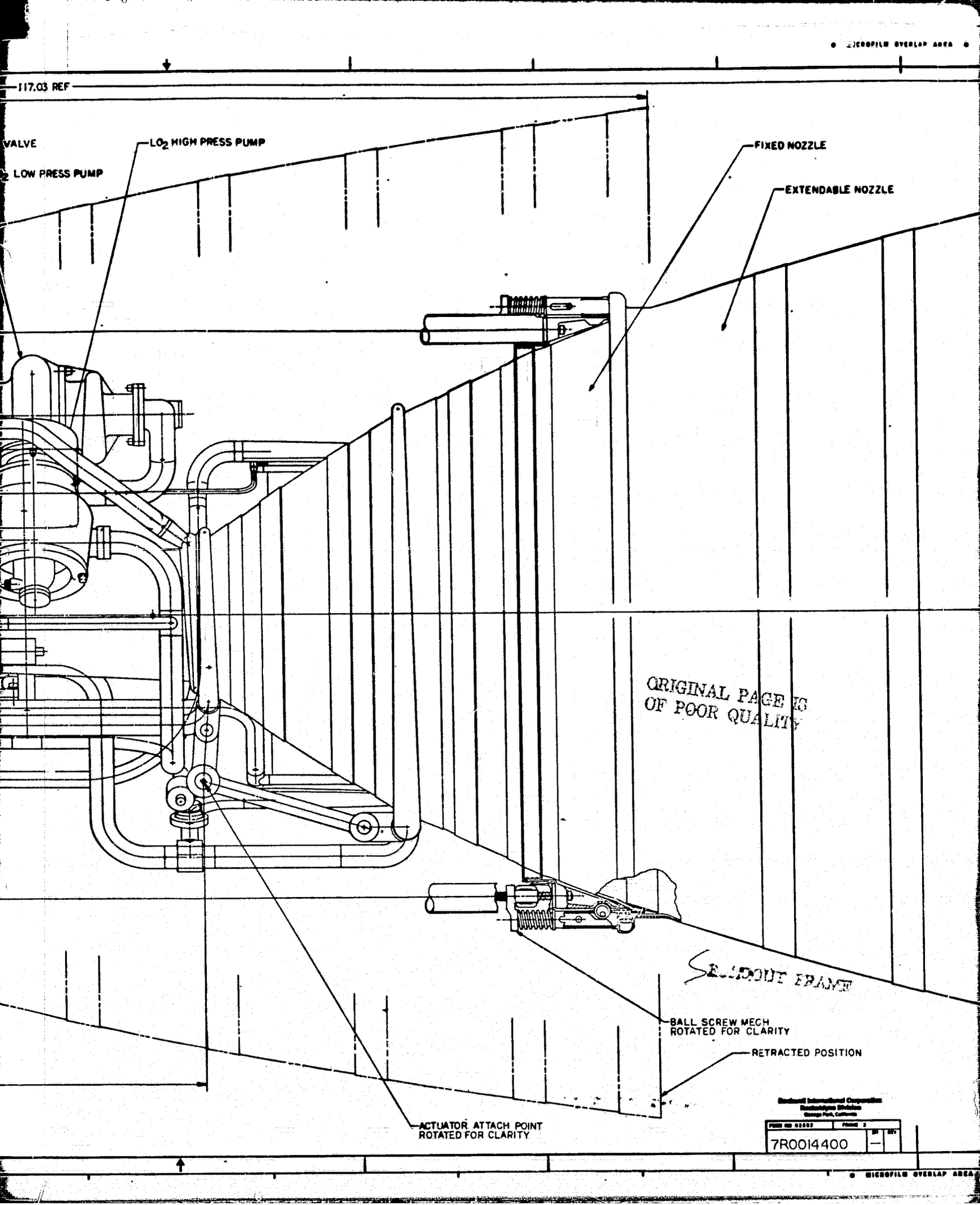

MICROFILM OVERLAP AREA
117.03 REF
VALVE
LO_2 HIGH PRESS PUMP
$_2$ LOW PRESS PUMP
FIXED NOZZLE
EXTENDABLE NOZZLE
ORIGINAL PAGE IS OF POOR QUALITY
SEE ABOUT FRAME
BALL SCREW MECH ROTATED FOR CLARITY
RETRACTED POSITION
ACTUATOR ATTACH POINT ROTATED FOR CLARITY
7R0014400
MICROFILM OVERLAP AREA

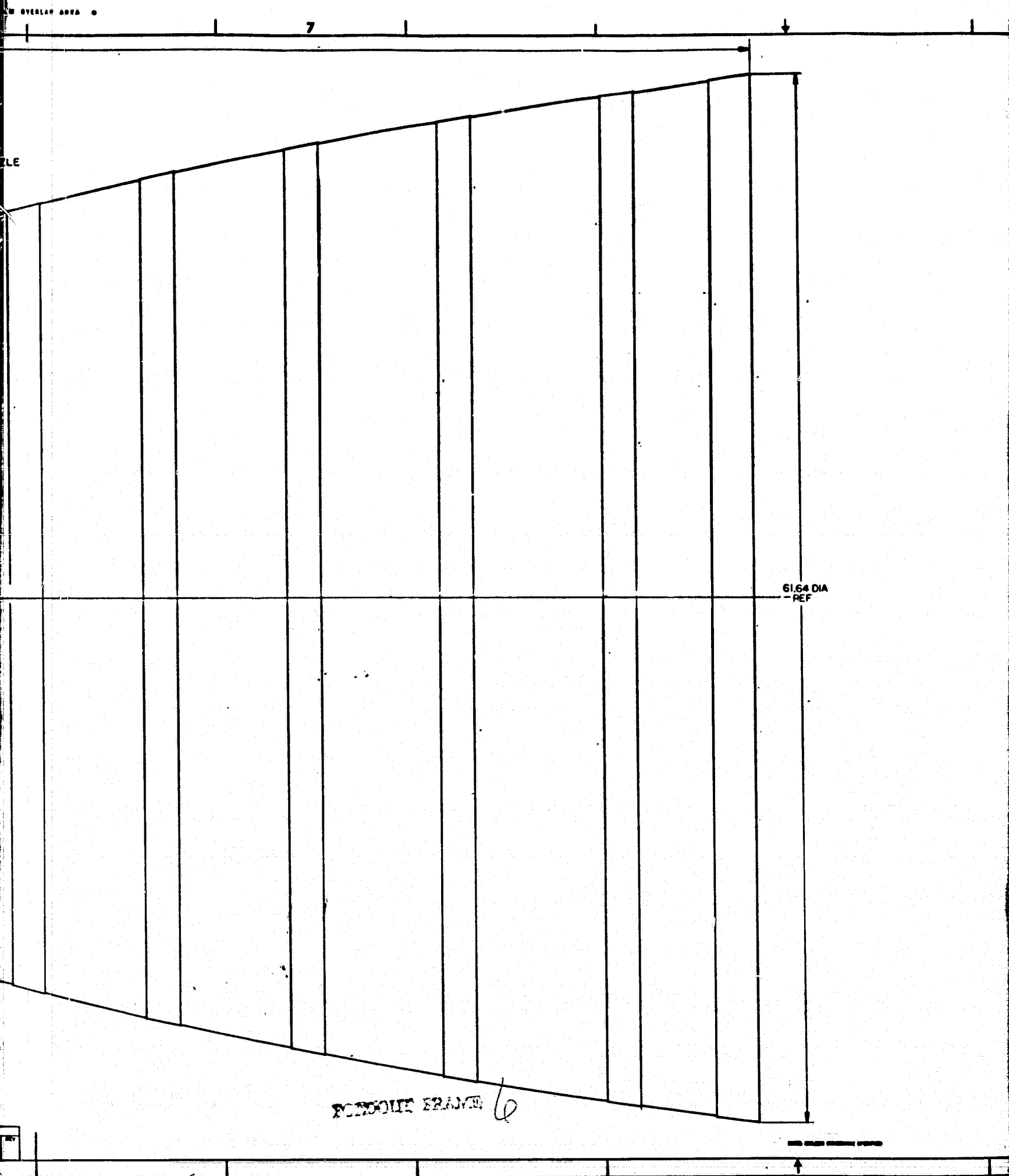

OVERLAP AREA
7
ZLE
61.64 DIA
REF
FOLDOUT FRAME 6
FILM OVERLAP AREA

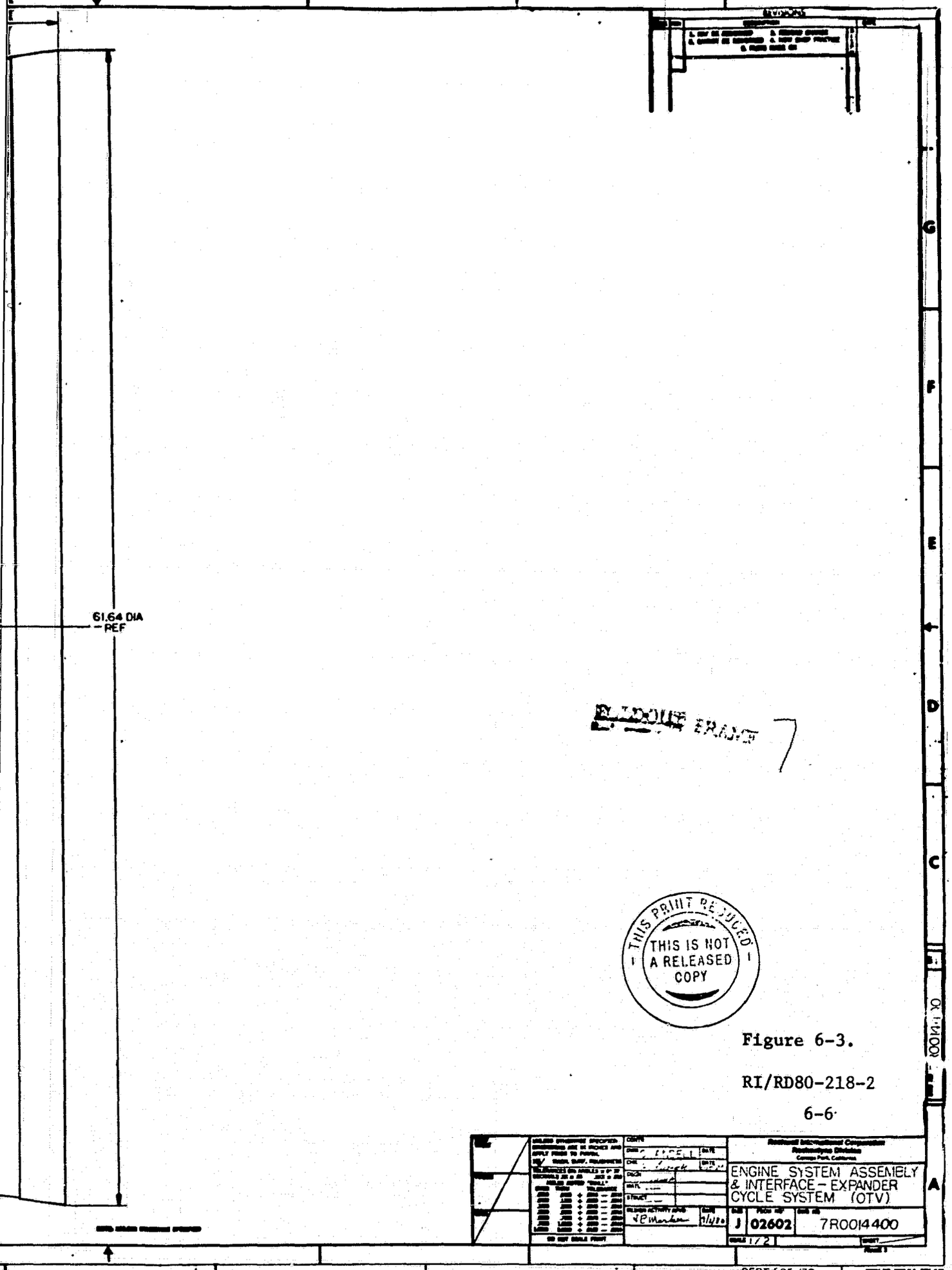

Figure 6-3.

DEPT 585-139
EXP. DESIGN

TABLE 6-1. PRELIMINARY OTV DUCTING DESIGN

FLUID	DUCT ROUTING	MATERIAL	O.D. (in.)	WALL (in.)	VELOCITY @ MR = 6 (ft/sec)
LH_2	Ext. Noz. Cool. Inlet	Flex Hose	.500	--	47
LH_2	Fuel Pump to Regen.	Inconel 718	1.000	.020	184
LH_2	Regen. to MCC Collant	Inconel 718	1.000	.020	314
GH_2	MCC Cool. to Noz. Cool.	Incoloy 903	1.250	.028	555
GH_2	Noz. Cool. to H.P. Fuel Turb.	Incoloy 903	1.250	.028	703
GH_2	Lox Gasifier Inlet	Incoloy 903	1.000	.028	112 (646 @ THI)
GH_2	H.P. Fuel Turb. to H.P. O_2 Turb.	Incoloy 903	1.375	.020	560
GH_2	L.P. Fuel Turb. Inlet	Incoloy 903	.625	.020	514
GH_2	O_2 Turb. Bypass	Incoloy 903	.625	.020	482
GH_2	L.P. Fuel Turb. to Regen.	Incoloy 903	.625	.020	612
GH_2	Regen. to Injector	Incoloy 903	1.750	.020	545
GH_2	Lox Gasifier to Ins.	Incoloy 903	1.000	.020	204 (729 @ THI)
Lox	Oxid. Pump to Ins.	Inconel 718	1.250	.020	47
Lox	LOX Gasifier Inlet	Inconel 625	.250	.020	14
GOX	LOX Gasifier to Inj.	Inconel 718	1.000	.020	2 (128 @ THI)

propellant inlet valves to ensure maximum pump performance. Placing the pumps further aft would have the undesirable effect of increasing the gimbaling moment. Location of the center of gravity was the primary reason for placing the pumps on opposite sides of the combustor. Each T-mounted pump consists of separate boost and high pressure turbopumps, but the T-mount design eliminates the ducting and associated joints required between them. This results in less weight, lower hydraulic losses, reduction in insulation requirements, higher reliability, and simple packaging.

The location of other system components was determined by the location of the pumps and thrust chamber assembly, a design effort to minimize duct routing, center of gravity and maintenance accessibility considerations, and the necessity to allow clearance with the retracted extendible nozzle. Welded joints are used to the extent possible in order to reduce weight and possible leak paths. Bolted flanged joints with seals will be used only to facilitate the removal of components when welding is not suitable. It is important to note that the valve bodies will be welded to the interconnect ducting; but, because the valve mechanism may still be easily removed, the valves may be considered to be line replaceable. Other components can become line replaceable by utilizing bolted flange joints in place of the appropriate welded joints and accepting a small weight penalty.

The turbine gas regenerator is located near the high pressure oxidizer pump turbine discharge in order to minimize system ducting without imposing excessive thermal loads. The regenerator may deflect with the oxidizer turbine housing, yet the ducting design permits independent thermal expansions in the fuel pump and the injector.

The liquid oxygen gasifier is of a curved flat plate design to permit it to be packaged next to the fixed nozzle, where it does not hamper the maintenance of other components. Ducting may also be easily routed to the gasifier when located in this position.

The gimbal/thrust mount assembly, Fig. 6-4 transmits all of the engine thrust to the vehicle and permits gimballing of the engine to the required 6° in three directions and +15° in pitch. The gimbal consists of a simple spherical bearing which used a teflon fabric liner between the races to reduce friction. The bellows around the gimbal provide torsional rigidity and protects the bearing from contaminants. A flange provided at the forward end of the gimbal is the vehicle attachment. The aft portion of the thrust mount is attached to the thrust chamber with bolts also used to secure the injector. Adequate clearance is provided inside the thrust mount for removal of the igniter and spark plugs.

The gimballing actuator attach points duplicate current Centaur Vehicle engine attach points. The attachment links are designed so as to permit expansion of the nozzle.

The engine nozzle consists of a fixed section and an extendible/retractable section in order to provide additional thrust without exceeding the permissible engine stowed length. Rocketdyne in-house studies have investigated the nature of the required nozzle extension mechanism by considering a variety of transport devices and by developing a unique latching method that also carries all thrust loads. These studies identified a triple ballscrew transport mechanism as satisfying all of the operational requirements in the most reliable, efficient manner. The nozzle extension mechanism is included in the Engine System Assembly and Interface Drawing, Fig. 6-3. Each ballscrew is encapsulated in a C-shaped Inconel 718 tube along its entire length. Teflon rings on the ballscrew nuts ride on the inner surface of the tubes. Retention of the ballscrews at each end is such that column loading is never incurred. These features provide a lightweight means of satisfying ballscrew ridity requirements because the ballscrew and nut size may be minimized. The ballscrews are rotated by a single D. C. motor with provisions for a manual override. The motor is located at the forward end of one ballscrew, with torque-tubes driving the other two screws. All three ballscrews are, except for mechanical tolerances, properly synchronized, providing correct alignment of the extendible nozzle at all times. Limit switches at the aft end of each transport

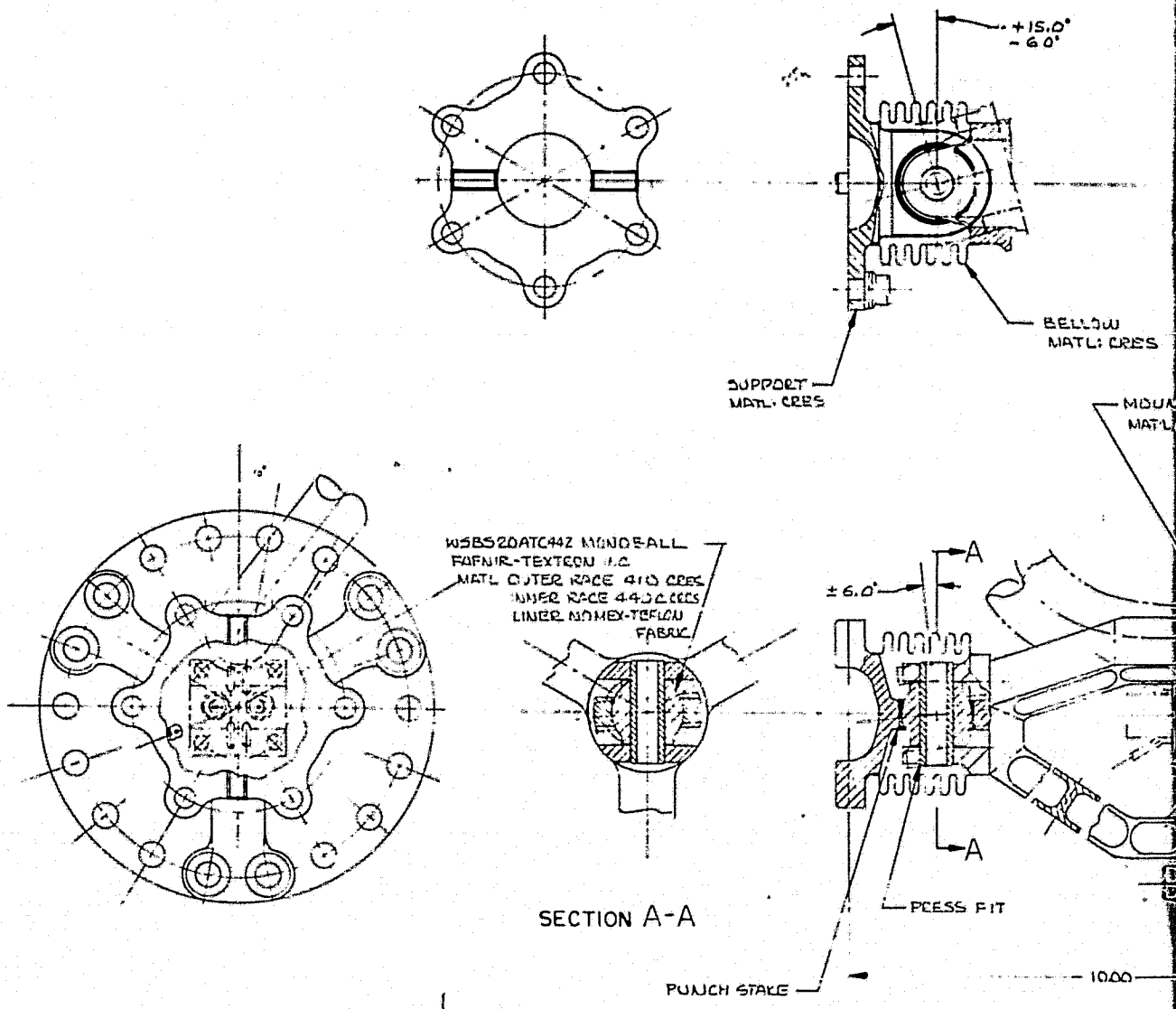

FOLDOUT FRAME

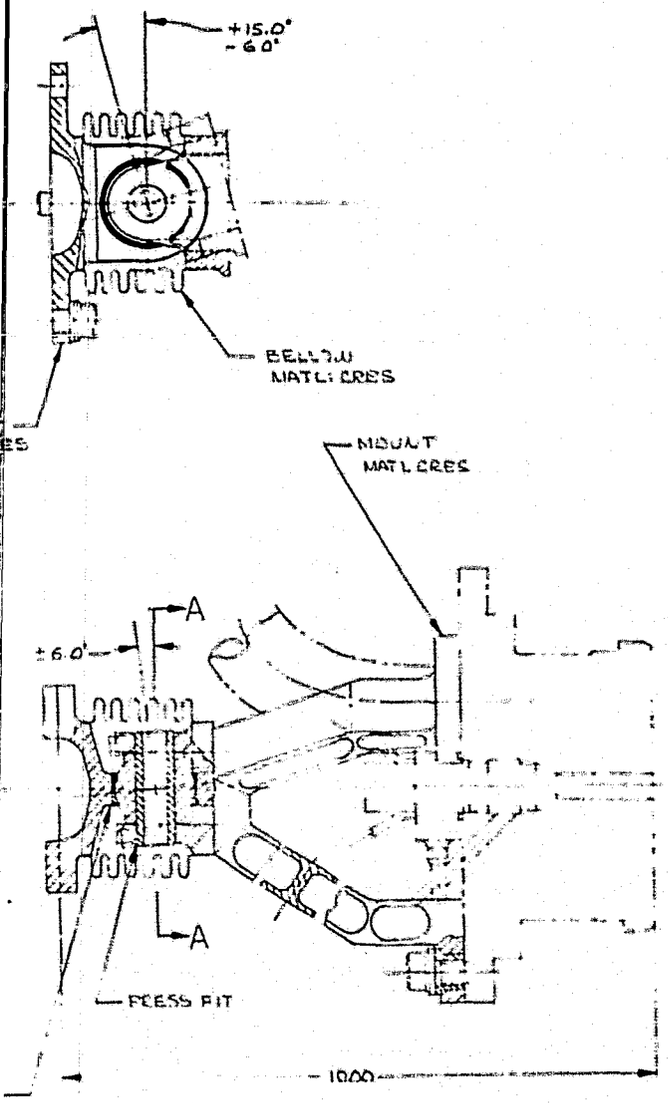

FOLDOUT FRAME 2

Figure 6-4.

INFORMATION COPY

Rockwell International Corporation
Rocketdyne Division
Canoga Park, California

V/B-L THRUST MOUNT LAYOUT

E 02602

screw indicate the locking of each latch and shut off the motor. A single switch at the forward end initiates motor shutoff during retraction.

The latching mechanism, Fig. 6-5 is simple and lightweight, yet it provides for both positive self-locking and self-unlocking, accommodation of transport mechanism tolerance, and the transmittal of the thrust loads from the extendible nozzle to the fixed nozzle. In the extension made, the three ballscrews rotate and cause the extendible nozzle to translate aft until a positioning lip is engaged, sealing the joint. Although the nozzle stops, the screws continue to rotate and the latching mechanisms continue to move aft; collapsing the transport springs and moving the cam-ramps along the locking cylinders. This forces the cylinders into the "V" grooves located in the fixed nozzle, thereby affecting a firm retention and reaction path for the extendible nozzle. The cam-ramps flatten out after engagement so that the accumulation of tolerances in the drive system may be accommodated. To retract the nozzle, the rotation of the ballscrews is reversed. As the latches move forward, the pins pressed into the cam-ramps engage the forward end of the slots located in the latch housings and the locking cylinders are forced out of the "V" grooves as the nozzle translates back into its stowed position.

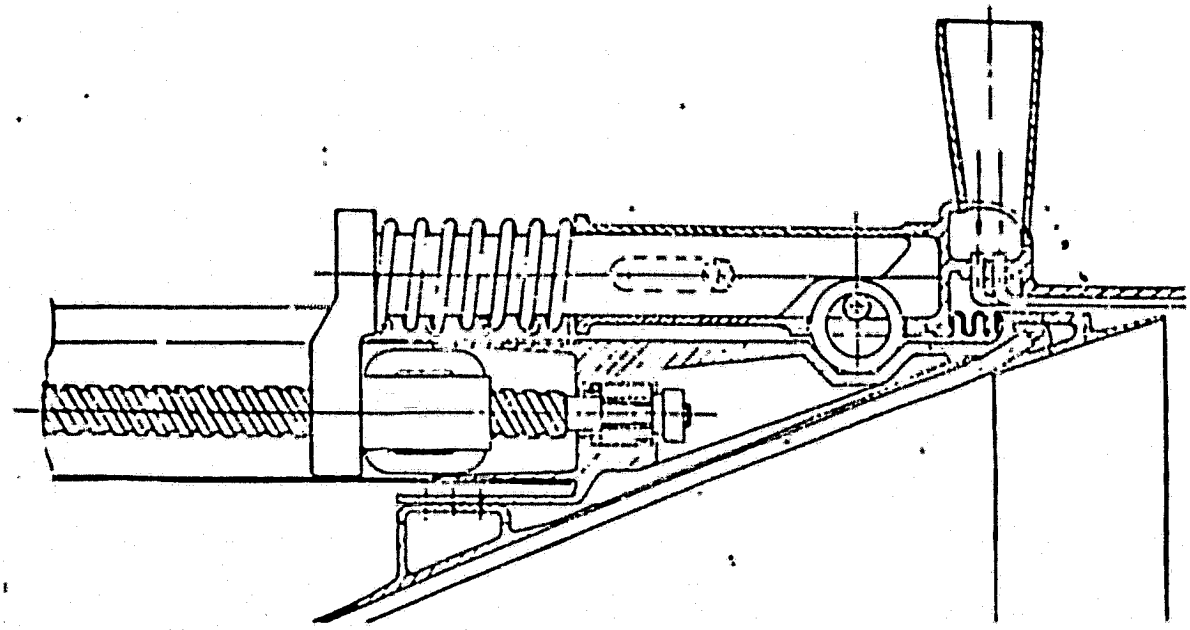

a) LATCHED

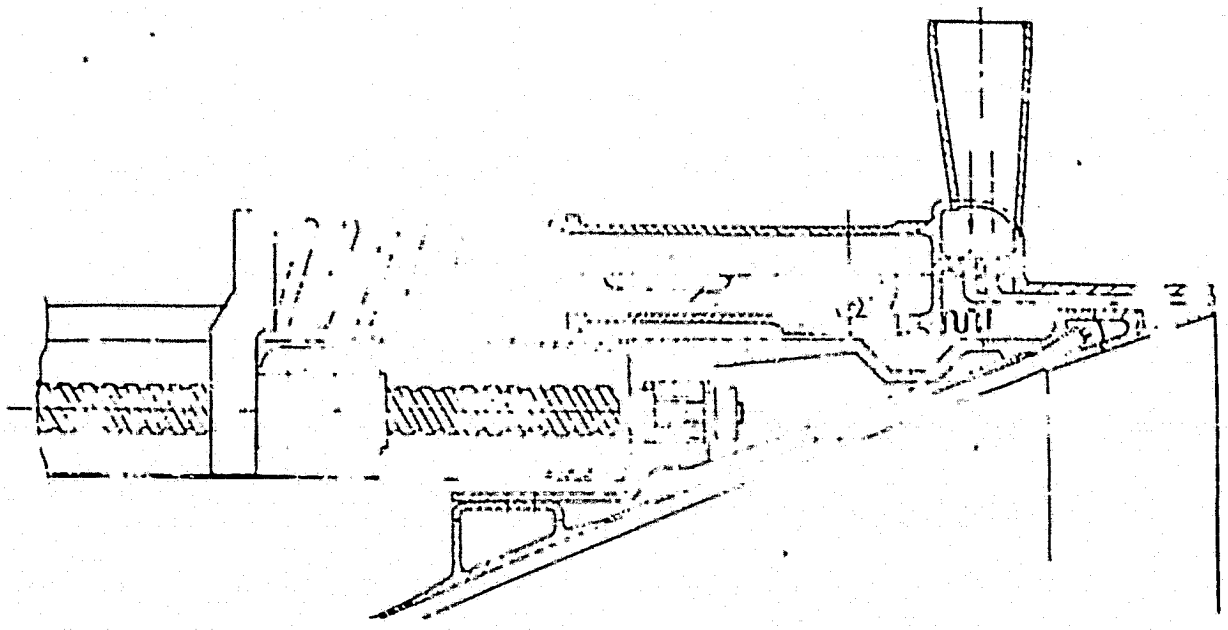

b) UNLATCHED

Figure 6-5. Latching Mechanism Details

ORIGINAL PAGE IS
OF POOR QUALITY

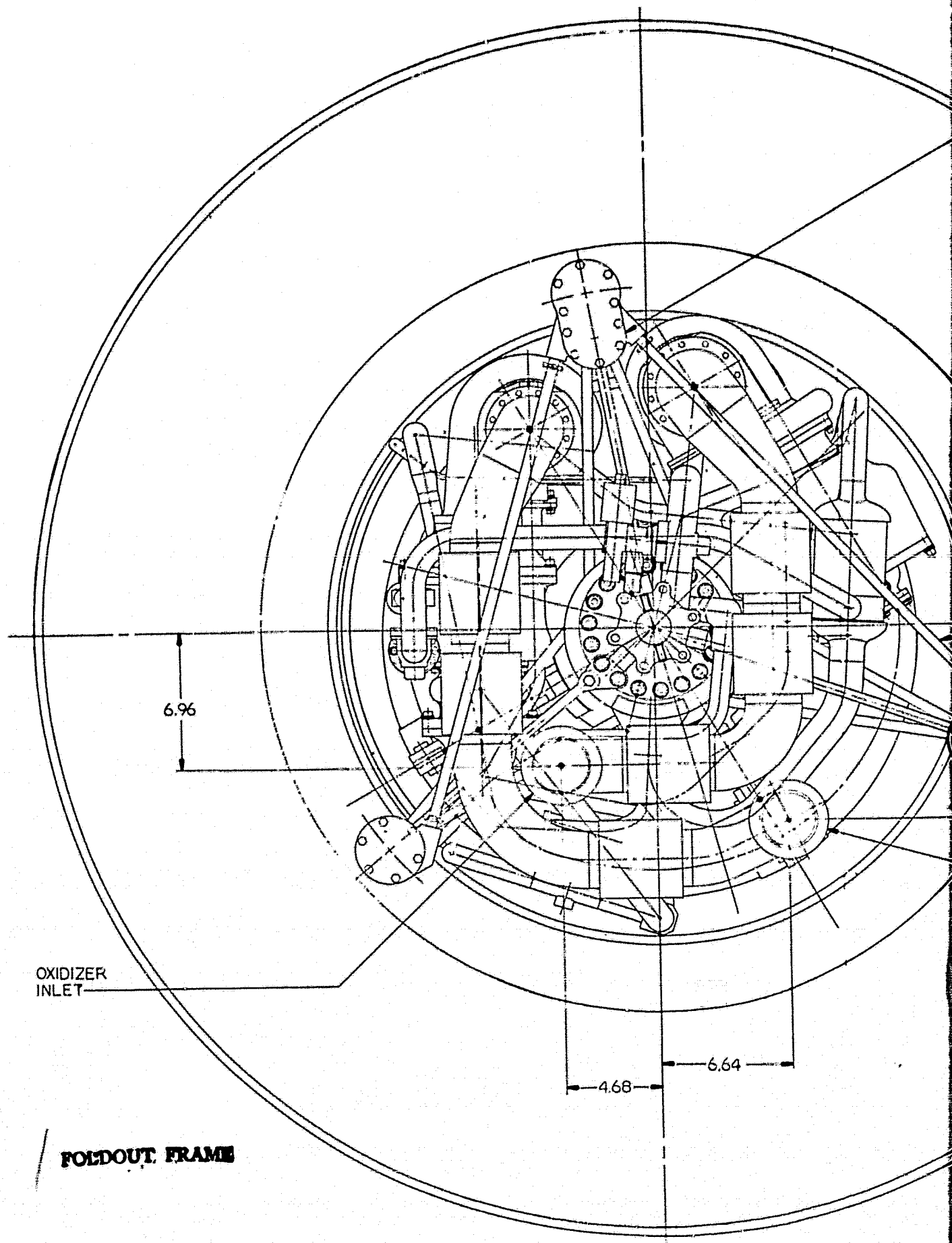

FOLDOUT FRAME

MICROFILM OVERLAP AREA

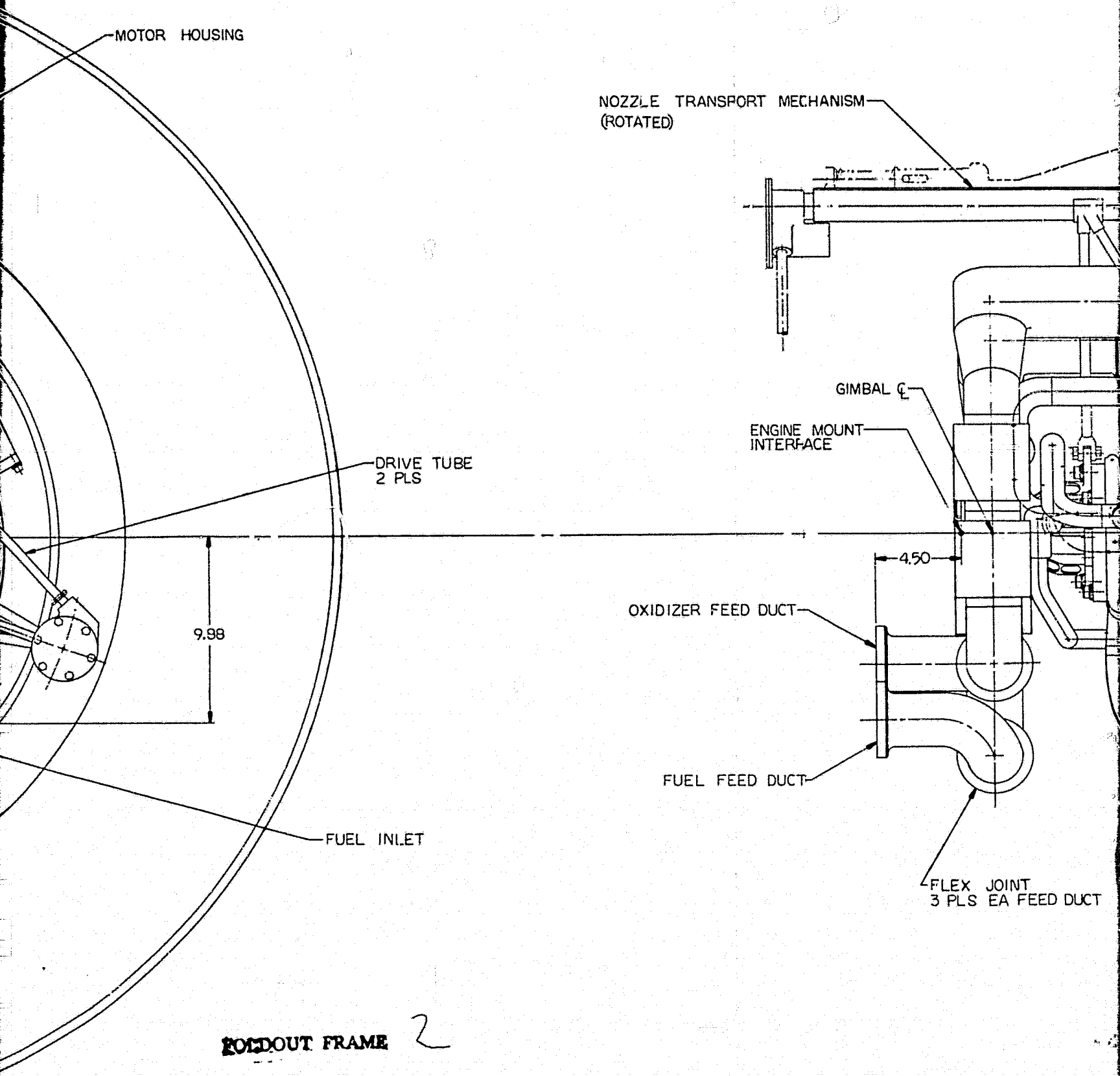

FOLDOUT FRAME 2

Rockwell International Corporation
Rocketdyne Division
Canoga Park, California
FSCM NO 07692 | FRAME 1 | SH | REV

MICROFILM OVERLAP AREA

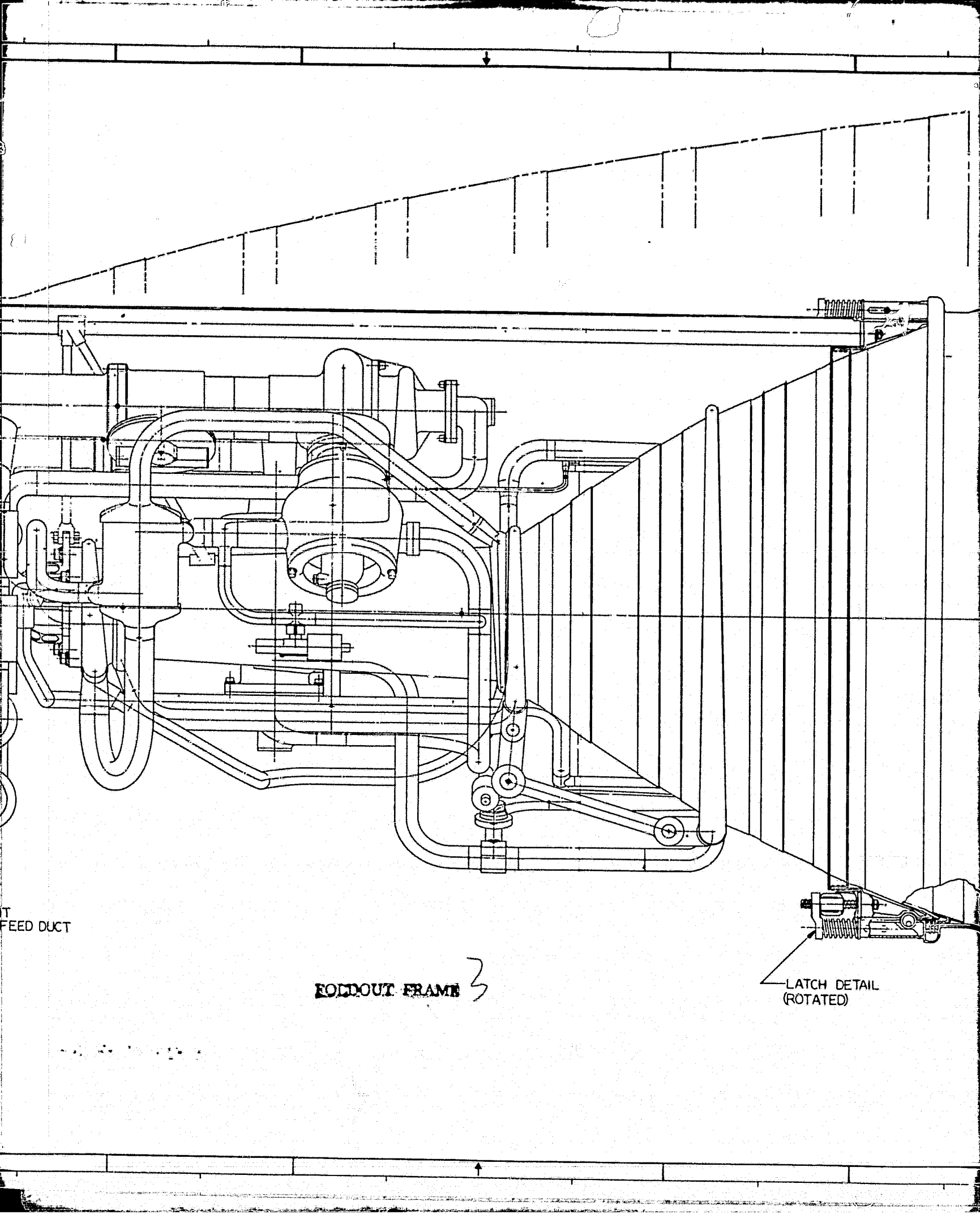

FOLDOUT FRAME 3

MICROFILM OVERLAP AREA

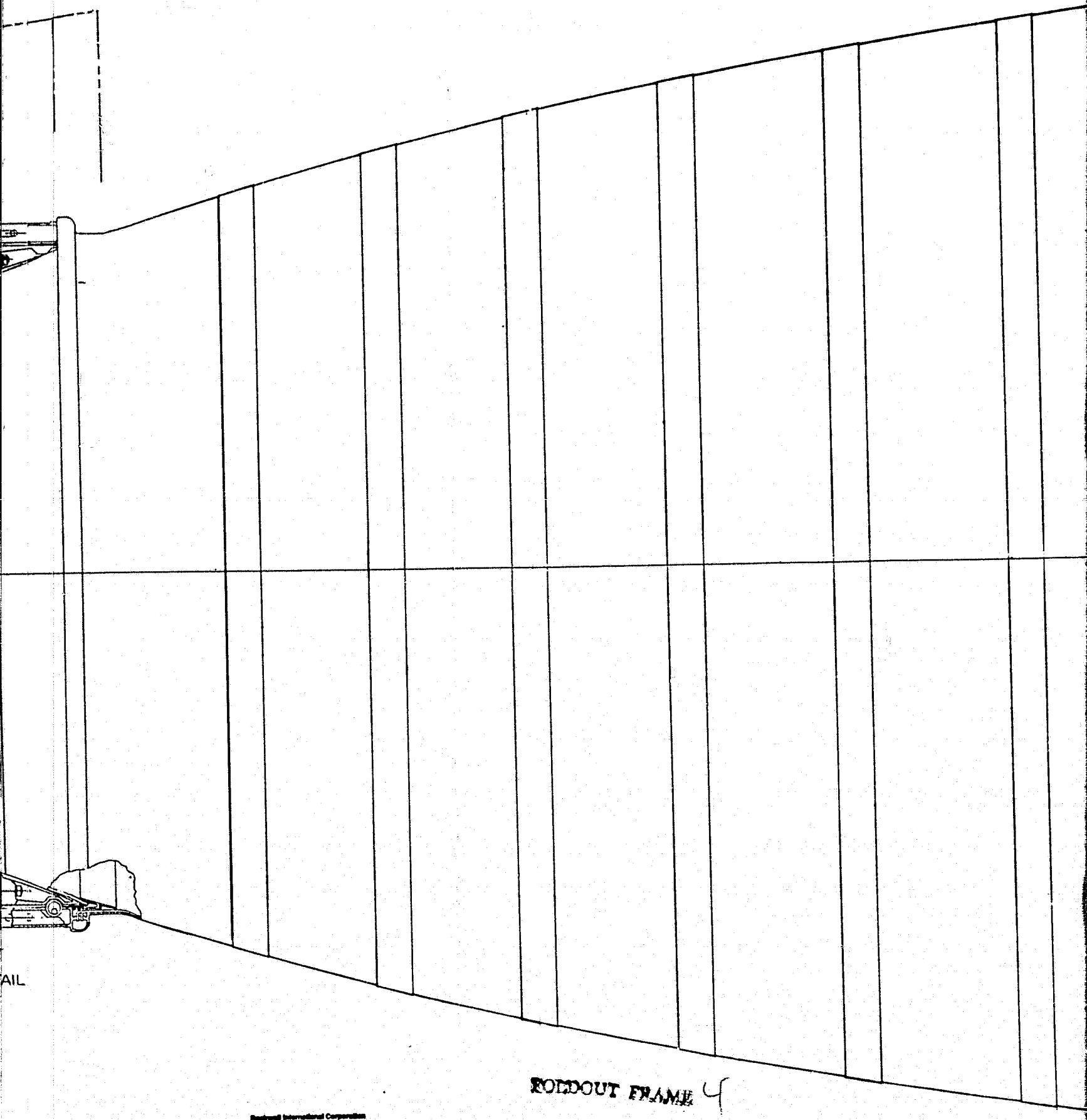

FOLDOUT FRAME 4

Rockwell International Corporation
Rocketdyne Division
Canoga Park, California

FSCM NO. 82693	FRAME 2		
		SH	REV

MICROFILM OVERLAP AREA

REVISIONS

Figure 6-6

FOLDOUT FRAME 5

THIS PRINT REDUCED
THIS IS NOT A RELEASED COPY

Rockwell International Corporation
Rocketdyne Division
Canoga Park, California

ENGINE SYSTEM
INSTALLATION-EXPANDER
CYCLE SYSTEM (CTV)

J 02602 7R0014399

DO NOT SCALE PRINT

ENGINE DATA SUMMARY (TASK 7)

In Task 7, thrust and mixture ratio for a low thrust operating point were defined and NASA's concurrence obtained. Mass and power balances were developed for all four of the required engine thrust and mixture ratio operating levels: full thrust (15K), off-design mixture ratio (7:1), pumped-idle mode, and tank-head idle mode. Performance predictions were prepared for both the high and the low thrust operating conditions at their respective mixture ratios , using simplified JANNAF performance methodology. The method employed to develop predicted performance has been substantiated by test data and comparison with rigorous standard computer codes. In similar manner, life performance prediction was performed for the high thrust and low thrust operating levels at their respective mixture ratios.

Engine component weights were determined from design drawings and layouts. A tabulation of individual weights is presented in this section, as well as engine overall weight and other mass property data, center of gravity moment of inertia.

Engine layouts and packaging studies provided inputs to define engine dimensions and envelope. Vehicle geometrical interfaces were also defined and are presented in this section.

Pump NPSH requirements were assessed and recommendations for achieving lower inlet NPSH values than nominal are made.

MAINSTAGE OPERATION

The design operating point is at a thrust level of 15,000 lb. and an engine mixture ratio of 6.0. The system flowrates, pressures, and temperatures are defined by steady-state engine balances performed during configuration definition and selection. Table 7-1 and Figure 7-1 display a summary of mainstage operation.

TABLE 7-1. ENGINE DESIGN POINT BALANCE

Design Variables	MR = 6 Value
General	
Thrust, lbf	15,000
Chamber Pressure, psia	1,540
Mixture Ratio, Engine	6.0
Mixture Ratio, Thrust Chamber	6.59
Specific Impulse (Engine) seconds	480.8
Specific Impulse (Thrust Chamber), seconds	481.3
Engine Fuel Flowrate, lb/sec	4.48 (1)
Thrust Chamber Fuel Flowrate, lb/sec	4.05
Engine Oxidizer Flowrate, lb/sec	26.88 (2)
Thrust Chamber Oxidizer Flowrate, lb/sec	26.71
Dump Coolant Fuel Flowrate, lb/sec	0.36
Turbomachinery	
Low-Pressure Oxidizer Pump Speed, rpm	6,475
Low-Pressure Oxidizer Pump Efficiency	0.692
Low-Pressure Oxidizer Pump Horsepower	10.09
Low-Pressure Oxidizer Pump Inlet Pressure	16.3
Low-Pressure Oxidizer Pump Outlet Pressure	86.3
Low-Pressure Oxidizer Pump Diameter, inches	3.60
Low-Pressure Fuel Pump Speed, rpm	28,486
Low-Pressure Fuel Pump Efficiency	0.731
Low-Pressure Fuel Pump Horsepower	20.01
Low-Pressure Fuel Pump Inlet Pressure, psia	18.8
Low-Pressure Fuel Pump Outlet Pressure, psia	73.8
Low-Pressure Fuel Pump Diameter, inches	3.14

(1) Includes 0.034 lb/sec pressurization flow
(2) Includes 0.134 lb/sec pressurization flow

TABLE 7-1. ENGINE DESIGN POINT BALANCE (Cont)

Design Variables	MR - 6 Value
General - Turbomachinery (cont)	
High-Pressure Oxidizer Pump Speed, rpm	52,837
High-Pressure Oxidizer Pump Efficiency	0.666
High-Pressure Oxidizer Pump Horsepower	384
High-Pressure Oxidizer Pump Outlet Pressure, psia	2,649
High-Pressure Oxidizer Pump Diameter, inches	2.55
High-Pressure Fuel Pump Speed, rpm	110,000
High-Pressure Fuel Pump Efficiency	0.635
High-Pressure Fuel Pump Horsepower	1,586
High-Pressure Fuel Pump Outlet Pressure, psia	4,671
High-Pressure Fuel Pump Diameter, inches	3.80
High-Pressure Oxidizer Turbine Diameter, inches	4.85
High-Pressure Oxidizer Turbine Flowrate, lb/sec	2.99
High-Pressure Oxidizer Turbine Admission, %	24.5
High-Pressure Oxidizer Turbine Tip Speed, ft/sec	1,188
High-Pressure Oxidizer Turbine Velocity Ratio	0.44
High-Pressure Oxidizer Turbine Efficiency	0.629
High-Pressure Oxidizer Turbine Pressure Ratio	1.21
High-Pressure Fuel Turbine Diameter, inches	3.00
High-Pressure Fuel Turbine Flowrate, lb/sec	3.65
High-Pressure Fuel Turbine Admission, %	33
High-Pressure Fuel Turbine Tip Speed, ft/sec	1,604
High-Pressure Fuel Turbine Velocity Ratio	0.48
High-Pressure Fuel Turbine Efficiency	0.636
High-Pressure Fuel Turbine Pressure Ratio	1.72

TABLE 7-1. ENGINE DESIGN POINT BALANCE (Concl.)

Design Variables	MR = 6 Value
Cooling Jacket	
Combustor Coolant Flowrate, lb/sec	4.09
Combustor Coolant Pressure Drop, psid	320
Combustor Heat Input, Btu/sec	7,445
Combustor Exit Temperature, R	696
Nozzle Coolant Flowrate, lb/sec	4.09
Nozzle Heat Input, Btu/sec	2,537
Nozzle Exit Temperature, R	872

At mainstage, all valves are at their defined design position. Table 7-2 summarizes valve position, resistance, flowrate, and pressure drop at the design operating point.

The design chamber pressure is 1540 psia. The thrust chamber, with a throat area of 4.697 square inches, develops 14,807 lb of thrust. The remaining 193 lb. of thrust is developed by the nozzle extension dump coolant.

Component Pressure Drop Allocation

Baseline component pressure drops for OTV engines were defined during the Phase A studies (NAS8-32996) and were refined in the Phase A Extension Component Drops defined including injectors, orifice, and valves. Injector drops were selected based on sound design practices for good feed system stability. Valve pressure drops were chosen to provide adequate control margins. Orifice resistance (inserted upstream of main turbines) provides a ΔP margin for correction of engine variations and contingencies.

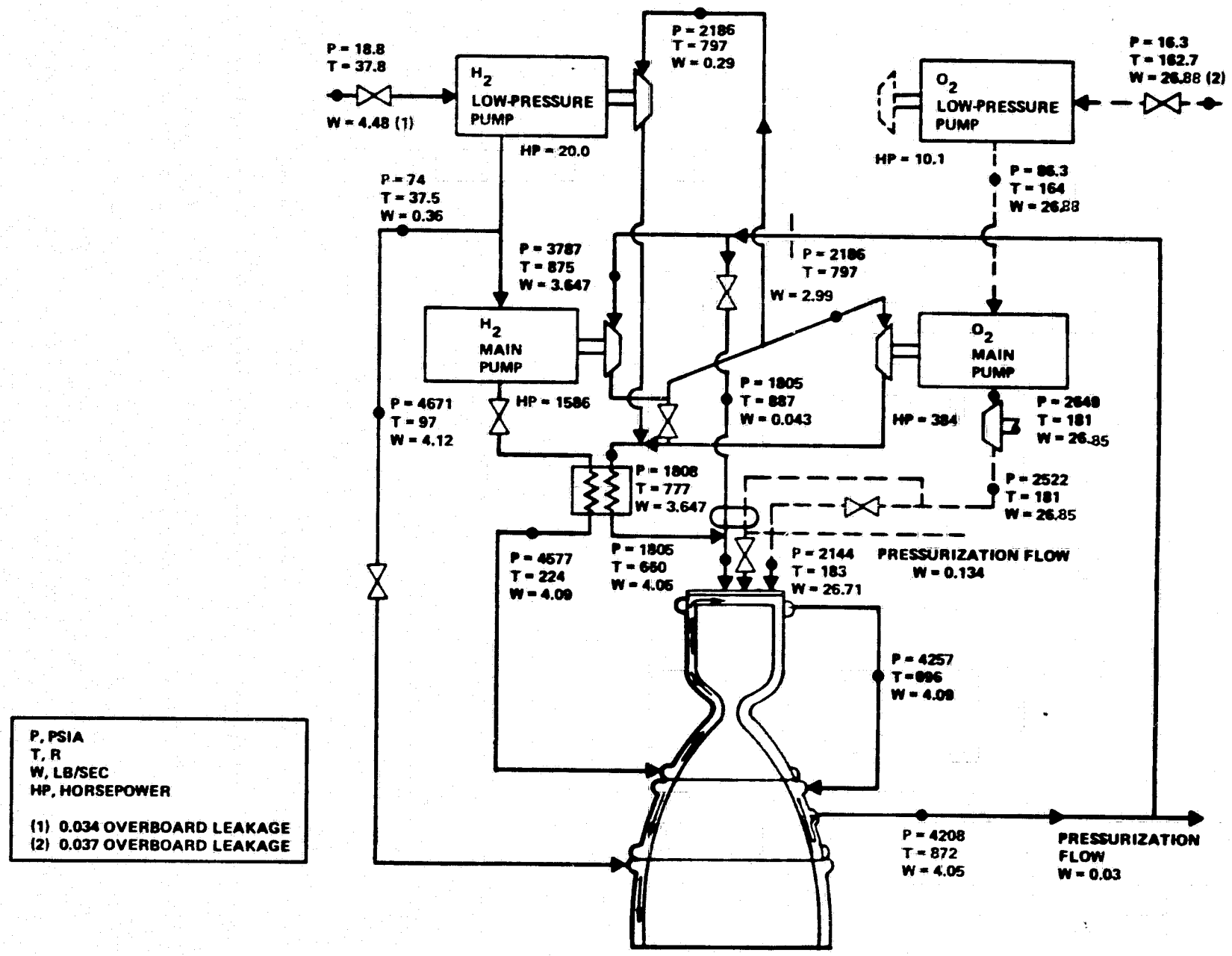

Figure 7-1. Flow, Pressure, Temperature and Power Schedule
F = 15K LB., MR = 6

TABLE 7-2. DESIGN-POINT VALVE CHARACTERISTICS

Valve	Position	Resistance $Sec^2/In^2\ Ft^3$	Flowrate Lb/Sec	Pressure Drop, psi
Main Fuel	100%	25.551	4.086	93.43
Main Oxidizer	80%	37.604	26.714	378.3
Main Turbine Bypass	50%	6599.1	0.405	1981.1
Oxidizer Turbine Bypass	80%	1246.44	0.365	376.61

Table 7-3 summarizes pressure drop groundrules in effect for the point design system. The oxidizer injector resistance is chosen at a relatively high design value (38% of chamber pressure) in order to assure sufficient delta-P at low-thrust operating points.

TABLE 7-3. COMPONENT ΔP ALLOCATION

Component	Minimum Pressure Drop, Design, %
Main Oxidizer Injector	37.9 (1)
Main Fuel Injector	16.0 (1)
Main Fuel Valve	2.0 (2)
Main Oxidizer Valve	15.0 (2)
Turbine Upstream Orifice	10.0 (2)

(1) Percentage of Chamber Pressure
(2) Percentage of Upstream Pressure

Engine Ducting Flow Velocities and Pressure Losses

Propellant ducts were sized with the object of achieving minimum pressure drop and minimum weight. Design-point mach numbers were kept below 0.2, in accordance with good design practice. Table 7-4 presents a summary of duct segments, diameters, materials, flow velocity, and estimated pressure drop. The pressure drops shown are based on preliminary estimates of line lengths and should be refined to include line expansion and contraction losses and line bends.

Pressure Loss Modeling. The line losses tabulated in Table 7-4 amount to 164 psi on the fuel side of the engine and 18 psi on the oxidizer side. Because these losses became defined at the conclusion of the design/analysis iteration, the schematic description used in the steady-state model did not contain the detailed loss breakdown presented in Table 7-4. Instead, duct losses were assumed to be lumped and included in the pressure drop of the "power margin" orifice placed upstream of the main turbines. The orifice is assumed to have a ΔP of 10% of the pressure upstream of the orifice. This amounts to 421 psia at the selected design point. The engine power balances shown in this section will therefore be consistent with the estimated ducting losses if the upstream orifice is thought of as a 257 psi drop. This leaves 164 psia for losses distributed elsewhere around the engine system. In effect, 3.89% of the 10% ΔP in the orifice is used to account for various duct losses and the remainig 6.1% is retained as a margin. The exact breakdown and remaining power margin balance will be obtained when detail duct loss calculations are performed.

Flowrates

Total engine flowrates are 4.48 lb/sec of hydrogen and 26.88 lb/sec of oxygen. Of this, 0.034 lb/sec of hydrogen and 0.13 lb/sec of oxygen are recirculated back to the tanks as pressurant gas. The net flows are therefore 4.45 lb/sec H_2 and 26.75 lb/sec O_2. The nozzle extension dump coolant requirement is 0.36 lb/sec. This flow is tapped off downstream of the fuel boost pump. Main fuel pump inlet flow is thus 4.12 lb/sec. Assumed overboard pump leakages are 0.037 lb/sec

TABLE 7-4. DESIGN ENGINE DUCTING PRELIMINARY CHARACTERISTICS

Fluid	Duct Routing	Material	O.D. Inches	Wall Thickness Inches	ΔP, Psid Estimate	Velocity @ MR = 6 Ft/Sec
LH_2	Extendible Nozzle Coolant Inlet	Flex Hose	0.500	—	—	47
LH_2	Fuel Pump to Regenerator	Inconel 718	1.000	0.020	16	184
LH_2	Regenerator to Combustor Jacket	Inconel 718	1.000	0.020	28	314
GH_2	Combustor Jacket to Nozzle Jacket	Incoloy 903	1.250	0.028	32	555
GH_2	Nozzle Jacket to HPFT	Incoloy 903	1.250	0.028	40	703
GH_2	LOX Gasifier Inlet	Incoloy 903	1.000	0.028	1	112
GH_2	HPFT to HPOT Inlet	Incoloy 903	1.375	0.020	17	560
GH_2	LPFT Inlet	Incoloy 903	0.625	0.020	14	514
GH_2	Oxidizer Turbine Bypass	Incoloy 903	0.625	0.020	13*	482
GH_2	LPFT to Regenerator	Incoloy 903	0.625	0.020	17	612
GH_2	Regenerator to Injector	Incoloy 903	1.750	0.020	14	545
GH_2	LOX Gasifier to Injector	Incoloy 903	1.000	0.020	2	204
LOX	Oxidizer Pump to Injector	Inconel 718	1.250	0.020	17	47
LOX	LOX Gasifier Inlet	Inconel 625	0.250	0.020	1.4	14
GOX	LOX Gasifier to Injector	Inconel 718	1.000	0.020	0	2

*Line only - does not include valve.

hydrogen.

All of the thrust chamber hydrogen is used to cool the chamber. Because the fuel pressurant is tapped off downstream of the cooling jackets, the coolant flow is 4.09 lb/sec (4.0535 + 0.034). Table 7-5 summarizes all secondary flows for the selected design point and for off-design operating points as well.

TABLE 7-5. EXPANDER CYCLE SECONDARY FLOWS

Flow Description	FLOWRATE, lb/sec		
	F = 15K MR = 6	F = 15K MR = 7	F = 1.8K MR = 4
Fuel Pressurization	0.034	0.339	0.016
Oxidizer Pressurization	0.130	0.134	0.09
Bearing Coolant - LPFTP	0.05	(1)	(1)
Bearing Coolant H_2 - HPFTP	0.078	(1)	(1)
Helium Purge - HPOTP	0.013	0.013	0.013
Bearing Coolant H_2 - HPOTP	0.15	(1)	(1)
Overboard Leakage - HPFTP	0.034	0.039	0.0059
Overboard Leakage - HPOTP	0.037	0.030	0.0042

(1) Not determined

The design main turbine bypass fraction is ten percent. This means that 90% of the thrust chamber flow is available to the turbines, while 10% (0.405 lb/sec) is bypassed through the main turbine bypass valve. The bypass flow is used to supply energy to vaporize the oxidizer tank pressurization flow in the GOX heat exchanger. This flow also constitutes one of the engine power margins.

The main oxidizer turbine requires 2.99 lb/sec of the hydrogen available at the fuel turbine discharge. The remaining 0.66 lb/sec is divided between the low pressure fuel turbine (0.29 lb/sec) and the oxidizer turbine bypass valve (0.37 lb/sec).

Pressures

The design chamber pressure of 1540 psia requires injector inlet pressures of 2144 psia for oxidizer and 1805 psia for hydrogen. On the oxidizer side, the pressure drop of the main oxidizer valve (378 psia) and hydraulic boost turbine (127 psia) result in an oxidizer pump discharge pressure of 2649 psia.

On the hydrogen side, the main oxidizer turbine pressure ratio of 1.21 leads to an inlet pressure of 2186 psia. A duct loss of 16.4 psi between the series turbines and the main fuel turbine pressure ratio of 1.72 result in a turbine inlet pressure of 3787 psia. An orifice with a design pressure drop of 10% of its upstream pressure is placed upstream of the main fuel turbine. This pressure drop (421 psi) provides the second source of engine power margin for engine-to-engine variations and contingencies. The required cooling jacket discharge pressure is 4208 psia. A net pressure drop of 369 psi across the series-connected jackets and a main fuel valve delta-p of 93 psi lead to a main fuel pump discharge pressure of 4671 psia.

Temperatures

Hydrogen compressive heating in the boost and main fuel pumps results in a pump discharge temperature of 97R, a 59.2 degree increase over the inlet temperature. Heating in the regenerator raises the temperature to 224R. In the cooling jackets, the hydrogen is heated to 696R in the combustor and then to 872R in the fixed nozzle. Throttling through the turbine upstream orifice raises the temperature to 875R at the turbine inlet. In the main fuel turbine, the hydrogen undergoes a temperature drop of 78R, so that the main oxidizer turbine inlet temperature is 797R. The final turbine discharge temperature is 773R. Mixing of the 773R oxidizer turbine flow with the 785R LPFT flow yields a temperature of 777R at the hot-side inlet to the regenerator. The regenerator heat transfer rate of 1815 Btu/sec results in a hot-side outlet temperature of 635R. This flow is mixed with the main turbine bypass flow at 870R to form the main injector hydrogen flow at 660R.

Performance Prediction

The simplified JANNAF performance procedures described in CPIA Publication 246 was used to determine the engine performance at all operating points, both on-design and off-design. The procedure is based on the efficiencies presented in Table 7-6, and a set of simpler computer programs than those required in the rigorous JANNAF performance procedures (Figure 7-2). This simpler procedure has the advantage of providing data more economically and of making use of the fact that the process efficiencies remain insensitive to certain sets of design parameters so that they need to be established only for those design parameters to which they are more sensitive. This procedure has been used in the analysis of the advanced thrust chamber performance.

TABLE 7-6. JANNAF METHODOLOGY THRUST CHAMBER PERFORMANCE EFFICIENCY FACTORS

$\eta_{IS_{TD}}$ and $\eta_{C^*_{TD}}$	Efficiency accounting primarily for two-dimensional flow effects
$\eta_{IS_{KIN}}$ and $\eta_{C^*_{KIN}}$	Efficiency accounting primarily for reaction kinetic (nonequilibrium effects)
$\eta_{IS_{VAP}}$ and $\eta_{C^*_{VAP}}$	Efficiency accounting for presence of uncombusted propellant drops
$\eta_{IS_{MIX}}$ and $\eta_{C^*_{MIX}}$	Efficiency accounting for incomplete mixing; made up of $\eta_{IS_{STRAT}}$ and $\eta_{IS_{EL\ MIX}}$
$\eta_{IS_{HL}}$ and $\eta_{C^*_{HL}}$	Efficiency to correct for all heat losses from the combustion gases not included in the boundary layer analysis (large-scale turbulence, radiation, etc.).
$\eta_{IS_{BL}}$ and $\eta_{C^*_{BL}}$	Efficiency accounting for boundary layer thrust decrement. The IS_{ODE} value may also have to be adjusted to account for boundary layer mass deficit.

• THRUST CHAMBER SPECIFIC IMPULSE $\left(I_{S_{T/C}}\right)$

$$I_{S_{T/C}} = I_{S_{ODE\ AVG\ MR}} \left[\eta I_{S_{TD}} \eta I_{S_{KIN}} \eta I_{S_{VAP}} \eta I_{S_{MIX}} \eta I_{S_{HL}} - \left(1 - \eta I_{S_{BL}}\right) \right]$$

ODE TDE ODK CICM CICM BLIMP ODE BLIMP

• SYSTEM SPECIFIC IMPULSE

$$I_{S_{SYSTEM}} = \frac{I_{S_{T/C}} \dot{M}_{T/C} + I_{S_{DUMP}} \dot{M}_{DUMP}}{\dot{M}_{SYSTEM}}$$

Figure 7-2. JANNAF Simplified Performance Procedures Performance Parameters and Computer Programs

Expander Cycle Point Design Performance

The JANNAF performance of the engine is indicated in Table 7-7 for an engine mixture ratio of 6.0 and rated thrust of 15,000 pounds. A complete mass and energy balance and resulting thrust chamber specific impulse is provided. Indicated in the table are the nonboundary layer heat transferred from the core flow to the regenerative-cooling hydrogen flow, heat transferred from the boundary layer to the regenerative-cooling hydrogen flow, and the heat transferred from the boundary layer to the dump-cooling hydrogen flow. The first of the above heat effects is reflected in the heat loss efficiency (η_{TSHL}), the second in the level of LOX/H_2 ODE specific impulse, and the third in the level of the heated hydrogen ODE specific impulse. Accounting for the remaining losses (vaporization, mixing, kinetics, two dimensional expansion, and boundary layer), a thrust chamber delivered specific impulse of 481.3 is predicted for a chamber pressure of 1540 psia and system mixture ratio of 6.0. The predicted engine specific impulse performance accounting for dump-coolant flow, and pump leakage flows is 480.8 sec. The individual process efficiencies used in the calculation of the engine performance are discussed below.

<u>Vaporization and Mixing Efficiency</u>. The primary injector performance characteristics are largely dictated by two parameters: the mixing/distribution efficiency, and the evaporation/reaction efficiency. The methods of performance prediction and performance analysis outlined by the JANNAF committees are based on these two parameters for the description of injector efficiency.

The overall efficiency of the injector can be denoted by the product of a mixing-limited efficiency ($\eta_{c^* \, mix}$) and a vaporization-limited efficiency ($\eta_{c^* \, vap}$), i.e.,

$$\eta_{c^*} = \eta_{c^*} \times \eta_{c^* \, vap}$$

The mixing efficiency of the individual elements is ensured by design features based on Rocketdyne experience with high-performance gas-liquid coaxial injectors. A high velocity ratio between the gaseous fuel and the liquid oxidizer

TABLE 7-7. ADVANCED EXPANDER CYCLE ENGINE POINT DESIGN PERFORMANCE (THRUST = 15K, MR = 6.0)

• FLOW AND ENERGY BALANCE	
CHAMBER PRESSURE, PSIA	1540
AREA RATIO	625
ENGINE MIXTURE RATIO	6.0
THRUST CHAMBER MIXTURE RATIO	6.59
INJECTOR OXYGEN FLOWRATE, LB/SEC	26.71
INJECTOR HYDROGEN FLOWRATE, LB/SEC	4.05
DUMP COOLANT HYDROGEN FLOWRATE, LB/SEC	0.36
INJECTOR HYDROGEN NET HEAT GAIN, BUT/SEC	9260
DUMP COOLANT HYDROGEN NET HEAT GAIN, BTU/SEC	2290
• PERFORMANCE	
ODE SPECIFIC IMPULSE, SECONDS	502.06
HEAT LOSS EFFICIENCY, $\eta_{I_{S_{HL}}}$	0.9982
VAPORIZATION EFFICIENCY, $\eta_{I_{S_{VAP}}}$	1.0000
MIXING EFFICIENCY, $\eta_{I_{S_{MIX}}}$	0.9990
REACTION KINETIC EFFICIENCY, $\eta_{I_{S_{KIN}}}$	0.9927
2-D EXPANSION EFFIENCY, $\eta_{I_{S_{TD}}}$	0.9907
BOUNDARY LAYER EFFICIENCY, $\eta_{I_{S_{BL}}}$	0.9779
DELIVERED SPECIFIC IMPULSE, DUMP-COOLED NOZZLE, SECONDS	534.6
DELIVERED THRUST CHAMBER SPECIFIC IMPULSE, SECONDS*	481.28
DELIVERED ENGINE SPECIFIC IMPULSE, SECONDS	480.8

*I_S FROM INJECTOR FLOWS ONLY

Comparative history of various injectors and local mixing efficiencies versus a velocity related mixing parameter is shown in Fig. 7-3 . As indicated in Fig. 7-3, the advanced expander injector will operate in a region of high mixing efficiency similar to the SSME and ASE main injectors.

For the advanced expander injector, at a mixing parameter value of 9 and above, and a cup recess/liquid jet diameter ratio of 1.0, a mixture ratio uniformity factor (E_m) above 99 is shown in Fig. 7-3. A generalized plot of E_m versus $\eta_{c^* mix}$, obtained from SSME and other injector cold-flow data in the mixture range of 5.0 to 7.0 (Fig. 7-4), shows that the predicted $\eta_{c^* mix}$ for this injector is 99.8% or above.

The coaxial injection combustion model (CICM) was used as a design tool in the selection of a high-performance coaxial element for the advanced expander cycle injector. CICM is an analytical model developed by Rocketdyne and used by JANNAF to describe the highly complex injection and combustion processes of gas-liquid propellant coaxial elements. The CICM computer model includes the effect of spray droplet atomization, heating, burning, and droplet drag from the injection post tip to the end of the propellant jet. A stream-tube model is utilized to simulate the combustion process within the combustion chamber. All propellant and combustion gas physical properties in the program are supplied by property table subroutines. The program utilizes an advanced droplet vaporization and heating model that includes real gas effects which are sensitive to vapor-liquid equilibrium and solubility of external gases into the droplet.

The advanced expander cycle injector design configuration was analyzed using the CICM model at mixture ratios of 6.0 and 7.0 for thrust levels of 15,000, at a mixture ratio of 6.0 for 1500 pounds thrust, and at a mixture ratio of 4.0 for 800 pounds thrust (Fig. 7-5). The results for the nominal thrust (15K) cases show that liquid atomization, vaporization, and reaction will occur well upstream of the combustion chamber throat, producing a predicted vaporization/

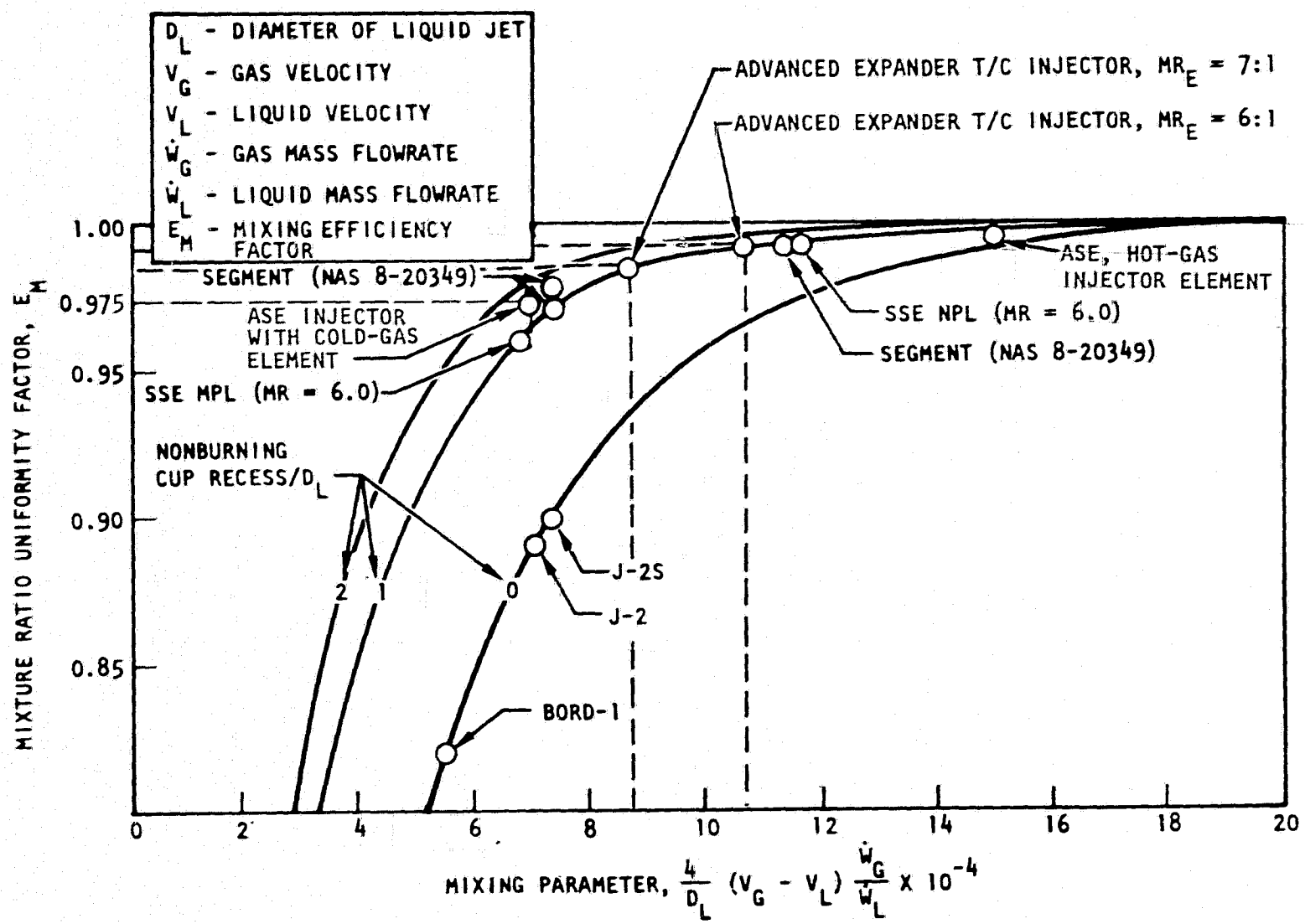

Figure 7-3. Injector Mixing Efficiency Comparison

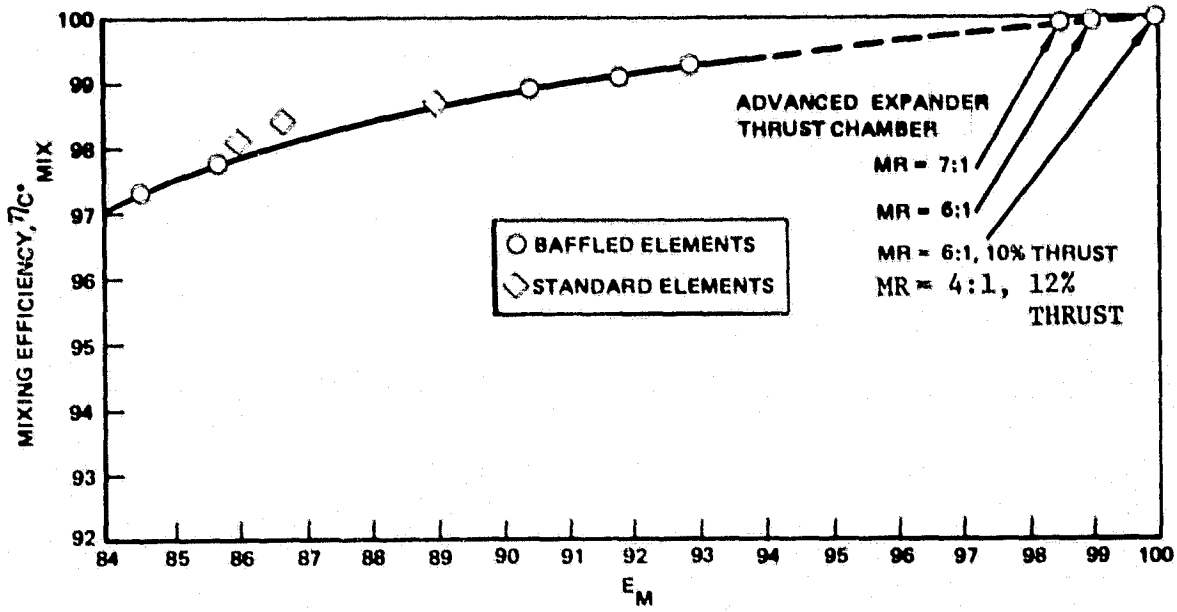

Figure 7-4. Generalized Plot of Mixing Efficiency (E_m) and $\eta_c{}^*{}_{mix}$ Based on SSME and Other Cold-Flow Data (o/f = 5 to 7)

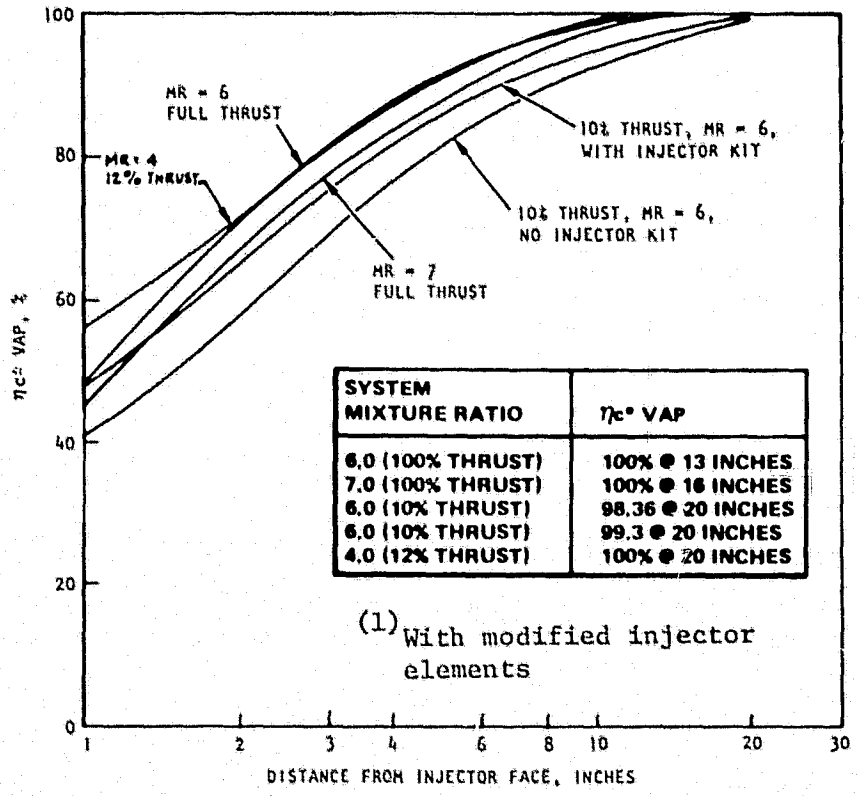

Figure 7-5. Injector Performance From CICM Model Analyses

reaction efficiency of 100%. For the pump idle mode thrust (1800 lb.) the 20 in. length is sufficient for attainment of 100% vaporization. The analysis for the 1500-pound-thrust (10% thrust) operating point was performed with both unmodified injector elements and with a smaller ID face retainer nut. The smaller retainer nut decreases the area of flow and increases the hydrogen velocity for improved vaporization. This change to the injector can be performed on a dedicated low thrust engine and constitutes a hardware kit.

Overall injection characteristic velocity efficiency is expressed as the product of the mixing efficiency, and the vaporization/reaction efficiency: $\eta_{c^* pred} = \eta_{c^* mix} \times \eta_{c^* vap}$. For the injection design, the overall predicted characteristic velocity efficiency values for all nominal thrust cases are in excess of 99.8% (Table 7-8). With the modified injector the 10% thrust case achieves an efficiency of 99.3%.

TABLE 7-8. EXPANDER INJECTOR η_{c^*} VALUES

Engine MR	Engine Thrust lb.	Characteristic Velocity Efficiency η_{c^*} %MIX,	Characteristic Velocity Efficiency η_{c^*} %VAP,	Characteristic Velocity Efficiency η_{c^*} %PRED,
6.0	15,000	99.9	100	99.9
7.0	15,000	99.8	100	99.8
4.0	1,800	100.0	100	100.0
6.0	1,500	99.9	98.36	98.26
6.0(1)	1,500	100.0	99.3	99.3

(1) With modified injector elements

Reaction Kinetics. Kinetic losses (η kinetics) arise from the fact that combustion gas equilibrium cannot change fast enough to follow the changes in pressure and temperature as the gases expand through the nozzle. Two JANNAF computer codes are used to calculate these losses. The One-Dimensional Kinetics Program (ODK) is used for simplified calculations. For cases where a more exact

analysis is required, TDK can be used to include the effects of two-dimensional flow in the calculations. Calculations made for the point-design engine using TDK at nominal conditions of 15K thrust and 6.59 mixture ratio are shown in Fig. 7-6 plotted with the parametric data curves from the cycle optimizer code. Excellent agreement is indicated.

Two-Dimensional Expansion Efficiency. Rocketdyne's nozzle analysis computer code is used to determine the flowfield in the nozzle. The transonic solution, discussed in the Nozzle Contour section, the wall contour, and the flow propellant properties are input to the code, which utilizes the method of characteristics to calculate the flowfield. The code is capable of handling variable flow properties. Two-dimensional or divergence losses from nonaxial flow at the nozzle exit plane are determined by integrating the pressure along the wall to calculate the nozzle thrust and comparing this result to the thrust produced by a one-dimensional expansion to the same area ratio. Output from the code includes properties along the wall and divergence efficiency of the nozzle. For the advanced expander point design nozzle, the Rocketdyne analysis code was used to determine the two-dimensional efficiency. The performance of the selected contour was then verified using the JANNAF standard TDK program.

TDK was developed to determine liquid rocket engine performance. The program calculates the inviscid two-dimensional nonequilibrium expansion of gaseous propellant mixtures. The method of characteristics is the basic analysis method. This code was used by Rocketdyne to calculate both the two-dimensional divergence and kinetic efficiency of the selected nozzle.

The two-dimensional efficiency determined for the ε = 625 advanced expander thrust chamber nozzle $\eta_{I_{STD}} = 0.9907$ is shown plotted in Fig. 7-7 with parametric values obtained from the cycle optimizer code built-in curve fit. The curve fit represents data obtained from detailed aerodynamic analysis of a family of nozzles similar to the design nozzle.

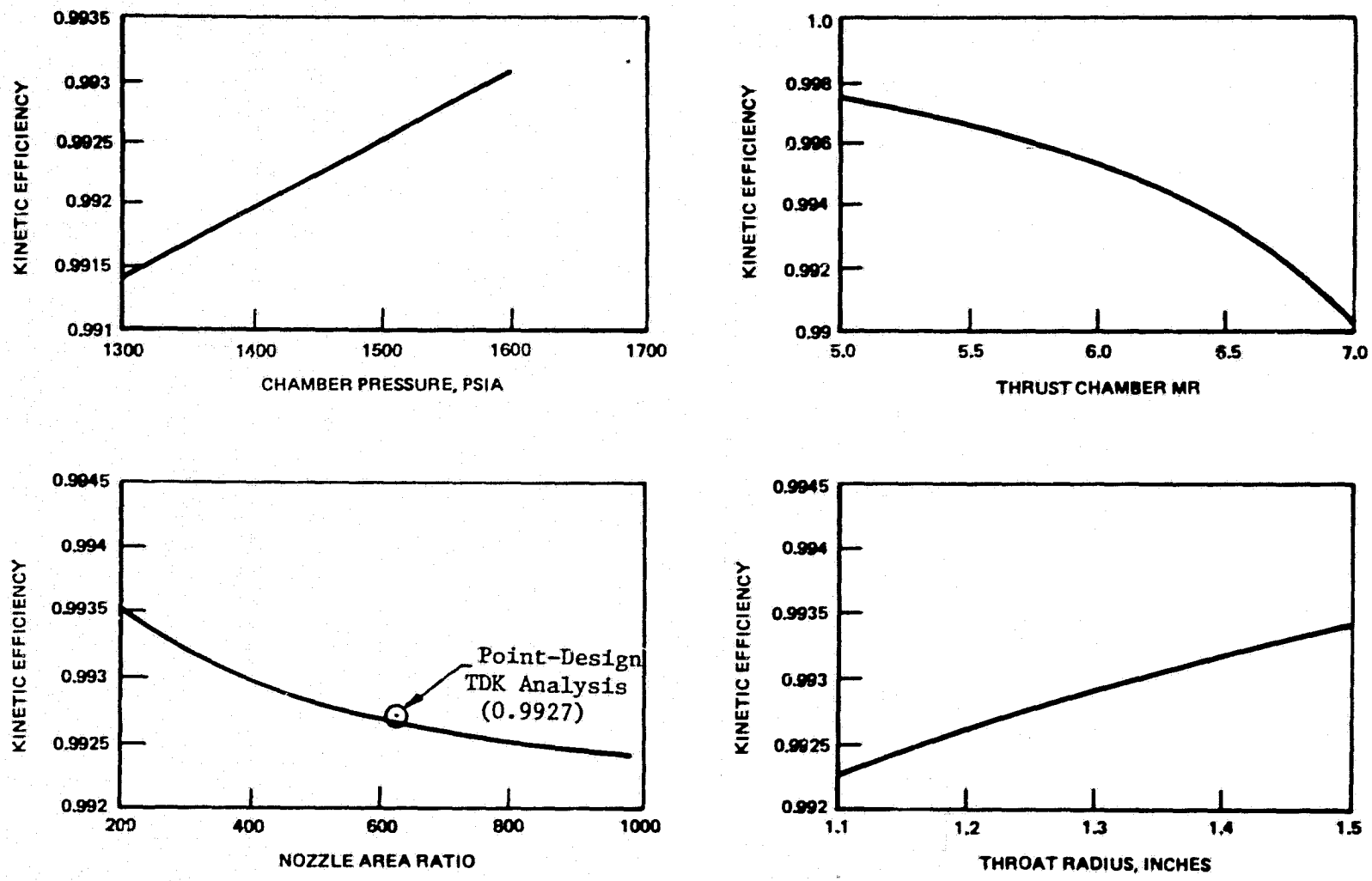

Figure 7-6. Parametric and Point-Design Kinetic Analysis

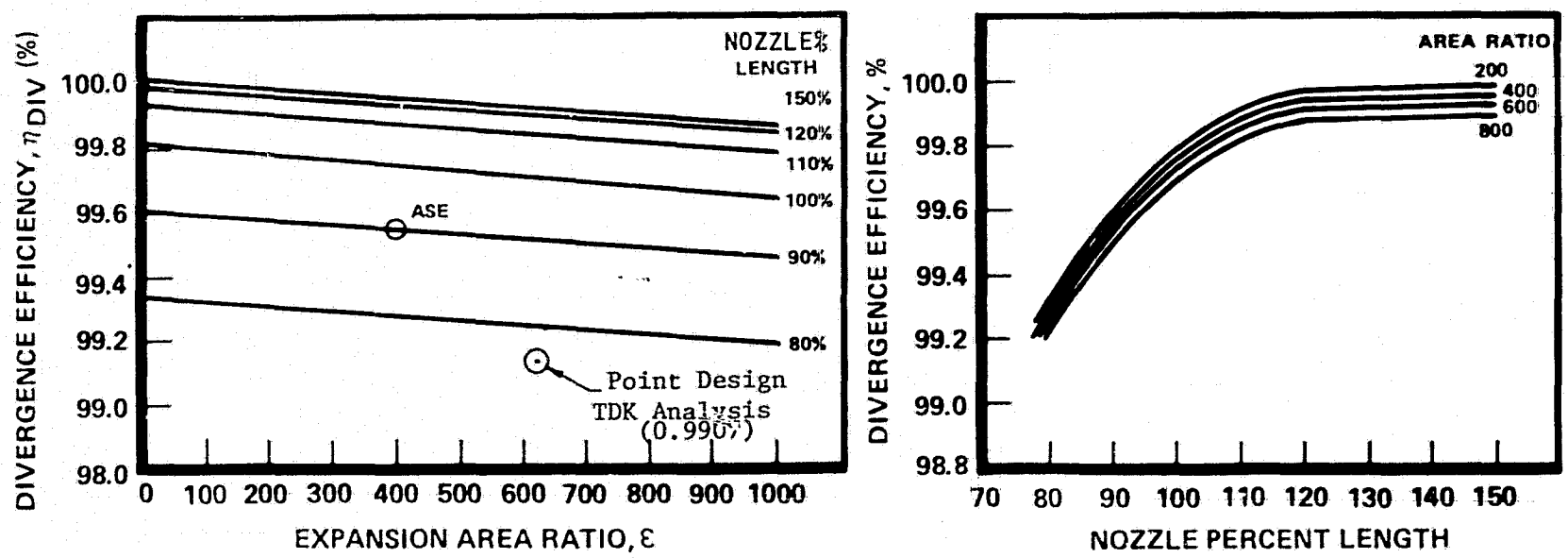

Figure 7-7. Parametric and Point-Design Two-Dimensional Nozzle Efficiency

235-339

Rockwell International
Rocketdyne Division

Boundary Layer Analysis. For moderate and high-thrust nozzles, analysis of the viscous flow near the nozzle wall can be separated from the potential flow core with negligible loss in analysis accuracy. Drag losses in the nozzle thrust result from shear between the gases and the wall and a resulting loss in flow momentum in this region. The region in the flow affected by the wall is the boundary layer.

Two boundary layer computer programs are used at Rocketdyne to calculate the drag loss in thrust chambers. The rigorous analytical procedure recommended by the JANNAF Performance Standardization Working Group is the Boundary Layer Integral Matrix Procedure (BLIMP). This computerized program uses a strip-integral procedure to solve a comprehensive set of equations describing fluid flow in a boundary layer. For turbulent flow, the time-averaged equations of motion are solved utilizing an eddy viscosity model to describe the Reynolds stress term, plus constant turbulent Prandtl and Schmidt numbers in the energy and species conservation equations.

The BLIMP computer program uses conditions from the outer streamline in the TDK program for the supersonic portion and ODK for the subsonic portion of the thrust chamber. The wall temperature, pressure, and thermochemical data are fed into the BLIMP program together with the geometry. The boundary layer is assumed to begin at the start of the converging section of the combustion chamber. The output of the program provides a complete set of data on the boundary layer thicknesses, wall heat fluxes, and heat transfer coefficients.

Rocketdyne's computer code for determining boundary layer and heat transfer characteristics for rocket thrust chambers is an integral method of solution for the von Karman boundary layer momentum equation and the energy equation. The solutions describe the wall skin friction and Stanton number behavior along the chamber wall. Laminar and turbulent flow involving favorable or adverse pressure gradients can be solved by this program. For the definition of the local gas-side heat transfer coefficient, a similarity between the nondimensional heat transfer coefficient and the skin friction coefficient is assumed.

Both cold-flow and full scale reacting flow experiments have been conducted to verify the accuracy of the Rocketdyne boundary layer analysis code. Agreement between the experimental results and Rocketdyne's analysis code was shown to be good in these tests.

Boundary layer experiments were also conducted as part of full-scale testing of the Rocketdyne ASE, $\varepsilon = 400$ nozzle. Pitot pressure and temperature rakes were installed at the exit of the nozzle. Measurements were made during a full-scale LOX/H_2 test. Drag losses determined from these measurements are indicated. The measured momentum loss was 2.25%, which compares favorably to the 2.6% loss predicted by the Rocketdyne computer code. Drag losses predicted by the JANNAF code BLIMP were higher -- 3.4%.

Typical analytical boundary layer drag losses are shown in Fig. 7-9 for OTV configurations. Drag losses range from 2 to 3% of the total thrust. Increased pressure decreases nozzle drag. Increased percent length increases drag because of the additional wall length for a fixed area ratio. Drag decreases with thrust increases because the flow in the boundary layer becomes a smaller percentage of the total flow. A small net decrease in drag losses results from increased area ratios because the flow is expanded more rapidly.

The Rocketdyne boundary layer code was used to predict drag losses for the advanced expander thrust chamber $\varepsilon = 625$ nozzle and adjusted for agreement between the code and the ASE $\varepsilon = 400$ experimental result conditions. Calculated drag efficiency for the advanced expander thrust chamber is:

$$\eta_{I_{s_{BL}}} = 0.9780$$

indicating that 2.2% of the possible thrust is lost due to drag on the wall.

<u>Nonboundary Layer Heat Loss Efficiency</u>. The boundary layer attaches approximately 3 inches from the injector face. At this station, 721 Btu/sec have been transferred to the hydrogen coolant from the core flow for a system

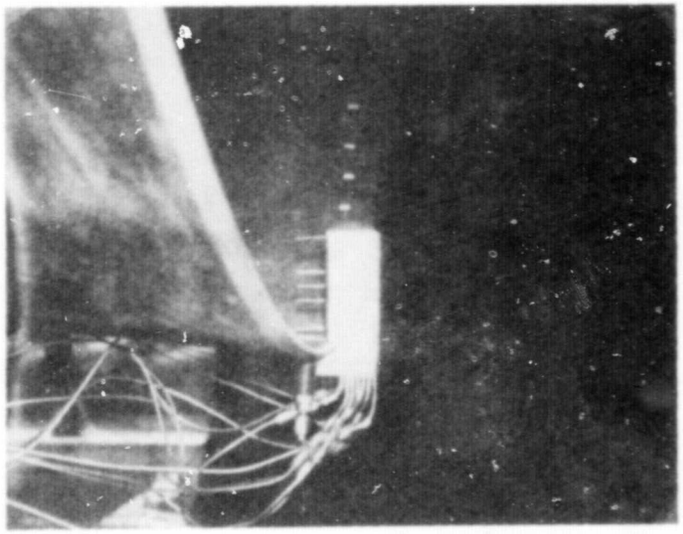

PRESSURE RAKE

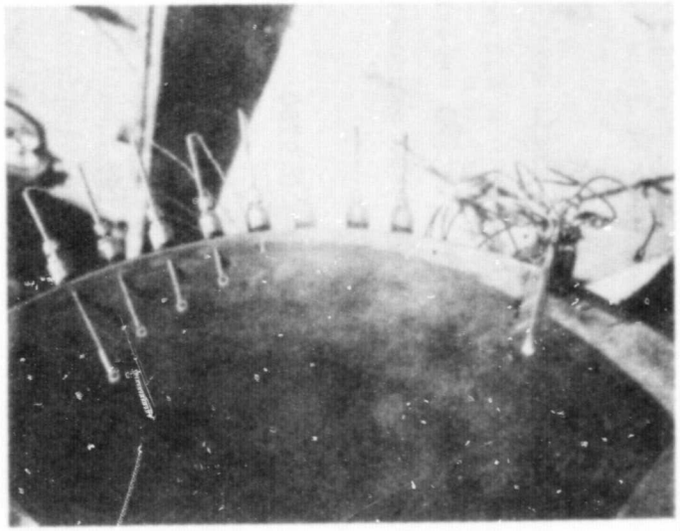

TEMPERATURE RAKE

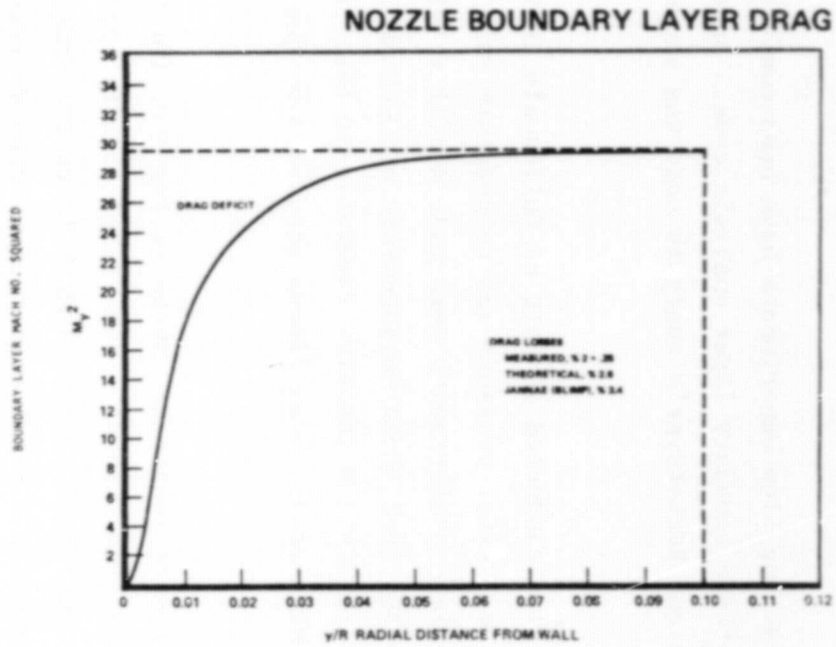

Figure 7-8. Nozzle Boundary Layer Drag Losses

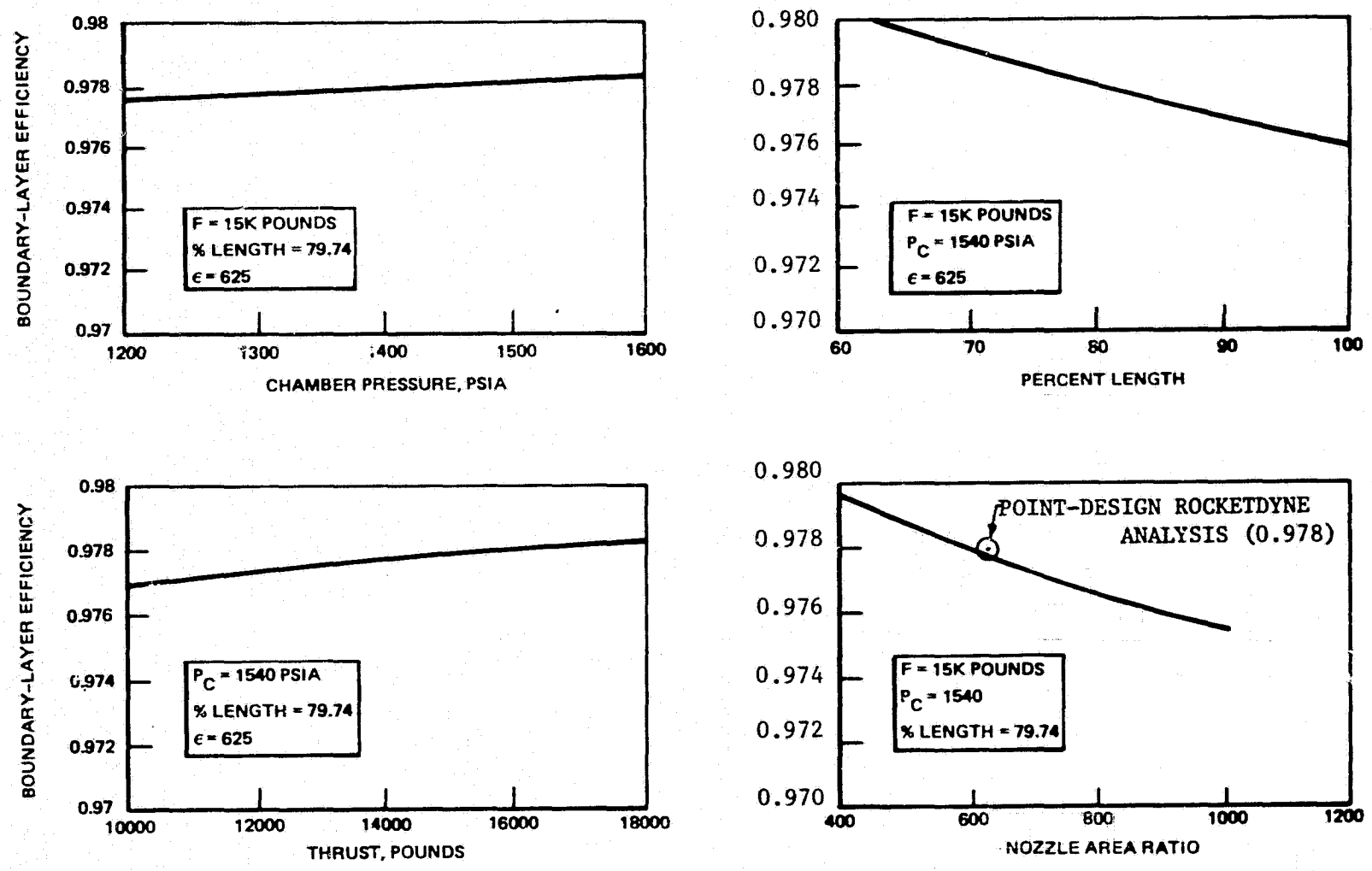

Figure 7-9. Boundary Layer Efficiency Correlation

mixture ratio of 6:1. This results in a net heat load of 9260 Btu/sec (Table 7-7) transferred to the coolant during regenerative cooling of the thrust chamber to an expansion area ratio of 225:1. Calculation of the one-dimensional specific impulse (ISPODE) for this heat load level leads to a heat loss efficiency of η_{ISPHL} of 0.9982. Similar values are calculated for the other thrust and mixture ratio conditions of Table .

Dump Coolant Specific Impulse. The baseline thrust chamber design utilizes dump-cooling between expansion area ratios of 225:1 and 625:1. Six percent of the total hydrogen flow is discharged through the 1080 tubes comprising the dump-cooled portion of the nozzle, and through small nozzles at the end of each tube, to the vehicle exterior. At a nominal system mixture ratio of 6.0, the dump-coolant hydrogen heats to a temperature of 2075.5 R. Expanding the heated hydrogen through a 30:1 expansion area ratio nozzle produces an ideal specific impulse of 5 52.8 seconds (Fig.7-10). Divergence and orientation losses result in a delivered dump coolant specific impulse of 534.6 seconds.

Life Evaluation - Mainstage

A detailed life evaluation was performed for the thrust chamber operating at design Pc and thrust. Calculations of cyclic fatigue life were correlated with results of Rocketdyne's regenerative cooling computer code. The code results were found to agree with those derived from rigorous finite-element stress analysis. Life at off-design thrust levels and mixture ratios was then assessed with the regenerative cooling analysis code.

Fatigue Life Evaluation Methodology. The fundamental theory used in the life prediction analysis is that failure depends on the accumulation of incremental damage caused by fatigue and creep mechanisms.

Where available, data obtained from material fatigue specimens and test data of actual hardware are used in life analysis. The life analysis is based on a

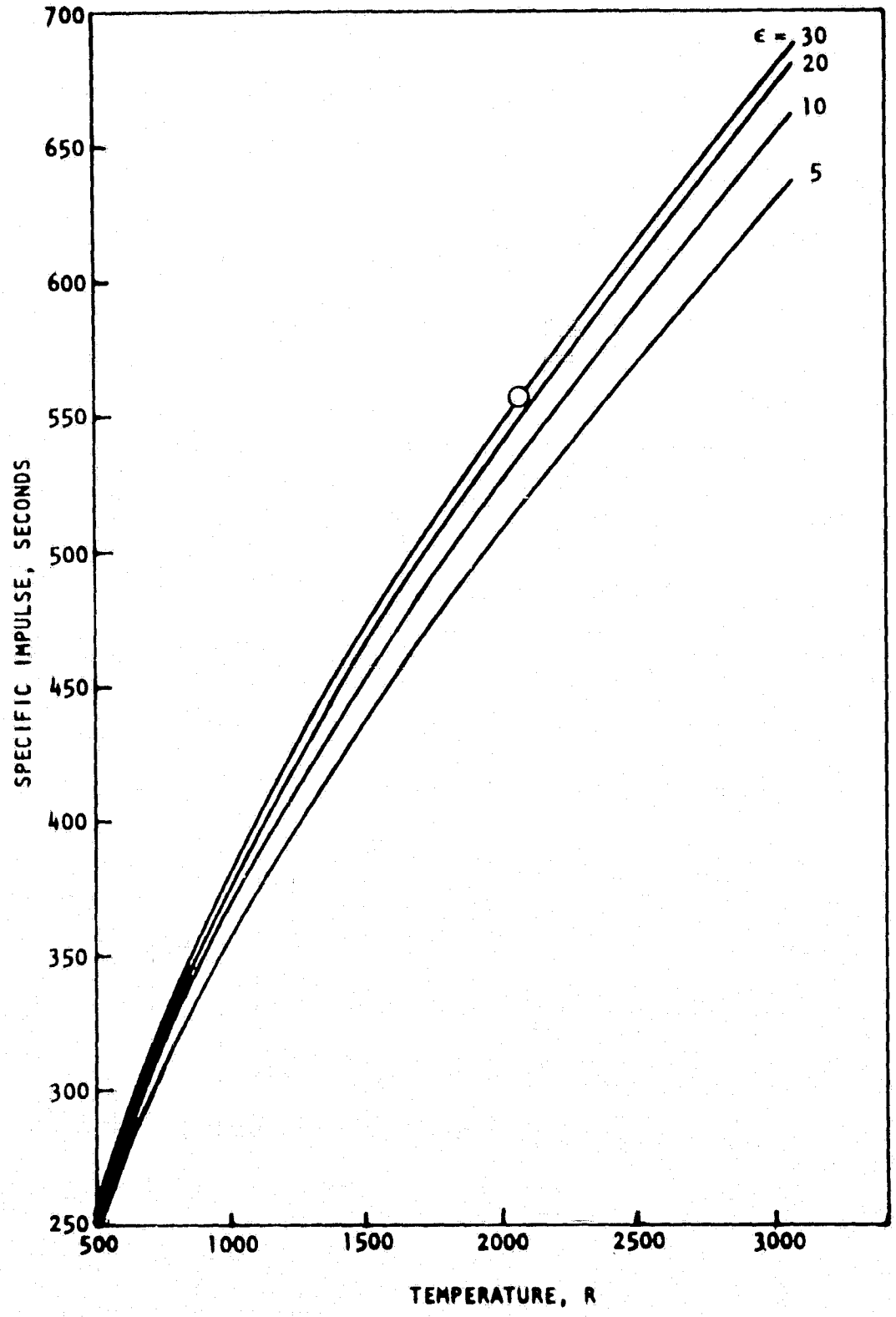

Figure 7-10. Heated Hydrogen Specific Impulse

definition of the stress-strain-time-temperature history during each operating cycle. Creep damage is evaluated from the stress-time-temperature cycle, and fatigue damage from the strain-time-temperature cycle.

The life analysis logic diagram is shown in Fig. 7-11.

Low-cycle fatigue damage is evaluated by a linear damage accumulation fraction,

$$\phi_f = \Sigma \frac{n_i}{N_{f_i}}$$

where n_i is the actual number of cycles at a particular stress or strain amplitude and N_{f_i} is the cycles to failure at the same amplitude (Miner's Rule).

A linear damage accumulation fraction is used to evaluate creep rupture damage,

$$\phi_c = \Sigma \frac{t_i}{T_{r_i}}$$

where t_i is the actual time at a particular stress and T_{r_i} is the time to rupture at that same stress. Lower bound fatigue property data are used to evaluate life.

Each component that experiences cyclic loading during operation is designed to the following fatigue criteria:

Low-Cycle Fatigue Limit Life = 4 X Service Life Operational Cycles

Limit life is the maximum expected usefulness of the structure expressed in time and/or cycles of loading. The service life for the expander cycle point-design components is defined as 300 start/shutdown cycles or 10 hours of accumulated run time.

The low-cycle fatigue criteria is applicable to cyclic stresses, including thermal, associated with steady-state and transient operating conditions such

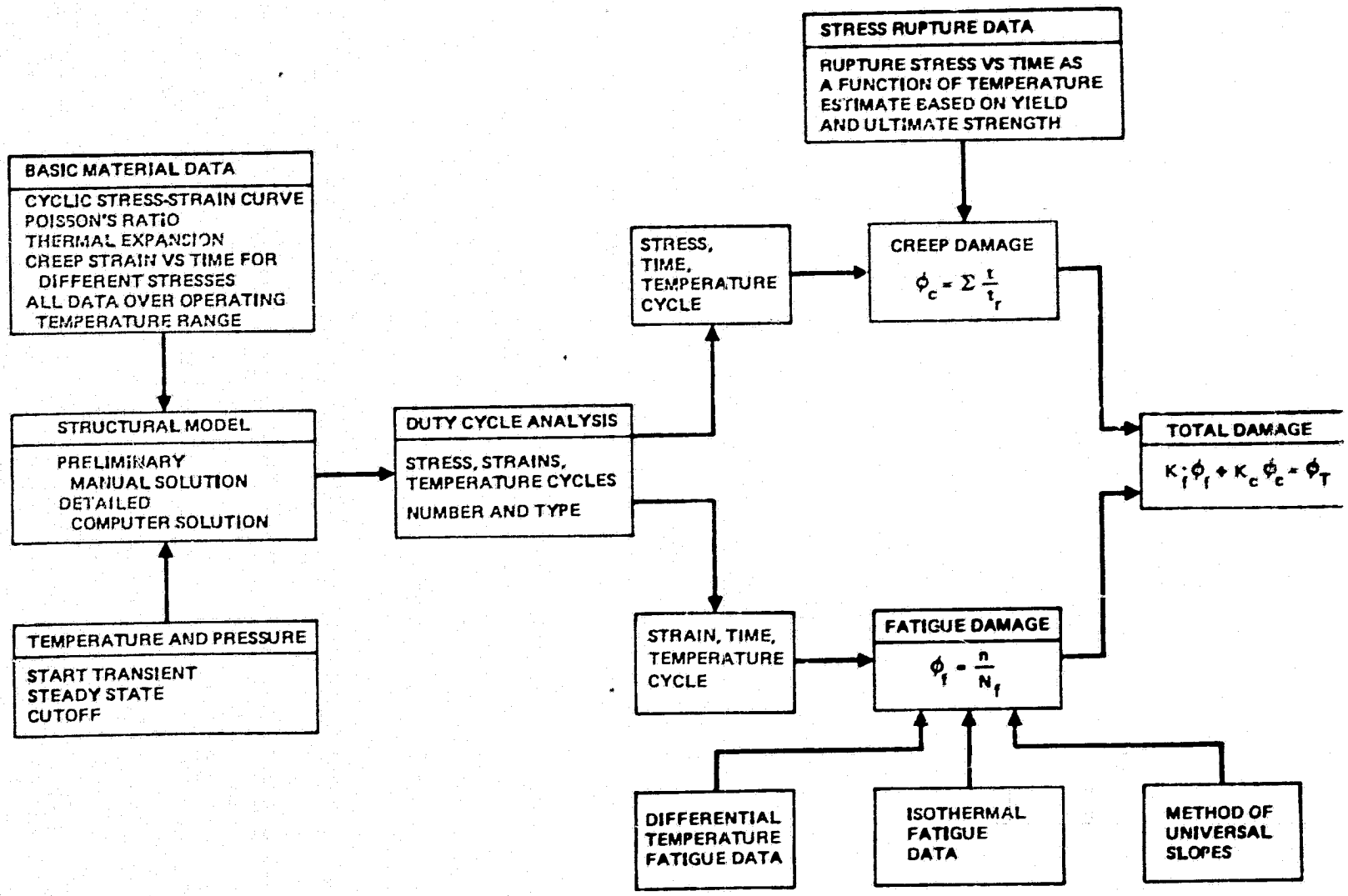

Figure 7-11. Life Analysis Logic Diagram

as an engine start/shutdown cycle. For those components experiencing low-cycle fatigue, the following generalized life equation is used to take into consideration the interaction of low-cycle fatigue and creep damage:

$$\text{Life Criteria} = 4\phi_{fL} + 4\phi_{c} \leq 1.0$$

Finite-Element Cyclic Life Analysis Results. Two finite-element structural models were used to establish the strain ranges of the combustor critical throat channel section. An axisymmetric model of the combustor channel/wall was run to establish the varying transverse strain profile to be used for the plane strain (second model) of a repeatable segment of the local channel cross section (Figure 2-21a). A cyclic program was used to subject the structural models to complete heatup and chilldown cycles. This was done to allow full strain hardening to occur and stabilize the strain range values at the critical locations.

The channel section analyzed was located approximately 0.18-inch forward of the geometric throat. A thermal excursion from steady-state operating temperature to a -100F post chill was used. Coolant and hot gas pressure were used as applicable. Figure 2-21b shows the steady-state temperature profile and typical contour plots of effective strain for the heatup and cooldown cycles.

Table 7-12 gives a life summary of the different materials of the coolant channel section at the critical throat region.

The results show that the minimum required life of 300 x 4 cycles is exceeded at the critical throat section of the combustor. The NARloy-Z hot-gas wall over the land has the lowest life of 1350 cycles. Analysis shows no creep damage at the channel wall maximum operating temperature and stress.

The total life criteria with safety factors, as previously defined, are as follows:

$$\text{Life Criteria} = 4\left(\frac{300}{1350}\right) + 0 = 0.89 \leq 1.0$$

TABLE 7-9. LIFE SUMMARY OF COOLANT CHANNEL SECTION AT CRITICAL THROAT REGION

LOCATION	CYCLIC STRAIN RANGE, %	LIMIT LIFE CYCLES	DAMAGE FRACTION
(A) NARloy-Z HOT GAS WALL OVER LAND	1.87	1350	0.222
(B) NARloy-Z HOT GAS WALL OVER CHANNEL	1.35	3500	0.086
(C) EDCu INTERFACE BETWEEN LAND AND BACK WALL	0.11	$>10^4$	0
(D) EDNi BACK WALL	0.12	$>10^4$	0

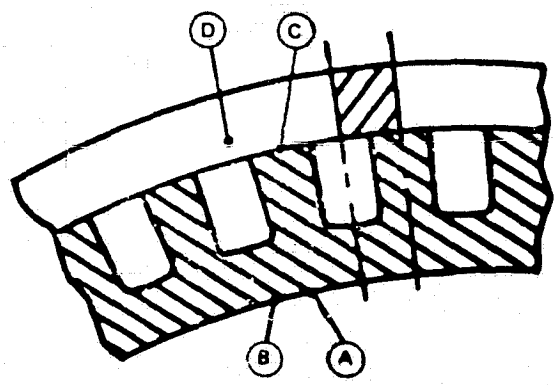

The cyclic strain range in the EDCu interface and the EDNi back wall are low and show no damage (Table 7-9).

Cycle Life Analysis - Regenerative Cooling Code. The finite element analysis provides an accurate prediction of the low cycle fatigue at the critical thrust chamber station near the throat. Which station in the combustor is critical is determined using the regenerative cooling analysis code. Wall temperature profile and pressure data from the latter code are input into the finite element analysis code. It would be an expensive undertaking to perform a finite element analysis on each station in the thrust chamber and from it select the low cycle fatigue limiting station. The regenerative cooling analysis program therefore

has been equipped with low cycle fatigue life equations similar to the finite analysis program which can be fine-tuned to the latter with coefficients which are applied to the strain ranges. Once a finite element analysis has been run for the critical station, the coefficients are obtained and used in the regenerative cooling analysis program to determine life at other stations in the combustor, nozzle, extendable nozzle at on-design and off-design conditions.

Cycle Life Without Regenerator. Eighty-two stations are sequentially analyzed for cooling parameters and life during a regenerative cooling model run of the combustor as shown in Table 7-10.. Combustor cycle life using no turbine gas regenerator is seen to range from a high value of 38,000 cycles at the coolant entrance (Station 0) to a low value of 1256 at Station 56, 0.18 inches upstream of the throat. Cycle life at the injector end (Station 82) is 9818 cycles. Strain and total damage fraction are printed at each station as well as creep and fatigue damage fractions, creep stress and hot-gas pressure. The value determined at the critical station (1256 cycles) is seen to agree within 10% of the cycle life determined with the finite element analysis (1350 cycles), with the rigorously determined cycle life being higher.

Cycle-Life With Regenerator. The turbine gas regenerator increases the coolant inlet temperature by approximately 100 R. A regenerative cooling model run was made for the combustor under coolant inlet conditions of 224 R. A computer printout showing the results of conditions in the vicinity of the throat is shown in Table 7-11. The higher coolant inlet temperature has in effect moved the critical (lower cycle life) station closer to the injector plane (Station 70) and has increased the life to 1365 cycles. This is caused by the coolant heat transfer coefficient peak with temperature occuring further in the coolant path from throat-to-injector as a result of the change in coolant inlet temperature. Cycle life is determined by hot-gas wall-to-back wall delta temperatures. The increased heat transfer coefficient has shifted this delta downstream.

TABLE 7-10 COMBUSTOR CYCLE LIFE ANALYSIS, MR = 6.45, STATIONS 0-29

HOURS OF FIRING TIME, T = 5.250E+00
DESIGN CYCLE LIFE, N, CYCLES = 2.500E+02
LIFE CYCLE SAFETY FACTOR = 4.000E+00
INITIAL JACKET TEMPERATURE, DEG F = -1.000E+02
INITIAL GAS-SIDE WALL TEMPERATURE, DEG F = -1.000E+02

STA.	X (IN)	HOT GAS PRESSURE (PSIA)	CREEP STRESS (PSIA)	CREEP DAMAGE FRACT.	FATIGUE DAMAGE FRACT.	DAMAGE FRACT.	UNIAX. STRAIN RANGE	CYCLE LIFE
0	3.858	15.18	8259.11	.00008	.00648	.02621	.00160	38154.78
1	3.590	16.78	8255.10	.00008	.00675	.02731	.00200	36616.45
2	3.132	20.86	8245.79	.00007	.00707	.02857	.00255	35004.62
3	2.927	22.04	8242.75	.00007	.00721	.02914	.00283	34319.90
4	2.564	25.92	8234.11	.00007	.00742	.02998	.00330	33360.08
5	2.250	30.07	8225.15	.00007	.00758	.03062	.00371	32653.79
6	2.109	32.20	8220.65	.00007	.00766	.03094	.00392	32317.55
7	1.856	36.70	8211.35	.00007	.00848	.03421	.00431	29228.95
8	1.739	39.00	8206.63	.00007	.00901	.03633	.00451	27523.41
9	1.525	43.86	8196.82	.00007	.00995	.04010	.00486	24939.59
10	1.334	48.78	8186.99	.00007	.01088	.04380	.00520	22832.84
11	1.246	51.33	8181.96	.00007	.01132	.04555	.00535	21954.59
12	1.078	56.67	8171.46	.00007	.01220	.04907	.00567	20380.25
13	.999	59.38	8166.15	.00007	.01265	.05086	.00582	19663.35
14	.850	65.04	3597.48	.00000	.00762	.03050	.00381	32791.03
15	.779	67.91	3593.99	.00000	.00766	.03063	.00391	32645.23
16	.643	73.81	3586.95	.00000	.00789	.03156	.00408	31684.32
17	.511	80.14	3579.62	.00000	.00830	.03320	.00424	30124.64
18	.382	86.94	3571.96	.00000	.00866	.03466	.00438	28852.23
19	.352	88.01	3570.62	.00000	.00867	.03469	.00438	28828.04
20	.342	96.44	3563.64	.00000	.00974	.03896	.00478	25666.71
21	.335	102.62	3558.55	.00000	.01043	.04171	.00503	23977.22
22	.321	115.72	3547.76	.00000	.01190	.04761	.00556	21005.43
23	.313	122.68	3542.03	.00000	.01269	.05078	.00584	19694.23
24	.298	137.52	3529.83	.00000	.01477	.05907	.00640	16928.74
25	.291	145.42	3523.34	.00000	.01607	.06430	.00672	15552.21
26	.276	162.11	6878.92	.00001	.01572	.06294	.00663	15888.52
27	.268	170.90	6864.81	.00001	.01711	.06849	.00696	14600.99
28	.252	189.51	6834.94	.00001	.02008	.08035	.00761	12445.48
29	.236	209.39	6803.07	.00001	.02366	.09468	.00829	10562.01

TABLE 7-10. COMBUSTOR CYCLE LIFE ANALYSIS, MR = 6.45, STATIONS 30-82 (Continued)

LIFE CYCLE PARAMETERS

HOURS OF FIRING TIME, T =	5.250E+00
DESIGN CYCLE LIFE, N, CYCLES =	2.500E+02
LIFE CYCLE SAFETY FACTOR =	4.000E+00
INITIAL JACKET TEMPERATURE, DEG F =	-1.000E+02
INITIAL GAS-SIDE WALL TEMPERATURE, DEG F =	-1.000E+02

STA.	X (IN)	HOT GAS PRESSURE (PSIA)	CREEP STRESS (PSIA)	CREEP DAMAGE FRACT.	FATIGUE DAMAGE FRACT.	DAMAGE FRACT.	UNIAX. STRAIN RANGE	CYCLE LIFE
30	.228	219.65	6613.69	.00001	.03495	.13996	.00997	7144.76
31	.212	241.73	6776.74	.00001	.04415	.17677	.01095	5657.12
32	.204	253.17	6780.69	.00001	.04913	.19657	.01142	5087.21
33	.188	277.14	6722.49	.00001	.05954	.23821	.01232	4198.03
34	.172	302.44	6682.17	.00001	.07203	.28814	.01324	3470.56
35	.164	315.64	6661.13	.00001	.08005	.32026	.01379	3122.47
36	.149	342.96	6617.59	.00001	.09837	.39232	.01488	2548.95
37	.141	357.22	6594.91	.00001	.10771	.43087	.01541	2320.84
38	.125	385.63	6548.10	.00001	.12888	.51557	.01637	1939.61
39	.117	401.76	6524.02	.00001	.14246	.56987	.01685	1754.79
40	.102	433.06	6474.22	.00001	.18230	.64922	.01776	1540.31
41	.087	465.61	6422.47	.00001	.16678	.74713	.01872	1338.46
42	.079	482.31	6389.69	.00001	.17772	.71089	.01844	1406.69
73	-9.769	1518.13	5140.70	.00000	.10915	.43662	.01549	2290.31
74	-10.973	1521.55	5124.42	.00000	.10728	.42912	.01539	2330.37
75	-12.178	1523.98	5109.52	.00000	.10862	.43448	.01537	2301.62
76	-13.383	1525.67	5099.10	.00000	.12028	.48111	.01570	2076.52
77	-14.588	1526.79	5091.62	.00000	.12459	.49836	.01574	2006.59
78	-15.794	1527.43	5081.75	.00000	.11437	.45749	.01532	2185.56
79	-17.000	1527.63	5075.08	.00000	.09623	.38494	.01456	2597.60
80	-18.000	1527.63	5070.55	.00000	.07981	.31923	.01377	3132.58
81	-19.000	1527.63	5063.92	.00000	.05678	.22713	.01210	4402.77
82	-20.000	1527.63	5057.37	.00000	.02546	.10185	.00858	9816.50

TABLE 7-10. COMBUSTOR CYCLE LIFE ANALYSIS, MR = 6.45, STATIONS 43-72 (Continued)

HOURS OF FIRING TIME, T = 5.250E+00
DESIGN CYCLE LIFE, N, CYCLES = 2.500E+02
LIFE CYCLE SAFETY FACTOR = 4.000E+00
INITIAL JACKET TEMPERATURE, DEG F = -1.000E+02
INITIAL GAS-SIDE WALL TEMPERATURE, DEG F = -1.000E+02

STA.	X (IN)	HOT GAS PRESSURE (PSIA)	CREEP STRESS (PSIA)	CREEP DAMAGE FRACT.	FATIGUE DAMAGE FRACT.	DAMAGE FRACT.	UNIAX. STRAIN RANGE	CYCLE LIFE
43	.065	516.58	6328.07	.00001	.17924	.71698	.01850	1394.73
44	.058	534.12	6300.15	.00001	.15681	.62726	.01751	1594.24
45	.044	569.96	6233.93	.00000	.12603	.50415	.01626	1983.52
46	.037	588.28	6204.75	.00000	.12410	.49644	.01619	2014.36
47	.024	625.54	6133.81	.00000	.11434	.45739	.01576	2186.31
48	.018	644.48	6103.60	.00000	.11664	.46657	.01588	2143.28
49	.006	682.94	5981.05	.00000	.11079	.44316	.01557	2256.54
50	0.000	717.36	5926.14	.00000	.18478	.73913	.01858	1352.95
51	-.035	832.28	5703.44	.00000	.18620	.74482	.01858	1342.60
52	-.070	891.85	5604.96	.00000	.19274	.77098	.01872	1297.05
53	-.105	942.91	5376.61	.00000	.11962	.47849	.01602	2089.90
54	-.140	984.96	5301.43	.00000	.13808	.55231	.01670	1810.59
55	-.175	1017.80	5240.70	.00000	.17377	.69508	.01811	1438.68
56	-.180	1036.24	5210.13	.00000	.19905	.79621	.01865	1255.94
57	-.282	1093.16	5094.09	.00000	.18348	.73393	.01830	1362.53
58	-.384	1132.46	5005.36	.00000	.16307	.65230	.01776	1533.04
59	-.485	1187.34	4937.22	.00000	.16066	.64265	.01770	1556.05
60	-.587	1199.00	4933.96	.00000	.16596	.66386	.01785	1506.35
61	-.683	1221.13	4912.05	.00000	.15834	.63338	.01758	1578.83
62	-.790	1240.27	4890.97	.00000	.15980	.63920	.01766	1564.46
63	-.891	1270.85	4850.75	.00000	.15469	.61874	.01740	1616.18
64	-.993	1284.94	4835.12	.00000	.15696	.62785	.01751	1592.73
65	-1.146	1297.17	4823.58	.00000	.15412	.61650	.01737	1622.06
66	-1.369	1324.54	4792.40	.00000	.15133	.60531	.01722	1652.06
67	-2.565	1412.78	4656.69	.00000	.11686	.46746	.01589	2139.22
68	-3.763	1456.22	10357.79	.00072	.16860	.67727	.01777	1476.53
69	-4.962	1481.04	10258.81	.00065	.14091	.56625	.01679	1766.00
70	-6.162	1496.40	10208.00	.00062	.15829	.63564	.01729	1573.21
71	-7.363	1506.47	5180.94	.00000	.14244	.56976	.01676	1755.13
72	-8.566	1513.32	5159.18	.00000	.11085	.47941	.01603	2085.89

ORIGINAL PAGE IS OF POOR QUALITY

TABLE 7-11. COMBUSTOR CYCLE LIFE ANALYSIS, MR = 6.45, STATIONS 43 - 72, WITH TURBINE GAS REGENERATOR

HOURS OF FIRING TIME, T = 5.250E+00
DESIGN CYCLE LIFE, N, CYCLES = 2.500E+02
LIFE CYCLE SAFETY FACTOR = 4.000E+00
INITIAL JACKET TEMPERATURE, DEG F = -1.000E+02
INITIAL GAS-SIDE WALL TEMPERATURE, DEG F = -1.000E+02

STA.	X (IN)	HOT GAS PRESSURE (PSIA)	CREEP STRESS (PSIA)	CREEP DAMAGE FRACT.	FATIGUE DAMAGE FRACT.	DAMAGE FRACT.	UNIAX. STRAIN RANGE	CYCLE LIFE
43	.065	516.66	6292.19	.00001	.10922	.43690	.01549	2288.83
44	.058	534.20	6264.19	.00000	.09511	.38045	.01471	2628.46
45	.044	570.05	6193.06	.00000	.07790	.31160	.01365	3209.25
46	.037	588.37	6163.79	.00000	.07704	.30819	.01359	3244.73
47	.024	625.63	6086.64	.00000	.07208	.28833	.01325	3468.31
48	.018	644.58	6056.33	.00000	.07368	.29474	.01336	3392.79
49	.006	683.04	5901.00	.00000	.07176	.28705	.01323	3483.70
50	0.000	717.48	5845.87	.00000	.11354	.45415	.01572	2201.90
51	-.035	832.41	5601.81	.00000	.11492	.45968	.01579	2175.43
52	-.070	891.98	5502.00	.00000	.11778	.47113	.01594	2122.56
53	-.105	943.05	5191.23	.00000	.08241	.32963	.01394	3033.71
54	-.140	985.11	5112.87	.00000	.09243	.36971	.01455	2704.79
55	-.175	1017.96	5048.98	.00000	.11228	.44912	.01565	2226.57
56	-.180	1036.40	5018.00	.00000	.12091	.48362	.01607	2067.73
57	-.282	1093.35	4892.73	.00000	.11704	.46818	.01590	2135.93
58	-.384	1132.64	4796.27	.00000	.11067	.44270	.01557	2258.86
59	-.485	1187.53	4743.47	.00000	.11142	.44570	.01561	2243.67
60	-.587	1199.18	4752.11	.00000	.11564	.46256	.01583	2161.90
61	-.683	1221.32	4740.15	.00000	.11303	.45212	.01569	2211.79
62	-.790	1240.46	4726.73	.00000	.11599	.46397	.01585	2155.30
63	-.891	1271.05	4693.07	.00000	.11351	.45404	.01572	2202.43
64	-.993	1285.14	4682.95	.00000	.11702	.46807	.01590	2136.42
65	-1.146	1297.38	4678.09	.00000	.11705	.46820	.01590	2135.86
66	-1.369	1324.75	4656.00	.00000	.11816	.47266	.01596	2115.69
67	-2.565	1413.00	4530.46	.00000	.10983	.43931	.01552	2276.31
68	-3.763	1456.44	10093.76	.00057	.17468	.70101	.01758	1426.52
69	-4.962	1481.27	9993.73	.00050	.15717	.63070	.01699	1585.54
70	-6.162	1496.63	9945.92	.00067	.18242	.73237	.01754	1365.43
71	-7.363	1506.70	5044.96	.00000	.16941	.67764	.01708	1475.71
72	-8.566	1513.56	5020.91	.00000	.14259	.57035	.01637	1753.31

TABLE 7-12. COMBUSTOR/NOZZLE TRANSITION SECTION CYCLE LIFE

ANALYSIS, MR = 6.45, 1-3/4 PASS NOZZLE

LIFE CYCLE PARAMETERS

HOURS OF FIRING TIME, T =	5.250E+00
DESIGN CYCLE LIFE, N, CYCLES =	2.500E+02
LIFE CYCLE SAFETY FACTOR =	4.000E+00
INITIAL JACKET TEMPERATURE, DEG F =	-1.000E+02
INITIAL GAS-SIDE WALL TEMPERATURE, DEG F =	-1.000E+02

STA.	X (IN)	HOT GAS PRESSURE (PSIA)	CREEP STRESS (PSIA)	CREEP DAMAGE FRACT.	FATIGUE DAMAGE FRACT.	DAMAGE FRACT.	UNIAX. STRAIN RANGE	CYCLE LIFE
0	3.858	15.18	2589.42	.00000	.00894	.03576	.00448	27966.11
1	4.484	12.22	2588.60	.00000	.00833	.03330	.00425	30029.91
2	4.843	10.86	2587.95	.00000	.00820	.03280	.00420	30490.00
3	6.198	7.39	2584.57	.00000	.00762	.03050	.00382	32787.50
4	7.165	5.87	2581.61	.00000	.00756	.03024	.00365	33063.75

TABLE 7-13. FIXED NOZZLE (1-3/4 PASS) CYCLE LIFE ANALYSIS, MR = 6

HOURS OF FIRING TIME, T =	1.000E+01
DESIGN CYCLE LIFE, N, CYCLES =	3.000E+02
LIFE CYCLE SAFETY FACTOR =	4.000E+00
INITIAL JACKET TEMPERATURE, DEG F =	7.000E+01
INITIAL GAS-SIDE WALL TEMPERATURE, DEG F =	7.000E+01

STA.	X (IN)	HOT GAS PRESSURE (PSIA)	CREEP STRESS (PSIA)	CREEP DAMAGE FRACT.	FATIGUE DAMAGE FRACT.	DAMAGE FRACT.	UNIAX. STRAIN RANGE	CYCLE LIFE
0	7.165	5.67	22[illegible].89	.00000	.02422	.09656	.00221	12385.64
1	9.360	3.70	2[illegible].27	.00000	.02381	.09520	.00211	12597.20
2	10.599	3.06	31[illegible].31	.00000	.02374	.09496	.00210	12634.29
3	13.431	2.14	3[illegible].42	.00000	.02355	.09424	.00205	12735.95
4	15.052	2.02	422[illegible]5.51	.00000	.02355	.09422	.00205	12736.15
5	18.774	1.26	49825.27	.00000	.02358	.09432	.00206	12722.19
6	20.906	1.06	53521.51	.00000	.02359	.09437	.00206	12716.55
7	25.839	.76	62247.36	.00002	.02362	.09457	.00207	12689.39
8	28.667	.64	66637.53	.00006	.02362	.09481	.00207	12657.14
9	30.000	.66	66561.68	.00013	.02367	.09521	.00208	12604.04
10	28.667	.64	66536.79	.00002	.02258	.09064	.00184	13239.04
11	25.839	.76	62294.77	.00002	.02369	.09483	.00208	12654.17
12	20.906	1.06	53216.14	.00000	.02372	.09486	.00209	12648.04
13	18.774	1.26	49815.[illegible]	.00000	.02373	.09491	.00209	12643.55
14	15.052	2.02	42156.93	.00000	.02373	.09493	.00209	12641.33
15	13.431	2.14	38570.29	.00000	.02375	.09496	.00210	12633.85
16	10.599	3.06	31763.[illegible]	.00000	.02393	.09[illegible]	.00214	12534.47
17	9.360	3.7[illegible]	2[illegible].76	.00000	.02402	.09633	.00213	12456.55
18	7.165	5.87	22387.18	.00000	.02459	.09635	.00229	12201.77

TABLE 7-14. NOZZLE EXTENSION CYCLE LIFE ANALYSIS, MR = 6

HOURS OF FIRING TIME, T = 1.000E+01
DESIGN CYCLE LIFE, N, CYCLES = 3.000E+02
LIFE CYCLE SAFETY FACTOR = 4.000E+00
INITIAL JACKET TEMPERATURE, DEG F = 7.000E+01
INITIAL GAS-SIDE WALL TEMPERATURE, DEG F = 7.000E+01

STA.	X (IN)	HOT GAS PRESSURE (PSIA)	CREEP STRESS (PSIA)	CREEP DAMAGE FRACT.	FATIGUE DAMAGE FRACT.	DAMAGE FRACT.	UNIAX. STRAIN RANGE	CYCLE LIFE
0	30.000	.60	397.91	.00000	.02639	.10555	.00306	11369.27
1	35.187	.45	435.99	.00000	.00839	.03355	.00014	35772.17
2	38.989	.38	460.49	.00000	.00788	.03151	.00012	38079.85
3	43.091	.32	484.34	.00000	.00723	.02892	.00010	41494.35
4	47.680	.27	507.75	.00000	.00693	.02770	.00009	43316.86
5	52.739	.22	530.38	.00000	.00629	.02515	.00007	47712.76
6	58.397	.19	552.49	.00000	.00572	.02287	.00005	52460.30
7	64.585	.15	573.36	.00000	.00532	.02126	.00004	56432.17
8	71.547	.13	593.31	.00000	.00520	.02080	.00004	57681.74
9	79.290	.10	611.84	.00000	.00469	.01876	.00003	63966.58
10	86.996	.09	627.02	.00000	.00444	.01777	.00003	67521.76

ORIGINAL PAGE IS
OF POOR QUALITY

TABLE 7-15. ENGINE BALANCE, MR = 7

Engine Variables	Values
General	
Thrust, lbf	15,000
Chamber Pressure, psia	1,515
Mixture Ratio, Engine	7.0
Mixture Ratio, Thrust Chamber	7.745
Specific Impulse (Engine), seconds	468.0
Specific Impulse (Thrust Chamber), seconds	468.3
Engine Fuel Flowrate, lb/sec	4.040 (1)
Thrust Chamber Fuel Flowrate, lb/sec	3.616
Engine Oxidizer Flowrate, lb/sec	28.140 (2)
Thrust Chamber Oxidizer Flowrate, lb/sec	28.045
Dump Coolant Fuel Flowrate, lb/sec	0.36
Turbomachinery	
Low-Pressure Oxidizer Pump Speed, rpm	7,238
Low-Pressure Oxidizer Pump Efficiency	0.692
Low-Pressure Oxidizer Pump Horsepower	11.9
Low-Pressure Oxidizer Pump Inlet Pressure	16.3
Low-Pressure Oxidizer Pump Outlet Pressure	95.5
Low-Pressure Oxidizer Pump Diameter, inches	3.6
Low-Pressure Fuel Pump Speed, rpm	19,804
Low-Pressure Fuel Pump Efficiency	0.565
Low-Pressure Fuel Pump Horsepower	6.2
Low-Pressure Fuel Pump Inlet Pressure, psia	18.8
Low-Pressure Fuel Pump Outlet Pressure, psia	33.0
Low-Pressure Fuel Pump Diameter, inches	3.15

(1) Includes 0.034 lb/sec pressurization flow
(2) Includes 0.134 lb/sec pressurization flow

TABLE 7-15. ENGINE BALANCE, MR = 7 (CONT)

Engine Variables	Value
General - Turbomachinery	
High-Pressure Oxidizer Pump Speed, rpm	50,327
High-Pressure Oxidizer Pump Efficiency	0.660
High-Pressure Oxidizer Pump Horsepower	357
High-Pressure Oxidizer Pump Outlet Pressure, psia	2,346
High-Pressure Oxidizer Pump Diameter, inches	2.55
High-Pressure Fuel Pump Speed, rpm	102,143
High-Pressure Fuel Pump Efficiency	0.639
High-Pressure Fuel Pump Horsepower	1,281
High-Pressure Fuel Pump Outlet Pressure, psia	4,153
High-Pressure Fuel Pump Diameter, inches	3.8
High-Pressure Oxidizer Turbine Diameter, inches	4.85
High-Pressure Oxidizer Turbine Flowrate, lb/sec	2.63
High-Pressure Oxidizer Turbine Admission, %	24.5
High-Pressure Oxidizer Turbine Tip Speed, ft/sec	1,132
High-Pressure Oxidizer Turbine Velocity Ratio	0.42
High-Pressure Oxidizer Turbine Efficiency	0.641
High-Pressure Oxidizer Turbine Pressure Ratio	1.19
High-Pressure Fuel Turbine Diameter, inches	3.0
High-Pressure Fuel Turbine Flowrate, lb/sec	2.95
High-Pressure Fuel Turbine Admission, %	33
High-Pressure Fuel Turbine Tip Speed, ft/sec	1,490
High-Pressure Fuel Turbine Velocity Ratio	0.46
High-Pressure Fuel Turbine Efficiency	0.692
High-Pressure Fuel Turbine Pressure Ratio	1.59

TABLE 7-15. ENGINE BALANCE, MR = 7 (CONCL.)

Engine Variables	Value
Cooling Jacket	
Combustor Coolant Flowrate, lb/sec	3.65
Combustor Coolant Pressure Drop, psid	292
Combustor Heat Input, Btu/sec	7,275
Combustor Exit Temperature, R	747
Nozzle Coolant Flowrate, lb/sec	3.65
Nozzle Coolant Pressure Drop, psid	47.2
Nozzle Heat Input, Btu/sec	2,453
Nozzle Exit Temperature, R	938

Nozzle and Nozzle Extension Cycle Life. The regenerative cooling program results obtained for the NARloy-Z channel-wall transition section of the 1-3/4 pass nozzle are shown in Table 7-12. Four stations were examined in this case. The lowest life determined is 27966 cycles at the entrance to the nozzle transition section (Station 0).

The cycle life results for the fixed tubular (A286 material) nozzle are shown in Table 7-13. Eighteen stations were examined in the fixed nozzle case. Life throughout the length of the nozzle is approximately equal, and averages at a value of 12500 cycles.

Cycle life analysis results for the extension nozzle are shown for 10 stations in Table 7-14. The lowest life is determined at Station 0, at the nozzle attach plane. The minimum life is 11,369 cycles. Life at exit is 67522 cycles.

OPERATION AT MR = 7

The advanced expander cycle engine is designed to be capable of operation at an alternate engine mixture ratio of 7.0. The higher mixture ratio is intended to provide mission flexibility for round-trip missions using the same vehicle tanks as a delivery mission at a mixture ratio of 6.0.

A tabular balance summary and flow schematic for MR = 7, similar to those shown above for the design mixture ratio of 6.0, are presented as Table 7-15 and Fig. 7-12 . The data shown results from steady-state off-design computer modeling.

Valve resistance changes required to accomplish operation at MR = 7 are as follows:

Main Oxidizer Valve: Opened to 41% of its design resistance

Main Turbine Bypass Valve: Opened to 25.6% of its design resistance

Oxidizer Turbine Bypass Valve: Closed to 24.2 times its design resistance

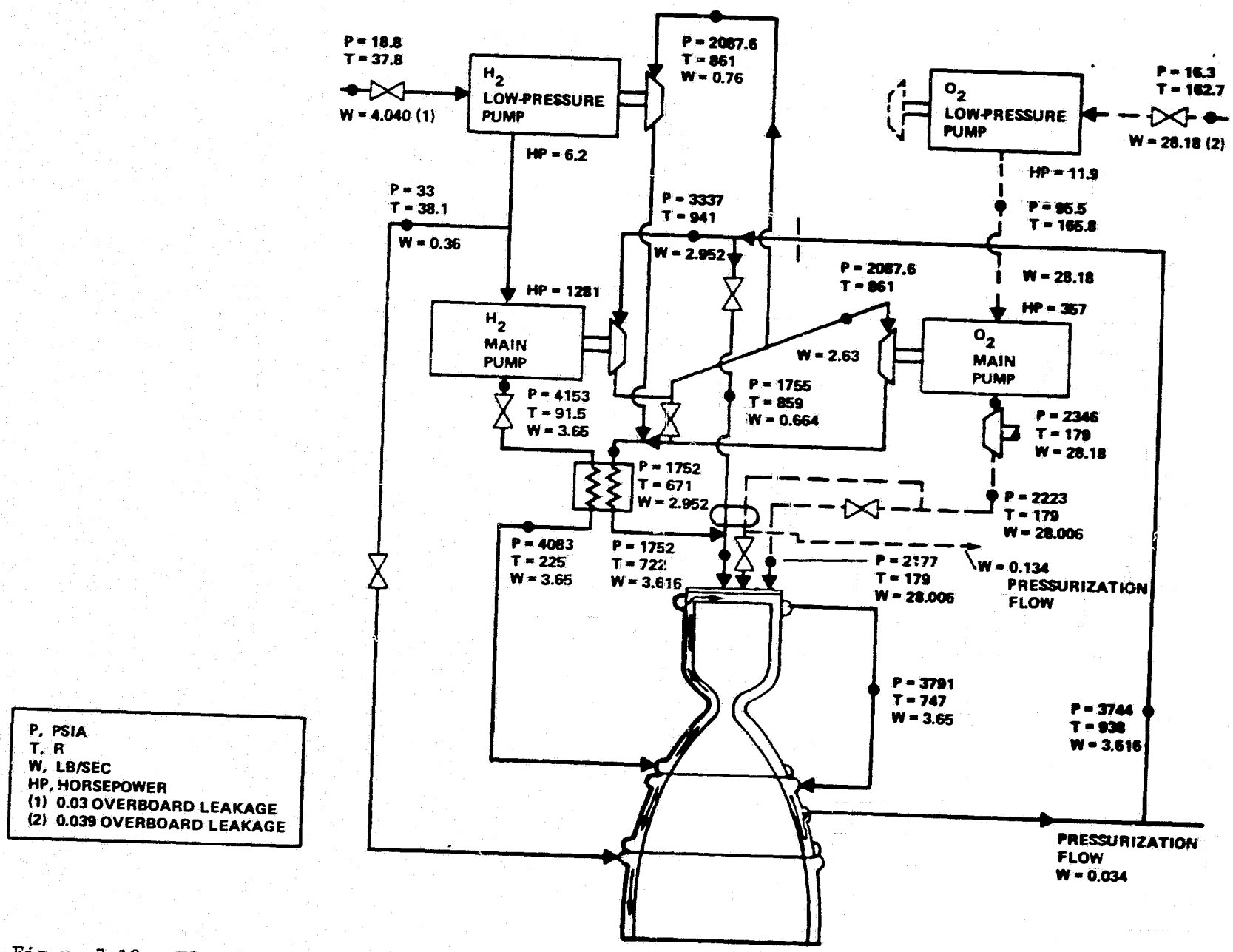

Figure 7-12. Flow, Pressure, Temperature and Power Schedule, F = 15K LB., MR = 7

The main fuel valve is left at its design resistance value.

Closing the OTBV and opening the MOV together serve to shift the engine mixture ratio higher by providing more power for pumping oxygen relative to fuel and by reducing the flow resistance downstream of the main oxidizer pump. Opening the main turbine bypass valve reduces net turbine power from the design level of 1970 HP to 1638 HP, a 17% reduction. The resulting turbine bypass fractions (as percent of thrust chamber hydrogen flow) are 18.4% for both turbines and 1.8% for the oxidizer turbine alone.

Performance Prediction - MR = 7

Table 7-16 presents a summary of performance calculations carried out for full-thrust operation at an engine mixture ratio of 7.0. The methods described above for design-point performance calculations were used to obtain the tabulated values.

The heat loss efficiency is slightly greater than the design value (0.9985 vs 0.998), reflecting the slight change in total heat load. Mixing efficiency is slightly poorer (See Table 7-7) than at on-design mixture ratio of 6:1. The major change is in kinetic losses which are significantly greater, due to the higher mixture ratio. Thrust chamber specific impulse has decreased 13 seconds from that obtained at MR = 6, mainly due to the lower kinetic efficiency at MR = 7 (-6 sec.) and the lower ideal specific impulse (-7 sec.) of the MR = 7 operation.

TABLE 7-16. ADVANCED EXPANDER ENGINE POINT DESIGN PERFORMANCE (THRUST = 15K, MR = 7.0)

• FLOW AND ENERGY BALANCE	
CHAMBER PRESSURE, PSIA	1515
AREA RATIO	625
ENGINE MIXTURE RATIO	7.0
THRUST CHAMBER MIXTURE RATIO	7.74
INJECTOR OXYGEN FLOWRATE, LB/SEC	28.006
INJECTOR HYDROGEN FLOWRATE, LB/SEC	3.616
DUMP COOLANT HYDROGEN FLOWRATE, LB/SEC	0.36
INJECTOR HYDROGEN NET HEAT GAIN, BTU/SEC	9024
DUMP COOLANT HYDROGEN NET HEAT GAIN, BTU/SEC	2555
• PERFORMANCE	
ODE SPECIFIC IMPULSE, SECONDS	495.74
HEAT LOSS EFFICIENCY, $\eta_{I_{S_{HL}}}$	0.9985
VAPORIZATION EFFICIENCY, $\eta_{I_{S_{VAP}}}$	1.0000
MIXING EFFICIENCY, $\eta_{I_{S_{MIX}}}$	0.9980
REACTION KINETIC EFFICIENCY, $\eta_{I_{S_{KIN}}}$	0.9791
2-D EXPANSION EFFIENCY, $\eta_{I_{S_{TD}}}$	0.9907
BOUNDARY LAYER EFFICIENCY, $\eta_{I_{S_{BL}}}$	0.9779
DELIVERED SPECIFIC IMPULSE, DUMP-COOLED NOZZLE, SECONDS	534.6
DELIVERED THRUST CHAMBER SPECIFIC IMPULSE, SECONDS*	468.3
DELIVERED ENGINE SPECIFIC IMPULSE, SECONDS	468.0

*I_S FROM INJECTOR FLOWS ONLY

Combustor Cycle Life at $M_R = 7$

The cycle life of the combustion chamber was analyzed at an engine mixture ratio of 7:1 using the regenerative cooling program. Table 7-17 presents the results. The minimum life is calculated for station 68, 3.76 inches from the throat. The calculated cycle life is 1284, a value which satisfies the safety factor required on life, i.e., 4 x 300 cycles.

Nozzle and Nozzle Extension Cycle Life at MR = 7

Table 7-18 details regenerative cooling code results for the transition section at the 7:1 mixture ratio. Minimum cycle life is 25,111 at station 0. A minimum cycle life of 12,072 (Table 7-19) is predicted for the fixed nozzle at Station 18, located at the exit plane of the fixed nozzle. The life of the extendible portion of the nozzle at this mixture ratio is expected to be very similar to that calculated at the design mixture ratio. This is due to the influence of the dump coolant valve (DCV) which keeps the nozzle extension dump coolant flow nearly constant at 0.36 lb/sec at $M_R = 7:1$.

The nozzle extension has excess cycle life at $M_R = 6:1$, similar to the case of the fixed nozzle. At $M_R = 7:1$, the fixed nozzle cycle life is reduced by only 129 cycles, or 1%. This supports the conclusion that the extendible nozzle cycle life will be more than adequate at the 7:1 mixture ratio, as a similar 1% reduction will result in more than adequate life for the extension.

LOW - THRUST OPERATION

Two reduced-thrust operating points have been defined for the Advanced Expander Engine. These include tank-head idle thrust and pumped idle thrust. Tank-head idle operation is accomplished with pumps locked (restrained from rotating). The engine operates in a purely pressure-fed mode. Tank-head idle operation is intended to provide for pump chill-down and conditioning.

TABLE 7-17. COMBUSTOR CYCLE LIFE ANALYSIS, MR = 7.7, WITH TURBINE GAS REGENERATOR

HOURS OF FIRING TIME, T = 5.250E+00
DESIGN CYCLE LIFE, N, CYCLES = 2.500E+02
LIFE CYCLE SAFETY FACTOR = 4.000E+00
INITIAL JACKET TEMPERATURE, DEG F = -1.000E+02
INITIAL GAS-SIDE WALL TEMPERATURE, DEG F = -1.000E+02

STA.	X (IN)	HOT GAS PRESSURE (PSIA)	CREEP STRESS (PSIA)	CREEP DAMAGE FRACT.	FATIGUE DAMAGE FRACT.	DAMAGE FRACT.	UNIAX. STRAIN RANGE	CYCLE LIFE
43	.065	505.21	5525.04	.00000	.12743	.50973	.01632	1961.80
44	.058	522.36	5497.69	.00000	.10956	.43824	.01551	2281.84
45	.044	557.42	5429.76	.00000	.09123	.36494	.01448	2740.17
46	.037	575.33	5401.17	.00000	.09026	.36103	.01442	2769.88
47	.024	611.77	5327.79	.00000	.08430	.33721	.01406	2965.52
48	.018	630.30	5298.18	.00000	.08618	.34473	.01418	2900.85
49	.006	667.91	5157.18	.00000	.08324	.33295	.01399	3003.50
50	0.000	701.58	5103.33	.00000	.13265	.53061	.01650	1884.63
51	-.035	813.96	4871.31	.00000	.13456	.53825	.01657	1857.88
52	-.070	872.22	4774.21	.00000	.13932	.55730	.01674	1794.37
53	-.105	922.16	4496.03	.00000	.09374	.37495	.01463	2667.02
54	-.140	963.28	4420.01	.00000	.10455	.41822	.01524	2391.11
55	-.175	995.40	4358.78	.00000	.13019	.52077	.01642	1920.23
56	-.180	1013.43	4328.70	.00000	.14342	.57369	.01688	1743.11
57	-.282	1069.12	4209.85	.00000	.13793	.55170	.01669	1812.57
58	-.384	1107.54	4117.72	.00000	.12787	.51149	.01633	1955.08
59	-.485	1161.21	4061.47	.00000	.12923	.51693	.01638	1934.49
60	-.587	1172.61	4066.09	.00000	.13608	.54433	.01663	1837.13
61	-.683	1194.25	4051.13	.00000	.13208	.52831	.01648	1892.83
62	-.790	1212.97	4035.35	.00000	.13694	.54775	.01666	1825.64
63	-.891	1242.88	4000.13	.00000	.13311	.53245	.01652	1878.12
64	-.993	1256.66	3988.24	.00000	.13921	.55684	.01673	1795.85
65	-1.146	1268.62	3982.08	.00000	.14017	.56069	.01677	1783.50
66	-1.369	1295.39	3957.96	.00000	.14257	.57030	.01684	1753.47
67	-2.565	1381.68	3811.11	.00000	.11445	.45779	.01577	2184.39
68	-3.763	1424.17	8476.07	.00015	.19451	.77865	.01788	1284.27
69	-4.962	1448.44	8377.36	.00012	.17745	.71032	.01733	1407.82
70	-6.162	1463.46	8322.97	.00017	.18962	.75915	.01747	1317.26
71	-7.363	1473.31	4215.23	.00000	.17778	.71113	.01705	1406.22
72	-8.566	1480.01	4199.03	.00000	.19348	.77393	.01723	1292.11

TABLE 7-18. COMBUSTOR NOZZLE TRANSITION SECTION, CYCLE LIFE

1-3/4 PASS, MR = 7.7, WITH TURBINE GAS REGENERATOR

LIFE CYCLE PARAMETERS

HOURS OF FIRING TIME, T =	5.250E+00
DESIGN CYCLE LIFE, N, CYCLES =	2.500E+02
LIFE CYCLE SAFETY FACTOR =	4.000E+00
INITIAL JACKET TEMPERATURE, DEG F =	-1.000E+02
INITIAL GAS-SIDE WALL TEMPERATURE, DEG F =	-1.000E+02

STA.	X (IN)	HOT GAS PRESSURE (PSIA)	C-EFF STRESS (PSIA)	CREEP DAMAGE FRACT.	FATIGUE DAMAGE FRACT.	DAMAGE FRACT.	UNIAX. STRAIN RANGE	CYCLE LIFE
0	3.858	14.84	2298.[illegible]	.00000	.00995	.03982	.00486	25111.38
1	4.484	11.95	2297.38	.00000	.00935	.03740	.00464	26737.79
2	4.843	10.62	2296.78	.00000	.00922	.03686	.00458	27126.28
3	6.198	7.23	2293.58	.00000	.00828	.03311	.00423	30201.34
4	7.165	5.74	2290.73	.00000	.00787	.03149	.00407	31758.04

ORIGINAL PAGE IS
OF POOR QUALITY

TABLE 7-17. FIXED NOZZLE CYCLE LIFE, 1-3/4 PASS,

MR = 7.7, WITH TURBINE GAS REGENERATOR

HOURS OF FIRING TIME, T = 1.000E+01
DESIGN CYCLE LIFE, N, CYCLES = 3.000E+02
LIFE CYCLE SAFETY FACTOR = 4.000E+00
INITIAL JACKET TEMPERATURE, DEG F = 7.000E+01
INITIAL GAS-SIDE WALL TEMPERATURE, DEG F = 7.000E+01

STA.	X (IN)	HOT GAS PRESSURE (PSIA)	CREEP STRESS (PSIA)	CREEP DAMAGE FRACT.	FATIGUE DAMAGE FRACT.	DAMAGE FRACT.	UNIAX. STRAIN RANGE	CYCLE LIFE
0	7.165	5.74	19691.56	.00000	.02472	.09886	.00233	12138.12
1	9.360	3.61	25177.63	.00000	.02448	.09790	.00227	12256.92
2	10.599	3.01	28082.06	.00000	.02445	.09782	.00226	12267.76
3	13.431	2.09	33994.34	.00000	.02438	.09753	.00225	12303.66
4	15.052	1.97	37100.55	.00000	.02443	.09770	.00226	12282.09
5	18.774	1.23	43870.59	.00000	.02453	.09811	.00228	12231.45
6	20.906	1.04	47389.58	.00000	.02457	.09827	.00229	12211.70
7	25.839	.74	54808.93	.00000	.02464	.09856	.00231	12175.84
8	28.667	.62	58674.67	.00001	.02465	.09862	.00231	12168.53
9	30.000	.58	60309.13	.00001	.02469	.09882	.00232	12143.36
10	28.667	.62	58673.93	.00001	.02359	.09441	.00206	12710.74
11	25.839	.74	54806.34	.00000	.02464	.09856	.00231	12174.81
12	20.906	1.04	47382.20	.00000	.02457	.09827	.00229	12211.62
13	18.774	1.23	43860.36	.00000	.02453	.09811	.00228	12231.70
14	15.052	1.97	37142.03	.00000	.02442	.09769	.00226	12283.19
15	13.431	2.09	33980.31	.00000	.02438	.09751	.00224	12306.51
16	10.599	3.01	27950.07	.00000	.02443	.09773	.00226	12281.06
17	9.360	3.61	25122.45	.00000	.02451	.09804	.00228	12240.09
18	7.165	5.74	19694.59	.00000	.02485	.09940	.00236	12072.42

ORIGINAL PAGE IS
OF POOR QUALITY

In both idle modes, it is desirable to achieve the highest possible mixture ratio in the interest of avoiding performance loss. Mixture ratios obtainable are limited by pump and feed-system stability. Engine modification to provide pump recirculation and adequate injector pressure drop is a potential means of increasing idle mode mixture ratio.

Tanked - Idle Operation

Predicted engine system operating parameters at tanked-idle are summarized in Table 7-20. Figure 7-13 presents schematically the flows, temperatures, and pressures resulting from computer balances at tank-head idle. Performance prediction data, obtained by the method described above, are presented in Table 7-21.

Valve positions for tank-head idle operation are summarized below.

TANK-HEAD IDLE CONTROL VALVE POSITION

VALVE	POSITION %	RESISTANCE $SEC^2/IN^2\ FT^3$
Main Fuel Valve	100.0	25.55
Main Oxidizer Valve	0.0	
Main Turbine Bypass Valve	100.0	55.76
Oxidizer Turbine Bypass Valve	73.0	713.7

Because the MOV is fully closed for tank-head idle operation, the thrust chamber is supplied with oxygen through the gaseous oxidizer valve, which is fully opened during this operating mode.

TABLE 7-20. ENGINE BALANCE AT TANKED IDLE

ENGINE VARIABLES	VALUES
General	
Thrust, lbf	61.3
Chamber Pressure, psia	7.2
Mixture Ratio, Engine	2.85
Mixture Ratio, Thrust Chamber	3.11
Specific Impulse (Engine), seconds	450.4
Specific Impulse (Thrust Chamber), seconds	456.2
Engine Fuel Flowrate, lb/sec	0.0353
Thrust Chamber Fuel Flowrate, lb/sec	0.03194
Engine Oxidizer Flowrate, lb/sec	0.1007
Thrust Chamber Oxidizer Flowrate, lb/sec	0.09934
Dump Coolant Fuel Flowrate, lb/sec	0.03
Turbomachinery	
Low-Pressure Oxidizer Pump Speed, rpm	0.0
Los-Pressure Oxidizer Pump Efficiency	--
Low-Pressure Oxidizer Pump Horsepower	0.0
Low-Pressure Oxidizer Pump Inlet Pressure	15.4
Low-Pressure Oxidizer Pump Outlet Pressure	15.4
Low-Pressure Oxidizer Pump Diameter, inches	3.6
Low-Pressure Fuel Pump Speed, rpm	0.0
Low-Pressure Fuel Pump Efficiency	--
Low-Pressure Fuel Pump Horsepower	0.0
Low-Pressure Fuel Pump Inlet Pressure, psia	18.3
Low-Pressure Fuel Pump Outlet Pressure, psia	18.3
Low-Pressure Fuel Pump Diameter, inches	3.14

TABLE 7-20. ENGINE BALANCE AT TANKED IDLE (Continued)

ENGINE VARIABLES	VALUE
General Turbomachinery	
High-Pressure Oxidizer Pump Speed, rpm	0.0
High-Pressure Oxidizer Pump Efficiency	--
High-Pressure Oxidizer Pump Horsepower	0.0
High-Pressure Oxidizer Pump Outlet Pressure, psia	15.4
High-Pressure Oxidizer Pump Diameter, inches	2.55
High-Pressure Fuel Pump Speed, rpm	0.0
High-Pressure Fuel Pump Efficiency	--
High-Pressure Fuel Pump Horsepower	0.0
High-Pressure Fuel Pump Outlet Pressure, psia	18.3
High-Pressure Fuel Pump Diameter, inches	3.8
High-Pressure Oxidizer Turbine Diameter, inches	4.85
High-Pressure Oxidizer Turbine Flowrate, lb/sec	0.010
High-Pressure Oxidizer Turbine Admission, %	24.5
High-Pressure Oxidizer Turbine Tip Speed, ft/sec	0.0
High-Pressure Oxidizer Turbine Velocity Ratio	0.0
High-Pressure Oxidizer Tubeine Efficiency	--
High-Pressure Oxidizer Turbine Pressure Ratio	1.08
High-Pressure Fuel Turbine Diameter, inches	3.0
High-Pressure Fuel Turbine Flowrate, lb/sec	0.033
High-Pressure Fuel Turbine Admission, %	33
High-Pressure Fuel Turbine Tip Speed, ft/sec	0.0
High-Pressure Fuel Turbine Velocity Ratio	0.0
High-Pressure Fuel Turbine Efficiency	--
High-Pressure Fuel Turbine Pressure Ratio	1.40

C-6

TABLE 7-20. ENGINE BALANCE AT TANKED IDLE
(Continued)

ENGINE VARIABLES	VALUE
Cooling Jacket	
Combustor Coolant Flowrate, lb/sec	0.032
Combustor Coolant Pressure Drop, psid	0.01
Combustor Heat Input, Btu/sec	84.3
Combustor Exit Temperature, R	633
Nozzle Coolant Flowrate, lb/sec	0.032
Nozzle Coolant Pressure Drop, psid	0.18
Nozzle Heat Input, Btu/sec	27.4
Nozzle Exit Temperature, R	661.4

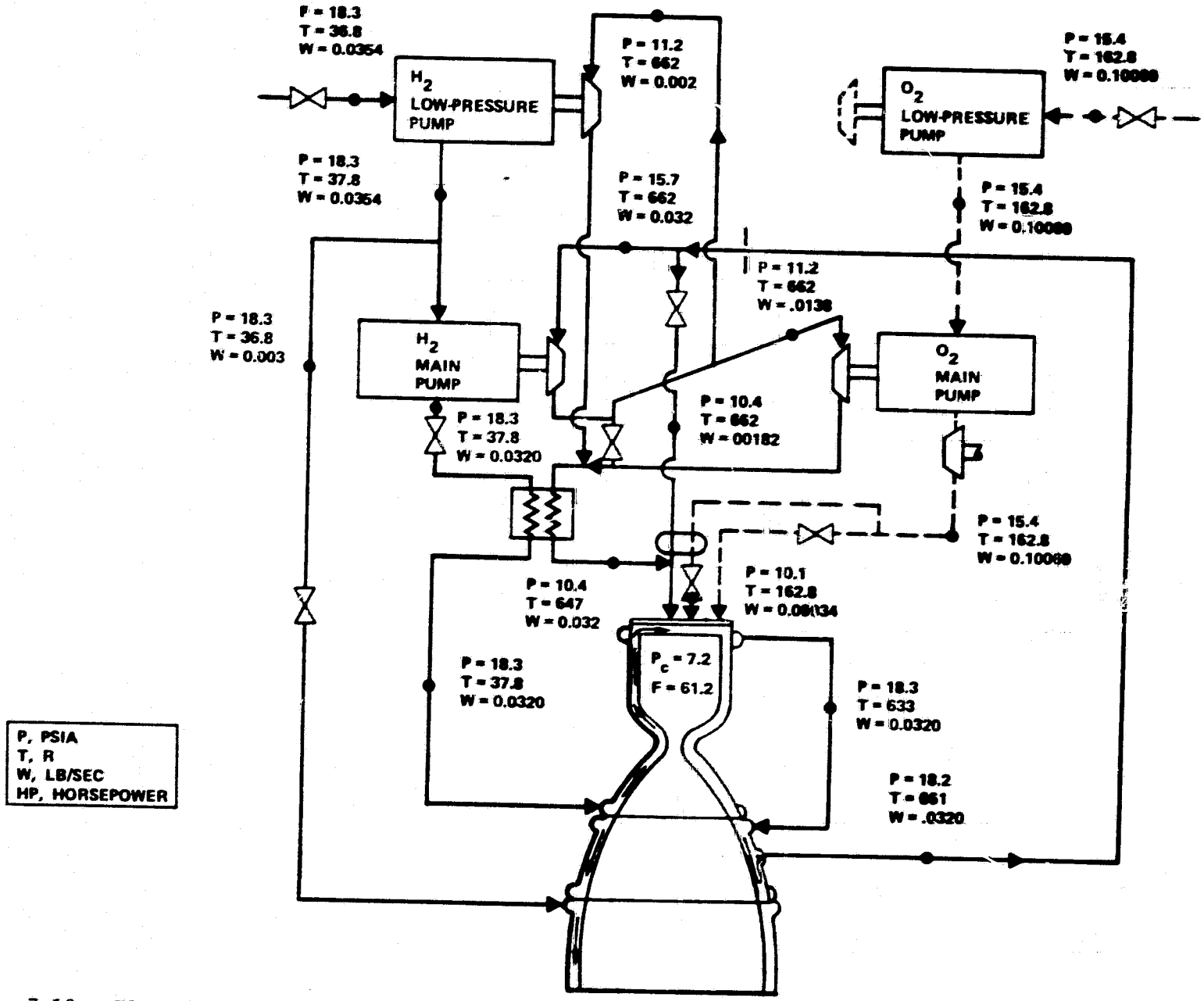

Figure 7-13. Flow, Pressure, and Temperature Schedules - Tank Head Idle

TABLE 7-21. ADVANCED EXPANDER PERFORMANCE AT TANKED IDLE

● FLOW AND ENERGY BALANCE	
CHAMBER PRESURE, PSIA	7.2
AREA RATIO	625
ENGINE MIXTURE RATIO	2.85
THRUST CHAMBER MIXTURE RATIO	3.11
INJECTOR OXYGEN FLOWRATE, LB/SEC	0.0993
INJECTOR HYDROGEN FLOWRATE, LB/SEC	0.0319
DUMP COOLANT HYDROGEN FLOWRATE, LB/SEC	0.003
INJECTOR HYDROGEN NET HEAT GAIN, BTU/SEC	111.7
DUMP COOLANT HYDROGEN NET HEAT GAIN, BTU/SEC	
● PERFORMANCE	
ODE SPECIFIC IMPULSE, SECONDS	503.2
HEAT LOSS EFFICIENCY, $\eta_{I_{S_{HL}}}$	1.00
VAPORIZATION EFFICIENCY, $\eta_{I_{S_{VAP}}}$	0.9980
MIXING EFFICIENCY, $\eta_{I_{S_{MIX}}}$	1.00
REACTION KINETIC EFFICIENCY, $\eta_{I_{S_{KIN}}}$	0.9833
2-D EXPANSION EFFICIENCY, $\eta_{I_{S_{TD}}}$	0.9907
BOUNDARY LAYER EFFICIENCY, $\eta_{I_{S_{BL}}}$	0.9344
DELIVERED SPECIFIC IMPULSE, DUMP-COOLED NOZZLE, SEC	534.6
DELIVERED THRUST CHAMBER SPECIFIC IMPULSE, SEC*	456.2
DELIVERED ENGINE SPECIFIC IMPULSE, SEC	450.4

*I_S FROM INJECTOR FLOWS ONLY

Pumped-Idle Operation

The results of steady-state model balances for pumped-idle operation are presented in Table 7-22 and in Figure 7-14 . A detailed performance prediction breakdown is provided in Table 7-23.

The pumped-idle thrust level is 1800 lb, or 12% of full thrust. Engine mixture ratio is 4.0. This mixture ratio was selected as the highest M_R which does not lead to instability as predicted by Transient model runs.

To achieve this operating state, engine system control valves are adjusted as follows:

Main Oxidizer Valve:	Closed to 17.2 times design resistance
Main Turbine Bypass Valve:	Fully opened to 1% of design resistance
Oxidizer Turbine Bypass Valve:	Opened to 39.4% of design resistance

The main fuel valve is left in its fully open position.

The net effect of these control inputs is to reduce available turbine flowrate by bypassing 60% of the heated hydrogen around both main turbines, and to adjust the power split between the turbines to match the mixture ratio. Increased MOV resistance helps lower the mixture ratio to 4.0.

Oxidizer-Side Pressure Drops. The design MOV ΔP is 378 psi, and the oxidizer injector ΔP is 604 psi at design. At the pumped-idle thrust level (12% of full thrust), the oxidizer injector ΔP is only 7 psi. In order to assure stability of the oxidizer flow at low thrust, additional flow resistance must be provided between the injector and pump discharge. This is accomplished by operating in pumped idle with the MOV closed to increase its resistance from 0.53 $sec^2/in^2 ft^3$ to 9.09 $sec^2/in^2\ ft^3$. This results in an MOV pressure drop of 84.6 psi at pumped idle.

TABLE 7-22. ENGINE BALANCE - PUMPED IDLE

ENGINE VARIABLES	VALUES
General	
Thrust, lbf	1800.
Chamber Pressure, psia	203.
Mixture Ratio, Engine	4.0
Mixture Ratio, Thrust Chamber	4.31
Specific Impulse (Engine), seconds	471.3
Specific Impulse (Thrust Chamber), seconds	471.8
Engine Fuel Flowrate, lb/sec	0.7796
Thrust Chamber Fuel Flowrate, lb/sec	0.7077
Engine Oxidizer Flowrate, lb/sec	3.14068
Thrust Chamber Oxidizer Flowrate, lb/sec	3.0507
Dump Coolant Fuel Flowrate, lb/sec	0.05
Turbomachinery	
Low-Pressure Oxidizer Pump Speed, rpm	808.
Low-Pressure Oxidizer Pump Efficiency	0.692
Low-Pressure Oxidizer Pump Horsepower	0.02
Low-Pressure Oxidizer Pump Inlet Pressure	16.33
Low-Pressure Oxidizer Pump Outlet Pressure	17.3
Low-Pressure Oxidizer Pump Diameter, inches	3.60
Low-Pressure Fuel Pump Speed, rpm	11280.
Low-Pressure Fuel Pump Efficiency	0.522
Low-Pressure Fuel Pump Horsepower	0.91
Low-Pressure Fuel Pump Inlet Pressure, psia	18.8
Low-Pressure Fuel Pump Outlet Pressure, psia	28.6
Low-Pressure Fuel Pump Diameter, inches	3.14

TABLE 7-22. ENGINE BALANCE - PUMPED IDLE
(continued)

ENGINE VARIABLES	VALUES
General Turbomachinery	
High-Pressure Oxidizer Pump Speed, rpm	15,976
High-Pressure Oxidizer Pump Efficiency	0.572
High-Pressure Oxidizer Pump Horsepower	5.63
High-Pressure Oxidizer Pump Outlet Pressure, psia	295.
HIgh-Pressure Oxidizer Pump Diameter, inches	2.55
High-Pressure Fuel Pump Speed, rpm	35,230.
High-Pressure Fuel Pump Efficiency	0.435
High-Pressure Fuel Pump Horsepower	46.6
High-Pressure Fuel Pump Outlet Pressure, psia	499.
High-Pressure Fuel Pump Diameter, inches	3.8
High-Pressure Oxidizer Turbine Diameter, inches	4.85
High-Pressure Oxidizer Turbine Flowrate, lb/sec	0.22
High-Pressure Oxidizer Turbine Admission, %	24.5
High-Pressure Oxidizer Turbine Tip Speed, ft/sec	305.9
High-Pressure Oxidizer Turbine Velocity Ratio	0.23
High-Pressure Oxidizer Turbine Efficiency	0.450
High-Pressure Oxidizer Turbine Pressure Ratio	1.06
HIgh-Pressure Fuel Turbine Diameter, inches	3.0
High-Pressure Fuel Turbine Flowrate, lb/sec	0.28
High-Pressure Fuel Turbine Admission, %	33.
High-Pressure Fuel Turbine Tip Speed, ft/sec	617.5
High-Pressure Fuel Turbine Velocity Ratio	0.25
High-Pressure Fuel Turbine Efficiency	0.58
High-Pressure Fuel Turbine Pressure Ratio	1.31

TABLE 7-22. ENGINE BALANCE - PUMPED IDLE
(Continued)

ENGINE VARIABLES	VALUES
Cooling Jacket	
Combustor Coolant Flowrate, lb/sec	0.724
Combustor Coolant Pressure Drop, psid	31.5
Combustor Heat Input, Btu/sec	1192.2
Combustor Exit Temperature, R	585
Nozzle Coolant Flowrate, lb/sec	0.724
Nozzle Coolant Pressure Drop, psid	4.18
Nozzle Heat Input, Btu/sec	460.3
Nozzle Exit Temperature, R	766.9

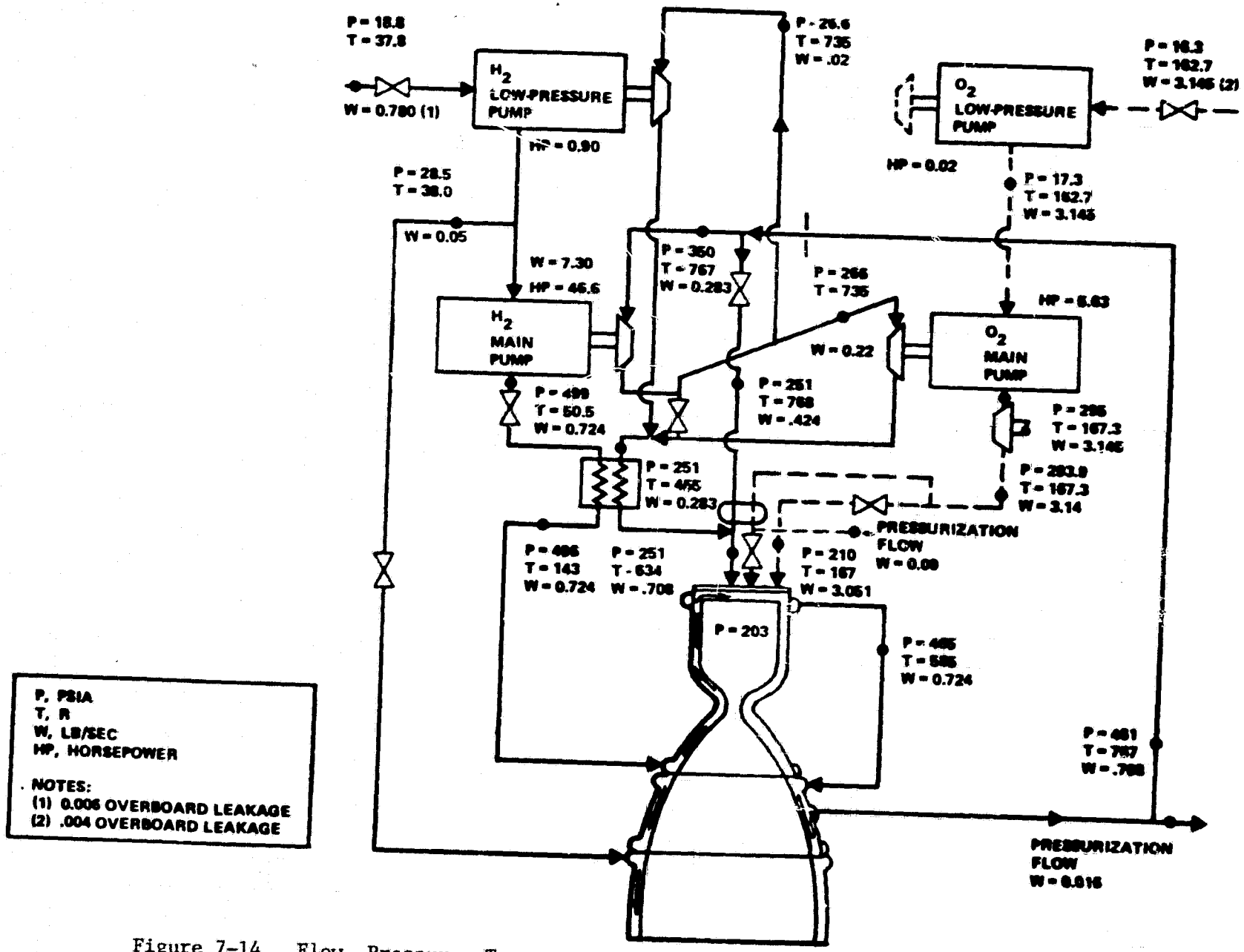

Figure 7-14. Flow, Pressure, Temperature, and Power Schedules, Pumped Idle

TABLE 7-23. ADVANCED EXPANDER THRUST CHAMBER PERFORMANCE (THRUST = 1.0K, MR = 4.0)

• FLOW AND ENERGY BALANCE	
CHAMBER PRESSURE, PSIA	203
AREA RATIO	625
ENGINE MIXTURE RATIO	4.0
THRUST CHAMBER MIXTURE RATIO	4.31
INJECTOR OXYGEN FLOWRATE, LB/SEC	3.0507
INJECTOR HYDROGEN FLOWRATE, LB/SEC	0.7707
DUMP COOLANT HYDROGEN FLOWRATE, LB/SEC	0.05
INJECTOR HYDROGEN NET HEAT GAIN, BTU/SEC	1530.5
DUMP COOLANT HYDROGEN NET HEAT GAIN, BTU/SEC	366.5
• PERFORMANCE	
ODE SPECIFIC IMPULSE, SECONDS	501.98
HEAT LOSS EFFICIENCY, $\eta_{I_{S_{HL}}}$	0.9975
VAPORIZATION EFFICIENCY, $\eta_{I_{S_{VAP}}}$	1.000
MIXING EFFICIENCY, $\eta_{I_{S_{MIX}}}$	1.000
REACTION KINETIC EFFICIENCY, $\eta_{I_{S_{KIN}}}$	0.9849
2-D EXPANSION EFFIENCY, $\eta_{I_{S_{TD}}}$	0.9907
BOUNDARY LAYER EFFICIENCY, $\eta_{I_{S_{BL}}}$	0.9665
DELIVERED SPECIFIC IMPULSE, DUMP-COOLED NOZZLE, SECONDS	534.6
DELIVERED THRUST CHAMBER SPECIFIC IMPULSE, SECONDS*	471.81
DELIVERED ENGINE SPECIFIC IMPULSE, SECONDS	471.35

*I_S FROM INJECTOR FLOWS ONLY

WEIGHT AND MASS-PROPERTY BREAKDOWNS

One of the design objectives for the expander point design studies was maintaining component weight at levels compatible with payload performance requirements. In keeping with this approach, weights were calculated for each component. Material selections were reviewed and substitution made where weight could be reduced. Excess material was scalloped from turbopump flanges and injector body. Manifold cross sectional areas were reduced and tapered. Minimum thickness thrust chamber tubes were utilized and jackets chem milled to minimum thickness. Inconel 718 and Incoloy 903 were used for propellant ducting to minimize wall thickness.

Some effort has already been expended toward weight reduction, but with further analysis and design effort, it is expected that significant improvements will be possible. This is due in part to designs which reflect conservative design philosophy as well as the fact that some weights are estimates based on past experience, where improved technology may permit more efficient designs.

Final component weights are presented in Table 7-24. Wrap-around inlet ducts (13.5 pounds) and engine controller (24 pounds) are not included in the point design weight. Mass properties are presented in Table 7-25, for the engine in the nozzle retracted (stowed position) and nozzle extended (operating position).

Stable oxidizer system operation is achieved at a penalty of increased oxidizer pump power requirement, relative to operation with smaller main valve resistance requirements.

Performance Prediction - Pumped Idle. The methodology described in the performance section was applied to predict thrust chamber and system performance at pumped-idle thrust. The resulting performance breakdown, Table 7-23 yields 471.3 seconds as the engine specific impulse. This value is approximately 9.5 seconds below the design performance of 480.8 seconds (Table 7-7). Theoretical (ODE) specific impulse at pumped idle is nearly equal to that at mainstage. Reductions in theoretical I_{sp} caused by the lower hydrogen injection temperature counterbalanced by improvements due to mixture ratio reduction. The heat loss efficiency term is slightly smaller than at design, because slightly more energy relative to the total is picked up prior to boundary layer attachment in pumped idle mode than at mainstage. C* efficiency, consisting of mixing and vaporization terms, is unity at this operating point, as shown in Figure 7-5 and Table 2-4. Kinetic losses are significantly greater than at mainstage, due to the lower chamber pressure. Approximately four seconds of additional loss are encountered at pumped idle. The 2-D expansion efficiency, a function of geometry and gas properties, remains at its design value. Boundary-layer losses are greater by about 5.5 seconds than at design, due to operation at lower thrust and chamber pressure.

TABLE 7-24. EXPANDER CYCLE ENGINE
POINT DESIGN WEIGHT CHARACTERISTICS

DESCRIPTION	WEIGHT POUNDS
Thrust Chamber	(205.4)
Injector	9.4
Combustor	50.7
Fixed Nozzle (1-1/2 Pass)	62.6
Extendible Nozzle	82.7
Turbopumps	(109.5)
Low Pressure H_2	13.8
High Pressure H_2	37.3
Low Pressure O_2	18.8
High Pressure H_2	39.6
Propellant Valves	23.7
Control Valves	4.9
Propellant Ducts	17.0
I.F., Purge & Control Lines	2.3
Gimbal Bearing	6.0
Actuator Struts	6.5
Extendible Mechanism	36.0
H_2 Regenerator	16.0
O_2 Heat Exchanger	21.0
Harness & Sensors	5.2
Ignition System	3.1
System Installation Parts	4.4
TOTAL POUNDS	461.0

TABLE 7-25. EXPANDER CYCLE ENGINE MASS PROPERTIES

DESCRIPTION	WEIGHT POUNDS
Thrust Chamber	(205.4)
Injector	9.4
Combustor	50.7
Fixed Nozzle (1-1/2 Pass)	62.6
Extendible Nozzle	82.7
Turbopumps	(109.5)
Low Pressure H_2	13.8
High Pressure H_2	37.3
Low Pressure O_2	18.8
High Pressure H_2	39.6
Propellant Valves	23.7
Control Valves	4.9
Propellant Ducts	17.0
I.F., Purge & Control Lines	2.3
Gimbal Bearing	6.0
Actuator Struts	6.5
Extendible Mechanism	36.0
H_2 Regenerator	16.0
O_2 Heat Exchanger	21.0
Harness & Sensors	5.2
Ignition System	3.1
System Installation Parts	4.4
TOTAL POUNDS	461.0

MASS PROPERTIES ABOUT GIMBAL AXIS - NOZZLE EXTENDED

WEIGHT POUNDS	$\bar{x}$ INCH	$\bar{y}$ INCH	$\bar{z}$ INCH	Ixx SLUG FT^2	Iyy SLUG FT^2	Izz SLUG FT^2
461.0	-34.7	0.3	1.12	21.7	205.0	206.0

MASS PROPERTIES ABOUT CENTER OF GRAVITY - NOZZLE EXTENDED

WEIGHT POUNDS	$\bar{x}$ INCH	$\bar{y}$ INCH	$\bar{z}$ INCH	Ixe SLUG FT^2	Iye SLUG FT^2	Ize SLUG FT^2
461.0	-34.7	0.3	1.12	21.6	85.0	86.7

MASS PROPERTIES ABOUT CENTER OF GRAVITY - NOZZLE RETRACTED

WEIGHT POUND	$\bar{x}$ INCH	$\bar{y}$ INCH	$\bar{z}$ INCH	Ixr SLUG FT^2	Iyr SLUG FT^2	Izr SLUG FT^2
461.0	-27.9	0.3	1.12	21.6	48.7	50.4

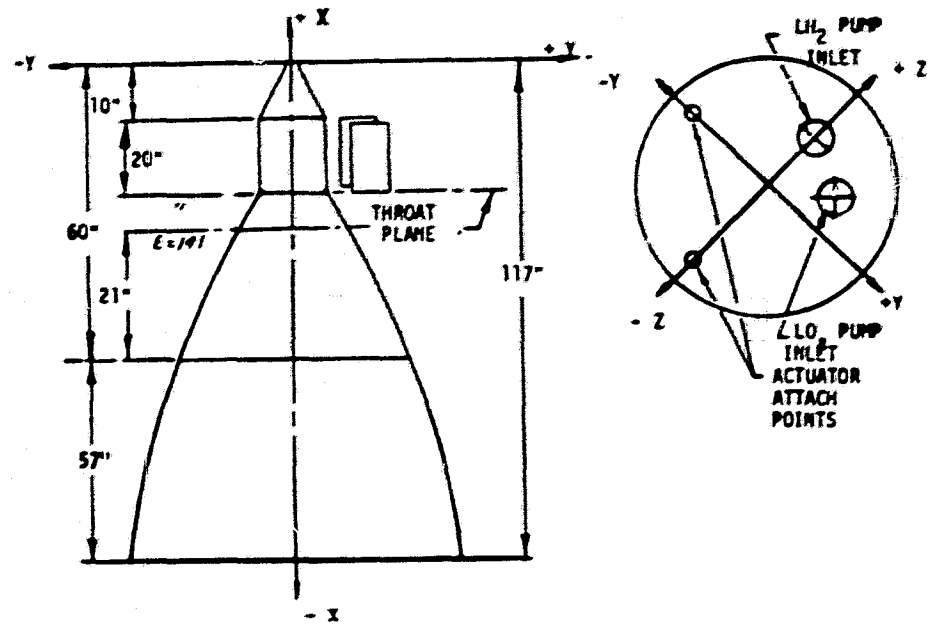

NPSH REQUIREMENTS AND CAPABILITIES

The original suction requirements that the OTV boost pumps were designed to accommodate are summarized in Table 7-26. The Net Positive Suction Head (NPSH) values are finite and positive, and the boost pumps will operate at these values without vapor in the flow.

TABLE 7-26. ORIGINAL OTV SUCTION REQUIREMENTS

Propellant	H_2	O_2
Tank Vapor Pressure, psia	18.4	15.6
Pump Inlet NPSH, Ft.	15	2

This means that the pump inlets were sized so that the NPSH's supplied at the pump inlets are equal to, or greater than, the inlet flow velocity head. However, it is also true that pumps designed to this criteron will often operate satisfactorily at zero tank NPSH, which is a two-phase (vapor-liquid) operating condition at the pump inlet (Ref.7-3,7-6,7-7,& 7-8. This is an advantage because it eliminates the constraint of having to pressurize the tanks. Therefore, an analysis was conducted to determine the tank vapor pressures under which those boost pumps would operate at zero tank NPSH.

Because unpressurized tanks are the ultimate goal of zero tank NPSH, the analysis must begin with saturated liquid in the tanks (which is zero tank NPSH by definition), and must include a treatment of the vehicle accelerations, the inlet line flow accelerations, and the inlet line losses. The assumed inlet line geometries are summarized in Table 7-27 and the method for calculating inlet line pressure drops is summarized in Table 7-28. It must be noted that this inlet line analysis is approximate because (1) the geometries in Table 7-27 are a function of the vehicle, which is not fully defined at this time, and (2) as implied in Table 7-28 , the pressure drop calculations were

simplified considerably by using constant values of liquid density, which produces results that are slightly optimistic. However, the results are close enough to give a good evaluation of potential capabilities.

For the existing preliminary designs of the OTV boost pumps, the pump inlet geometries, and the operating conditions at both full thrust and pump idle modes, are summarized in Table 7-29. This zero NPSH evaluation was conducted for both operating modes, because both are contractual requirements. As discussed in detail below, the results of the analysis indicate that these designs will operate at zero tank NPSH with little or no modifications if the tank vapor pressures are equal to, or greater than, those shown in Table 7-26. If the tank vapor pressures are reduced to a very low value of 10 psia, relatively minor design modifications would be required. These modifications are: (1) on the LOX side, a 20% increase in inlet line and boost pump inlet tip diameters in orde r to accommodate full thrust operation, and (2) on the LH_2 side, a 25% decrease in rotational speed when operating at pump idle mode. No modifications are required to operate the LH_2 boost pump at full thrust, or the LOX boost pump at pump idle mode.

TABLE 7-27. FEED LINE GEOMETRIES

Propellant	H_2	O_2
Line Lengths, Ft.	18-20	3-4
Acceleration, G's (Full Thrust)	.1-.2	.1-.2

TABLE 7-28. ASSUMPTIONS FOR PREDICTING PUMP INLET CONDITIONS

Line Diameter = Pump inlet tip diameter

Line Losses:

One bell mouthed inlet, K_L = .04

Two vaned mitered elbows, K_L = .2/elbow

Pipe friction

Acceleration:

Flow accelerates to operating point in 5 sec.

Entire line length is in direction of motion

Pressure Drop:

$$C_m = \frac{\dot{w}}{\rho A}$$

$$\Delta P = \frac{\rho}{144} \left[\frac{C_m^{\,2}}{2g} (1 + K_L) + L \left(\frac{a_L}{g} - \frac{a_V}{g} \right) \right]$$

TABLE 7-29. OTV BOOST PUMP OPERATING CONDITIONS

Operating Mode	Parameter	H_2	O_2
All	D_{1T}, In.	3.14	3.6
	D_{1R}, In.	1.57	1.25
Full Thrust	$\dot{w}$, Lb/Sec	4.45	26.71
	N, RPM	28,490	6475
Idle	$\dot{w}$, Lb/Sec	0.76	3.02
	N, RPM	11,780	784

Cavitation Evaluation

Because operation at zero tank NPSH usually results in two-phase flow at the pump inlet, the first condition to assess is the effect of cavitation when these operating conditions are being approached. If cavitation effects are negligible, the analysis need only consider two-phase flow. However, if cavitation effects are considerable under some conditions, the analysis must also consider cavitation effects on pumping capability.

The impact of cavitation was assessed by predicting the NPSH required at 2% loss in head due to cavitation. This is done by deducting the thermodynamic suppression head (TSH) from the NPSH in cold water ($NPSH_{H_2O}$), as shown in Equation 1:

EQUATION 1

$$NPSH = NPSH_{H_2O} - TSH$$

The NPSH in water is the NPSH required at 2% head loss in water and the TSH is the correction in the subject propellant that, when deducted from the water NPSH, produces the NPSH that would give the same vapor cavity size and, consequently, the same head loss in the subject propellant (References 4, 5, and 6). Based on correlations made at Rocketdyne, the TSH's are expressed by Equations 2 and 3 for LH_2 and LO_2, respectively.

EQUATION 2

$$TSH_{LH_2} = \frac{.000691\ (d/Z)^{.16}\ U^{.85}\ \tan^2\beta(\beta_{HYDROGEN})}{\phi^4}$$

EQUATION 3

$$TSH_{LO_2} = .0986\ (d/Z)^{.16}\ U^{.85}\ \beta_{LO_2}$$

Where:

d	=	inducer inlet tip diameter, in.
Z	=	number of inducer blades at inlet
U	=	inducer inlet tip speed, ft/sec
β	=	inducer blade angle at inlet tip, degrees
ϕ	=	inducer inlet tip flow coefficient, C_m/U
C_m	=	flow axial velocity entering inducer, ft/sec
$\beta_{HYDROGEN}$	=	thermal factor for liquid hydrogen
β_{LO_2},	=	thermal factor for liquid oxygen

The two thermal factors, $\beta_{HYDROGEN}$ and β_{LO_2}, are purely a function of the propellant physical properties and are shown in Fig. 7-15as a function of propellant vapor pressure. These NPSH's were calculated for the operating conditions shown in Table 7-29 at both the design vapor pressures (Table 7-26) and at the low vapor pressures of 10 psia. The results are summarized in Table 7-30. In all cases, the thermodynamic suppression head is considerably greater than the NPSH capability in water, which means that the inducer vapor cavities are small under the anticipated flow conditions. Therefore, cavitation would have little impact on the performances of these pumps under these operating conditions. As a result, cavitation limits can be ignored and the pumping limits and capabilities are governed primarily by two-phase flow phenomena.

Two-Phase Evaluation

The two-phase flow pumping capability was evaluated by first estimating the flow conditions at the pump inlet, and then comparing those flow conditions with the flow conditions at the two-phase pumping limits. These activities are discussed separately below.

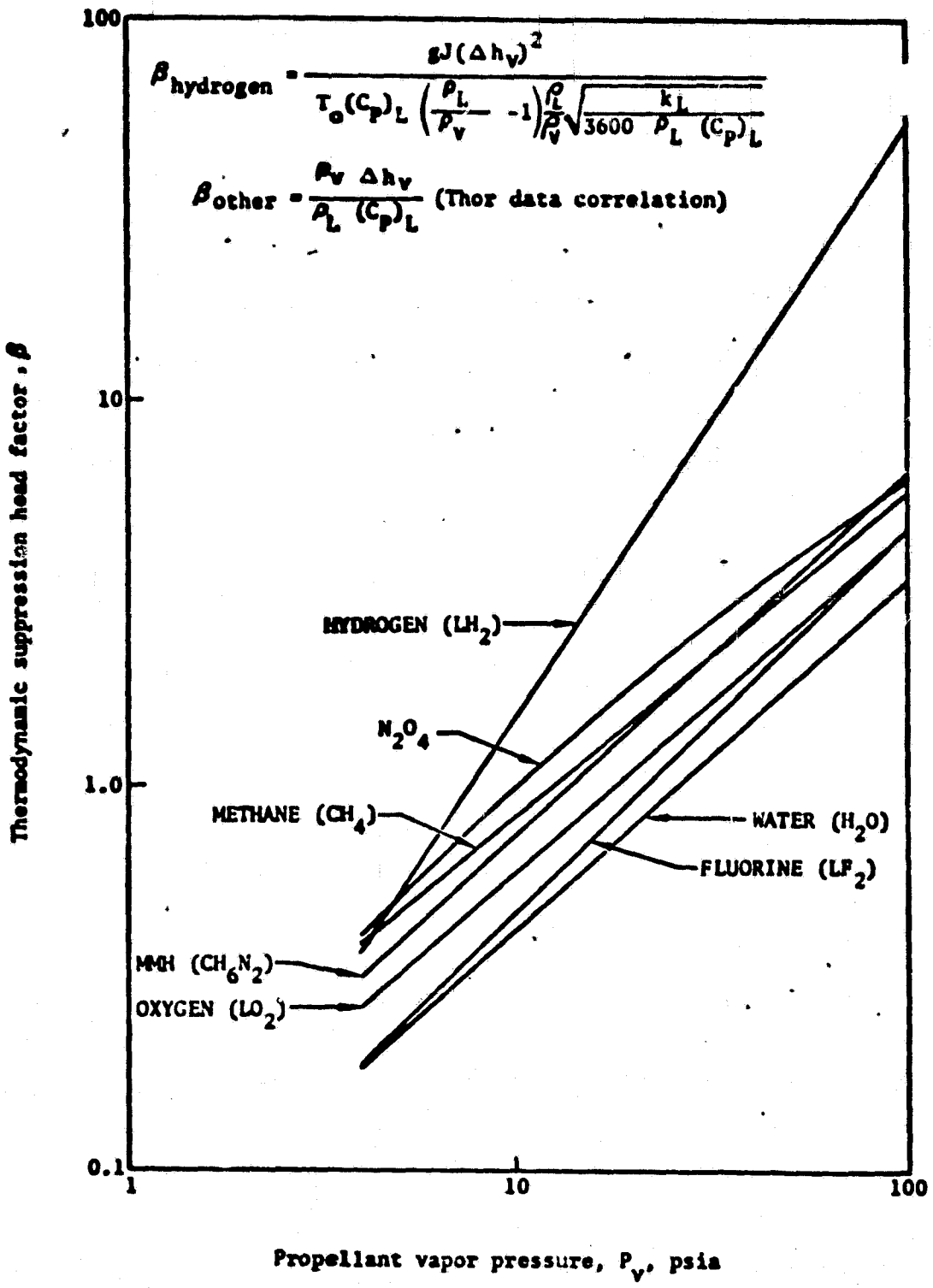

Figure 7-15. Thermodynamic Suppression Head Factor for Various Propellants as a Function of Vapor Pressure

TABLE 7-30. THERMODYNAMIC SUPPRESSION HEAD EFFECTS

Operating Mode	Fluid	Tank P_v, psia	NPSH Capability In H_2O, Ft.	TSH, Ft.	NPSH Capability In Fluid, Ft
Full Flow	H_2	18.4	2.03	4.44	-2.41
	H_2	10	2.01	2.96	- .95
	O_2	15.6	31.3	363	-332
	O_2	10	30.7	117.3	-127
Pump Idle	H_2	18.4	.029	.737	-.71
	H_2	10	.029	.492	-.46
	O_2	15.6	5.22	5850	-5840
	O_2	10	5.29	2570	-2560

Pump Inlet Conditions. As discussed earlier, the inlet line assumptions used in predicting the pump inlet conditions are summarized in Table 7-28. The first one was used to relate the line velocity to the pump inlet velocity. It is reasonable because (1) the line size should be minimized in order to minimize weight, and (2) the line cross sectional area should be at least as large as the pump inlet area in order to minimize losses and (in two0phase flow) avoid choking.

Also shown in Table 7-28 is that the line losses are the sum of the line component and the friction losses. With the inlet line geometries indicated in Tables 7-27, 7-28 and 7-29, the total inlet line loss coefficients are 1.74 in hydrogen and .67 in oxygen.

Two accelerations are involved in the calculations, the flow acceleration relative to the vehicle (which drops the pump inlet pressure) and the vehicle acceleration itself (which tends to increase the pump inlet pressure). The first acceleration assumption was determined from typical start transients predicted for the OTV engine. The second acceleration assumption indicates the amount of the inlet line that the vehicle acceleration acts on. The vehicle acceleration itself was assumed to be .1 G (minimum was selected from Table 7-27 in order to be conservative) for full thrust operation, which was ratioed down by the flowrates in order to get the pump idle mode value of .0121 G.

Finally, the indicated equations were used to estimate the inlet line pressure drop. Liquid flow density was assumed in order to simplify the calculation. This is somewhat optimistic because, for a given weight flowrate, the inlet line pressure drop would be (roughly) inversely proportional to average flow density.

As indicated in Table 7-28, the four components of inlet line pressure drop are the initial expansion to the line velocity, the inlet line losses, the value that accelerates the flow in the inlet line, and the pressure head value caused by vehicle acceleration. The first three decrease the pressure, and

the last increases it. These four components were assumed to be additive because the constant entropy lines on the temperature-entropy charts are almost parallel to the constant enthalpy lines at low vapor weight fractions. As a result, a pressure drop along a constant enthalpy line (which represents a loss) results in about the same amount of vapor as the same pressure drop along a constant entropy line (which represents an ideal expansion to a finite velocity). As a result, very little error is introduced by adding the pressure drops and determining the vapor fraction along a constant entropy line. This greatly simplifies the calculation.

This procedure was used to estimate the inlet line pressure drops. The liquid flow densities were obtained from Ref. 7-4 and 7-5 and are shown as a function of vapor pressure in Fig. 7-16. The line pressure drop and the differential change of quality with pressure at constant entropy (Fig.7-17, derived from Ref. 7-4 and 7-5 were used in Equation 4 to estimate the vapor weight fraction at the pump inlet.

EQUATION 4

$$X = \left[- \left(\frac{\partial X}{\partial P} \right)_s \right] \Delta P$$

This and the vapor to liquid density ratio (Fig.7-18) were then used to estimate the vapor volume fraction at the pump inlet (Equation 5).

EQUATION 5

$$\alpha = \frac{1}{\frac{\rho_L}{\rho_V} \left(\frac{1}{X} - 1 \right) + 1}$$

The resulting pump inlet flow conditions (static pressure, vapor volume fraction supplied, and flow velocity) are summarized in Tables 7-31 and 7-32 at the full thrust and the pump idle modes, respectively.

Two-Phase Limits. The parameters that permit the evaluation of the two phase pumping limits were then determined to indicate the feasibility of the predicted

Pump Inlet Conditions. As discussed earlier, the inlet line assumptions used in predicting the pump inlet conditions are summarized in Table 7-28. The first one was used to relate the line velocity to the pump inlet velocity. It is reasonable because (1) the line size should be minimized in order to minimize weight, and (2) the line cross sectional area should be at least as large as the pump inlet area in order to minimize losses and (in two-phase flow) avoid choking.

Also shown in Table 7-28 is that the line losses are the sum of the line component and the friction losses. With the inlet line geometries indicated in Tables 7-27, 7-28 and 7-29, the total inlet line loss coefficients are 1.74 in hydrogen and .67 in oxygen.

Two accelerations are involved in the calculations, the flow acceleration relative to the vehicle (which drops the pump inlet pressure) and the vehicle acceleration itself (which tends to increase the pump inlet pressure). The first acceleration assumption was determined from typical start transients predicted for the OTV engine. The second acceleration assumption indicates the amount of the inlet line that the vehicle acceleration acts on. The vehicle acceleration itself was assumed to be .1 G (minimum was selected from Table 7-27 in order to be conservative) for full thrust operation, which was ratioed down by the flowrates in order to get the pump idle mode value of .0121 G.

Finally, the indicated equations were used to estimate the inlet line pressure drop. Liquid flow density was assumed in order to simplify the calculation. This is somewhat optimistic because, for a given weight flowrate, the inlet line pressure drop would be (roughly) inversely proportional to average flow density.

As indicated in Table 7-28, the four components of inlet line pressure drop are the initial expansion to the line velocity, the inlet line losses, the value that accelerates the flow in the inlet line, and the pressure head value caused by vehicle acceleration. The first three decrease the pressure, and

the last increases it. These four components were assumed to be additive because the constant entropy lines on the temperature-entropy charts are almost parallel to the constant enthalpy lines at low vapor weight fractions. As a result, a pressure drop along a constant enthalpy line (which represents a loss) results in about the same amount of vapor as the same pressure drop along a constant entropy line (which represents an ideal expansion to a finite velocity). As a result, very little error is introduced by adding the pressure drops and determining the vapor fraction along a constant entropy line. This greatly simplifies the calculation.

This procedure was used to estimate the inlet line pressure drops. The liquid flow densities were obtained from Ref. 7-4 and 7-5 and are shown as a function of vapor pressure in Fig. 7-16. The line pressure drop and the differential change of quality with pressure at constant entropy (Fig.7-17, derived from Ref. 7-4 and 7-5 were used in Equation 4 to estimate the vapor weight fraction at the pump inlet.

EQUATION 4

$$X = \left[- \left(\frac{\partial X}{\partial P} \right)_s \right] \Delta P$$

This and the vapor to liquid density ratio (Fig.7-18) were then used to estimate the vapor volume fraction at the pump inlet (Equation 5).

EQUATION 5

$$\alpha = \frac{1}{\frac{\rho_L}{\rho_G} \left(\frac{1}{X} - 1 \right) + 1}$$

The resulting pump inlet flow conditions (static pressure, vapor volume fraction supplied, and flow velocity) are summarized in Tables 7-31 and 7-32 at the full thrust and the pump idle modes, respectively.

Two-Phase Limits. The parameters that permit the evaluation of the two phase pumping limits were then determined to indicate the feasibility of the predicted

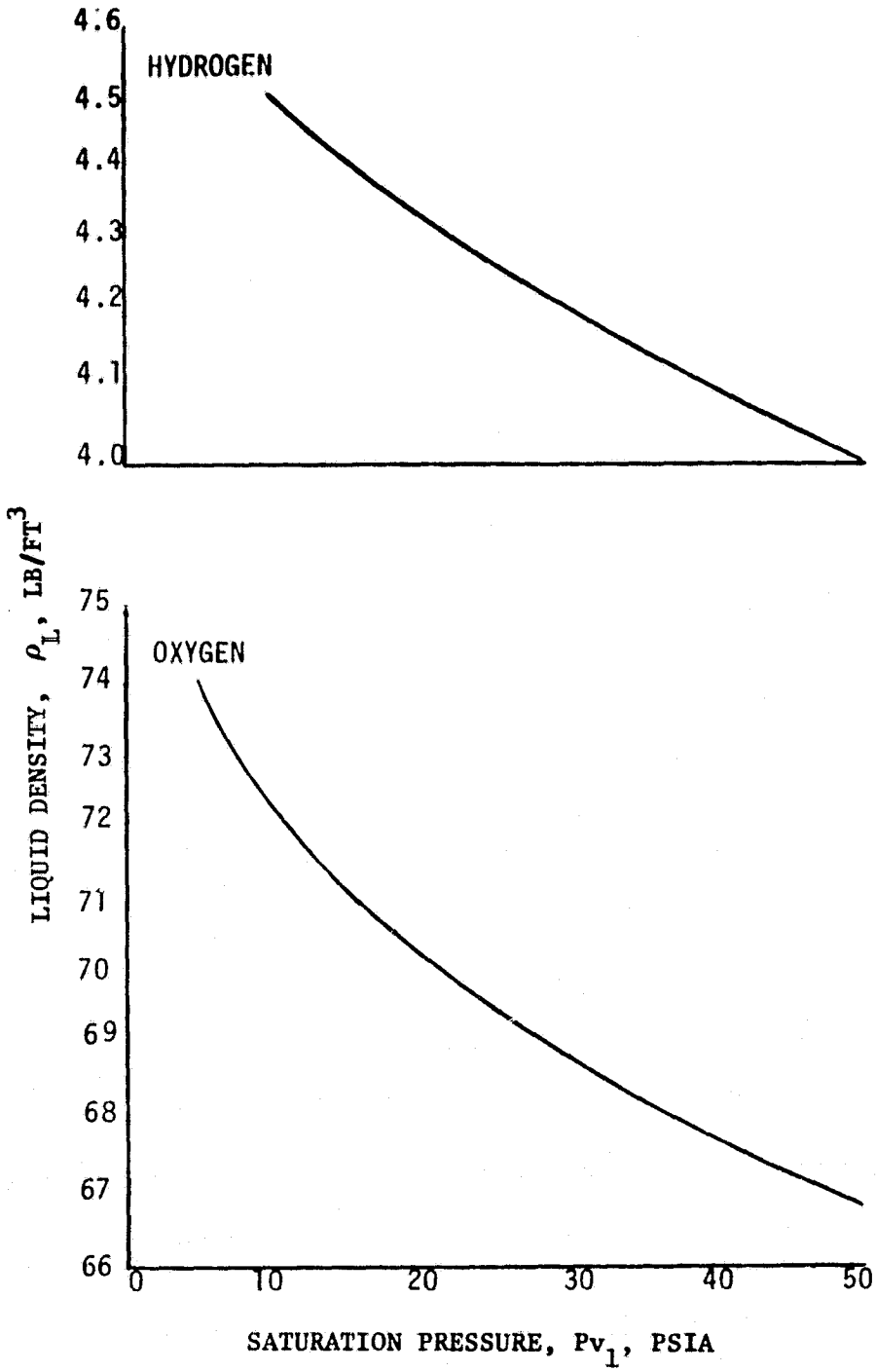

Figure 7-16. Liquid Flow Densities

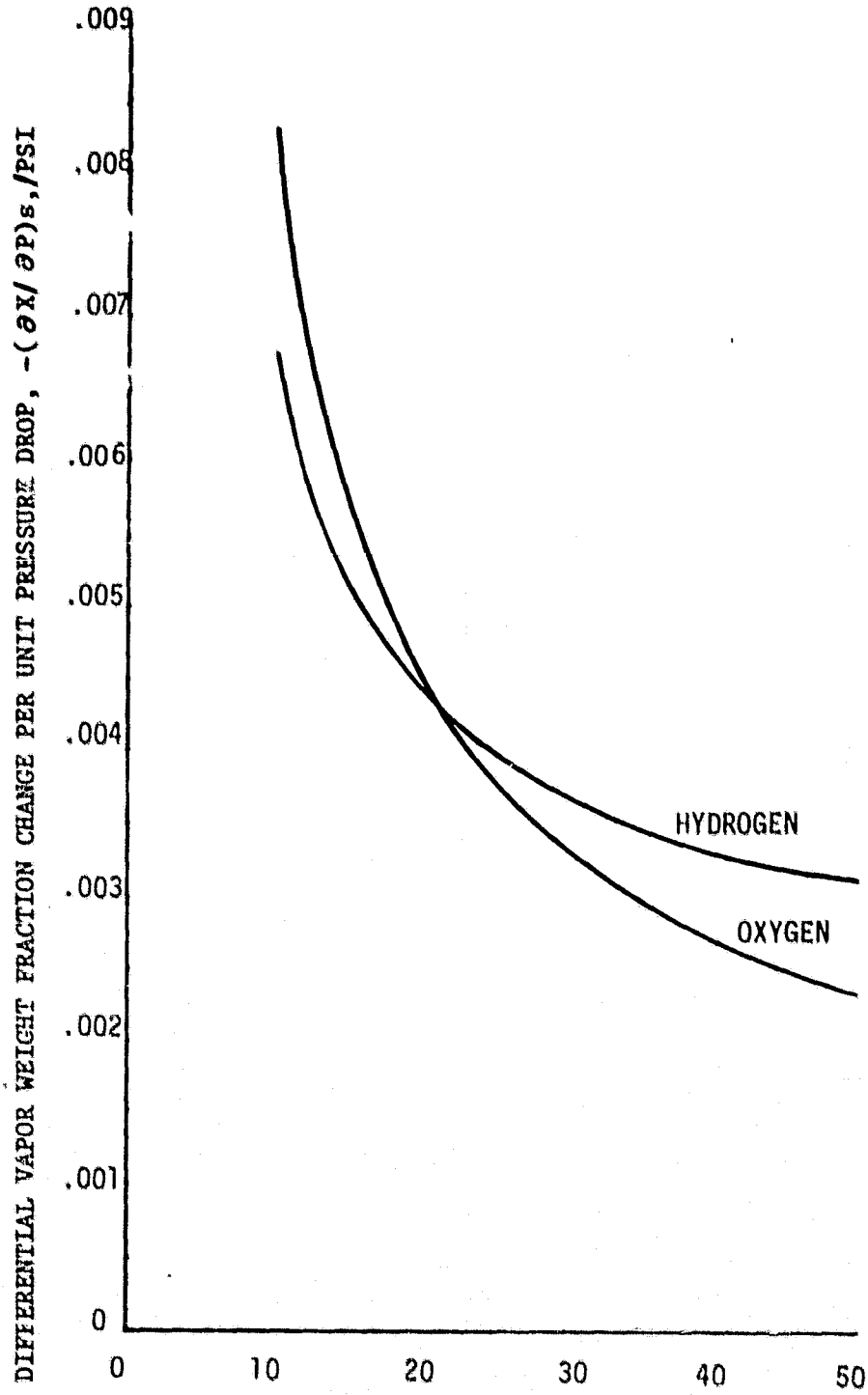

Figure 7-17. Vapor Fraction Differential Changes For Isentropic Expansions from a Saturated Liquid

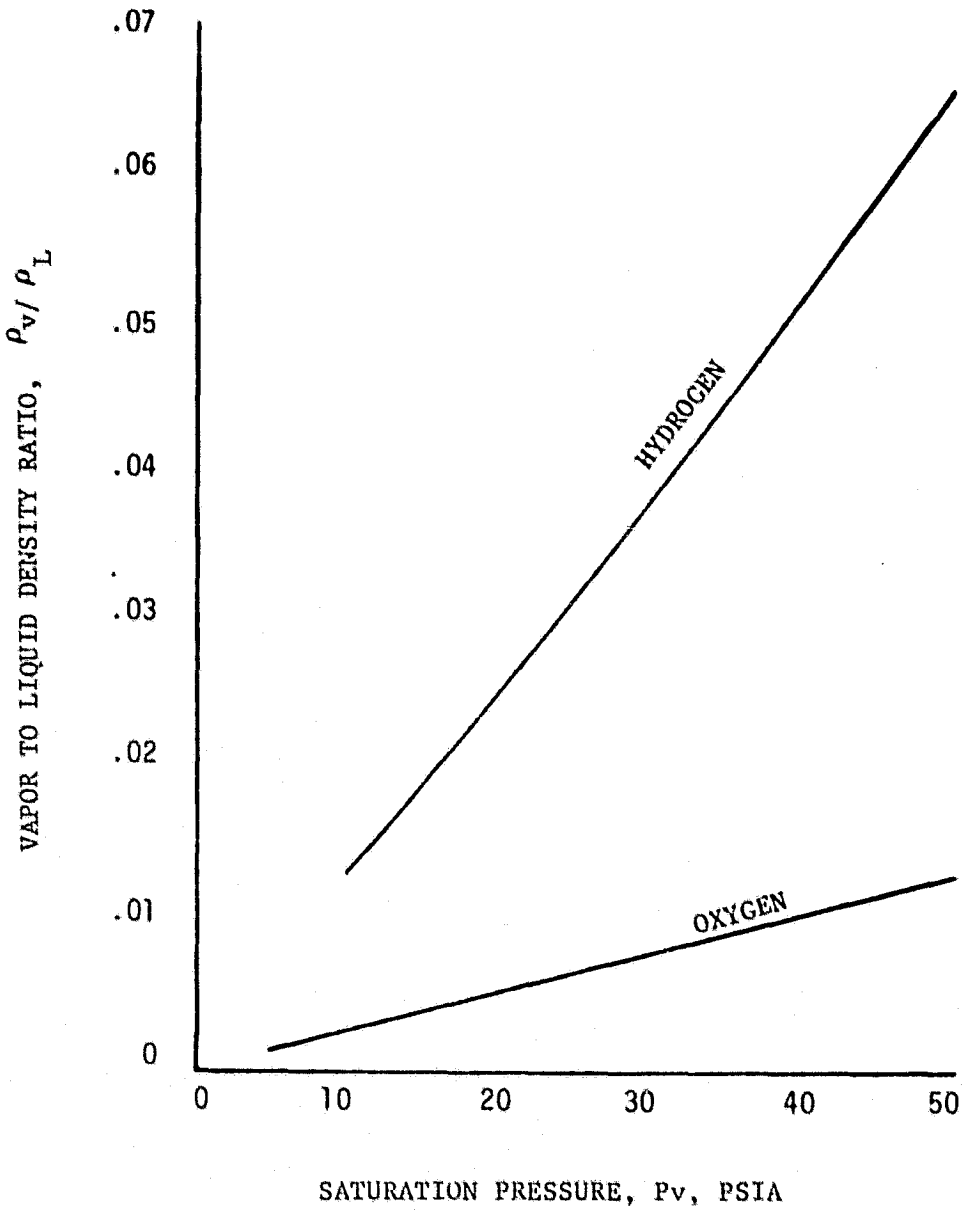

Figure 7-18. Vapor to Liquid Density Ratios

TABLE 7-31. OTV BOOST PUMP TWO PHASE* PUMPING EVALUATION UNDER FULL FLOW CONDITIONS

Fluid	Tank P Vapor, psia	Duct Loss Coef., K_L	Flow Accel. Time, Sec.	Vehicle Accel., G's	P Static, psia	Vapor Vol. Fraction α, %		Flow Velocity C_m, Ft/Sec	Flow Mach Number, M
						Supplied	Blade Capacity		
H_2	18.4	1.74	5	.1	17.85	9.9	27.5	22.6	.27
H_2	10	1.74	5	.1	9.47	21.5	29.8	25.2	.44
O_2	15.6	.67	5	.1	15.31	27.5	33.5	7.89	.82
O_2	10	.67	5	.1	9.72	46.1	34.7	10.43	1.23

* Tank NPSH = 0 (Sat. Liquid in Tank)

TABLE 7-32. OTV BOOST PUMP TWO PHASE* PUMPING EVALUATION UNDER PUMP IDLE MODE FLOW CONDITIONS

Fluid	Tank P Vapor, psia	Duct Loss Coef., K_L	Flow Accel. Time, Sec.	Vehicle Accel., G's	P Static psia	Vapor Vol. Fraction, α, %		Flow Velocity, C_m, Ft/Sec	Flow Mach Number, M
						Supplied	Blade Capacity		
H_2	18.4	1.74	5	.0121	18.38	.42	**	3.48	.047
H_2	10	1.74	5	.0121	9.98	1.05	**	3.38	.075
O_2	15.6	.67	5	.0121	15.61	0	38	.647	.00022
O_2	10	.67	5	.0121	10.01	0	39	.635	.00021

*Tank NPSH = 0 (Sat. Liquid in Tank)

**$(i/\beta)_L$ = .77, Which is beyond the angle of attack limit for two-phase flow

pump inlet conditions. As shown in Table 7-33 these limit indicating parameters are the inlet line Mach number under equilibrium flow conditions, the inducer blade vapor pumping capacity, and the inducer blade inlet liquid flow incidence to blade angle ratio.

The inlet line Mach numbers are the ratio of the flow velocity to the acoustic velocity (Equation 6).

EQUATION 6

$$M = \frac{C_m}{c} = \frac{\dot{w}}{\rho_L A \frac{\rho}{\rho_L} c} \approx \frac{\dot{w}}{\rho_L A\, c(1-\alpha)}$$

It is apparent that the product of the acoustic velocity (c) and one minus the vapor volume fraction $(1-\alpha)$ are required to make this calculation. Equation 7 is the expression for acoustic velocity in terms of flow desnities, quality, and the acoustic velocities of the individual phases.

EQUATION 7

$$c = \frac{\rho_L / \rho}{\sqrt{\frac{1-x}{c_L^2} + \left(\frac{\rho_L}{\rho_v}\right)^2 \frac{x}{c_v^2} + \frac{\rho_L}{144g}\left(\frac{\rho_L}{\rho_v} - 1\right)\left[-\left(\partial x / \partial P\right)_s\right]}}$$

However, treating the vapor as a void fraction, and noting that the large single phase acoustic velocities and the low qualities cause the first two terms in the denominator to be small, Equation 7 reduces to:

EQUATION 8

$$c(1-\alpha) \approx \frac{1}{\sqrt{\frac{\rho_L}{144g}\left(\frac{\rho_L}{\rho_v} - 1\right)\left[-\left(\partial x / \partial P\right)_s\right]}}$$

TABLE 7-33. TWO PHASE PUMPING LIMITS

. INLET LINE CHOKING

EQUILIBRIUM MACH NO. < 1.0

. BLADE CHOKING

$$\alpha \leq \alpha_{MAX} = 1 - \frac{\phi_L}{\phi_{MAX}} = 1 - \frac{\phi_L}{.93\ TAN(\beta_{1T} - 1.5)}$$

$$i_L / \beta_b \leq .7$$

This parameter utilizes fluid physical property data from Fig. 7-16, 7-17 and 7-18. The resulting values are shown in Fig. 7-19. Referring back to Equation 6, it is apparent that the ratio of the liquid flow velocity (the flow velocity if the flow were a pure liquid) to the acoustic parameter in Figure is the approximate inlet line Mach number. Tables 7-31 & 7-32 indicate that this value exceeds 1.0 for only one condition, the oxygen line under full flow conditions at a tank saturation pressure of 10 psia. This indicates that the inlet line would be choked and, therefore, would have to be enlarged to accommodate the flow condition. The inlet line Mach numbers for the other 7 cases in Tables 7-31 & 7-32 are all less than 1.0 and, therefore, those inlet lines are sufficiently large to pass the flow.

The other major two-phase flow limit in Table 7-33 is the inducer blade choking limit which sets the inducer blade vapor pumping capacity. At the flow conditions existing at the leading edges of the inducer blades, very little area convergence is required to cause choking and, therefore, the inducer blade choking limit occurs (approximately) when the fluid angle of the two-phase flow is equal to the blade angle (References 7-6, 7-7 & 7-8). This is the limit because operation at a larger fluid angle (larger two-phase inlet flow coefficient) would result in an area convergence which, as stated earlier, would result in choking. As a result, the vapor volume fraction pumping capacity is proportional to the difference between the flow coefficient at the limit and the liquid flow coefficient (the flow coefficient if the entering flow were a pure liquid). With appropriate allowances for boundary layer and blade thickness, this is expressed by Equation 9.

EQUATION 9

$$\alpha_{MAX} = 1 - \frac{\phi_L}{.93 \tan(\beta_{1T} - 1.5)}$$

Since the inlet tip blade angles for both OTV boost pumps are around 7°, this reduces to Equation 10.

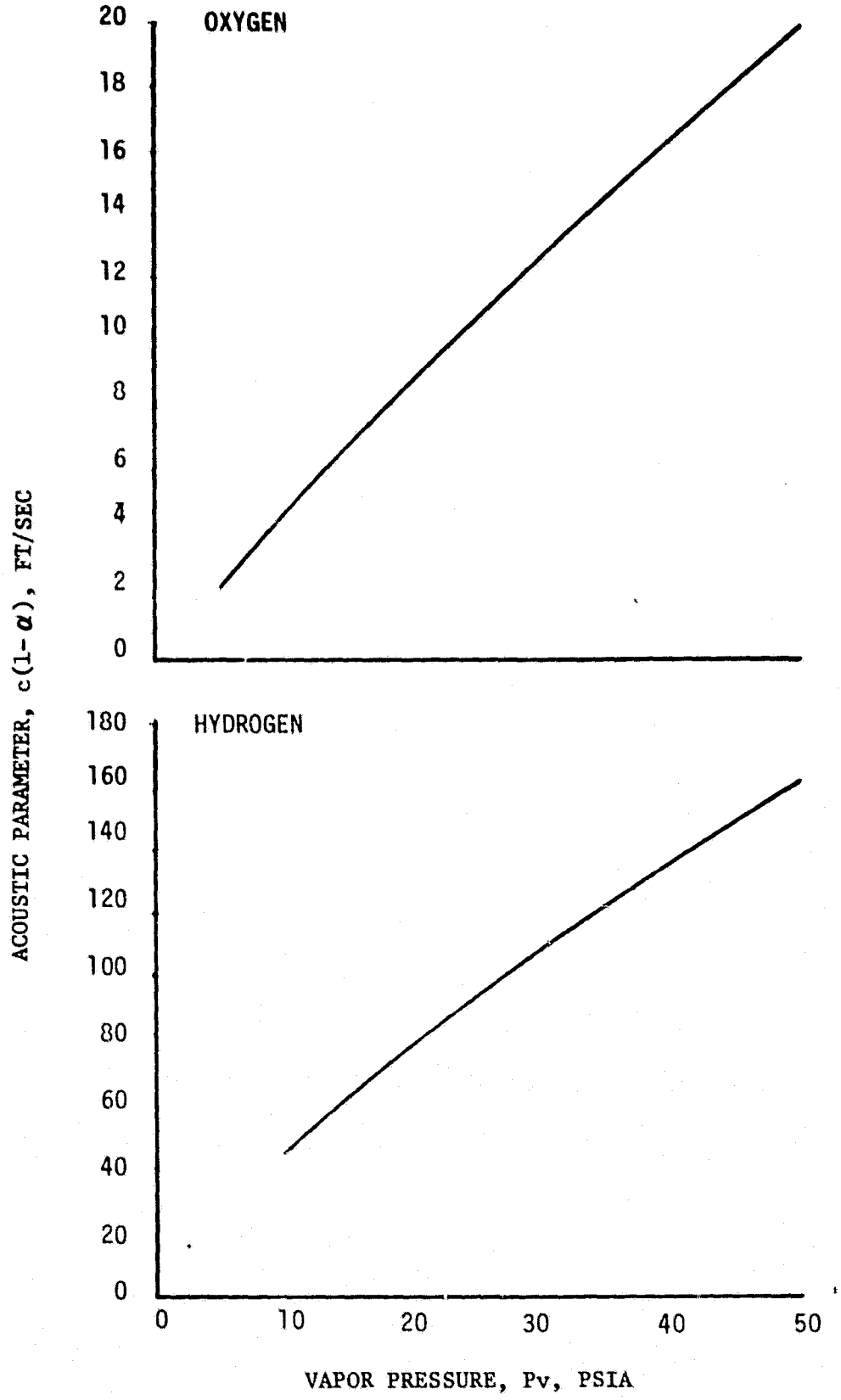

Figure 7-19. Approximate Acoustic Parameter

EQUATION 10

$$\alpha_{MAX} = 1 - \frac{\phi_L}{.0895}$$

The upper limit to this vapor pumping capacity occurs when the ratio of the liquid angle of attack (the angle of attack, on the inducer blade leading edge tips, that the flow would have if it were a pure liquid) to the blade angle exceeds 0.7. Reference 7-8 indicated that vapor capacity becomes unpredictable at larger values. Equation 11 is the expression for this ratio.

EQUATION 11

$$(i/\beta)_L = \frac{\beta_{1T} - \text{Arc Tan}\left(\frac{\phi_L}{.93}\right)}{\beta_{1T}}$$

The vapor capacities of the OTV boost pumps, which are predicted by Equations 10 and 11, are shown in Fig. 7-20. It should be noted that some vapor capacity is probable at flow coefficients below .034 (beyond the $(i/\beta)_L$ limit); zero is indicated because the value is unpredictable and, under some conditions, appears to approach zero. These vapor capacities are compared with the supplied vapor fractions in Tables 7-31 and 7-32.

Evaluation of Results

The changes recommended to obtain zero tank NPSH operation with the OTV boost pumps are summarized in Table 7-34. They are discussed below at both the OTV tank vapor pressures (Table 7-36) and 10 psia tank vapor pressures.

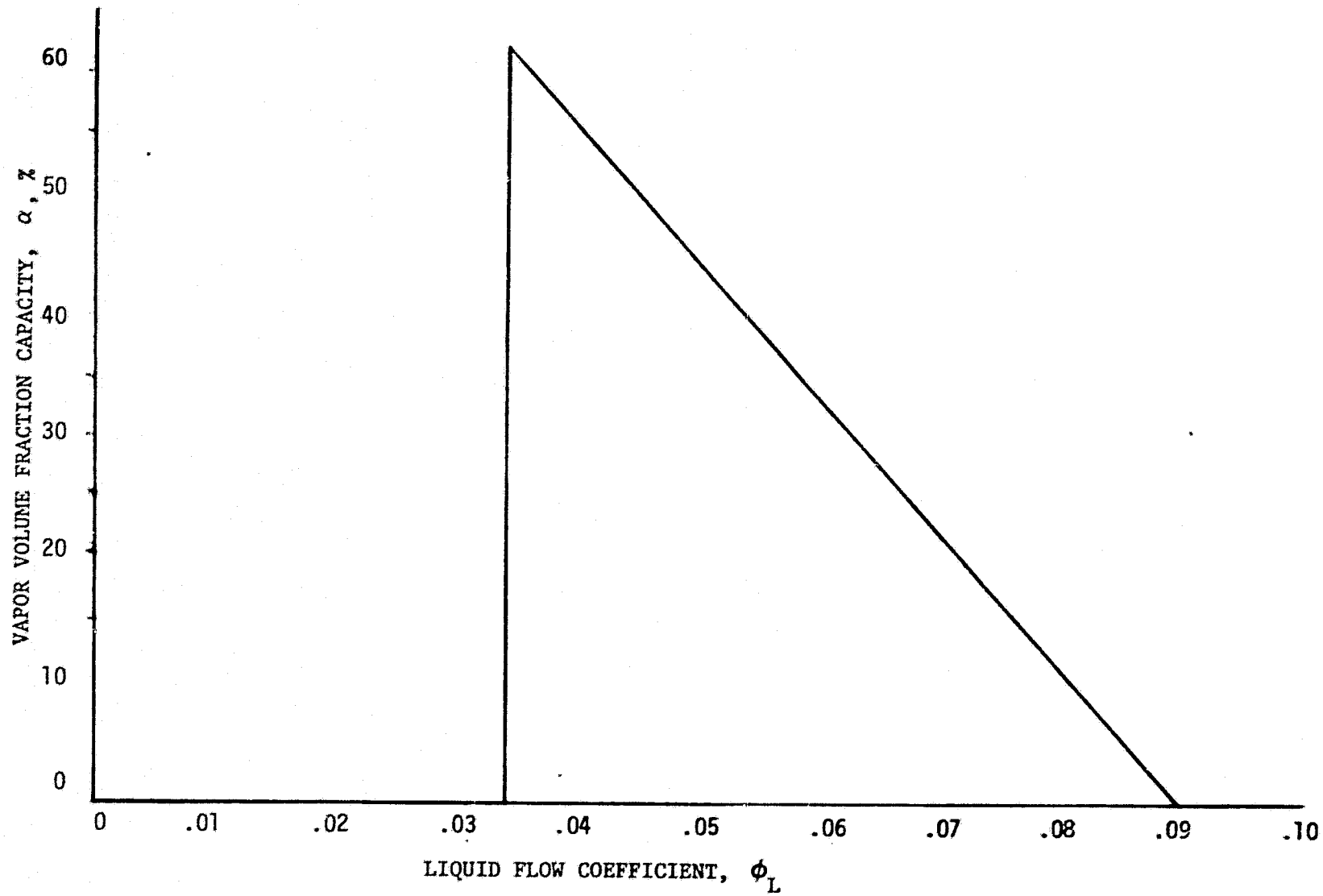

Figure 7-20. Inducer Blade Vapor Pumping Capacity for OTV Boost Pumps

TABLE 7-34. CONCLUSIONS AND RECOMMENDATIONS

Operating Mode	Tank Vapor Pressure, Psia	Recommended Changes to Boost Pumps	
		H_2	O_2
Full Thrust	Existing	None	None
	10 Psia	None	Increase Diameter 20%
Idle Mode	Existing	Decrease Speed 25%*	None
	10 Psia	Decrease Speed 25%*	None

*Probably Not Mandatory

OTV Tank Vapor Pressure. As discussed earlier, the inlet line Mach numbers at the OTV tank vapor pressures are all less than 1.0 (Tables 7-31 and 7-32) and, therefore, the presently anticipated inlet lines are sufficiently large to pass the flow. As also shown in Table 7-31 , the vapor capacities exceed the supplied values under all full flow operating conditions at OTV vapor pressure. This is also true for the O_2 boost pump during idle mode (Table 7-32). However, the angle of attack on the hydrogen boost pump blades during idle mode is beyond the limit for two-phase flow. This is probably not a problem because the vapor volume fraction is less than 1%, and some vapor capacity is usually possible at angles of attack beyond the limit (Ref. 7-8). It may be concluded that the hydrogen boost pump speed during idle mode should be reduced 25% if it can be done easily without compromising other operating requirements. However, if difficulty is encountered, it would probably be satisfactory to leave the idle mode speed as it is.

10 Psia Tank Vapor Pressure. As shown in Table 7-31, the hydrogen inlet line for full flow operation is sufficiently large because the Mach number is at a very safely subsonic value of .44. However, this is not true for the oxygen inlet line because the approximation of inlet line Mach number exceeds 1, which means that the flow would be choked. Therefore, to avoid this with a safe margin, the oxygen inlet line diameter and, to be safe, the oxygen boost pump inlet tip diameter, should both be increased 20% in order to operate at full thrust at a tank saturation pressure of 10 psia.

As far as idle mode is concerned, Table 7-32 shows that the situation is almost identical to that at the OTV tank vapor pressures, i.e., the oxygen side is satisfactory and the hydrogen side is probably satisfactory but, to be safe, the speed should be reduced 25% if it can be done easily without seriously compromising something else.

REFERENCES

1-1 AFRPL-TR-72-27, July 1972, Orbit to Orbit Shuttle Engine Design Study, Pratt and Whitney Aircraft.

2-1 NASA-CR134908, High-Temperature, Low-Cycle Fatigue of Copper-Base Alloys for Rocket Nozzles; Part I - Data Summary for Materials Tested in Prior Programs, November 1975.

2-2 AGARD-CP-243, An Application of Strainrange Partitioning to Copper-Base Alloys.

2-3 AFRPL-TR-73-10, Investigation of Thermal Fatigue in Non-Tubular Regeneratively Cooled Thrust Chambers; Final Report, Vol II, 1973.

2-4 NASA-TMX-73665, Experimental Fatigue Life Investigation of Cylindrical Thrust Chambers.

2-5 Rao, G. V. R.: "Exhaust Nozzle Contour for Optimum Thrust," Jet Propulsion, June 1958.

7-1 J. K. Jakobsen, "On the Mechanism of Head Breakdown in Cavitating Inducers", ASME Paper No. 63-AHGT-29, March, 1963.

7-2 T. F. Gelder, R. S. Ruggeri, and R. D. Moore, Cavitation Similarity Considerations Based on Measured Pressure and Temperature Depressions in Cavitated Regions of Freon-114, NASA TN D-3509, July, 1966.

7-3 W. R. Bissell and A. J. Sobin, Turbopump Systems for Liquid Rocket Engines, NASA Space Vehicle Design Criteria Monograph, NASA SP-8107, August, 1974.

7-4 R. D. McCarty and Lloyd A. Weber, Thermophysical Properties of Oxygen from Freezing Liquid Liner to 600R for Pressures to 5000 psia, NBS Technical Note 384, July, 1971.

7-5 R. D. McCarty, Hydrogen Technological Survey-Thermophysical Properties, NASA SP-3089, 1975.

7-6 W. R. Bissell, G. S. Wong, and T. W. Winstead, "Analysis of Two-Phase Flow in LH_2 Pumps for O_2/H_2 Rocket Engines", AIAA Joural of Spacecraft and Rockets, June 1970, pp. 707-713.

7-7 J. A. King, Design of Inducers for Two-Phase Oxygen-Final Report, R-8832, Rocketdyne, January, 1972.

7-8 J. A. King, Design of Inducers for Two-Phase Operation-Final Report, R-8283, Rocketdyne, January, 1971.

APPENDIX A

This Appendix contains the specifications for each of the valves of the Advanced Expander Cycle Point Design Engine.

Table No.	Name	Page No.
A-1	Main Oxidizer Valve	A-2
A-2	Main Fuel Valve	A-3
A-3	Turbine Bypass Valve	A-4
A-4	Oxidizer Turbine Bypass Valve	A-5
A-5	Gaseous Oxidizer Valve	A-6
A-6	Dump-Coolant Control Valve	A-7
A-8	Igniter Fuel Valve	A-8
A-9	Igniter Oxidizer Valve	A-9
A-10	Fuel Tank Pressurization Valve	A-10
A-11	Oxidizer Tank Pressurization Valve	A-11
A-12	28 Vdc Electric Actuator	A-12
A-13	Oxidizer Inlet Valve	A-13
A-14	Fuel Inlet Valve	A-14

VALVE SPECIFICATION

PROJECT: OTV EXPANDER

ITEM NUMBER: 1 **DATE:** 4-30-80

7-21-80 REV. A

1. NAME/TYPE: Main Oxidizer Valve (MOV) Modulating Sector Ball Valve (6:1 MR/7:1 MR-80% Window Area/12%)
2. FLUID SERVICE: LOX
3. PRESSURE, PSIA: 2498 - Max. Operating
4. TEMPERATURE: 160°R Min. Fluid, 560°R Max. Ambient
5. FLOW RATE, LB/SEC: 26.70/28.06/3.02
6. DELTA P, PSI: 345.3/126.2/91.4
7. MAX INTERNAL LEAK He, SCIM: 100.
8. MAX EXTERNAL LEAK He, SCIM: 1.0
9. ACTUATION: Electric Motor - (See Spec. 12)
10. RESPONSE, Sec: (See Spec. 12)
11. EQUIVALENT ORIFICE DIAMETER, IN: 0.735/0.969/0.345
12. LINE SIZE, IN: 1.25 I.D.
13. ENVELOPE: Ball Dia. - 1 1/2 In.; Hole Dia. - 3/4 In.; 90° Cone Inlet Contraction, No outlet diffuser.
14. MAX WEIGHT, LB: 3.5
15. FEATURES: 600 PSIG Pneumatic Actuator for Failsafe Closure in 150 MSEC. Max. with Override Cluth, Welded End Fittings.

VALVE SPECIFICATION

PROJECT: OTV EXPANDER

ITEM NUMBER: 2 **DATE: 4-30-80**

7-21-80 REV. A

1. NAME/TYPE: Main Fuel Valve (MFV) / Sector Ball Valve
2. FLUID SERVICE: LH_2
3. PRESSURE, PSIA: 4186 Max. Operating
4. TEMPERATURE: 43.0°R Min. Fluid, 560°R Max. Ambient
5. FLOW RATE, LB/SEC: 4.06 at 6:1 M.R. (Max.)
6. DELTA P, PSI: 25, Max. at 6:1 MR
7. MAX INTERNAL LEAK He, SCIM: 100
8. MAX EXTERNAL LEAK He, SCIM: 1.0
9. ACTUATION: Electric Motor - (See Spec. 12)
10. RESPONSE, SEC: (See Spec. 12)
11. EQUIVALENT ORIFICE DIAMETER, IN: 1.83
12. LINE SIZE, IN: 1.0 I.D.
13. ENVELOPE: Ball Dia. - 1 1/2 In.; Hole dia. - 3/4 In.; 1 3/4 In. Exit Diffuser
14. MAX WEIGHT, LB: 3.3
15. FEATURES: Welded End Fittings.

VALVE SPECIFICATION

PROJECT: OTV EXPANDER

ITEM NUMBER: 3 **DATE:** 4-30-80

7-21-80 REV. A

1. NAME/TYPE: Turbine Bypass Valve (TBV)/Modulating Rotary Plug Valve (6:1 MR/7:1 MR/12% - 80% Window Area)
2. FLUID SERVICE: GH_2
3. PRESSURE, PSIA: 3697 - Max. Operating
4. TEMPERATURE: 160°R Min., 750°R Max. Fluid
5. FLOW RATE, LB/SEC: 0.41 / 0.46 / 0.43
6. DELTA P, PSI: 1908 / 1669 / 175
7. MAX INTERNAL LEAK He, SCIM: No shutoff required
8. MAX EXTERNAL LEAK He, SCIM: 1.0
9. ACTUATION: Electric Motor (See Spec. 12)
10. RESPONSE, SEC: (See Actuator Spec.)
11. EQUIVALENT ORIFICE DIAMETER, IN: 0.195 / 0.219 / 0.589
12. LINE SIZE, IN: 1.0 ID
13. ENVELOPE: Hole Dia. - 1/2 In.; Cylinder Dia. - 0.72 In.; 90° Cone Inlet Contraction, no Exit Diffuser
14. MAX WEIGHT, LB: 3.5
15. FEATURES: 600 PSIG Penumatic Actuator for Failsafe Closure in 150 MSEC. Max. with override clutch. Welded end Fittings.

VALVE SPECIFICATION

PROJECT: OTV EXPANDER

ITEM NUMBER: 4 **DATE: 4-30-80**

7-21-80 REV. A

1. NAME/TYPE: Oxidizer Turbine Bypass Valve (OTBV)/Modulating Rotary Plug Valve (6:1MR/7:1MR/Window Area 12%-80%)
2. FLUID SERVICE: GH_2
3. PRESSURE, PSIA: 2155 - Max. Operating
4. TEMPERATURE: $160^{o}R$ Min., $750^{o}R$ Max. Fluid
5. FLOW RATE, LB/SEC: 0.45 / 0.18 / 0.06
6. DELTA P, PSI: 348 / 350 / 21
7. MAX INTERNAL LEAK He, SCIM: No Shutoff Required
8. MAX EXTERNAL LEAK He, SCIM: 1.0
9. ACTUATION: Electric Motor (See Spec. 12)
10. RESPONSE, Sec: (See Actuator Spec.)
11. EQUIVALENT ORIFICE DIAMETER, IN: 0.329/0.211/0.387
12. LINE SIZE, IN: 0.625 I.D.
13. ENVELOPE: Hole Dia. - 0.325 In.; Cylinder Dia. - 0.47.; 90° Cone Inlet Contraction, No Exit Diffuser
14. MAX WEIGHT, LB: 2.0
15. FEATURES: Welded End Fittings

VALVE SPECIFICATION

PROJECT: OTV EXPANDER

ITEM NUMBER: 5 **DATE: 4-30-80**

1. NAME/TYPE: Gaseous Oxidizer Valve (GOV)/ Normally Open, Self-Actuated
2. FLUID SERVICE: GOX
3. PRESSURE, PSIA: 2498 - Max. Operating
4. TEMPERATURE: 160°R Min. Fluid, 560°R Max. Ambient
5. FLOW RATE, LB/SEC: 0.13
6. DELTA P, PSI: 8.2
7. MAX INTERNAL LEAK He, SCIM: 3000 @ 2450 PSIA, 300 PSID, 530°R
8. MAX EXTERNAL LEAK He, SCIM: 1.
9. ACTUATION:
10. RESPONSE, SEC.:
11. EQUIVALENT ORIFICE DIAMETER, IN: 0.575
12. LINE SIZE, IN:
13. ENVELOPE:
14. MAX WEIGHT, LB: 3.0
15. FEATURES: Valve is Open at Tank Head Idle and Closed at Pumped Idle (∿206 PSIA). Welded End Fittings.

VALVE SPECIFICATION

PROJECT: OTV EXPANDER

ITEM NUMBER: 6 DATE: 4-30-80

1. NAME/TYPE: Dump Fuel Valve (DFV)/Normally Closed, Self Actuated (6:1 MR / 7:1 MR / 12%)
2. FLUID SERVICE: LH_2
3. PRESSURE, PSIA: 71.2 / 73.8 / 29.5
4. TEMPERATURE: 38°R Min. Fluid, 560°R. Max. Ambient
5. FLOW RATE, LB/SEC: 0.36 / 0.37 / 0.05
6. DELTA P, PSI: 33.7 / 34.2 / 28.8
7. MAX INTERNAL LEAK He, SCIM: Internal Orifice for Tank Head Flow
8. MAX EXTERNAL LEAK He, SCIM: 1.0
9. ACTUATION: Inlet Pressure (See Item 3.)
10. RESPONSE, SEC.
11. EQUIVALENT ORIFICE DIAMETER, IN: 0.306 / 0.309 / 0.119
12. LINE SIZE, IN: 0.5 I.D.
13. ENVELOPE:
14. MAX WEIGHT, LB: 1.0
15. FEATURES: Internal Orifice to provide Tank Head Idle Flow Requirement; Valve to Modulate Open at Pumped Idle & go to Full Open at Main-Stage; Welded End Fittings.

VALVE SPECIFICATION

PROJECT: OTV EXPANDER

ITEM NUMBER: 8 **DATE: 4-30-80**

1. NAME/TYPE: Igniter Fuel Valve (IFV) / 2-way Solenoid Valve
2. FLUID SERVICE: GH_2
3. PRESSURE, PSIA: 3908 - Max. Operating
4. TEMPERATURE: 160°R Min., 600°R Max. Fluid
5. FLOW RATE, LB/SEC: 0.055 @ 576°R (Mainstage)
6. DELTA P, PSI: 2120 (Mainstage)
7. MAX INTERNAL LEAK He, SCIM: 10.
8. MAX EXTERNAL LEAK He, SCIM: 1.0
9. ACTUATION: 28 VDC Solenoid, 1.5 AMP
10. RESPONSE, SEC.: 0.050
11. EQUIVALENT ORIFICE DIAMETER, IN: 0.065
12. LINE SIZE, IN: 1/4 O.D.
13. ENVELOPE:
14. MAX WEIGHT, LB: 1.0
15. FEATURES: Unbalanced Direct Operated Solenoid Valve NOTE: <0.001 lb/sec Flow Estimated with this ESEOD at Tank Head Idle. Welded End Fittings.

VALVE SPECIFICATION

PROJECT: OTV EXPANDER

ITEM NUMBER: 9 **DATE: 4-30-80**

1. NAME/TYPE: Igniter Oxidizer Valve (IOV)/2-way Solenoid Valve
2. FLUID SERVICE: GOX
3. PRESSURE, PSIA: 2498 - Max. Operating
4. TEMPERATURE: 160°R. Min. Fluid, 560°R. Max. Ambient
5. FLOW RATE, LB/SEC: 0.045 @ 530°R (Mainstage)
6. DELTA P, PSI: Estimate 200
7. MAX INTERNAL LEAK He, SCIM: 10
8. MAX EXTERNAL LEAK He, SCIM: 1.0
9. ACTUATION: 28 VDC Solenoid, 1.5 Amp.
10. RESPONSE, SEC: 0.050
11. EQUIVALENT ORIFICE DIAMETER, IN: 0.060
12. LINE SIZE, IN: 1/4 O.D.
13. ENVELOPE:
14. MAX WEIGHT, LB: 1.0
15. FEATURES: Unvalanced Direct Operated Solenoid Valve

    NOTE: <0.001 lb/sec Flow Estimated with this ESEOD at Tank Head Idle, Welded End Fittings.

VALVE SPECIFICATION

PROJECT: OTV EXPANDER

ITEM NUMBER: 10 DATE: 4-30-80

1. NAME/TYPE: Fuel Tank Pressurization Valve (FTPV)/ Check Valve
2. FLUID SERVICE: GH_2
3. PRESSURE, PSIA: 4000 - Max. Operating
4. TEMPERATURE: 160°R Min., 600°R Max. Fluid
5. FLOW RATE, LB/SEC: 0.0255
6. DELTA P, PSI: 30 @ Full Open
7. MAX INTERNAL LEAK He, SCIM: 10.
8. MAX EXTERNAL LEAK He, SCIM: 1.0
9. ACTUATION: 6 to 10 PSID Cracking Pressure
10. RESPONSE, SEC:
11. EQUIVALENT ORIFICE DIAMETER, IN: 0.12
12. LINE SIZE, IN: 1/4 O.C.
13. ENVELOPE:
14. MAX WEIGHT, LB: 0.2
15. FEATURES: Welded End Fittings

VALVE SPECIFICATION

PROJECT: OTV EXPANDER

ITEM NUMBER: 11 **DATE: 4-30-80**

1. NAME/TYPE: Oxidizer Tank Pressurization Valve (OTPV)/ Check Valve
2. FLUID SERVICE: GOX
3. PRESSURE, PSIA: 2500. Max. Operating
4. TEMPERATURE: 160°R. Min. Fluid, 560°R. Max. Ambient
5. FLOW RATE, LB/SEC: 0.1005
6. DELTA P, PSI: 14 PSID @ Full Open
7. MAX INTERNAL LEAK He, SCIM: 10
8. MAX EXTERNAL LEAK He, SCIM: 1.0
9. ACTUATION: : 6 to 10 PSID Cracking Pressure
10. RESPONSE, SEC:
11. EQUIVALENT ORIFICE DIAMETER, IN: 0.12
12. LINE SIZE, IN: 1/4 O.C.
13. ENVELOPE:
14. MAX WEIGHT, LB: 0.2
15. FEATURES: Welded End Fittings

ACTUATOR SPECIFICATION

PROJECT: OTV

ITEM NUMBERS: 12 DATE: 4-30-80 7-21-80, REV. A

1. NAME/TYPE: 28 FDC ELECTRIC ACTUATOR/90 DEGREE ROTATION FROM DUAL REDUNDANT TORQUE MOTORS DRIVING BALL SCREW, LEVEL/LINK
2. MIN. TORQUE, IN-LB: 35
3. MAX OVERLOAD TORQUE, IN-LB: 70
4. MIN. SPEED, DEG/SEC: 90
5. MAX REACTION TIME, SEC.: 0.015
6. MAX OUTPUT BACKLASH, DEG: 0.1
7. MAX POWER, WATTS: 98
8. MAX 10 SEC. OVERLOAD POWER, WATTS: 500
9. OPERATING TEMPERATURE: °F: -300 to + 100
10. DUTY & LIFE CYCLE: RAMP TO 10% & DWELL, 80% & HOLD 2000 SEC., RAMP CLOSED, 1000 CYCLES
11. MAX HOLD TORQUE, IN-LB: 10
12. POSITION INDICATION LVDT OFF BALL SCREW
13. WEIGHT, LB: 1.4
14. FEATURES: 1-1/2" OD, 5/8" ID. 0.53" WIDTH RARE EARTH BRUSH TYPE MOTORS DESIGNED FOR SPACE VACUUM: 5/8" OD, 3/8" SHAFT, 3/4" WIDTH BALL SCREW WITH 0.1 INCH LEAD: 0.5" LEVEL/LINK

VALVE SPECIFICATION

PROJECT: OTV EXPANDER

ITEM NUMBER: 13

DATE: 6-16-80
7-21-80 REV. A

1. NAME/TYPE: OXIDIZER INLET/BALL VALVE, ON/OFF

2. FLUID SERVICE: Liquid Oxygen (ρ= 71.2 lb/ft^3)

3. PRESSURE, PSIA: 16.

4. TEMPERATURE: 163°R Propellant, 560°R Max. Ambient

5. FLOW RATE, LB/SEC: 28.06 @ 7:1 MR

6. DELTA P, PSI: 0.1

7. MAX INTERNAL LEAK He, SCIM: 10.

8. MAX EXTERNAL LEAK He, SCIM: 1.0

9. ACTUATION: Spring Closed, 600 PSIG Actuator Open 100. SCIM He Max. Leakage

10. RESPONSE, SEC. 2.0

11. EQUIVALENT ORIFICE DIAMETER, IN: -

12. LINE SIZE, IN: 3.600 ID Straight Through

13. ENVELOPE: 5.4 In. Max. Length

14. MAX WEIGHT, LB: 4.4

15. FEATURES: Open/Close Position Indication Off Actuator, TFE Triangle Seals, Flange Inlet, Welded Tube Outlet, All Aluminum Construction

VALVE SPECIFICATION

PROJECT: OTV EXPANDER

ITEM NUMBER: 14

DATE: 6-16-80

7-21-80 REV. A

1. NAME/TYPE: Fuel Inlet/ Ball Valve, ON/OFF
2. FLUID SERVICE: Liquid Hydrogen (σ- 4.37 lb/ft^3)
3. PRESSURE, PSIA: 19.
4. TEMPERATURE: 37.8^{o}R Propellant, 560°R Max. Ambient
5. FLOW RATE, LB/SEC: 4.46 @ 6:1 MR
6. DELTA P, PSI: 0.1
7. MAX INTERNAL LEAK He, SCIM: 10.
8. MAX EXTERNAL LEAK He, SCIM: 1.0
9. ACTUATION: Spring Closed, 600 PSIG Actuator Open 100. SCIM He Max.Leakage
10. RESPONSE, SEC: 2.0
11. EQUIVALENT ORIFICE DIAMETER, IN: -
12. LINE SIZE, IN: 3.14 ID Straight Through
13. ENVELOPE: 4.7 In. Max. Length
14. MAX WEIGHT, LB: 4.0
15. FEATURES: Open/Close Position Off Actuator; TFE Triangle Seals, Flange Inlet, Welded Tube Outlet, All Aluminum Construction

VALVE SPECIFICATION

PROJECT: OTV EXPANDER

ITEM NUMBER: 15,16,17,18,19 **DATE:** 7-21-80 REV. A

1. NAME/TYPE: CONTROL SOLENOID VALVES/3-Way, Normally Closed
2. FLUID SERVICE: Gaseous, Nitrogen, Helium, Hydrogen
3. PRESSURE, PSIA: 600
4. TEMPERATURE: 160°R Min. Fluid, 560°R Max. Ambient
5. FLOW RATE, LB/SEC:
6. DELTA P, PSI:
7. MAX INTERNAL LEAK He, SCIM: 1.0
8. MAX EXTERNAL LEAK He, SCIM: 1.0
9. ACTUATION: 28 VDC Solenoid, 0.8 Amp.
10. RESPONSE, SEC: 0.02
11. EQUIVALENT ORIFICE DIAMETER, IN: 0.03
12. LINE SIZE, IN: 1/4 OD
13. ENVELOPE:
14. MAX WEIGHT, LB: 0.3
15. FEATURES: Unbalanced, direct operated valve with hermetic sealed solenoid; flat, metal-to-metal seating.